SYSTEM-LEVEL PERFORMANCE ASSESSMENT OF THE PROPOSED REPOSITORY AT YUCCA MOUNTAIN USING THE TPA VERSION 4.1 CODE

Prepared for

**U.S. Nuclear Regulatory Commission
Contract NRC–02–02–012**

Prepared by

**Sitakanta Mohanty (CNWRA)
Richard Codell (NRC)
Jose M. Menchaca (SwRI®)
Ronald Janetzke (CNWRA)
Michael Smith (CNWRA)
Patrick LaPlante (CNWRA)
Meraj Rahimi (NRC)
Albert Lozano (SwRI)**

**Center for Nuclear Waste Regulatory Analyses
San Antonio, Texas**

**September 2002
Revised December 2002
Revised March 2004**

ABSTRACT

The U.S. Nuclear Regulatory Commission (NRC), with the technical assistance from the Center for Nuclear Waste Regulatory Analyses, developed the Total-system Performance Assessment (TPA) code. This code was developed as a tool to assist NRC in its evaluation of performance assessments in any potential license application by the U.S. Department of Energy (DOE) for a repository at Yucca Mountain, Nevada. This report describes a series of computations performed using the TPA Version 4.1 code to calculate long-term repository performance estimates in light of uncertainty in conceptual models and associated input parameters. This report includes (i) system-level and process-level modeling results (e.g., intermediate results) to understand the influence of trends and variabilities in outputs; (ii) system-level sensitivity and uncertainty analysis results based on a variety of analysis techniques to understand the influence of parameters, alternative conceptual models, and subsystems (especially repository components) on repository performance; (iii) capability of barriers to reduce the flow of water and delay transport of radionuclides; (iv) consequence of human intrusion; and (v) synthesis of results to apply risk insights to assess the relative importance of the integrated subissues used by NRC to review the DOE total system performance assessment.

An influential parameter, alternative conceptual model, or subsystem is one that either produces significant uncertainty in performance estimates or one to which performance measures (e.g., regulatory compliance limits) are sensitive. Sensitivity and uncertainty analyses were conducted using numerous TPA Version 4.1 code runs for each sensitivity analysis technique. Results of system-level analyses are based on the peak dose from any realization and the peak expected dose to a receptor group 20 km [12.4 mi][1] from the repository during the 10,000-year compliance period. Limited results are presented for a 100,000-year time period to understand system characteristics that may not become apparent in the 10,000-year modeling results because of the calculated long life of the waste package.

For the basecase modeling scenario, which includes the seismic and climatic activity, peak risks of 0.21 µSv/yr [0.021 mrem/yr] and 90 µSv/yr [9 mrem/yr] were obtained for the 10,000- and 100,000-year simulation periods, respectively. The faulting scenario changed the peak expected dose negligibly. The igneous activity scenario increased the peak expected risk in 10,000 years to 3.6 µSv/yr [0.36 mrem/yr]. For the stylized human intrusion scenario, a peak risk of 1µSv/yr [0.1 mrem/yr] was obtained for the 10,000-year period. Only initially defective waste package failures contribute to the basecase risk because the performance calculations show that no waste packages in the repository fail from corrosion within 10,000 years. The geologic properties of the unsaturated and saturated zones limit releases to the accessible environment to only a few, long-lived, nonsorbing radionuclides. Np-237 is the only sorbing radionuclide contributing to dose estimates in this time period. Only a fraction of the precipitating water (0.002 percent of the precipitation or 0.0037 percent of the infiltration) was estimated to contact the waste form, which reflects diversion processes of the unsaturated zone, drip shield, and waste package.

Sensitivity analyses show that conceptual models of colloidal transport, spent nuclear fuel dissolution, spent nuclear fuel wetting, and wetted fuel surface area may substantially influence

---

[1]The analyses presented in this report were completed before the location of the receptor group was defined to be 18 km [11.2 mi] in 10 CFR Part 63.

estimated risk from the basecase scenario. The direct release of radioactivity to the surface of the earth for extrusive basaltic volcanism uses a geometry-based model, which estimates the number of waste packages affected directly from the width of the volcanic conduit intersecting the repository. Alternative, explicit models for the interaction of magma with waste packages, based on physics of magma flow, can show an increased risk of an order of magnitude.

Limited distributional sensitivity analyses conducted in this report with the most influential parameters suggest a 10 percent change to the mean of a parameter's distribution can increase risk by as much as 150 percent. Performance results show comparable sensitivity to both the engineered and the natural repository component groups. The influential parameters, alternative conceptual models, and repository components were then compared to the current integrated subissues, which are used by the NRC to focus work on items important to repository performance. Five of 14 integrated subissues did not show up as significant.

Parametric sensitivity analysis serves an important purpose in identifying the effect of input parameter uncertainty on system performance to obtain risk insights. Repository component and alternative conceptual model sensitivity analyses provide additional key information about the importance of integrated subissues that can be used as a starting point by the analyst to determine why certain parameters or models do or do not show up as important.

The analyses and results are limited by simplifications in models and assumptions regarding parameter values. As a consequence, these results are for illustration and are not indicative of repository safety. However, the estimates resulting from this study will assist the staff to focus its attention on phenomena that may be most important relative to repository performance. The manner in which these analyses were conducted or the assumptions and approaches used should not be construed to express the views, preferences, or positions of the NRC staff regarding implementation of regulations for Yucca Mountain or the ability of a potential Yucca Mountain repository to comply with those regulations.

CONTENTS

CONTENTS (continued)

CONTENTS (continued)

CONTENTS (continued)

CONTENTS (continued)

CONTENTS (continued)

FIGURES

FIGURES (continued)

FIGURES (continued)

TABLES

TABLES (continued)

EXECUTIVE SUMMARY

The U.S. Nuclear Regulatory Commission (NRC), with technical assistance from the Center for Nuclear Waste Regulatory Analyses (CNWRA), developed the Total-system Performance Assessment (TPA) Code. This code was developed as a tool to assist NRC in its evaluation of performance assessments in any potential license application by the U.S. Department of Energy (DOE) for a repository at Yucca Mountain, Nevada. To date, four reports have been written by the NRC staff about performance assessment for the proposed Yucca Mountain repository. The first, referred to as Iterative Performance Assessment Phase 1 (Codell, et al., 1992), assembled and demonstrated the NRC assessment methodology. The second NRC total system performance assessment, Iterative Performance Assessment Phase 2 (Wescott, et al., 1995), used the TPA Version 2.0 code to investigate the features, events, and processes influencing performance of the proposed Yucca Mountain repository. Information obtained in these iterative performance assessment analyses was used in NRC reviews of early DOE total system performance assessments of Yucca Mountain. The third NRC total system performance assessment (Mohanty, et al., 1999) used the TPA Version 3.1 code (Mohanty and McCartin, 2001) to assist the NRC to evaluate the DOE viability assessment. The fourth NRC Total System Performance Assessment (Mohanty, et al., 1999) used the TPA Version 3.2 code (Mohanty and McCartin, 1998), which implemented the Total System Performance Assessment–Viability Assessment design changes. This allowed an independent, in-depth analysis at the system and subsystem levels to attribute risk significance to integrated subissues. Revisions were made to the TPA Version 3.2 code to implement the DOE Enhanced Design Alternative II, new and revised NRC conceptual models and risk assessment methods leading to the development of the TPA Version 4.1 code (Mohanty, et al., 2002). The revised code was a tool used by the staff in evaluating the Total System Performance Assessment–Site Recommendation. This report documents the most recent overall system- and process-level sensitivity and uncertainty analyses performed by NRC and CNWRA using models and conditions similar to the Total System Performance Assessment–Site Recommendation. This report presents

- A brief description of the conceptual models implemented in the TPA Version 4.1 code and a formal presentation of the method for combining the disruptive event scenario results with the basecase scenario (Chapters 2 and 3)

- An indepth discussion of deterministic and stochastic results for the basecase and disruptive scenario cases based on peak risk and capability of barriers to reduce flow of water and to prevent or delay radionuclide transport (Chapters 3 and 7)

- The results of system-level parametric sensitivity and uncertainty analyses using statistical and nonstatistical techniques to determine the parameters and barrier components that most influence repository performance (Chapters 4, 5, and 6)

- The results from the alternative conceptual model sensitivity analysis using either models explicitly incorporated in the TPA Version 4.1 code or models that can be mimicked through adjustment of input parameters to determine model and parameter uncertainties (Chapters 2, 3, and 4)

- An estimation of the relative importance of the integrated subissues to focus staff efforts (Chapter 7)

- A documentation of improvements in NRC staff capabilities in performance assessment based on the insights gained from process- and system-level results and sensitivity analyses (Chapter 8)

System-level performance was evaluated using the basecase data set in which 330 of 950 parameters were sampled to represent data uncertainty and variability. The chosen parameters were screened from the larger list on the basis of staff experience with the models, to include those parameters most likely to have a significant impact on the results. To develop a better understanding of the trends of the outputs at a process level, results from a single realization (using the mean value data set) were also analyzed. Calculations to date using the basecase data set (the basecase is defined as the undisturbed scenario along with the effects of rockfall due to seismicity) indicate peak expected doses of 2.1×10^{-4} mSv/yr [0.021 mrem/yr] in 10,000 years, the compliance period. For a simulation period, three radionuclides (I-129, Tc-99, and Np-237) consistently are the primary contributors to the peak expected dose. The gap fraction does not substantially influence peak expected dose. Igneous activity is the primary disruptive scenario contributing to the peak expected dose, estimated to be 3.6 µSv/yr [0.36 mrem/yr]. The faulting disruptive event is a negligible contributor to the peak expected dose (Chapter 3).

The consequences of human intrusion were evaluated using a stylized, bounding analysis. One waste package was assumed to fail non-mechanistically, resulting in a peak dose of 0.001 mSv/yr [0.1 mrem/yr] during the compliance period.

Subsystem capabilities for reducing the water flow rate and preventing or delaying radionuclide transport were derived from the total system performance assessment results. The analyses showed that only a fraction of the precipitating water contacts the drip shield and the waste package (0.02 percent of the precipitation) and enters the failed waste packages in the basecase (0.002 percent of the precipitation) showing the capability of the unsaturated zone above the repository (Chapters 3 and 7).

The sensitivity and uncertainty analyses were conducted using numerous (several thousand for each analysis method) TPA Version 4.1 code runs. The sensitivity and uncertainty of repository performance to specific parameters were evaluated using different statistical and nonstatistical tests. These tests examined the sensitivity of repository performance to individual parameters to identify those most important to repository performance. Although the report identifies and presents influential parameters for both 10,000- and 100,000-year simulation periods, risk insights are summarized for only the 10,000-year compliance period. Limited results are presented for a 100,000-year time period to understand system characteristics that may not become apparent in the 10,000-year modeling results because of the calculated long life of the waste packages. An influential parameter, alternative conceptual model, or repository component is one that either drives uncertainty in repository performance, or one to which the estimated performance is sensitive. Several parameters were found most influential for the basecase (in order of influence on the peak dose for each realization): (i) mean annual infiltration at start, (ii) drip shield failure time, (iii) the preexponential term for the spent nuclear fuel dissolution rate calculation, (iv) areal fraction of the repository wetted by water infiltrating into the repository, (v) the focusing factor that modifies the flow reaching a wetted waste package, (vi) the well

pumping rate at the 20-km [12.4-mi][1] receptor group location, (vii) alluvium sorption properties for Np-237, (viii) length of the alluvium pathway in the saturated zone, (ix) fraction of the condensate from thermal reflux moving toward the repository, and (x) fraction of waste packages that are initially defective (Chapters 4 and 7).

The two orders of magnitude higher risk (i.e., probability-weighted dose) from the igneous activity case compared to the basecase implies that the igneous activity related parameters can play a dominant role in the performance though the risk is still small. The influential parameters include (i) airborne mass load above the fresh ash blanket, (ii) wind speed, (iii) diameter of volcanic conduit, (iv) volcanic event power, (v) volcanic event duration, (vi) time of next volcanic event in the region of interest, and (vii) ash mean particle diameter (Chapters 4 and 7).

Distributional sensitivity analyses were conducted to investigate the impact of distribution function shape on the dose responses. Using the 10 most influential parameters identified by the parametric sensitivity analysis, the distributional sensitivities showed that the choice of distribution function plays an important role in the performance assessment estimation. For example, a 10-percent change to the mean of the distribution function representing the uncertainty in the flow multiplication factor that modifies the flow reaching a wetted waste package results in a 150-percent change in the peak expected dose. Performance calculations also showed high sensitivity to the choice of the distribution function for the drip shield failure time parameter. The types of errors in constructing a distribution function that could lead to the improper choice of a distribution function have been highlighted (Chapter 5 and 7).

Alternative conceptual model sensitivity studies were conducted on a case-by-case basis with appropriate consideration of uncertainty in the model parameters. Analyses used peak expected dose as the performance measure. Alternative conceptual model sensitivity analyses showed that colloidal transport (if plausible, in the Yucca Mountain environment) and the spent nuclear fuel dissolution rate, in combination with the spent nuclear fuel wetting mode and the surface area over which water contacts spent nuclear fuel, could substantially influence basecase scenario risk. An alternative process-based model for magma-tunnel interaction increased the estimate of number of waste packages contributing to direct release and the consequent peak risk by one order of magnitude (Chapters 2, 3, 4, and 7). All alternative conceptual models were assumed to be as probable as the basecase conceptual models.

Repository component sensitivity analyses were performed for two reasons: (i) obtaining sensitivity at an easily understood subsystem level such as a physical repository component and (ii) estimating the importance of the subsystem when parametric sensitivity analysis did not lead to failure (e.g., waste package) during the compliance period or the conservativeness in the conceptual model prevented noticeable dose response to the data range. Analyses showed that repository performance is very sensitive to the waste package repository component. Also, the group of natural repository components (i.e., unsaturated zone and saturated zone together) showed approximately the same level of sensitivity as the waste package repository component. This suggests that analyses should focus on determining if any undesirable constraints in parameters and models for waste package life prediction are responsible for the long waste package life. The repository component sensitivity analysis described in this report is not

---

[1]The analyses presented in this report were completed before the location of the receptor group was defined to be 18 km [11.2 mi] in 10 CFR Part 63.

intended to provide either guidance to DOE or to describe a preferred approach for demonstrating the capability of a barrier. These analyses were performed to further the staff efforts to understand the TPA Version 4.1 code and to explore where to improve understanding of the repository system (Chapter 6 and 7).

The influential parameters were traced back to the integrated subissues used by NRC to focus its high-level waste program on aspects important to repository performance (NRC, 1998). Nine out of 14 integrated subissues have at least one influential parameter (including the integrated subissues related to disruptive scenarios), based on the results of the TPA Version 4.1 code. The integrated subissues that showed up as important to performance are (i) volcanic disruption of waste packages (DIRECT1), (ii) airborne transport of radionuclides (DIRECT2), (iii) radionuclide transport in the saturated zone (SZ2), (iv) degradation of engineered barriers (ENG1), (v) flow paths in the unsaturated zone (UZ2), (vi) quantity and chemistry of water contacting waste packages and waste forms (ENG3), (vii) radionuclide release rates and solubility limits (ENG4), (viii) climate and infiltration (UZ1), and (ix) mechanical disruption of engineered barriers (ENG2). The integrated subissues that did not show up as important are (i) radionuclide transport in the unsaturated zone (UZ3), (ii) flow rates in the saturated zone (SZ1), (iii) representative volume (DOSE1), (iv) redistribution of radionuclides in soil (DOSE2), and (v) biosphere characteristics (DOSE3). DOSE1 has a one-to-one linear effect on estimated dose, however, this integrated subissue is moot because the pumping rate is now specified in the regulation. Note that DOSE2 and DOSE3 integrated subissues were determined to be unimportant only on the basis of parametric sensitivity. Alternative conceptual models may alter this finding (Chapter 7).

This total system performance assessment aids the NRC staff by focusing their review of DOE total system performance assessments on those models and parameters that most affect estimated system performance. It should be noted that the results presented in the following chapters are based on numerous simplifying assumptions and use only limited site-specific data. Parametric sensitivity analysis sometimes fails to show the importance of processes or parameters, especially those associated with radionuclides that never arrive at the pumping well within the regulatory period. Therefore, several analyses in this report were conducted using data outside the range (e.g., alternative conceptual model and repository component sensitivity) to identify areas where the analyst should focus.

Conclusions drawn from the analyses presented in this report may change as the models and assumptions are updated based on revised design, ongoing site characterization, recommendations from reviewers and experts, and improved model conceptualization and data interpretation by staff. The analyses also contain uncertainties regarding conceptual models for consequences and scenarios. Finally, this report should be considered as an interim application of some of the methods the NRC staff developed to review a performance assessment submitted by DOE as part of any potential license application.

This report was prepared to document work performed by CNWRA for NRC under Contract No. NRC–02–02–012. The activities reported here were performed on behalf of the NRC Office of Nuclear Material Safety and Safeguards, Division of High-Level Waste Repository Safety. The report is an independent product of CNWRA and does not necessarily reflect the views or regulatory position of NRC.

References

Codell, R.B, N. Eisenberg, D. Fehringer, W. Ford, T. Margulies, T. McCartin, J. Park, and J. Randall. NUREG–1327, "Initial Demonstration of the NRC's Capability to Conduct a Performance Assessment for a High-Level Waste Repository." Washington, DC: NRC. May 1992.

Mohanty, S. and T.J. McCartin. "NRC Sensitivity and Uncertainty Analyses for a Proposed High Level Waste Repository at Yucca Mountain, Nevada, Using TPA 3.1." San Antonio, Texas: CNWRA. February 2001.

Mohanty, S. and T.J. McCartin. "Total-system Performance Assessment (TPA) Version 3.2 Code: Module Description and User's Guide." San Antonio, Texas: CNWRA. 1998.

Mohanty, S., T.J. McCartin, and D.W. Esh. "Total-system Performance Assessment (TPA) Version 4.0 Code: Module Descriptions and User's Guide." San Antonio, Texas: CNWRA. 2002.

Mohanty, S., R. Codell, R.W. Rice, J. Weldy, Y. Lu, R.M. Byrne, T.J. McCartin, M.S. Jarzemba, and G.W. Wittmeyer. "System-Level Repository Sensitivity Analyses Using TPA Version 3.2 Code." CNWRA 99-002. San Antonio, Texas: CNWRA. 1999.

NRC. "Issue Resolution Status Report Key Technical Issues: Total System Performance Assessment and Integration." Revision 1.0. Washington, DC: NRC. 1998.

Wescott, R.G., M.P. Lee, N.A. Eisenberg, T.J. McCartin, and R.G. Baca, eds. NUREG–1464, "NRC Iterative Performance Assessment Phase 2." Washington, DC: NRC. October 1995.

ACKNOWLEDGMENTS

QUALITY OF DATA, ANALYSES, AND CODE DEVELOPMENT

DATA: CNWRA-generated data contained in this report meet quality assurance requirements described in the CNWRA Quality Assurance Manual. Data from other sources are freely used. The respective sources of non-CNWRA data should be consulted for determining levels of quality assurance.

ANALYSES AND CODES: The TPA Version 4.1k code and variations have been developed following the procedures described in the CNWRA Technical Operating Procedure (TOP–018), which implements the quality assurance requirements contained in the CNWRA Quality Assurance Manual. The TPA Version 4.1.1 code reflects a minor modification to the Version 4.1k code to produce additional information for Chapter 7. Codes used in conducting sensitivity analyses have also been developed following procedures described in TOP–018.

1 INTRODUCTION

In accordance with the provisions of the Nuclear Waste Policy Act of 1982 (1982), the U.S. Nuclear Regulatory Commission (NRC) is responsible for evaluating any license application for a proposed geologic repository constructed for emplacement of high-level nuclear waste [i.e., commercial spent nuclear fuel, several types of U.S. Department of Energy (DOE)-owned high-level nuclear waste from the production of nuclear weapons, spent nuclear fuel from weapon production reactors, research reactors, and U.S. Navy reactors] at Yucca Mountain, Nevada. In support and preparation of the regulatory review activities outlined in the Nuclear Waste Policy Act of 1982, the NRC staff is conducting detailed technical performance assessments to understand the potentially important isolation characteristics and capabilities of the proposed repository system at Yucca Mountain.

The performance assessment activity is a part of an ongoing iterative process at the NRC to prepare for the review of a potential DOE license application. As part of these iterative performance assessment activities, NRC and its support contractor, the Center for Nuclear Waste Regulatory Analyses (CNWRA), are using the TPA code. The TPA code is not meant to demonstrate compliance (that is the responsibility of the DOE), but is a tool to allow NRC to perform an independent analysis of a license application for the proposed repository and to support review capability. The TPA code, which evolves with each iterative performance assessment phase, is designed to simulate the behavior of the repository system, taking into account the essential characteristics of the natural and engineered barrier subsystems and changes in knowledge about the geologic setting and design. To support identification of features, events, and processes of the repository important to safety, this document presents a variety of estimates of the sensitivity of repository performance to uncertainty in the repository system using the latest version of the TPA code, Version 4.1.[1] For this report, sensitivity is defined as the relative change in model response (i.e., output) for a unit change of input, and uncertainty is defined as the comparative change in overall output range because of input value uncertainty.

NRC previously conducted analyses of repository performance (Codell, et al., 1992; Wescott, et al., 1995; Mohanty, et al., 1999). For the latest iteration, Version 4.1 of the TPA code was developed to accommodate changes to the design of the proposed repository and incorporate the latest understanding of features, events, and processes at Yucca Mountain. This latest version includes (i) a much finer spatial discretization capability for the repository and geologic system; (ii) incorporation of the DOE Enhanced[2] Design Alternative II, including the drip-shield barrier; (iii) an alternative waste package failure mode that accounts for complex igneous processes; (iv) variable length flow paths in the alluvium to account for uncertainties in site saturated zone hydrology; and (v) enhanced biosphere dose modeling capabilities that incorporate biosphere parameter uncertainties.

---

[1]TPA Version 4.0 code is the last iteration of the user's guide, however, Version 4.1, more specifically, Version 4.1j was used for calculations in this report. Despite several changes to the code in moving from Version 4.0 to 4.1j, the documentation in the user's guide for Version 4.0 remains applicable. Most revisions pertain to replacing old with new data as these were made available through the course of developing this report.

[2]DOE has modified the Enhanced Design Alternative II several times. The particular modified design used in this report is the one that was available at the early stage of the development of this report.

1.1　Background

Performance assessments for geologic repositories are based on conceptual models of physical processes and parameters derived from field and laboratory data or expert elicitation. Because of measured data being sparse and spatially variable and the inherent uncertainty involved in simulating physical processes for many thousands of years, the results of performance assessment are uncertain. Therefore, an important aspect of conducting a performance assessment is quantifying the sensitivity of the results to the uncertainty associated with the input parameters and alternative conceptual models. Such an analysis will provide information delineating those input parameters, alternative conceptual models, and subsystems that most affect the model results. Knowing which parameters, models, and subsystems most influence model results allows the analyst to improve the conceptualization of the repository system and improve confidence in the numerical results. Likewise, identification of the parameters, models, and subsystems that produce the most uncertainty in results provides a means of comparing and evaluating different performance assessment models and indicates where future design, site characterization, and analysis activities should be focused.

Staff developed a systematic, hierarchical approach to reviewing the DOE total system performance assessments, illustrated in Figure 1-1. The focal point is the overall repository system where the performance measure is the expected annual dose to the reasonably maximally exposed individual during the 10,000-year time period of interest. Analysis of overall repository system performance results using a variety of techniques provides useful insights to the contribution of subsystems and components to overall performance. To facilitate review of the DOE total system performance assessments, staff will examine the contribution to performance from each of three repository subsystems—engineered, geosphere, and biosphere—as shown in the second tier of Figure 1-1. Each of these subsystems is further subdivided into discrete components that include the engineered barriers that make up the engineered system, unsaturated zone flow and transport, saturated zone flow and transport, direct release to the biosphere, and dose calculation for the biosphere. Recognizing there are many different ways of dividing the overall system into smaller, analyzable components, this particular division is primarily based on the natural progress of radionuclide release and transport to a receptor group at the Yucca Mountain site and takes advantage of the results of past NRC total system performance assessments and reviews of the DOE total system performance assessments. At the base of the hierarchy are the key elements of the repository system (integrated subissues) that need to be abstracted into a total system performance assessment.

1.1.1　Previous Iterative Performance Assessment Analyses

To date, four reports have been written by the NRC staff on performance assessment for the proposed Yucca Mountain repository. The first, referred to as Iterative Performance Assessment Phase 1 (Codell, et al., 1992), developed and demonstrated the NRC assessment methodology. Iterative Performance Assessment Phase 1 examined the sensitivity and uncertainty in radionuclide releases to the accessible environment for a geologic repository in unsaturated tuff. The second NRC total system performance assessment, Iterative Performance Assessment Phase 2 (Wescott, et al., 1995), was performed using the TPA Version 2.0 code to investigate the features, events, and processes influencing isolation performance of the proposed Yucca Mountain repository.
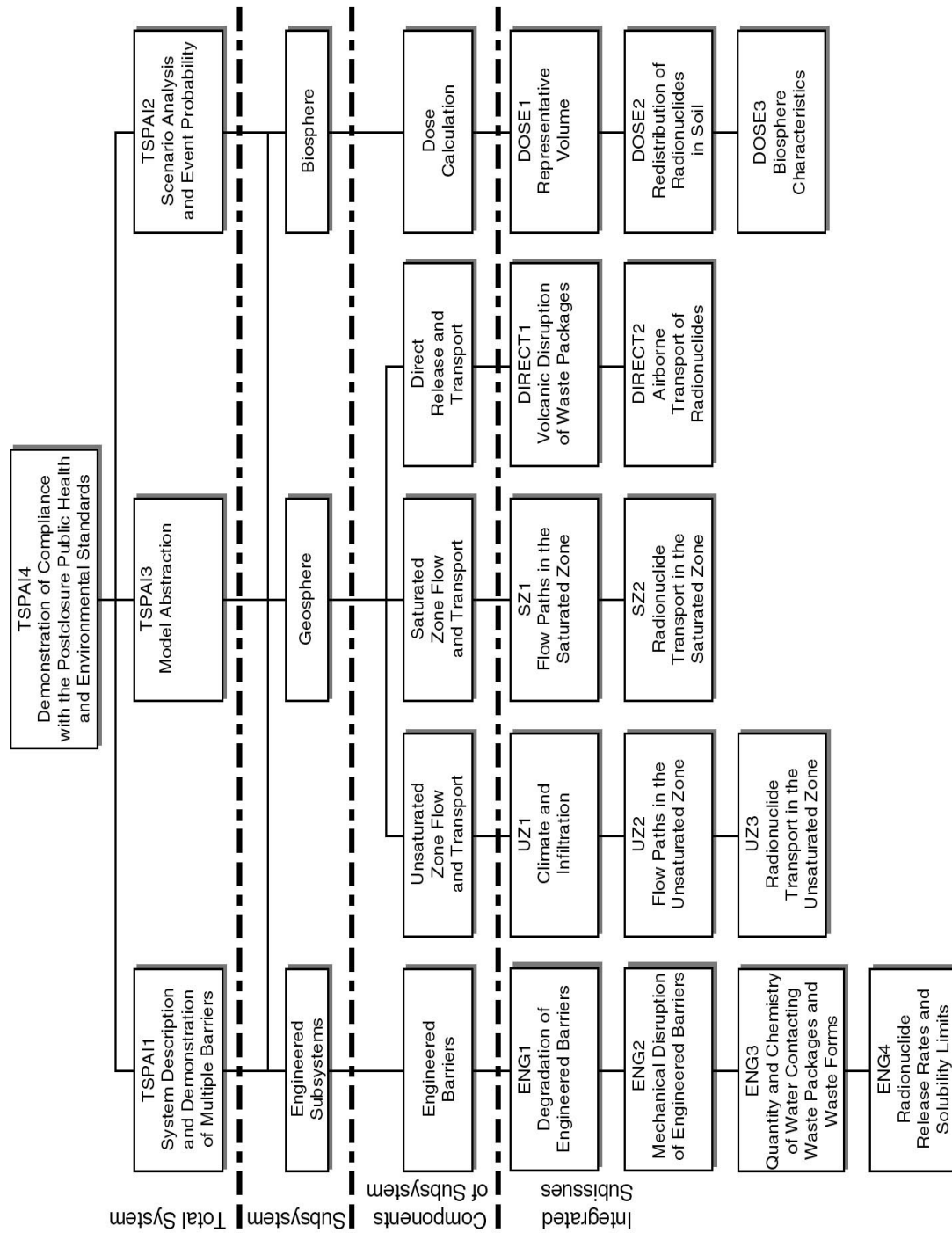
Figure 1-1. Flowdown Diagram Showing the Subsystems and the Integrated Subissues

Information obtained in these iterative performance assessment analyses was used in NRC reviews of early DOE total system performance assessments for Yucca Mountain. At the time Phase 2 analyses were completed in 1993, the overall performance measures for the geologic repository used in the iterative performance assessment were cumulative total releases of radionuclides (normalized release) to the accessible environment and radiation dose (effective dose equivalent) to the exposed population. These performance measures were consistent with regulations in 40 CFR Part 191 (Code of Federal Regulations, 2003) and 10 CFR Part 60 (Code of Federal Regulations, 2003) in effect at the time. The third NRC total system performance assessment (NRC, 1999b) was performed a few years later using the TPA Version 3.1 code to determine whether or not the NRC would be able to quantitatively evaluate the conclusions reached by DOE in its viability assessment. During this period, the focus of performance estimates emphasized radiation dose as a primary performance measure in anticipation of forthcoming U.S. Environmental Protection Agency standards for Yucca Mountain in 40 CFR Part 197 (Code of Federal Regulations, 2001). Subsequent to developing and testing the TPA Version 3.1 code, detailed sensitivity and uncertainty analyses were undertaken (NRC, 1999a) that indicated the need for further refinement of the TPA code prior to its use to evaluate the DOE Total System Performance Assessment–Viability Assessment [Civilian Radioactive Waste Management System Management and Operating Contractor (CRWMS M&O), 1998]. Revisions made to the TPA code led to the TPA Version 3.2 code (Mohanty and McCartin, 1998), which was used to evaluate the Total System Performance Assessment–Viability Assessment (CRWMS M&O, 1998). This version of the TPA code was used to conduct additional sensitivity analyses documented in the fourth of the aforementioned performance assessment reports (Mohanty, et al., 1999). Analyses using the TPA Version 3.1 code and above were based on the new regulation [10 CFR Part 63 (Code of Federal Regulations, 2002), which is based on the risk-informed, performance-based approach. The new regulation provides site-specific criteria (including design criteria) and eliminates detailed requirements such as quantitative subsystem performance objectives in Part 60.

In addition, the total system performance assessment analyses are used to focus NRC activities on factors of greatest importance to repository performance. The site-specific regulations developed by NRC for the Yucca Mountain repository are risk-informed and performance-based. Therefore, the NRC review of a potential license application to build and operate a deep geologic repository at Yucca Mountain will focus on those physical aspects of the repository system of greatest importance to radiological safety. The results from this study, in part, will be used to assist development of the review strategy outlined by the NRC in its Yucca Mountain Review Plan (NRC, 2002).

1.1.2   Iterative Performance Assessment Phase 1 Sensitivity and Uncertainty Analyses

Four sensitivity or uncertainty analyses were performed for Iterative Performance Assessment Phase 1 (Codell, et al., 1992): (i) demonstration of the effect of individual parameters on the resultant complementary cumulative distribution function of cumulative release to the accessible environment, (ii) use of stepwise linear regression to estimate sensitivity of key parameters in the consequence models, (iii) determination of relative importance of individual radionuclides in the waste, and (iv) sensitivity of complementary cumulative distribution functions to the performance of the natural and engineered barriers. The sensitivity and uncertainty analyses considered only groundwater pathway releases. Gaseous release of radionuclides was not part

of the Iterative Performance Assessment Phase 1 total system performance assessment results but was included as an auxiliary analysis.

Although Iterative Performance Assessment Phase 1 conducted full sensitivity and uncertainty analyses for the groundwater pathway, only complementary cumulative distribution functions for cumulative release [as required by 40 CFR Part 191 (Code of Federal Regulations, 2000) and 10 CFR Part 60 (Code of Federal Regulations, 2000)] were generated for the scenario cases (basecase, basecase with human intrusion, and basecase with pluvial conditions with and without human intrusion). Cumulative release refers to the sum of releases to the accessible environment of all radionuclides during the time period of interest. Cumulative distribution functions reflected the uncertainty in the sampled parameters propagated through the analysis. Peak dose was not calculated as a performance measure for the Iterative Performance Assessment Phase 1 study.

1.1.3   Iterative Performance Assessment Phase 2 Sensitivity and Uncertainty Analyses

In Iterative Performance Assessment Phase 2 (Wescott, et al., 1995), model results were evaluated to develop regression equations describing total system performance assessment model output and to analyze input parameter sensitivity. Techniques used to develop a regression equation that emulated the total system performance assessment model included transformation of data (Iman and Conover, 1979; Seitz, et al., 1991); test for heteroscedasticity (residual variation—Draper and Smith, 1981; Bowen and Bennett, 1988; Sen and Srivastava, 1990); and Mallows' C_p statistic (Sen and Srivastava, 1990). In addition to techniques used in previous performance assessments (e.g., the stepwise linear regression), several techniques were evaluated to determine parameter importance and sensitivity, including Kolmogorov-Smirnov and Signs tests (Bowen and Bennett, 1988) and differential analysis (Helton, et al., 1991).

Phase 2 Iterative Performance Assessment also included igneous activity, seismicity, faulting, climate change, and exploratory drilling. Sensitivity and uncertainty analyses were conducted for the undisturbed case as well as for the aforementioned disruptive scenarios. These analyses were conducted with radionuclide release to the accessible environment and integrated population dose as the output variables.

1.1.3   TPA Version 3.1 Code Sensitivity and Uncertainty Analyses

For the TPA Version 3.1 code (NRC, 1999b), a variety of analytical procedures were implemented to assess sensitivity of the estimated peak dose because of variations in the values of model parameters as well as changes resulting from use of alternative conceptual models. Scaled sensitivity coefficients were obtained by univariate and stepwise, multiple linear regression, and by standard differential analysis. To make linear regression models as accurate as possible, the dependent (peak dose) and independent (sampled inputs) variables were transformed using four methods: (i) normalization, in which the variable is divided by its mean; (ii) standardization, in which the difference between the variable and its mean is divided by the standard deviation of the variable; (iii) rank transformation, in which the value of the variable is replaced by its numerical rank; and (iv) logarithmic transformation, in which a multiplicative model is converted to an additive model. The statistical significance of the scaled sensitivity coefficients obtained by stepwise regression was determined using student t-statistic.

The importance or influence of each parameter was ranked by the order in which the stepwise procedure selected the parameter for inclusion as an explanatory variable in the regression equation and by the use of Kolmogorov-Smirnov and Sign tests (Bowen and Bennett, 1998).

Sensitivity coefficients were calculated for both 10,000- and 50,000-year time periods and for waste canisters constructed with an inner corrosion-resistant layer of either Alloy 625 or Alloy 22 leading to the identification of four distinct sets of important parameters. The effects of employing alternative conceptual models were also investigated for a variety of repository subsystems. Descriptions of alternative conceptual models considered include (i) backfilling of the repository, (ii) diffusion in the rock matrix, (iii) credit for protection of the fuel provided by zircalloy cladding, (iv) focusing the flow of water to a smaller number of waste packages, (v) use of the flowthrough model for spent nuclear fuel dissolution and transport, (vi) radionuclide release rates based on natural analogs for spent nuclear fuel, (vii) no credit for sorption of radionuclides, and (viii) instantaneous failure of all waste packages.

Based on the results of the sensitivity and uncertainty analyses, preliminary conclusions were drawn about the relative importance of the integrated subissues. For the 10,000-year simulation period, the most important integrated subissues are those for waste package corrosion and the quantity and chemistry of water contacting the waste packages. When Alloy 22 is used, corrosion of the waste packages is minimal during the 10,000-year simulation period, and mechanical disruption of the waste packages is the most important integrated subissue. For the 50,000-year time period, the integrated subissues related to dilution of radionuclides in groundwater through well pumping and retardation in water production zones and alluvium are most important.

1.1.5   TPA Version 3.2 Code Sensitivity and Uncertainty Analyses

The TPA Version 3.2 code sensitivity and uncertainty analyses (Mohanty, et al., 1999) emphasized step-by-step evaluation of total system performance using intermediate code results that reflected the behavior of individual processes and subsystems. Analyses of results were based on TPA Version 3.2 code runs involving (i) a single realization with all sampled parameters fixed at mean values and (ii) multiple realizations where uncertain parameters were sampled from assigned data ranges. Effects of parametric uncertainty on performance results were analyzed using scatterplot and stepwise multiple linear regression techniques (as previously done), however, the application of additional techniques such as the Morris method, Fourier Amplitude Sensitivity test, and Parameter Tree method diversified the suite of methods used to gain insight to parameter sensitivities. The sensitivity and uncertainty analyses were conducted using numerous TPA Version 3.2 code runs (several thousand realizations) for each sensitivity analysis technique. Results of system-level analyses were based on peak dose and peak expected dose to a receptor group 20 km [12.4 mi] from the repository during the 10,000 (compliance period), 50,000, or 100,000 years after closure (a longer period was used for investigating any significant effects that may not be evident because of the calculated long life of the waste package).

System-level results indicated the igneous activity scenario presented a greater risk than the basecase scenario representing undisturbed repository performance. Influential parameters for the 10,000- and 50,000-year time periods were mapped to the integrated subissues, and seven of the integrated subissues were identified as not significant for the 10,000-year period. The most sensitive integrated subissues identified for 10,000 years included (i) waste package

degradation, (ii) quantity and chemistry of water contacting waste packages and waste forms, (iii) spatial and temporal distribution of water flow, (iv) retardation in the water production zone and alluvium, (v) dilution of radionuclides in groundwater because of well pumping, (vi) volcanic disruption of waste packages, and (vii) airborne transport of radionuclides. Staff working on various key technical issues used this information to improve models and data supporting parameter uncertainty distributions.

1.2   Purpose of Current Analysis

The current sensitivity and uncertainty analyses involve a variety of techniques used in the aforementioned previous iterations. The objectives of the analyses described in this report build on the goals of previous iterations and include

- Inform staff reviews of the DOE TPA on those factors most significant to total system performance.

- Within the framework of the total system performance assessment model, determine the extent repository barriers reduce water flow and prevent or delay radionuclide transport to the receptor location.

- Explain the performance of the repository system based on modeled repository behavior at the process, subprocess, and subsystem levels.

- Estimate the risk and associated uncertainty to an average individual at the receptor location from the basecase scenario (a scenario where the deterioration of the engineered system takes place through a naturally slow process) and from disruptive event scenarios (where rare acute natural events can impact repository performance).

- Determine the input parameters (range and type of distribution), alternative conceptual models, and subsystems in the TPA Version 4.1 code that have the greatest effect on the estimated peak dose for the time period of interest at the receptor location by using a variety of techniques. This report summarizes analyses conducted to determine the parameters, alternative conceptual models, and subsystems that have the greatest influence on total system performance.

- Estimate the relative importance of the integrated subissues or key elements of subsystem abstraction.

- Continue improving staff capabilities, including the TPA code, for independent evaluation of future DOE total system performance assessments for the site recommendation and license application for the proposed Yucca Mountain repository.

Since the release of the TPA Version 3.2 code, which was used in the last published sensitivity analysis report (Mohanty, et al., 1999), several major improvements were incorporated into the TPA code and associated input data sets that affect sensitivity analysis results. Although most changes were based on new information provided by DOE after completion of the TPA Version 3.2 code, major modifications made to the TPA Version 4.1 code include

- Incorporation of the DOE Enhanced Design Alternative II and drip-shield barrier into performance calculations

- Addition of waste package failure modes resulting from complex igneous process calculations performed outside the TPA Version 4.1 code

- Improvements of the matrix diffusion model for saturated zone hydrologic transport calculations

- Variation of length for the tuff and alluvium groundwater flow paths to incorporate current uncertainties in site hydrology

- Addition of time dependency to the calculation of resuspension of ash deposits for the inhalation dose calculations following a postulated igneous event

- Enhancement of biosphere dose modeling capabilities to improve integration with total system calculations, propagate input uncertainties to dose results, and provide greater flexibility in parameter input and output

- Inclusion of much finer discretization capability for the repository and geologic setting

A detailed list of modifications made for the TPA Version 4.1 code is provided in Mohanty, et al. (2002).

1.3   Report Organization

This report documents the most recent system-level analyses performed by NRC and CNWRA that were conducted using the TPA Version 4.1 code. Chapter 2 provides a brief description of the conceptual models in the TPA Version 4.1 code. Chapter 3 presents an analysis of total system behavior. Analyses using the mean value data set to explain the trend in the intermediate and final outputs are presented in this chapter for the basecase and for the disruptive events cases. Results from multiple realizations using basecase data and data associated with disruptive events are explored in this chapter to highlight how variability in sampled parameters leads to variability in dose. These results have been used to analyze the extent to which the barriers in the repository reduce flow of water and delay transport of radionuclides.

Chapter 4 describes the system-level sensitivity studies, which were conducted in two parts. The sensitivity and uncertainty of repository performance to specific parameters were evaluated using a variety of statistical tests because no single test is comprehensive. The use of numerous methods (described in this chapter and Appendixes A–D) to examine the sensitivity of repository performance to individual parameters is intended to identify, as comprehensively as possible, those parameters most important for understanding repository performance. The parameters identified as important are also verified to provide additional confidence in the results. Alternative conceptual models and disruptive scenario cases were compared to evaluate the relative importance of specific components and assumptions used in the model. Analyzing the influence of individual components of the model using the full set of parameter values and a comprehensive model of repository behavior allows the relative importance of the components to be investigated.

Chapter 5 describes distributional sensitivity analysis methods and results. This chapter investigates if the repository performance is sensitive to the selected distribution type for a parameter. The choice of distribution function, which is greatly influenced by the lack of sufficient data, can affect significantly the dose responses. Chapter 6 presents the subsystem sensitivity analysis approach and results used to understand the influence of the subsystems on performance assessment results. Chapter 7 provides a synthesis of all results, including risk insights, gained from the analyses. Risk insights are presented through (i) the description of barrier capabilities in reducing flow of water and preventing or delaying movement of radionuclides, (ii) the identification of parameters that are important based on parametric and distributional sensitivity analyses, (iii) subsystems that are influential based on repository component sensitivity analyses, (iv) conceptual models that are important based on alternative conceptual model studies, and (v) results that are mapped to the integrated subissues. Chapter 8 presents the summary and conclusions. Appendix E describes the abbreviated parameter names used throughout the report, and Appendixes F and G provide additional details supporting performance calculations of human intrusion and in-package criticality.

1.4   Caveats

Because it is not practical to model a system as complex as a geologic repository in a complete and exhaustive manner, numerous assumptions and simplifications are used directly, or are implicit. Consequently, there are limitations associated with any models that makes assumptions and simplification. Even if it includes assumptions and simplifications, the objective of a performance assessment model is to provide a reasonable representation of repository performance. These assumptions and limitations for the analyses presented in this report are listed next.

- Any underlying assumptions, limitations, and bases used to construct the models in the TPA Version 4.1 code also apply to these analyses. These models are described in Chapter 2 and discussed in greater detail in the TPA Version 4.0 code user's guide (Mohanty, et al., 2002).

- The results are limited by the use of simplifying assumptions and models, and parameters based on limited data. As a consequence, these results are for illustration only. Moreover, the manner in which these analyses were conducted or the assumptions and approaches used should not be construed to express the views, preferences, or positions of the NRC staff regarding implementation of regulations at Yucca Mountain.

2 OVERVIEW OF THE TOTAL SYSTEM PERFORMANCE ASSESSMENT CONCEPTUAL MODELS IN THE TPA VERSION 4.1 CODE

The TPA Version 4.1 code focuses on the postclosure performance of the proposed high-level waste repository at Yucca Mountain for long time periods (e.g., 10,000 years). To quantify the uncertainty in estimating repository performance during long time periods, the total system performance assessment analysis is conducted in a probabilistic manner in which many realizations are simulated using input parameter sets sampled from probability distributions. Detailed simulation models that include all the process couplings, heterogeneities, and complexities are not incorporated into the code to maintain reasonable computer execution times with modest hardware resources.

The TPA Version 4.1 code is used in this analysis to obtain deterministic and probabilistic estimates of dose for specified time periods (e.g., regulatory compliance simulation period and beyond) at designated receptor locations {e.g., 20 km [12.4 mi] downgradient of Yucca Mountain}. The TPA Version 4.1 code, which is specifically tailored for evaluation of performance of the proposed repository at Yucca Mountain, is an update of the code used in the review of the U.S. Department of Energy (DOE) Total System Performance Assessment–Viability Assessment Phase 2 study (Mohanty, et al., 1999). Conceptual models used in the previous version of the TPA code have been documented in Mohanty and McCartin (1998) and for the 4.0 version in Mohanty, et al. (2002).

The TPA Version 4.1 code user's guide contains additional detailed information on the conceptual and mathematical models and the code structure. A simplified flowchart illustrating the structure of the TPA Version 4.1 code is presented in Figure 2-1. The total system performance assessment input parameter values and the bases for their selection are presented in Appendix A of the same user's guide.

2.1 Conceptualizations of the Repository and its Geologic Setting

For ease of use and computational efficiency, the TPA Version 4.1 code replaces the intricate repository layout and the complex geologic setting with relatively simple conceptual representations. The repository layout, for example, is represented by an idealized planar feature discretized into a set of subareas, while the geology is replaced by a sequence of laterally homogeneous layers. Properties and environmental conditions for each subarea are assumed uniform. Except for the influence of the climatic conditions (e.g., precipitation) and thermal load, flow and transport processes in and below a given subarea are independent of processes in other subareas. Thus, flow is entirely vertical with no lateral diversion in the unsaturated zone.

As illustrated in Figure 2-2, quadrilateral subareas of uniform thickness are used to represent individual subregions of the repository. In the current application, the repository is divided into 10 subareas; however, the TPA Version 4.1 code has the capability to use much finer discretizations of both the repository and the geologic setting beneath it. The number of waste packages in each subarea is assumed proportional to the fraction of the total repository area represented. Radionuclide releases from the engineered barrier subsystem are calculated by modeling a single prototypical waste package for each subarea and for each failure type. Performance characteristics of the waste package and subsequent release in each subarea are
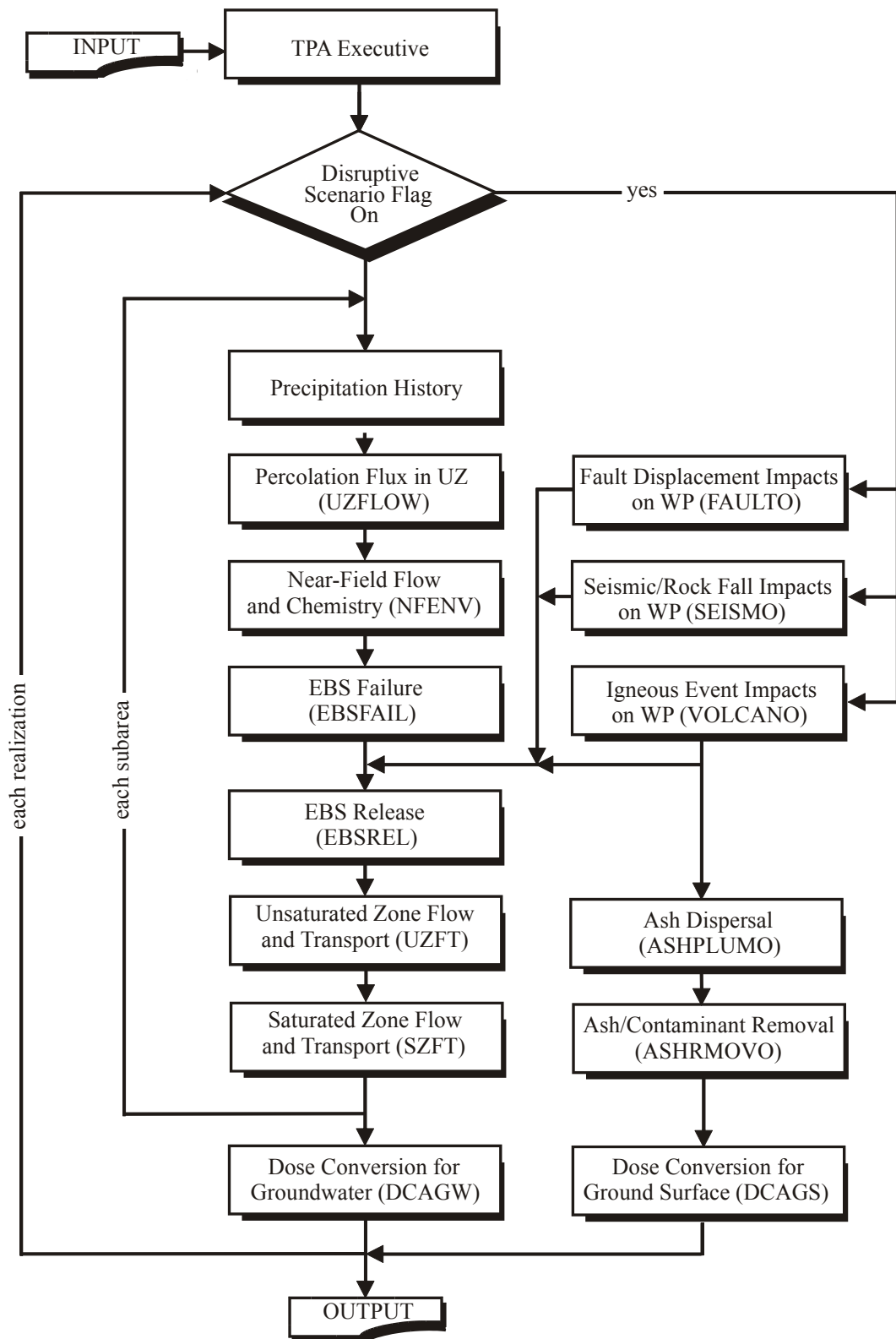
Figure 2-1. Flow Diagram for TPA Version 4.1 Code
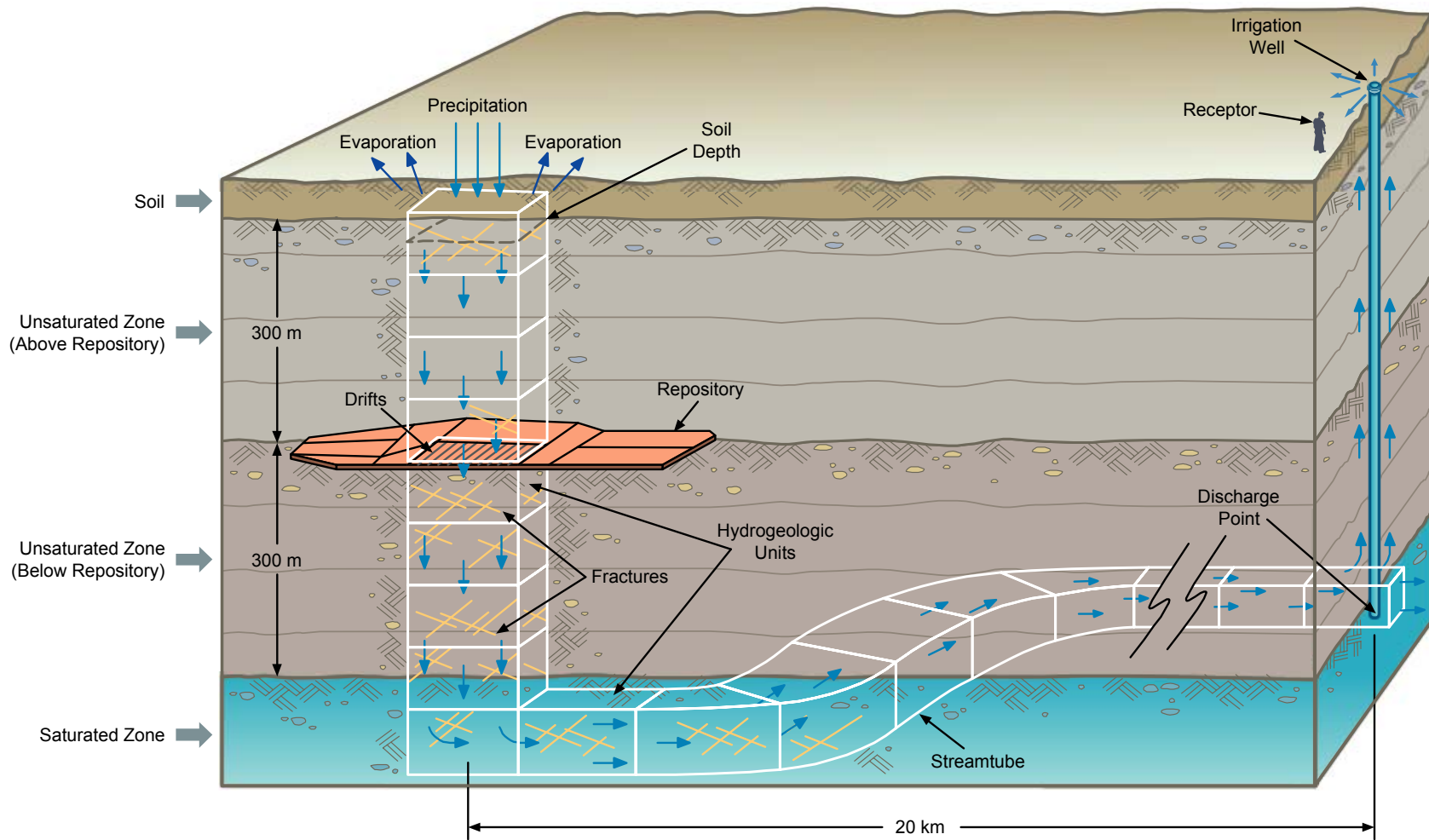
Figure 2-2. Conceptualization of the Repository System

calculated by considering the evolution of such characteristics as climatic conditions, water flux, thermal and chemical conditions, and geologic processes (e.g., seismicity, fault displacement, and igneous activity). Breaching of the waste package by human intrusion and the associated release are considered separately.

The geologic setting is composed of the unsaturated zone (i.e., geologic media between the ground surface and the water table) and the saturated zone (i.e., groundwater aquifer beneath the repository, extending to the location of the receptor group). For simplicity, the stratigraphy is assumed laterally continuous and uniform within a subarea, but differing from subarea to subarea. This simplification implies that, in general, flow in the unsaturated zone is primarily vertical with little or no lateral diversion of flow along hydrostratigraphic units. This simplification is based on the assumptions that the shallow infiltration does not vary substantially among subareas and the near-field thermohydrologic processes do not show substantial subarea-scale variation. The geologic setting also includes features, events, and processes, such as seismicity, tectonism (faulting), and igneous activity (intrusive and extrusive) that may adversely affect the performance of the repository. Seismicity, tectonism, and intrusive igneous activity affect the performance characteristics of the waste package and contribute to groundwater releases.

To model flow and transport in the saturated zone, the total system performance assessment conceptual model consists of three distinct streamtubes over the width of the repository footprint normal to unsaturated zone flow. Each of the 10 subareas in the unsaturated zone is connected to 1 of the 3 streamtubes in the saturated zone, based on proximity. Radionuclide releases from each of the unsaturated zone streamtubes provide the source term to the saturated zone streamtubes. The saturated zone streamtubes are treated as separate conduits and have flow velocities that vary along the individual flow paths. The mass flowrate of radionuclides exiting all saturated zone streamtubes at the well head is used to calculate annual dose to the average member of the receptor group. The annual dose computation accounts for all releases in the groundwater pathway at the location of the receptor group, the spatial extent of the releases in the saturated zone at the location of the receptor group, the extent of the production zone containing the radionuclides (all radionuclides are assumed released in one production zone), and the influence of the pumping rate attributed to water use by the receptor group.

Direct release of radionuclides to the accessible environment because of an extrusive igneous event is also modeled in the TPA Version 4.1 code. The physical characteristics of the extrusion and the assumption of a uniform distribution of waste packages in the repository are used to determine the number of waste packages affected by the event. Alternative modeling is also used to capture the complex magma-repository interaction in determining the waste packages affected by the extrusive event. Radionuclides are transported to the receptor location, based on characteristics of the eruption and meteorological conditions. The areal density of radionuclides in the soil, resulting from the deposition of volcanic ash containing spent nuclear fuel particles, is then calculated. This soil concentration is used in computing the annual dose to the average member of the receptor group.

2.2 Conceptual Models Implemented in the TPA Version 4.1 Code

In developing the TPA Version 4.1 code, several conceptual models were formulated, integrated, and implemented through abstracted mathematical models. These basic conceptual

models, which describe the interactions and couplings of physical and chemical processes believed present in a proposed geologic repository at Yucca Mountain, can be grouped into the following generic categories:

- Infiltration and deep percolation
- Near-field environment
- Radionuclide releases from the engineered barrier subsystem
- Aqueous-phase radionuclide transport through the unsaturated and saturated zones
- Airborne transport from direct radionuclide releases
- Exposure scenario and reference biosphere

The conceptual models are designed to apply to the current DOE repository design and specific site characteristics of the Yucca Mountain area and provide flexibility for examining alternative designs and uncertainties in site and engineered material performance. In some generic categories, alternative conceptual models have also been incorporated into the code.

These conceptual models are used to represent a range of system states including disruptive events. The consequences of disruptive events (e.g., fault displacement and igneous activity) are evaluated with the TPA Version 4.1 code by assessing the effects on engineered barrier failure (producing releases to groundwater), direct releases of radionuclides (airborne releases to the biosphere), or both. Disruptive event consequences are weighted by the probability of the event affecting the repository to calculate a risk versus time curve as explained in Chapter 3.

The following discussion provides a general overview of the key aspects of the major conceptual models implemented in the TPA Version 4.1 code. Detailed descriptions of these models, including the mathematical basis, assumptions, and calculational methodologies, are presented in the TPA Version 4.0 code user's guide (Mohanty, et al., 2002).

2.2.1   Infiltration and Deep Percolation

A one-dimensional modeling approach is used in the TPA Version 4.1 code to describe how meteoric water at the land surface moves vertically downward through the unsaturated zone, to the repository horizon, and ultimately to the water table. In the conceptual model, the deep percolation flux (q_{perc}) is assumed equal to the shallow infiltration rate (q_{infil}). The annual average q_{infil} is estimated based on

- Present-day shallow-infiltration rate
- Change in climate with time
- Elevation, vegetation, evapotranspiration, and soil depth for the repository subarea

Uncertainty in the present-day infiltration rate estimate is accounted for in the TPA Version 4.1 code by treating it as a statistically sampled input parameter. Temporal variations are incorporated by varying the present-day infiltration rate for the 100,000-year period assumed for long-term climatic changes. The effects of site-specific soil cover thickness, vegetation, and elevation are used to reflect the spatial variation for each of the subareas.

The variation of q_{infil} from changes in climate was developed through consideration of paleo-climatic information and results from detailed process-level auxiliary analysis (Stothoff, et al., 1997; Stothoff, 1999). The q_{infil} response function depends on two independent variables,

present-day mean annual precipitation and temperature, as well as the present-day infiltration rate. After computing q_{infil}, the water flux at the repository horizon is then partitioned into

- Water flux diverted around the failed waste package
- Water flux entering the failed waste package

Thus, for the purposes of the TPA Version 4.1 code, the net water flux carrying dissolved radionuclides is a fraction of the total water flux arriving at the repository. It is this net water flux that is used in the TPA Version 4.1 code to calculate the radionuclide source term for each subarea.

2.2.2 Near-Field Environment

Physical and chemical processes in the near field of the repository, such as heat transfer, water-rock geochemical interactions, and refluxing of condensate water, are expected to affect waste package performance. In the TPA Version 4.1 code, a range of near-field characteristics is included in the abstracted mathematical models for heat and water flow, while table look-ups are used for chemical parameters. For estimating waste package failure times and radionuclide release rates, the near-field environment is characterized by

- Surface temperatures of the drift wall rock and waste package
- Relative humidity in the region between the waste package and drift wall
- Water chemistry (e.g., pH, chloride concentration, and carbonate ion concentration)
- Water reflux during the thermal phase

The average rock temperature in the repository horizon is calculated using a conduction-only model that considers the time history of temperature for each subarea calculated from the amount of emplaced waste. The waste package surface temperature is calculated using a multimode heat transfer (i.e., conduction, convection, and radiation) model based on thermal output from the waste package and the repository horizon temperature. Temperature calculations account for ventilation during the preclosure period that could potentially reduce peak waste package temperature and the presence of the drip shield. Water vapor pressure is computed using the standard thermodynamic equation relating vapor pressure to temperature.

Estimates of the pH and chloride concentration histories of water films on the waste package surface were developed in a separate analysis using the multicomponent geochemical module of the MULTIFLO code (Lichtner, et al., 2000). Because the chloride concentration in the water film is likely to be higher than that in the rock mass, the chloride history is scaled by a statistically sampled parameter. The TPA Version 4.1 code provides the option of either using a look-up table that uses the temperature-dependent pH (not currently used) and chloride concentration generated with the MULTIFLO code or specifying constant values in the input file.

The amount of water percolating through the drifts varies with time primarily because of the coupled processes of heat transfer and fluid flow (e.g., vaporization, condensation, and refluxing). Water refluxing produced by these thermohydrologic effects is important for the first few thousand years, after which natural percolation wholly determines the rate of water flow into the repository. Three lumped-parameter water reflux models are included in the TPA Version 4.1 code. The first model considers episodic reflux associated with time-dependent perching above the repository. The second model assumes the volume of

refluxing water will always be sufficient to depress the boiling isotherm in fractures and reach the waste package during the times the surface temperature exceeds the boiling point of water. In the third model, the degree to which the boiling isotherm is depressed is a function of the temperature, the thickness of the dryout zone, and the volume of reflux water. These functions vary with time. Each reflux model produces estimates of the total water flux into the repository during the thermal period.

2.2.3　　　Radionuclide Releases from the Engineered Barrier Subsystem

The specific layout of the underground repository facility is based on the DOE new Enhanced Design Alternative II (CRWMS M&O, 1999). The key engineered barriers for Enhanced Design Alternative II include the waste package and drip shield. The waste package design for high-level waste disposal consists of a large cylindrical cask {i.e., approximately 1.8-m [5.9-ft] diameter and 5.6-m [18.4-ft] length} surrounded by a 15-mm [0.59-in] thick Alloy 22 outer overpack around a 50-mm [1.97-in] thick Type 316L inner overpack, designed to prevent mechanical failure as a result of rockfall. The waste package will be emplaced in the drift on a v-shaped Alloy 22 pallette held together by stainless steel supports. The Alloy 22 and stainless steel supports rest on an invert of sand or gravel ballast held in place by a carbon steel frame.

A 1.5- to 2-cm [0.6- to 0.8-in] thick drip shield, made of Titanium Grade 7, covers the top and sides of the waste package and extends the length of the emplacement drift. The drip shield is intended to protect the waste package surface from dripping water, especially during the thermal reflux period when the environmental conditions could be conducive to crevice corrosion of the Alloy 22 outer overpack. Backfill, however, is not present in the Enhanced Design Alternative II used in the TPA Version 4.1 code.

In the TPA Version 4.1 code, the performance of a prototypical waste package (including the presence of a drip shield) is modeled for each repository subarea for each of the eight waste package failure categories and subcategories. When this prototypical waste package fails, all waste packages in that subarea for a specified failure category are assumed to have failed. The estimation of both waste package failure times and liquid releases is dependent on the nature and extent of corrosion, effectiveness of the drip shield, the near-field environment, the percolation flux in the drift, and external processes that may impose static loads or dynamic loads. Waste package failures are grouped into three basic categories: (i) corrosion and mechanical failure, (ii) disruptive event, and (iii) initially defective waste package failure. After determining the waste package failure time, the TPA Version 4.1 code calculates the aqueous-phase radionuclide releases from the waste package by considering the dissolution of radionuclides from the spent nuclear fuel matrix, advective transport from the waste package (based on the amount of water contacting and entering the waste package, which can be influenced by assumptions for the drip shield), and advective and diffusive transport through the invert directly to the unsaturated zone beneath the repository.

Corrosion failure of the waste package is defined to occur at the time when the outer overpack is fully penetrated by a single pit and the waste form is exposed to water. The abstracted corrosion model uses a conceptual framework that assumes the formation of a water film containing a salt solution (concentrations before and after drip-shield failure are different) but does not explicitly consider water dripping on the container. The corrosion processes considered in the model abstraction include dry air oxidation, humid air corrosion, and aqueous corrosion.

In the Enhanced Design Alternative II, the dry air oxidation and humid air corrosion modes have much smaller contributions to the failure of the waste packages compared with the aqueous corrosion, especially of the Alloy 22 outer overpack. Nevertheless, the TPA Version 4.1 code has retained the capability to evaluate dry air oxidation and humid air corrosion. Waste package surface temperature and the chloride concentration in the water film influence the mode and, hence, the rate of corrosion. The predominant mode of corrosion depends on environmental factors and the container material. Mechanical failure of the waste package, also included in the TPA Version 4.1 code, is considered the result of fracture of the steel overpack because of thermal embrittlement arising from prolonged exposure at temperatures sufficiently elevated to cause substantial degradation of mechanical properties. To estimate mechanical waste package failure in the TPA Version 4.1 code, it is assumed that both overpacks have the properties of steel and, therefore, fail together. In adopting Enhanced Design Alternative II, the consideration of mechanical failure of both the outer and inner overpacks is still incorporated in the TPA Version 4.1 code even if the average waste package temperature is relatively low compared to the spent nuclear fuel design. Failure of the drip shield is not mechanistically modeled in the TPA Version 4.1 code, instead, the drip-shield failure time is specified by an input parameter that is either a constant or is sampled.

Disruptive event waste package failures are caused by seismicity, fault displacement, and igneous activity. In the case of seismicity, waste package failures are caused by rockfalls that mechanically load and deform the waste package (drip shield assumed not present for seismic rockfall failure of waste package). Movements along undetected faults or new faults that exceed a preestablished displacement threshold are assumed to fail waste packages within the fault zone. For igneous activity, all waste packages contacted by magma are assumed to fail. Waste packages within a drift penetrated by a dike, but outside the volcanic conduit, are assumed to fail and expose the spent nuclear fuel to water while those within the conduit are assumed entrained in the magma and released directly to the biosphere. Alternatively, a range of waste package failures from entrainment by magma can be specified and determined as external to the TPA code using a one-dimensional hydrodynamic model for magma movement in the drifts. For fault displacement, failures are modeled by superimposing the physical dimensions of the perturbation (i.e., length, width, and orientation of the fault) on the repository footprint to determine the total number of waste packages potentially affected in each repository subarea. Separate failure times are calculated for seismicity, fault displacement, and igneous activity. Multiple seismic events occur during the compliance simulation periods; however, seismic failure occurrences are collected into four distinct failure times.

For most applications of the TPA Version 4.1 code, it is assumed that a small number of waste packages have failed by the time of repository closure. These initially failed waste packages are attributed to fabrication defects or damage to the waste package as a result of improper emplacement. The number of initially defective waste packages is typically assumed to be 0.01 to 1.0 percent of the total number of containers.

Radionuclide releases from the waste package are calculated by considering the alteration rate of spent nuclear fuel (i.e., rate at which radionuclides in fuel become available for release), radionuclide solubility limits, and transport mechanisms out of the waste package. The TPA Version 4.1 code incorporates numerous parameters, such as the fraction of spent nuclear fuel that is wet, particle size of the spent nuclear fuel, alteration rate of UO_{2+x}, and credit for cladding, that control the release of radionuclides from the spent nuclear fuel matrix. The effects of the formation of secondary minerals such as schoepite on spent nuclear fuel

2-8

dissolution are treated separately. After radionuclides are leached from the spent nuclear fuel waste form, the calculated releases are adjusted to ensure consistency with the radioelement solubility limits. The gap fraction inventory of radionuclides is available for instantaneous release and, therefore, may be a major contributor to early dose.

A parameter value in the input file is used to specify the fraction of failed waste packages in the subarea that is wetted and available to contribute to the source term. To compute the time-dependent source term, the TPA Version 4.1 code provides two conceptual models: (i) a bathtub model—the waste package must fill with water before the radionuclides are released and (ii) a flowthrough model—radionuclides are released by water dripping on the waste form. For the bathtub model, the waste package is treated as a stirred tank, with the tank capacity dependent on the statistically sampled water outlet height. Water will fill the waste package until the capacity (height) is reached and, thereafter, the amount of water entering the waste package will equal the amount of water flowing out. The water capacity of the bathtub is assumed to be unique to the failure modes and to subareas (except for faulting and igneous activity failures). Releases from waste packages will travel through the invert before exiting the engineered barrier subsystem and entering the unsaturated zone below the repository. If the physical properties of the invert are conducive, the radionuclide species could be sorbed, thus providing an additional barrier to radionuclide release. The flowthrough model is a variant of the bathtub model except water does not have to first fill the bathtub before release, and the fraction of fuel wetted is independent of the water level. The user has the option of selecting the mode of water retention in the waste package (bathtub or flowthrough) for each failure type.

2.2.4　　　　Treatment of Transport in the Unsaturated and Saturated Zones

Movement of aqueous-phase radionuclides from the repository horizon through the unsaturated and saturated zones to the receptor group is modeled in the TPA Version 4.1 code using the streamtube approach. Each streamtube encompasses one or more repository subareas and is composed of a vertical section from the repository to the water table and horizontal sections in the saturated zone. The transport module NEFTRAN II (Olague, et al., 1995) simulates the spectrum of processes (e.g., advection, dispersion, matrix diffusion, sorption, and decay) occurring within individual streamtubes. Currently, 20 radionuclides, including the most important contributors to dose, are specified for groundwater transport; however, the TPA Version 4.1 code has the capability to model up to 43 radionuclides, if necessary.

Time-dependent flow velocities in the unsaturated zone are calculated using the hydraulic properties of each major hydrostratigraphic unit. The transport module simulates the transport of radionuclides through either the porous rock matrix or fractures.[1] Radionuclide retardation by chemical sorption in the rock matrix can significantly reduce the transport rates and is, therefore, included in the model. Retardation on fracture surfaces, however, is neglected because the significance of this mechanism has yet to be demonstrated.

Although groundwater flow in the saturated zone is assumed at steady state, radionuclide transport within individual streamtubes is time dependent because the source term varies with

---

[1]Transport though rock matrix takes place if the percolation rate, q_{perc}, is less than the hydraulic conductivity of the rock matrix, K_{matrix}, or through fractures when q_{perc} exceeds K_{matrix}.

time. Streamtubes in the saturated zone exhibit variable cross sections along the flow path; this variable streamtube geometry was based on a separate two-dimensional modeling study of the subregional flow. The conceptual model of the saturated zone assumes that flow in the tuff aquifer is in localized conductive zones (i.e., permeable fracture zones) while flow in the alluvium is presumed uniformly distributed in the alluvial aquifer. Although the streamtube approach neglects dilution effects arising from lateral dispersion, credit is taken for sorption in the alluvium, which is likely to retard aqueous phase transport of many radionuclides. The length of the flow path for the alluvium can have a significant effect on radionuclide retardation in the alluvium. The TPA Version 4.1 code uses a variable distance for the length of the alluvium flow path because the location of the transition from the tuff aquifer to the valley-fill aquifer is not well defined. Additionally, matrix diffusion from flowing pores and fractures into the more-or-less stagnant matrix pore water within the rock is included in the saturated zone transport model.

2.2.5 Airborne Transport for Direct Releases

Radiologic risks associated with the volcanic component of igneous activity are calculated in the TPA Version 4.1 code by modeling airborne releases of radionuclides for simulated volcanic eruptions. The volcanism modules assume that the magma intercepts waste packages, moves upward to the land surface, and then ejects the tephra and spent nuclear fuel mixture into the atmosphere. The physical characteristics of each simulated eruption (e.g., vent size and event power and duration) and atmospheric conditions are treated as statistical parameters in calculations of tephra dispersal and deposition patterns, tephra deposit thickness, and radionuclide soil concentrations. Three primary factors determining the tephra plume geometry and transport rates include

- Power and duration of the eruption
- Wind speed and direction
- Spent nuclear fuel particle sizes

The ash transport model developed by Suzuki (1983) was modified by Jarzemba, et al. (1997) and incorporated into the TPA Version 4.1 code to calculate the distribution of the released radionuclides. The time-dependent radionuclide areal densities are calculated taking into account the thickness of the tephra deposit, leaching and erosion rates, and radionuclide decay rates. The calculated doses attributed to direct releases are strongly influenced by the time of the event (early events result in larger doses, partly caused by the contribution to the estimated doses from short-lived fission and activation products present in the spent nuclear fuel).

2.2.6 Exposure Pathways and Reference Biosphere

Dose calculations are performed in the TPA Version 4.1 code for exposure pathways applicable to a dose receptor approximating the reasonably maximally exposed individual defined in 10 CFR 63.312 (henceforth will be referred to as reasonably maximally exposed individual). Considering local characteristics of the Amargosa Valley, Nevada, area, the dose receptor is represented as a member of a farming community located 20 km [12.4 mi] south of the repository location (note that changes to the TPA code to use an 18-km [11.2-mi] receptor location consistent with the final 10 CFR Part 63 rulemaking were not implemented prior to conducting calculations for this report). The dose receptor is assumed exposed to radionuclides transported through the groundwater pathway, air pathway, or both as a result of direct releases

arising from the volcanic component of igneous activity. Results of these calculations are expressed by the total effective dose equivalent.

Geographic location and lifestyle characteristics assigned to the dose receptor are primary aspects defining the dose receptor specified in the TPA Version 4.1 code. The farming community is assumed to include persons that use contaminated water for

- Drinking {i.e., 2 L/day [0.528 gal/day]}
- Agriculture typical of Amargosa Valley area practices (e.g., growing alfalfa and gardening)

The farming community is assumed exposed to surface contamination through

- Consumption of contaminated farm products (i.e., ingestion)
- Breathing air with ash-spent nuclear fuel particles (i.e., inhalation)
- Direct contact

Site-specific dose conversion factors for each radionuclide and pathway are used to convert radionuclide concentrations in the groundwater and soil to total effective dose equivalent values. The individual dose conversion factors are generated through separate pathway calculations using the GENTPA code, a module in the TPA 4.1 Version code. A variety of parameters (e.g., irrigation rates and diet) are used to provide flexibility in defining biosphere and exposure scenario. Two separate sets of parameters are included to represent two distinct reference biospheres associated with the present arid climate and the projected future pluvial climate. In addition to computing the annual dose history for each stochastic simulation, the TPA Version 4.1 code scans these dose calculations to identify the magnitude and timing of the peak dose.

2.3   Basecase Definition and Alternative Conceptual Models

The conceptual models available in the TPA Version 4.1 code are briefly presented in the previous sections. The option to evaluate alternatives to the basecase conceptual models is included in the TPA Version 4.1 code. The following sections list the set of conceptual models selected for the basecase studies and also describe the alternatives to the basecase models analyzed at a process level in Chapter 3. The effects of these models on the total system are discussed in Chapter 4.

2.3.1   Basecase

The basecase input data set reflects current repository design features and likely parameter-range estimates for evaluation of processes affecting repository performance. The set of conceptual models that constitute the basecase against which alternative conceptual models are evaluated in the sensitivity/uncertainty analyses include

- No cladding protection
- Dissolution of spent nuclear fuel based on J–13 Well water chemistry
- Bathtub model (i.e., pooling of water in the waste package after failure) to determine water mass balance and fuel wetting of the failed waste package
- Matrix diffusion of contaminants in the saturated zone

A complete list of the input parameters used for the basecase can be found in Appendix A in the TPA Version 4.0 code user's guide (Mohanty, et al., 2002). Climate change and seismicity are considered as integral components of the basecase and, therefore, alternative conceptual models to the components are not considered in the analyses.

2.3.2 Alternative Conceptual Models

Various alternative conceptual models are investigated to determine the sensitivity of repository performance to changes in waste package design, radionuclide release mechanisms, and radionuclide transport models. These alternative model runs are conducted with the TPA Version 4.1 code and do not include disruptive events. The alternative models used in this analysis are grouped according to fuel wetting assumptions, fuel-dissolution models, and transport assumptions. For the analyses presented in this report, the repository performance is defined as the peak of the expected dose from the multiple-realization calculation.

2.3.2.1 Fuel-Dissolution Models

The TPA Version 4.1 code contains four models (Models 1–4) for the dissolution rate of the spent nuclear fuel that has contacted water. The basecase model uses Model 2 (Mohanty and McCartin, 1998), which is based on the dissolution rate of spent nuclear fuel in J–13 Well water containing silica and calcium ions. The alternative dissolution models—some of which are combined with fuel wetting alternatives—are listed next.

2.3.2.1.1   Fuel-Dissolution Model 1

The first alternative fuel-dissolution model (Model 1) has an increased spent nuclear fuel dissolution rate at high carbonate concentrations (Mohanty, et al., 2002) and reduced silicate and calcium concentrations in the water entering the waste package.

2.3.2.1.2   Fuel-Dissolution Model 3 (Natural Analog)

In this alternative conceptual model, fuel dissolution and contaminant release rates are based on maximum likely rates inferred from measurements at the Peña Blanca, Mexico, natural analog site (Murphy and Codell, 1999). For this alternative, the uranium dissolution rate for fully exposed fuel is 24 kg/yr [53 lb/yr] from the entire repository but is further limited by the fraction of wetted waste packages and the fuel wetting factors, which range from 0 to 1. This alternative conceptual model is invoked by setting Model 3.

2.3.2.1.3   Fuel-Dissolution Model 4 (Schoepite Dissolution)

The schoepite-alternative conceptual model assumes that all radionuclides released from the spent nuclear fuel matrix are captured in the secondary uranium mineral schoepite (Murphy and Codell, 1999) and are subsequently released at a limit controlled by schoepite solubility. This model is specified by setting Model 4. Although there is evidence of incorporation into secondary minerals of some radionuclides (notably Np-237), it is unlikely that other radionuclides important to dose such as I-129 and Tc-99 would be so incorporated. Therefore, this model may be overly optimistic.

2.3.2.2   Fuel Wetting Assumptions

This grouping includes alternative conceptual models related to the way spent nuclear fuel in the waste package is contacted by water. These five alternative models use combinations of the flowthrough and dissolution-rate models and also the TPA Version 4.1 code input parameters for the amount of water and fraction of the subarea wetted by impinging water.

2.3.2.2.1   Flowthrough Model with Fuel-Dissolution Model 2

This alternative conceptual model evaluates the flowthrough option in which water enters waste packages through corrosion pits but does not pool in the container. In the bathtub model used in the basecase, the bathtub height is determined by the fraction of fuel wetted (determined by the position of the exit port, which is a corrosion pit), which is sampled and ranges from 0 to 1. In the flowthrough model, the fraction of fuel wetted is unrelated to the water level in the waste package. Additionally, the fraction of fuel wetted is likely much smaller than in the bathtub model and depends on poorly understood phenomena such as dripping patterns, surface tension, and vapor-phase wetting. This flowthrough conceptual model is invoked by setting the appropriate Water Contact Mode flags to 1. In this model, the fraction of fuel wetted is equivalent to the fraction immersed in the bathtub model. In this model, solubility limits for the radionuclides might become important because of the limited amount of water in contact with the fuel.

2.3.2.2.2   Flowthrough Model with Fuel-Dissolution Model 1

This alternative conceptual model uses the flowthrough model described in the last paragraph but with the Model 1 (carbonate-dissolution model), which assumes that silica and the calcium ion will be depleted from much of the water entering the waste package by reaction with the fuel and metal in their path.

2.3.2.2.3   Focused Flow

The basecase conceptual model assumes that all of the water infiltration into a subarea will be received by only a fraction of the subarea. There is a large uncertainty in the fractional area within a subarea that will receive water. The focused flow alternative conceptual model accounts for the possibility that the fractional area within a subarea that receives water could be much smaller because a few discrete fractures will carry the bulk of the water and will focus or funnel the water heavily on fewer waste packages. The net effect will be higher infiltration onto fewer waste packages compared to lower infiltration onto a larger number of waste packages in the basecase. This alternative model is invoked by increasing the range of WastePackageFlowMultiplicationFactor parameter by a factor of four (from $3.15 \times 10^{-2} - 1.05 \times 10^3$ to $1.26 \times 10^{-1} - 4.20 \times 10^3$), while decreasing the fraction of waste packages wetted by a factor of one-fourth (from 0–1 to 0–0.25). This setting has the effect of funneling the same quantity of water for each subarea to one-fourth the number of waste packages.

2.3.2.2.4   Cladding Credit Plus Spent Nuclear Fuel-Dissolution Model 1

The basecase conceptual model assumes that once the inner and outer overpacks have been breached, spent nuclear fuel is exposed and available for dissolution and transport. This assumption implies that 100 percent of the cladding is ineffective in preventing water from contacting spent fuel, dissolving radionuclides, and transporting radionuclides out of the waste

form. The alternative conceptual model assumes that the cladding allows release from only one percent of the waste form (i.e., 99 percent of the cladding prevents release from occurring during the simulation period).

2.3.2.2.5   Grain-Size Model with Fuel-Dissolution Model 1

This conceptual model uses the grain size from the uranium dioxide fuel instead of the particle size to determine surface area, which leads to a higher dissolution rate because of the increased surface area. This alternative conceptual model combines the fuel-dissolution Model 1 for relatively fast dissolution by carbonate water, with the large surface area of the grain size.

2.3.2.3   Transport Alternatives

The transport assumptions in the basecase unsaturated zone and saturated zone conceptual models are investigated with three alternative models. These assumptions affect the releases and times of releases from the engineered barrier subsystem, unsaturated zone, and saturated zone.

2.3.2.3.1   No Retardation of Plutonium, Americium, and Thorium

This alternative conceptual model indicates the contribution to repository performance of retardation of plutonium, americium, and thorium in the geosphere and the effect on the groundwater doses if chemical conditions resulted in no sorption. Once released from failed waste packages, plutonium, americium, and thorium are assumed to travel at the same speed as water through the engineered barrier subsystem, unsaturated zone, and saturated zone to the receptor location. This alternative model is invoked by setting partition coefficients (K_d) to zero and retardation coefficients (R_d) to unity for these elements. This model approximates the potential effect of colloids that could move through the geosphere unretarded if filtration processes were not considered radioactive.

2.3.2.3.2   No-Solubility Limit Model

This alternative conceptual model indicates the contribution of the solubility limit of each radionuclide and the effect on the groundwater doses if this limit was removed for each radionuclide. Once the spent nuclear fuel is dissolved, the radionuclides are assumed to remain dissolved in the water in the waste package and exit with the water flowing out of the waste package. The model is invoked by setting the solubility limits at high values {100 kg/m^3 [6.24 lb/ft^3]}. This calculation provides an estimate of the capability of the solubility limit in delaying the release of groundwater radionuclides. The effect of the solubility limit in delaying releases has been studied for the bathtub water fuel wetting mode separately from the flowthrough fuel wetting mode.

2.3.2.3.3   No Matrix Diffusion

This conceptual model assumes that no matrix diffusion will occur in the tuff saturated zone transport legs where there is fracture flow. No matrix diffusion is specified by setting the parameter DiffusionRateSTFF as a constant value of 0.0 yr^{-1}.

3 ANALYSIS OF TOTAL SYSTEM BEHAVIOR

In this chapter, the relationships among repository performance, key input parameters, and intermediate results for deterministic and probabilistic cases are presented. For the probability case, most techniques rely on the Monte Carlo method for determining system performance. The performance measure of the system in the U.S. Nuclear Regulatory Commission (NRC) Yucca Mountain repository performance assessment exercises is the peak dose in the simulation period to an exposed individual located 20 km [12.4 mi] from the repository. Many of the input parameters are not precisely known and are spatially variable so their values are described by probability distributions. The Monte Carlo technique makes repeated calculations (called realizations) of the possible states for the system, choosing values for the input parameters from their probability distributions. Although 330 input parameters[1] are sampled in the TPA Version 4.1 code, only a few of these parameters contribute significantly to the uncertainty in peak dose because of the great sensitivity of peak dose to the parameters, the large variability of the parameters, or both. The mean values and distributions for the uncertain total system performance assessment input parameters are summarized in Tables 3-1 to 3-18.

In the single-realization case, mean values for the input parameters are used. The mean-value simulation establishes a quantitative baseline demonstration of the behavior of the total system at the process level and of repository performance as measured by groundwater dose. Additionally, the repository performance is related to the key input parameters and intermediate results in a deterministic mode.

After the discussion of results from the mean-value simulation, a description of the variability in the total system performance assessment results from multiple realizations is presented. The variability in the behavior of the total system at the components level and the system level are analyzed in multiple realizations using distributions for the input parameters. For example, the variability in dose is related to variability in the release rate from the engineered barrier subsystem. Both the single- and multiple-realization basecase analyses provide background information and form the framework to evaluate the sensitivity of repository performance to input parameters presented in Chapter 4. After the multiple-realization results, the outputs from alternative conceptual models and disruptive events are presented. This chapter concludes with a discussion of a methodology used to calculate risks from the disruptive events. Results are primarily evaluated for the 10,000-year regulatory compliance period. To better understand several processes, results are also evaluated out to 100,000 years.

3.1　　　　Single-Realization Deterministic Analyses

This section examines repository behavior for a single realization to illustrate how a repository component influences both the dose and the behavior of other repository components. For the single realization, all input parameters are specified at their mean values. It should be emphasized that the annual dose obtained from using the mean value data set is not the same as the expected annual dose (which is the performance measure) obtained from multiple realizations because of the nonlinear dependency of dose on input parameters.

---

[1]The actual number of parameters contributing to the variability in peak dose is fewer than 330, depending on which group of conceptual models is used in the calculation. The Latin Hypercube Sampling module in the TPA Version 4.1 code samples all parameters that are not constant, regardless of their use in a specific run.

The following is a description of how the repository is described for the calculations. The waste emplaced at Yucca Mountain is assumed to total 70,040 MTU[2] in an area of 5,400,000 m^2 [2.1 mi^2] {approximately 5,000 m [3.1 mi] long and 1,000 m [0.6 mi] wide}. Assuming an average of 7.89 MTU per waste package and an equivalence between the spent nuclear fuel and other types of wastes, such as U.S. Department of Energy (DOE) spent nuclear fuel and glass high-level waste, approximately 8,877 waste packages will be needed for waste disposal. The initial inventory activity is approximately 6.65×10^{20} Bq [1.8×10^{10} Ci]. Waste packages with a 5.275-m [17.3-ft] length and a 1.579-m [5.2-ft] diameter are emplaced in drifts 5.5 m [18.0 ft] in diameter, spaced 81.0 m [266 ft] apart. The average age of the spent nuclear fuel is 26 years. The descriptions of the mean values for the key parameters used in various process-level calculations are presented in each of the following sections.

3.1.1   Unsaturated Zone Flow

Detailed modeling (Stothoff, 1999) suggests that climate conditions could significantly affect the flow of water in the unsaturated zone and into the repository. As a consequence, the amount of water contacting a waste package, which affects the release rate of radionuclides from the engineered barrier subsystem and the transport of the radionuclides in the unsaturated zone, may also be significantly influenced.

In the TPA Version 4.1 code,[3] precipitation is assumed to vary from present-day to pluvial conditions for 100,000 years. Although the compliance period is just 10,000 years, simulation up to 100,000 years shows possible wetter conditions for the site, and furthers the understanding of performance of the repository if estimates of infiltration, heat-induced evaporation and diversion are beyond the expected ranges. For the mean value data set, Figure 3-1 shows the mean annual precipitation changes from approximately 160 to 330 mm/yr [6.29 to 12.99 in/yr], whereas the infiltrating water entering the unsaturated zone changes from 7 to 37 mm/yr [0.3 to 1.5 in/yr]. At a user-specified time in the TPA Version 4.1 code, the climatic condition switches from nonpluvial to pluvial and back to pluvial at a later time. The nonpluvial to pluvial transition takes place at 13,000 years (based on the Milankovich cycle), which is outside the regulatory period. In a 100,000-year period, the climatic condition is characterized by pluvial conditions approximately 74 percent of the time and by present-day condition 26 percent of the time. Because the onset of the pluvial period lies beyond 10,000 years, the pluvial climates will not affect the waste package failure and the release of radionuclides in the regulatory period of interest.

For higher flow rates, there are generally larger releases because of the greater amount of water available to dissolve and transport radionuclides out of the waste package. Increasing flow rates in the unsaturated zone are not only expected to transport a larger mass of radionuclides from the engineered barrier subsystem, but also lead to higher doses. The mean values of the parameters used to calculate the time-varying infiltration rates in the unsaturated zone are presented in Table 3-1.

---

[2]The repository design specification uses 70,000 MTU. The additional 40 MTU only reflects a numerical artifact associated with the waste specification on a per waste package basis.

[3]The specific version of the TPA code used in developing this chapter is 4.1k.
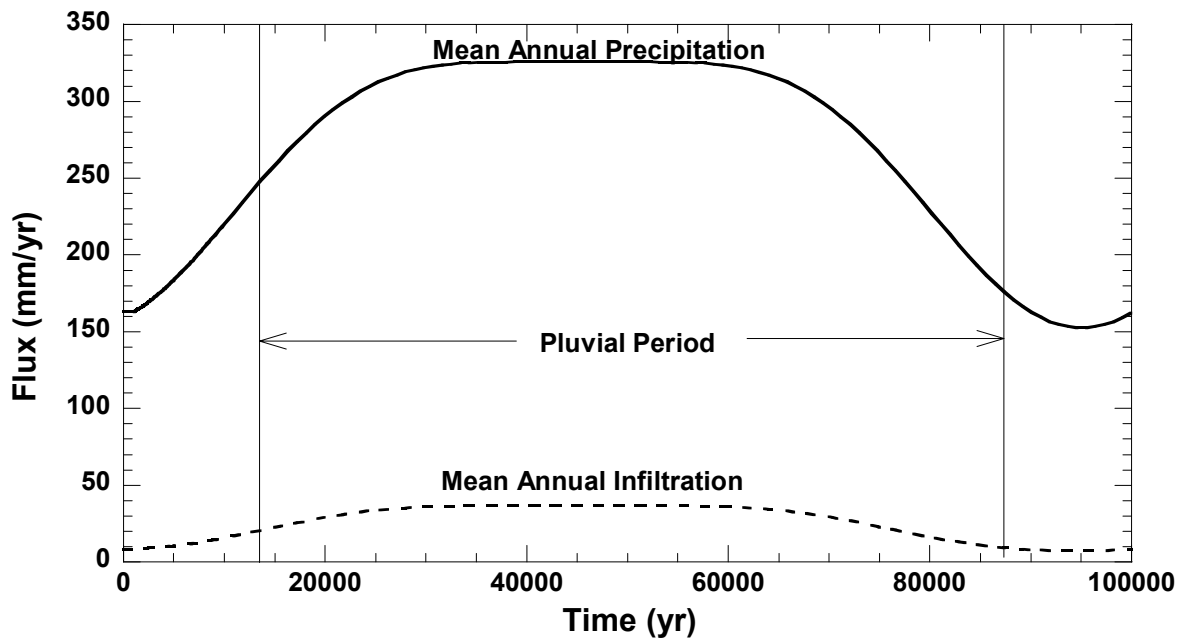
**Figure 3-1. Mean Annual Precipitation and Infiltration of the Repository Horizon
Averaged Over all Subareas and Encompassing Both the Current and
Pluvial Periods for the Mean Value Data Set**

Table 3-1. Mean Values and Distributions of Parameters for Infiltration Calculations		
Parameter	Mean Value	Distribution
Areally averaged mean annual infiltration for the initial (current) climate	8.5 mm/yr	Uniform; 4.0, 13.0
Mean average precipitation multiplier at glacial maximum	2.00	Uniform; 1.5, 2.5
Mean average temperature increase at glacial maximum	−7.5 °C	Uniform; −10.0, −5.0

3.1.2   Near-Field Environment

Near-field thermal conditions may alter the flow of water into the repository, which influences the quantity of water that contacts, dissolves, and transports the spent nuclear fuel out of the engineered barrier subsystem. The near-field chemical environment, in conjunction with the thermal environment, affects waste package corrosion and determines the quantity and time history of water entering the waste package. These near-field conditions and the flow of water onto the waste packages are discussed in the following sections.

3.1.2.1   Repository-Scale Thermohydrology

Radioactive decay of spent nuclear fuel generates heat that perturbs ambient percolation conditions. The heat evaporates water and creates a dryout zone around the drift. Above the repository horizon, the water vapor condenses and flows back toward the repository by gravity, thus creating a reflux zone. The reflux zone is maintained until the near-field temperature falls

3-3

below boiling. When the temperature falls below boiling or water from the condensate zone penetrates the dryout zone through fast fracture paths, water flows into the drift. Water entering the drift may impinge on the drip shield and contribute to drip-shield corrosion. Water flowing into the drift could change the humidity condition in the drift and, after the drip shield fails, can change the environment at the waste package contributing to waste package corrosion failure, radionuclide release, and transport out of the engineered barrier subsystem into the unsaturated zone.

Of the three reflux models in the TPA Version 4.1 code described in Chapter 2, the third model was used in the basecase. This model estimates the depth of the boiling isotherm (as a function of dryout zone thickness) that water will penetrate and the volume of water flowing from the condensate zone. Table 3-2 presents the mean values of parameters used in the reflux calculations.

Figure 3-2(a) presents subarea-to-subarea variations (see Figure 4-2 in the TPA Version 4.0 code user's guide) in the volume of water contacting waste packages for 100,000 years, which behaves similarly to the infiltration rates in Figure 3-1. Figure 3-2 also shows differences in the seepage flux between subareas and a consistency in the general behavior of the seepage flux for all 10 subareas, with subarea 1 having the largest seepage flow rate, which is attributable to the effects of high elevation and thin soil cover.

The sudden drop in the rate in Figures 3-2(b) and (c) at early times (100–800 years) illustrates a large change in the seepage flux that occurs because of the temperature increase subsequent to the repository closure. Although this thermal perturbation takes place before the corrosion failure of waste packages and drip shields, the modified infiltration rate could affect releases from initially defective failures or seismically induced failures as soon as the drip shield fails. The duration of the thermal perturbation may be significant for the 10,000-year simulation period. The jump in the seepage flux in Figure 3-2(a) at 10,000 years is an artifact of the assumption made in the TPA Version 4.1 code that the thermal perturbation is negligible after 10,000 years, which was made to improve code efficiency. The assumption that the thermal perturbation is negligible beyond 10,000 years, has only a small impact on the peak dose (less than 3 percent), for the 100,000-year simulation. The subarea average infiltration rate in the unsaturated zone is provided in Figure 3-3. Water flowing into the drift and water entering the waste package are also illustrated in this figure. The effects of the thermal perturbation on the flow rate are evident in this figure for approximately 10,000 years. Significant infiltration into the repository is delayed until approximately 900 years and the thermal effects reduce seepage above the repository until just after 10,000 years.

3.1.2.2   Drift-Scale Thermohydrology

Waste package surface temperature, drift wall temperature, and waste package surface relative humidity are computed for each subarea. The mean input parameters used to compute these values are presented in Table 3-2. Figures 3-4(a) and (b) illustrate the subarea-to-subarea differences in the waste package surface temperature, and Figure 3-5 shows waste package surface relative humidity. For the mean value data set presented in Table 3-2, the highest temperature of approximately 170 °C [340 °F] is observed at approximately 100 years, after which the temperature drops almost exponentially to 50 °C [122 °F] at 10,000 years. The
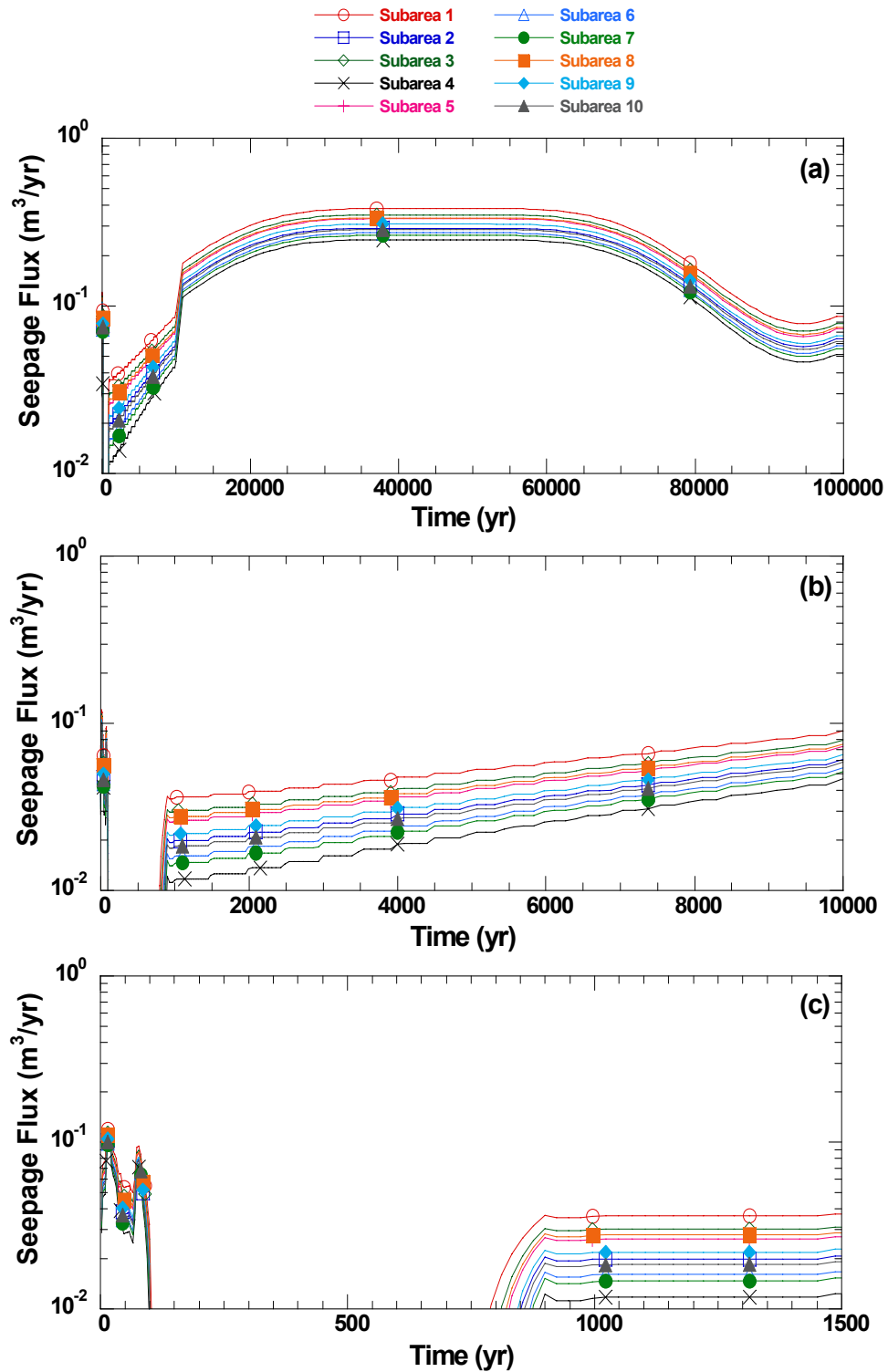
Figure 3-2. Effect on the Thermal Perturbation on the Near-Field Seepage Rate in Each Subarea for the Mean Value Data Set During (a) 100,000-, (b) 10,000-, and (c) 1,500-Year Periods
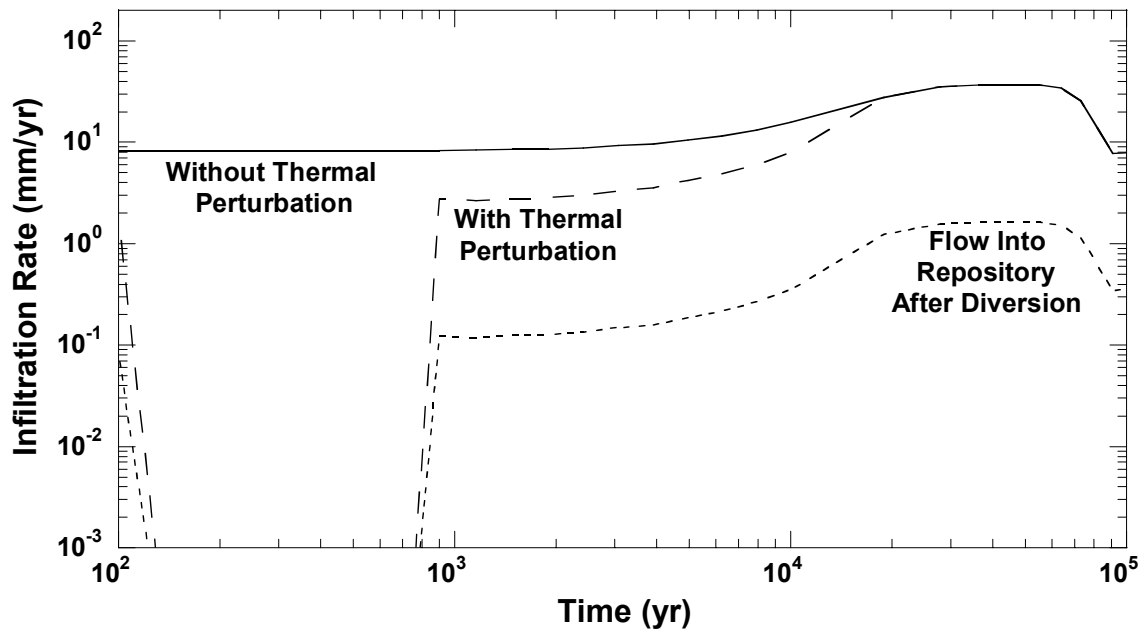
Figure 3-3. Subarea Average Infiltration Rate, Flow into the Drift, and Amount of Water Hitting the Drip Shield (or Entering the Waste Package after the Drip Shield Failure) for the Mean Value Data Set

boiling point, 97 °C [210 °F] at the repository, is reached at 1,500 years, and the temperature drops to ambient temperature, 23 °C [73 °F], at 80,000 years. The sharp rise in the temperature in Figure 3-4(b) from 85 °C [200 °F] at 50 years to 165 °C [329 °F] at 80 years corresponds to the repository closure at 50 years when the ventilation stops. Subareas 1 and 2 are the largest subareas, and Subarea 7 is the smallest (located away from the center of the repository and having an elongated shape). Thus, in the largest two subareas (i.e., Subareas 1 and 2), waste packages cool slower compared with the smallest subarea (i.e., Subarea 7) because Subarea 7 suffers more from the edge cooling effect than Subareas 1 and 2. Cooling is the slowest in Subarea 8 because the exposed surface area for cooling is much smaller than the cooling surface area for Subareas 1 and 2, leading to a much smaller edge cooling effect. At any given time, Subarea 7 exhibits the lowest temperature and Subarea 8 exhibits the highest temperature. Because the temperature for a subarea is determined at its center, the distance of this point from the cooling edge strongly influences predicted temperature in a subarea.

Subarea-dependent temperature and relative humidity values from the near field are also used by the waste package degradation model to determine the waste package failure time. Consequently, the waste package failure time may be different for each subarea. Depending on the selection of the model, spent nuclear fuel dissolution also can be a function of temperature. Therefore, the spent nuclear fuel dissolution rate and, thus, the quantity of radionuclides

3-6

Table 3-2. Mean Values and Distributions of Parameters for Determining Repository Scale and Drift Scale Thermohydrology		
Parameter	**Mean Value**	**Distribution**
Length of reflux zone*	2.00×10^1 m	—†
Maximum flux in reflux zone*	1.00×10^{-9} m/s	—
Perched bucket volume per subarea-area*	5.00×10^{-1} m^3/m^2	—
Emplacement drift spacing	81 m	—
Waste package spacing along emplacement drift	6.4 m	—
Total waste emplaced in repository	70040 MTU	—
Fraction of condensate removed	0.125/yr	Uniform; 0.0, 0.25
Fraction of condensate toward repository	0.525/yr	Uniform; 0.05, 1.0
Fraction of condensate toward repository removed	0.00	—
Density of water at boiling	9.61×10^2 kg/m^3	—
Enthalpy of phase change for water	2.40×10^6 J/kg	—
Temperature gradient in vicinity of boiling isotherm	5.05×10^1 K/m	Uniform; 1.0, 100.0
Waste package pay load	7.89 MTU	—
Age of waste	26.0 yr	—
Ambient repository temperature	2.00×10^1 °C	—
Mass density of Yucca Mountain rock	2.58×10^3 kg/m^3	—
Specific heat of Yucca Mountain rock	8.40×10^2 J/(kg-K)	—
Thermal conductivity of Yucca Mountain rock	1.56 W/(m-K)	Triangular; 1.34, 1.59, 1.75
Emissivity of drift wall	8.00×10^{-1}	—
Emissivity of drip shield	0.63	—
Emissivity of waste package	8.70×10^{-1}	—
Thermal conductivity of floor	6.00×10^{-1} W/(m-°C)	—
Effective thermal conductivity of unbackfilled drift*	9.00×10^{-1} W/(m-°C)	—
Factor for ventilation heat losses	0.70	—
Time of emplacement of backfill	50.0 yr	—
Effective thermal conductivity of backfill*	0.27 W/(m-°C)	—
Thermal conductivity of inner overpack wall	1.50×10^1 W/(m-°C)	—
Thermal conductivity of outer overpack	11.1 W/(m-°C)	—
Effective thermal conductivity of basket and spent nuclear fuel in waste package	1.00 W/(m-°C)	—
Elevation of repository horizon	1.07×10^3 m	—
Elevation of ground surface	1.40×10^3 m	—
*Not used in Reflux 3 Model †Dash in the last column indicates a constant value for the parameter distribution		
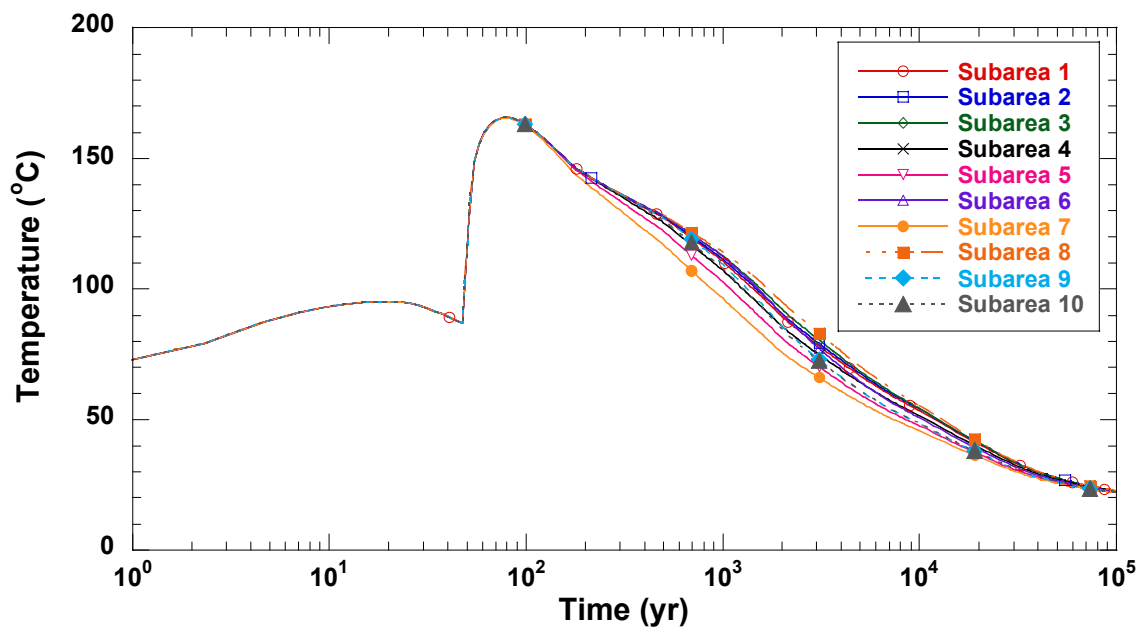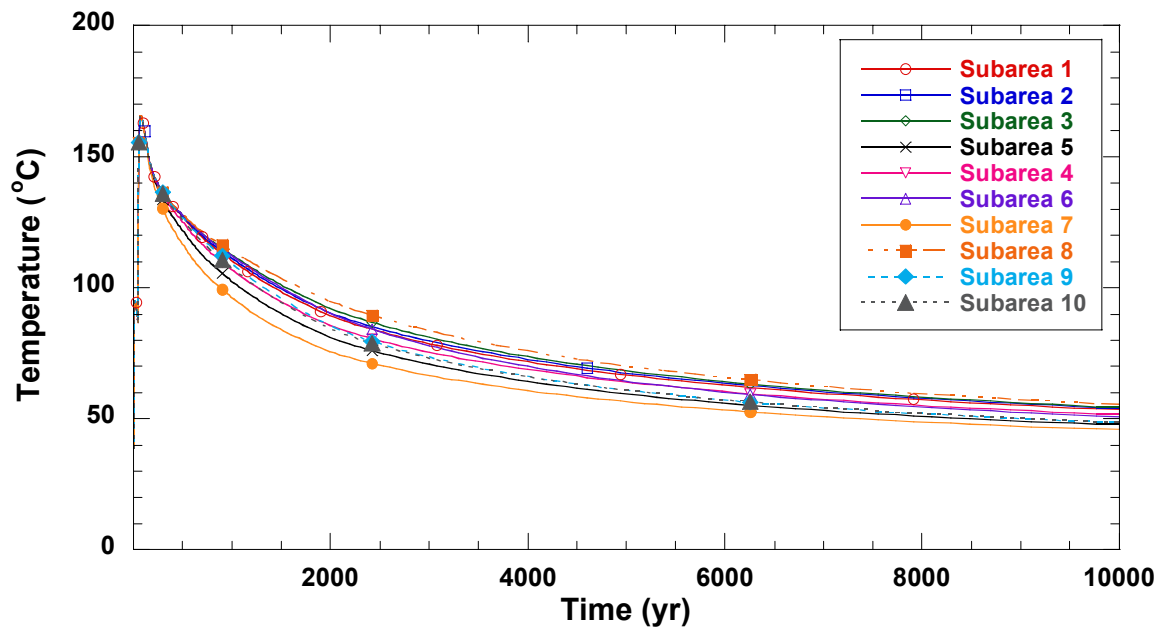
Figure 3-4. Waste Package Surface Temperature in Each Subarea for the Mean Value Data Set (a) in Linear Scale for 10,000 Years, and (b) in Log Scale for 100,000 Years

available for release, can be different for each subarea. For the drift-scale thermohydrology, the climatic conditions were found insignificant in the detailed calculations using equivalent continuum modeling conducted outside the TPA Version 4.1 code.

3.1.2.3 Near-Field Geochemical Environment

The near-field geochemical environment is represented by the time-dependent chloride concentration in water that interacts with the waste package and waste form. The geochemical environment is also characterized by oxygen partial pressure, the solution pH, and the total dissolved carbonate, but these characteristics are assumed not to change with time. Figure 3-6 shows the time history of chloride concentration used by the TPA Version 4.1 code, which is calculated with the MULTIFLO (Lichtner, et al., 2000) computer code outside the TPA Version 4.1 code. Uncertainty in the chloride concentration is presented in Table 3-3 along with the other parameters used to calculate waste package corrosion. The chloride concentration is calculated based on an initial fluid composition corresponding to J–13 Well water and represents the time-dependent composition of water available at the drift wall. The fractures dry out quickly and remain dry until approximately 800 years. During this dryout period and within the context of a continuum model, it is not possible to represent the return of liquid water to the waste package and the associated chloride concentration, because this flow would presumably take place along open fractures in the form of gravity-driven flow manifested as dripping. As shown in Figure 3-6, when the fracture system above the drift becomes wet again at approximately 800 years, the chloride concentration at that time has a value that is four orders of magnitude larger than the initial value. The concentration decreases in a nearly exponential fashion to its initial value of 2×10^{-4} mol/L [7.58×10^{-4} mol/gal] beyond 1,500 years after a small rise between 800 and 1,500 years. During the dryout phase, the chloride
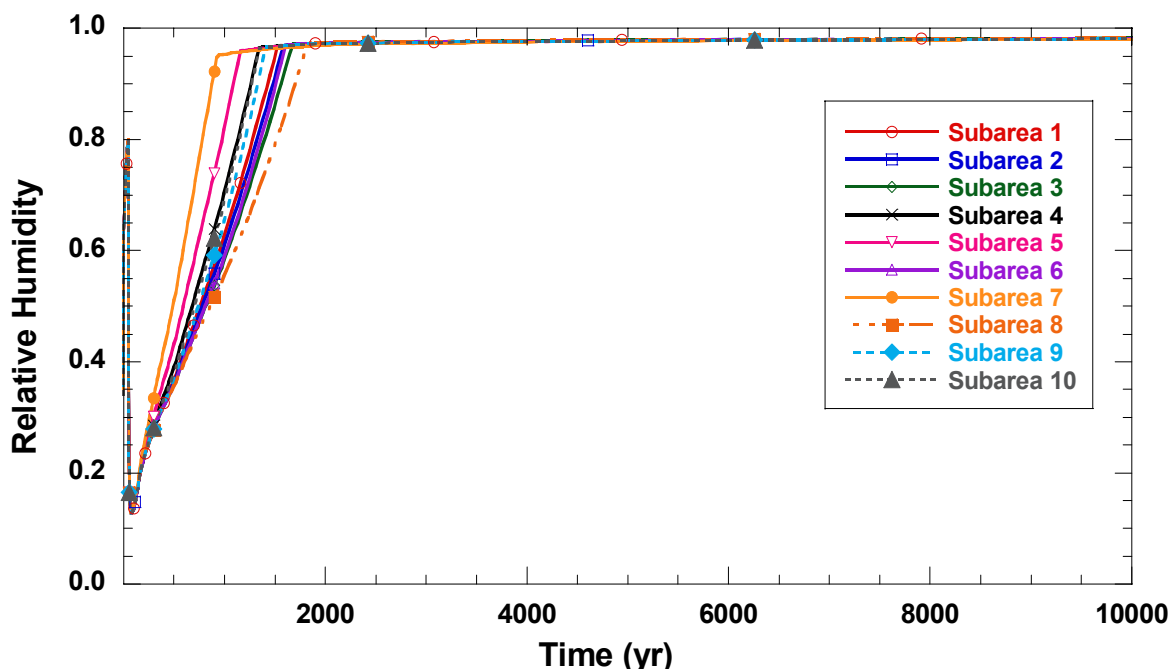
Figure 3-5. Waste Package Surface Relative Humidity in Each Subarea for the Mean Value Data Set

Table 3-3. Parameters for Determining the Corrosion Failure of Waste Packages		
Parameter	Mean Value	Distribution
Outer waste package thickness	0.02 m	—
Inner waste package thickness	0.05 m	—
Metal grain radius	1.38×10^1 μm	—
Grain boundary thickness	7.00×10^{-4} μm	—
Dry oxidation constant	9999.00	—
Critical relative humidity humid air corrosion	5.50×10^{-1}	—
Critical relative humidity aqueous corrosion	0.625	Normal; 0.6 0.65
Thickness of water film	2.00×10^{-3} m	Uniform; 0.001, 0.003
Boiling point of water	9.70×10^1 °C	—
Outer overpack E_{rp} intercept	2006.00	—
Temperature coefficient of outer overpack E_{rp} intercept	−15.2	—
Outer overpack E_{rp} slope	−590.7	—
Temperature coefficient of outer pack E_{rp} slope	4.30	—
Inner overpack E_{rp} intercept	−10,000	—
Temperature coefficient of inner overpack E_{rp} intercept	0.00	—
Inner overpack E_{rp} slope	0.00	—
Outer waste package beta kinetics parameter for oxygen	7.50×10^{-1}	—
Outer waste package beta kinetics parameter for water	5.00×10^{-1}	—
Inner waste package beta kinetics parameter for oxygen	7.50×10^{-1}	—
Inner waste package beta kinetics parameter for water	5.00×10^{-1}	—
Outer waste package rate constant for oxygen reduction	3.00×10^{10} C-m/mol/yr	—
Outer waste package rate constant for water reduction	3.20 C-m/m²/yr	—
Inner waste package activation energy for oxygen reduction	4.0×10^4 J/mol	—
Inner waste package activation energy for water reduction	2.50×10^4 J/mol	—
Passive current density for waste package outer overpack	9.30×10^3 C/m²/yr	Normal 1.6×10^3, 1.7×10^4
Passive current density for waste package inner overpack	1.00×10^{10}	—
Temperature coefficient of inner overpack E_{rp} slope	0.00	—

Table 3-3. Parameters for Determining the Corrosion Failure of Waste Packages (continued)		
Parameter	**Mean Value**	**Distribution**
Measured galvanic couple potential	0.00	—
Coefficient for localized corrosion of outer overpack	2.5×10^{-4}	—
Exponent for localized corrosion of outer overpack	1.00	—
Coefficient for localized corrosion of inner overpack	1.00	—
Exponent for localized corrosion of inner overpack	1.00	—
Humid air corrosion rate	1.00×10^{-15} m/yr	—
Fractional coupling strength	0.0	—
Factor for defining choice of critical potential	0.0	—
Critical chloride concentration for first layer (Alloy 22)	0.5 mol/L	—
Critical chloride concentration for second layer (316L SS)	1.00×10^{-10} mol/L	—
Chloride multiplication factor	2.30	Uniform; 1.0, 3.6
Chloride multiplication factor prior to failure of the drip shield	1.0	—
Time of failure of the drip shield	7422.0	Lognormal 2700, 20400
Reference pH	9.0	—
Tortuosity of scale on waste package	1.0	—
Porosity of scale on waste package	1.0	—
Yield strength	370 MPa	—
Safety factor	1.4	—
Fracture toughness	1.00×10^7 MPa/m^2	—
Waste package surface scale thickness	0.0 m	—

concentration is assumed in equilibrium with respect to halite. The chloride multiplication factor in Table 3-3 (mean value of 2.3) modifies the time-dependent chloride concentration curve presented in Figure 3-6. The chloride multiplication factor is intended to account for the uncertainty in estimating the water chemistry; the parameter values (chloride concentration) and MULTIFLO results are considered the lower bound for chloride concentration.

3.1.3 Degradation of Engineered Barriers

The engineered barrier subsystem primarily includes two barriers: a drip shield and the waste package. Because the radionuclide release can begin only after waste package failure, the lifetime of a drip shield and a waste package significantly affects repository performance. The failure mechanisms for these two barriers are described in the following sections.
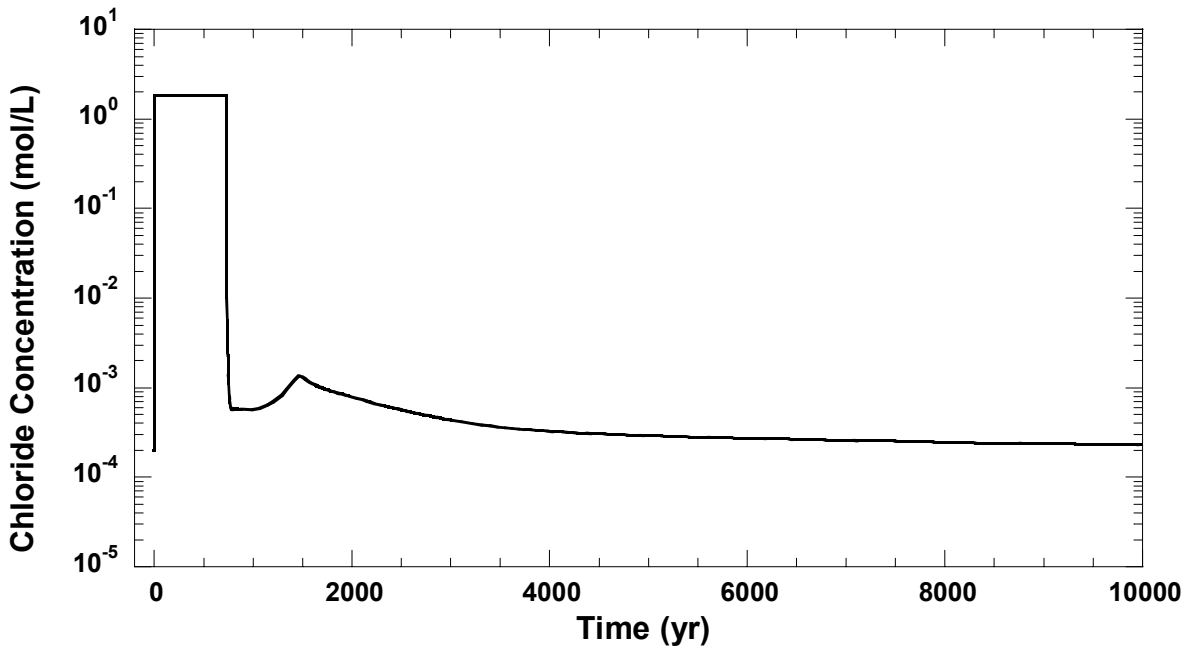
Figure 3-6. Time History of Chloride Concentration Computed by MULTIFLO

3.1.3.1 Drip Shield Degradation

The 15-mm [0.59-in] thick drip shield is intended to protect the waste package from water dripping on the waste package surface (also protects the waste package from rockfall), especially during the thermal reflux period when environmental conditions could be conducive to crevice corrosion of the waste package outer overpack. The drip-shield failure time is estimated outside the TPA Version 4.1 code and is provided to the code as a distribution function. Because of the high level of uncertainty in determining the geometry of failure of the drip shield, it is assumed that the drip shield is completely removed at the time of its failure. The average drip shield failure time is 7,422 years (Table 3-3).

3.1.3.2 Waste Package Degradation

The waste package degradation rate is strongly dependent on the behavior of the inner and outer waste package materials. The outer waste package material is Alloy 22, and the inner material is Type 316L stainless steel. The mean values of the parameters used in computing the waste package failure time are presented in Table 3-3. Figure 3-7 provides a time evolution of the waste package wall thinning and shows waste package wall thinning of less than 4 percent (or 13 percent of the Alloy 22 overpack thickness) by year 10,000. Figure 3-8 shows that, for the mean value data set, 45 waste packages are initially defective at year zero. The number of initially defective failures ranges from 2 to 8 waste packages in the 10 subareas. No seismically induced failure occurs for the mean value data set. The first corrosion failures take place in Subareas 4, 5, 7, and 10 at 69,400 years, and the next corrosion failure occurs in Subareas 1, 2, 3, 6, 8, and 9 at 70,300 years. A total of 2,392 waste packages fail at the time of first failure, and 6,440 fail at the time of second failure. All waste packages in a subarea available for corrosion failure are assumed to fail simultaneously.
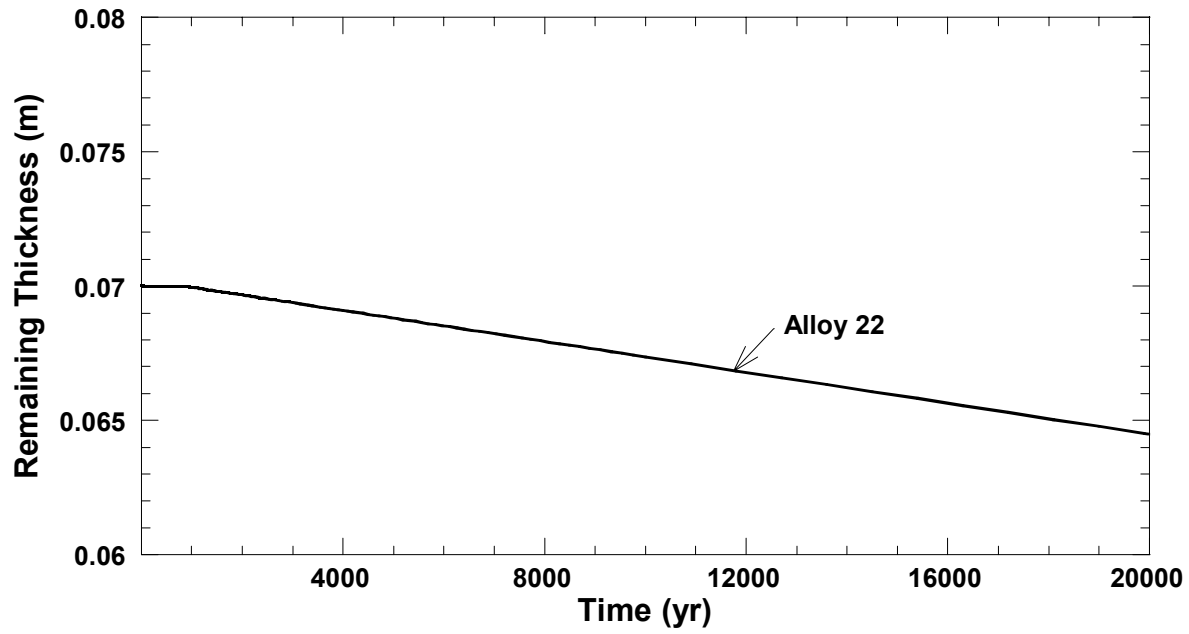
Figure 3-7. Waste Package Wall Thickness as a Function of Time for the Mean Value Data Set
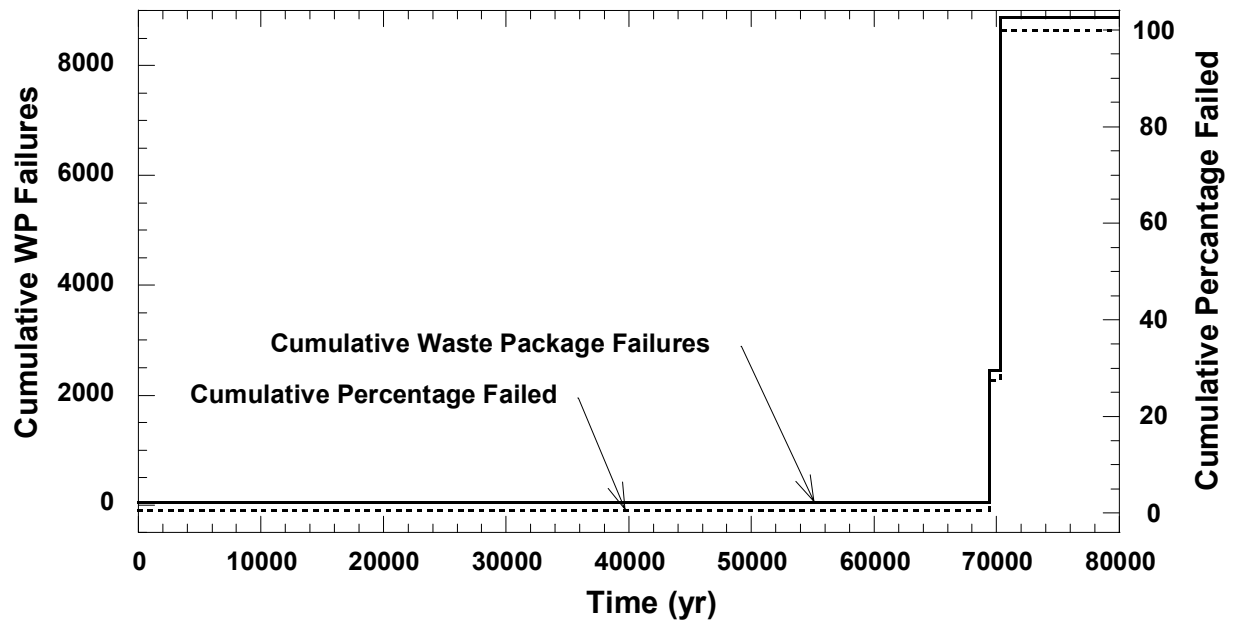
Figure 3-8. Cumulative Number and Percentage of Failed Waste Packages for the Mean Value Data Set

3.1.4   Releases from Waste Package

The main processes that control releases of radionuclides from the spent nuclear fuel to the boundary with the geosphere in the model are (i) protection of the spent nuclear fuel by cladding, (ii) degradation of the spent nuclear fuel by air and water vapor, (iii) contact of the spent nuclear fuel by liquid water, (iv) mobilization of radionuclides from the spent nuclear fuel to the liquid water, (v) transport of dissolved or otherwise mobilized (colloids) radionuclides in the water to the outside of the waste package, and (vi) transport of dissolved radionuclides in the water through the invent material to the outside of the engineered barrier subsystem.

Radionuclide releases are modeled assuming advective mass transfer out of the waste package from incoming water. The volume of water contacting the spent nuclear fuel is computed from a combination of flow in the near-field environment and three flow factors. The first flow factor represents the fraction of dripping water, which may be focused to reach the waste package. The second flow factor represents the fraction of the water that reaches the waste package, which enters the waste package. The first two factors are fixed, time-dependent variables read in from a data file; so a third factor, WastePackageFlowMultiplicationFactor, was added with an uncertainty distribution. The flow rate into the waste package is used in the bathtub model to determine radionuclide release rates. The mean value parameters used in the calculation of radionuclide release rates from the engineered barrier subsystem are presented in Tables 3-4 and 3-5.

Because radionuclides have different chemical, physical, and biological properties that affect the mobilization and radiotoxicity, not every radionuclide in the spent nuclear fuel is an important contributor to dose. Furthermore, because modeling all radionuclides in the spent nuclear fuel significantly increases the computation time, a screening process, employing criteria such as contribution to dose, was used to determine a list of 20 radionuclides. The 20 radionuclides and the decay chains evaluated in the total system performance assessment analysis are presented in Table 3-6.

3.1.4.1   Cladding Degradation

Cladding must fail for water to contact the spent nuclear fuel. Because of limited knowledge, no explicit mechanism for cladding failure is included in the TPA Version 4.1 code. To capture the potential effect of cladding degradation, however, a fraction of the rods inside a waste package may be specified to have failed at the time of waste package failure. In the basecase, cladding failure is specified at 100 percent of the fuel rods, indicating no cladding protection for the spent nuclear fuel (see Table 3-4).

3.1.4.2   Spent Nuclear Fuel Dissolution and Mobilization

The spent nuclear fuel is present in the waste package in pellet form. Water must contact the pellet surface and the internal surfaces in the accessible fractures and pores. Spent nuclear fuel dissolution is modeled by defining rate equations for the spent nuclear fuel exposed after waste package failure and cladding degradation. Of the four spent nuclear fuel dissolution models, the one for which the rate equation is based on laboratory data in the presence of calcium and silicon is selected (Model 2). The data follow an Arrhenius-type trend that uses the time-varying temperature as the independent parameter. The dissolution rate is calculated from a mass balance on the water flowing into the waste package. Because the flow rate is subarea dependent, the dissolution rate varies from subarea to subarea.

Table 3-4. Parameters Used in Determining Radionuclide Releases from the Engineered Barrier Subsystem		
Parameter	Mean	Distribution
Water contract mode for initial failure (0 = Bathtub, 1 = Flowthrough)	0	—
Water contract mode for faulting failure (0 = Bathtub, 1 = Flowthrough)	1	—
Water contract mode for volcanic failure (0 = Bathtub, 1 = Flowthrough)	1	—
Water contact mode for seismic failure interval1 (0 = Bathtub, 1 = Flowthrough)	0	—
Water contact mode for seismic failure interval2 (0 = Bathtub, 1 = Flowthrough)	0	—
Water contact mode for seismic failure interval3 (0 = Bathtub, 1 = Flowthrough)	0	—
Water contact mode for seismic failure interval4 (0 = Bathtub, 1 = Flowthrough)	0	—
Water contact mode for corrosion failure (0 = Bathtub, 1 = Flowthrough)	0	—
WastePackageFlowMultiplicationFactor	6	lognormal; 3.15×10^{-2}, 1.05×10^{3}
Subarea wet fraction	5.0×10^{-1}	Uniform; 0.0, 1.0
Initial failure time	0.00 yr	—
Defective fraction of waste packages per cell	5.05×10^{-3}	Uniform; 1.0×10^{-4}, 1.0×10^{-2}
Number of SEISMO waste package failure intervals	4.00	—
Beginning of seismic waste package failure intervals	0, 2000, 5000, 10,000 yr	—
Waste package internal volume	4.83 m^3	—
Spent nuclear fuel density	1.06×10^{4} kg/m^3	—
Surface area model	1.00	—
Spent nuclear fuel dissolution model	2.00	—
Oxygen partial pressure	2.10×10^{-1} atm	—
Negative log10 carbonate concentration	3.71 mol/L	—
User leach rate	2.50×10^{-6} kg/yr/m^2	—
Preexponential factor for spent nuclear fuel dissolution rate for dissolution Model 2	3.79×10^{-4} (mg m^{-2}d^{-1})	Log-uniform; 1.2×10^{3}, 1.2×10^{6}
Initial radius of spent nuclear fuel particle	1.85×10^{-3} m	Normal; 7.0×10^{-4}, 3.0×10^{-3}
Radius of spent nuclear fuel grain	1.25×10^{-5} m	—
Cladding correction factor	1.0	—
Subgrain fragment radius of UO$_2$ particle after transgranular fracture	1.25×10^{-6} m	Normal; 5.0×10^{-7}, 2.0×10^{-6}
Thickness of cladding	6.1×10^{-4} m	—
C-14 inventory of spent nuclear fuel	7.2×10^{-4} Ci/kg	—

Table 3-4. Parameters Used in Determining Radionuclide Releases from the Engineered Barrier Subsystem (continued)		
Parameter	**Mean**	**Distribution**
Clad C-14 inventory of spent nuclear fuel	4.89×10^{-4} Ci/kg	—
Zirconium oxide and crud C-14 inventory of spent nuclear fuel	2.48×10^{-5} Ci/kg	—
Gap and grain boundary inventory of spent nuclear fuel	6.2×10^{-6} Ci/kg	—
Spent nuclear fuel wetted fraction for all failure types	5.0×10^{-1}	Uniform; 0.0, 1.0
Invert bypass (0 = use ebsfilt, 1 = bypass ebsfilt)	0.00	—
Invert rock porosity	3.0×10^{-1}	—
Invert thickness	7.5×10^{-1} m	—
Invert diffusion coefficient	4.4×10^{-5} m^2/yr	—
Invert matrix permeability	2.0×10^{-17} m^2	Lognormal; 2.0×10^{-18}, 2.0×10^{-16}
Unsaturated zone minimum velocity change factor (fraction)	4.0×10^{-1}	—
Maximum matrix longitudinal dispersivity specified as a fraction of layer thickness	0.06	—
Maximum fracture longitudinal dispersivity specified as a fraction of layer thickness	0.06	—
Invert RD		
Am	3.00×10^3	—
C	6.10×10^1	—
Cl	1.00	—
Cm	6.00×10^3	—
Cs	1.21×10^2	—
I	7.00	—
Nb	6.10×10^2	—
Ni	6.10×10^1	—
Np	1.20×10^3	—
Pb	3.01×10^2	—
Pu	3.00×10^3	—
Ra	6.01×10^3	—
Se	1.00	—
Tc	1.00	—
Th	3.00×10^3	—
U	6.01×10^2	—

Table 3-5. Distributions of Solubility Limits		
Element	Mean Value (kg/m^3)	Distribution (kg/m^3)
Am	1.20×10^{-4}	Uniform; 2.4×10^{-8}, 2.4×10^{-4}
C	1.40×10^{1}	—
Cl	3.60×10^{1}	—
Cm	2.40×10^{-4}	—
Cs	1.35×10^{2}	—
I	1.29×10^{2}	—
Nb	9.30×10^{-7}	—
Ni	1.10×10^{-1}	—
Np	2.14×10^{-2}	Log triangular; 1.2×10^{-3}, 3.4×10^{-2}, 2.4×10^{-1}
Pb	6.60×10^{-5}	—
Pu	1.21×10^{-4}	Uniform; 2.4×10^{-6}, 2.4×10^{-4}
Ra	2.30×10^{-5}	—
Se	7.90×10^{1}	—
Tc	9.93×10^{1}	—
Th	2.30×10^{-4}	—
U	7.60×10^{-3}	—

Table 3-6. Radionuclide Decay Chains	
Chain Number	Chain
1	Cm-246 → U-238
2	Cm-245 → Am-241 → Np-237
3	Am-243 → Pu-239
4	Pu-240
5	U-234 → Th-230 → Ra-226 → Pb-210
6	Cs-135
7	I-129
8	Tc-99
9	Ni-59
10	C-14
11	Se-79
12	Nb-94
13	Cl-36

The average temperature of the waste package surface, calculated in the drift-scale thermohydrology model, is used in the dissolution rate equation. This assumption that the temperature of the waste package surface is close to the temperature at the interior of the waste package is justified because, after the waste package failure, the temperature difference between the inside and outside of the waste package is expected to be small. The total surface area of the spent nuclear fuel available for dissolution is approximately 600 m^2 [6,460 ft^2] per waste package based on the spent nuclear fuel particle size, grain density, and the spent nuclear fuel wetted fraction.

As with spent nuclear fuel dissolution, mobilization of spent nuclear fuel also depends on the initial inventory instantaneously released from the gap between spent nuclear fuel and cladding

into the contacting water as soon as the waste package fails. The radionuclides available for instantaneous release are assumed held loosely on the grain boundaries, cladding/fuel gap, and cladding, referred to collectively as gap inventories. These inventories could be a major contributor to early dose. The gap and grain boundary inventories for each radionuclide are specified as input parameters as shown in Table 3-7.

3.1.4.3 Transport in the Engineered Barrier Subsystem

The TPA Version 4.1 code models advective transport out of the waste package and advective and diffusive transport through the invert below the waste package. Two different flow rates are used in these transport calculations. The volumetric flow rate of water into the waste package is calculated by multiplying the seepage flux into the drift by the surface area of the holes (pits and crevices). The volumetric flux through the invert is based on the volume of water entering the drift rather than on the volume of water entering the waste package.

Inside the waste package, high-solubility nuclides released from the solid matrix are transported out of the waste package. Low-solubility nuclides, however, precipitate out of solution if released from the solid matrix at a concentration exceeding the carrying capacity of water (or solubility limit of a particular nuclide). The volume of water available for dissolution of waste is the amount of water in the failed waste package and the difference between the volume of water flowing in and out of the failed waste package. Table 3-5 provides solubility limits of the radioelements evaluated in the TPA Version 4.1 code.

Releases from the waste package will travel through the invert before entering the tunnel wall. Current design shows the waste package on a pallet (consisting of two cradles and a steel

Table 3-7. Initial Inventory, Gap Inventory, and Half-Life of Radionuclides in Spent Nuclear Fuel for Groundwater Release			
Radionuclide	Inventory at 10 Years from Reactor (Ci/WP)	Gap Inventory (%)	Half-Life (yr)
Am-241	16411.20	0.00	4.32×10^2
Am-243	208.30	0.00	7.38×10^3
C-14	11.36	10.00	5.73×10^3
Cl-36	0.09	12.00	3.01×10^5
Cm-245	2.89	0.00	8.50×10^3
Cm-246	0.60	0.00	4.73×10^3
Cs-135	4.23	6.00	2.30×10^6
I-129	0.28	6.00	1.57×10^7
Nb-94	6.69	0.00	2.03×10^4
Ni-59	19.25	0.00	8.00×10^4
Np-237	3.42	0.00	2.14×10^6
Pb-210	4.47×10^{-7}	0.00	2.23×10^1
Pu-239	2911.41	0.00	2.41×10^4
Pu-240	4292.16	0.00	6.54×10^3
Ra-226	3.24×10^{-6}	0.00	1.60×10^3
Se-79	0.21	6.00	1.10×10^6
Tc-99	114.41	1.00	2.13×10^5
Th-230	1.08×10^{-3}	0.00	7.70×10^4
U-234	9.31	0.00	2.45×10^5
U-238	2.49	0.00	4.47×10^9

support) over a porous invert made of sand or gravel ballast in between a carbon steel frame. Water running off or passing through the waste package would fall onto the invert. The invert material could sorb some of the radionuclide species, thereby providing an additional barrier to their release into the geosphere proper.

In the invert, advective and diffusive transport is modeled through 0.75 m [2.5 ft] of invert (slightly thicker than the value used in the Total System Performance Assessment—Site Recommendation) having a 30-percent porosity. The determination of whether flowthrough the invert occurs in the matrix or fast paths (such as fractures that could potentially form with time as a result of consolidation of sand and gravel) is based on the invert matrix permeability and the average flow rate of water through the invert. Radionuclide sorption is modeled in the sand or gravel ballast invert, and the mean values of the Rds are presented in Table 3-4, together with values for other parameters used to compute transport in the engineered barrier subsystem. Colloidal transport of radionuclides is not considered in this calculation.

3.1.5 Unsaturated Zone Transport

Radionuclides released from the engineered barrier subsystem must pass (or be transported) through the unsaturated zone to reach the saturated zone. The main attributes of the unsaturated zone that control transport of radionuclides are (i) velocity of radionuclides in groundwater (fracture versus matrix flow), (ii) radionuclide sorption, (iii) matrix diffusion, and (iv) hydrologic stratigraphy. The transport velocity within a specific hydrostratigraphic unit (e.g., Calico Hills nonwelded zeolitic) is determined by assuming vertical flow below the repository and comparing the vertical flow to the saturated hydraulic conductivity of the matrix; if the vertical flow exceeds the saturated conductivity any time during the simulation, fracture transport velocities are used. Although this approach does not account for spatial variability of flow caused by heterogeneities in the hydrologic properties of the fractures and matrix, or the episodic nature of infiltration, the approach generally yields short traveltimes to the saturated zone, using current hydraulic properties and infiltration estimates.

In unsaturated zone transport calculations, the NEFTRAN II code (Olague, et al., 1995) models one-dimensional advection and retardation of radionuclides with chain decay. Inputs to the unsaturated zone transport model are the release rates of radionuclides from the engineered barrier subsystem, the time-varying flow results from the unsaturated zone shown in Figure 3-1, and the chemical and physical properties of the hydrostratigraphic units between the repository and the water table (see Figure 3-9 and Table 3-8). The water table elevation remains constant in the total system performance assessment calculations. Thus, the thickness of the unsaturated zone does not change with time even during the pluvial climate. Sorption in fractures is neglected because of the fast traveltimes, whereas sorption in the matrix is modeled using the sorption coefficients presented in Table 3-8. The effects of matrix diffusion on transport in the unsaturated zone are not modeled.

Figure 3-10 shows the release rate for Cl-36. Because Cl-36 moves unretarded, comparison of the times of the release rates in this figure indirectly illustrates the unsaturated zone. The engineered barrier subsystem and unsaturated zone release rates are nearly the same, with only approximately 100 years difference, indicating the unsaturated zone does not significantly delay groundwater transport in those subareas where the Calico Hills vitric unit is absent.
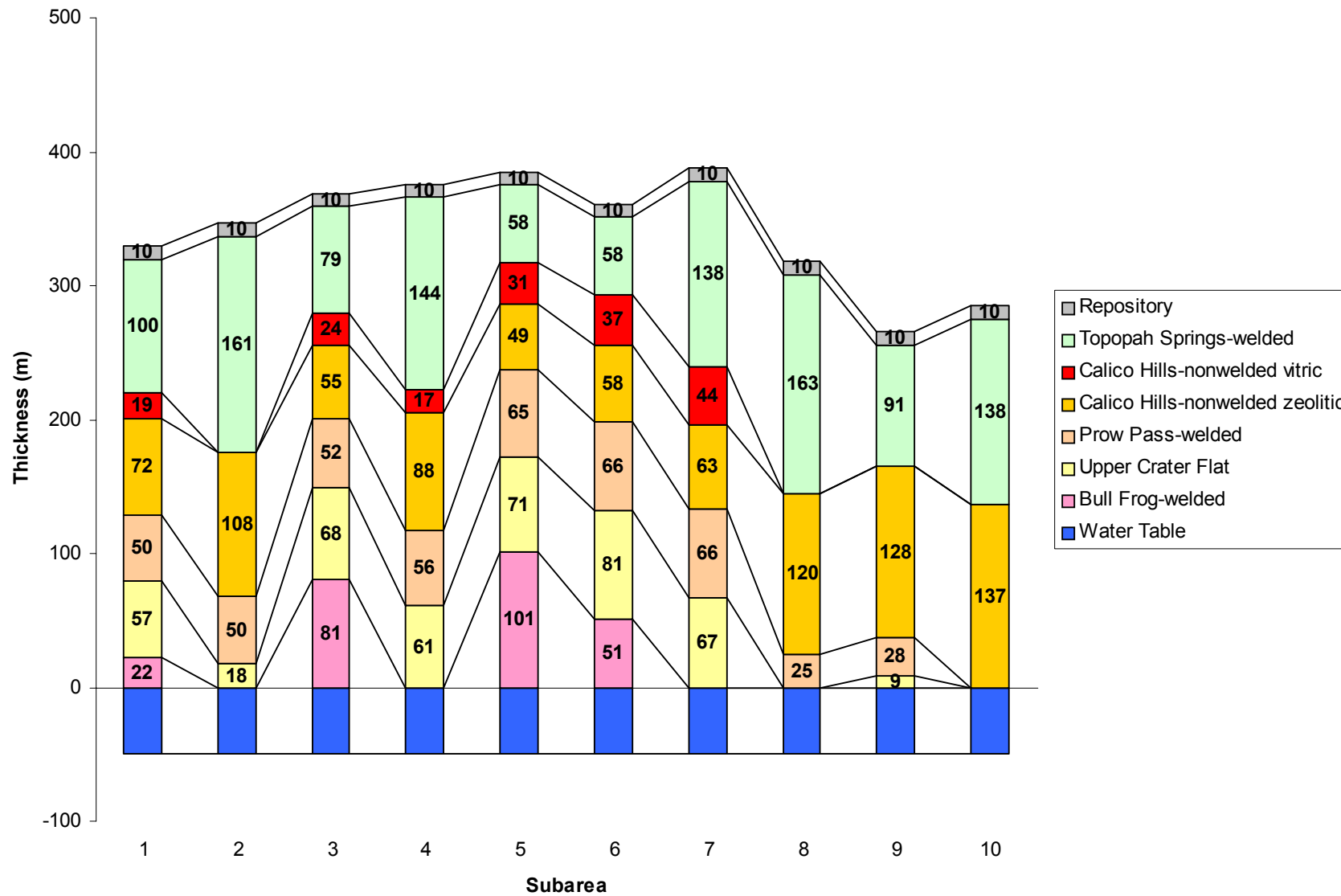
Figure 3-9. Thickness of Subarea Stratigraphic Units

Table 3-8. Mean Values and Distributions of Sorption Coefficient, K_d (m³/kg), Parameters (Other Parameters for Unsaturated Zone Radionuclide Transport Are Also Included.)

Element	Bull Frog Welded Unit	Calico Hills Nonwelded Vitric Unit	Calico Hills Nonwelded Zeolitic Unit	Prow Pass Welded Unit	Topopah Spring Welded Unit	Upper Crater Flat Unit
Am	10,993 (Lognormal; 1,699; 71,123)	34,549 (Lognormal; 5,340; 223,529)	31,410 (Lognormal; 4,855; 203,209)	25,912 (Lognormal; 4,005; 167,647)	11,386 (Lognormal; 1,760; 73,663)	27,090 (Lognormal; 4,187; 175,267)
C	0.00 —	0.00 —	0.00 —	0.00 —	0.00 —	0.00 —
Cl	0.00 —	0.00 —	0.00 —	0.00 —	0.00 —	0.00 —
Cm	0.00 —	0.00 —	0.00 —	0.00 —	0.00 —	0.00 —
Cs	0.51 (Uniform; 0.020, 1.0)	0.055 (Uniform; 0.010, 0.10)	2.75 (Uniform; 0.50, 5.0)	0.51 (Uniform 0.020, 1.0)	0.51 (Uniform 0.020, 1.0)	0.51 (Uniform 0.020, 1.0)
I	0.00 —	0.00 —	0.00 —	0.00 —	0.00 —	0.00 —
Nb	0.00 —	0.00 —	0.00 —	0.00 —	0.00 —	0.00 —
Ni	0.2500025 (Uniform; 5.0×10^{-6}, 0.50)	0.0500005 (Uniform; 1.0×10^{-6}, 0.10)	0.2500025 (Uniform; 5.0×10^{-6}, 0.50)	0.2500025 (Uniform; 5.0×10^{-6}, 0.50)	0.2500025 (Uniform; 5.0×10^{-6}, 0.50)	0.2500025 (Uniform; 5.0×10^{-6}, 0.50)
Np	9.408×10^{-3} (Lognormal; 3.04×10^{-3}, 2.71×10^{-2})	2.96×10^{-2} (Lognormal; 9.91×10^{-3}, 8.84×10^{-2})	2.690×10^{-2} (Lognormal; 9.01×10^{-3}, 8.03×10^{-2})	2.219×10^{-2} (Lognormal; 7.43×10^{-3}, 6.63×10^{-2})	9.740×10^{-3} (Lognormal; 3.26×10^{-3}, 2.91×10^{-2})	2.320×10^{-2} (Lognormal; 7.77×10^{-3}, 6.93×10^{-2})
Pb	0.3 (Uniform; 0.10, 0.50)	0.3 (Uniform; 0.10, 0.50)	0.3 (Uniform; 0.10, 0.50)	0.3 (Uniform; 0.10, 0.50)	0.3 (Uniform; 0.10, 0.50)	0.3 (Uniform; 0.10, 0.50)
Pu	1.036 (Lognormal; 0.36; 2.98)	3.252 (Lognormal; 1.13; 9.36)	2.961 (Lognormal; 1.03; 8.51)	2.443 (Lognormal; 0.85; 7.02)	1.068 (Lognormal; 0.37; 3.08)	2.556 (Lognormal; 0.89; 7.34)

Table 3-8. Mean Values and Distributions of Sorption Coefficient, K_d (m³/kg), Parameters (Other Parameters for Unsaturated Zone Radionuclide Transport Are Also Included.) (continued)

Element	Bull Frog Welded Unit	Calico Hills Nonwelded Vitric Unit	Calico Hills Nonwelded Zeolitic Unit	Prow Pass Welded Unit	Topopah Spring Welded Unit	Upper Crater Flat Unit
Ra	0.3 Uniform; (0.1, 0.5)	0.075 (Uniform; 0.050, 0.10)	3 (Uniform; 1.0, 5.0)	0.3 Uniform; (0.1, 0.5)	0.3 Uniform; (0.1, 0.5)	0.3 Uniform; (0.1, 0.5)
Se	1.5×10^{-2} (Uniform; 3.0×10^{-7}, 3.0×10^{-2})	1.0×10^{-2} (Uniform; 2.0×10^{-7}, 2.0×10^{-2})	7.5×10^{-3} (Uniform; 1.5×10^{-7}, 1.5×10^{-2})	1.5×10^{-2} (Uniform; 3.0×10^{-7}, 3.0×-10^{-2})	1.5×10^{-2} (Uniform; 3.0×10^{-7}, 3.0×10^{-2})	1.5×10^{-2} (Uniform; 3.0×10^{-7}, 3.0×10^{-2})
Tc	0.00 —	0.00 —	0.00 —	0.00 —	0.00 —	0.00 —
Th	76.05 (Lognormal; 12; 482; 500; 3.557×10^{-3})	240.0 (Lognormal; 38; 1,516; 1.064×10^{-2})	216.5 (Lognormal; 34; 1,378, 1.014×10^{-2})	178.4 (Lognormal; 28; 1,137, $8,380 \times 10^{-3}$)	77.46 (Lognormal; 12; 500, 3.682×10^{-3})	188.8 (Lognormal; 30; 1,188, 8.745×10^{-3})
U	1.78×10^{5} (Lognormal; 7.11×10^{-1})	5.58×10^{-5} (Lognormal; 5.58×10^{-5}, 2.03)	1.014×10^{-2} (Lognormal; 5.07×10^{-5}, 2.03)	4.18×10^{-5} (Lognormal; 1.68)	1.34×10^{-5} (Lognormal; 7.37×10^{-1})	4.37×10^{-5} (Lognormal; 1.75)

Table 3-8. Mean Values and Distributions of Sorption Coefficient, K_d (m³/kg), Parameters (Other Parameters for Unsaturated Zone Radionuclide Transport Are Also Included) (continued)

Parameter	Mean	Distribution
Matrix Permeability		
Topopah Spring—welded	2.00×10^{-19} m²	Lognormal; 2.0×10^{-20}, 2.0×10^{-18}
Calico Hills—nonwelded vitric	2.00×10^{-14} m²	Lognormal; 2.0×10^{-15}, 2.0×10^{-13}
Calico Hills—nonwelded zeolitic	5.00×10^{-18} m²	Lognormal; 5.0×10^{-19}, 5.0×10^{-17}
Prow Pass—welded	1.00×10^{-17} m²	Lognormal; 1.0×10^{-18}, 1.0×10^{-16}
Upper Crater Flat	3.00×10^{-18} m²	Lognormal; 3.0×10^{-19}, 3.0×10^{-17}
Bull Frog—welded	2.00×10^{-19} m²	Lognormal; 2.0×10^{-20}, 2.0×10^{-18}
Unsaturated Fracture Zone	1.94×10^{-17} m²	Lognormal; 1.8×10^{-18}, 2.1×10^{-16}
Matrix Porosity		
Topopah Spring—welded	1.20×10^{-1}	—
Calico Hills—nonwelded vitric	3.30×10^{-1}	—
Calico Hills—nonwelded zeolitic	3.20×10^{-1}	—
Prow Pass—welded	2.80×10^{-1}	—
Upper Crater Flat	2.80×10^{-1}	—
Bull Frog—welded	1.20×10^{-1}	—
Unsaturated Fracture Zone	1.20×10^{-1}	—
Matrix Beta		
Topopah Spring—welded	1.5	—
Calico Hills—nonwelded vitric	1.3	—
Calico Hills—nonwelded zeolitic	2.30	—
Prow Pass—welded	1.50	—
Upper Crater Flat	1.40	—
Bull Frog—welded	1.70	—
Unsaturated Fracture Zone	2.30	—
Matrix Grain Density		
Topopah Spring—welded	2.46×10^{3} kg/m³	—
Calico Hills—nonwelded vitric	2.26×10^{3} kg/m³	—

Table 3-8. Mean Values and Distributions of Sorption Coefficient, K_d (m³/kg), Parameters (Other Parameters for Unsaturated Zone Radionuclide Transport Are Also Included) (continued)

Parameter	Mean	Distribution
Calico Hills—nonwelded zeolitic	2.40×10^3 kg/m³	—
Prow Pass—welded	2.54×10^3 kg/m³	—
Upper Crater Flat	2.42×10^3 kg/m³	—
Bull Frog—welded	2.57×10^3 kg/m³	—
Unsaturated Fracture Zone	2.63×10^3 kg/m³	—
Fracture Permeability		
Topopah Spring—welded	8.00×10^{-13} m²	Lognormal; 8.0×10^{-15}, 8.0×10^{-11}
Calico Hills—nonwelded vitric	8.00×10^{-13} m²	Lognormal; 8.0×10^{-15}, 8.0×10^{-11}
Calico Hills—nonwelded zeolitic	6.00×10^{-13} m²	Lognormal; 6.0×10^{-15}, 6.0×10^{-11}
Prow Pass—welded	6.00×10^{-13} m²	Lognormal; 6.0×10^{-15}, 6.0×10^{-11}
Upper Crater Flat	6.00×10^{-13} m²	Lognormal; 6.0×10^{-15}, 6.0×10^{-11}
Bull Frog—welded	3.00×10^{-13} m²	Lognormal; 3.0×10^{-15}, 3.0×10^{-11}
Unsaturated Fracture Zone	1.00×10^{-12} m²	Lognormal; 1.0×10^{-13}, 1.0×10^{-11}
Fracture Porosity		
For Topopah Spring—welded and Unsaturated Fracture zone	3.16×10^{-3}	Lognormal; 1.0×10^{-3}, 1.0×10^{-2}
For all other units	3.16×10^{-4}	Lognormal; 1.0×10^{-4}, 1.0×10^{-3}
Fracture beta		
For all units	2.00	—
For Unsaturated Fracture Zone	1.60	—
Dispersivity		
Matrix longitudinal dispersivity as a fraction of unit	0.06	—
Fracture longitudinal dispersivity as a fraction of unit	0.06	—
Note: Dash in last column indicates a constant value for the parameter distribution		
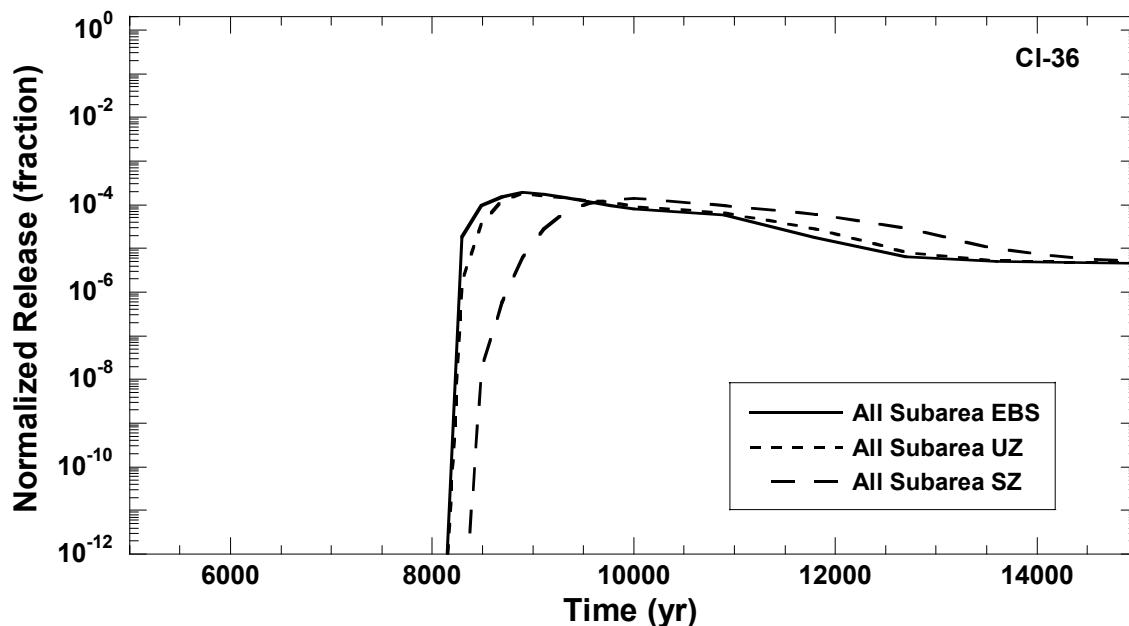
Figure 3-10. Cl-36 Normalized Release Rates from the Engineered Barrier Subsystem, Unsaturated Zone, and Saturated Zone

3.1.6 Saturated Zone Flow and Transport

The transport of radionuclides from the location at which radionuclides from the unsaturated zone enter the water table immediately below the repository to a receptor location takes place in the saturated zone. Transport of radionuclides in the saturated zone is complicated by (i) spatial variability in the geochemical properties of the fracture surfaces and rock matrix, (ii) heterogeneity in formation-scale transport pathways, (iii) temporal variations in the flow field caused by climatic change and pumping for water use, and (iv) variability in the rate at which radionuclides transiting the unsaturated zone reach the water table. Although the abstracted model neglects many of the high-resolution spatial and temporal variations in transport processes, the model does include (i) advective transport through the tuff and alluvial aquifers, (ii) longitudinal dispersion during transport, (iii) chemical sorptive processes that retard the transport of radionuclides in the alluvial aquifer and in the matrix of the tuff aquifer, and (iv) diffusion of radionuclides from the fractures to the matrix in the tuff aquifer. Three one-dimensional streamtubes originating at the water table below the repository and terminating at a receptor location connecting to one or more unsaturated zone streamtubes are used for representing saturated zone transport. Radionuclide transport is simulated using the NEFTRAN II code (Campbell and Leigh, 1991), which calculates the radionuclide release rate (Bq/yr) at the down-gradient receptor location. For each subarea, radionuclide transport out of the engineered barrier subsystem and into the unsaturated and saturated zones is conceptualized as occurring in a single streamtube that originates in the repository, extends to the water table, and continues to the receptor location. Streamtubes begin at the water table directly below the repository and continue to the receptor location. Each subarea in the repository is assigned to the nearest streamtube. Subareas 1, 2, 3, 4, and 8 are mapped to

Streamtube 2; Subareas 5, 6, and 7 are mapped to Streamtube 1; and Subareas 9 and 10 are mapped to Streamtube 3.

Figure 3-11 shows the subareas and streamtubes used for the saturated zone transport model, and Table 3-9 provides the length of the saturated zone flow path by subarea. The groundwater traveltimes from the point where the radionuclides enter the saturated zone to the receptor location are 536 years for Subareas 1, 2, 3, 4, and 8 (Streamtube 2); 596 years for Subareas 5, 6, and 7 (Streamtube 1); and 766 years for Subareas 9 and 10 (Streamtube 3) for the mean value data set. Variations in the groundwater traveltimes are primarily the result of variations in the streamtube length, width, and flow rates. The total saturated zone flow rate in all the streamtubes is 1.78×10^5 m^3/yr [6.29×10^6 ft^3/yr]. The relative contributions of Streamtubes 1, 2, and 3 to the total saturated zone flow are 33, 41, and 26 percent. The release rate at the outlet of the streamtubes is determined using the sum of the release rates from all the streamtubes and is dependent on the time-varying concentration at the inlet. Figure 3-10 shows the saturated zone release rates for Cl-36, which is not retarded in the saturated zone.

The source term for the saturated transport model is the time-varying radionuclide release rate from the unsaturated zone calculations. Other inputs to the saturated zone transport model include the physical and chemical properties of the tuff and alluvium and the streamtube flow rates, widths, and lengths. The mean values for the saturated zone input parameters are presented in Table 3-9. The correlation coefficients for the alluvium matrix retardation factors are presented in Table 3-10.

3.1.7   Dose to the Receptor Group

The radionuclide concentrations in groundwater in the saturated zone at the receptor location are used to calculate the annual total effective dose equivalent to a reasonably maximally exposed individual. The groundwater concentrations are converted to doses by taking into consideration (i) the location of the receptor group, (ii) the lifestyle characteristics of the receptor group and the exposure pathways, (iii) processes that determine fate and transport of contaminants in the biosphere, (iv) calculation of human doses from factors that convert exposure to contaminated media to effective dose equivalents, and (v) well pumping rates. The activity released from the saturated zone per unit time is converted to activity per unit volume of water by dividing by the pumping rate. Dose conversion factors are then calculated and used to determine dose to the reasonably maximally exposed individual. At each timestep, total doses are the sum of the product of each radionuclide concentration and dose conversion factor within and among groundwater pathways.

The receptor location for the basecase data set is 20 km [12.4 mi] from the repository. At 20 km [12.4 mi], the mean value for the pumping rate is 1.21×10^7 m^3/yr [4.3×10^8 ft^3/yr], which is sufficient to capture the entire contaminant plume. Because the TPA Version 4.1 code assumes the volume of water pumped is constant throughout the simulation period, values for the concentration of the well water exhibit the same behavior as the saturated zone release rates. For example, to convert from Cl-36 release rates in Figure 3-10 to concentration, the release rates are divided by the well pumping rate to compute the wellwater concentrations. Note that in the saturated zone transport model, the well pumping rate does not change the velocity field, thus does not alter the rate of radionuclide transport.

3-26
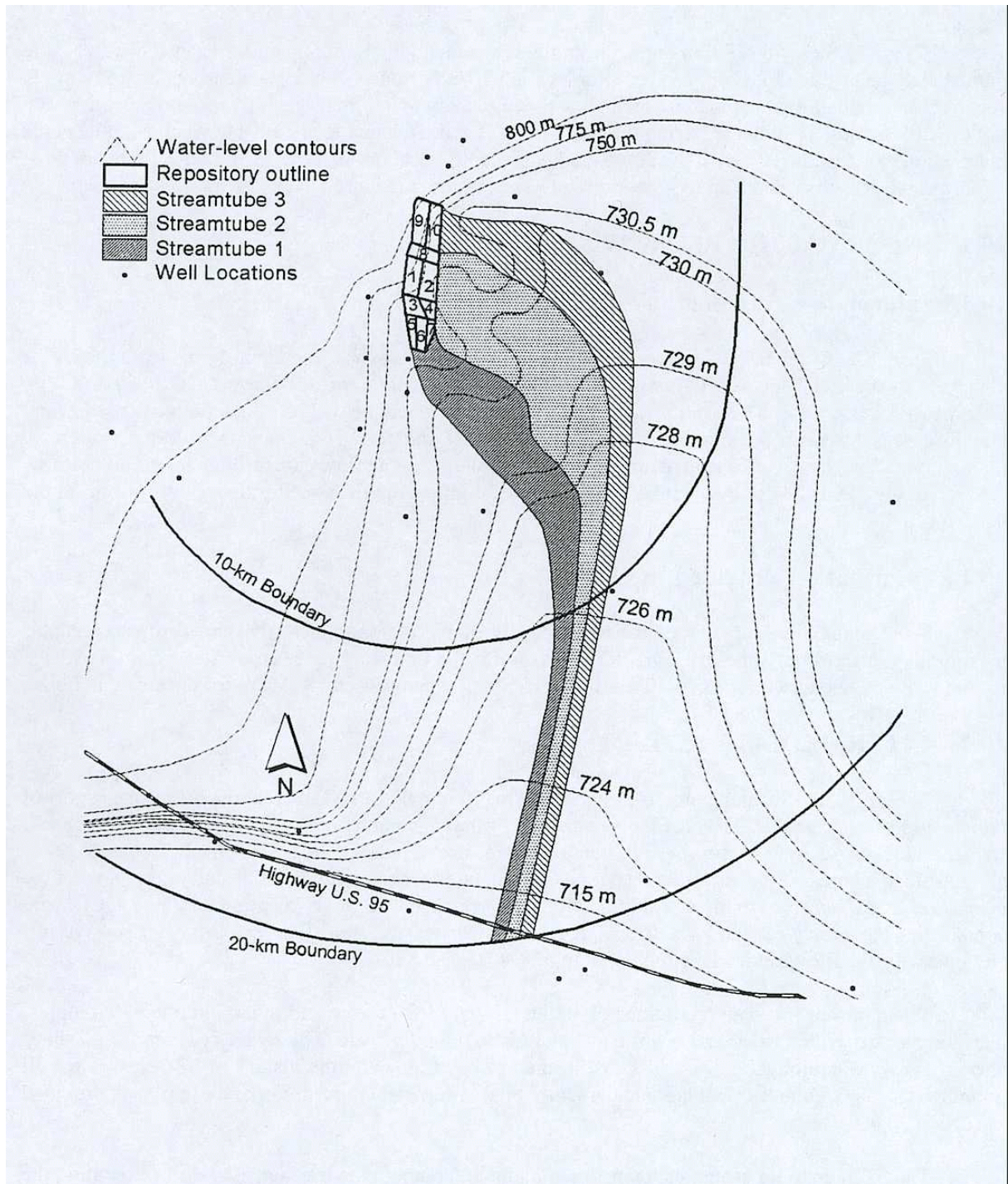
Figure 3-11. Saturated Zone Streamtubes Assigned to Each Subarea

Table 3-9. Mean Values and Distributions Used for Saturated Zone Flow and Radionuclide Transport in Total System Performance Assessment		
Parameter	**Mean**	**Distribution**
Mixing zone dispersion fraction	1.00×10^{-2}	—
Tuff dispersion fraction	1.00×10^{-2}	—
Alluvium dispersion fraction	1.00×10^{-1}	—
Tuff fracture porosity	3.16×10^{-3}	Log-uniform; 1.0×10^{-3}, 1.0×10^{-2}
Alluvium matrix porosity	1.25×10^{-1}	Uniform; 1.0×10^{-1}, 1.5×10^{-1}
Immobile R_d for tuff		
Am	1.80×10^4	—
Np	19.00	—
I	1.00	—
Tc	1.00	—
Cl	1.00	—
Cm	1.8×10^4	—
U	37.00	—
Pu	1.8×10^3	—
Th	1.8×10^4	—
Ra	5.4×10^3	—
Pb	5.4×10^3	—
Cs	9.0×10^3	—
Ni	1.8×10^3	—
C	1.00	—
Se	55.00	—
Nb	1.8×10^4	—
Immobile porosity for tuff	2.00×10^{-1}	—
Diffusion rate for tuff	0.001	—
Fracture R_d for tuff for all nuclides	1.00	—
Minimum residence time for tuff	1.00×10^1 yr	—
Minimum residence time for alluvium	1.00×10^1 yr	—
Distance to tuff alluvium interface	14.95 km	Uniform; 10.0, 19.9
Distance to receptor group	20.00 km	—
Pluvial well pumping rate at receptor group 20 km [gal/day]	6.215×10^6	Uniform; 3.2×10^6, 9.23×10^6
Pluvial switch time	13000.00	—
Well pumping rate at receptor group at 20 km	8.75×10^6 gal/day	Uniform 4.5×10^6, 1.3×10^7
Mixing zone thickness at 20 km	1.25×10^2 m	Uniform 50.00, 200.0
Alluvium Matrix R_d (For Correlations See Table 3-11)		
Am	7.14×10^7	Lognormal; 7.5×10^4, 6.8×10^{10}
C	1.00	—
Cl	1.00	—
Cm	7.50×10^4	—
I	1.00	—
Np	6.24×10^1	Lognormal; 1.0, 3.9×10^3
Pu	1.28×10^4	Lognormal; 4.2×10^2, 3.9×10^5

Table 3-9. Mean Values and Distribution Used for Saturated Zone Flow and Radionuclide Transport in Total System Performance Assessment (continued)		
Parameter	**Mean**	**Distribution**
Se	2.24×10^1	Log-uniform; 1.0, 500.0
Tc	1.00	—
Th	9.25×10^3	Lognormal; 1.9, 4.5×10^7
U	1.38×10^2	Lognormal; 1.0, 1.9×10^4
Ra	4.0×10^3	Log-uniform; 2.0×10^3, 8.0×10^3
Pb	4.0×10^3	Log-uniform; 2.0×10^3, 8.0×10^3
Cs	9.49×10^4	Log-uniform; 9.0×10^4, 1.0×10^5
Ni	8.94×10^1	Log-uniform; 1.0×10^0, 8.0×10^3
Nb	7.75×10^3	Log-uniform; 2.0×10^3, 3.0×10^4
Streamtube Flow Properties		
Subarea	**Saturated Zone Streamtube**	**Length (m)**
1	2	26,900
2	2	26,100
3	2	26,900
4	2	25,900
5	1	22,500
6	1	22,200
7	1	21,800
8	2	26,600
9	3	30,000
10	3	29,300

Table 3-10. Correlated Parameters and Correlation Coefficients for the Multiple Realizations		
Correlated Parameter 1	**Correlated Parameter 2**	**Correlation**
SubAreaWetFraction	ArealAverageMeanAnnualInfiltrationAtStart[mm/yr]	0.631
SubAreaWetFraction	MatrixPermeability_TSw_[m2]	−0.623
AlluviumMatrixRD_SAV_Am	AlluviumMatrixRD_SAV_Pu	0.964
AlluviumMatrixRD_SAV_Am	AlluviumMatrixRD_SAV_U	0.346
AlluviumMatrixRD_SAV_Am	AlluviumMatrixRD_SAV_Np	0.837
AlluviumMatrixRD_SAV_Am	AlluviumMatrixRD_SAV_Th	0.112
AlluviumMatrixRD_SAV_Pu	AlluviumMatrixRD_SAV_U	0.489
AlluviumMatrixRD_SAV_Pu	AlluviumMatrixRD_SAV_Np	0.881
AlluviumMatrixRD_SAV_Pu	AlluviumMatrixRD_SAV_Th	0.109
AlluviumMatrixRD_SAV_Np	AlluviumMatrixRD_SAV_Th	0.260
AlluviumMatrixRD_SAV_Np	AlluviumMatrixRD_SAV_U	0.610
AlluviumMatrixRD_SAV_Th	AlluviumMatrixRD_SAV_U	0.165

The groundwater dose is determined by multiplying the concentration of the nuclides in the pumped water with the dose conversion factor. The mass of radionuclides captured by pumping is diluted in the volume of water extracted from the pumping well and converted from a groundwater concentration to a dose using dose conversion factors. The dose to an individual of the receptor group originates from drinking and irrigation waters used by an average adult living in Amargosa Valley. The groundwater pathway dose conversion factors for the 20 radionuclides used in the basecase mean value data set are summarized in Table 3-11.

3.2　　　　Results From The Mean Value Data Set

This section describes the behavior of the total system and explains how the individual dose is influenced by the various subsystem models and parameters. Time history plots of key system parameters for both doses and release rates at various subsystem boundaries are presented in this section for the mean value, single-realization case.

The dose to an average individual residing 20 km [12.4 mi] downgradient of the repository is presented in Figure 3-12 for radionuclides with doses greater than 10^{-8} mSv/yr [10^{-6} mrem/yr] for 10,000 and 100,000 years. The period of 100,000 years is chosen so the effects of one cycle of the pluvial climate and the effects of waste package corrosion, which occur after the 10,000-year simulation period, can be studied.

A peak total dose of 3.5×10^{-4} mSv/yr [0.035 mrem/yr] occurred during the 10,000-year simulation period. The dose is dominated in the 10,000-year simulation period by I-129, Tc-99, and, to some extent, Cl-36 (more than two orders of magnitude less than I-129 or Tc-99 doses). These nuclides are nonsorbing and have relatively long half-lives.

For the 100,000-year simulation period, a peak total dose of 3.8×10^{-2} mSv/yr [3.8 mrem/yr] occurred at 100,000 years, and the dose was dominated by Np-237, but also had significant contributions from I-129 and Tc-99. To 28,000 years, dose contribution is primarily from Tc-99 and I-129. At 28,000 years, Np-237 starts contributing noticeably to dose and immediately becomes the dominant contributor. The average breakthrough time for Np-237 from the engineered barrier subsystem and unsaturated zone is approximately 8,700 years. The average breakthrough time for Np-237 from the saturated zone is 31,400 years with its earliest breakthrough occurring at 25,300 years. The ramp-up in dose between 30,000 and 40,000 years is related to the delayed breakthrough of Np-237 released from initially defective waste packages. The peak occurring near 70,000 years is a result of the waste packages failing from corrosion at 69,400 years. The main contributors to this peak are I-129, Tc-99, and, to a lesser extent, Cl-36. The peak near 100,000 years is from the delayed release of Np-237 from failed waste packages from corrosion at 70,000 years. A discussion of the total system performance assessment results from the 10,000- and 100,000-year simulation periods, with and without the faulting and igneous activity disruptive events, follows in the next two sections.

3.2.1　　　　10,000-Year Releases and Dose

As evident from Figure 3-8 and as explained in Section 3.1.3.2, all basecase releases in 10,000 years are from the initially defective waste package failures. Although the initially defective failures take place at the zero year, releases do not occur until 8,300 years. Before 8,300 years, the drip shield fails at 7,422 years and then refluxing water enters and fills

Table 3-11. Biosphere Dose Conversion Factors for Groundwater at the 20-km Receptor Location		
Radionuclide	Nonpluvial Dose Conversion Factor (rem/year)/(Ci/m^3)	Pluvial Dose Conversion Factor (rem/year)/(Ci/m^3)
Ac-227	1.53×10^7	2.64×10^5
Ag-108m	8.26×10^3	3.79×10^6
Am-241	3.91×10^6	3.44×10^6
Am-242m	3.78×10^6	3.61×10^6
Am-243	3.89×10^6	3.29×10^6
C-14	2.93×10^3	2.92×10^5
Cl-36	5.09×10^3	5.62×10^5
Cm-243	2.69×10^6	1.39×10^6
Cm-244	2.16×10^6	5.60×10^6
Cm-245	4.02×10^6	2.57×10^6
Cm-246	3.97×10^6	3.71×10^6
Cs-135	7.62×10^3	3.63×10^6
Cs-137	5.38×10^4	2.74×10^5
I-129	2.95×10^5	1.09×10^7
Mo-93	1.92×10^3	1.45×10^7
Nb-94	7.80×10^3	3.84×10^6
Ni-59	2.42×10^2	7.02×10^4
Ni-63	6.64×10^2	3.74×10^6
Np-237	4.75×10^6	4.55×10^6
Pa-231	1.14×10^7	2.98×10^5
Pb-210	5.88×10^6	3.71×10^6
Pd-107	1.81×10^2	2.06×10^6
Pu-238	3.44×10^6	3.63×10^6
Pu-239	3.79×10^6	2.76×10^5
Pu-240	3.79×10^6	1.36×10^6
Pu-241	7.35×10^4	4.00×10^2
Pu-242	3.60×10^6	5.14×10^4
Ra-226	1.47×10^6	7.27×10^3
Se-79	9.43×10^3	2.82×10^5
Sm-151	4.20×10^2	2.06×10^4
Sn-121m	1.95×10^3	1.82×10^3
Sn-126	2.18×10^4	7.87×10^3
Sr-90	2.07×10^5	1.67×10^2
Tc-99	1.91×10^3	1.74×10^3
Th-229	3.89×10^6	1.71×10^3
Th-230	5.88×10^5	7.44×10^3
U-232	1.44×10^6	1.71×10^3
U-233	3.15×10^5	1.83×10^5
U-234	3.09×10^5	8.99×10^3
U-235	2.90×10^5	6.23×10^2
U-236	2.93×10^5	2.26×10^2
U-238	2.80×10^5	4.45×10^3
Zr-93	1.79×10^3	2.60×10^3
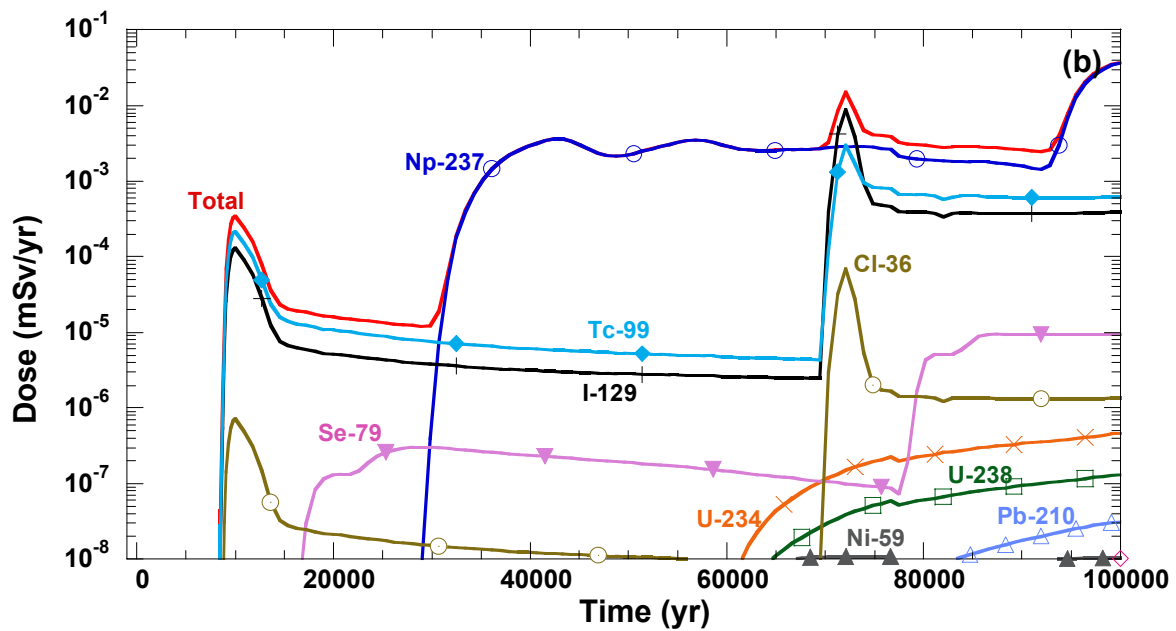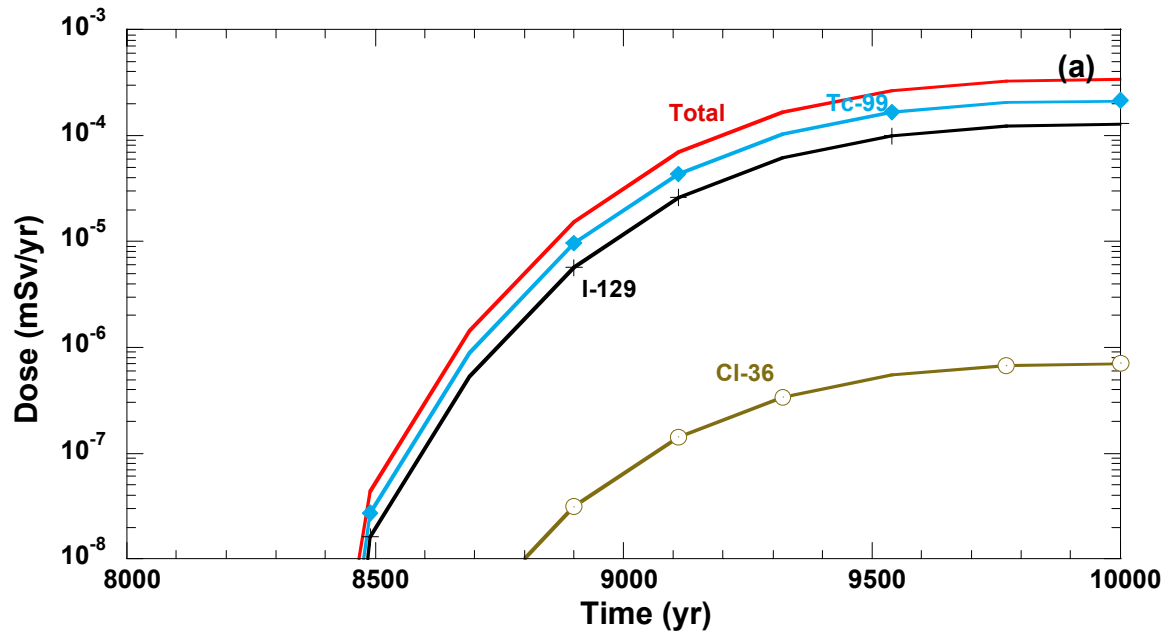
Figure 3-12. Groundwater Dose to an Average Individual as a Function of Time at the Receptor Location 20 km [12.4 mi] Downgradient of the Repository, for the Mean Value Data Set in the (a) 10,000-Year, and (b) 100,000-Year Simulation Period

the failed waste package. Water accumulates in the failed waste package with time and eventually overflows, releasing radionuclides.

Time histories of radionuclide releases at the outflow boundaries of the engineered barrier subsystem, the unsaturated zone, and the saturated zone are shown in Figure 3-13. In general, the release rates from the engineered barrier subsystem in Figure 3-13(a) for the soluble radionuclides drop after the peak release is reached because of inventory depletion due to radioactive decay and the removal of radionuclides from the waste package due to release. Other radionuclides, such as U-238, U-234, Np-237, Pu-239, Nb-94, and Th-230, which are less soluble and have relatively longer half-lives, exhibit increasing release rates throughout the 10,000-year simulation period. Am-241 also has low solubility; however, with a half-life of only 432 years, the inventory decreases rapidly.

There is only a small increase {~ 1.0×10^{-5} mSv/yr [1.0×10^{-3} mrem/yr]} in the engineered barrier subsystem release rates from the instantaneous release of the gap fraction inventory. The increase in infiltration rate for the 10,000-year simulation period shown in Figure 3-1 is only marginal compared with the period beyond 10,000 years. Therefore, climatic change from current to pluvial conditions is a key event that affects release rates only beyond 10,000 years.

The similarity between engineered barrier subsystem and unsaturated zone releases shown in Figures 3-13(a) and (b) indicates the unsaturated zone as modeled apparently does not significantly delay the releases into the saturated zone for the mean value data set. One might expect the unsaturated zone to delay the transport of radionuclides because the radionuclides must be transported 300 m [984 ft] from the repository to the water table.

The unsaturated zone releases are directly related to the presence of the Calico Hills vitric layer. The groundwater traveltime through the unsaturated zone is 11–21 years for Subareas 2, 8, 9, and 10 (i.e., fracture flow); the remaining subareas are between 200 and 700 years (i.e., matrix flow). Subareas 2, 8, 9, and 10 show a fast path because, in the absence of the Calico Hills nonwelded vitric layer, the flow is predominately in fractures. Consequently, for Subareas 2, 8, 9, and 10, which encompass almost 48.3 percent of the spent nuclear fuel inventory, the unsaturated zone does not delay radionuclide transport subsequent to release from the engineered barrier system. For the remaining 51.7 percent of the spent nuclear fuel inventory, the 200–700 years of groundwater traveltime somewhat delays the non-retarded radionuclides, however, retarded radionuclides will be effectively held up for greater than 10,000 years in those subareas where the Calico Hills vitric unit is present.

The saturated zone release illustrated in Figure 3-13(c) reveals releases of only non-retarded Tc-99, I-129, and Cl-36 in the 10,000-year simulation period. The saturated zone release rates presented in Figure 3-13(c) also can be compared with Figure 3-13(b) to evaluate the effects of flow and transport in the saturated zone. The groundwater traveltime computed using the streamtube flow rates and lengths in the saturated zone is 570 years (see Table 3-12). However, sorption in the alluvium significantly increases the traveltime for most radionuclides.

As illustrated in Figure 3-12(a), the groundwater pathway dose at 10,000 years is dominated by I-129, Tc-99, and to some extent, Cl-36. These nuclides contribute the most to dose because of no retardation during transport in alluvium, a large initial inventory {1.32×10^9, 5.37×10^{11}, and 4.26×10^8 Bq/MTU [0.0357, 14.5, and 0.0115 Ci/MTU]}, long half-lives compared with the 10,000-year timeframe of interest (1.57×10^7, 2.13×10^5, 3.01×10^5 year), moderate to high dose conversion factors, and moderate to high solubilities {129, 99.3, and 36 kg/m^3 [8.05, 6.20, and 2.25 lb/ft^3]}. Tables 3-5 and 3-7 through 3-10 provide a summary of
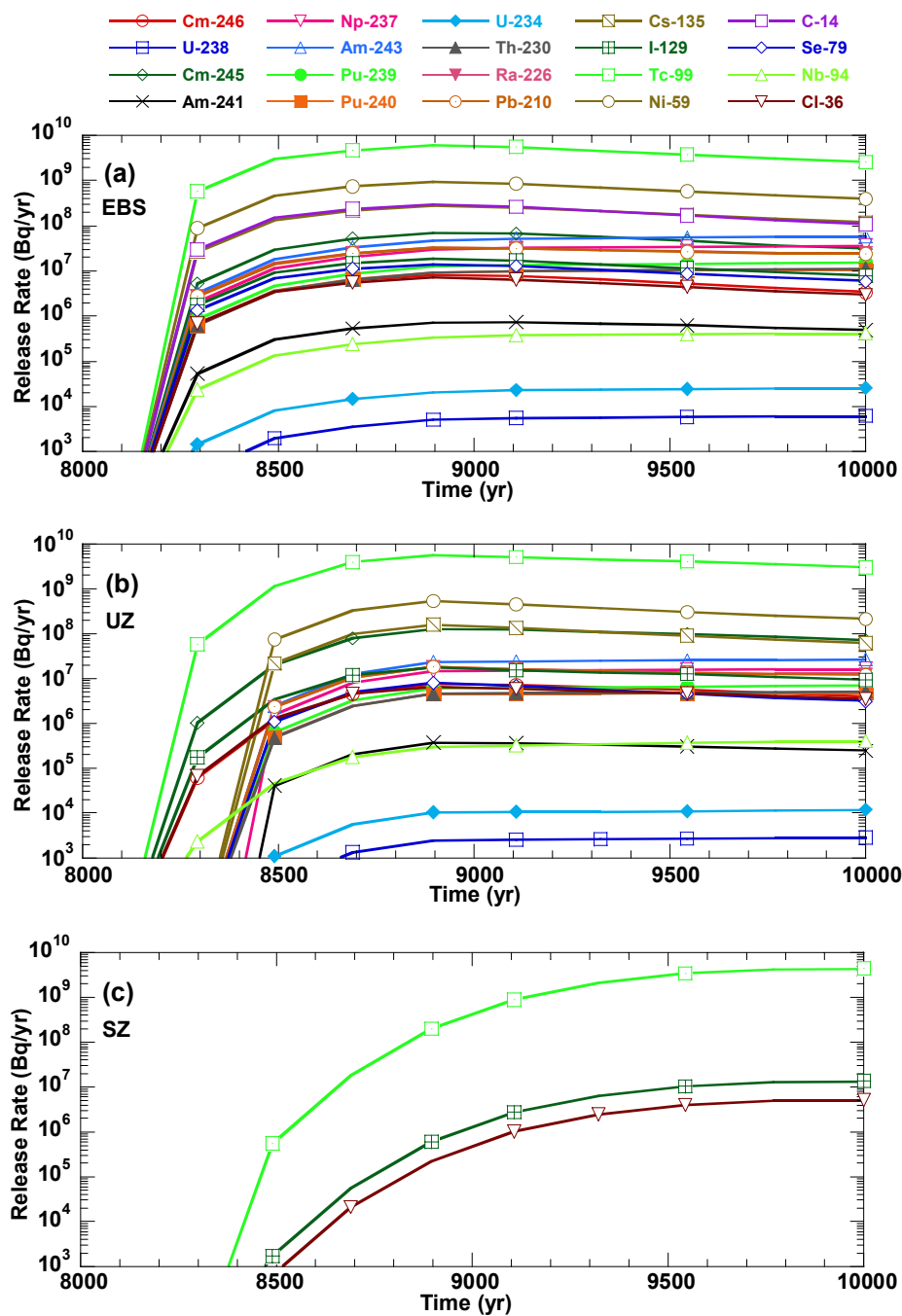
Figure 3-13. Release Rates in the 10,000-Year Time Period of Interest from the (a) Engineered Barrier Subsystem, (b) Unsaturated Zone, and (c) Saturated Zone for the Mean Value Data Set

Table 3-12. Average, Maximum, and Minimum Saturated Zone Groundwater Traveltimes and the Average from 350 Realizations				
		Groundwater Traveltimes (yr)		
Streamtube	**Subarea**	**Minimum**	**Maximum**	**Average**
1	5	58	1,356	629
	6	57	1,352	627
	7	57	1,350	626
2	1	76	1,261	592
	2	72	1,234	578
	3	74	1,249	586
	4	72	1,234	578
	8	72	1,239	581
3	9	80	1,790	821
	10	78	1,781	816
Average (all subareas)		70	1,385	644

the mean values for these parameters corresponding to all radionuclides. To obtain a perspective of the magnitude of the dose, a total dose of 10^{-11} Sv/yr [1 nanorem/yr] does not appear until 8,490 years in the time evolution of the dose curve in Figure 3-12(a). Furthermore, the saturated zone release rate for I-129 corresponding to 74,000 Bq/yr [2 μCi/yr] occurs at 8,300 years, at which time there is no measurable dose from any nuclide. The only nuclides that contribute more than 10^{-11} Sv/yr [1 nanorem/yr] to dose in 10,000 years are I-129, Tc-99, and Cl-36, which exhibit the peak doses at the end of the 10,000-year simulation period.

The dose histories for a particular faulting event and a particular igneous event are presented in Figures 3-14(a) and (b). The purpose of the following discussion is not to compare the incremental risk posed by the faulting or the igneous event, but rather to illustrate the behavior of the underlying model abstractions for faulting and igneous activity. To determine the risk, one would need to multiply the additional doses caused by faulting and igneous activity by their respective annual probabilities of occurrence [5×10^{-6} and 1×10^{-7} (see Mohanty, et al., 2002, pp. 12-2 and 14-2, for details)]. For the mean value data set, there are no faulting events because the mean value of the threshold displacement is greater than the mean value of the credible displacement along a fault. If the threshold is made smaller than the mean value of the credible displacement, however, the faulting event occurs at approximately 4,900 years and causes the failure of 208 waste packages. Figure 3-14(a) shows that the compliance period peak groundwater dose from the forced faulting event occurs approximately 1,400 years earlier and more than 2.5 times the basecase compliance period peak dose. The earlier release is because waste packages failed from faulting events do not experience bathtub behavior and thus have rapid release. The difference between the results arises solely from the release of spent nuclear fuel from waste packages failed by faulting.

The groundwater dose from igneous activity in Figure 3-14(b) behaves similarly to the dose from faulting events. The increase in groundwater dose from igneous activity is smaller than that for faulting events because only 53 waste packages are failed by the intrusive igneous activity compared with 208 waste packages failed by the faulting event in the mean value, single-realization case. Extrusive igneous events also result in a peak ground surface dose of

Figure 3-14. Groundwater Dose in 10,000-Year Simulation Period With and Without (a) Faulting and (b) Igneous-Activity Disruptive Events, for the Mean Value Data Set, Without Probability Weighting. (The Ground-Surface Dose is Shown for Releases Caused by Extrusive Igneous Activity.)

approximately 0.1 Sv/yr [10,000 mrem/yr] at 4,900 years, which is the time of the volcanic event, and the dose exponentially decreases thereafter.

3.2.2   100,000-Year Releases and Dose

This section presents a discussion of the total system performance assessment results from the 100,000-year simulation period for dose, release rates, and other intermediate values such as corrosion failure time using the mean value data set. The results for the 100,000-year simulation period are different from the results for the 10,000-year simulation period, in part because waste packages fail from corrosion only after 10,000 years.

Calculations beyond 10,000 years help us understand the effect of processes beyond the anticipated behavior of the repository for the regulatory period (e.g., failure of the waste packages by corrosion, wetter environment).

Figure 3-8 provides the performance of the engineered barrier subsystem showing the number of failed waste packages during the 100,000-year simulation period. Initially defective failures in all subareas account for 45 waste packages, whereas, of those remaining, 2,392 waste packages in Subareas 4, 5, 7, and 10 fail from corrosion at 69,400 years; and 6,440 waste packages in Subareas 1, 2, 3, 6, 8, and 9 fail from corrosion at 70,300 years (i.e., 900 years after the first corrosion failure). Thus, all 8,877 waste packages in the repository fail by 70,300 years. Table 3-3 provides a summary of the total system performance assessment input parameters that determine the waste package failure time.

The release rate histories for all 20 radionuclides at the three boundaries (i.e., engineered barrier subsystem, unsaturated zone, and saturated zone presented in Figure 3-15) reflect the time required for the drip shield to fail, and initially defective waste packages to fill with water (8,300 years) and release radionuclides, together with the final corrosion failure time of 70,300 years. The waste packages failed by corrosion fill relatively faster and release radionuclides relatively faster than the initially defective failures because the thermal reflux period has passed, the drip shields have failed, and the pluvial period has taken effect. The first peak releases begin at approximately 8,300 years, corresponding to the initially defective failure, and the second peak begins just after 70,000 years, corresponding to the corrosion failure of waste packages. Just as with the 10,000-year simulation period in Figure 3-13, release rates of radionuclides are impacted by sorption, half-lives, initial inventories, gap inventories, solubilities, and dose conversion factors. Values for these parameters are presented in Tables 3-5 and 3-7 through 3-10. The gap fraction inventory has a larger impact on dose in the 100,000-year simulation period (a 300 percent increase in dose 2,700 years after the first corrosion failures at 69,000 years) compared with the 10,000-year simulation period (a 12-percent increase in the peak dose which occurs at 10,000 years). This is primarily the result of a larger gap inventory being available from 8,832 waste packages failing from corrosion compared to 45 waste packages that are initially defective. The gap fraction inventory, however, influences the 10,000-year simulation period peak while it does not affect the 100,000-year simulation period peak since the localized corrosion peak from the gap fractions of 3.76×10^{-3} mSv/yr [0.379 mrem/yr] occurs earlier than and is an order of magnitude less than the period peak of 3.79×10^{-2} mSv/yr [3.79 mrem/yr].

For the waste package failure modes in which the waste package behaves as a bathtub, the releases of Tc-99, I-129 and the other highly soluble radionuclides represent the accumulation of the radionuclides in water that occurs as the waste package fills. In the nominal case
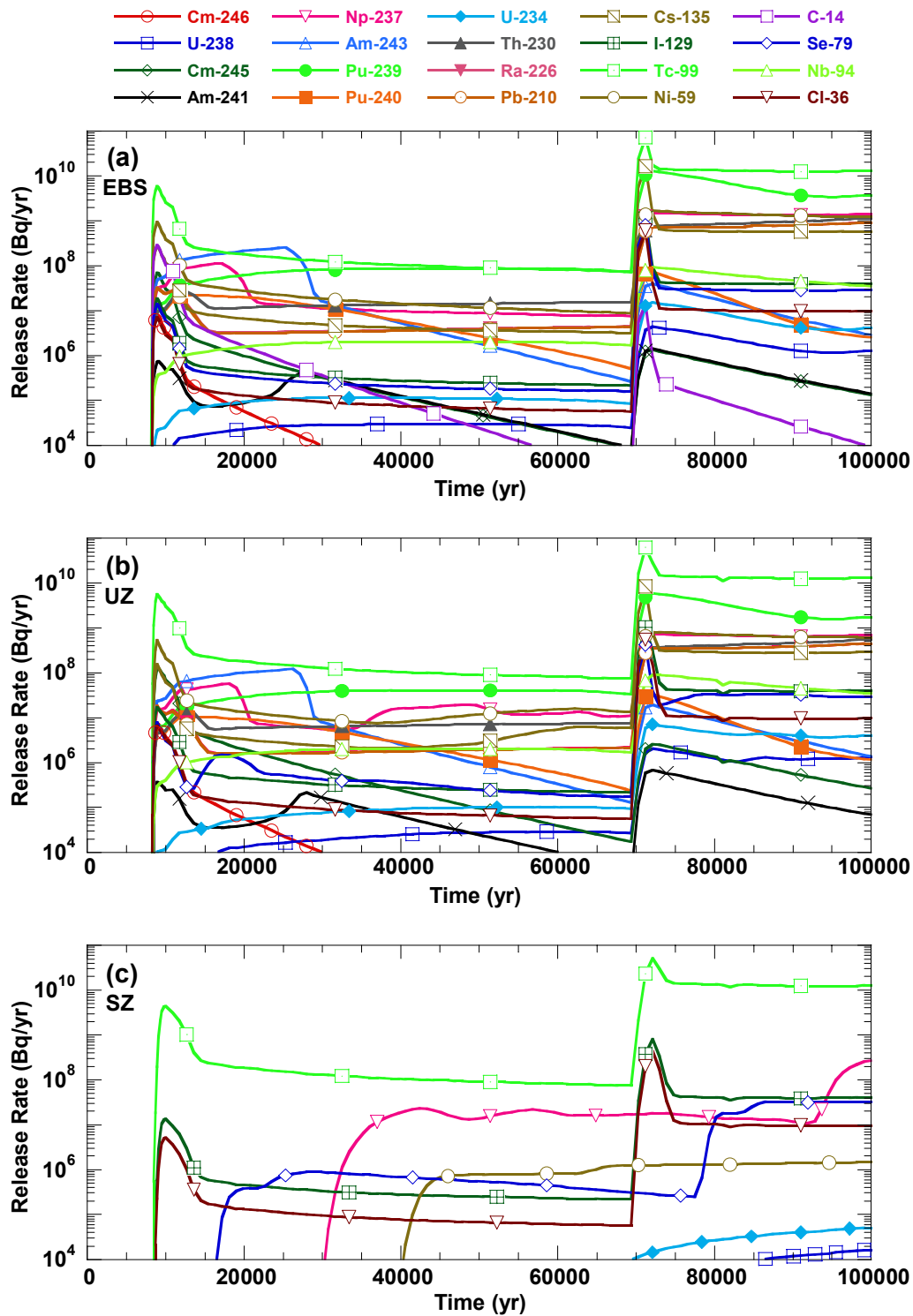
Figure 3-15. Release Rates up to 100,000 Years from the (a) Engineered Barrier Subsystem, (b) Unsaturated Zone, and (c) Saturated Zone for the Mean Value Data Set

scenario, bathtub behavior occurs for initially defective, corrosion, and seismic failures. Because seismic failure does not occur with the mean value data set, bathtub behavior occurs before 10,000 years because of initially defective failure and after 10,000 years because of corrosion failure. The peak releases for these highly soluble radionuclides from initially defective waste packages occur after the waste package fill with water at 8,300 years. As Figure 3-15 shows, the release rates of less soluble radionuclides such as Np-237 from the initially defective waste packages peak at 17,000 years. This time delay of 8,700 years after the Tc-99 and I-129 peak release is because the solubility limit controls the release rate. Because Np-237 leaves the waste package at the solubility limit, the release rate from the waste package is proportional to the rate of water flowing through the waste package. Further discussions on the impact of solubility limits on Np-237 can be found in Chapter 7. With a half-life of 2.14×10^6 years and an initial inventory of 1.27×10^{11} Bq [3.42 Ci] per waste package, the Np-237 inventory is available for release throughout the simulation period. After 17,000 years, the solubility limit's control on release rate decreases as the flow rate increases (because of the reduced rate of radionuclide mass accumulation in the bathtub caused by inventory depletion), implying that the release becomes more controlled by the dissolution rate. Therefore, the decrease in the Np-237 release rate until the next waste package failure time can be attributed to a higher infiltration rate during the pluvial period. This effect is observable in Figure 3-15(a), from 17,000 years to the corrosion failure time at 70,000 years. After 70,000 years, radionuclide releases decrease (i.e., not solubility-limited) following the peak releases at approximately 70,000 years. The decrease in release rates for the radionuclides with low solubilities can also be attributed to high flow rates during the pluvial period that switches the release mode from solubility-limited to dissolution limited. Pu-239 is another actinide that is solubility-limited in ambient Yucca Mountain pore waters. Therefore, its release rates from the engineered barrier subsystem should be similar to Np-237, as Figure 3-15(a) shows.

The plot in Figure 3-15(b) represents the release rates at the water table for each radionuclide summed over all 10 subareas. A comparison of the engineered barrier subsystem and unsaturated zone release rates in Figures 3-15(a) and (b) shows that the unsaturated zone has little delaying effect, not only on the transport of Tc-99, a nonsorbing nuclide, but also on the transport of the other 19 radionuclides. Those subareas that do not contain the Calico Hills vitric layer do not significantly affect the release rates because for those subareas, transport occurs mainly in fractures. For the subareas containing the Calico Hills vitric layer, however, release rates would be significantly lowered, especially for retarded radionuclides.

Figure 3-15(c) illustrates the performance of the saturated zone in the 100,000-year simulation period. In the saturated zone, sorption significantly affects the release rates. The only radionuclides that arrive at the receptor location with a release rate greater than an arbitrarily chosen low value of 37,000 Bq/yr [10^{-6} Ci/yr] are Tc-99, Np-237, I-129, Se-79, Cl-36, Ni-59, and U-234. Either retardation of the remaining 13 radionuclides in the alluvium delays the time of arrival past the 100,000-year simulation period or the inventory decays during transit because the half-lives are short relative to the transport time. The saturated zone alluvium sorption coefficients for all radionuclides are provided in Table 3-9.

The radionuclides dominating the 100,000-year dose are different from those dominating the 10,000-year dose. For the 100,000-year simulation period, the dose shown in Figure 3-12(b) is dominated by Np-237, Tc-99, and I-129, with smaller contributions from Cl-36, Se-79, and others. The radionuclides contributing the most to the peak dose at 72,000 years are I-129, Np-237, and Tc-99, with minor contributions from Cl-36. Although Cl-36 has a relatively long half-life at 3.01×10^5 years, the inventory is small (see Table 3-7). Thus, although contributing

with some significance to peak dose at 72,000 years, Cl-36 rapidly becomes an insignificant contributor to dose. Figure 3-12(b) also illustrates the impact of retardation in the alluvium portion of the saturated zone on the arrival of radionuclides at the 20-km [12.4-mi] receptor location. The retardation factors for Cl-36, I-129, Tc-99, Se-79, and Np-237 are 1.0, 1.0, 1.0, 22.4, and 62.4. The reasons Tc-99 and I-129 dominate the dose in Figure 3-12(b) are (i) high solubility in the water contacting the spent nuclear fuel, (ii) no retardation, (iii) long half-lives, and (iv) relatively large dose conversion factors. Np-237 has comparatively low solubility, but has a relatively large dose conversion factor. Tables 3-5 and 3-7 through 3-10 provide summaries of the values for these parameters. Note that the flow in the remainder of the saturated zone (i.e., tuff) is in fractures which are assumed to have no retardation. Retardation in the tuff occurs only after radionuclides diffuse into the matrix but the effect is much smaller compared to the retardation in the alluvium.

Figures 3-16 and 3-17 show the Tc-99 and Np-237 release rates and the Tc-99 dose, by individual subarea and the entire repository. The engineered barrier subsystem release rates for Tc-99 and Np-237 in Figure 3-16(a) and (b) exhibit similar behavior with the subareas having the largest inventory contributing the most to the total release. The number of waste packages in each subarea, which are directly related to the inventory, are 1,455; 1,568; 775; 426; 760; 851; 323; 846; 977; and 896 for Subareas 1–10. Subareas 1 and 2 contain the most waste packages and show the highest release rates, whereas subareas 4 and 7 contain the fewest waste packages and have the lowest release rates.

The plots of the unsaturated zone releases in Figure 3-16(c) indicate that the Tc-99 release rates are essentially the same as the engineered barrier subsystem releases in Figure 3-16(a). Np-237 release rates [Figure 3-16(d)] vary considerably between unsaturated zone release and engineered barrier subsystem release especially in Subareas 1, 3, 4, 5, 6, and 7, which have the Calico Hills nonwelded vitric unit (Figure 3-9) that has relatively high matrix permeability compared with other units. At the infiltration rate corresponding to the mean value data set, only matrix flow can occur in this unit. Flow occurs in the fractures for Subareas 2, 8, 9, and 10 with groundwater traveltimes of approximately 20 years and no retardation. For Subareas 1, 3, 4, 5, 6, and 7, however, the transport of Np-237 is retarded in the matrix and the effects of the time-varying unsaturated zone flow change the Tc-99 and Np-237 release rates. As evident in Figure 3-16(b), (c), and (d), retardation in the matrix produces a greater effect on the Np-237 unsaturated zone release rates than on those radionuclides that are not retarded.

The saturated zone release rates for Tc-99 in Figure 3-16(e) exhibit a delay when compared with the Tc-99 unsaturated zone release rates in Figure 3-16(c). The general characteristics of the engineered barrier and unsaturated zone releases are preserved insofar as the peak releases arising from initially defective failures and corrosion failures are apparent in the plot. The variability by subarea is also consistent for the Tc-99 release rates. There is lower Np-237 release from the saturated zone because of retardation in the saturated zone alluvium.

The groundwater doses for Tc-99 by subarea are shown in Figure 3-17. The characteristics of these dose curves are identical to the corresponding saturated zone release rate curves for Tc-99 in Figure 3-16(e) because the dose is obtained from the release rates using several multipliers. For 100,000 years, the subareas with the largest Tc-99 release rates and doses
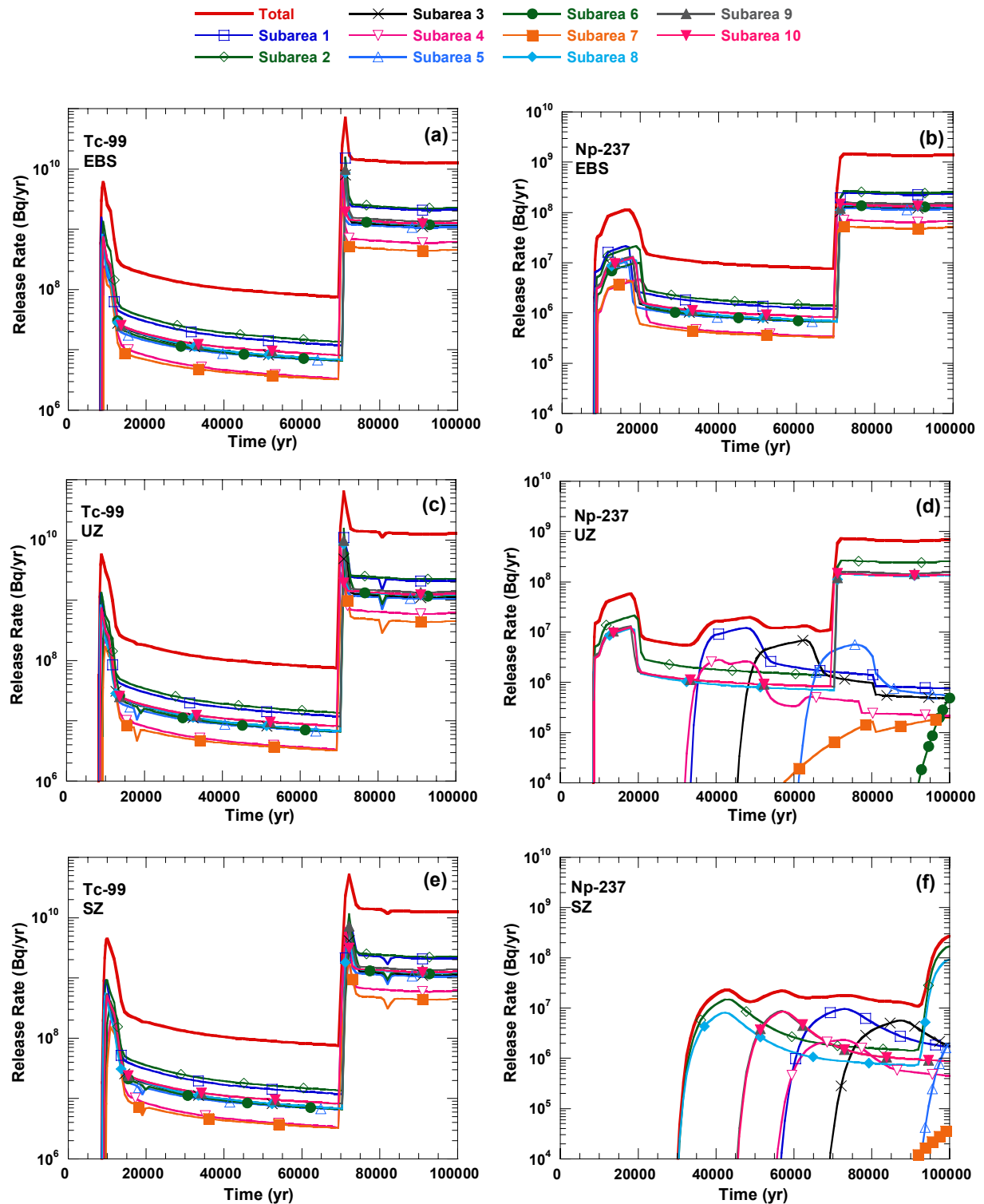
Figure 3-16. Tc-99 and Np-237 Total Releases by Subarea in 100,000 Years from the (a) and (b) Engineered Barrier Subsystem, (c) and (d) Unsaturated Zone, and (e) and (f) Saturated Zone for the Mean Value Data Set

3-41
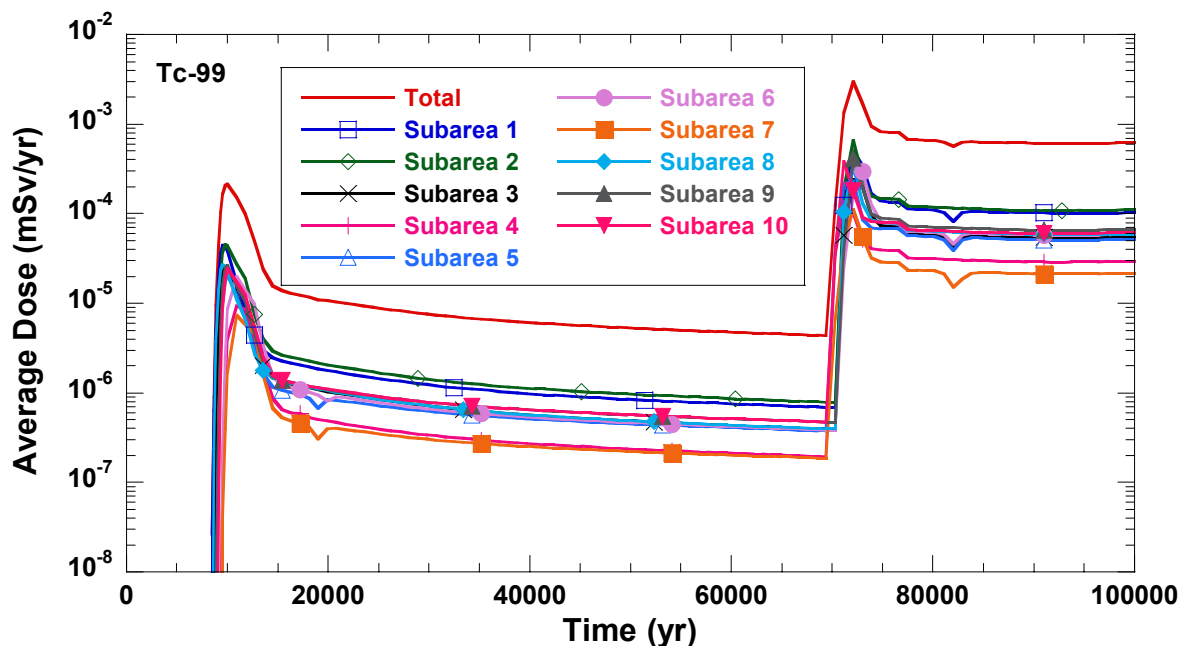
Figure 3-17. Tc-99 Groundwater Doses, Total and by Subarea, in 100,000 Years, for the Mean Value Data Set

(shown in Figure 3-17) contain the greatest amount of spent nuclear fuel (i.e., the subareas listed from the largest to the smallest amount of spent nuclear fuel are Subareas 2, 1, 9, 10, 6, 8, 3, 5, 4, and 7). The saturated zone traveltimes vary by subarea because groups of subareas are connected to different streamtubes. Subareas 1, 2, 3, 4, and 8 are connected to Streamtube 2 and exhibit the shortest saturated zone traveltimes, whereas Subareas 5, 6, and 7 are assigned to Streamtube 1, and Subareas 9 and 10 use Streamtube 3. The longest traveltimes are found in Streamtube 3 (see Table 3-9 for streamtube lengths), which is at the outer edge of the saturated zone pathway. The groundwater doses for all radionuclides by subarea are shown in Figure 3-18. The combined effects of retardation, solubility limit and groundwater traveltime are evident in the variations shown in the figure. The dose history for faulting events and igneous activity[4] for 100,000 years is presented in Figure 3-19. As with the results for the 10,000-year simulation period, the mean value data set results show no faulting events because the mean value of the threshold displacement is greater than the mean value of the credible displacement along a fault. But if a faulting event were to occur (i.e., emulated by making the threshold smaller than the credible displacement), the faulting event would occur at approximately 4,900 years and fail 208 waste packages. Figure 3-19(a) shows the groundwater dose from the faulting event (before probability weighting) is greater than the dose without a faulting event from approximately 10,000 to 18,000 years.

The groundwater dose from igneous activity for the 100,000-year simulation period [shown in Figure 3-19(b)] behaves similarly to the dose from faulting events. As with the results for the

---

[4]These results are presented only to show the process-level trends and must be used in proper context. Because these results are not weighted by appropriate probabilities, the dose values are much larger than they should be when appropriately weighted by the event probability. The annual probability for the faulting event is 5×10^{-6} and for the igneous event is 1×10^{-7} years^{-1}(Mohanty, et al., 2002).
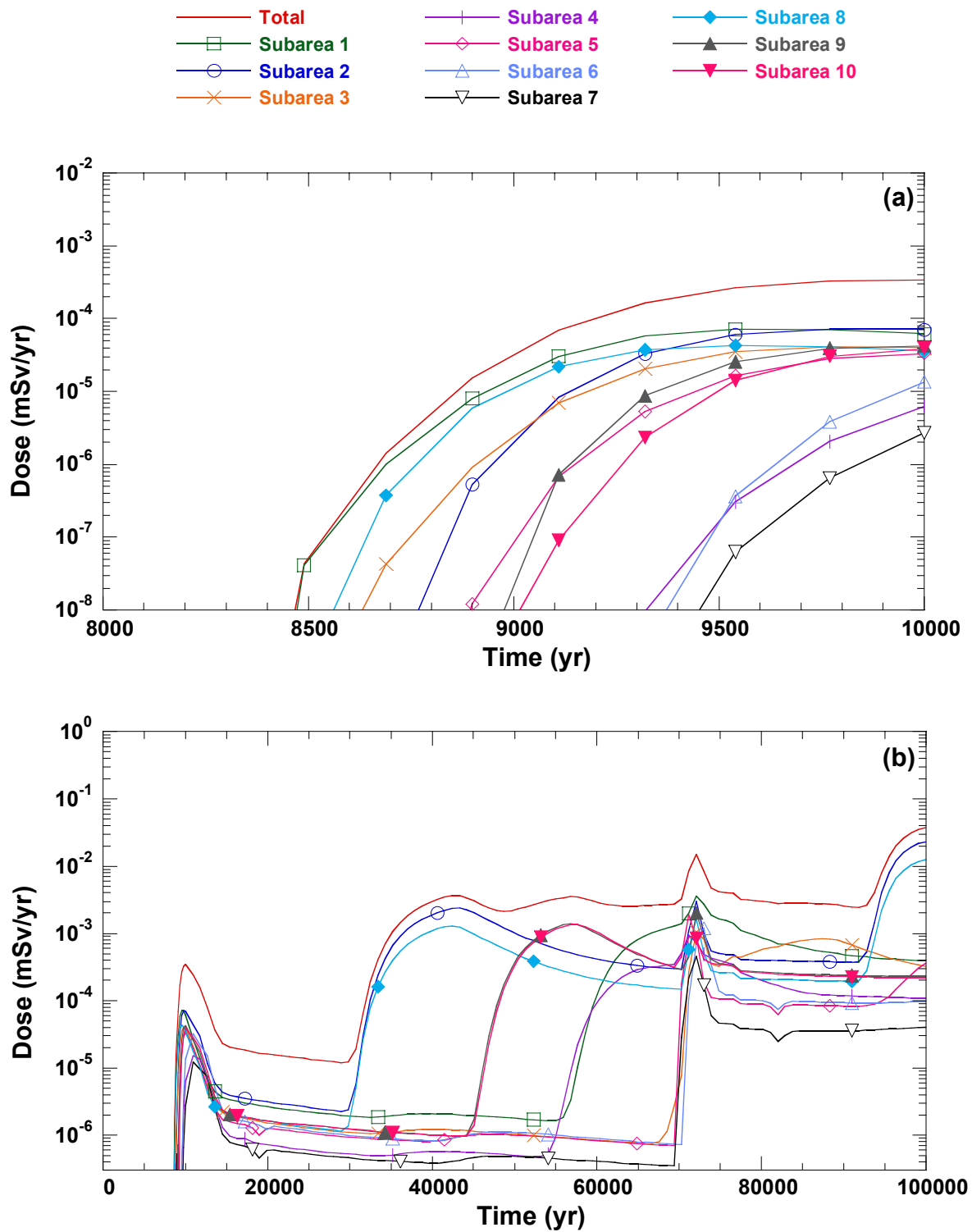
Figure 3-18. Groundwater Dose, Total and by Subarea, in (a) 10,000, and (b) 100,000 Years, for the Mean Value Data Set

3-43

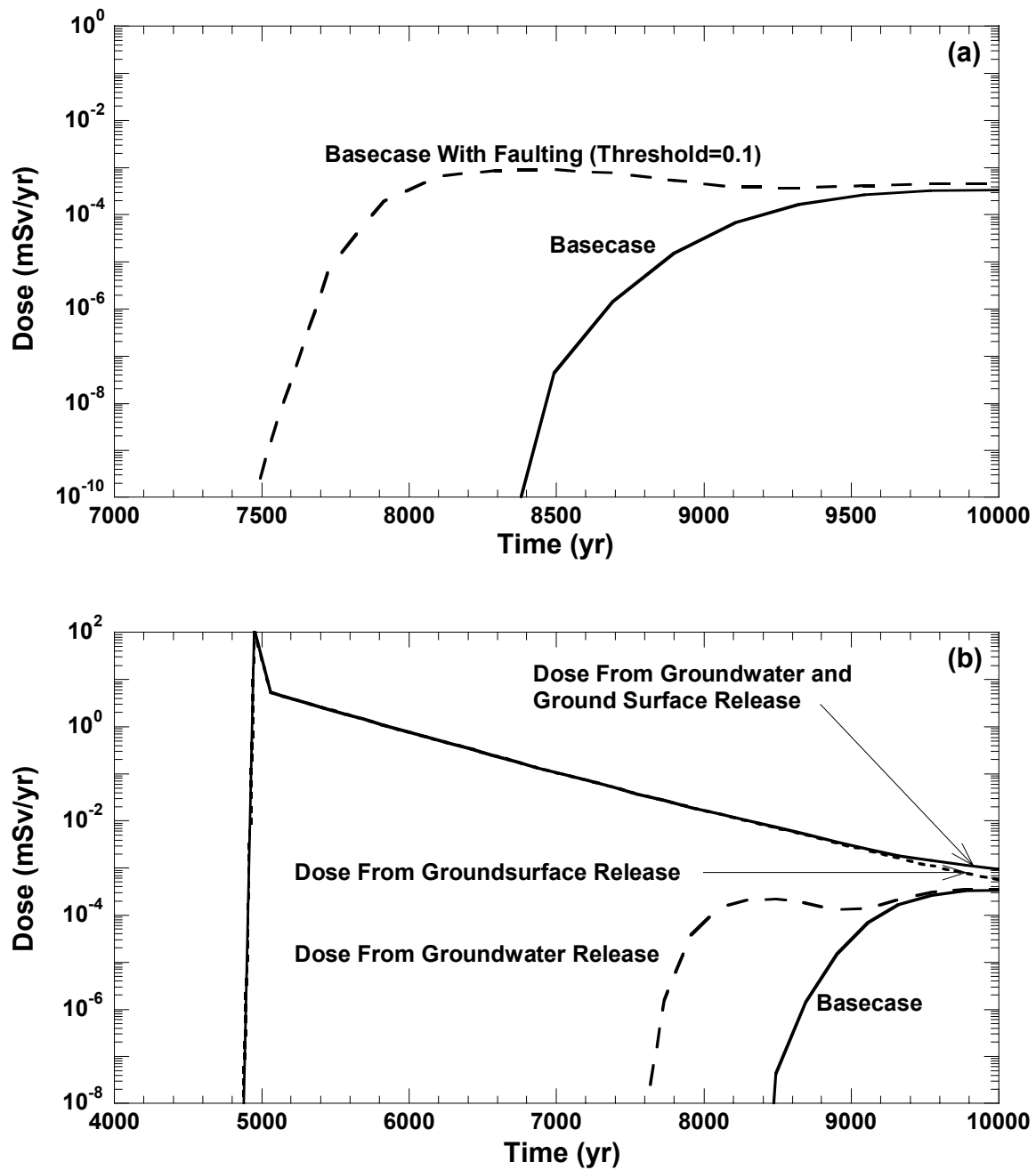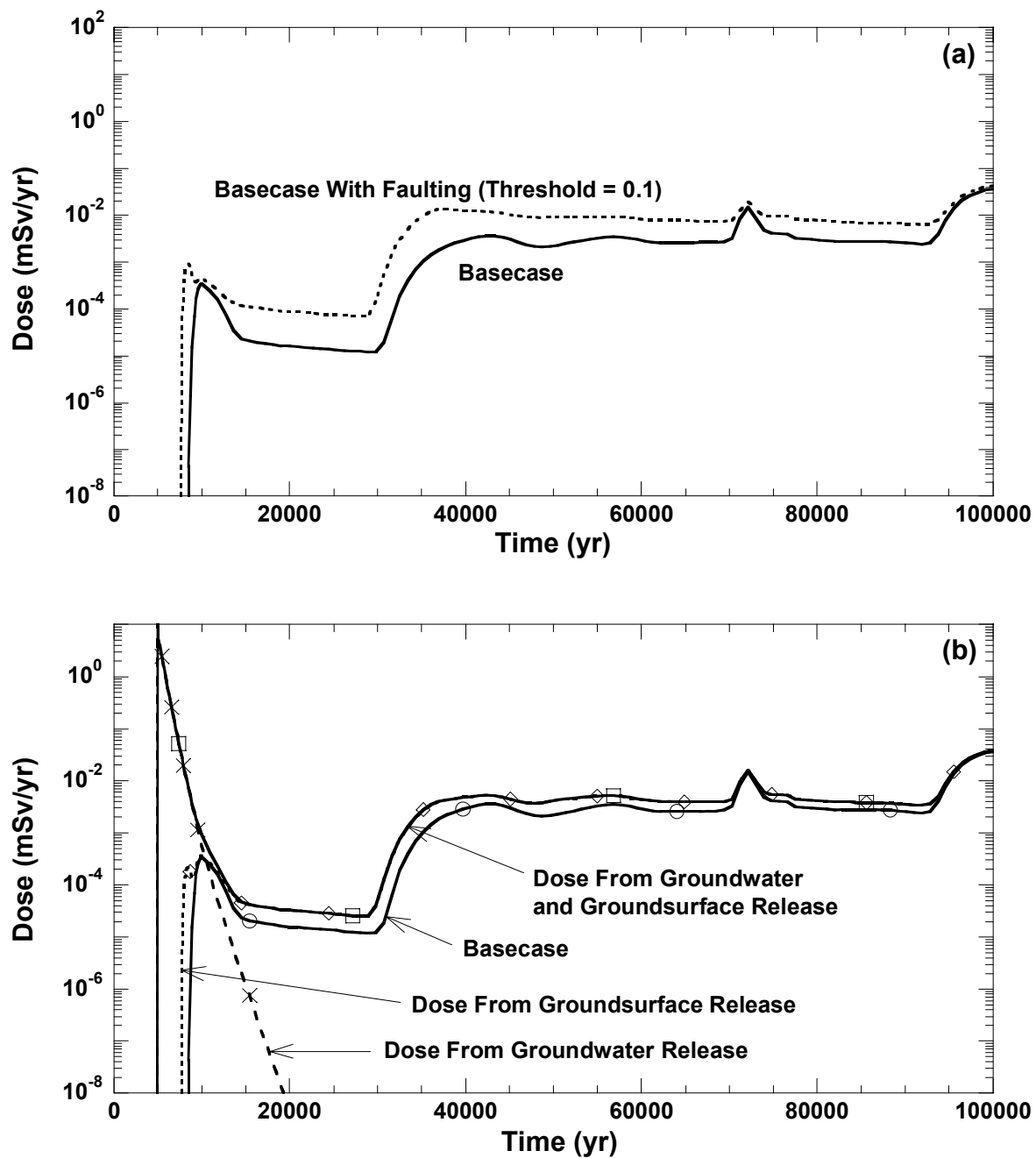**Figure 3-19. Groundwater Dose in 100,000 Years With and Without (a) Faulting and (b) Igneous-Activity Disruptive Events for the Mean Value Data Set, Without Probability Weighting. (The Ground-Surface Dose is Shown for Releases Caused by Extrusive Igneous Activity.)**

10,000-year simulation period, the increase in groundwater dose from igneous activity for 100,000 years is smaller than that for faulting events because only 53 waste packages are failed by the intrusive igneous activity, compared with 208 waste packages failed by the faulting event. Extrusive igneous events also result in a ground-surface dose that peaks at approximately 100 mSv/yr [10,000 mrem/yr] when the volcanic events occur at 4,900 years and exponentially decreases thereafter. At approximately 12,000 years, the groundwater and ground-surface contributions to dose are equal. For the remainder of the 100,000-year period, the igneous activity groundwater doses stay above the basecase (except for a short period corresponding to the corrosion failure at 70,000 years) because of the release from the 53 waste packages that failed from intrusive igneous activity. The doses presented in Figure 3-19 are not probability weighted.

3.3　　　Multiple-Realization Analysis

The performance of the Yucca Mountain repository is evaluated with a probabilistic (i.e., stochastic) approach that averages the results from multiple realizations. This approach uses the probabilistic sampling of input data to compute dose at a receptor location 20 km [12.4 mi] from the repository during 10,000 and 100,000 years. Although the deterministic approach (runs with the mean value data described in the previous section) was presented to illustrate in detail how the behavior of the various components or processes influences other components or dose, the probabilistic analysis provides results that show the variation in the output resulting from the combined effects of the uncertainty and variability in the input data. Also, trends and relationships not evident in the results from the deterministic simulation are revealed in the probabilistic results.

Probabilistic sampling is conducted using Latin Hypercube Sampling (Iman, et al., 1980) for the 350 realizations, which is theoretically large enough to obtain convergence in results while maintaining computational efficiency (see Appendix H for further discussion on convergence). Each realization uses a set of values generated from probability distribution functions specified in the total system performance assessment input file. Probability distribution functions are constructed for the input parameters whose true values are uncertain or vary spatially and temporally. Uncertainty arises from a lack of complete information, whereas variability is the natural or inherent variance in the value of a parameter.

In the basecase data set, of the 950 parameters, 620 are defined as constants, and 330 are defined by probability distribution functions. The basis for assigning a constant value or a probability distribution to the parameter depends on various factors. For example, constant values are assigned to parameters that are either well characterized or have negligible variability. Probability distribution functions are assigned to parameters not well known or where variability has been observed in data. The subject matter experts have provided a valid basis to assign a constant value or a probability distribution function to a parameter though no formal elicitation process was used. Selection of the particular distribution type, such as normal, uniform, or beta, depends on the information available for the parameter and may involve either the best fit of data to a distribution or a reasonable assumption of the distribution type. Specification of a probability distribution function in the TPA Version 4.1 code consists of a distribution type and limits (e.g., uniform with a minimum of 0 and a maximum of 100, or log-triangular, with a minimum of 1.0×10^{-5}, a maximum of 1.0×10^{-1}, and a peak of 1.0×10^{-3}). The limits are set at 0.01^{th} percentile and at the 99.99^{th} percentile for unbounded distributions.

These values are required by the Latin Hypercube Sampling model in the TPA Version 4.1 code. The impact of assuming a particular distribution for a parameter is evaluated in Chapter 5.

When the TPA Version 4.1 code is executed for a realization of the parameters, dose to the receptor is calculated for that realization. The results from all Monte Carlo realizations using Latin Hypercube Sampling are plotted to evaluate the repository performance. For example, dose to the receptor is presented in a scatterplot of peak dose versus time of peak dose, a time history of dose for all realizations, and a complementary cumulative distribution function of peak dose. The expected dose is computed by averaging the doses at each time step from all realizations. The resulting curve is a time-dependent curve that represents the expected dose. The peak expected dose is the largest expected dose obtained from the expected dose curve versus time. For example, groundwater dose from a single realization using the mean value data set is shown in Figure 3-18 (total dose curve), and the expected dose from multiple realizations is presented in Figure 3-20, which also shows the dose from individual realizations. Peak dose obtained from the expected dose curve is shown in Figure 3-20. Additionally, the relationship between dose and intermediate results, such as waste package failure time, flow of water into a waste package, and radionuclide release rates, is presented for all realizations.

3.3.1   Unsaturated Zone Flow

The variation in the mean, minimum, and maximum infiltration rates is illustrated in Figure 3-21. For the mean infiltration rates, a present-day climate exists from 0 to approximately 13,000 years, and 87,000 to 100,000 years, with the pluvial climate occurring between 13,000 and 87,000 years. Figure 3-21 shows that the infiltration rate ranges between 4 and 30 mm/yr [0.16 and 1.2 in/yr] in the first 10,000 years, with the infiltration rate steadily rising from 0th year to $10,000^{th}$ year. The average infiltration is 8 mm/yr [0.31 in/yr] at the 0th year and doubles in the first 10,000 years. The peak infiltration rate ranges approximately two orders of magnitude {4–96 mm/yr [0.16–3.8 in/yr]} in the 100,000-year simulation period. This range is related to the total system performance assessment input parameter for the present-day areal average mean infiltration rate, which has a uniform distribution from 4 to 13 mm/yr [0.158 to 0.512 in/yr].

As shown earlier using the mean value data set, subarea 1 exhibits the largest infiltration rates (see Figure 3-2) because of higher infiltration at the ground surface above Subarea 1, which is attributable to near-surface processes such as elevation and soil depth. Subareas 4, 6, and 7, however, have the lowest infiltration rates. In any single realization, the subarea-to-subarea variability in infiltration rates is substantial. The largest subarea-to-subarea variation observed in 10,000 and 100,000 years are 0.040 m^3/yr and 0.134 m^3/yr [1.42 ft^3/yr and 4.73 ft^3/yr]. The minimum and maximum pluvial infiltration rates, which occur between approximately 13,000 and 87,000 years, vary from approximately 10 to 85 mm/yr [0.394 to 3.35 in/yr] for all realizations and subareas.

3.3.2   Near-Field Environment

The time history of average waste package temperature for each subarea is shown in Figure 3-22(a). The subarea-to-subarea variability in the waste package temperature from 0 to 400 years and from 10,000 to 100,000 years is less than 10 °C [50 °F]. The subarea-to-subarea variability in the waste package temperature in the 400- to 10,000-year time period is greater than 10 °C [50 °F] with a maximum temperature difference of 20 °C [68 °F] at 1,600 years. This period corresponds to the greatest amount of heat generated from the radioactive decay of
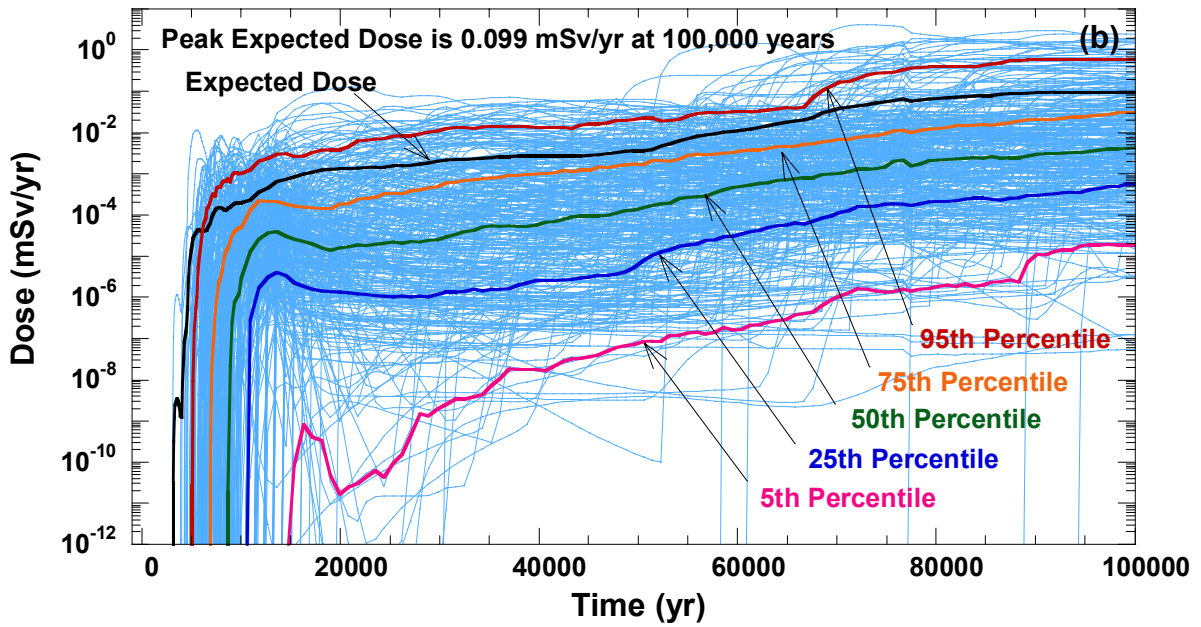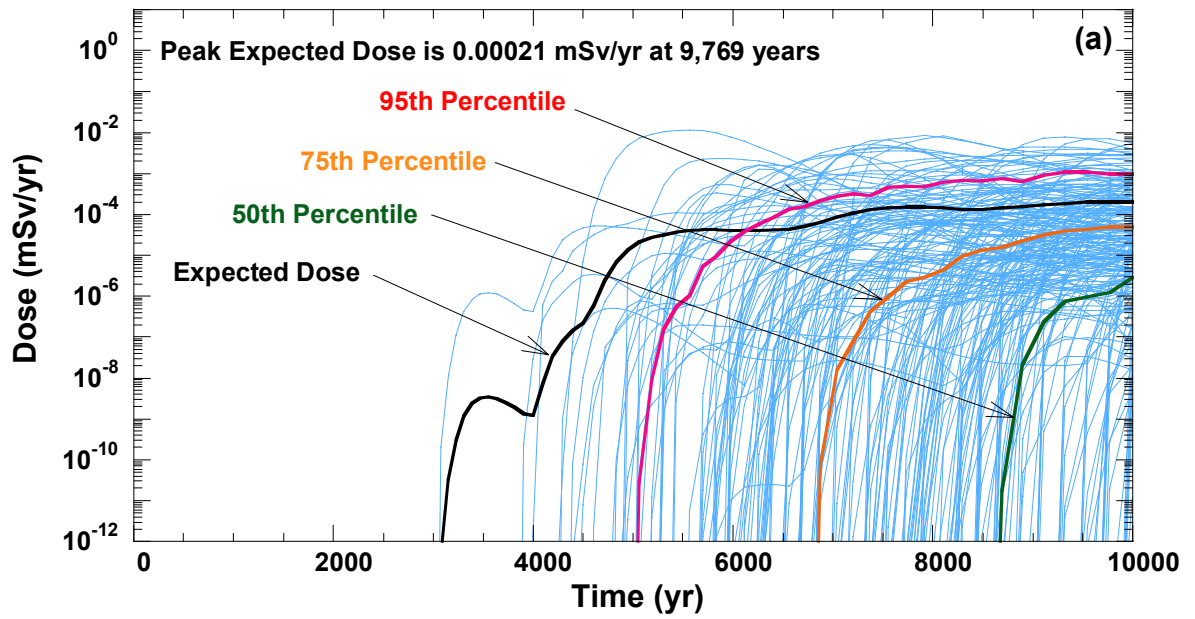
Figure 3-20. Groundwater Dose in (a) 10,000 and (b) 100,000 Years, Including the
Average Dose for 350 Realizations
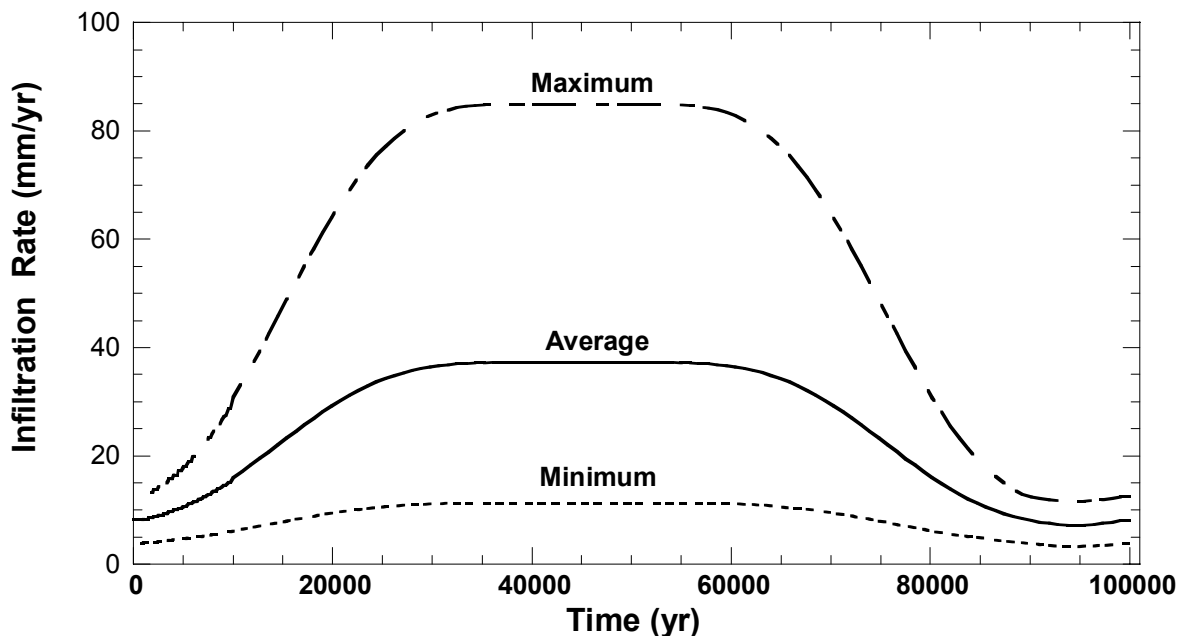
Figure 3-21. Mean, Maximum, and Minimum Infiltration Rates in the Unsaturated Zone for All Subareas. (The Subarea Average Infiltration Rate is Obtained by Averaging Over All 350 Realizations.)

spent nuclear fuel. Note that the subarea-to-subarea variability in temperature shown here may not be fully reflective of the edge effect (i.e., heat losses at the periphery of the subarea) because of the limited number of subareas used and the temperature is estimated only at the center of each subarea.

Figure 3-22(b) shows the average, minimum, and maximum waste package temperatures for Subarea 1. The range between the minimum and maximum temperatures is approximately 20 °C [68 °F] for the time period of 100–1,000 years. Subareas 2–10 exhibit the same general variability in the average, minimum, and maximum waste package temperatures as Subarea 1. The largest minimum to maximum difference within a subarea for all 350 realizations is 25 °C [77 °F] for all subareas, and this difference occurs around 90 years. These large differences indicate the parameters sampled in the basecase data set (e.g., thermal conductivity of the rock surrounding the repository) have an influence on the range of computed waste package temperatures. This difference could affect the spent nuclear fuel dissolution and corrosion calculations because the corrosion rate is sensitive to the waste package temperature especially if localized corrosion is a possibility.

3.3.3   Waste Package Degradation

Figure 3-23 presents results from all realizations and the expected failure curve of waste packages failed by corrosion. The time of waste package failure by corrosion ranges from approximately 37,900 to beyond 100,000 years, with an average corrosion failure time for 350 realizations of approximately 68,000 years. For the computation of the average waste

3-48
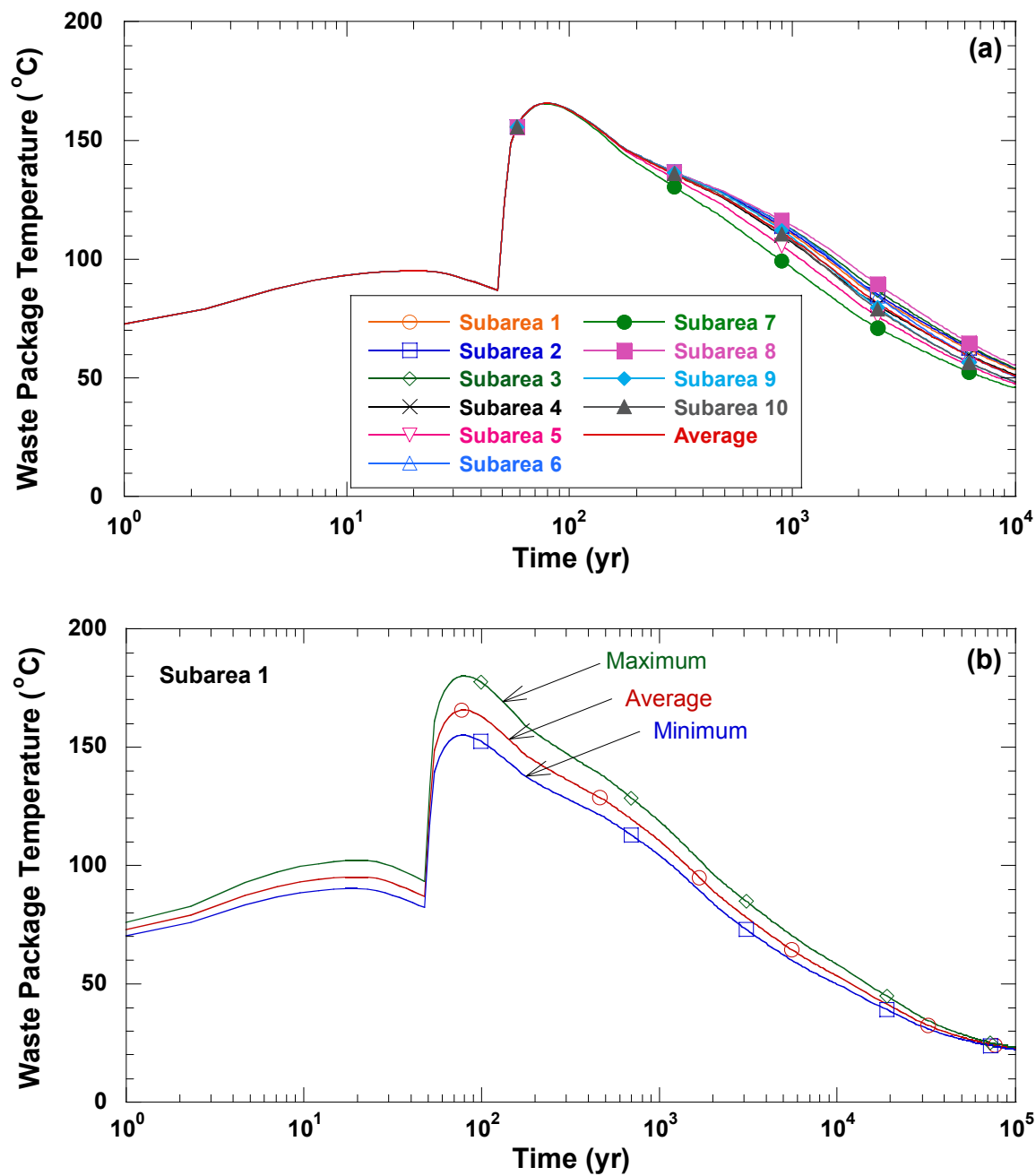
Figure 3-22. Waste Package Surface Temperature: (a) Averaged over the Repository and for Each Subarea; and (b) in Subarea 1, the Average, Minimum, and Maximum Values, for 350 Realizations
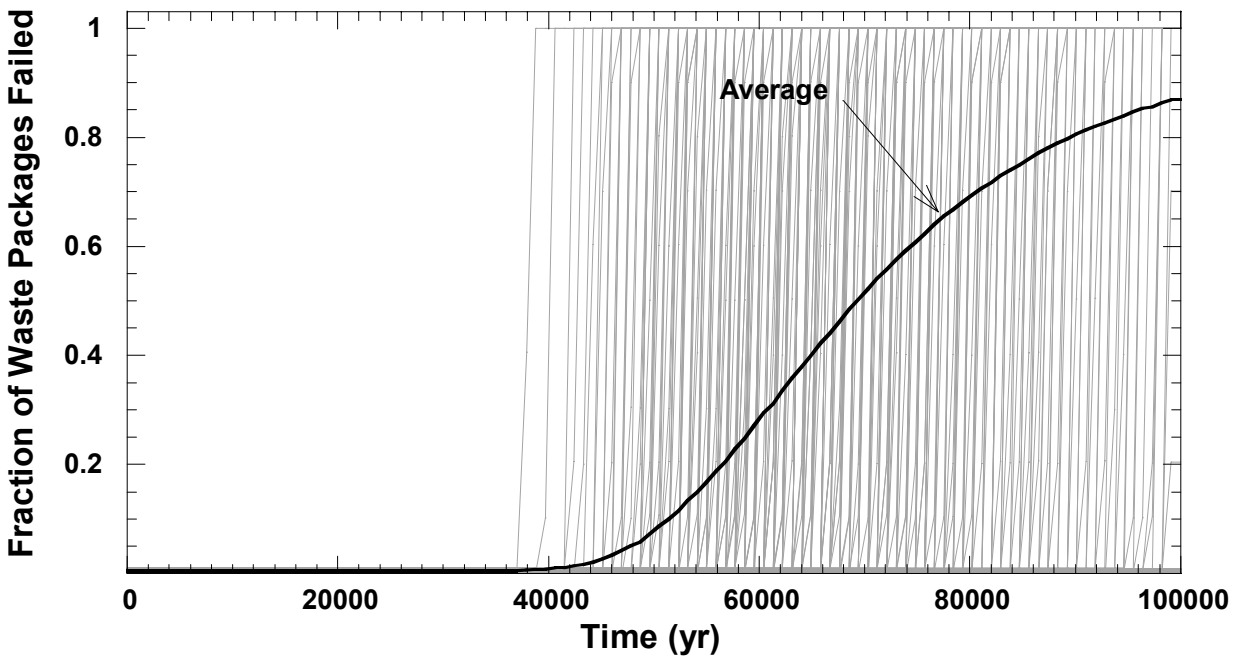
Figure 3-23. Fraction of Waste Packages Failed by Corrosion for Each of the 350 Realizations, and the Average Fraction of Failed Waste Packages

package failure time, it is assumed that all waste packages lasting longer than 100,000 years also failed at 100,000 years. Based on the models used and the assumption made in the TPA 4.1 code, even with 4,000 realizations, the earliest failure time is 37,900. It should be noted that effects of failure at welds and closures, which could substantially decrease waste package failure time, have not been considered in this calculation.

Note that not all waste packages fail from corrosion in 100,000 years. When the waste package failure time is delayed, more of the spent fuel inventory decays, and the transport time through the unsaturated zone and saturated zone is delayed. Thus, the peak groundwater dose is generally expected to be lower for a longer waste package life. In most instances, the peak groundwater dose occurs after the average waste package failure time for the 100,000-year analyses. For 27 percent (95 out of 350) of the realizations, however, the peak groundwater dose occurs at times equal to or greater than 100,000 years. Because the waste package does not fail until 37,900 years, no groundwater peak dose corresponding to the corrosion failure of waste package is observed in 10,000 years.

3.3.4   Radionuclide Release

Water transports radionuclides out of the waste package and into the unsaturated and saturated zones to the receptor location. The release from the engineered barrier subsystem should be positively correlated with the flow rate of water in the unsaturated zone above the repository. Higher flow rates into the waste package lead to early release from the bathtub formed in the waste package and promotes dissolution-limited release. Higher release rates contribute to greater peak groundwater doses, as shown in Figure 3-24, for Tc-99 and Np-237, in Subarea 1.
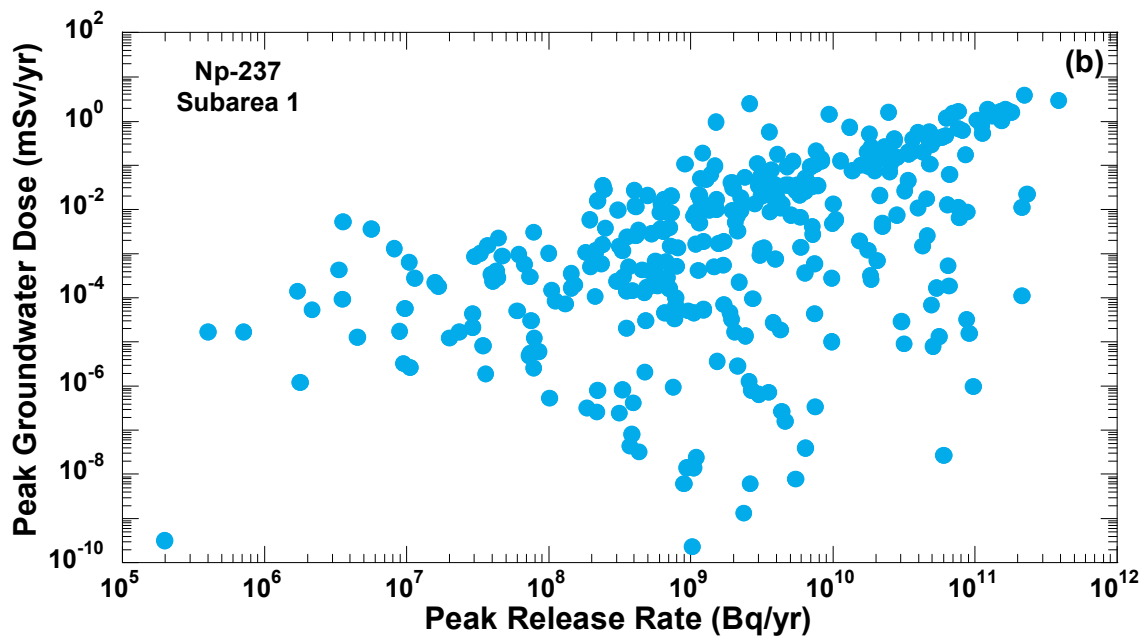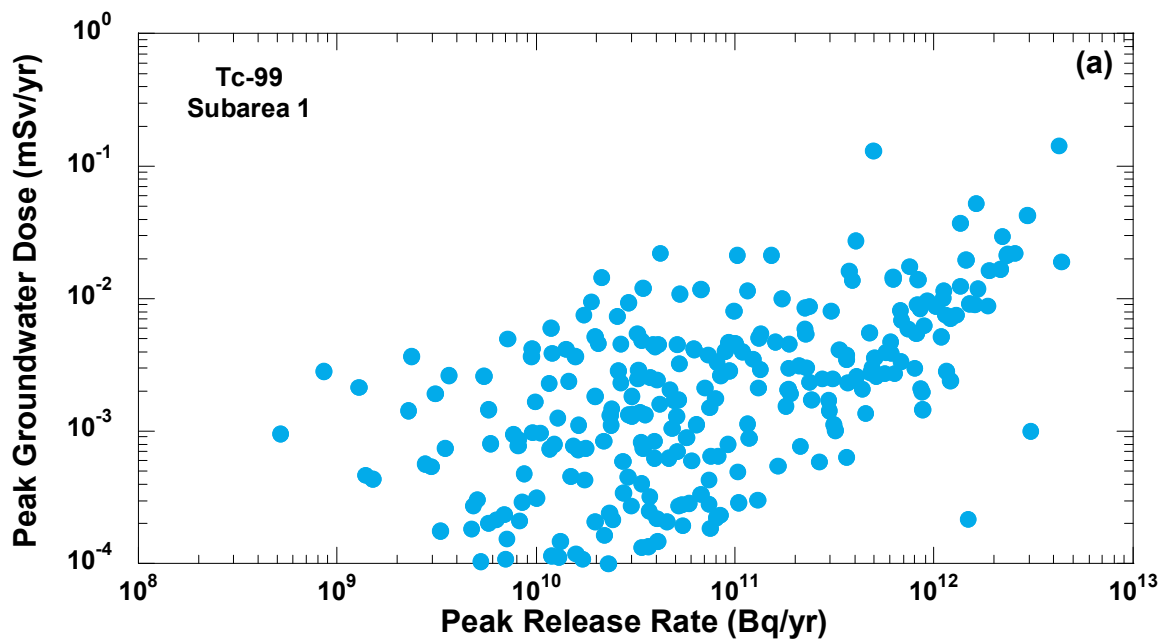
Figure 3-24. Peak Groundwater Dose and the (a) Tc-99 and (b) Np-237, Peak Release Rates from Subarea 1, for 350 Realizations

The Subarea 1 release rates presented in these figures are representative of release rates from Subareas 2–10. Factors that influence the radionuclide transport from the engineered barrier subsystem to the receptor location, such as retardation, cause greater variability in the groundwater dose than the release rate from the engineered barrier system.

Figure 3-25 shows the release rate of Tc-99 from Subarea 1 for 10,000 and 100,000 years. The figure shows a large variability in the engineered barrier subsystem release rates. The peak release rates corresponding to initially defective failure at the 0th year are spread from 3,700 to 32,000 years and beyond, and the peaks corresponding to the corrosion failure are spread from 41,000 to 100,000 years. The variability can be attributed to factors such as lower flow rates at times less than 40,000 years, retardation of radionuclides, time of waste package failure, and time to fill the waste package. The variability in the magnitude of the releases extends more than six orders of magnitude.

The cumulative release of radionuclides from the engineered barrier subsystem as a function of time is plotted in Figure 3-26 along with the initial inventory, the unsaturated and saturated zone releases, and the expected failure curve of waste packages failed from corrosion with its own axis displayed at the right-hand axis. This graph shows a sharp rise in the activity level at less than 5,000 years, which corresponds to the initially defective failure. An increase in activity level after 45,000 years is caused by the waste packages failing from corrosion. Radionuclides with a combination of higher solubility, half-life, initial inventory and gap fraction (e.g., Tc-99) contribute to the largest release rates. The figure shows approximately 1.11×10^{13} Bq [300 Ci] of radionuclides have been released in 10,000 years at the engineered barrier subsystem, of which approximately 5.9×10^{12} Bq [160 Ci] have been released from the saturated zone (which is 5×10^{-5} percent of the initial inventory). The figure also shows that at the end of 100,000 years, 1.33×10^{15} Bq [36,000 Ci] have been released from the saturated zone, which is 0.01 percent of the initial inventory and 1.25 percent of the 100,000-year no-release inventory. No-release inventory is the remaining inventory at any given time up to which decay and ingrowth take place but no releases occur.

3.3.5 Unsaturated Zone Transport

Figure 3-27 presents the Tc-99, Np-237, and Pu-239 average release rates and the expected failure curve of waste packages failed from corrosion for the basecase data set. In the first 37,900 years, releases result from initial waste package failures. The failure of waste packages from corrosion begins at approximately 37,900 years, and a corresponding increase in the release rates is evident in Figure 3-27, after 40,000 years, with the peak average release rate for 350 realizations occurring at approximately 80,000 years.

The results in Figure 3-26 indicate that the simulated unsaturated zone releases are only slightly less than the engineered barrier subsystem releases. Such a small difference between the two curves suggests the effects of the hydrostratigraphic units beneath the repository on the radionuclide release rates are not significant. Although there is substantial hold-up of radionuclides (~ 50 percent of the inventory) in the subareas where the Calico Hills vitric layer is present, still a large fraction of the release to the saturated zone comes from the subareas where the unit is thin or missing.
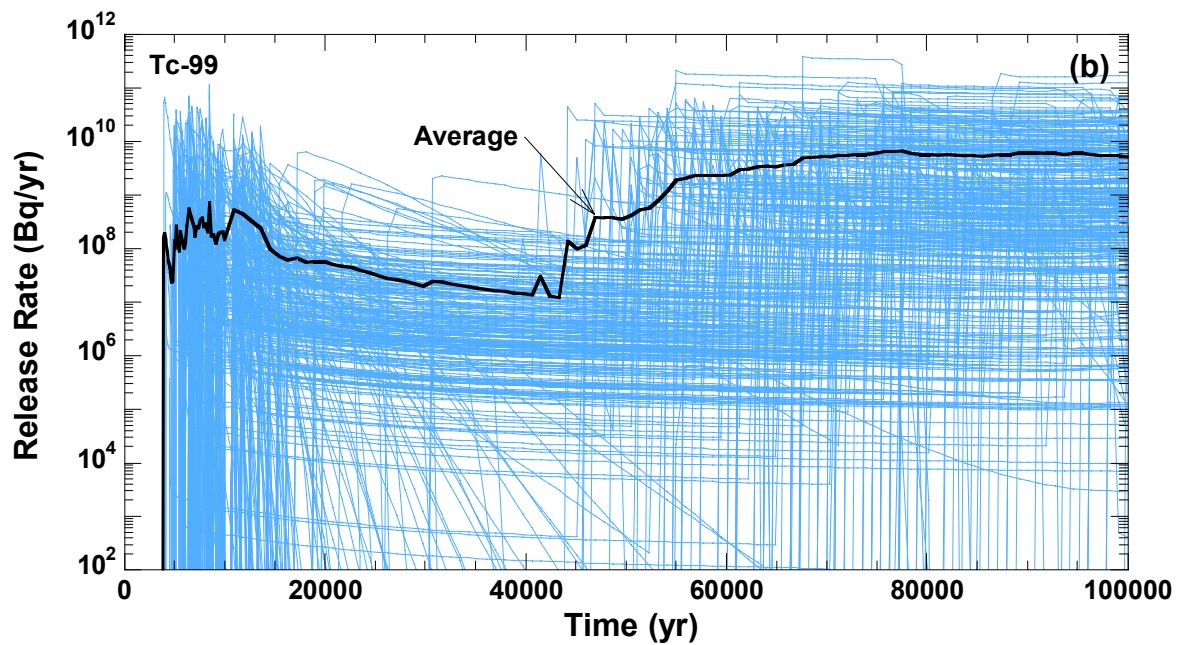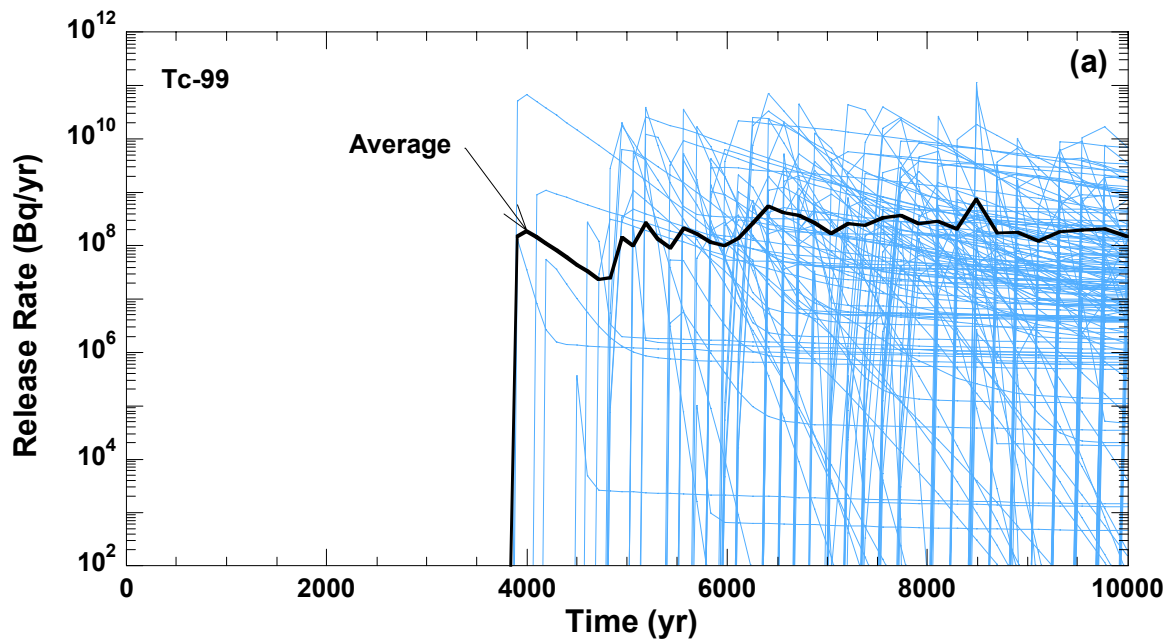
Figure 3-25. TC-99 Release Rates from the Engineered Barrier Subsystem Over (a) 10,000 and (b) 100,000 Years, Including the Average Release Rate, in Subarea 1, for 350 Realizations
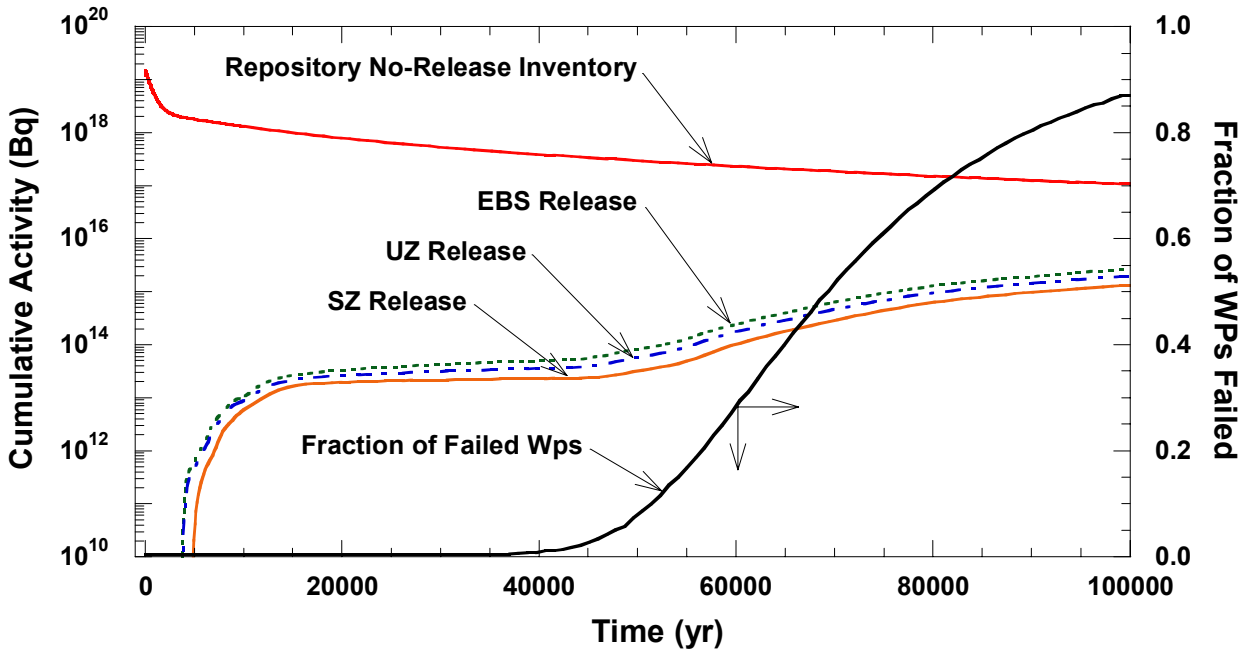
Figure 3-26. Cumulative Releases from the Engineered Barrier Subsystem, the Unsaturated Zone, and the Saturated Zone Together with the Initial Inventory in the Repository
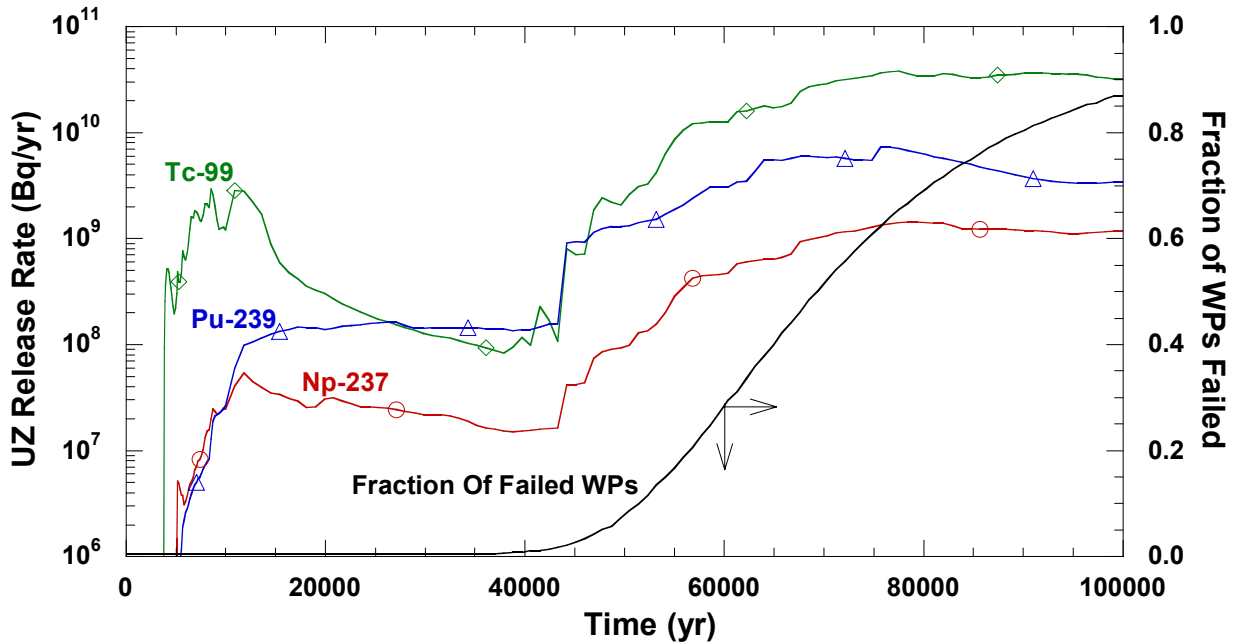
Figure 3-27. Unsaturated Zone Average Release Rates of Tc-99, Np-237, and Pu-239, for 350 Realizations

Figure 3-28 shows the Tc-99 release rate from the unsaturated zone from Subarea 1 over 10,000 and 100,000 years. Figure 3-29 is a composite plot of the average engineered barrier subsystem, unsaturated zone and saturated zone release and shows that the average release rate versus time curve for Tc-99 for the unsaturated zone does not significantly lag behind the release rate curve for the engineered barrier subsystem. As with the engineered barrier subsystem, releases from the unsaturated zone before 40,000 years are from initially failed waste packages, whereas the peak releases observed after 40,000 years result mainly from corrosion failures. The magnitude of the releases extends six to seven orders of magnitude and arises partly from the variability in the flow rate, retardation in the unsaturated zone, and matrix versus fracture flow.

The inference that the unsaturated zone reduces by only a small amount the engineered barrier subsystem release rates is further supported by Figure 3-30, which shows the complementary cumulative distribution function of the unsaturated zone traveltimes.
The average unsaturated zone traveltime is approximately 282 years with a range of 150–800 years. Subareas 2, 8, 9, and 10 exhibit the fastest groundwater traveltimes with averages varying from 12 to 27 years. The remaining subareas (1, 3, 4, 5, 6,and 7) exhibit average groundwater traveltime from 245 to 769 years. Differences in the traveltimes arise mainly from the presence of the Calico Hills vitric layer.

3.3.6   Saturated Zone Flow and Transport

Average release rates from the saturated zone are presented in Figure 3-31 for Tc-99, Np-237, and Pu-239. The Tc-99, Np-237, and Pu-239 unsaturated zone and saturated zone release rates can be significantly different because of the flow path length and retardation in the saturated zone alluvium. The path length in the saturated zone alluvium ranges from 134 to 12,000 m [440 to 39,400 ft], whereas the unsaturated zone path length is approximately 350 m [984 ft]. The average retardation factors for Tc-99, Np-237, and Pu-239 are 1; 137; and 14,900 in the unsaturated zone matrix and 1; 62; and 13,000 in the saturated zone alluvium where saturated zone retardation occurs. Consequently, the longer flow path, combined with greater retardation, has a larger effect on the saturated zone release rates than on the unsaturated zone release rates. These effects can be seen in the unsaturated zone and saturated zone release rates plotted in Figures 3-27 and 3-31. Compared with the releases from the unsaturated zone, Tc-99 and Np-237 releases are smaller from the saturated zone and, because of a larger retardation factor, Pu-239 is released from the saturated zone in 100,000 years.

Figure 3-32 shows the saturated zone release rates from 350 realizations and the average of these realizations for Tc-99 in Subarea 1. The effect of the flow path length on the Tc-99 saturated zone release rates for Subarea 1, from 10,000 and 100,000 years, is evident when comparing the saturated zone release rates with the unsaturated zone release rates in Figure 3-29. Because Tc-99 is specified as nonsorbing, and the flow is essentially quasi steady state, the difference in release rates is primarily a function of groundwater traveltime.
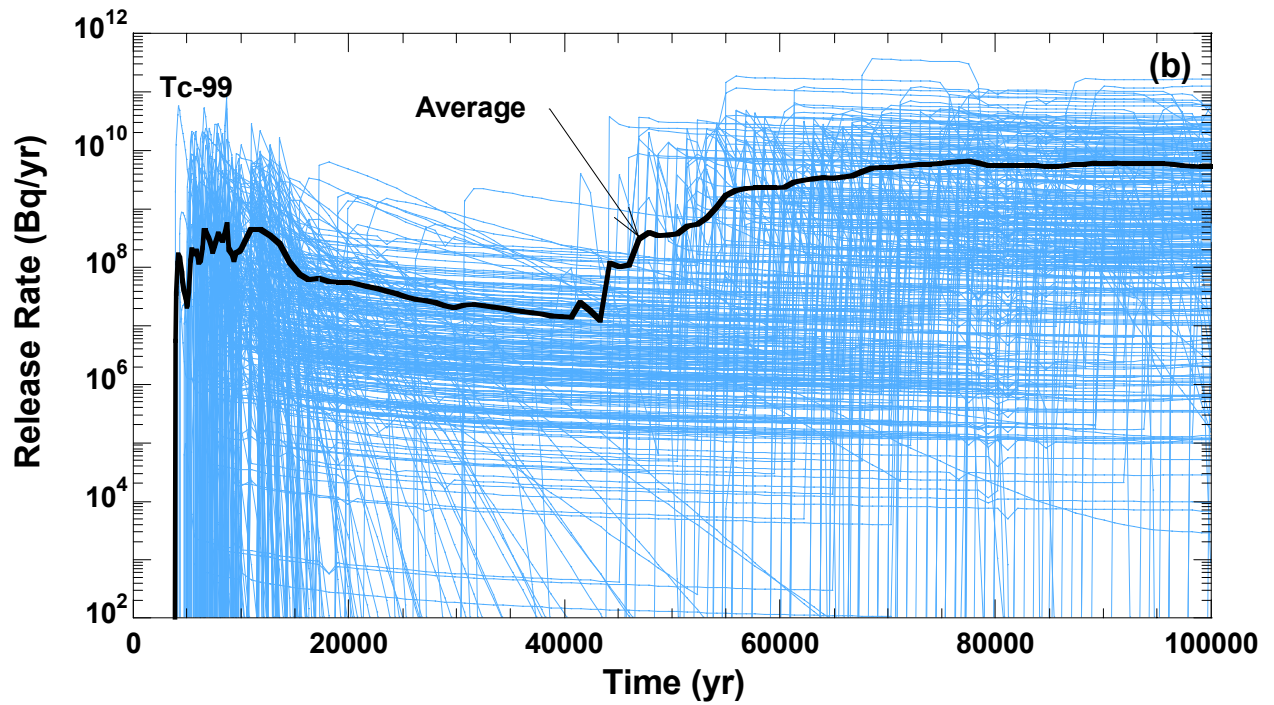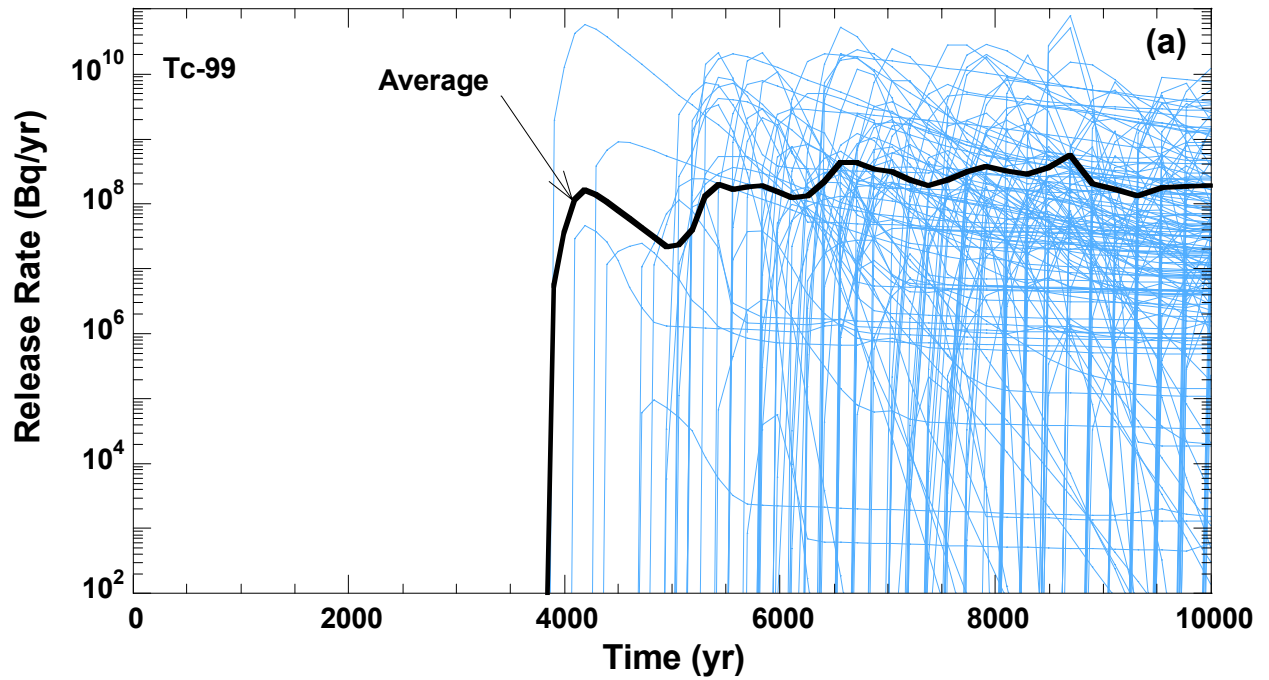
Figure 3-28. Unsaturated Zone Release Rates of Tc-99 Over (a) 10,000 and (b) 100,000 Years, Including the Average Release Rate, in Subarea 1, for 350 Realizations
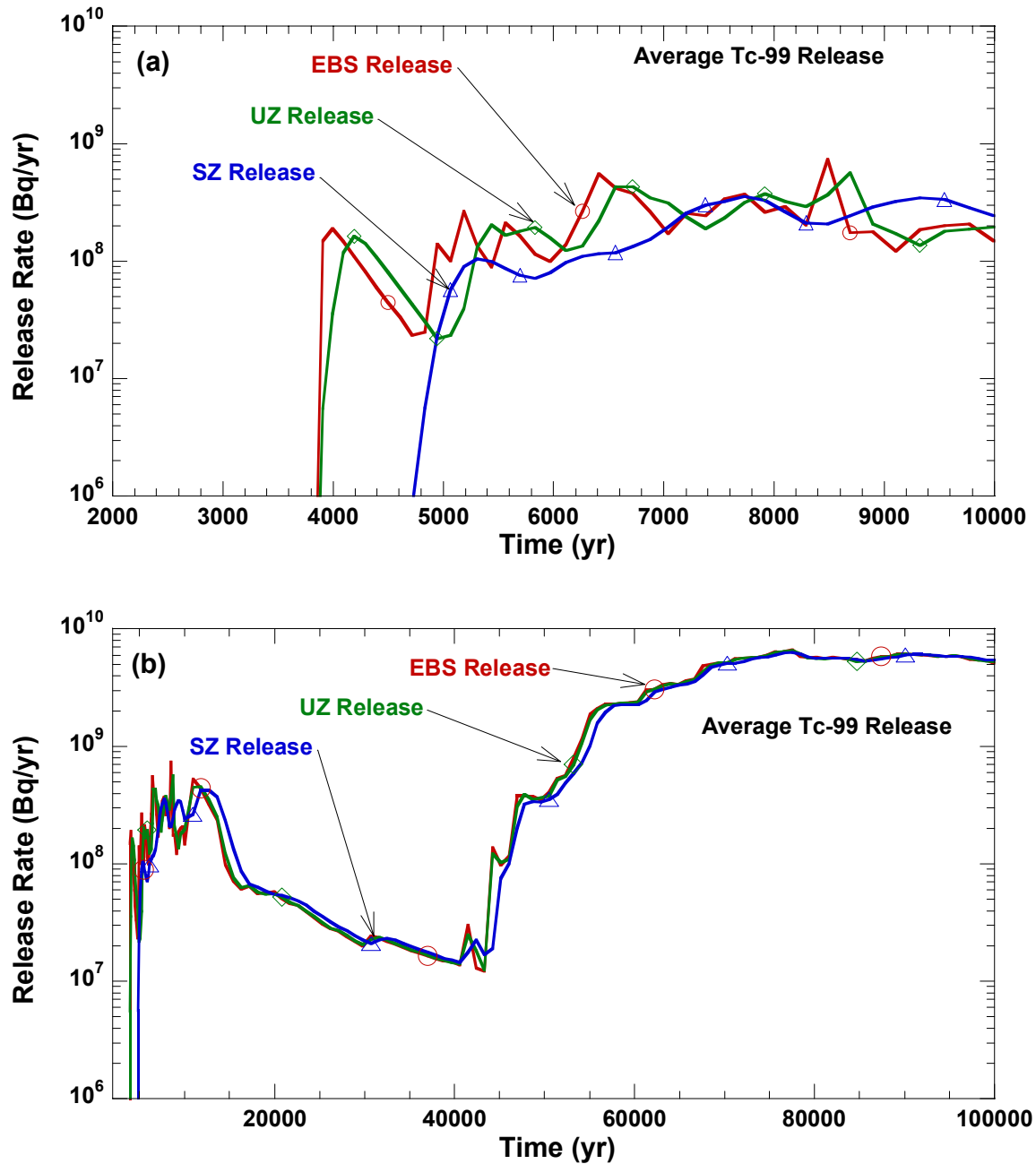
Figure 3-29. Tc-99 Average Release Rate from the Engineered Barrier Subsystem, the Unsaturated Zone and the Saturated Zone over (a) 10,000 and (b) 100,000 Years in Subarea 1 for 350 Realizations
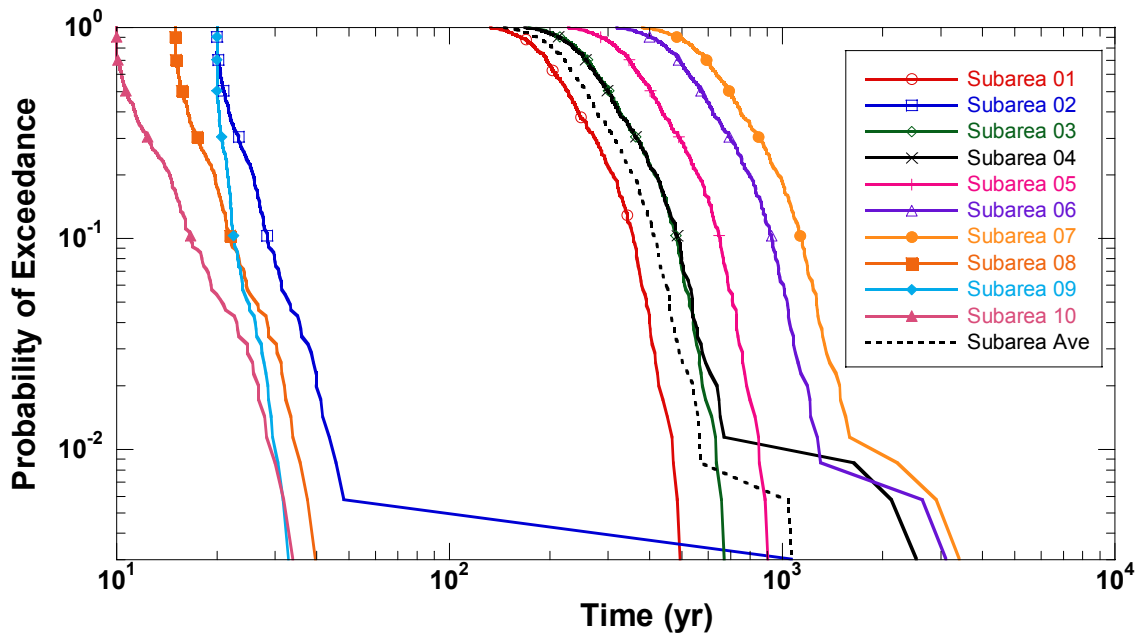
Figure 3-30. Complementary Cumulative Distribution Function of Unsaturated Zone Groundwater Travel Times for 350 Realizations
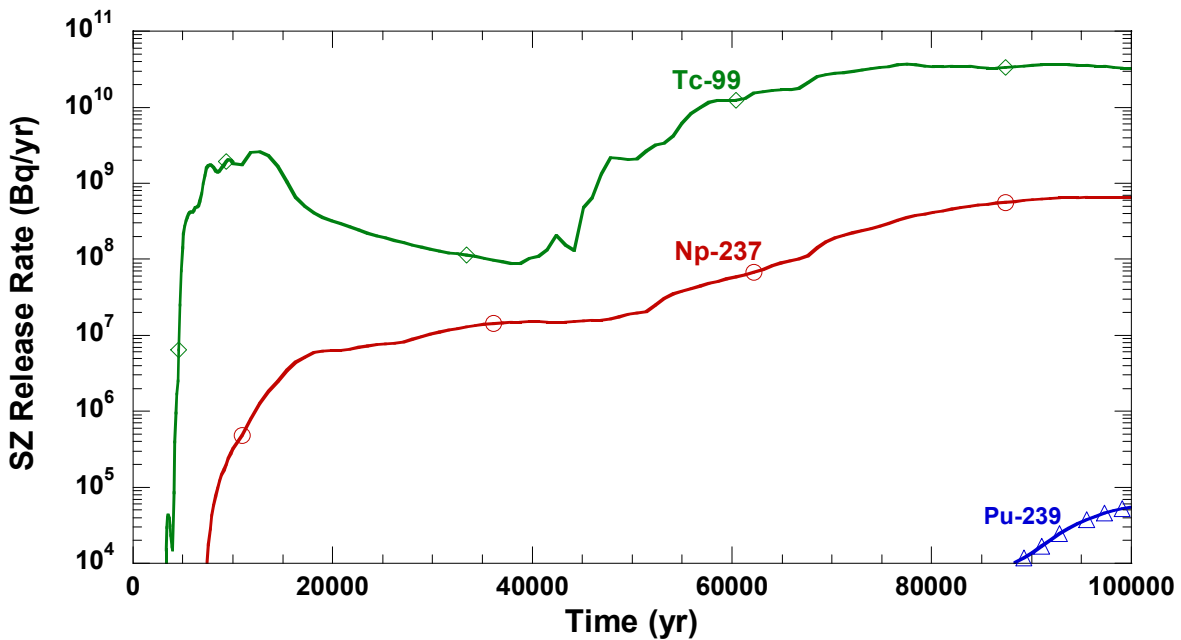
Figure 3-31. Saturated Zone Average Release Rates of Tc-99, Np-237, and Pu-239, for 350 Realizations
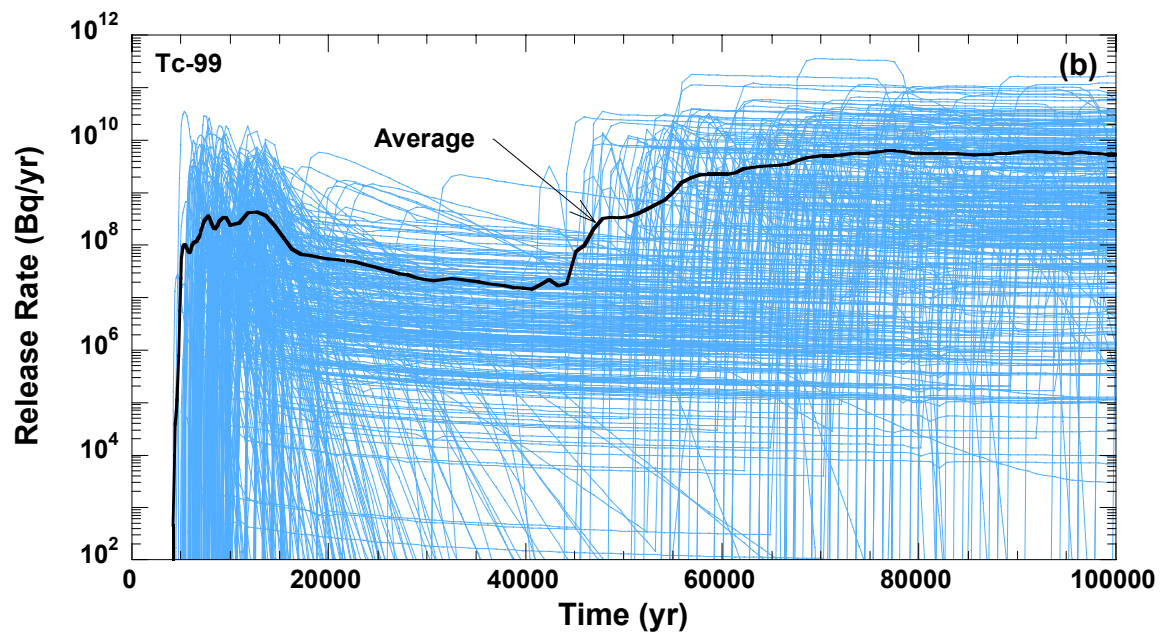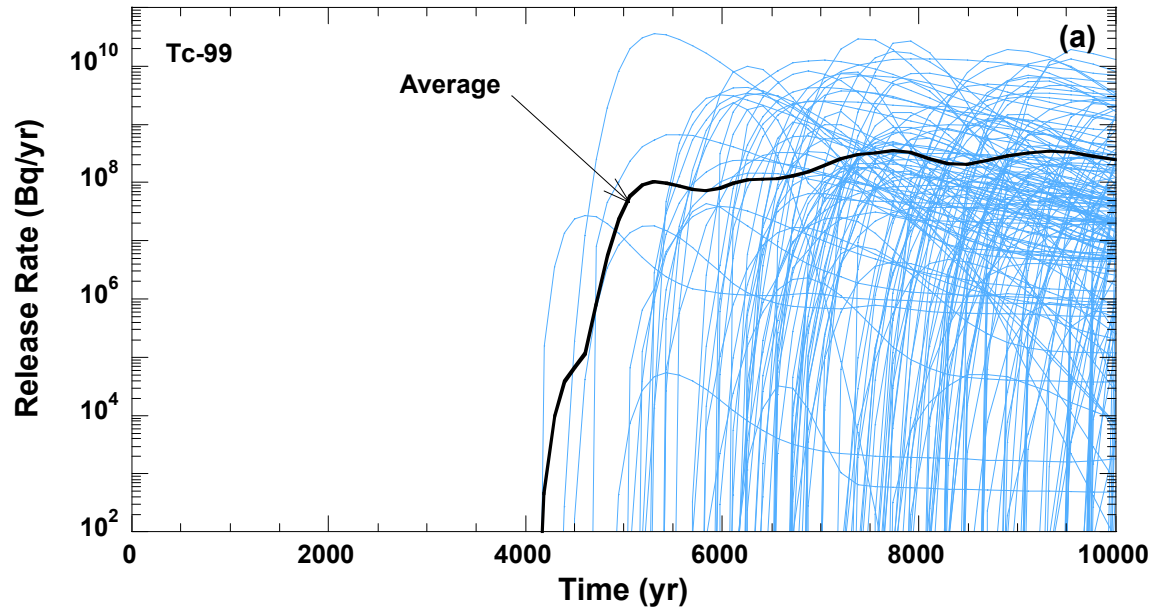
Figure 3-32. Saturated Zone Release Rates of Tc-99 Over (a) 10,000 and (b) 100,000 Years, Including the Average Release Rate, in Subarea 1, for 350 Realizations

The complementary cumulative distribution function of the saturated zone average groundwater traveltimes for all 350 realizations and for each subarea is presented in Figure 3-33. The groundwater traveltime in the saturated zone ranges between 57 and 1,790 years, with an average of 640 years (see Figure 3-33), compared with the approximately 280-year average groundwater traveltime for the unsaturated zone (see Figure 3-30). The streamtube connections given in Table 3-9 are clearly evident in Figure 3-33 because the subarea groundwater traveltime falls into three distinct groups corresponding to the saturated zone streamtubes. Variation in groundwater traveltime among subareas connected to the same streamtube are because of the subarea location in the repository footprint; the subareas located further west have the longest traveltime. The subarea-to-subarea variation in the minimum traveltimes ranges between 57 to 80 years, whereas the maximum traveltimes range between 1,234 and 1,790 years. Table 3-12 provides a summary of the average (of all realizations), minimum, and maximum saturated zone groundwater traveltimes for the repository and for each subarea. The average for each subarea is obtained using equal weighting of groundwater traveltimes from each realization. Similarly, the repository average (from all subareas and realizations) is the mean of subarea averages. The subarea-to-subarea variability in the average (from 350 realizations) saturated zone traveltimes is approximately three times less than for the unsaturated zone. The realization-to-realization variation in the repository averaged saturated zone groundwater traveltimes ranges between 580 to 820 years; for the unsaturated zone, the range is 12 to 770 years.

3.4　　　　Dose to the Receptor Group from Multiple Realization Set

The peak expected dose for the multiple realization case for the 10,000-year simulation period is 2.1×10^{-4} mSv/yr [0.021 mrem/yr]. For the 100,000-year simulation period, the peak expected dose is 9.9×10^{-2} mSv/yr [9.9 mrem/yr]. Table 3-13 provides the primary radionuclides contributing to peak expected dose for the 10,000- and 100,000-year simulation periods. The main contributors to the dose for both simulation periods are Np-237, I-129, and Tc99. Np-237 is the third largest contributor at 10,000 years but becomes the dominant contributor at the 100,000-year simulation period.

The variability in dose among all 350 realizations is shown in Figure 3-20, for 10,000 and 100,000 years, together with the average dose and the 5th, 25th, 50th, 75th, and 95th percentiles. The minimum and maximum peak doses vary from no release {i.e., $< 1.0 \times 10^{-22}$ mSv/yr [1.0×10^{-20} mrem/yr]} to 1.15×10^{-2} mSv/yr [1.15 mrem/yr], for 10,000 years, and 2.9×10^{-6} mSv/yr [2.9×10^{-4} mrem/yr] to 4.10 mSv/yr [410 mrem/yr] for 100,000 years. The doses occurring before 37,900 years are from initially defective waste packages. After 37,900 years, corrosion failures occur and contribute to increased dose.

The groundwater dose from each of the radionuclides considered for groundwater transport (Cm-246, U-238, Cm-245, Am-241, Np-237, Am-243, Pu-239, Pu-240, U-234, Th-230, Ra-226, Pb-210, Cs-135, I-129, Tc-99, Ni-59, C-14, Se-79, Nb-94, and Cl-36) is illustrated in Figure 3-34 for all 350 realizations. Figure 3-34 is a box plot representation of each radionuclide contribution to the total dose as a percentage. Each box contains half of the radionuclide percentage values with the top and bottom lines of the box showing the ±25 percent limits of the values. The median radionuclide percentage value is represented by
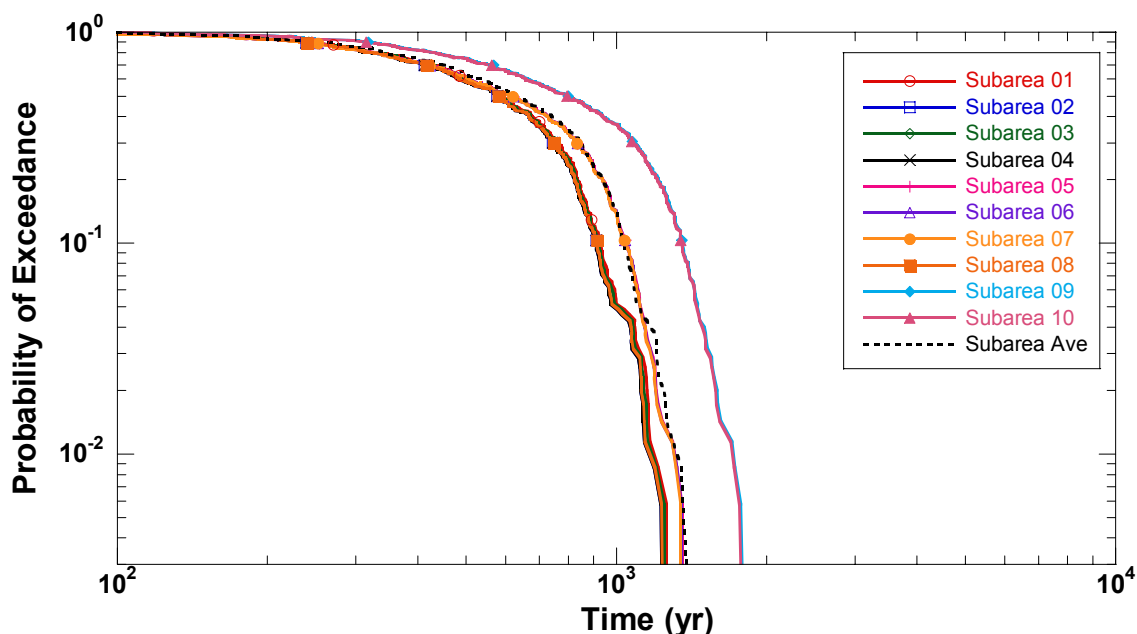
Figure 3-33. Complementary Cumulative Distribution Function of Saturated Zone Groundwater Traveltimes for 350 Realizations

Radionuclide	10,000 Years Mean Value Data Set (mSv/yr)	10,000 Years Multiple-Realization Data Set (mSv/yr)	100,000 Years Mean Value Data Set (mSv/yr)	100,000 Years Multiple-Realization Data Set (mSv/yr)
Table 3-13. Primary Radionuclides Contributing to Peak Expected Dose				
Np-237	0	4.29×10^{-5}	3.69×10^{-2}	9.54×10^{-2}
I-129	1.30×10^{-4}	5.34×10^{-5}	3.90×10^{-4}	1.33×10^{-3}
Tc-99	2.15×10^{-4}	1.09×10^{-4}	6.17×10^{-4}	2.09×10^{-3}
U-234	0	1.77×10^{-9}	4.62×10^{-7}	6.80×10^{-5}
Cl-36	7.11×10^{-7}	2.64×10^{-7}	1.35×10^{-6}	5.10×10^{-6}
Se-79	0	3.74×10^{-8}	9.31×10^{-6}	1.14×10^{-5}

the horizontal line inside the box. Values in the data set that remain within a specified limit (e.g., 95th percentile) are indicated by the line extending from the top of the box. The circles are labeled "outliers" by the statistical test, which are values beyond three standard deviations from the mean, but are nevertheless significant values. In Figure 3-34a, all Np-237 values are outliers, because, of the 350 realizations, 286 realizations (82 percent) have no contribution from Np-37. Eleven of the realizations have Np-237 contributions that exceed 80 percent. Of the 350 realizations, the highest percentage contribution of I-129 to total dose is 70 percent. In 3 of the realizations, Tc-9 contributes at least 80 percent to the total dose. The median value for I-129 is 31.7 percent and for Tc-99 is 41.6 percent. In Figure 3-34b, representing the
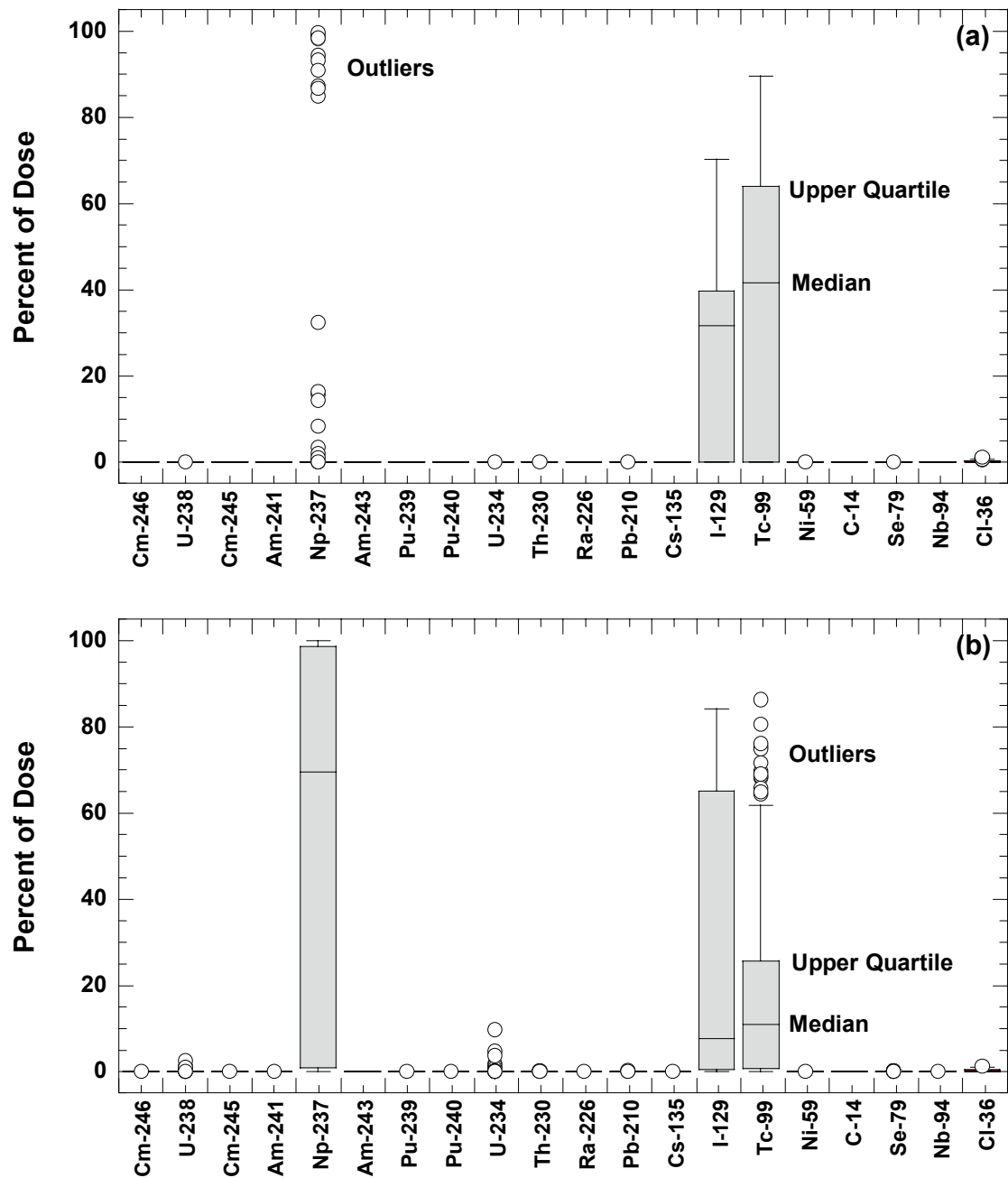
Figure 3-34. Percent Each Radionuclide Contributes to the Peak Groundwater Dose in (a) 10,000 and (b) 100,000 Years for 350 Realizations

100,000-year case, Np-237, I-129, and Tc-99 contribute at least 1 percent to the groundwater dose for any single realization. Of the 350 realizations, Np-237 exceeds 80 percent of the contribution for 177 realizations and exceeds 90 percent of the contribution in 166 of those realizations. Contributions to total dose exceeds 80 percent in only 7 realizations for I-129, and in only 2 realizations for Tc-99. The median values for Np-237, I-129 and Tc-99, are 69.6, 7.7 and 11 percent. Radionuclides U-238, U-234, Se-79, and Cl-36 contribute at least 0.01 percent to the total. The remaining nuclides (Cm-246, Cm-245, Am-241, Am-243, Pu-239, Pu-240, Th-230, Ra-226, Pb-210, Cs-135, Ni-59, C-14, and Nb-94) contribute negligibly to the groundwater dose. The radionuclides with the greatest consistency in contributing to peak dose in all realizations are I-129 and Tc-99 for 10,000 years and Np-237, followed by I-129 and Tc-99, for 100,000 years. The results (plotted in Figure 3-35) of the expected dose for each nuclide show similar behavior for the 10,000- and 100,000-year simulation periods, as does Figure 3-34, with the same nuclides having the largest contribution to the groundwater dose.

3.5 Alternative Conceptual Models

This section compares repository performance, as measured by expected dose, for the basecase data set, with the expected dose computed for the alternative conceptual models described in Section 2.3. Only the general trends in the groundwater dose of the alternative models relative to the basecase are described in this section. Additional discussion of the sensitivity of TPA output to a conceptual model, using multiple realizations, is provided in Section 4.4.

Conceptual models can be activated with flags in the TPA Version 4.1 code input file, by modifying TPA input parameters, or by a combination of both setting appropriate flags and changing TPA input parameters. All three approaches are used in this section to specify a conceptual model and to analyze the influence of the conceptual model on the expected dose. Conceptual models activated with flags in the TPA input file include the four dissolution rate models, bypassing invert transport, and the particle and grain surface-area models. Conceptual models evaluated by modifying the parameter values in the TPA input file are the focused flow, matrix diffusion, and no retardation module. Conceptual models activated using a combination of flags and changes to TPA input parameters include the flowthrough models and cladding protection.

Figures 3-36 through 3-38 present expected groundwater dose in 10,000 and 100,000 years for the basecase data set, together with expected groundwater doses from the total system performance assessment alternative conceptual models. For the conceptual models evaluated using the basecase data set, peak expected dose spans 4 orders of magnitude for the 10,000-year simulation period. The general trend in groundwater expected dose exhibited in Figures 3-36 through 3-38 indicates a wide range in the sensitivity of groundwater expected dose to the conceptual model. The alternative models with the most deviation from the basecase data set peak dose are the no-retardation case, which is 2 orders of magnitude greater than the basecase peak dose, and the schoepite and Clad-M1 cases, which are 2 orders of magnitude less than the basecase peak dose, for 10,000- and 100,000-year
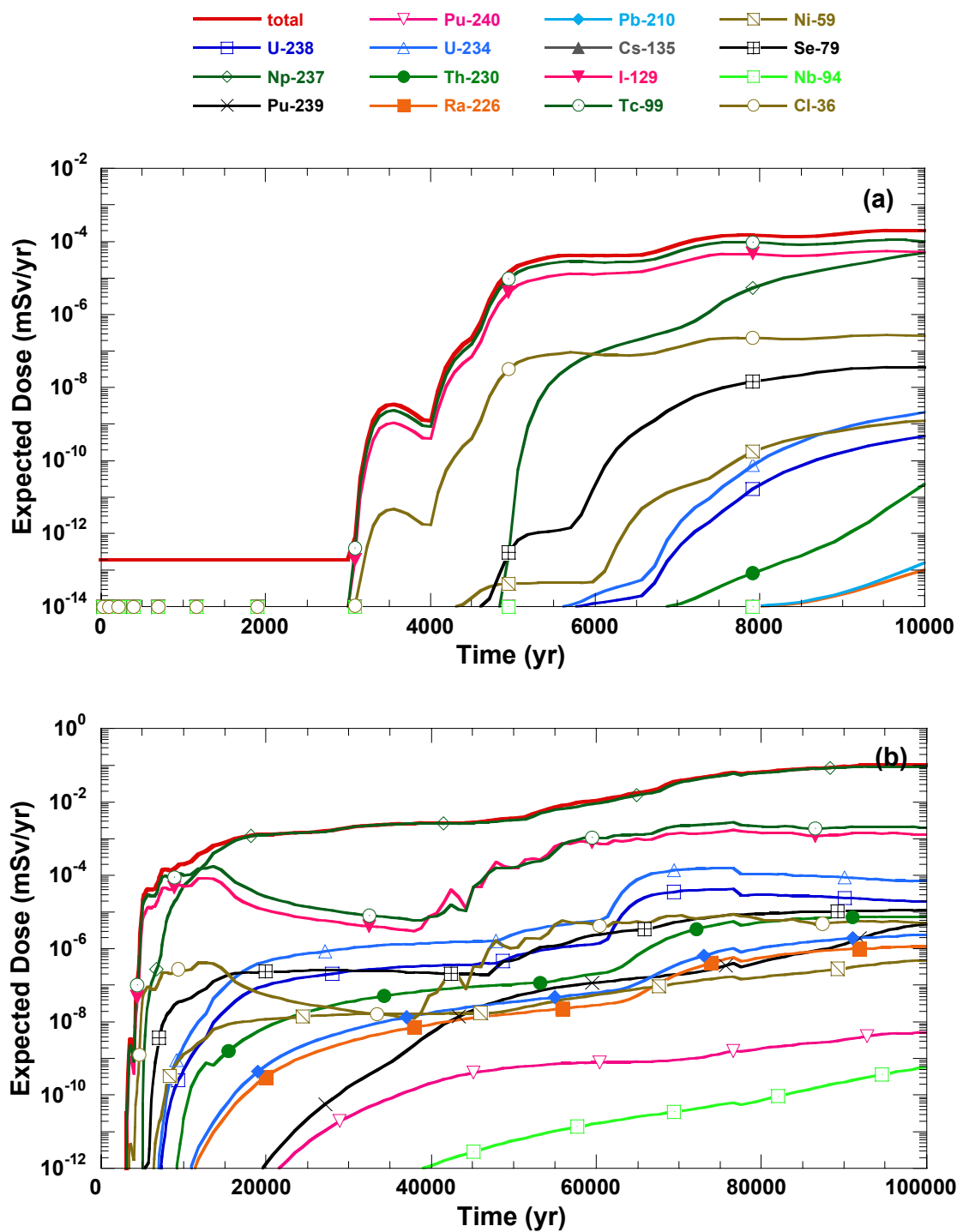
Figure 3-35. Average Groundwater Dose in (a) 10,000 and (b) 100,000 Years for Each Nuclide, Including the Total Dose, for 350 Realizations
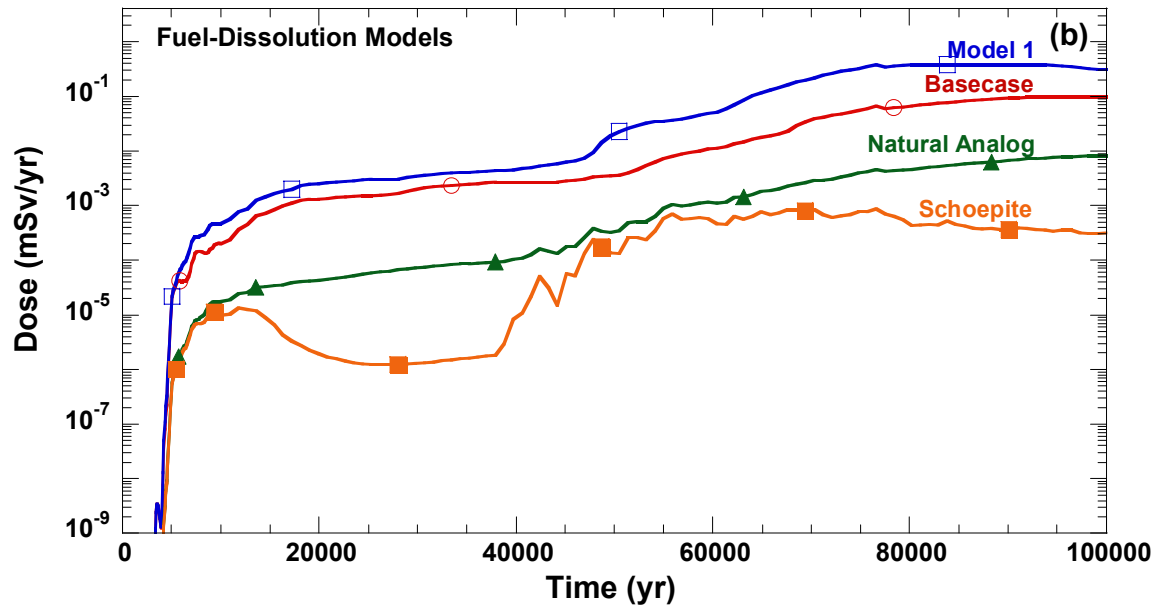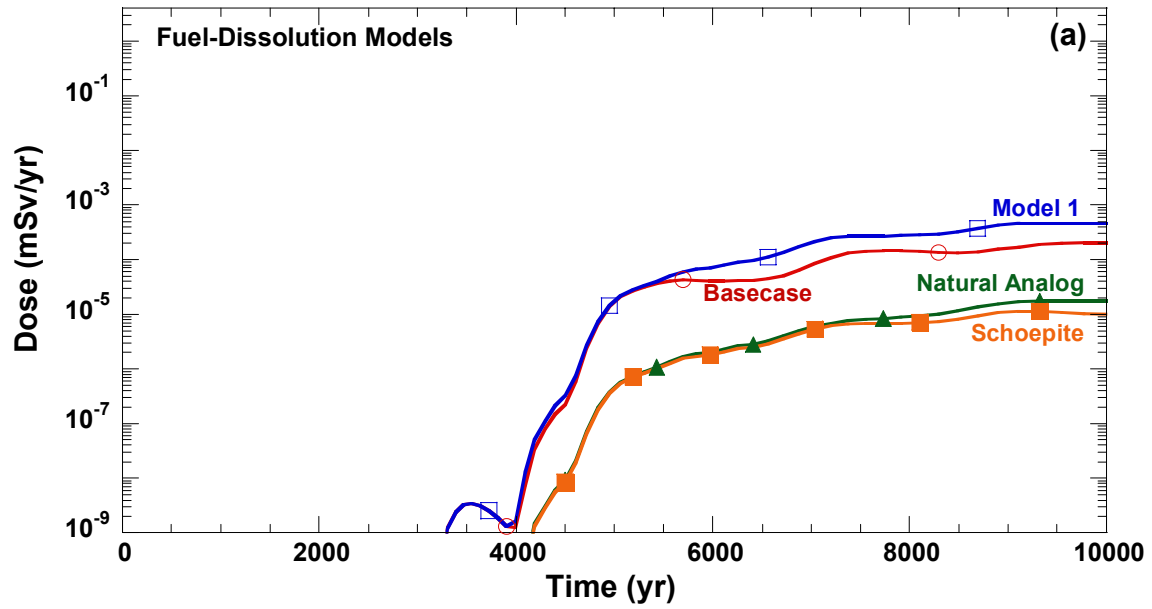
Figure 3-36. Average Groundwater Dose from the Basecase and the Fuel-Dissolution Alternative Conceptual Models in (a) 10,000 and (b) 100,000 Years, for 350 Realizations
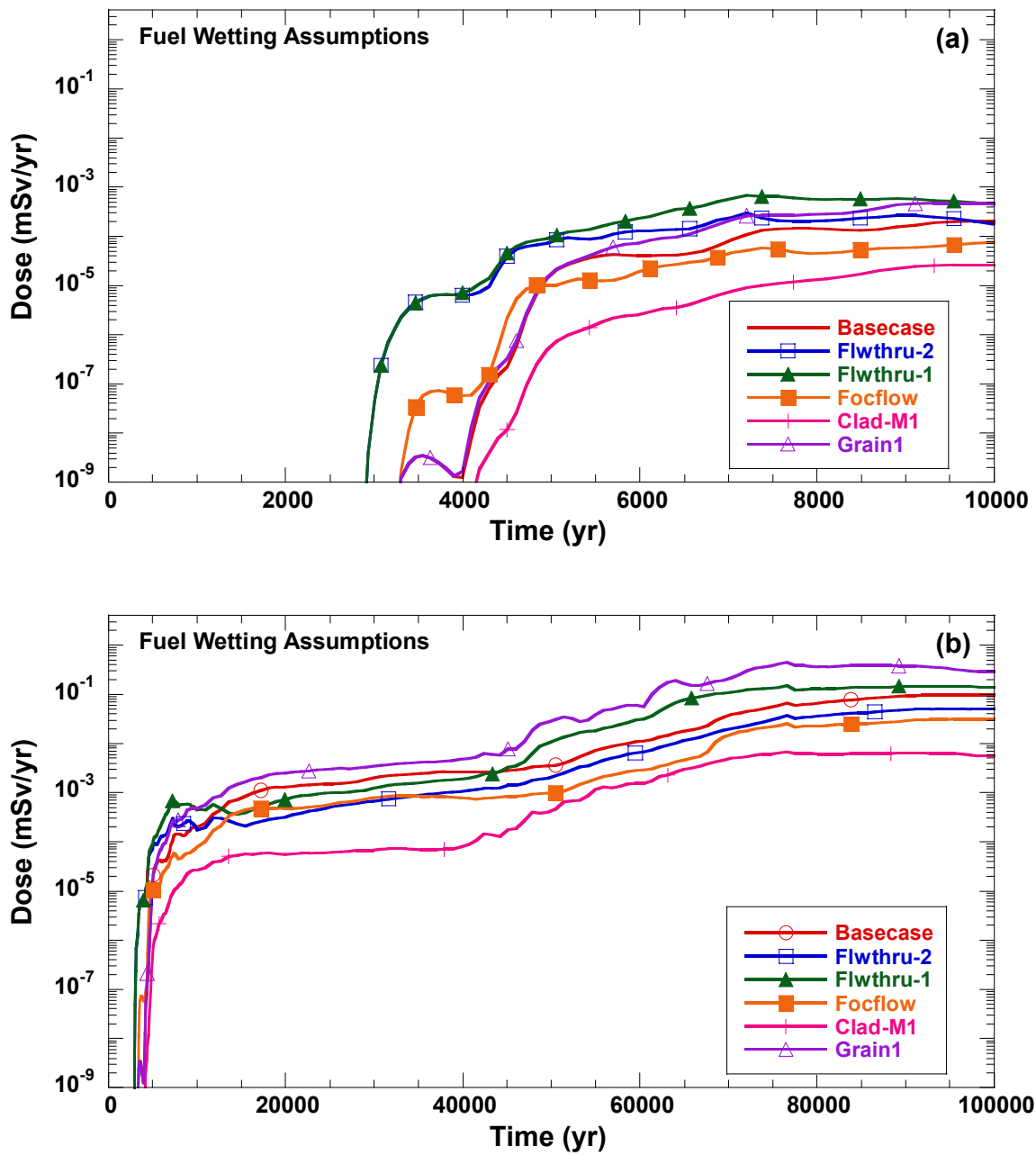
Figure 3-37. Average Groundwater Dose from the Basecase and the Fuel-Wetting Alternative Conceptual Models in (a) 10,000 and (b) 100,000 Years, for 350 Realizations

3-66
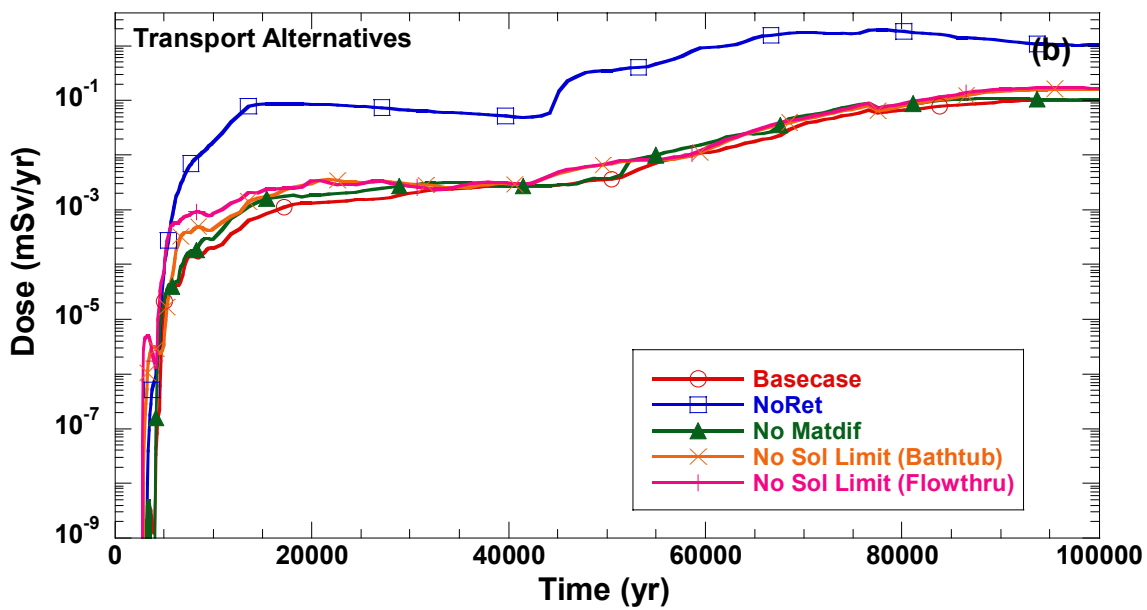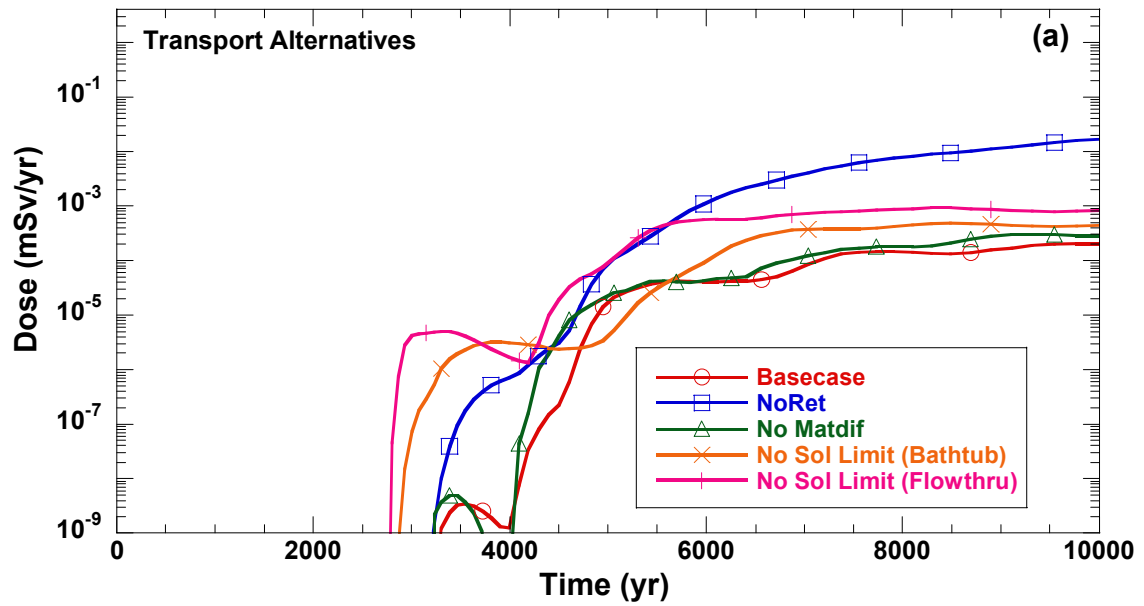
Figure 3-38. Average Groundwater Dose from the Basecase and the Transport Alternative Conceptual Models in (a) 10,000 and (b) 100,000 Years, for 350 Realizations

simulation periods. The following sections discuss the alternative conceptual models grouped by fuel dissolution, fuel wetting, and transport assumptions and compare the groundwater expected dose for the basecase. The TPA Version 4.1 code user's guide presents a description of these models.

3.5.1 Fuel-Dissolution Models

Results from total system performance assessment simulations, using three different fuel dissolution models, are evaluated by comparing the expected groundwater dose from each of the models with the basecase expected groundwater doses. The expected groundwater dose from the basecase, and from the three fuel dissolution alternative conceptual models, is shown in Figure 3-36.

3.5.1.1 Fuel-Dissolution Model 1

The expected groundwater dose in Figure 3-36 (labeled as Model 1) shows an earlier release and higher dose than the basecase after 5,500 years. The small increase in dose between 5,500 and 10,000 years in Figure 3-36(a) for Model 1 is attributable to the delayed release and ingrowth of Np-237 in the saturated zone from initially defective failures. From 50,000 to 100,000 years, the Model 1 dose maintains a dose output approximately 3 to 7 times the basecase model. Compared with Model 2, dissolution Model 1 is characterized by a higher release rate resulting from faster dissolution.

3.5.1.2 Fuel-Dissolution Model 3 (Natural Analog)

The groundwater expected dose in Figure 3-36 (labeled as Natural Analog), which displays similar dose results from the schoepite dissolution model for the first 7,000 years, shows later release with lower doses throughout the 100,000-year simulation period, than the basecase dose, indicating a slower dissolution rate. After 40,000 years, this model exhibits slight fluctuations that dissipate after 80,000 years. As stated in Section 2.3.2.1.2, this model uses a fixed dissolution rate of 24 kg/yr [53 lb/yr] and is limited by the fraction of wetted waste packages and the fuel wetting factors.

3.5.1.3 Fuel-Dissolution Model 4 (Schoepite Dissolution)

The groundwater expected dose in Figure 3-36 (labeled as Schoepite) displays the lowest dose of all the fuel dissolution models for the 10,000- and 100,000-year simulation periods. The variations in dose after 40,000 years for this dissolution model are similar to Model 3. The variations display larger displacement but at a reduced dose than that of Model 3.

3.5.2 Fuel-Wetting Assumptions

The amount of water contacting a waste package affects the engineered barrier subsystem release rate and the time of the release. This section presents results that investigate the assumptions for fuel wetting with five alternative conceptual models. The groundwater expected doses computed using these models and the basecase results are provided in Figure 3-37.

3.5.2.1   Flowthrough Model with Fuel-Dissolution Model 2

The groundwater expected dose in Figure 3-37 (labeled as Flwthru-2) has an earlier release and higher dose than the basecase (expected) dose for the first 10,000 years. An earlier dose is expected because in the flowthrough model, release from the waste package occurs instantaneously (i.e., no time to fill waste package). Beyond 10,000 years, the basecase dose is higher than the flowthrough model dose because release is limited by solubility over a longer period in the flowthrough than in the bathtub water contact mode.

3.5.2.2   Flowthrough Model with Fuel-Dissolution Model 1

Groundwater expected dose in Figure 3-37 (labeled as Flwthru-1) indicates an earlier release and corresponding dose than the basecase (expected) dose at the beginning of the simulation. During 13,000 to 44,000 years, the basecase dose exceeds the flowthrough Model 1 dose because the release is limited by solubility over a longer period in the flowthrough water contact mode compared to the bathtub water contact mode in the basecase. Beyond 44,000 years, the relative increase in dose occurs following the onset of waste package corrosion failure. The dose from flowthrough Model 1 is higher than the basecase dose after 44,000 years for the same reason as for the dose resulting from initially defective waste packages.

3.5.2.3   Focused Flow

As presented in Figure 3-37, the groundwater expected dose (labeled as Focflow), computed using a focused flow of water onto the waste package, is greater than the basecase dose, before approximately 5,000 years. The basecase groundwater expected dose is approximately 2 to 4 times more than the expected dose from the focused flow model for the remainder of the 100,000-year simulation period. These results are consistent with solubility-limited releases associated with higher flows at earlier times and lower doses thereafter, which is the net result of fewer waste packages receiving more water.

3.5.2.4   Cladding Credit with Model 1

The groundwater expected dose in Figure 3-37 (labeled as Clad-M1), calculated for this conceptual model, is approximately 2 orders of magnitude less than the groundwater expected dose for the basecase during the entire simulation period. Such reduction in dose in spite of a higher dissolution rate is expected, because the faster dissolution rate is compensated by the reduction in dissolution surface area resulting from the specified level of cladding protection.

3.5.2.5   Grain-Size Model with Fuel-Dissolution Model 1

The groundwater expected dose in Figure 3-37 (labeled as Grain1) produces higher doses than the basecase after 5,500 years. The higher release for this model is caused by faster leaching rate associated with dissolution Model 1 and water contacting a larger surface area of spent nuclear fuel.

3.5.3 Transport Alternatives

The three alternative conceptual models that test assumptions about transport in the engineered barrier subsystem, the unsaturated and the saturated zones are assessed in this section. Figure 3-38 presents the groundwater expected doses for these conceptual models and the basecase dose.

3.5.3.1 No Retardation of Plutonium, Americium, and Thorium

As presented in Figure 3-38, the groundwater expected dose (labeled as NoRet), calculated assuming no retardation for plutonium, americium, and thorium in the unsaturated and saturated zones, is greater than the basecase expected dose for the entire 100,000-year simulation period. Moreover, the general characteristics of the groundwater expected dose are consistent with the dose with no retardation and are approximately one to three orders of magnitude greater than the basecase dose throughout the 100,000-year simulation period.

3.5.3.2 No-Solubility Limit Model

The groundwater expected dose presented in Figure 3-38 [labeled No Sol Limit(Bathtub)] has earlier release and higher dose than the basecase prior to 4,700 years. After 4,700 years it has similar dose levels to the basecase expected dose. During the remaining 10,000-year simulation period, the two dose curves cross at least three times, and the levels are never more than approximately one order of magnitude apart. The three main contributors to early dose (I-129, Tc-99, and Cl-36) have relatively high solubilities {129 kg/m^3 [8.05 lb/ft^3], 99.3 kg/m^3 [6.20 lb/ft^3], and 36.0 kg/m^3 [2.25 lb/ft^3]} for the basecase, so additional increases had little effect on the expected dose. Other contributors such as Np-237 have low solubilities {0.00024 kg/m^3 [1.50 × 10^{-5}]}, and increases in their solubility did have an effect on the expected dose. If the water contact models are changed from bathtub to flowthrough [labeled No Sol Limit(Flowthru)], the expected dose curve displays earlier release and is increased by one to two orders of magnitude for early times (2,700 to 7,000 years).

3.5.3.3 No Matrix Diffusion

The groundwater expected dose presented in Figure 3-38 [labeled No Matdif] has earlier release and higher does than the basecase. The peak expected dose for the no matrix diffusion case {3.1 × 10^{-4} mSv/yr [0.031 mrem/yr]} occurs approximately 450 years earlier and is 50-percent greater than the basecase peak expected dose {2.1 × 10^{-4} mSv [0.021 mrem/yr]}.

The increase in the peak expected dose resulting from the no matrix diffusion case is a direct result of the early arrival time of the radionuclides at the pumping well. For example, Np-237 breaks through 3,600 years earlier for the no-matrix diffusion case compared with the basecase in which the matrix diffusion coefficient is specified as 10^{-3} per year. In the basecase, matrix diffusion not only contributes to increased traveltime but also exposes matrix surface for radionuclide sorption. In this regard, the sorbing radionuclides (e.g., Np-237) are delayed longer than the nonsorbing radionuclides (e.g., Tc-99).

3.6 Disruptive Events

The TPA Version 4.1 code results from faulting and igneous activity are presented in this section for single and multiple realizations. The disruptive events and the ground surface doses from igneous activity are compared with doses computed using the basecase data set.

3.6.1 Single-Realization Analysis of Disruptive Events

To determine the number of waste packages ruptured by seismically induced rockfall, which is part of the basecase, the time evolution of seismicity that includes the number, time, and magnitude of seismic events is obtained using the seismic hazard curve presented in Figure 3-39. The vertical extent of rockfall associated with different categories of seismic events (Figure 3-40), and the joint spacing information (Figure 3-41) for computing the rockfall area, are used in determining the rockfall volume. The rockfall volume is then used to compute impact stress which, if it induces a plastic strain on the waste package at the contact of impact exceeding 2 percent, will fail the waste package. Other associated information is presented in Table 3-14 and Figure 3-42.

To determine the number of waste packages failed by a faulting disruptive event, the TPA Version 4.1 code uses the time of the faulting event and the fault length and width information summarized in Table 3-15. Faults modeled in the TPA Version 4.1 code are hidden faults (i.e., either unknown and unmapped faults or underestimated faults), and thus the total system performance assessment calculations recognize that the waste packages will be emplaced with an appropriate setback distance from known faults. The recurrence rate for a faulting event is 5×10^{-5} per year (Mohanty, et al., 2002). Igneous activity contributes to waste package failures for both extrusive and intrusive events. As modeled, extrusive events result in the direct release of radionuclides to the ground surface, whereas intrusive events contribute to groundwater releases. The igneous event occurs between 100- and 10,000-years postclosure, with a recurrence rate of 1×10^{-7} per year. The parameters corresponding to the determination of the timing of future igneous events, the subsurface area affected by a volcanic event, and the number of waste packages affected by intrusions extending laterally from the volcanic conduit are presented in Table 3-16.

After the volcanic event penetrates the repository and exhumes spent nuclear fuel, the areal density of deposited ash and radionuclides is computed at the compliance point. Input parameters, such as eruption height, wind velocity, and parameters that determine the transport and deposition of radionuclides in ash are presented in Table 3-16. The radionuclides modeled for extrusive releases, in addition to those evaluated for groundwater transport, are listed in Table 3-17 with corresponding initial inventories and half-lives. Parameters associated with surface erosion of radionuclides from the ash blanket deposited after an extrusive igneous event are presented in Table 3-18. For the ground surface pathway, the areal densities calculated for each radionuclide, computed with the ASHPLUME (Jarzemba, et al., 1997) ash transport model, are used in determining the total effective dose equivalents. Dose conversion factors are computed internally in the TPA Version 4.1 code by using GENTPA, a modification of the GENII computer code (Napier, et al., 1988). Table 3-19 presents only the mean of the values used in the TPA Version 4.1 code.
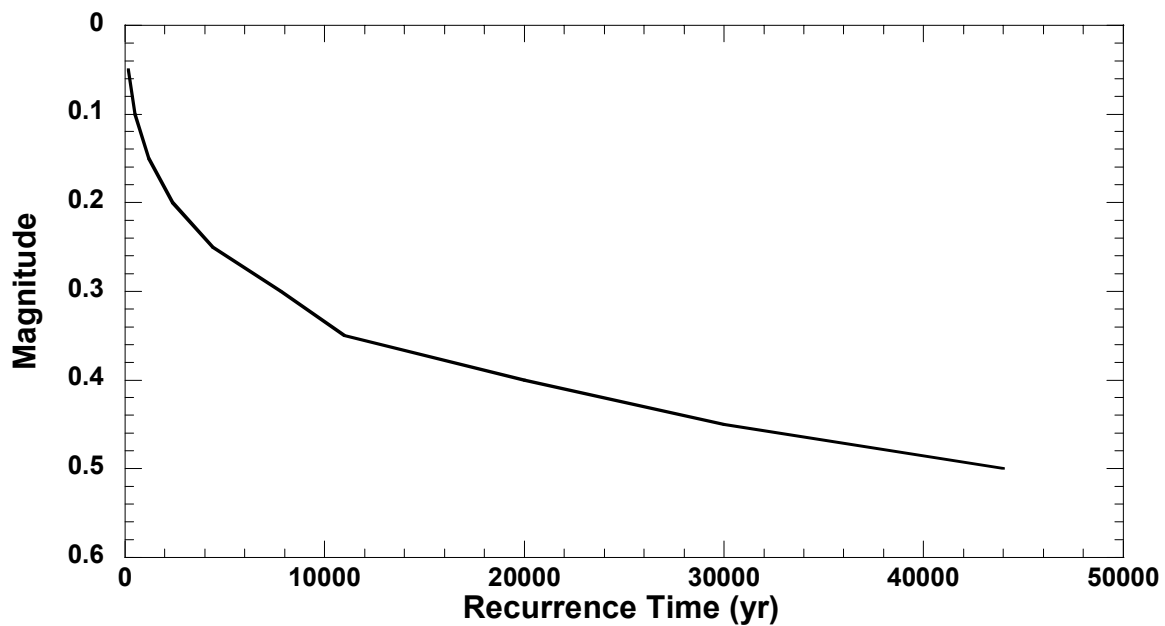
Figure 3-39. Seismic Hazard Curve Comprises Ground Accelerations and Recurrence Times Used to Determine the Time of Seismic Events
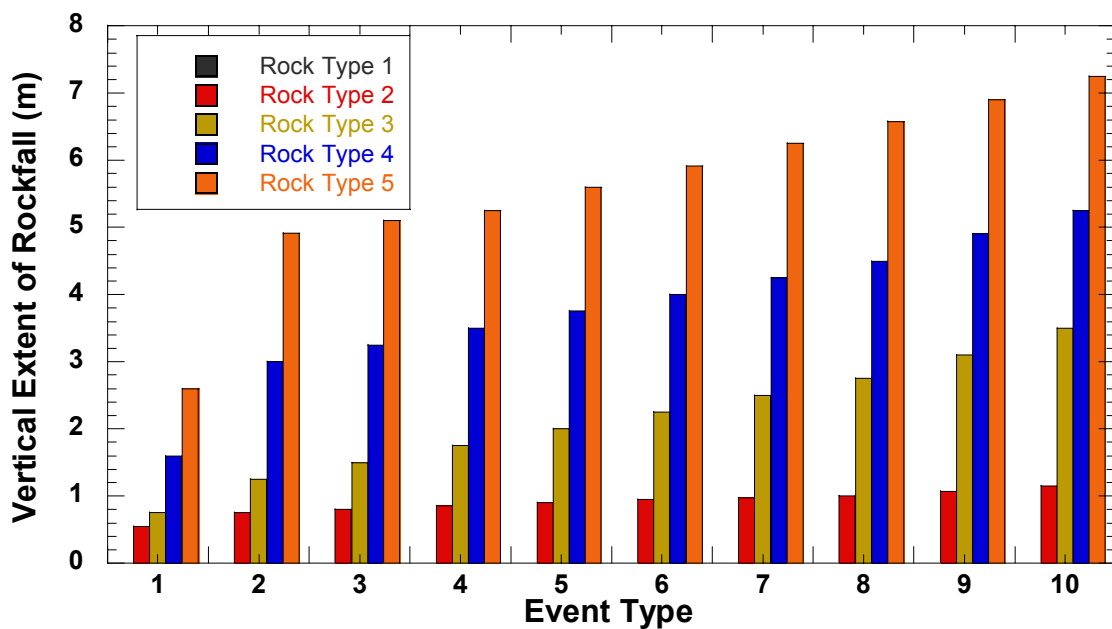
Figure 3-40. Vertical Extent of Rockfall Associated with the 5 Rock Types and 10 Seismic Events Defined by the Seismic Hazard Curve
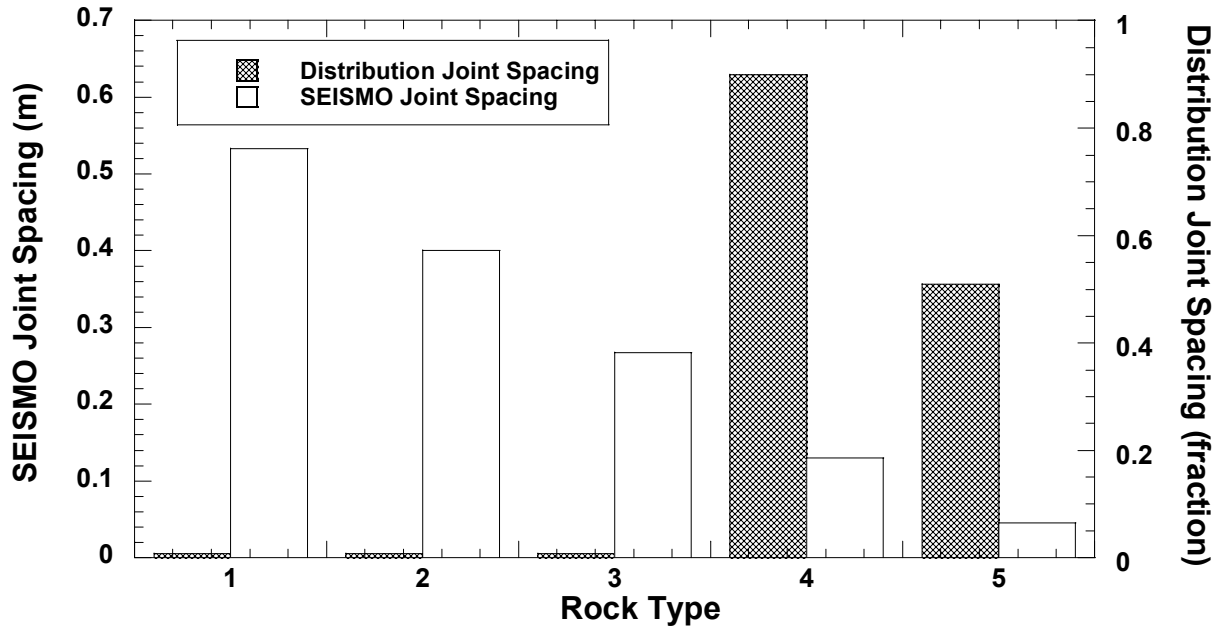
Figure 3-41. Joint Spacing of the 5 Rock Types and 10 Seismic Events

Table 3-14. Parameters Used in Determining Seismic Failure of Waste Packages		
Parameter	**Mean Value**	**Distribution**
Waste package stiffness for SEISMO	1.21×10^{10} Pa m	—
Waste package modulus of elasticity for SEISMO	1.76×10^{11}	—
Rock modulus of elasticity for SEISMO	3.45×10^{10} Pa	Normal; 2.76×10^{10}, 4.14×10^{10}
Waste package Poisson ratio for SEISMO	2.00×10^{-1}	—
Rock Poisson ratio for SEISMO	2.00×10^{-1}	Normal; 0.15, 0.25
Rock falling distance for SEISMO	2.00 m	—
Waste package falling distance for SEISMO	3.00×10^{-1} m	—
Waste package number of support pair for SEISMO	2.00	—
Waste package support stiffness for SEISMO	5.50×10^{9} Pa m	—
Waste package ultimate strength	6.20×10^{8} Pa	—
Grain density for Topopah Spring-welded for SEISMO	2.55 g/cm³	—
Waste package yield point	2.00×10^{-3}	—
Waste package plastic elongation	0.05	—
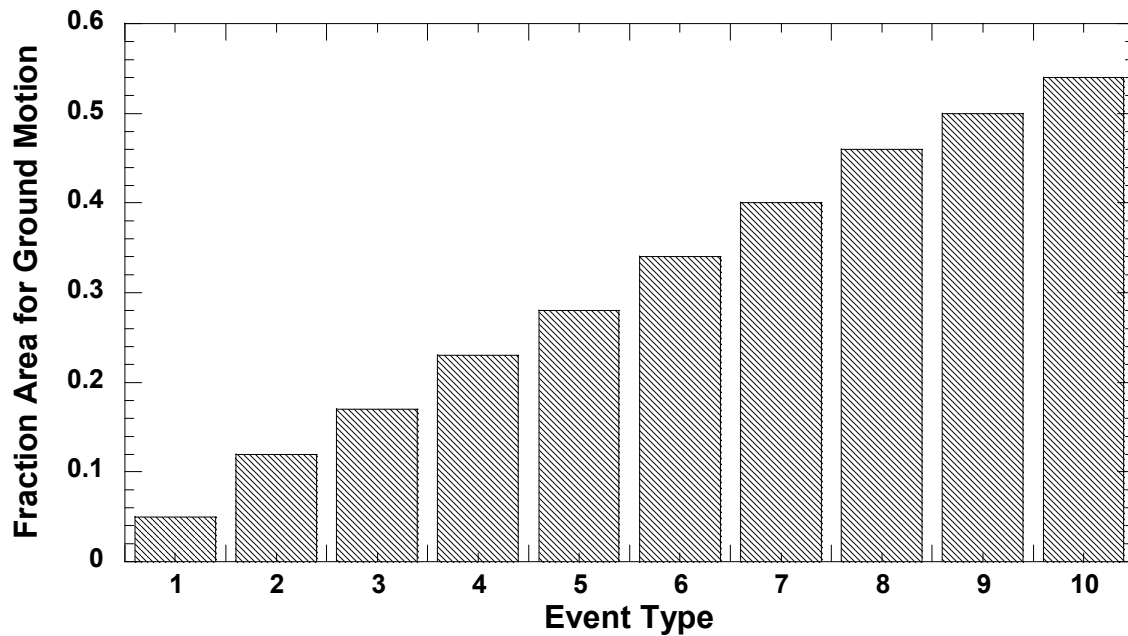
Figure 3-42. Fraction of the Area with Ground Motion for Each of the 10 Seismic Events Defined by the Seismic Hazard Curve

Table 3-15. Faulting Disruptive Event Parameters		
Parameter	**Mean Value**	**Distribution**
Time of next faulting event in region of interest	4.89×10^3 years	Finite exponential; 100.0, 10,000.0, 2.0×10^{-5}
Threshold displacement for fault disruption of waste package	2.00×10^{-1} m	User distribution; 4 values: 0.1, 0.2, 0.3, 0.4
X coordinate of faulting event in region of interest	5.48×10^5 m	Uniform; 547,400.0, 548,600.0
Y coordinate of faulting event in region of interest	4.08×10^6 m	Uniform; 4,076,000.0, 4,079,600.0
Probability for NW orientation of faults	5.00×10^{-2}	—
Random number to determine fault orientation	5.00×10^{-1}	Uniform; 0.0, 1.0
NW fault strike orientation measured from north—clockwise	$-32.5°$	—
NE fault strike orientation measured from north—clockwise	$10°$	—
NW fault trace length	4.00×10^3 m	—
NE fault trace length	4.00×10^3 m	—
NW fault zone width	2.16×10^1 m	Beta; 0.5, 275.0, 1.25, 15.0
NE fault zone width	2.85×10^1 m	Beta; 0.5, 365.0, 1.25, 15.0

Table 3-15. Faulting Disruptive Event Parameters (continued)		
Parameter	Mean Value	Distribution
NW amount of largest credible displacement	1.34×10^{-1} m	Lognormal; 5.41×10^{-2}, 3.30×10^{-1}
NW cumulative displacement rate	5.00×10^{-5} mm/yr	—
NE cumulative displacement rate	5.00×10^{-5} mm/yr	—

Table 3-16. Igneous Activity Parameters		
Parameter	Mean Value	Distribution
Volcano model (1 = geometric, 2 = distribution)	1	—
Time of next volcanic event in region of interest	5.05×10^3 years	Finite exponential; 100.0, 10,000.0, 1.0×10^{-7}
X location in region of interest	5.48×10^5 m	—
Y location in region of interest	4.08×10^6 m	—
Random number to determine if extrusive or intrusive volcanic event	5.00×10^{-1}	Uniform; 0.0, 1.0
Fraction of time volcanic event is extrusive	9.99×10^{-1}	—
Angle of volcanic dike measured from north—clockwise	$7.50°$	Uniform; 0.0, 15.0
Length of volcanic dike	6.50×10^3 m	Uniform; 2,000.0, 11,000.0
Width of volcanic dike	5.50 m	Uniform; 1.0, 10.0
Diameter of volcanic conduit	5.13×10^1 m	Uniform; 24.6, 77.9
Density of air at standard pressure	1.29×10^{-3} g/cm^3	—
Viscosity of air at standard pressure	1.80×10^{-4} g/cm-s	—
Constant relating fall time to eddy diffusivity	4.00×10^2 cm^2/sec$^{5/2}$	—
Maximum particle diameter for particle transport	1.00×10^1 cm	—
Minimum fuel particulate size	1.00×10^{-4} cm	—
Mode fuel particulate size	1.00×10^{-3} cm	—
Maximum fuel particulate size	1.00×10^{-2} cm	—
Minimum ash density for variation with size	0.8 g/cm^3	—
Maximum ash density for variation with size	1.60 g/cm^3	—
Minimum ash log diameter for density variation	-2.00	—
Maximum ash log diameter for density variation	-1.00	—
Particle shape parameter	5.00×10^{-1}	—
Incorporation ratio	3.00×10^{-1}	—
Wind direction	$-90°$	—
Wind speed	1.20×10^3 cm/sec	Exponential; 8.3×10^{-4}

Table 3-16. Igneous Activity Parameters (continued)		
Parameter	**Mean Value**	**Distribution**
Volcanic event duration	4.85×10^5 sec	Log-uniform; 1.80×10^5, 1.30×10^6
Volcanic event power	4.31×10^{10} W	Log-uniform; 3.59×10^9, 5.30×10^{11}
Volcanic column constant beta	1.00×10^1	—
Ash mean particle log diameter	1.00×10^{-1} cm	Log triangular; 0.01, 0.1, 1.0
Ash particle size distribution standard deviation	1.00	—
Relative rate of blanket removal	0.0007	—
Fraction of precipitation lost to evapotranspiration	6.80×10^{-1}	—
Fraction of irrigation lost to evapotranspiration	5.00×10^{-1}	—
Fraction of year soil is saturated from precipitation	5.40×10^{-3}	—
Fraction of year soil is saturated from irrigation	2.00×10^{-1}	—
Ash bulk density	1.40 g/cm^3	—
Ash volumetric moisture fraction at saturation	4.00×10^{-1}	—
Depth of the rooting zone	1.50×10^{-1} m	—
Subarea of volcanic event (Model 2)	2.00	—
Number of waste packages contained by ejecta (Model 2)	50.677	Beta 1.0, 150, 1.0, 2.0
Number of magma induced mechanical failures remaining in drift (Model 2)	37.40	Log uniform; 1.0, 1402.0

Table 3-17. Initial Inventory and Half-Life of Additional Radionuclides Considered for Ground Surface Release, But Not for Groundwater Release		
Radionuclide	**Inventory at 10 Years from Reactor (Ci/WP)**	**Half-Life (Years)**
Ac-227	5.93×10^{-5}	2.18×10^1
Ag-108m	9.94×10^{-1}	4.18×10^2
Am-241	1.64×10^4	4.32×10^2
Am-242m	1.96×10^2	1.52×10^2
Am-243	2.08×10^2	7.38×10^3
C-14	1.14×10^1	5.73×10^3
Cl-36	9.07×10^{-2}	3.01×10^5
Cm-243	2.01×10^2	2.85×10^1
Cm-244	2.11×10^4	1.81×10^1
Cm-245	2.89×10^0	8.50×10^3
Cm-246	6.01×10^{-1}	4.73×10^3
Cs-135	4.23×10^0	2.30×10^6
Cs-137	7.22×10^5	3.00×10^1
I-129	2.82×10^{-1}	1.57×107

Radionuclide	Inventory at 10 Years from Reactor (Ci/WP)	Half-Life (Years)
Mo-93	1.19×10^{-1}	3.50×10^{3}
Nb-94	6.69×10^{0}	2.03×10^{4}
Ni-59	1.93×10^{1}	8.00×10^{4}
Ni-63	2.94×10^{3}	9.20×10^{1}
Np-237	3.42×10^{0}	2.14×10^{6}
Pa-231	2.12×10^{-4}	3.28×10^{4}
Pb-210	4.47×10^{-7}	2.23×10^{1}
Pd-107	1.03×10^{0}	6.50×10^{6}
Pu-238	2.97×10^{4}	8.77×10^{1}
Pu-239	2.91×10^{3}	2.41×10^{4}
Pu-240	4.29×10^{3}	6.54×10^{3}
Pu-241	7.27×10^{5}	1.44×10^{1}
Pu-242	1.66×10^{1}	3.87×10^{5}
Ra-226	3.24×10^{-6}	1.60×10^{3}
Se-79	2.14×10^{-1}	1.10×10^{6}
Sm-151	3.38×10^{3}	9.00×10^{1}
Sn-121m	8.21×10^{0}	5.00×10^{1}
Sn-126	6.98×10^{0}	1.00×10^{5}
Sr-90	4.93×10^{5}	2.91×10^{1}
Tc-99	1.14×10^{2}	2.13×10^{5}
Th-229	2.17×10^{-6}	7.34×10^{3}
Th-230	1.08×10^{-3}	7.70×10^{4}
U-232	3.10×10^{-1}	7.20×10^{1}
U-233	2.71×10^{-4}	1.59×10^{5}
U-234	9.31×10^{0}	2.45×10^{5}
U-235	1.35×10^{-1}	7.04×10^{8}
U-236	2.22×10^{0}	2.34×10^{7}
U-238	2.49×10^{0}	4.47×10^{9}
Zr-93	1.95×10^{1}	1.53×10^{6}

Table 3-18. Parameters Used in Computing Ash and Radionuclide Removal from the Ground Surface

Element	K_d in Volcanic Ash (cm³/g)	Solubility in Volcanic Ash (mol/L)
Ac	4.50×10^{2}	1.00×10^{-6}
Am	1.90×10^{3}	1.00×10^{-6}
C	5.00	1.00
Cs	2.80×10^{2}	1.00
Cl	0.25	1.00
Cm	4.00×10^{3}	1.00×10^{-6}
I	1.00	1.00
Pb	2.70×10^{2}	3.20×10^{-7}
Mo	1.00×10^{1}	1.00
Np	5.00	1.00×10^{-4}
Ni	4.00×10^{2}	2.00×10^{-3}
Nb	1.60×10^{2}	1.00×10^{-8}
Pd	5.50×10^{1}	9.50×10^{-4}

Table 3-18. Parameters Used in Computing Ash and Radionuclide Removal from the Ground Surface (continued)		
Element	**K_d in Volcanic Ash (cm^3/g)**	**Solubility in Volcanic Ash (mol/L)**
Pu	5.50×10^2	5.00×10^{-6}
Pa	5.50×10^2	3.20×10^{-8}
Ra	5.00×10^2	1.00×10^{-7}
Sm	2.45×10^2	5.00×10^{-6}
Se	1.50×10^2	1.00
Au	5.50×10^1	1.00
Sr	1.50×10^1	1.30×10^{-4}
Tc	1.00×10^{-1}	1.00
Th	3.20×10^3	3.20×10^{-9}
Sb	1.30×10^2	5.00×10^{-8}
U	3.50×10^1	4.50×10^{-5}
Zr	6.00×10^2	3.20×10^{-10}
Sn	1.30×10^2	5.00×10^{-8}
Ag	5.50×10^1	1.00
Other Parameters		
Parameter	**Mean Value**	**Distribution**
Distance cutoff for dose conversion duality in DCAGS module	19.99	—
Airborne mass load for igneous activity dose calculation	1.00×10^{-3} g/m^3	Log-uniform; 1.2×10^{-3}, 1.6×10^{-2}
Occupancy factor for igneous activity dose calculation	0.605	—
Depth of resuspendable layer	3.00×10^{-1} cm	—
Airborne mass load above fresh ash blanket	4.30×10^{-3}	Log-uniform; 1.2×10^{-3}, 1.6×10^{-2}
Airborne mass load above soil	1.20×10^{-4}	Log-uniform; 5.0×10^{-5}, 3.0×10^{-4}
Rate of reduction of mass loading factor	0.70	—

Table 3-19. Biosphere Dose Conversion Factors of All 43 Nuclides for Ground Surface at the 20-km [12.4-mi] Receptor Location				
Nonpluvial and Pluvial Dose Conversion Factors				
Radionuclide	**Direct Exposure (rem/yr)/(Ci/m^2)**	**Inhalation (rem/yr)/(Ci/m^3)**	**Ingestion of Animal Products (rem/yr)/(Ci/m^2)**	**Ingestion of Crops (rem/yr)/(Ci/m^2)**
Ac-237	7.60	1.40×10^{14}	4.46×10^2	6.44×10^4
Ag-108m	1.24×10^5	5.94×10^9	5.40	5.00×10^1
Am-241	1.34×10^3	9.32×10^{12}	3.00×10^1	1.58×10^4
Am-242m	1.46×10^2	8.92×10^{12}	2.82×10^1	1.52×10^4
Am-243	2.60×10^3	9.24×10^{12}	3.00×10^1	1.58×10^4
C-14	7.80×10^{-1}	4.38×10^7	0.00	3.40×10^{-1}
Cl-36	3.40×10^1	4.60×10^8	4.20×10^3	1.52×10^4
Cm-243	6.20×10^3	6.44×10^{12}	5.60×10^1	1.10×10^4
Cm-244	4.40×10^1	5.20×10^{12}	4.60×10^1	8.80×10^3
Cm-245	4.20×10^3	9.54×10^{12}	8.40×10^1	1.62×10^4
Cm-246	3.80×10^1	9.46×10^{12}	8.40×10^1	1.62×10^4
Cs-135	1.66	9.54×10^7	1.40×10^1	7.00×10^1
Cs-137	2.60×10^4	6.70×10^8	9.60×10^1	4.80×10^2
I-129	1.24×10^3	3.64×10^9	4.00×10^2	1.32×10^3

3-78

Radionuclide	Direct Exposure (rem/yr)/(Ci/m^2)	Inhalation (rem/yr)/(Ci/m^3)	Ingestion of Animal Products (rem/yr)/(Ci/m^2)	Ingestion of Crops (rem/yr)/(Ci/m^2)
Mo-93	2.60×10^2	5.98×10^8	6.20	7.40×10^1
Nb-94	7.40×10^4	8.70×10^9	1.36×10^{-3}	4.60×10^1
Ni-59	0.00	5.66×10^7	3.80×10^{-1}	2.20
Ni-63	0.00	1.32×10^8	1.06	6.00
Np-237	1.46×10^3	1.13×10^{13}	1.30×10^3	3.80×10^4
Pa-231	1.96×10^3	2.70×10^{13}	7.60×10^1	4.80×10^4
Pb-210	1.24×10^2	2.84×10^{11}	5.58×10^2	2.66×10^4
Pd-107	0.00	2.68×10^8	1.58×10^{-1}	2.40
Pu-236	1.66×10^1	8.22×10^{12}	9.00×10	1.38×10^4
Pu-239	1.76×10^1	9.00×10^{12}	1.00×10^1	1.52×10^4
Pu-240	4.00×10^1	9.00×10^{12}	1.00×10^1	1.52×10^4
Pu-241	2.60×10^{-1}	1.73×10^{11}	1.90×10^{-1}	3.00×10^2
Pu-242	3.40×10^1	8.62×10^{12}	9.40×10	1.46×10^4
Ra-226	3.20×10^2	1.80×10^{11}	1.06×10^2	6.60×10^3
Se-79	1.02	2.06×10^8	1.98×10^1	5.00×10^1
Sm-151	2.40×10^{-1}	6.28×10^8	3.40×10^{-2}	1.94
Sn-121m	2.40×10^2	2.42×10^8	3.86	1.42×10^1
Sn-126	2.60×10^3	2.10×10^9	3.38×10^2	1.31×10^2
Sr-90	1.34×10^1	2.72×10^{10}	2.94×10^2	6.72×10^3
Tc-99	3.80	1.75×10^8	3.80×10^1	5.60×10^3
Th-229	4.20×10	4.50×10^{13}	1.71×10^2	1.66×10^4
Th-230	3.60×10^1	6.84×10^{12}	2.60×10^{-1}	2.40×10^3
U-232	5.00×10^1	1.38×10^{13}	1.18×10^2	7.24×10^3
U-233	3.60×10^1	2.84×10^{12}	1.80×10^2	1.58×10^3
U-234	3.60×10^1	2.78×10^{12}	1.76×10^2	1.54×10^3
U-235	7.20×10^3	2.58×10^{12}	1.64×10^2	1.45×10^3
U-236	3.20×10^1	2.64×10^{12}	1.66×10^2	1.46×10^3
U-238	2.60×10^1	2.48×10^{12}	1.61×10^2	1.41×10^3
Zr-93	0.00	6.76×10^9	5.68×10^{-4}	7.24

Table 3-19. Biosphere Dose Conversion Factors of All 43 Nuclides for Ground Surface at the 20-km [12.4-mi] Receptor Location (continued)

Nonpluvial and Pluvial Dose Conversion Factors

3.6.2 Multiple-Realization Analysis of Disruptive Events

The variability in the average dose arising from faulting events and igneous activity for the multiple-realization simulations is presented in this section. The dose history for faulting events for the 100,000-year simulation period without probability weighting is presented in Figure 3-43(a). The average groundwater dose from the faulting events is approximately 50- to 100-percent greater than the dose without a faulting event from 5,000 to 50,000 years. After 70,000 years, the groundwater dose with faulting and the basecase in the 100,000-year simulation period are not distinguishable.

Figure 3-43(b) shows the probability-weighted expected dose curve (or, the risk curve) for the igneous activity scenario together with the groundwater expected dose curve (or, the risk curve) computed using the basecase data set. For the igneous activity scenario, peak dose occurs much earlier than the basecase. Dose from the igneous activity scenario at early times is several orders of magnitude greater than the basecase. The difference between the igneous
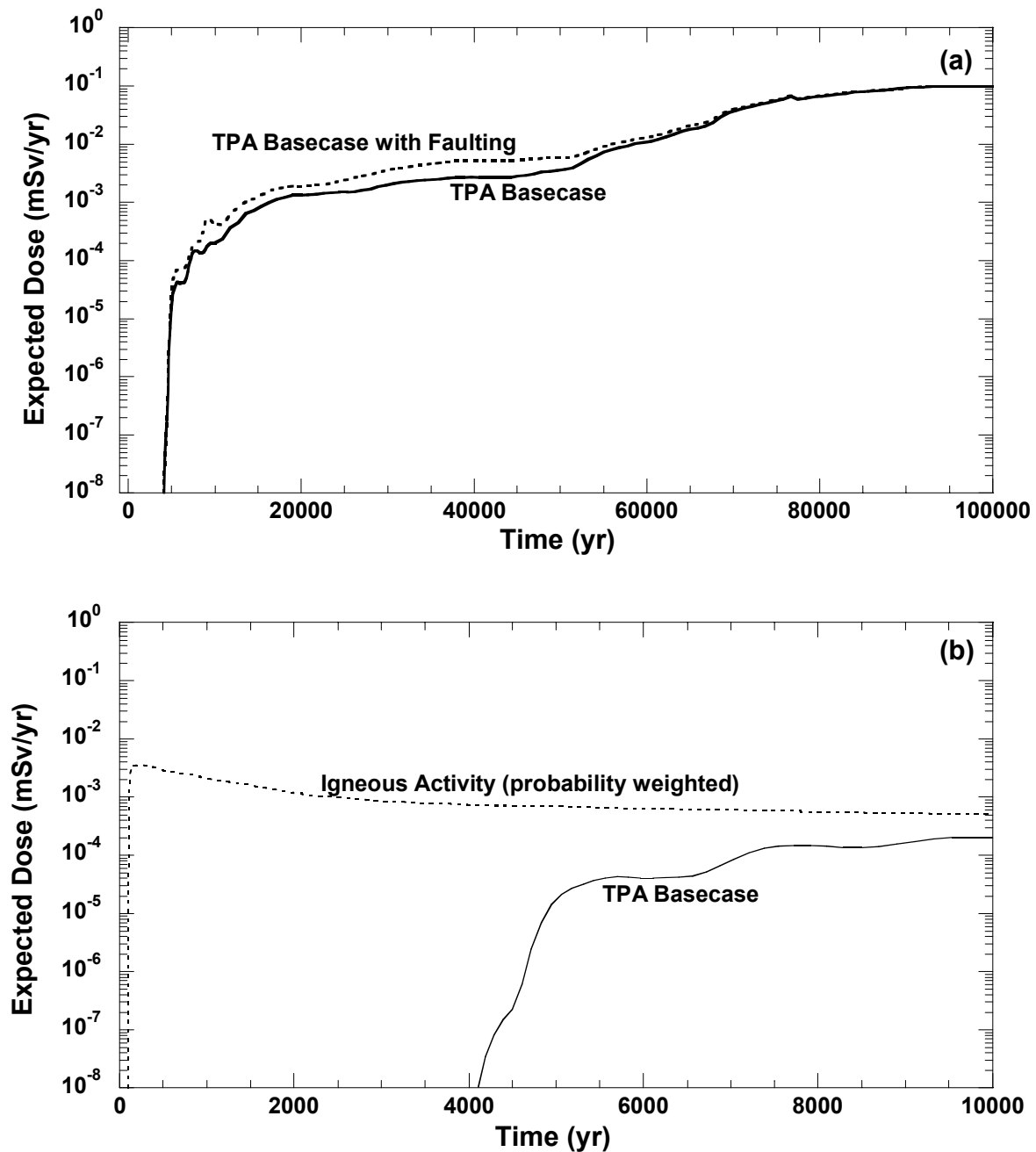
Figure 3-43. Groundwater Dose for (a) Faulting (Shown for 100,000 Years) and (b) Igneous Activity (Shown for 10,000 Years), for 350 Realizations. (Only the Ground-Surface Dose for Releases Caused by Extrusive Igneous Activity in (b) is Probability Weighted. Faulting Dose is not Probability Weighted.)

activity and the basecase scenario doses gradually decreases with time, down to approximately an order of magnitude at 10,000 years. The peak risk from igneous activity, which occurs at 225 years, is 3.6 mSv/yr x 10^{-3} mSv/yr [0.36 mrem/yr]. This risk value is a 16-fold increase over the basecase risk of 2.1 x 10^{-4} mSv/yr [0.021 mrem/yr], which occurs close to 10,000 years in a 10,000-year simulation period.

3.7 Calculation of Risk

Risk is defined in this report as the probability-weighted dose. Doses are calculated from three scenario classes: (i) basecase with seismicity, (ii) faulting, and (iii) igneous activity. The probability of the three scenario classes sums to unity; this implies these scenario classes are assumed exhaustive.

The average risk to a receptor can be computed by summing contributions to dose from each Monte Carlo simulation, weighted by the scenario probability and the conditional probability of each realization within the scenario. The methodology for computing conditional risk (i.e., assuming the scenario has a probability of one) from scenarios other than extrusive igneous activity is presented in Section 3.7.1. The methodology used to determine the conditional risk from scenarios with extrusive igneous activity is described in Section 3.7.2. The methodology for combining the conditional risks to an overall risk is presented in Section 3.7.3.

3.7.1 Scenarios Other Than Extrusive Igneous Activity

The risk or expected effective dose equivalent is the product of the consequence (i.e., dose) and the probability that the dose has occurred. Estimates of dose are uncertain because the models and their input parameters are uncertain, as are the times of occurrence of the disruptive events such as faulting and intrusive igneous activity. Monte Carlo analysis is used to account for the uncertainty in parameters and events. Monte Carlo analysis propagates the uncertainty in model inputs through the conceptual models by evaluating a model repeatedly, using input values randomly selected. The output of the Monte Carlo analysis is a set of results, such as dose versus time, for each randomly chosen input set of values. Generally, each Monte Carlo output result has equal probability. Thus, each dose curve from the Monte Carlo analysis has a probability of occurrence equal to 1/N, where N is the number of Monte Carlo samples. The analysis in this section does not explicitly include conceptual model uncertainty other than that captured by changes in the input parameters.

The expected dose-versus-time relationship for scenario j (e.g., intrusive volcanic scenario) can be developed by summing, for all realizations, the probability-weighted contributions from the family of dose relationships produced by the N Monte Carlo samples. The mathematical representation of this calculation is

$$\overline{D}_j(t) = \sum_{i=1}^{N} p_i C_{i,j}(t)$$
(3-1)

where

$\overline{D}_j(t)$ — average annual dose to the receptor individual as a function of time for the jth scenario.

$C_{i,j}$ — dose as a function of time for the ith realization of the jth scenario

p_i — probability assigned to the dose curve for the jth realization; for Monte Carlo sampling, $p_j = (1/N)$

N — number of model simulations that compose the family of dose curves (i.e., N Monte Carlo samples of the model inputs are used to generate N model outputs in the form of dose curves)

The index indicates the event can occur at any time between $[0,t]$.

3.7.2 Extrusive-Igneous Activity Scenario

Disruptive events, such as a volcanic eruption through the repository block, are generally of short duration (several years) compared to the nominal case (tens of thousands of years). Although the standard Monte Carlo approach is suitable for the nominal case that has long-term, gradually evolving consequences, and relatively high probability of occurrence, the method is not well suited to the incorporation of the effects of low-probability, high-consequence disruptive events such as volcanism.

For a typical nominal case evaluation of the proposed Yucca Mountain repository performance, the number of Monte Carlo samples, which must be greater than the number of sampled variables, is generally 350 or more to generate a stable mean dose curve. On the other hand, a standard Monte Carlo simulation involving low-probability volcanism of short duration would require an unreasonably large number of realizations to generate a stable risk curve. For example, if the probability of extrusive volcanism through the repository is 10^{-7} per year, there would have to be approximately 1,000 realizations per simulated volcanic event in 10,000 years. Also, there would have to be many hundreds or thousands of events to produce a tolerably stable mean dose curve, given that the duration of the volcanic release is relatively short. A Monte Carlo simulation with such a large number of realizations would be prohibitively expensive because each realization could take several minutes to compute.

The current NRC staff approach to generate the risk curve for low-probability events is to convolute the conditional mean dose curves generated assuming the event has taken place at a time after repository closure, t_e. A person living at time t' will be at risk from all events taking place prior to or at t'. For the volcanism scenario, the average annual dose, D, to a person living at time t' who is exposed to a volcano occurring at time t_e would be

$$\overline{D} = af(t_e, t' - t_e) \tag{3-2}$$

where a is the peak amplitude of the dose if the event happened at time $= 0$, $f(t_e, t'-t_e)$ is a function expressing the relative dose occurring at time t' from an event at time t_e. The relative

dose, *f*, is a function both of the time of the event after site closure and the time between the event and the evaluation time. Considering the volcanic event has a fixed probability of occurring in any year, the risk to a person living at *t´* is the convolution of all possible prior volcanic events multiplied by the annual probability, *p*

$$\overline{D}(t') = \int_{t_{min}}^{t'} apf(\tau, t'-\tau) d\tau \qquad (3\text{-}3)$$

where t_{min} is the earliest time that volcanism is considered to occur (e.g., 100 years after closure in this analysis, which reflects an effective control period that would limit radiological exposures).

For the igneous-activity scenario, dose consequences are largest for events that occur soon after repository closure, while the relatively short-lived, but high-activity, radionuclides, such as Am-241, are still present in significant quantities. Radionuclides can reach the affected population in short times (hours to days) but persist in the environment and also can cause lower levels of exposure long after the event (hundreds to thousands of years). The procedure for developing the expected dose curve for the igneous-activity scenario involves the following steps:

• Conduct probabilistic analyses at specific event times.

Dose consequences of igneous activity are calculated at specific event times rather than randomly selecting occurrence times in a Monte Carlo approach. In the present model, the event times t_e are 100 years; 500 years; and 1,000–10,000 years, in 1,000-year steps (Figure 3-44).

• Generate conditional expected dose curves for specific event times.

Each of the separate probabilistic analyses described previously is used to develop a separate conditional expected dose versus time curve as in Eq. (3-2) for the specific event time t_e.

• Generate an overall expected dose curve.

The expected dose at any given time t′ is determined by cumulating the mean dose curves at the 12 specified event times. Equation (3-3) describes how the expected annual dose to the receptor individual is convoluted from the conditional dose curves. In practice, the function f within the integrand of Eq. (3-3) is generated from the 12 mean dose curves at fixed values of t_e using linear interpolation to generalize to any value of t_e.

The probability-weighted dose curve calculated with this more efficient approach is presented in Figure 3-45. As expected, the consequences of an igneous event are highest at early times. The probability-weighted dose curve goes through a maximum at approximately 225 years, which results from the accumulation of risk from earlier events.
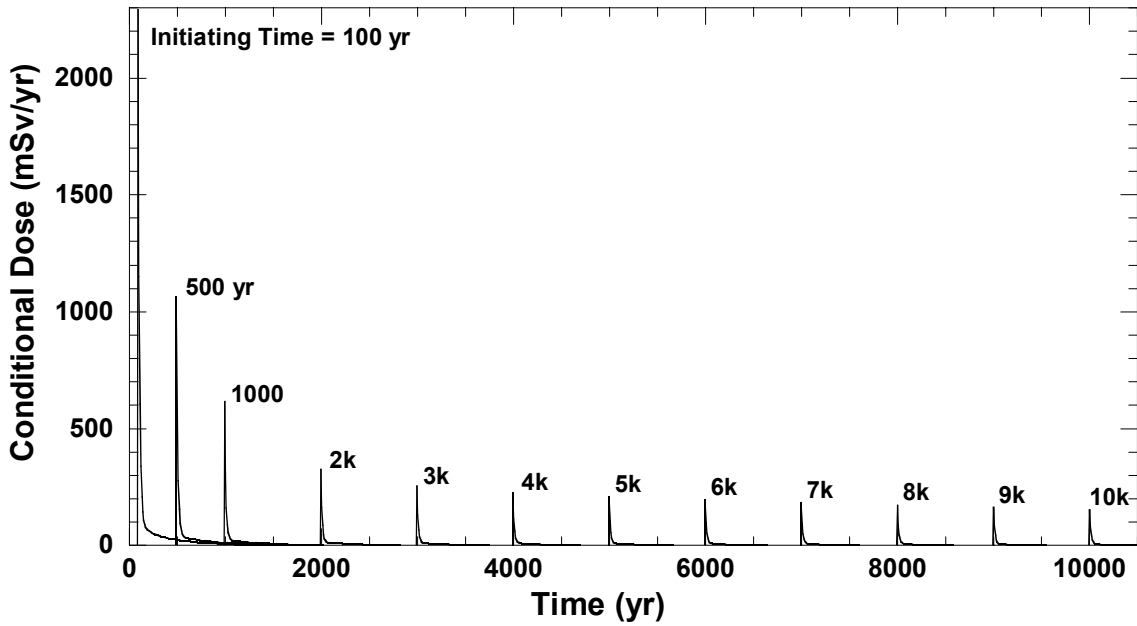
Figure 3-44. Mean Dose Arising from Extrusive Igneous Activity Shown with Various Times for the Volcanic Event in 350 Realizations
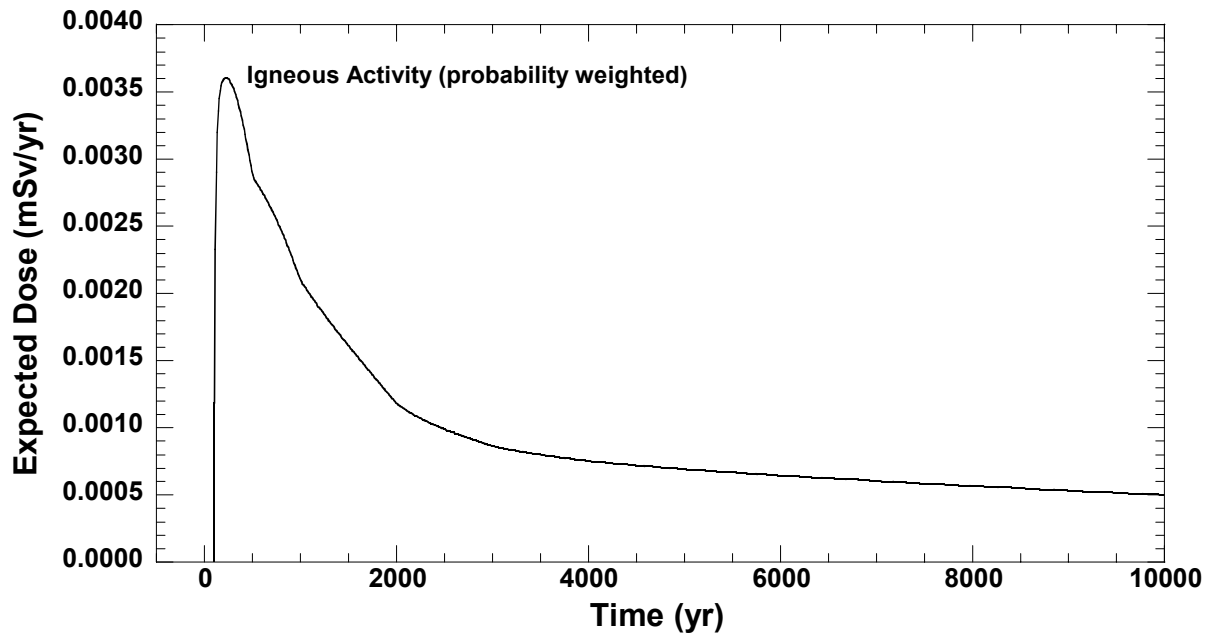
Figure 3-45. Contribution of Extrusive Igneous Activity to the Total Dose, Weighted by an Annual Probability for the Volcanic Event of 10^{-7}

3.7.3 Combining Conditional Risks into an Overall Risk

The overall risk, $\overline{D}(t)$, is calculated by summing the scenario mean doses weighted by the scenario probability, P_j. The mathematical representation of this calculation is

$$\overline{D}_j(t) = \sum_{j=1}^{M} \overline{D}_j(t) P_j \qquad (3\text{-}4)$$

where

$\overline{D}_j(t)$ — dose rate from scenario j, averaged for the Monte Carlo realizations

M — number of scenario classes

P_j — annual probability of scenario j

4 SYSTEM-LEVEL SENSITIVITY STUDIES

This chapter describes the sensitivity and uncertainty analysis techniques used in conjunction with results of the TPA Version 4.1 code[1] system-level calculations. In general, a sensitive parameter[2] is defined as one that produces a relatively large change in the output variable for a unit of change in an input parameter. The goal of the sensitivity analyses presented in this report is to determine the parameters to which peak dose for the simulation period shows the most sensitivity. The goal of the uncertainty analyses is to determine the parameters driving uncertainty (i.e., variation) in peak dose output. The analyses were conducted primarily for the basecase; limited analyses were conducted for the igneous activity and faulting disruptive events.

The sensitivity analyses in this report use peak dose as the output variable for each realization because this result is most likely to demonstrate sensitivity relationships among the independent and dependent variables. The performance measure in the Yucca Mountain implementing regulation 10 CFR Part 63 (Code of Federal Regulations, 2002) is stipulated to be the peak of the average dose history within the 10,000-year simulation period. Although there is an important distinction between these two measures of performance, the peak dose for each realization during the simulation period was used. The rationale for doing so is established in Section 4.3.1.

4.1 Sensitivity Analysis Techniques

This section describes the techniques used to determine which input parameters in the TPA Version 4.1 code most influence the results. It is noted that not all the techniques described were applied to all cases.

The output from the TPA Version 4.1 code is given by y, which is a function of random parameters, x_i, deterministic parameters, d_k; and model assumptions, a_m

$$y_j = f(x_{1_j}, x_{2_j}, \ldots, x_{l_j}, d_k, a_m)$$

(4-1)

where j represents the jth realization and l is the total number of sampled parameters in the model. It is assumed that the behavior of the system is simulated by appropriately sampling the random parameters and then computing the system output, y, for each realization of the parameters (Figure 4-1). To outline a method for analyzing simulation output, to identify important random parameters, and to develop understanding of their relationship to the output, it is assumed that the decisions about appropriate model assumptions and fixed parameters have been made *a priori*. As a result, the dependence of y on fixed parameters and model assumptions is not considered further and focus is on the dependence of y on the sampled parameters.

---

[1]The specific version of the TPA code used in this chapter is 4.1k.

[2]The terms "parameter" and "variable" are used interchangeably.
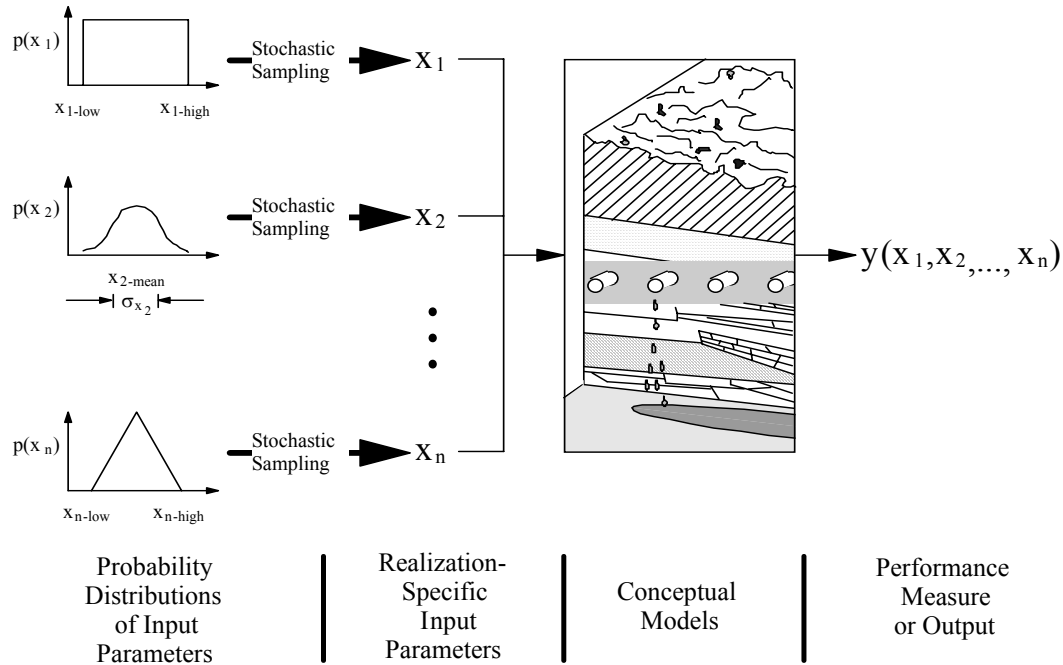
Figure 4-1. A Diagram Illustrating the Use of the Monte Carlo Method in Performance Assessment

4.1.1 Regression Analyses Methods

4.1.1.1 Single Linear Regression on One Variable

Single linear regression (i.e., regression with only the first power of one input variable and an intercept) of the output variable, with respect to each of the input parameters, can give a quantitative measure of the correlation through the coefficient of determination, R^2. This measure can be misleading, however, in cases where the dependencies are not purely of the first order with respect to the input variable. It is noted in this section and throughout this chapter that linear refers to the functional form of the regression and not the order to which the fitting parameters appear (although the regressions are also linear in the fitting parameters). Even when the output variable is linearly dependent on the input variable being studied, univariate linear regression of Monte Carlo results may fail to show unambiguous correlation because other sampled parameters that affect the output are varying at the same time, and the fitted model is clearly underspecified (i.e., the results depend on more than one variable).

The coefficient of determination, R^2, is small for most variables in the current analyses and is not necessarily a good indicator of the importance of the variables. A better indication of influence is to determine the probability that the slope of the linear regression line is significantly different from zero. This probability is determined with a t-test as described in succeeding sections.

4.1.1.1.1   Use of the t-Test To Determine Significance of Regression Parameters

The t-test is generally used to determine with a specified confidence level that an estimated parameter value differs from another value. A parameter, x_i, is deemed influential if there is a specified (e.g., 95 percent) confidence that the slope of its regression curve, m_i, is different from zero (Benjamin and Cornell, 1970).

The t-statistic of the slope of a single-variable regression line is defined as

$$t_i = m_i \sqrt{n \frac{S_{i,x}^2}{S^2}}$$ (4-2)

where

t_i —   t-statistic for regression coefficient m_i

m_i —   estimated value of regression coefficient i (i.e., slope of the best-fit line for dose versus the independent variable, x_i)

S —   estimated standard deviation of dose

$S_{i,x}$ —   estimated standard deviation of independent variable, x_i

n —   number of samples

For the analyses conducted herein, the number of realizations is large (4,000), which provides essentially an infinite number of degrees of freedom for the t-statistic. The critical value to ensure 95-percent confidence that m_i differs from zero for these conditions is 1.96 (Mason, et al., 1989). Equation (4-2) is used, therefore, to determine if the absolute value of the t-statistic for each independent variable is greater than 1.96. If not, the hypothesis that the independent variable was significant is rejected.

The t-statistic was used for the single-variable regressions and multiple linear regressions as described in Eq. (4-2).

4.1.1.2   Variable Transformations and Their Attributes

The correlation between input and output variables can be enhanced by transforming the variables. In general, variable transformations are used to (i) eliminate dimensionality of the variables, (ii) reduce the role of points at the tails of the distributions, and (iii) properly scale the resulting sensitivities to the variability of the input variables. Although transformations generally increase the goodness of the fit analyses, they distort the meaning of the results. For example, transformations such as rank and logarithmic applied to the dependent variable (dose) frequently give unfair weight to small doses, which do not affect the mean results as much as the higher doses. Because the proposed regulations are based on mean doses, regression results based on transformed variables should be used cautiously.

4.1.1.2.1　　　　Normalization

In normalization, the input variable, x_i, is transformed by dividing it by its mean value (or another baseline value such as the median or 90th percentile)

$$x_i^* = \frac{x_i}{\overline{x}_i}$$ (4-3)

Normalized variables are dimensionless and are scalar multiples of their baseline values. Dimensionless variables allow the comparison of sensitivities to other independent variables with different dimensions. Other types of normalization can also be used and will be shown later in this chapter.

Sensitivity measures based on normalized variables describe only the relative change in the dependent variable (peak dose) to changes in the independent variables. Although normalization allows a useful measure of sensitivity, it does not consider the ranges of the variability of the independent and dependent variables (see standardization, following).

4.1.1.2.2　　　　Rank Transformation

Rank transformation, a dimensionless transform, replaces the value of a variable by its rank (i.e., the position in a list that has been sorted from largest to smallest values) (Iman and Conover, 1979). Analyses with ranks tend to show a greater sensitivity than results with untransformed variables. If the distribution of doses is skewed toward the low end, which is usually the case, rank transformation can give unfair weights to lower doses.

4.1.1.2.3　　　　Logarithmic Transformation

For situations in which input and output variables range many orders of magnitude, it may be advantageous or even necessary to perform analyses on the logarithm of the variables instead of on the variable values themselves. The log transformation is also valuable for creating regression equations, where the subprocesses of the model multiply each other to form the output variable. For the present situation in which the dose calculation results from radionuclide releases from the waste form, transport through the geosphere, and uptake by humans, the processes are indeed largely multiplicative rather than additive. Log transforms, therefore, tend to give better fits to the Monte Carlo results than untransformed variables, but again at the expense of unfairly weighting the smaller doses. The log transformation may be used in conjunction with normalization.

4.1.1.2.4　　　　Standardization

The independent and dependent variables can be standardized by subtracting the mean and dividing by the standard deviation

$$x_i^* = \frac{x_i - \overline{x}}{\sigma_x}$$ (4-4)

Sensitivity measures based on standardized variables (standardized sensitivities) have the advantage of considering the range of the independent variable. Standardized variables can be greater or less than zero, hence, they cannot be used directly in the regression analyses using the log-transformed variables. Instead, the standardized sensitivities can be derived from sensitivities based on logs of the normalized variables

$$\frac{\partial y^*}{\partial x^*} = \frac{\sigma_{x_i}}{\sigma_y} \left(\frac{\partial y}{\partial x_i} \frac{x_i}{y} \right) \frac{y}{x_i}$$

(4-5)

where y^* and x^* are the standardized dependent and independent variables as defined by Eq. (4-4). The quantity in parentheses is the sensitivity derived from regression analysis with the logs of the normalized variables. Direct linear regression with standardized variables properly weights all doses.

A modified form of the standardized sensitivities approach was also used in the differential analysis described in Section 4.1.2. In this case, only seven points were defined for the parameter space, so the independent variables were standardized by the same standard deviations used in the regression analyses (i.e., the standard deviation based on 4,000 samples generated in the Monte Carlo analyses). Peak dose did not need to be standardized to show the relative sensitivities to the standardized independent variable. Therefore, those sensitivities have units of dose.

4.1.1.3 Stepwise Multiple Linear Regression

Stepwise multiple linear regression (stepwise regression) determines the most influential input parameters according to how much each input parameter reduces the residual sum of squares (Helton, et al., 1991). The form of the regression equation is

$$y = m_1 x_1 + m_2 x_2 + m_i x_i + m_n x_n + b$$

(4-6)

where

y	—	dependent variable
x_i	—	independent variables
m_i	—	regression coefficients
b	—	intercept

The regression coefficients, m_i, are measures of the linear sensitivity of y to input x_i (Draper and Smith, 1981). The variables may be the raw variables, transformed variables, or ranks. The stepwise algorithm calculates the reduction in the residual sum of squares for the independent variables in the order that gives the greatest reduction first. In the implementation of the procedure, a multiple linear regression model is fitted to the data in an iterative fashion. The procedure starts with the variable, x_i, which explains most of the variations in the model output, y. Then it adds additional variables (one at a time) to maximize the improvement in fit of the model according to the R^2 value. In the regression model, R^2, the coefficient of determination indicates the fraction of variability in the data explained by all the variability in the model. The sequence in which the inputs are selected is a useful measure of their uncertainty importance, as is the increment in R^2 they produce. Iman and Conover (1979) also suggest the

use of partial correlation coefficients, which are measures of the contribution of each uncertain input to the output uncertainty, after removing the effects attributable to other inputs. These coefficients are useful when there are significant correlations between the inputs (Morgan and Henrion, 1990).

The regression coefficients, m_i, are the partial derivatives of the dependent variable with respect to each of the independent variables. The correlation coefficient reflects the fractions of the variability explained by the individual variables (Zimmerman, 1991). The form of the linear regression equation that gave the best fit used the log of the normalized peak dose and the log of the normalized independent variables, x_n

$$\log \frac{y}{\bar{y}} = b + m_1 \log \frac{x_1}{\bar{x}_1} + m_2 \log \frac{x_2}{\bar{x}_2} + \ldots + m_i \log \frac{x_i}{\bar{x}_i} + \ldots + m_n \log \frac{x_n}{\bar{x}_n} \qquad (4\text{-}7)$$

where b is the intercept, m_i is the coefficient of the regression, and the overbars denote the value of the quantities used for normalization (generally the mean value).

When the antilog of both sides of Eq. (4-7) is computed, the resulting equation becomes

$$\frac{y}{\bar{y}} = 10^b \left(\frac{x_1}{\bar{x}_1} \right)^{m_1} \left(\frac{x_2}{\bar{x}_2} \right)^{m_2} \ldots \left(\frac{x_n}{\bar{x}_n} \right)^{m_n} \qquad (4\text{-}8)$$

After computing the partial derivative of both sides of Eq. (4-8) with respect to the independent variables and rearranging, the equation is reduced to

$$\frac{x_i}{y} \frac{\partial y}{\partial x_i} = m_i \qquad (4\text{-}9)$$

Therefore, the normalized sensitivities are exactly the coefficients of the regression equation using the logs of the normalized peak dose and independent variables. The form of the sensitivities shown by Eq. (4-9) is the same measure calculated by the differential method of Eq. (4-11) in Section 4.1.2.

4.1.1.4   Application of the Kolmogorov-Smirnov and Sign Tests for Determining Important Parameters

The Kolmogorov-Smirnov and Sign tests differ from regression because they are nonparametric; that is, these tests do not require the assumption that the data have prespecified functional forms (e.g., normal).

4.1.1.4.1   The Kolmogorov-Smirnov Test

The Kolmogorov-Smirnov test determines if a set of samples was drawn from a given distribution (Bowen and Bennett, 1988). This test is used to determine if an independent variable is influential by comparing the distribution of a subset of the independent variables,

corresponding to the values from the highest 10 percent of the peak dose realizations, to the theoretical distribution of that variable. If the two distributions are equivalent, peak dose is not sensitive to the variable in question. Conversely, if the distributions are different, the variable in question does have an effect on peak dose. For the present study, there are 4,000 vectors in the entire set, and the subset consists of the 400 vectors corresponding to the top 10 percent of the peak doses. The distribution of the variable in the 4,000-vector set is taken as the theoretical distribution, although it would also be possible to get the theoretical distribution directly from the generating function specified in the Latin Hypercube Sampling routine. The significance of the Kolmogorov-Smirnov test was determined at the 95-percent confidence level.

4.1.1.4.2   The Sign Test

The Sign test is another nonparametric test used to determine if a set of data corresponds to a given theoretical distribution (Bowen and Bennett, 1988). This test is used in a manner similar to the Kolmogorov-Smirnov test. In the Sign test, each observation of the input variable is represented by either a plus sign (+) or a minus sign (−), depending if the variable is greater than or less than the median value estimated by the theoretical distribution. The subset of the input parameter values corresponds to the highest 10 percent of the calculated peak doses. The subset is compared to the theoretical distribution, which, in this case, is assumed represented by the entire set of 4,000 vectors. The significance of the Sign test was determined at the 90-percent confidence level to be consistent with previous total system performance assessment analyses. The Sign test was combined with the Kolmogorov-Smirnov test so that both tests must pass to conclude the hypothesis that the variable is significant is not rejected.

4.1.2   Differential Analysis Technique

Regression analysis of the Monte Carlo results can only determine the most influential parameters when those parameters also have large enough regression coefficients that they are distinguishable from the confounding effects of the simultaneous sampling of all other independent variables. Differential analysis determines sensitivity unambiguously because it deals with changes in only one independent variable at a time. Differential analysis determines sensitivity of parameters only at local points in parameter space and does not consider the wide range of parameter variations like the Monte Carlo method does. However, by determining local sensitivities at several points using the Monte Carlo sampling framework, the local effects can be partially mitigated.

Differential analysis tests were conducted through multiple deterministic runs in which a single input parameter was changed by a known amount compared to its initial baseline value, while all other input parameters were held at a baseline value. The baseline value for this report is a sampled value for the input parameter. The sensitivity of a performance measure (in this case, peak dose for the simulation period) to a parameter is estimated as the first derivative of the performance measure with respect to that parameter

$$\frac{\delta y}{\delta x_i} = \frac{y(x_i, x_2, \ldots, x_i + \Delta x_i, \ldots x_I)}{\Delta x_i} = \frac{y(x_1, x_2, \ldots x_i, \ldots x_I)}{\Delta x_i} \tag{4-10}$$

Usually Δx_i is relatively small (e.g., 10 percent of the parameter value). These estimates of sensitivity are local (i.e., the value of the derivative may change at different points in the sample space). To partially alleviate this concern, the derivative may be evaluated at several points in the sample space. In the analyses presented herein, the derivative is transformed in one of two ways to allow comparison of sensitivity coefficients between parameters with different units. The first transformation is described by

$$S_i = \frac{\delta y}{\delta x_i} \frac{\overline{x}_i}{\overline{y}}$$

(4-11)

where S_i is the dimensionless normalized sensitivity coefficient. These normalized sensitivity coefficients are in the same form as the sensitivities defined by the regression analyses with the log of the normalized variables. Because S_i does not account for the range of the input parameter, a second transformation of the derivative is also performed. In the second transformation, the derivative is multiplied by the standard deviation of the input parameter distribution. This transformation is described by

$$S_\sigma = \frac{\delta y}{\delta x_i} \sigma_{x_i}$$

(4-12)

Baseline cases were run with input parameter values set at seven random points within each parameter distribution range selected using the Latin Hypercube Sampling technique. Seven points may not cover the whole space, but this limitation was imposed for expediency.

4.1.3   Morris Method Technique

The Morris Method (Morris, 1991) considers $\partial y / \partial x_i$ [3] as a random variable and uses the mean and standard deviation of the random variable to determine the sensitivity of y to x_i. A large mean value for $\partial y / \partial x_i$ implies that x_i has a large overall influence on y. A large standard deviation value for $\partial y / \partial x_i$ implies that either x_i has significant interactions with other input parameters or its influence on the y is highly nonlinear. Therefore, both the mean and standard deviation of $\partial y / \partial x_i$ are used to rank the influence of input parameters.

In the Morris method, the random variable, $\partial y / \partial x_i$, is evaluated using the current and previous values of y

$$\frac{\partial y}{\partial x_i} = \frac{y(x_1 + \Delta x_1, x_2, \ldots, x_i + \Delta x_i, \ldots, x_I)}{\Delta x_i}$$

(4-13)

$$- \frac{y(x_1 + \Delta x_1, x_2 + \Delta x_2, \ldots, x_i, \ldots, x_I)}{\Delta x_i}$$

---

[3] Strictly speaking, $\partial y / \partial x$ should be denoted as $\Delta y / \Delta x$ because Δx_i is not necessarily a small value as in the case of differential analysis. Here, the notation is maintained to simplify the comparison with the differential analysis method.

This method is in contrast to the differential analysis method in which $\partial y / \partial x_i$ is evaluated using the current and baseline values of y, as presented in Eq. (4-10).

To compute $\partial y / \partial x_i$, a design matrix was constructed using input variables as shown

$$
\begin{bmatrix}
x_1 & x_2 & \cdots & x_{i-1} & x_i & x_{i+1} & \cdots & x_I \\
\cdots & \cdots & \cdots & \cdots & \cdots & \cdots & \cdots & \cdots \\
x_1 + \Delta_1 & x_2 + \Delta_2 & \cdots & x_{i-1} + \Delta_{i-1} & x_i & x_{i+1} & \cdots & x_I \\
x_1 + \Delta_1 & x_2 + \Delta_2 & \cdots & x_{i-1} + \Delta_{i-1} & x_i + \Delta_i & x_{i+1} & \cdots & x_I \\
x_1 + \Delta_1 & x_2 + \Delta_2 & \cdots & x_{i-1} + \Delta_{i-1} & x_i + \Delta_i & x_{i+1} + \Delta_{i+1} & \cdots & x_I \\
\cdots & \cdots & \cdots & \cdots & \cdots & \cdots & \cdots & \cdots \\
x_1 + \Delta_1 & x_2 + \Delta_2 & \cdots & x_{i-1} + \Delta_{i-1} & x_i + \Delta_i & x_{i+1} + \Delta_{i+1} & \cdots & x_I + \Delta_I
\end{bmatrix}
\begin{matrix}
1 \\ \\ i \\ i+1 \\ i+2 \\ \\ I
\end{matrix}
$$

where $\Delta_i = \Delta x_i$. To construct this matrix, the range of each variable is subdivided into (*p*-1) intervals using *p* equally spaced points. Then x_i values are randomly sampled from these *(p*-1) intervals. It should be noted that each interval represents the left-most value in the original distribution. The increment, Δ ,is now represented by $\Delta_i = p/2(p-1)$.

To implement the Morris Method, the input variables are first normalized using the following

$$
x_i^* = \frac{x_i - x_{i_{min}}}{x_{i_{max}} - x_{i_{min}}}, \quad i = 1, 2, ..., I \tag{4-14}
$$

transformation so the transformed input parameter, x_i^* , ranges from 0 to 1.

To minimize the localization effect from the selection of the baseline value, seven random points in the jointly distributed sample space were selected using the Latin Hypercube Sampling technique for each random variable, $\partial y / \partial x_i$. The steps necessary to obtain the design matrix, which includes these samples, are presented in Appendix A.

4.1.4   The Fourier Amplitude Sensitivity Test Method

Both the differential analysis and the Morris Method handle one input parameter at a time. For a nonlinear computational model, input parameters are likely to have strong interactions. It would be desirable, therefore, to have a sensitivity analysis method that would investigate the influence of all input parameters at the same time. The Fourier Amplitude Sensitivity Test method (Cukier, et al., 1973) does this by first applying trigonometric transforms to the input parameters

$$
x_i = g_i\left(\sin\omega_i s\right), i = 1,2,\ldots,I \tag{4-15}
$$

The trigonometric transforms relate each input parameter, x_i, to a unique integer frequency, ω_i. All transforms have a common parameter, s, where $0 \leq s \leq 2\pi$. As s varies from 0 to 2π, all the input parameters vary through their ranges simultaneously at different rates controlled by the integer frequencies assigned to them through Eq. (4-15). Equally spaced values of s between 0 and 2π are chosen to generate values of x_i in Eq. (4-15). Because trigonometric transforms and integer frequencies are used in Eq. (4-15), the output, y, becomes periodic in s, and discrete Fourier analysis can be used to obtain the Fourier coefficients of y with respect to each integer frequency (Appendix B). The sensitivity of y to x_i is measured by the magnitudes of the Fourier coefficients for ω_i, and y is considered sensitive to the input parameters if the Fourier coefficients are relatively large.

The use of integer frequencies causes some errors because of aliasing among Fourier coefficients. The integer frequencies in Eq. (4-15) were chosen to minimize interactions among Fourier coefficients to ensure, as much as possible, that the particular coefficient, A_i (Appendix B), through the particular integer frequency, ω_i, represents only the influence of the corresponding input parameter, x_i. Appendix B explains how the integer frequencies are selected and how the Fourier Amplitude Sensitivity Test method is implemented. Assuming $0 \leq x_i \leq 1$, the trigonometric transformation functions used here were

$$x_i = \frac{1}{2} + \frac{1}{\pi}\arcsin\left[\sin\left(\omega_i s + r_i\right)\right], i = 1, 2, \ldots, I \qquad (4\text{-}16)$$

where r_i and i = 1, 2, ..., I are random numbers. If the range of variation of a parameter is different from [0, 1], Eq. (4-16) can be modified easily.

Currently, implementation of the Fourier Amplitude Sensitivity Test method is limited to 50 input parameters. According to Cukier, et al. (1975), as many as 43,606 realizations are needed to perform a satisfactory analysis on 50 input parameters to avoid aliasing among any 4 Fourier amplitudes.

4.1.5   Parameter Tree Method

The parameter tree method (Appendix C) examines total system output relative sensitivity (i.e., sensitivity of one parameter compared with another) and correlations of output to subgroups of input parameters. In this technique, the Monte Carlo (or Latin Hypercube Sampling) method is used to examine the possible outcomes of a combination of parameter sets. Bins of realizations are constructed based on their input parameter states (e.g., all sampled input parameters above their median value).

To analyze the outputs, y_j, in Eq. (4-1) to determine the sensitivity and correlations of output, y, to subgroups of the input parameters, x_n, n = 1, 2, ..., N, where $N<I$, a tree structure is developed. The parameter tree partitions input parameter space into bins, each bin forming a branch of the tree based on a partitioning (or branching) criterion. The simplest branching criterion is a classification based on parameter magnitude that treats sampled input values as either a $+$ or a $-$ depending on if the sampled value is greater or less than the branching criterion value.

Figure 4-2 depicts a general parameter tree. To explain Figure 4-2 using a system model, numerous realizations are generated for a given scenario class. Next, the realizations are partitioned into two subsets determined by whether the first influential parameter, x_i, is greater than or less than a specified level. Realizations with high values are all treated as $+$ and low values as $-$, regardless of their position within the subset.

Let the number of realizations associated with the two branches be N_{1+} and N_{1-}. Next, the output variable is examined for realizations associated with each branch of the tree. The number of realizations with y greater than a criterion (e.g., mean) are counted for both branches. Let these numbers be L_{1+} ($L_{1+} \leq N_{1+}$) and L_{1-} ($L_{1-} \leq N_{1-}$). The difference between L_{1+}/N_{1+} and L_{1-}/N_{1-} is a measure of the sensitivity of y to x_1. The procedure is repeated in each of these two subsets with the next influential parameter to be considered (and so on) until each of the influential parameters is considered. This procedure determines 2^M bins of realizations where M is the number of influential parameters. Note that not every sampled parameter in the system model needs to be considered if a subset of the sampled parameters satisfactorily explains the system behavior of interest. Sensitivity measures similar to those explained for one parameter are developed for a set of parameters (Jarzemba and Sagar, 2000).

4.1.6   Fractional Factorial Method

Factorial methods are used in designing experiments (Box and Hunter, 1961) and more recently, in testing computer codes and models (Schmidt and Launsby, 1991). The basic approach is to sample each of the parameters at 2 or 3 fixed values (e.g., for two parameter values, perhaps choosing the 5th and 95th percentile of the distribution to represent low and high values), and then run the model to determine the response. A full-factorial design looks at all possible combinations of sampled input variables; (e.g., for two parameter values, there would have to be 2^N samples, where N is the number of variables). Because the current problem has as many as 330 sampled variables, and each run requires several minutes of computer time, a full-factorial design is infeasible.

Fractional factorial designs require fewer than 2^N runs, but may produce ambiguous results. For example, a so-called level-4 design for 330 variables requires 2,048 runs. Such a level-4 experimental design can yield results for which the main effects of all variables are distinct from each other and two-way interactions of other variables but can be confounded by some 3-way or higher interactions of other variables. It is possible, however, to use other information generated in the runs to determine, in many cases, if the results of the fractional factorial design are truly measuring main effects or higher-order interactions.

In general, the fractional factorial analysis for this report was conducted in the following steps: (i) develop a fractional factorial design for all variables in the problem considering the largest number of runs that reasonably can be handled; (ii) from the results of the preliminary screening, perform an analysis of variance (ANOVA) to determine those variables that appear significant at a specified significance level; (iii) screen further the list of statistically significant variables on the basis of information other than the ANOVA results; and (iv) repeat the analyses with a refined set of variables and higher-resolution designs until results are acceptably unambiguous.

Results are presented as the F statistical parameter, which is a measure of the probability that the variable, or interaction of several variables, is significant to a specified degree of confidence,
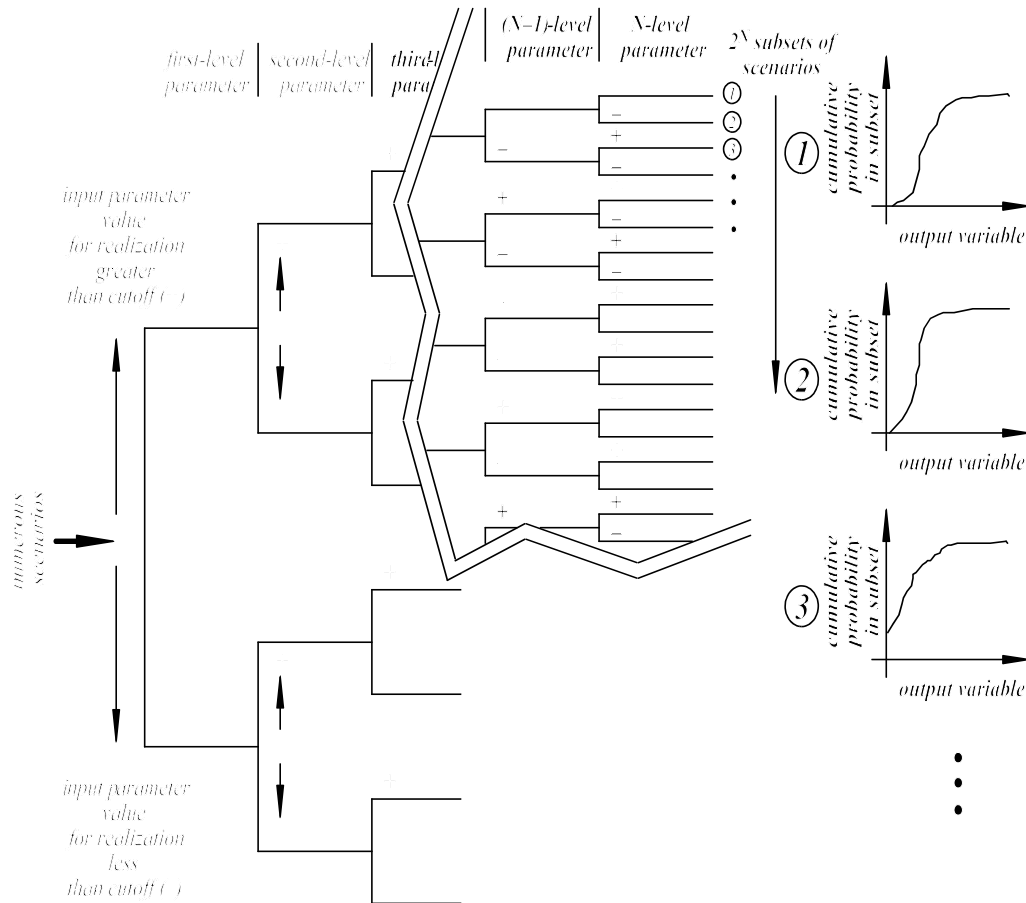
Figure 4-2. General Parameter Tree

with a large *F* being higher confidence. The full-factorial results are also used to draw detailed tree diagrams that show explicitly the direct effect of the high and low parameters in combination on peak dose.

4.1.7 Cumulative Distribution Function-Based Sensitivity Method

The cumulative distribution function sensitivity method is a fast and accurate method for analysis of results from computationally intensive and numerically complex models with large numbers of variables. The framework of the method is based on a hybrid approach that combines sampling that explores the parameter space and advanced reliability methods that focus the analysis at the tail of the probability distribution (Wu, 1994; Mohanty and Wu 2001). The details of this method can be found in Appendix D. The method is briefly described next.

The cumulative distribution function of a response function $Y = Y(X)$ can be represented as

$$p = F_Y(y_0) = P(Y < y_0) = \int \cdots \int_\Omega f_x(x)dx \qquad (4\text{-}17)$$

where $x = (x_1, x_2, \cdots, x_L)$ is a vector of L input parameters, and Ω is the region of X for $Y(X)<y_0$. From Eq. (4-17), the sensitivity of p with respect to a distribution parameter, θ, can be formulated as

$$\frac{\partial p}{\partial \theta} = \int \cdots \int_\Omega \frac{\partial f_x}{\partial \theta}dx \qquad (4\text{-}18)$$

which can be presented by an expectation function

$$\frac{\partial p | p}{\partial \theta | \theta} = \int \cdots \int_\Omega \frac{\theta \partial f_x}{f_x \partial \theta}\left(\frac{f_x}{p}\right)dx = E\left[\frac{\theta \partial f_x}{f_x \partial \theta}\right]_\Omega \qquad (4\text{-}19)$$

in which (f_x / p) is the sampling density function that corresponds to the sampling region, Ω.

The expected value in Eq. (4-19) is estimated using the samples in Ω. By applying this method for different percentiles, the sensitivities for the entire cumulative distribution function of Y can be estimated.

Based on Eq. (4-19), the two sensitivity measures developed are S_{σ_i} (standard deviation sensitivity) and S_{μ_i} (the mean sensitivity). These sensitivities are defined as

$$S_{\sigma_i} = \frac{\partial p / p}{\partial \sigma_i / \sigma_i} \qquad (4\text{-}20)$$

$$S_{\mu_i} = \frac{\partial p / p}{\partial \mu_i / \sigma_i} \qquad (4\text{-}21)$$

where μ_i is the mean and σ_i is the standard deviation of the random variable x_i. In Eqs. (4-20) and (4-21), the standard deviations, σ_i, are used as standardization factors to make the sensitivities dimensionless.

The function within the expectation operator in Eq. (4-19) can be computed by using standard numerical methods to differentiate the density function. The computation of the function, however, becomes difficult when the random variables x_i's are nonnormal and correlated. The sensitivity analysis can be simplified if the original random variables are transformed to standard normal variables using

$$u_i = \Phi^{-1}\left(F_{x_i}(x_i)\right) \qquad (4\text{-}22)$$

4-13

The transformation results in generating u_i samples for each random variable for the sensitivity analyses. For correlated x_i's, the variables produced remain correlated, and their sensitivities are correlated as well. The correlation, however, does not affect the identification of the significant variables because the adopted identification procedure was based on testing whether a variable has a zero sensitivity. The hypothesis can be tested without using the correlations.

By applying Eq. (4-22) to define the joint probability distribution function in Eq. (4-19), the sensitivities in Eqs. (4-20) and (4-21) can be simplified to (Wu, 1994)

$$S_{\sigma_i} = E\left[u_i^2\right]_\Omega - 1 \tag{4-23}$$

$$S_{\mu_i} = E\left[u_i\right]_\Omega \tag{4-24}$$

These sensitivities can be used to identify important variables. Note that each sampled parameter is treated as a random variable and is represented through x_i. Two new sensitivity measures that are consistent with the peak expected dose regulatory criterion are $\overline{S}_{Y_\mu}$ and $\overline{S}_{Y_\sigma}$. These two measures are referred to as performance mean-based measures. These measures were originally developed in an internal research and development project at Southwest Research Institute and have been applied in this report to the performance assessment results. These two sensitivity measures can be expressed as

$$\overline{S}_{Y_\mu} = \partial\mu_Y / \partial\mu_{x_i} = \frac{1}{k}\sum_{j=1}^{k}\left[u_i Y\right]_j \tag{4-25}$$

and

$$\overline{S}_{Y_\sigma} = \partial\mu_Y / \partial\sigma_{x_i} = \frac{1}{k}\sum_{j=1}^{k}\left[\left(u_i^2 - 1\right)Y\right]_j \tag{4-26}$$

To implement the method, the following steps are followed. A value, k, for random sampling is selected. Based on k, confidence limits are constructed for $\overline{S}_{Y_\sigma}, \overline{S}_{Y_\mu}$, or other sensitivity measures for non-participating random variables. Then k realizations of the response variable are computed based on the k sets of random input parameters. The k realizations of sampled values are then sorted and divided into a variety of regions. In each region, each set of an input parameter that corresponds to the realizations of the response variable is identified. For each input parameter, the identified samples are mapped to standardized normal variables. The standardized normal samples are used to compute sensitivities. The computed sensitivities are compared with the confidence limits to identify the influential random variables. If the calculated sensitivities are outside the acceptance limits (Mohanty and Wu, 2001), the alternative hypothesis is accepted that the sensitivities are greater than zero at the corresponding confidence level. If the calculated point lies well outside the limits, the variable is likely important. In such cases, the magnitudes of the sensitivities may be used to rank the important variables. The number of samples can be adaptively increased to reduce the sampling error and identify the important variables and their ranking with confidence.

4.2 Sensitivity Analysis Results from Monte Carlo Runs

This section presents the sensitivity and uncertainty analyses results generated using methods described in Section 4.1. Statistical results of the 4,000-vector Monte Carlo runs, which are treated separately from the differential analysis, Morris method, and the Fourier amplitude sensitivity test method, will be presented first in this section. A comparison of the results of the different methods will be presented in subsequent sections.

4.2.1 Procedure for Screening Monte Carlo Sensitivity Results

The Monte Carlo simulation results were screened to estimate which variables were likely to be influential and provide an estimate of the sensitivity coefficients.

The first part of the analyses involved preliminary screening. This stage of the analyses used a variety of techniques to determine in gross terms if an independent variable affects dose. All variables that passed any of the screening tests were included in the subsequent analyses. For all analyses, zero values of dose were eliminated from the data sets because they cannot be log transformed. For each simulation period (10,000 or 100,000 years), the following procedures were employed:

- t-statistic test for single linear regression of dose versus each variable
  — Raw variables
  — Rank of variables

- Stepwise linear regression
  — Normalized variables
  — Log of normalized variables
  — Ranks of variables

- Nonparametric tests
  — Kolmogorov-Smirnov test and Sign test combined

4.2.1.1 Sensitivity Results from Monte Carlo Analysis

This section presents the sensitivity results from the statistical analysis of a 4,000-vector Monte Carlo analysis of the basecase for 10,000- and 100,000-year simulation periods. The screening and regression analyses are summarized in Tables 4-1 and 4-2 for the 10,000- and 100,000-year simulation periods. The column headings in Tables 4-1 and 4-2 have the following explanations:

- Variable Name—The abbreviated name of the independent variable appearing potentially sensitive in any of the screening analyses. A complete list of the variable names is in Appendix E.

- Kolmogorov-Smirnov + Sign Test—The rank of variables that passed both the Kolmogorov-Smirnov and Sign tests.

- t-Norm—The rank of the t-value of a single-variable regression of the normalized variables greater than 1.96 (95-percent confidence level).

Variable Name	KS + Sign Test	t-Norm	Step Raw	Step Rank	t-Rank	Step Lnorm	Overall Rank
AAMAI@S	5	5	—	4	4	7	7
MAPM@GM	—	—	—	10	—	15	—
FOC-R	10.5	10	9	5	5	6	8
FOCTR	7	9	8	3	3	8	6
TempGrBI	—	—	—	7	8	10	—
DSFailTi	3.5	4	4	1	1	4	1
WPFlowMF	2	8	6	2	2	1	3
SbArWt%	3.5	1	1	9	6	3	2
WP-Def%	6	2	2	8	9	5	5
PSFDM1	1	3	3	6	7	2	4
MPrm_TSw	8	12	—	—	10	—	—
ARDSAVNp	12	—	—	4	—	—	—
DTFFAVIF	10.5	6	5	11	12	9	9
WPRRG@20	9	7	7	12	15	11	10
gen_dwc5	—	13	11	—	—	—	—
genKDsl	—	11	10	—	—	—	—

Table 4-1. Ranks of Significant Variables for 10,000 Years from Statistical Tests. Appendix E Provides a Description of the Variables.

- Step Raw—The rank of the variables from stepwise regression of the normalized variables.

- Step Rank—The rank of the variables from stepwise regression of the ranks of the variables.

- t-Rank—The rank of the t-value of a single-variable regression of the rank-transformed variables greater than 1.96 (95-percent confidence level).

- Step Lnorm—The rank of the variables from stepwise regression of the log of the normalized variables.

- Overall Rank—The reciprocal ranks of the six sensitivity tests. For each variable, take the reciprocal of each non-zero rank from each of the six tests and sum over all six tests. The overall rank is the rank of the sum of the reciprocals.

Variable Name	K-S+Sign Test	t-Norm	Step Raw	Step Rank	t-Rank	Step Lnorm	Overall Rank
AAMAI@S	8.5	4	—	—	4	8	8
MAPM@GM	2.5	—	—	11	18	9	9
AA_1_1	—	3	3	3	3	3	3
WPFlowMF	11	22	9	5	7	4	6
SbArWt%	4	2	2	2	1	1	2
PSFDM1	1	1	1	1	2	2	1
InitRSFP	—	10	7	9	—	15	—
Solbl-Np	15.5	14	8	8	—	10	—
SFWt%S44	—	17	12	13	—	—	—
SFWt%C2	—	25	—	—	16	17	—
MPrm_TSw	—	8	—	—	6	—	—
FPrs_CHz	—	18	—	15	—	—	—
IPPFSTFF	12.5	11	10	11	19	14	—
ARDSAVAm	6	16	—	—	9	—	—
ARDSAVNp	2.5	6	—	—	5	5	4
ARDSAV_U	9.5	15	—	—	10	—	—
ARDSAVPu	5	5	4	—	8	—	7
ARDSAVRa	14	29	—	14	—	—	—
DTFFAVIF	7.5	7	5	6	11	7	5
WPRRG@20	14	9	6	7	17	13	—
PWPRRG20	—	—	—	—	15	12	—
gen_ifi	16.5	12	11	10	13	11	10
genovitC	—	27	—	16	—	19	—

Table 4-2. Ranks of Significant Variables for 100,000 Years from Statistical Tests

Results for 10,000-Year Simulation Period

For each of the statistical tests, the resulting regression coefficients were sorted; the highest values received the best scores. Parameter sensitivities that ranked below the 95th percentile, either as t-statistic or F-statistic, were eliminated from consideration (rank = ∞). The overall rank for a variable consisted of two parts: (i) the number of times the variable appeared in the six tests with a finite rank (0 to 6) and (ii) the sum of the reciprocal of the rank for the six tests. A variant of the second test replaced the rank with its square, but the results did not change the conclusions. The top 10 variables in order of apparent importance from statistical measures are (i) DSFailTi, (ii) SbArWt%, (iii) WPFlowMF, (iv) PSFDM1, (v) WP-Def%, (vi) FOCTR, (vii) AAMAI@S, (viii) FOC-R, (ix) DTFFAVIF, and (x) WPRRG@20. The description of these variables can be found in Appendix E.

Results for 100,000-Year Simulation Period

Like with the 10,000-year results, the regression results were combined to give a single overall score that included the number of times the variable appeared in the six tests and the sum of the reciprocal of the rank for the six tests. The top 10 variables in order of apparent importance are (i) PSFDM1, (ii) SbArWt%, (iii) AA_1_1, (iv) ARDSAVNp, (v) DTFFAVIF, (vi) WPFlowMF, (vii) ARDSAVPu, (viii) AAMAI@S, (ix) MAPM@GM, and (x) WPRRG@20.

Regression Results for Extrusive Volcanism Parameters

The sensitivity analyses for volcanism parameters were treated separately because, in most cases, extrusive volcanic doses would be much larger than nonvolcanic groundwater doses, and, therefore, the groundwater doses can be neglected. It is important to note that the sensitivity analyses for igneous activity parameters in this report use conditional dose (i.e., does not factor in the volcanism event probability). The influential parameters may be different if the igneous activity event probability is accounted for. With probability weighting, the large ground surface dose with low probability can be comparable to small groundwater dose with high probability. Several groundwater dose parameters may then be more important than the ground surface dose parameters when the igneous activity contribution to the peak expected dose is reduced.

The extrusive volcanism model was run for 1,000 Latin Hypercube Sampling vectors, varying the parameters VC-Dia, WindSpd, VE-Durat, VE-Power, AshMnPLD, ABMLAAsh, and AMLASoil. Because there were only seven variables, only a stepwise regression of the raw variables and single parameter t-test were run for sensitivity, and both gave the same results. The tests showed six significant parameters in the following order: VE-Power, VC-Dia, WindSpd, VE-Durat, ABMLAAsh, and AshMnPLD. The variable AMLASoil was below the 5-percent significance level for inclusion.

4.3 Analysis of Sensitivity from Nonparametric Methods

4.3.1 Results from Differential Analyses

Differential analyses were performed using the TPA Version 4.1 code with the basecase. A total of 330 input parameter values were perturbed for each series. The input parameters perturbed are the sampled parameters in the TPA code.

Seven random sets (considered adequate for obtaining a stable average) of input parameters were evaluated. Perturbations to the parameters in these random sets were selected so that the parameter values were maintained in their defined ranges. The selection of random values yields calculations similar to one realization of a probabilistic TPA code run. The perturbations (1 percent) are applied to the baseline (i.e., local) parameter value. The percentage is that of the range of the distribution [i.e., (maximum value – minimum value) × 0.01] rather than that of the baseline value.

In the TPA Version 4.1 code, transport through the unsaturated zone stratigraphic units is not considered for units where the groundwater residence time is less than 10 years or 10 percent of the residence time for the entire unsaturated zone below the repository (Mohanty and McCartin, 1998). Differential analyses will result in the peak dose showing no sensitivity to parameters that describe unsaturated zone properties in those stratigraphic units excluded from the transport calculations. For example, when all parameters were set at their mean values, the unsaturated zone portion of NEFTRAN was omitted for a majority of the subareas. Thus, sampled unsaturated zone flow and transport parameters did not show any sensitivity in these calculations. When the transport times in the subunits of the unsaturated zone that control the bulk of the unsaturated zone transport are short, however, it is unlikely that any of the unsaturated zone parameters would have a substantial effect on the peak dose, therefore the aforementioned exclusion of stratigraphic units should not significantly affect results of the differential analyses.

For all sets of the random parameters, the waste packages did not fail from either seismicity or corrosion in the 10,000-year simulated period but did fail from corrosion within the 100,000-year simulated period. The baseline dose values in these cases are solely caused by initially defective waste packages.

The results of the differential analysis are shown for simulation periods of 10,000 and 100,000 years in Tables 4-3 and 4-4 for the basecase. The top 10 parameters are based on the mean of S_σ as shown in Eq. (4-12). These sensitivities were calculated using the arithmetic mean of the derivative weighted by the standard deviation of the input parameter. This measure was used to sort the input parameters in descending order because it reflects both the absolute value of peak dose and the uncertainty in the independent variables. This sensitivity measures the response of peak dose to each of the independent variables weighted by their standard deviation. The standard deviations are determined by the parameter range and distribution used in the Monte Carlo analyses. This measure considers the magnitude of the change in peak dose and the uncertainty in the independent variables. For comparison, the normalized sensitivity measure, S_i, in Eq. (4-11) is a relative sensitivity where the slope is scaled by the local values of dose and the independent variable. Therefore, S_i does not depend on whether the baseline dose is small or large, but only on the change in dose relative to the change in the independent variable.

4.3.2　　　　Results from the Morris Method

The Morris Method was applied to the TPA Version 4.1 code results from the basecase scenario. A total of 330 input parameters were investigated. A 2,317 × 330 matrix was generated and used in sampling input parameters for the 2,317 [(330 + 1) × 7] realizations,

Table 4-3. Top 10 Influential Parameters from Statistical and Nonstatistical Analyses for the 10,000-Year Simulation Period						
Rank	Statistics/ Regression	Differential Analysis	Fractional Factorial	Morris Method	Fourier Amplitude Sensitivity Test Method	Parameter Tree Method	Cumulative Distribution Function Sensitivity
1	DSFailTi	WPFlowMF	DSFailTi	AAMAI@S	DSFailTi	PSFDM1	WPFlowMF
2	SbArWt%	PSFDM1	WPFlowMF	MAPM@GM	gen_PUSF	WPFlowMF	PSFDM1
3	WPFlowMF	DSFailTi	FOCTR	DSFailTi	WPRRG@20	SbArWt%	SbArWt%
4	PSFDM1	SbArWt%	SbArWt%	WPFlowMF	gen_ifi	DSFailTi	WP-Def%
5	WP-Def%	genKDsTc	WP-Def%	gen_PUSF	ARDSAVNp	FOCTR	AAMAI@S
6	FOCTR	SFWt%I2	PSFDM1	WPRRG@20	InvMPerm	*Chlorid	DSFailTi
7	AAMAI@S	AAMAI@S	AAMAI@S	ARDSAVNp	MPrm_PPw	Solbl-Np	DTFFAVIF
8	FOC-R	SFWt%I1	WPRRG@20	IPPFSTFF	AAMAI@S	gen_hirP	WPRRG@20
9	DTFFAVIF	SFWt%I10	DTFFAVIF (*)	PSFDM1	SFWt%I2	SSMOV404	ARDSAVNp
10	WPRRG@20	WPRRG@20	InvMPerm (*)	SbArWt%	IPPFSTFF	AAMAI@S	FOCTR

Abbreviation	Description		Abbreviation	Description
AAMAI@S	ArealAverageMeanAnnualInfiltrationAtStart[mm/yr]		PSFDM1	Preexponential_SFDissolutionModel2
ARDSAVNp	AlluviumMatrixRD_SAV_Np		SbArWt%	SubAreaWetFraction
DSFailTi	DripShieldFailureTime[yr]		SFWt%I1	SFWettedFraction_Initial_1
DTFFAVIF	DistanceToTuffAlluviumInterface[km]		SFWt%I2	SFWettedFraction_Initial_2
FOC-R	FractionOfCondensateRemoved[1/yr]		SFWt%I10	SFWettedFraction_Initial_10
FOCTR	FractionOfCondensateTowardRepository[1/yr]		SFWt%S17	SFWettedFraction_SEISMO1_7
gen_hirP	HomeIrrigationRatePB[in/yr]		Solbl-Np	SolubilityNp[kg/m3]
gen_ifi	InterceptionFraction/Irrigate		SSMOV404	VerticalExtentOfRockFall4_4[m]
gen_PUSF	PlantUptakeScaleFactor		TempGrBI	TemperatureGradientInVicinityOfBoilingIsotherm[K/m]
genKDsTc	KD_Soil_Tc[cm3/g]		WP-Def%	DefectiveFractionOfWPs/cell
InvMPerm	InvertMatrixPermeability[m^2]		WPFlowMF	WastePackageFlowMultiplicationFactor
IPPFSTFF	ImmobilePorosityPenetrationFraction_STFF		WPRRG@20	WellPumpingRateAtReceptorGroup20km[gal/ day]
MAPM@GM	MeanAveragePrecipitationMultiplierAtGlacialMaximum		*Chlorid	ChlorideMultFactor
MPrm_PPw	MatrixPermeability_PP2_[m2]			
MPrm_TSw	MatrixPermeability_TSw_[m2]			

*These parameters are included for reference, but are below the 5-percentile cutoff from analysis of variance probability.

	Table 4-4. Top 10 Influential Parameters from Statistical and Nonstatistical Analyses for the 100,000-Year Simulation Period					
Rank	Statistics/ Regression	Differential Analysis	Fractional Factorial	Morris Method	Fourier Amplitude Sensitivity Test Method	Parameter Tree Method
1	PSFDM1	WPFlowMF	PSFDM1	ARDSAVNp	PSFDM1	PSFDM1
2	SbArWt%	PSFDM1	WPFlowMF	WPRRG@20	gen_ifi	SbArWt%
3	AA_1_1	ARDSAVNp	ARDSAVNp	gen_ifi	InvMPerm	ARDSAVNp
4	ARDSAVNp	SbArWt%	SbArWt%	DTFFAVIF	SFWt%C9	AA_1_1
5	DTFFAVIF	genKDsTc	SFWt%C2	MPrm_PPw	gen_PUSF	WPFlowMF
6	WPFlowMF	WP-Def%	gen_ifi	InvMPerm	WPFlowMF	SSMO-RPR
7	ARDSAVPu	AA_1_1	WPRRG@20	gen_PUSF	ARDSAVNp	ARDSAVAm
8	AAMAI@S	Solbl-Np	AAMAI@S	AAMAI@S	WPRRG@20	SFWt%S29
9	MAPM@GM	DSFailTi	—	genlvitC	SFWt%C1	AAMAI@S
10	WPRRG@20	gen_AUSF	—	InitRSFP	genlvitC	MAPM@GM

Abbreviation	Description		Abbreviation	Description
AA_1_1	AA_1_1[C/m2/yr]		InvMPerm	InvertMatrixPermeability[m^2]
AAMAI@S	ArealAverageMeanAnnualInfiltrationAtStart[mm/yr]		MPrm_PPw	MatrixPermeability_PP2_[m2]
ARDSAVNp	AlluviumMatrixRD_SAV_Np		PSFDM1	Preexponential_SFDissolutionModel2
DSFailTi	DripShieldFailureTime[yr]		SbArWt%	SubAreaWetFraction
DTFFAVIF	DistanceToTuffAlluviumInterface[km]		SFWt%C1	SFWettedFraction_Corrosion_1
gen_AUSF	AnimalUptakeScaleFactor		SFWt%C9	SFWettedFraction_Corrosion_9
gen_ifi	InterceptionFraction/Irrigate		Solbl-Np	SolubilityNp[kg/m3]
gen_PUSF	PlantUptakeScaleFactor		WP-Def%	DefectiveFractionOfWPs/cell
genKDsTc	KD_Soil_Tc[cm3/g]		WPFlowMF	WastePackageFlowMultiplicationFactor
genlvirtC	LeafyVegetableIrrigationTimeCB[mo/yr]		WPRRG@20	WellPumpingRateAtReceptorGroup20km[gal/day]
InitRSFP	InitialRadiusOfSFParticle[m]			
	Note new entries in table ARDSAVPu, SFWt%C2, MAPM@GM			

which produced 7 samples for each $\partial y / \partial x_i$. These samples were used to calculate the mean and standard deviation for each $\partial y / \partial x_i$. Seven samples were chosen to be consistent with the differential analysis method.

Figures 4-3 and 4-4 show graphs for the values of mean (abscissa) and standard deviation (ordinate) of $\partial y / \partial x_i$ values for the 10,000-and 100,000-year simulated periods. As described earlier, the greater the distance $\partial y / \partial x_i$ for parameter x_i is from zero, the more influential parameter x_i is. A point with large values of both mean and standard deviation suggests that the corresponding input parameter has a strong nonlinear effect itself and also strong interactive effects with other parameters on the output.

The top 10 most influential input parameters identified by the Morris Method are listed in Table 4-3 for the 10,000-year simulation period and in Table 4-4 for the 100,000-year simulation period, where each parameter was normalized according to Eq. (4-14). For the 10,000-year simulation period, the top 10 parameters are (i) AAMAI@S, (ii) MAPM@GM, (iii) DSFailTi, (iv) WPFlowMF, (v) gen_PUSF, (vi) WPRRG@20, (vii) ARDSAVNp, (viii) IPPFSTFF, (ix) PSFDM1, and (x) SbArWt%. The majority of these parameters are flow parameters that control the volume of water contacting spent nuclear fuel and the time at which the contact begins. The remaining parameters are related to calculations regarding the spent nuclear fuel-dissolution rate, transport properties in alluvium, dilution of radionuclide concentrations, and plant uptake in the biosphere.

For the 100,000-year simulated period, 3 of the parameters are related to biosphere calculations, and 2 are flow rate parameters that also were ranked for the 10,000-year simulated period. The parameter WPRRG@20 {well pumping rate for farming receptor group located at or beyond 20 km [12.4 mi] from Yucca Mountain} appears in both 10,000- and 100,000-year simulated periods, as well as some parameters related to transport properties in alluvium and spent nuclear fuel dissolution. The sensitivity of dose to the well pumping rate may no longer be relevant because this value is fixed at 10,140 m³/day [3,000 acre-ft/yr] in the final regulation.

The most influential parameters from the Morris Method analysis for the igneous activity disruptive event scenario in the 10,000-year simulated period are shown in Table 4-5. The top 10 influential parameters identified by the Morris method are (i) ABMLAAsh, (ii) WindSpd, (iii) VC-Dia, (iv) VE-Power, (v) VE-Durat, (vi) VEROI-Tn, (vii) AshMnPLD, (viii) VEi/e-R#, (ix) SFWt%V0, and (x) PSFDM1.

The results contrast with the regression-method-based results presented in Section 4.2.1.1 because the latter section used only the peak dose from direct releases resulting from extrusive igneous activity. The top six parameters identified by this method are identical to the top six identified by the statistical method in Section 4.2.1.1, though the ranking is different. As mentioned earlier, these six parameters pertain to dose from ground surface release caused by extrusive igneous events. The Morris Method also identified SFWt%V0 and PSFDM1 among the top 10 parameters, which are relevant to dose from groundwater release from intrusive igneous activity. Table 4-5 also shows that most parameters among the top 10 parameters from the basecase also appear as important among the top 20 parameters in the conditional igneous activity dose calculation. It is important to note that the sensitivity analyses for igneous activity
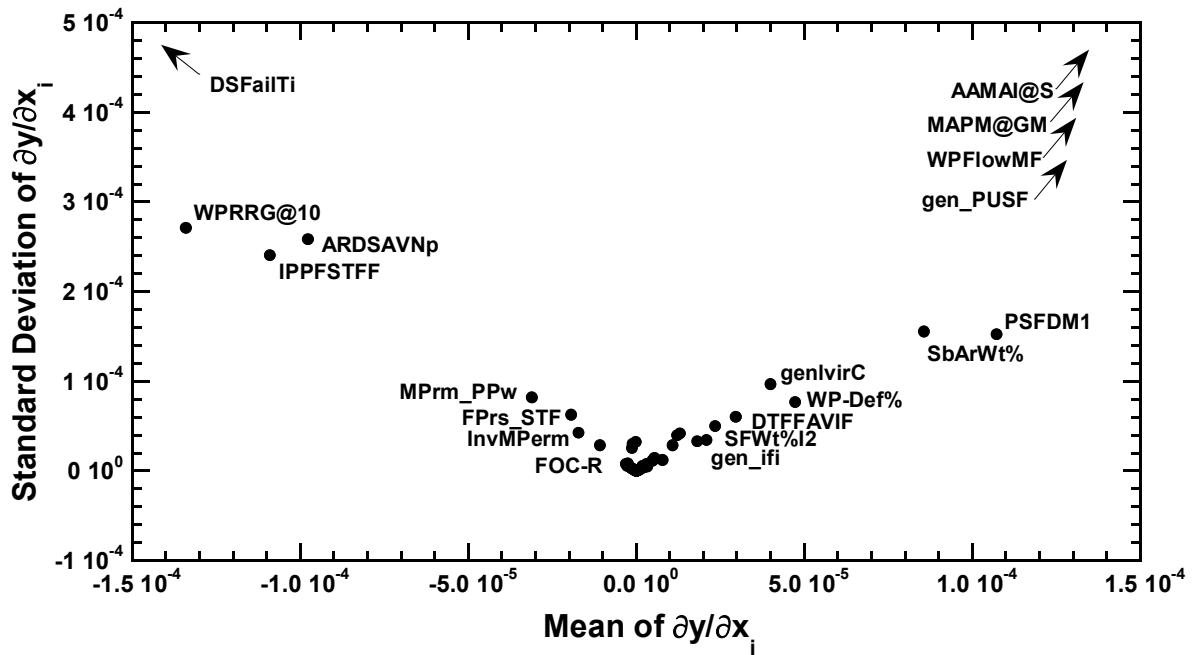
Figure 4-3. Results from the Morris Method from the Basecase for the 10,000-Year Simulation Period. Arrows Indicate the Associated Points are Outside the Graph.
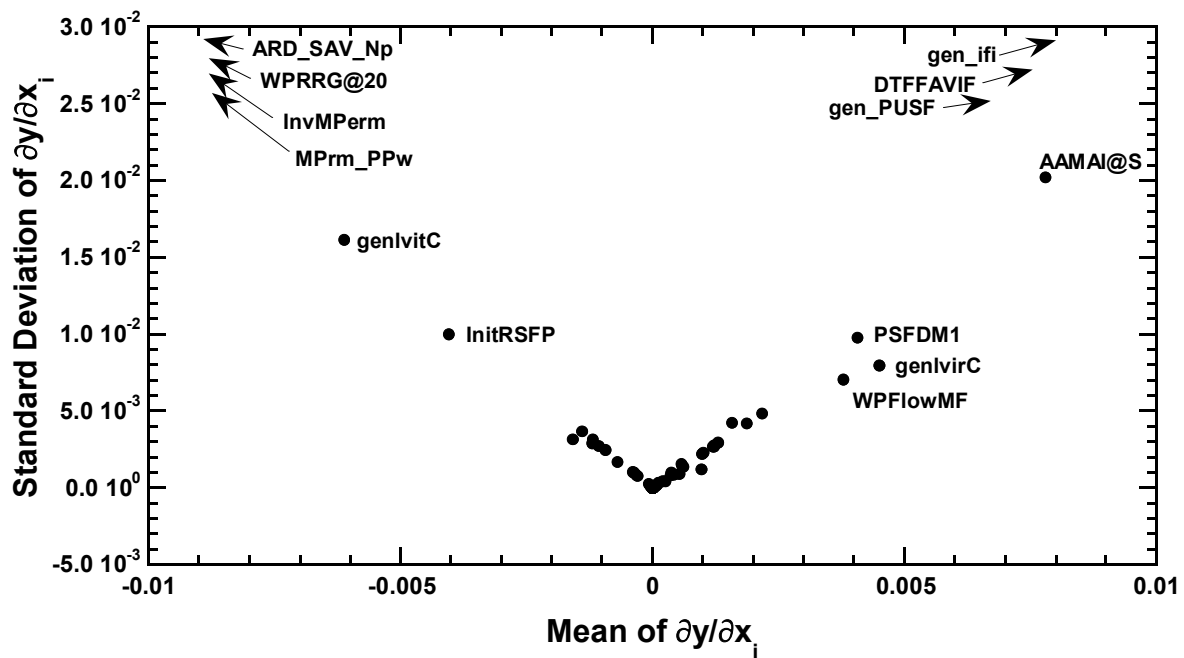
Figure 4-4. Results from the Morris Method from the Basecase for the 100,000-Year Simulation Period. Arrows Indicate the Associated Points are Outside the Graph.

parameters used conditional dose (i.e., did not factor in the volcanism probability). The influential parameters may be different if the igneous activity event probability is accounted for, that is, several groundwater parameters become more important (see explanation in Section 4.2.1.1).

For comparison purposes, sensitivities were computed using two performance measures: (i) the contribution of each realization to the overall peak risk (the overall peak risk will occur at a single point in time, and each realization will contribute to this single overall peak) and (ii) the peak dose from each realization. The relative sensitivity for the top 20 influential parameters identified using these 2 performance measures is presented in Figures 4-5 and 4-6. The relative sensitivity on the y-axis shows the relative influence the parameter has on the output variability. Although many similarities are identified in the results comparing both methods, the few differences provide useful insights. Four variables (SFWt%I10, SFWt%I5, SFWt%I3, and SFWFI1 in Figure 4-6) do not appear in the sensitivity analysis of dose corresponding to the peak expected dose shown in Figure 4-5. Four parameters (genlvirc, Morm-PPw, DTFFAVIF, and Fprs-STF in Figure 4-5) identified by the first method do not appear in the list identified by the second method. The rankings from the two methods were also somewhat different. For example, parameter DSFailTi in Figure 4-5, which appears as the 3rd most important parameter in the 1st method, is ranked 20th using the second method (Figure 4-6). No change in rank was observed only for AAMAI@S and MAPM@GM, the top two parameters in both methods.

In Figures 4-5 and 4-6, the variable DSFailTi ranks high in importance for peak of the realizations and low in importance for time of the peak expected dose. When using the criterion for peak of the expected dose, parameters like DSFailTi, which determine mainly the time of the peak dose within a realization, will show less sensitivity than parameters that determine mainly the amplitude of the peak. This is because a parameter that causes the peaks to be dispersed in time leads to a temporal nonalignment of the realization peaks that, when averaged over the realizations, leads to a lower peak of the expected dose curve.

4.3.3   Results from the Fourier Amplitude Sensitivity Test Method

In this report, the Fourier amplitude sensitivity test method is applied to the 20 parameters identified by the Morris Method presented in Table 4-6 for the two simulation periods. For the 20 parameters, only 4,174 realizations are needed to avoid aliasing among any 4 Fourier amplitudes (Appendix B). To account for the range of an input parameter, each Fourier amplitude was multiplied by the standard deviation of the corresponding input parameter as defined by Eq. (4-12). Ranking for the top 10 parameters using the Fourier amplitude sensitivity test method is listed in Tables 4-3 and 4-4 for the 10,000- and 100,000-year simulation periods.

It should be noted that the analysis presented here is limited by the initial selection of 20 parameters from the Morris Method analysis. Thus, some influential parameters may be identified by other nonstatistical methods but not by the Fourier amplitude sensitivity test method.

Rank	Parameter Identification	Parameter Abbreviation	Parameter Description
			Table 4-5. Top 20 Influential Parameters Identified by the Morris Method in the Igneous Activity Case Contributing to Both Groundwater and Ground Surface Releases
1	329	ABMLAAsh	Mass of soil in the air above a fresh volcanic ash blanket
2	325	WindSpd	Wind speed
3	322	VC-Dia	Conduit diameter
4	327	VE-Power	Volcanic event power
5	326	VE-Durat	Volcanic event duration
6	317	VEROI-Tn	Time of next volcanic event
7	328	AshMnPLD	Relative size of ash and spend nuclear fuel particulates from a volcanic event
8	318	VEi/e-R#	Random number to determine volcanic event type
9	80	SFWt%V0	Spent nuclear fuel wet fraction for volcanic events
10	63	PSFDM1	Preexponential factor for spent nuclear fuel-dissolution rate from ($mgm^{-2}d^{-1}$)
11	64	InitRSFP	Initial radius of spent nuclear fuel particle—affects spent nuclear fuel alteration rate and transport out of a failed waste package in EBSREL
12	239	WPRRG@20	Well pumping rate for residential receptor group located less than 20 km [12.4 mi] from Yucca Mountain
13	61	SbArWt%	Subarea wet fraction
14	223	IPPFSTFF	Effective fraction of saturted rock matrix accessible to matrix diffusion; during the time scale for transport from source to receptor, used to calculate effective immobile porosity and matrix diffusion mass-transfer rate coefficient in NEFTRAN
15	4	FOC-R	Fraction of water condensate removed in each reflux3 time step
16	1	AAMAI@S	Mean areal average infiltration into the subsurface at the start of a TPA Version 4.1 code run

Table 4-5. Top 20 Influential Parameters Identified by the Morris Method in the Igneous Activity Case Contributing to Both Groundwater and Ground Surface Releases (continued)			
Rank	Parameter Identification	Parameter Abbreviation	Parameter Description
17	244	gen_ifi	Irrigation interception fraction
18	12	DSFailTi	Time of failure of the drip shield
19	235	FPrs_STF	Fracture of saturated tuff porosity
20	203	MPrm_CHv	Calico Hills–nonwelded vitric matrix permeability

4.3.4   Results from the Parameter Tree Method

Figure 4-7 shows the parameter tree based on median values as the branching criterion. A set of 4,000 realizations of the TPA Version 4.1 code was used, and 330 input parameters were sampled for the basecase. In Figure 4-7, column A is the number of realizations of peak dose above the overall median value (i.e., of the 4,000 realizations) in that bin. For example, row 3 in column A shows that 127 of 4,000 realizations have 4 of the important parameters with values above the median, and 1, DSFailTi is below the median. Of these 127 realizations, 123 have peak doses above the median value for all 4,000 realizations $\{3.63 \times 10^{-9}$ Sv/yr $[3.63 \times 10^{-7}$ rem/yr]$\}$. Column B shows that for these 127 realizations, the mean value of peak dose is $\{5.57 \times 10^{-6}$ Sv/yr $[5.57 \times 10^{-4}$ rem/yr]$\}$, and column C shows these 127 realizations accounted for 33.4 percent of the population mean of peak doses. This analysis reinforces the notion that these are indeed influential parameters because slightly less than 3.2 percent of the realizations account for more than 33 percent of the mean from all realizations.

Column D shows an importance factor, R, which is determined as the ratio of the contribution to the overall mean from realizations in that bin to the average contribution of the same number of realizations to the overall mean, that is,

$$R = \frac{\text{fractional contribution to the overall mean dose (Column C)}}{\left(\dfrac{\text{number of realizations in bin}}{\text{total number of realizations}}\right)}$$

$$= \frac{\text{mean peak dose in bin (ColumnB))}}{\text{mean peak dose over all realizations}}$$

(4–27)

Data in columns A–D serve as figures of merit for characterizing the group of realizations in a bin. Two other interesting observations can be made about Figure 4-7. First, the realizations where none or one of the input parameters is a minus (–), account for 51.6 percent of the mean from all realizations (includes 740 of 4,000 realizations). Second, only 6 of 32 bins have importance factors above unity, indicating the output variable distribution is skewed (the 6 bins include 763 of 4,000 realizations). Symbols x_1 to x_5 for this column correspond to the five influential parameters shown in Figure 4-7.
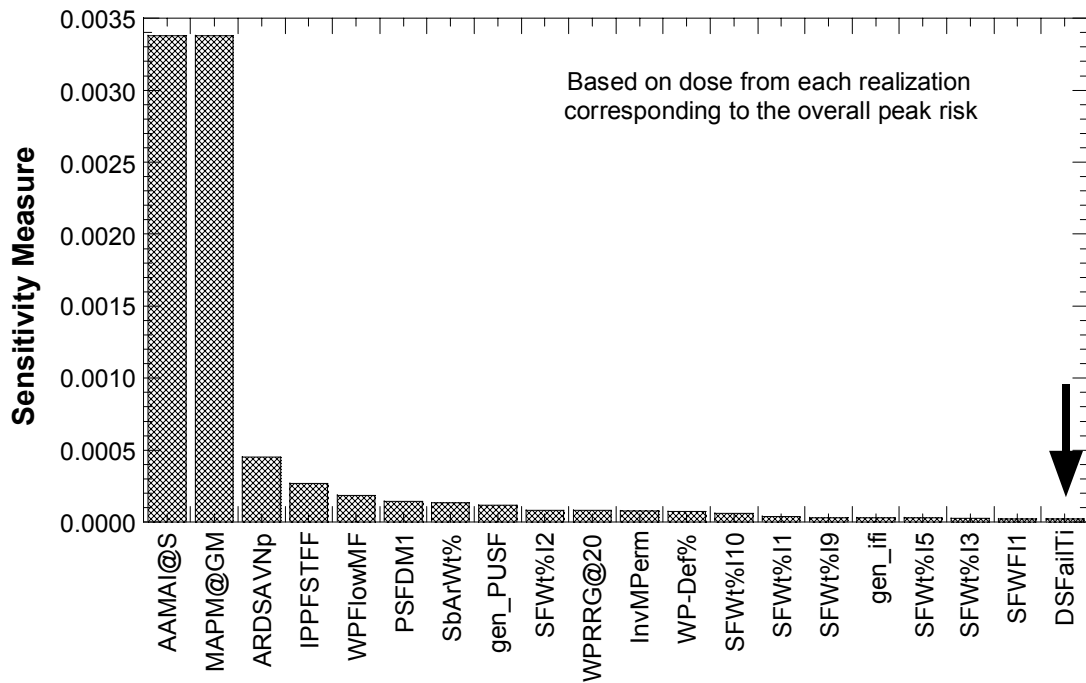
Figure 4-5. Influential Parameters Identified Using the Dose from Each Realization Corresponding to the Time the Peak Expected Dose Occurs

Figure 4-6. Influential Parameters Identified Using the Peak Dose from Each Realization

	10,000 Years		100,000 Years	
Rank	Based on Peak Dose	Based on Dose Corresponding to Peak Expected Dose	Based on Peak Dose	Based on Dose Corresponding to Peak Expected Dose
1	AAMAI@S (*)	AAMAI@S	ARDSAVNp (*)	DTFFAVIF
2	MAPM@GM	MAPM@GM	WPRRG@20	WPRRG@20
3	DSFailTi	ARDSAVNp	gen_ifi	gen_ifi
4	WPFlowMF	IPPFSTFF	DTFFAVIF	ARDSAVNp
5	gen_PUSF	WPFlowMF	MPrm_PPw	IPPFSTFF
6	WPRRG@20	PSFDM1	InvMPerm	InvMPerm
7	ARDSAVNp (*)	SbArWt%	gen_PUSF	MPrm_PPw
8	IPPFSTFF	gen_PUSF	AAMAI@S (*)	AAMAI@S
9	PSFDM1	SFWt%I2	genIvitC	genIvitC
10	SbArWt% (*)	WPRRG@20	InitRSFP	APrs_SAV
11	genIvirC	InvMPerm	PSFDM1	MKDCHvNp
12	WP-Def%	WP-Def%	genIvirC	PSFDM1
13	MPrm_PPw	SFWt%I10	WPFlowMF	InitRSFP
14	DTFFAVIF	SFWt%I1	SFWt%C2	genIvirC
15	FPrs_STF	SFWt%I9	SFWt%C1	FPrs_STF
16	SFWt%I2	gen_ifi	MAPM@GM	SFWt%C2
17	InvMPerm	SFWt%I5	DSFailTi	SFWt%C1
18	SFWt%I9	SFWt%I3	AA_1_1	SFWt%C9
19	SFWt%I1	SFWFI1	APrs_SAV	SFWt%C6
20	gen_ifi	DSFailTi	SFWt%C9	SFWFC1

Abbreviation	Description	Abbreviation	Description
AA_1_1	AA_1_1[C/m2/yr]	InvMPerm	InvertMatrixPermeability[m^2]
AAMAI@S	ArealAverageMeanAnnualInfiltrationAtStart[mm/yr]	MPrm_PPw	MatrixPermeability_PP2_[m2]
ARDSAVNp	AlluviumMatrixRD_SAV_Np	PSFDM1	Preexponential_SFDissolutionModel2
DSFailTi	DripShieldFailureTime[yr]	SbArWt%	SubAreaWetFraction
DTFFAVIF	DistanceToTuffAlluviumInterface[km]	SFWt%C1	SFWettedFraction_Corrosion_1
gen_AUSF	AnimalUptakeScaleFactor	SFWt%C9	SFWettedFraction_Corrosion_9
gen_ifi	InterceptionFraction/Irrigate	Solbl-Np	SolubilityNp[kg/m3]
gen_PUSF	PlantUptakeScaleFactor	WP-Def%	DefectiveFractionOfWPs/cell
genKDsTc	KD_Soil_Tc[cm3/g]	WPFlowMF	WastePackageFlowMultiplicationFactor
genIvirtC	LeafyVegetableIrrigationTimeCB[mo/yr]	WPRRG@20	WellPumpingRateAtReceptorGroup20km [12.4 mi]
InitRSFP	InitialRadiusOfSFParticle[m]		

*Correlated parameters

Table 4-6. Morris Results Derived from Peak Dose and Dose Corresponding to Peak Expected Dose for 10,000- and 100,000-Year Simulation Periods

Using the parameter tree based on median values as the branching criterion, the influential parameters are obtained for 10,000 and 100,000 years. Parameters identified as influential in the 10,000-year simulation period are PSFDM1, WPFlowMF, SbArWt%, DSFailTi, FOCTR, *Chlorid, Solbl-Np, gen_hirP, SSMOV404, and AAMAI@S. Parameters identified as influential in the 100,000-year simulation period are PSFDM1, SbArWt%, ARDSAVNp, AA_1_1, WPFlowMF, SSMO-RPR, ARDSAVAm, SFWt%S29, AAMAI@S, and MAPM@GM. Several parameters, such as SSMOV404 and SSMO-RPR, should be considered spurious because no waste package failures from seismic activity take place in 10,000 years. It should be noted the variables that can be captured by this method are limited by the number of realizations because each new branch of the tree cuts the number of samples by approximately half. Therefore, as the depth of the tree increases, the precision of the method decreases. In this regard it appears that more confidence can be attributed to the first 5 than the last 5 of these 10 influential parameters.

4.3.5 Results from the Fractional Factorial Design Method

The initial screening with the fractional factorial method used a level-4 design for 330 input variables and 2,048 runs. There were two values for each of the input parameter models chosen as the 5th and 95th percentiles of the parameter distributions. The TPA Version 4.1 code was run for this experimental design to calculate the peak doses for the 10,000- and 100,000-year simulation periods. Results from the set of 2,048 were analyzed by ANOVA, using a 95-percent confidence level.

4.3.5.1 Results for the 10,000-Year Simulation Period

The ANOVA yielded a set of 100 potentially important variables for the 10,000-year simulation period. The results for the 10,000-year simulation period were refined to a list of 37 variables by observations from other information generated by the code; for example, it was possible to eliminate all variables related to seismic failure of the waste packages by observing from other code outputs that there were no seismic failures in any of the runs.

Using the reduced set of 37 variables from the initial screening, another level-4 factorial design, which requires 2,048 runs was set up. With only 37 variables, it was possible to observe 2- and 3-way interactions that are combinations of the main effects and to make inferences about the 4th and higher-order interactions of those variables that might be explored by additional factorial designs. Several possible variables that showed significant main effects were eliminated by examining their aliases and judging that they were likely 3-way or higher-order effects. This intermediate list consisted of eight variables: AAMAI@S, FOCTR, DSFailTi, WPFlowMF, SbArWt%, WP-Def%, PSFDM1, and WPRRG@20. From this list of eight variables, a full-factorial design of 256 runs was constructed. ANOVA performed on the results led to the conclusion that all eight variables were significant and that there were significant interactions, up to six way. Table 4-7 shows the main and largest multiway interactions among the variables. The column labeled fstat is the F statistic, which is a measure of the strength of the effect.
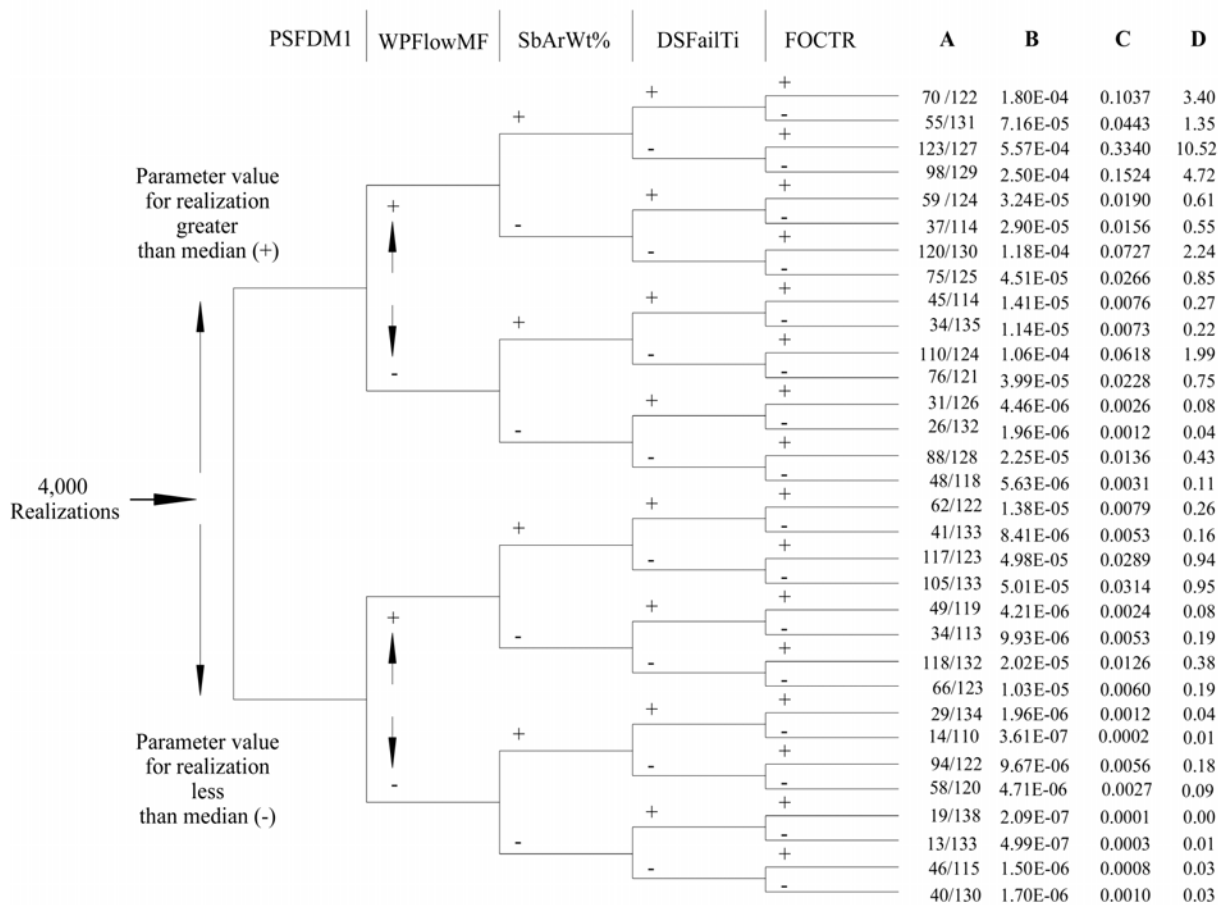
Figure 4-7. Median-Based Parameter Tree Describing the Technique for Examining System Sensitivity to Groups of Parameters

Figure 4-8 also shows the full-factorial results as a regression tree. This figure demonstrates clearly the relationships among the independent variables and the order of the variables in importance to the peak doses for 10,000 years.

4.3.5.2 Results of the 100,000-Year Factorial Design Experiments

The same level-4 design used for the 10,000-year results was used for 100,000 years. For the 100,000-year results, the initial ANOVA indicated that there are as many as 29 variables of the 330 that could be important. This list was further reduced to 17 variables based on information other than direct sensitivity from the ANOVA (e.g., all variables dealing with rockfall, volcanism, and seismicity were eliminated from the list because additional output from the code indicated there were no waste package failures from these mechanisms). Results showing sensitivity to these variables were caused by confounding of main effects with 3-way and higher parameter interactions, which are known to be present in the level-4 fractional factorial design.

Table 4-7. Main Effects and Strongest 2-Way Through 6-Way Interactions for the 10,000-Year Full-Factorial Design (Appendix E Provides Full Description of Parameters)							
FOCTR	DSFailTi	WPFlowMF	SbArWt%	WP-Def%	PSFDM1	WPRRG@20	Fstat
x							36
	x						36
		x					36
			x				29
				x			31
					x		29
						x	7
x	x						36
x		x					36
x			x				29
x				x			30
x					x		31
	x	x					36
	x		x				29
	x			x			30
	x				x		31
		x	x				29
		x		x			30
		x			x		31
			x	x			24
			x		x		26
				x	x		26
x	x	x					36
x	x		x				31
x	x			x			31

FOCTR	DSFailTi	WPFlowMF	SbArWt%	WP-Def%	PSFDM1	WPRRG@20	Fstat
x		x	x				29
x		x		x			30
x		x			x		31
x			x	x			24
x			x		x		26
x				x	x		26
	x	x	x				29
	x	x		x			30
	x	x			x		31
	x		x	x			26
	x		x		x		26
	x			x	x		26
			x	x	x		24
			x	x		x	26
		x		x	x		26
			x	x	x		21
x	x	x	x				29
x	x	x		x			30
x	x	x			x		31
x	x		x	x			24
x	x		x		x		26
x	x			x	x		26
x		x	x	x			24
x		x	x		x		26
x		x		x	x		26

Table 4-7. Main Effects and Strongest 2-Way Through 6-Way Interactions for the 10,000-Year Full-Factorial Design (Appendix E Provides Full Description of Parameters) (continued)							
FOCTR	DSFailTi	WPFlowMF	SbArWt%	WP-Def%	PSFDM1	WPRRG@20	Fstat
x			x	x	x		21
	x	x	x	x			24
	x	x	x		x		26
	x	x		x	x		26
	x		x	x	x		21
		x	x	x	x		21
x	x	x	x	x			24
x	x	x	x		x		26
x	x	x		x	x		26
x	x		x	x	x		21
x		x	x	x	x		21
	x	x	x	x	x		21
x	x	x	x	x	x		21

The 17 variables are AAMAI@S, MAPM@GM, MATI@GM, AA_1_1, WPFlowMF, SbArWt%, WP-Def%, PSFDM1, SFWt%C1, SFWt%C2, SFWt%C3, ARDSAVAm, ARDSAVNp, ARDSAV_U, ARDSAVPu, PWPRRG20, and gen_ifi.

The next fractional factorial design for 100,000 years was of level-5 resolution, requiring 2,048 vectors. From the level-5 design, the number of possible factor interactions is manageable; therefore, it was possible to judge whether a main effect associated with a particular variable was actually an alias caused by a multiple-way effect of other variables. While investigating the possible main effects and their aliases, 10 variables, which are most likely to be important were screened from the ANOVA result.

The final full-factorial design for 100,000 years looks at the 1,024 possible combinations of the 10 screened variables. Results of the full-factorial design show that eight of the variables are likely to be important. The eight variables are AAMAI@S, WPFlowMF, SbArWt%, PSFDM1, SFWt%C2, ARDSAVNp, PWPRRG20, and gen_ifi. In addition, the ANOVA on these eight variables shows there are many important interactions up to 6-way. Table 4-8 shows the eight significant variables and the strongest 2-way to 6-way combinations that could be important for the 100,000-year simulation period. The columns of the table show the variable in the interaction. Like the 10,000-year results, there are many other smaller, but credible,

Low parameter value ←——————————→ High parameter value

DSFailTi

WPFlowMF

0 mSv

0 mSv

FOCTR

5.3e-12 mSv

PSFDM1

1.16e-4 mSv

WP-Def%

3e-4 mSv

6.6e-3 mSv
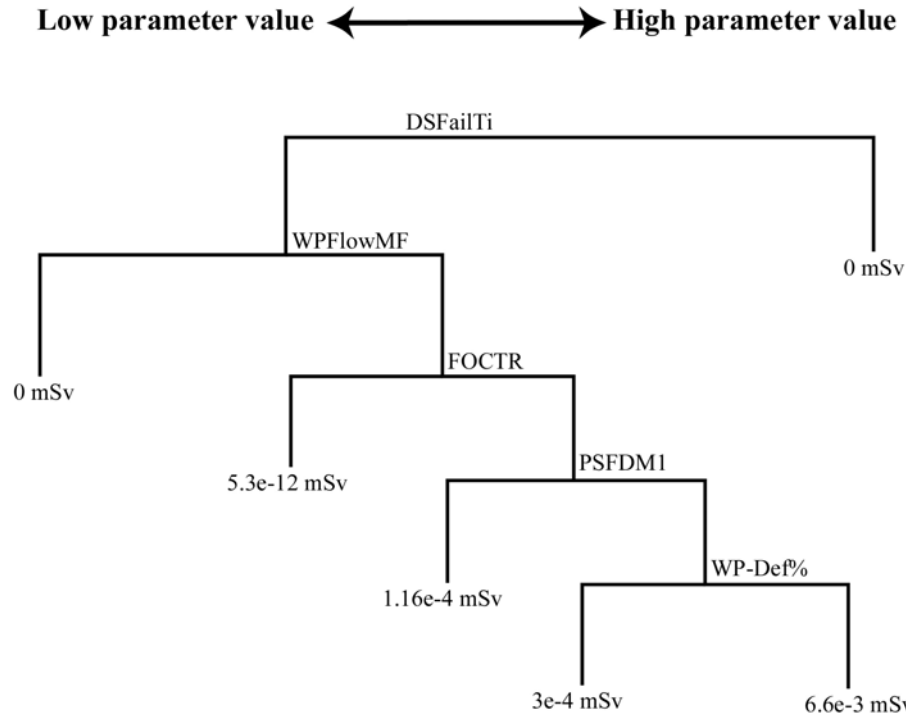
Figure 4-8. Factorial Design Results for 10,000-Year Simulation Period

interactions not listed. Figure 4-9 also shows the full-factorial results as a regression tree. This figure demonstrates clearly the relationships among the independent variables and the order of the variables in importance to the peak doses for 100,000 years.

The fractional factorial design method is a useful addition to the other sensitivity methods. It formally addresses the problem encountered in other sensitivity methods of confounding (mistaking true sensitivities with spurious results that may be caused by interactions of other variables). The factorial method allows the formal demonstration of the interaction among variables that can only be inferred by some of the other methods (e.g., the parameter tree method can show combinations of variables that lead to high doses, but only to a limited extent). The full-factorial results of the reduced set of variables from screening provides valuable information about the combination of extreme values of input variables (i.e., 5th- and 95th-percentile values) that could lead to the poorest repository performance. The tree diagrams that can be drawn from the full-factorial results on the reduced set of variables are explicit and show the exact relationship between the values of the variables and performance. Factorial design methods, however, are difficult to implement and, with the available tools, require a significant expenditure of staff and computer resources. The successive screening of variables is particularly demanding of staff time as is setting up the TPA Version 4.1 code to accept input from the factorial designs produced externally to the code. Another potential disadvantage of the factorial design is the reliance in this application to only two levels of sampling. This limitation presents the possibility of misidentification of variables for which the greatest

Table 4-8. Main Effects and Strongest 2-Way Through 6-Way Interactions for the 100,000-Year Full-Factorial Design (Appendix E Provides Full Description of Parameters)

AAMAI@S	WPFlowMF	SbArWt%	PSFDM1	SFWt%C2	ARDSAVNp	PWPRRG20	gen_ifi	F-Stat
X								37
	X							57783
		X						55989
			X					63135
				X				7812
					X			57703
						X		48
							X	5174
	X	X						47954
	X		X					54907
	X				X			53561
		X	X					52398
		X			X			47887
			X		X			57578
	X	X	X					45568
	X	X			X			44445
	X		X		X			53629
		X	X		X			47783
	X	X	X	X				6314
	X	X	X		X			44501
	X	X	X				X	3499
	X	X		X	X			6158
	X	X		X			X	432
	X	X			X		X	3434
	X		X	X	X			7407

AAMAI@S	WPFlowMF	SbArWt%	PSFDM1	SFWt%C2	ARDSAVNp	PWPRRG20	gen_ifi	F-Stat
	X		X	X			X	496
	X		X		X		X	4140
	X			X	X		X	479
		X	X	X	X			6047
		X	X	X			X	411
		X	X		X		X	3719
		X		X	X		X	396
			X	X	X		X	473
	X	X	X	X	X			6154
	X	X	X	X			X	415
	X	X	X		X		X	3447
	X	X		X	X		X	400
	X		X	X	X		X	480
	X	X	X	X	X		X	401

Table 4-8. Main Effects and Strongest 2-Way Through 6-Way Interactions for the 100,000-Year Full-Factorial Design (Appendix E Provides Full Description of Parameters) (continued)

sensitivities or most adverse results occur in the middle of the ranges rather than at the extremes. This limitation could be mitigated by including a midrange sample so there are 3 levels rather than two, but this would further increase the computational effort.

4.3.6 Results from the Cumulative Distribution Function— Sensitivity Method

Cumulative distribution function sensitivities have been evaluated at 9 performance (i.e., peak dose) cumulative distribution function values, ranging from 10th to 90th percentiles, with a 10-percent increment. Figure 4-10 shows S_μ sensitivity results for the top 10 influential parameters. The figure also shows the 90-percent test-of-hypothesis confidence limits. As noted earlier, the parameters not influential are close to the zero sensitivity line and within the 90 percent confidence limits. The farther the curve is outside the test-of-hypothesis acceptance limits, the more sensitive the performance cumulative distribution function is to the corresponding input parameter. The influential parameters can be ranked based on this departure from the zero line, which could be different for a given random variable at different cumulative distribution function levels.

Low parameter value ⟵————————⟶ **High parameter value**
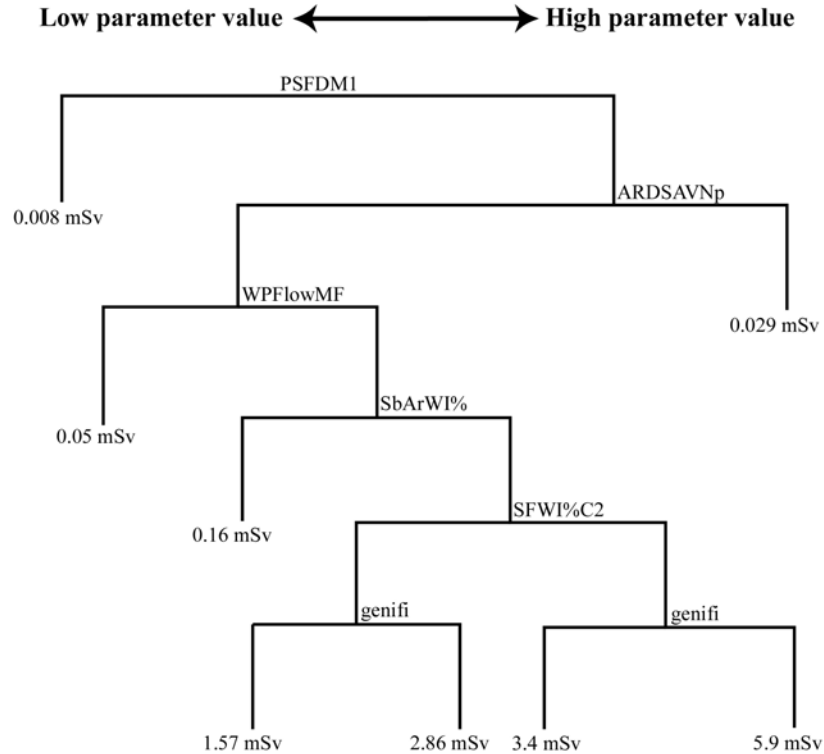
Figure 4-9. Factorial Design Results for the 100,000-Year Simulation Period

Table 4-9 and Figures 4-10 through 4-12 present influential parameters identified by the S_μ sensitivity at cumulative distribution function = 0.9, the S_μ sensitivity at average cumulative distribution function, and the $\overline{S}_{Y_\mu}$ sensitivity. These sensitivities have been calculated using a 4,000-vector TPA Version 4.1 code run. At the 90-percent confidence level, more than.10 parameters are identified as influential, but only the top 10 are shown in Table 4-9.

Figures 4-10 and 4-11 show that the ranking varies for different cumulative distribution function levels. This ranking implies that the functional relationship between the performance and the input variables is not linear (i.e., the sensitivity varies for the range of performance). For example, in Figure 4-11, the variable DSFailTi parameter (drip-shield failure time) has a higher sensitivity at cumulative distribution function = 0.1 than at cumulative distribution function = 0.9. In contrast, PSFDM1 (preexponential term for the spent nuclear fuel-dissolution Model 2) has the highest sensitivity at cumulative distribution function = 0.9, low sensitivity at cumulative distribution function = 0.1, and no acceptable sensitivity (i.e., <90-percent confidence) between the cumulative distribution function values of 0.25 and 0.45. Figure 4-12 shows results for $\overline{S}_{Y_\mu}$ sensitivity at the 90 percent confidence level. The top 10 influential parameters from $\overline{S}_{Y_\mu}$ sensitivity are presented in Table 4-3 for the 10,000-year simulation period. These parameters from $\overline{S}_{Y_\mu}$ sensitivity are (i) WPFlowMF, (ii) PSFDM1, (iii) SbArWt%, (iv) WP-Def%, (v) AAMAI@S, (vi) DSFailTi, (vii) DTFFAVIF, (viii) WPRRG@20, (ix) ARDSAVNp, and (x) FOCTR. These 10 parameters were ultimately selected to represent the cumulative distribution function sensitivity analysis method for comparison against other methods, primarily

Table 4-9. Top 10 Parameters from the Cumulative Distribution Function, Sensitivity Method with 1,000 Samples Using Various Sensitivity Measures (Appendix E Provides a Full Description of the Parameters)					
S_μ Sensitivity (At-Cumulative Distribution Function = 0.9)		S_μ Sensitivity (Averaged-over-Cumulative Distribution Function)		$\overline{S}_{Y_m}$ Sensitivity	
Variable Identification Number	Variable Abbreviation	Variable Identification Number	Variable Abbreviation	Variable Identification Number	Variable Abbreviation
63	PSFDM1	12	DSFailTi	60	WPFlowMF
60	WPFlowMF	60	WPFlowMF	63	PSFDM1
61	SbArWt%	5	FOCTR	61	SbArWt%
1	AAMAI@S	1	AAMAI@S	62	WP-Def%
12	DSFailTi	63	PSFDM1	1	AAMAI@S
62	WP-Def%	61	SbArWt%	12	DSFailTi
521	FOCTR	62	WP-Def%	237	DTFFAVIF
202	MPrm_TSw	4	FOC-R	239	WPRRG@20
239	WPRRG@20	6	TempGrBl	225	ARDSAVNp
237	DTFFAVIF	202	MPrm_TSw	5	FOCTR

because the $\overline{S}_{Y_\mu}$ sensitivity represented the sensitivity consistent with the peak expected dose regulatory basis. These parameters are similar to those identified by the S_μ sensitivity averaged-over-cumulative distribution function and S_μ sensitivity at cumulative distribution function = 0.9, with a few exceptions. Parameter TempGrBl is identified as important by the S_μ averaged-over-cumulative distribution function sensitivity but does not show up with the $\overline{S}_{Y_\mu}$ sensitivity or the S_μ at-cumulative distribution function = 0.9 sensitivity. Parameter MPrm_TSw appears in the S_μ at-average-cumulative distribution function sensitivity and the S_μ at-cumulative distribution function = 0.9 sensitivity but does not appear with the $\overline{S}_{Y_\sigma}$ sensitivity.

The ranking based on S_σ was different from that based on S_μ. The influential parameters identified by the $\overline{S}_{Y_\sigma}$ sensitivity were also substantially different from those identified by the $\overline{S}_{Y_\mu}$ sensitivity when analyzing the results from the TPA Version 4.1 code. Therefore, the results are not discussed in this report. An investigation of the implication of the S_σ and $\overline{S}_{Y_\sigma}$ sensitivity results is currently under way. When these two measures were applied to the previous version of the TPA code, the difference between the two sets of influential variables was small.
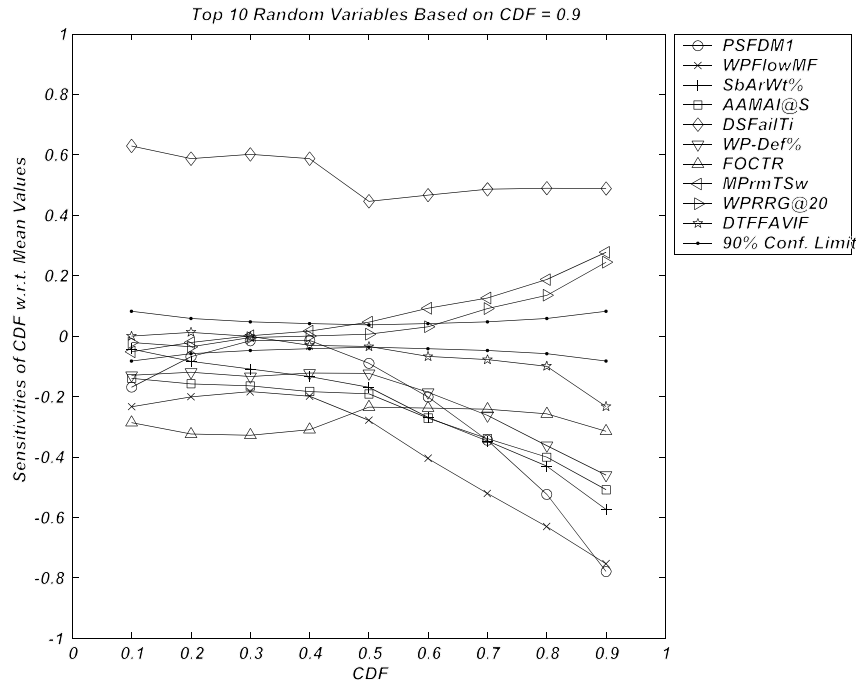
Figure 4-10. Sensitivity of Performance Cumulative Distribution Function to Input Variable Mean for Top 10 Variables Having Highest Average

The peak dose values showed, on an average, 1 potential outlier per 1,000 realizations. Conducting sensitivity analyses using the cumulative distribution function sensitivity method with and without the outliers had a profound effect on the response statistics, the sensitivities, and the rankings. One particular example is the 265th realization in the 1,000-vector run. In this run, the peak dose was nearly 238 times larger than the average peak dose. Further analysis revealed that in the 265th realization there were several influential variables with large parameter values that led to a very large peak dose value. Consequently, one must use as many realizations as feasible to compute the sensitivities no matter what method is used. Fortunately, the top five random variables in the $\overline{S}_{y_\mu}$ sensitivity remain on the top even though they are in a different order when more realizations are systematically considered.

4.4 Influential Parameters Based on Parametric Sensitivity

In the previous section, seven different sensitivity analysis methods were used to determine the most influential parameters. Several of these methods scale parameters so the sensitivity results reflect the variability of the inputs. Several methods do not standardize but scale parameters because their results are based on ranking the input variables using a set of predetermined criteria. The seven methods have different approaches for determining sensitivity. For example, regression with log-transformed variables places greater emphasis on smaller doses than regression with untransformed variables. The cumulative distribution
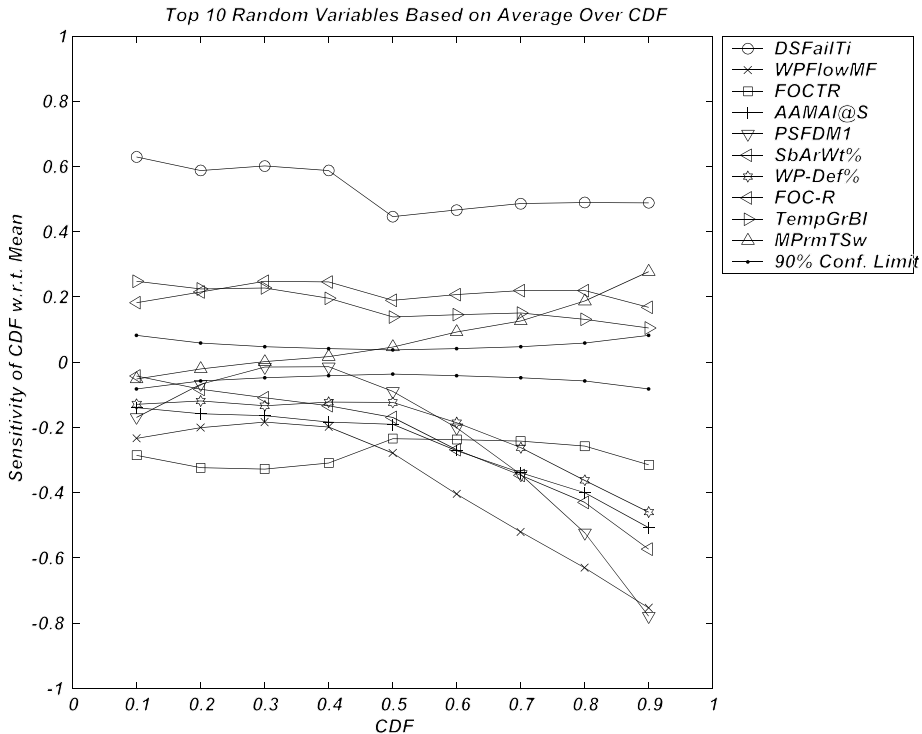
**Figure 4-11. Sensitivity of Performance Cumulative Distribution Function to
Input Variable Standard Deviation for Top 10 Variables Having
Highest Average; Sensitivity Calculated for
Averaged-Over-Cumulative Distribution Function**

function sensitivity method uses 3 different types of sensitivity measures, though the mean-mean sensitivity is used because it is consistent with the peak expected dose regulatory criterion. It is not clear that any one method was superior to another for this determination of sensitivity (or influence), and, consequently, no method can be fully relied on to provide a unique ranking of parameters. Therefore, the final list of parameters was selected on the basis of frequency of occurrence among various methods.

The selected parameters are presented in Table 4-10 for 10,000 years. The scores in these tables specify the number of methods that select a particular parameter among the top 10. For example, a score of 7/7 for the "areal average mean annual infiltration at start" parameter, AAMAI@S, implies the parameter ranks among the top 10 in all 7 methods. Also note that, among the seven methods, there is one statistical/regression method that relies on the combined results of Monte Carlo input-output response using linear and stepwise linear regressions of raw, rank, normalized, or log of normalized variables for parameter screening. Two other methods (parameter tree and cumulative distribution function sensitivity) are also based on Monte Carlo results. The other 4 methods are nonstatistical (differential analysis, fractional factorial design method, Morris Method, and Fourier amplitude sensitivity test method), for which the sampled parameters were determined specifically for the method. It should be noted that the Fourier amplitude sensitivity test method selects only the most
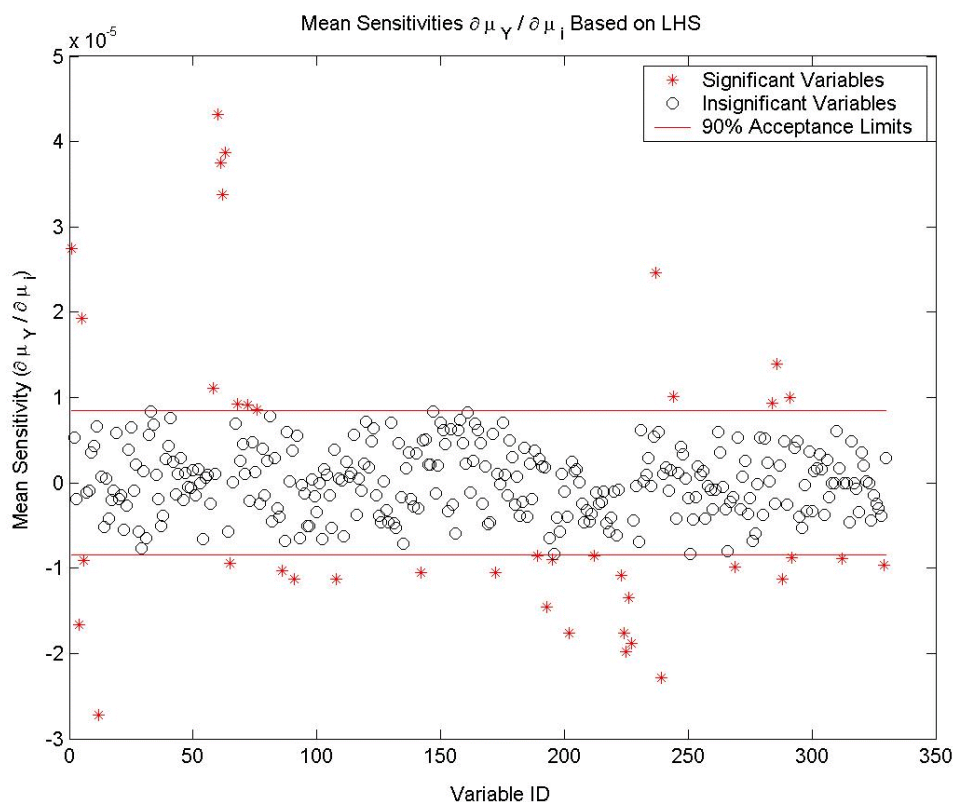
Figure 4-12. Important Variables Identified by the $S_{Y_\mu}(\partial\mu_Y/\partial\mu_{Z_i})$ **Sensitivity. The Top 10 Parameters Identified with Asterisks (Farthest from the Confidence Limit) are Shown in last Column of Table 4-9.**

No.	Parameter Abbreviation	Parameter Name	Score
	Table 4-10. Influential Parameters for the 10,000-Year Simulation Period from Sensitivity Analysis Studies		
1	AAMAI@S	Areal average mean annual infiltration at start	7/7
2	DSFailTi	Drip shield failure time	7/7
3	PSFDM1	Preexponential term for spent nuclear fuel-dissolution Model 2	6/7
4	SbArWt%	Subarea wet fraction	6/7
5	WPFlowMF	Waste package flow multiplication factor	6/7
6	WPRRG@20	Well pumping rate at 20-km [12.4-mi] receptor group	6/7
7	FOCTR	Fraction of condensate toward repository	4/7
8	ARDSAVNp	Alluvium R_d for Np-237	3/7
9	DTFFAVIF	Distance to Tuff-alluvium interface	3/7
10	WP-Def%	Waste package initially defective fraction	3/7

influential parameters of the top 20 listed in the peak dose column for the 10,000-year case of Table 4-6. The parameters that do not make the final list include those selected as influential by only one or two of the seven methods.

4.5 Verification of Sensitivity Analysis Results

Because most of the sensitivity analysis methods neither guarantee that the parameters are influential nor establish a degree of influence, it is important to verify if the group of parameters identified by various methods is truly influential. Because the system response is most affected by the most influential parameters identified with the sensitivity analysis, it is intuitive that the variance of the system response will be significantly reduced if the input variances of the influential parameters are reduced.

In the following sections, the variance reduction is shown for the entire complementary cumulative distribution functions when all influential parameters are treated as a group. When the influential variables were studied individually, however, only the overall reduction in variance was computed. Variance reductions were computed using 350 Latin Hypercube Sampling realizations for each case. The performance value used in the variance reduction calculations was the realization peak dose.

For convenience, the variance reduction for the group of influential parameters is shown as a change in the shape of a complementary cumulative distribution function. A cumulative distribution function was constructed from N performance values. Each value of y was assumed to have a probability of occurrence of $1/N$. If, by holding the influential parameters at their mean values, there is a decrease in the spread of N values of y, it can be concluded that the parameters are indeed influential. If the ranking produced by the majority rule is correct, the transition between the highest and lowest probability of exceedance values is expected to be sharp.

4.5.1 Verification of the Basecase Influential Parameters as a Group

Figure 4-13 shows complementary cumulative distribution functions of peak doses for 3 cases: (i) basecase—all 330 input parameters were allowed to be sampled within their ranges of variation, (ii) top 10 influential parameters were held fixed at their mean values while the remaining 320 input parameters are allowed to be sampled within their ranges of variation, and (iii) all but the top 10 influential input parameters were frozen at their mean values. For each case, results were plotted for the 10,000-year simulation period. Each curve represents the output from 350 runs using Latin Hypercube Sampling.

Case 1 in Figure 4-13 is the complementary cumulative distribution function of peak doses from the basecase run. Case 2 resulted in a sharp drop in variance of the peak doses. The standard deviation dropped from {1.32×10^{-3} to 1.9×10^{-4} mSv/yr [1.32×10^{-1} to 1.90×10^{-2} mrem/yr]}, which is nearly a two-orders-of-magnitude decrease. A large drop like that is expected if the influential parameters are truly important. Moreover, Case 3 results are similar to the Case 1 results. This similarity is expected if the influential parameters are truly important, because fixing the less influential parameters is expected to make little difference.
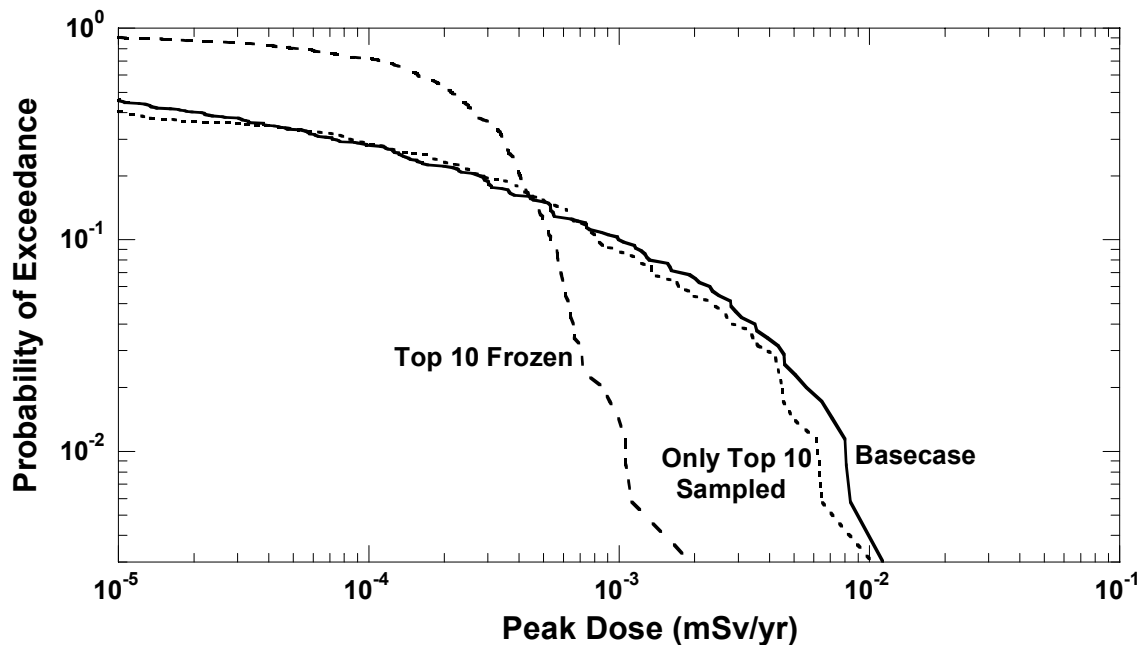
Figure 4-13. Conditional Complementary Cumulative Distribution Function of Peak Total Effective Dose Equivalents for the 10,000-Year Simulation Period from the Basecase, Conditioned by Holding 0 (Basecase) and 10 Most Influential Parameters Fixed at Their Mean Values and Fixing All but 10 Most Influential Variables

The slight difference between Case 1 and Case 2 indicates there may be more than 10 parameters that could be influential. Based on Figure 4-13, it appears the scoring method ranked the top parameters correctly.

4.5.2   Verification of the Igneous Activity Case Influential Parameters as a Group

Figure 4-14 shows complementary cumulative distribution functions of peak doses for 3 cases: (i) igneous activity conditional dose case—all 330 input parameters were allowed to be sampled within their ranges of variation, (ii) top 9 influential parameters were held fixed at their mean values while the remaining 321 input parameters were allowed to be sampled within their ranges of variation, and (iii) top 9 influential parameters were allowed to be sampled within their ranges of variation while the remaining 321 influential input parameters were frozen at their mean values. Only 9 parameters were selected because parameter 10 had already been considered in the basecase. For each case, results were plotted for a 10,000-year simulation period. The outputs were conditioned by holding the parameters fixed at their mean values and sampling the remaining 321 input parameters within their ranges of variation. Each curve represents the output from 350 runs using Latin Hypercube Sampling. Case 1 is the complementary cumulative distribution function of peak doses from the nominal case run. Case 2 resulted in a sharp drop in variance of the peak doses. The standard deviation dropped six orders of magnitude from {8.98×10^2 to 9.42×10^{-3} mSv/yr [8.98×10^4 to 9.42×10^{-1} mrem/yr]}. This drop was expected if the influential parameters were truly important. Moverover, the Case 3 results in Figure 4-5 are close to the Case 1 results. This correlation was expected if the influential parameters are truly important, because fixing the less influential parameters is expected to make little difference to

4-43
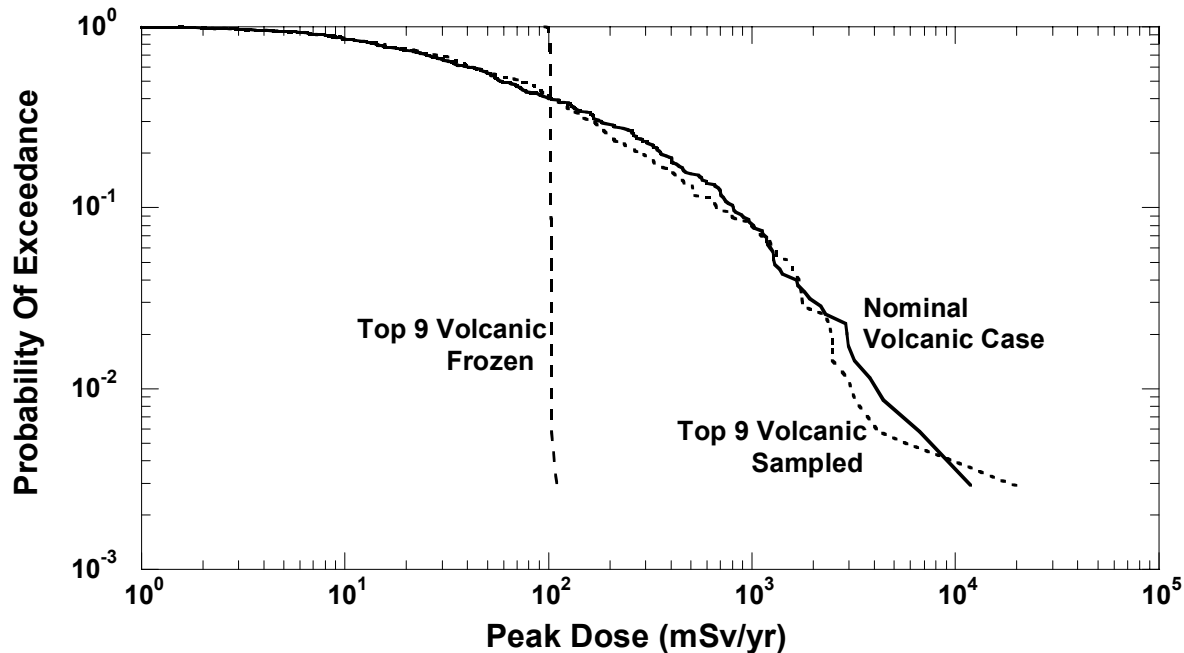
Figure 4-14. Conditional Complementary Cumulative Distribution Function of Peak Total Effective Dose Equivalents for the 10,000-Year Simulation Period from the Igneous Activity Case (Not Probability Weighted) Conditioned by Holding Zero and Nine Most Influential Parameters Fixed at Their Mean Values and Fixing All but Nine Most Influential Variables

the nominal case complementary cumulative distribution function. The slight difference between Case 1 and Case 2 indicates there may be more than nine parameters that could be influential. Based on Figure 4-14, it appears the scoring method ranked the top parameters correctly.

4.5.3 Verification of Individual Basecase Influential Parameters

For the analysis of variance reduction for individual influential parameters, each influential parameter was held fixed at its mean value while the remaining input parameters were sampled. The results of this analysis are presented in Table 4-11.

One finding from this analysis is that freezing an influential parameter at its mean value does not always lead to a corresponding reduction in output variance for the peak doses from each realization (see last 3 columns of Table 4-11). For example, freezing drip-shield failure time at a fixed value increases response (i.e., output) variability. This result implies that the scaled variability (i.e., coefficient of variation) displayed in the complementary cumulative distribution function for Case 2 (see Figure 4-13) would have been reduced further by fixing some of the top 10 influential parameters at their mean values.

Table 4-11. Variance Reduction for Most Influential Parameters in the Basecase					
Abbreviation	**Description of Influential Parameters**	**Mean of Peak Doses (mrem/yr)**	**Variance of Peak Doses (mrem/yr)²**	**Standard Deviation of Peak Doses (mrem/yr)**	**Coefficient of Variation (Unitless)**
Basecase	—	4.24×10^{-5}	1.76×10^{-8}	1.32×10^{-4}	3.124
AAMAI@S	Areal average mean annual infiltration at stat	4.23×10^{-5}	1.90×10^{-8}	1.38×10^{-4}	3.261
MAPM@GM	Mean average precipitation multiplier at glacial maximum	4.28×10^{-5}	1.86×10^{-8}	1.37×10^{-4}	3.188
DSFailTi	Drip shield failure time	7.20×10^{-5}	4.02×10^{-8}	2.00×10^{-4}	2.783
WPFlowMF	Waste package flow multiplication factor	3.61×10^{-5}	1.07×10^{-8}	1.03×10^{-4}	2.864
gen_PUSF	Plant uptake scale factor	4.20×10^{-5}	1.72×10^{-8}	1.31×10^{-4}	3.123
WPRRG@20	Well pumping rate at receptor group 20 km [12.4 mi]	4.07×10^{-5}	1.59×10^{-8}	1.26×10^{-4}	3.093
ARDSAVNp	Retardation factor for Np in saturated zone alluvium matrix	4.00×10^{-5}	1.64×10^{-8}	1.28×10^{-4}	3.207
IPPFSTFF	Immobile porosity penetration fraction for STFF	4.36×10^{-5}	1.89×10^{-8}	1.38×10^{-4}	3.160
PSFDM1	Preexponential term for spent nuclear fuel dissolution Model 2	2.57×10^{-5}	4.77×10^{-9}	6.90×10^{-5}	2.684
SbArWt%	Subarea wet fraction	3.85×10^{-5}	1.33×10^{-8}	1.15×10^{-4}	2.993
genlvirC	Leafy vegetable irrigation rate at compliance boundary	4.21×10^{-5}	1.72×10^{-8}	1.31×10^{-4}	3.116
WP-Def%	Defective fraction of waste packages per subarea	4.02×10^{-5}	1.42×10^{-8}	1.19×10^{-4}	2.967
MPrm_PPw	Matrix permeability for PPw	4.24×10^{-5}	1.76×10^{-8}	1.32×10^{-4}	3.124
DTFFAVIF	Distance to tuff-alluvium interface	4.02×10^{-5}	1.75×10^{-8}	1.30×10^{-4}	3.284
FPrs_STF	Fracture porosity in STFF	4.25×10^{-5}	1.68×10^{-8}	1.30×10^{-4}	3.056
SFWt%I2	Spent nuclear fuel wetted fraction for initially defective failure in Subarea 2	4.30×10^{-5}	1.77×10^{-8}	1.33×10^{-4}	3.094
InvMPerm	Invert matrix permeability	4.24×10^{-5}	1.76×10^{-8}	1.33×10^{-4}	3.122
SFWt%I9	Spent nuclear fuel wetted fraction for initially defective failure in Subarea 9	4.33×10^{-5}	1.88×10^{-8}	1.37×10^{-4}	3.164
SFWt%I1	Spent nuclear fuel wetted fraction for initially defective failure in Subarea 1	4.33×10^{-5}	1.78×10^{-8}	1.27×10^{-4}	3.081
gen_ifi	Irrigation interception fraction	3.95×10^{-5}	1.62×10^{-8}	1.27×10^{-4}	3.230

It is also important to note that some top influential parameters influence the mean, others influence the variance, and some affect both mean and variance. The process-level analyst must be aware of this aspect and set the goal before embarking on the process of acquiring new data for uncertainty reduction. The effect of the parameter distributional assumption on dose should also be considered.

Reduction of uncertainties in parameters PSFDM1, DSFailTi, WPFlowMF, and WP-Def% influenced the output uncertainty most (i.e., >5 percent). Reduction of uncertainties in parameters DSFailTi, PSFDM1, WPFlowMF, SbArWt%, ARDSAVNp, WP-Def%, and DTFFAVIF influenced the output mean most (i.e., >5 percent). All but DSFailTi decreased the mean. For parameters DSFailTi, PSFDM1, WPFlowMF, and WP-Def%, both mean and standard deviations of the output changed (i.e., >5 percent) when the uncertainty in the parameters was suppressed. Reduction of uncertainties in 14 out of 20 parameters reduced scaled variability in dose whereas the remaining 6 increased scaled variability.

4.5.4   Verification of Individual Igneous Activity Influential Parameters

For the variance reduction analysis of individual influential parameters in the igneous activity case, each influential parameter was held fixed at its mean value while the remaining input parameters were sampled. A conditional dose calculation was then performed corresponding to each influential parameter by holding each parameter fixed at the mean value and performing a 350-realization Monte Carlo run. Changes to the mean, variance standard deviation, and coefficient of variation of the peak dose values are presented in Table 4-12.

The largest output uncertainty reduction occurred for parameters VEROI-Tn and VE-Power (~30 percent), followed by WindSpd and VE-Durat (~15 percent). The largest increase to scaled variability resulted from fixing parameter ABMLAAsh at its mean value. The ABMLAAsh parameter increased the scaled variability by approximately 34 percent. Table 4-12 shows that parameters VEi/e-R# and SFWt%V0 affected neither the output scaled variability nor the output mean. The lack of variability reduction for VEi/e-R# (random number to determine volcanic event type) can be attributed to the fact that in the model, the sampled event is nonvolcanic if this parameter value exceeds 0.999. Because all sampled values in the basecase are less than 0.999 and because for the variance reduction calculation this parameter is set at 0.5, in both cases the volcanic event occurred. Therefore, no difference was observed in the basecase or the variance reduction case**.**

4.6   Alternative Conceptual Models and Scenario Cases Studied at the System Level

Alternative conceptual models are either explicitly specified in the TPA Version 4.1 code or are created by assigning a set of predetermined values to input parameters to mimic an alternative conceptualization. Analyses include full ranges of parameter variations for all parameters (i.e., similar to the nominal case). This process is a departure from the analyses using the previous versions of the TPA code in which parameters were set at their respective mean values. The results reflect model runs that compare the basecase with alternative conceptual models. First, the basecase was evaluated with a 350-vector run. Alternative conceptual model tests were conducted with 350-vector runs, and the results were compared with the basecase. The alternative conceptual models were selected to evaluate (i) the effect on repository performance of several repository design features currently being considered by U.S. Department of Energy, (ii) the effect on repository performance of plausible alternate thermo

			Mean of Peak Doses (mrem/yr)	Variance of Peak Doses (mrem/yr)^2	Standard Deviation of Peak Doses (mrem/yr)	Coefficient of Variation (Unitless)
No.	**Abbreviation**	**Description of Influential Parameters**				
N/A[*]	Igneous Activity Case	Basecase with igneous activity	32.45	8,056.48	89.76	2.766
1	ABMLAAsh	Airborne mass load above fresh ash blanket	28.93	11,412.68	106.83	3.693
2	WindSpd	Wind speed	43.55	8,922.01	94.46	2.169
3	VC-Dia	Diameter of volcanic cone	29.12	4,607.78	67.88	2.331
4	VE-Power	Volcanic event power	20.25	1,338.06	36.58	1.806
5	VE-Durat	Volcanic event duration	28.73	4,234.55	65.07	2.265
6	VEROI-Tn	Time of next volcanic event in region of interest	19.56	1,119.61	33.46	1.711
7	AshMnPLD	Ash mean particle log diameter	32.33	7,990.29	89.39	2.765
8	VEi/e-R#	Random number to determine if extrusive or intrusive volcanic event	32.45	8,056.48	89.76	2.766
9	SFWt%V0	Spent nuclear fuel wetted fraction for intrusive igneous activity	32.45	8,056.48	89.76	2.766

Table 4-12. Variance Reduction for Most Influential Parameters in the Igneous Activity Case Identified by the Morris Method; Analysis Results Are Presented Using Conditional Dose (i.e., No Probability Weighting)

[*]NA — Not applicable

hydrological conditions in the repository near field, and (iii) bounding engineered or natural system behaviors.

For each alternative conceptual model, only the noted changes, as described in Section 2.7.2 to the total system performance assessment input file, were made, with all other input parameters set to the values used in the basecase. Results are presented as the percentage change of peak expected dose with respect to the basecase peak expected dose.

Figure 4-15 shows the results for the 10,000-year simulation period, while Figure 4-16 is for the 100,000-year results.

Various observations can be made based on the results shown in this section.

- The largest mean doses resulted from the NoRet assumption for both the 10,000- and 100,000-year simulation periods, demonstrating the importance of retardation of plutonium, americium, and thorium in the alluvium.

- The No Sol Limit Flowthru alternative conceptual model (i.e., no solubility limit + flowthrough spent nuclear fuel wetting mode) led to a 353-percent increase in dose compared to the basecase during the 10,000-year simulation period. In the 100,000-year simulation period, this alternative conceptual model led to a 75-percent increase in dose compared to the basecase. This increase suggests that the solubility limit controls the release from the spent nuclear fuel.

- The No Sol Limit (Bathtub) conceptual model (i.e., no solubility limit + bathtub spent nuclear fuel wetting mode) had less effect on the peak expected dose than the No Sol Limit (Flowthru) alternative conceptual model. The peak expected dose changed by 141 percent for 10,000 years and by 67 percent for 100,000 years.

- The Flwthru-1 alternative conceptual model (i.e., flowthrough spent nuclear fuel wetting mode + spent nuclear fuel-dissolution Model 1) increased the peak expected dose by 240 percent in the 10,000-year simulation period and by 50 percent in the 100,000-year simulation period.

- Fast dissolution in the case of Model 1 (i.e., spent nuclear fuel-dissolution Model 1) and Grain 1 (i.e., particle size model) alternative conceptual models led to an increase in the peak expected dose for the 10,000-year simulation period, but the increase is not proportional to the increased rate of dissolution. In some cases, the high rate of dissolution does not contribute to an overall increase of dose for the 100,000-year simulation period. This increase probably indicated that the high dissolution rate of the fuel led to near-total depletion of the spent nuclear fuel.

- Alternatives based on natural analog data (Natan) and assumptions about the behavior of radionuclides in secondary uranium minerals (Schoepite) led to much smaller peak doses.

- Protection of the fuel by cladding (Clad-M1) led to a large reduction in peak doses.

- Removing matrix diffusion increases the peak expected dose by 50 percent for the 10,000-year simulation period and by 10 percent for the 100,000-year simulation period.
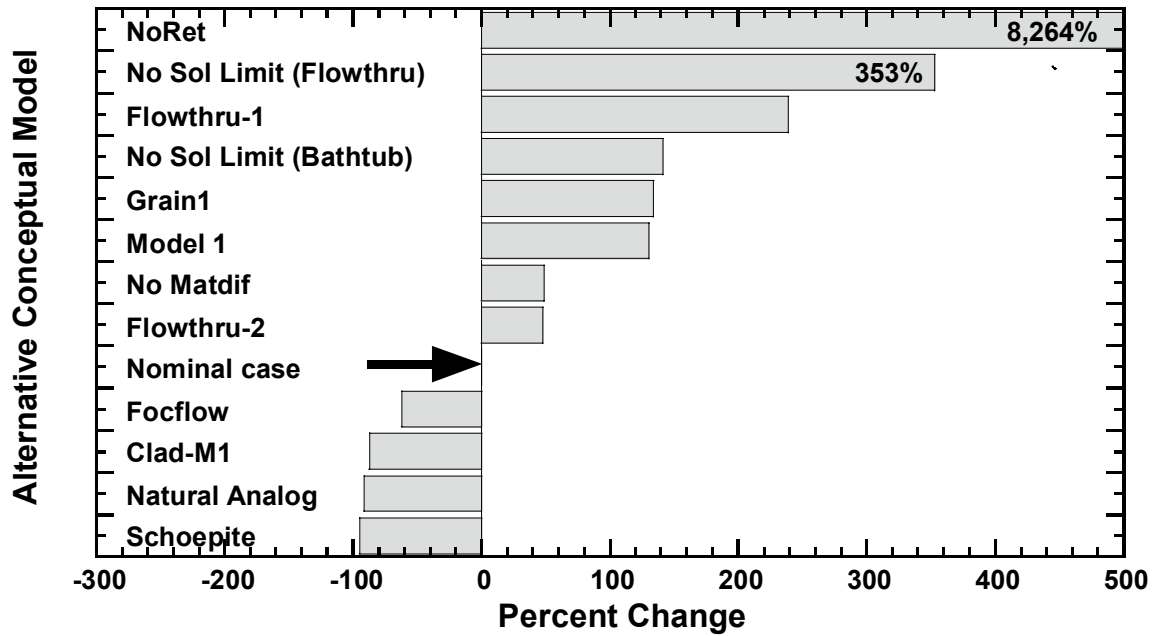
Figure 4-15. Bar Chart Showing the Effects of Alternative Conceptual Models at 10,000 Years
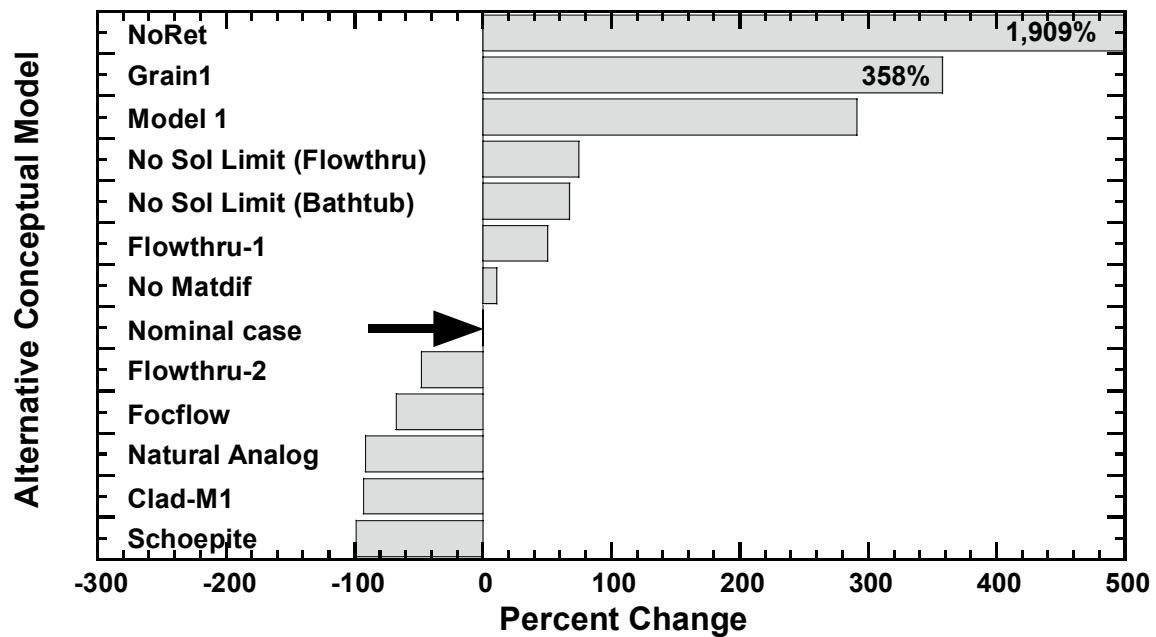
Figure 4.16 Bar Chart Showing the Effects of Alternative Conceptual Models at 100,000 Years

5 DISTRIBUTIONAL SENSITIVITY ANALYSIS

5.1 Background

The quality of performance assessment results depends in part on the process used for determining the probability distribution function for each sampled input parameter. The effect of distributional uncertainty is studied by conducting sensitivity or relative impact analyses of the uncertainty in the distribution functions on the peak expected dose as well as the shape of the peak dose cumulative distribution function. Because of the large number of sampled parameters in the TPA Version 4.1 code, only a small set of parameter distributions was evaluated. For the analyses presented in this report, only the shape of the distribution function is varied, the parameter range remains unchanged. In the following sections, the analysis method is presented, the results from the implementation of the method are presented, and some recommendations are made for future studies.

5.2 Analysis Method

The general approach for distributional sensitivity involves determination of the relative change to the performance measure for a prespecified perturbation to the distribution function. The direct (i.e., brute force) method involves performing several Monte Carlo runs corresponding to each change to the distribution function (i.e., the basecase and the sensitivity cases). Only one parameter is changed at a time. Each Monte Carlo run set corresponds to and is identical to the basecase run except that one input parameter has a distribution function different from the basecase. The relative change to the performance measure is expressed as (i) the difference between the old (i.e., the basecase) and the new (i.e., sensitivity case) peak expected dose and (ii) an effective distance between the old and new output distributions. Several notable methods have been proposed in the past by Beckman and McKay (1987) for fast computation focusing on improvement to the computational efficiency by eliminating the need to perform any Monte Carlo runs additional to a standard basecase run. One of these methods is based on the weighing method (Kahn and Marshall, 1953), and another method is the rejection method (Kennedy and Gentle, 1980). These methods, however, appear to have some limitations that could lead to approximations in the analysis if used outside the recommended limits. The efficiency of each method has been shown to decrease rapidly as large differences occur between the old and the new probability density functions. For this report, the direct (i.e., brute force) method was used because of these limitations.

The two measures used for estimating the sensitivity of performance on the distributional change to a parameter were (i) change in the peak expected dose and (ii) change to the peak dose cumulative distribution function. For the first measure, the expected dose was computed as a function of time from the Monte Carlo run set; the peak expected dose was then computed from the expected dose curve. The second measure was useful especially for cases where the peak expected dose remains the same as the basecase dose. Where the variance of peak dose is different, however, one could use complementary cumulative distribution functions instead of cumulative distribution functions—this will only add extra computational steps without any change in the results.

The change in output distribution in the second distributional sensitivity measure can be measured simply by measuring the area between two cumulative distribution functions, one for

the basecase and one for the sensitivity case. Chun, et al. (2000) used metric distance to represent this shaded region based on a Minkowski norm. Other measures can be found in Iman and Hora (1990); Khatib-Rahbar, et al. (1989); and Park and Ahn (1994). The metric distance, D, is defined as

$$D = \left[\sum_{x \in X} \left| F_1(x) - F_2(x) \right|^w \right]^{\frac{1}{w}}, w > 1 \qquad (5\text{-}1)$$

where

$F_1(x)$ — the basecase output cumulative distribution function
$F_2(x)$ — the sensitivity case output cumulative distribution function
w — an exponent

When $w = 2$, D represents the Euclidian metric distance between the two cumulative distribution functions

$$D = \left[\int_0^1 \left| F_1(x) - F_2(x) \right|^2 dx \right]^{\frac{1}{2}} \qquad (5\text{-}2)$$

The two cumulative distribution functions are normalized with the mean of the original cumulative distribution function. The parameter x represents the quantile. Then as noted earlier, the sensitivity case output cumulative distribution function refers to the case where the input distribution of only one of the parameters is changed by a prespecified value. Normalization with the mean value of the basecase makes the metric distance dimensionless.

Metric distance reflects the degree of impact an input parameter makes on the output distribution when the input distance is changed. A large value of the metric distance represents a large impact of the change in the input distribution on the output distribution.

For Monte Carlo or Latin hypercube sampling results, the metric distance can be expressed as

$$D = \left[\frac{1}{N} \sum_{n=1}^{N} \left[F_1^i(x) - F_2^i(x) \right]^2 \right]^{\frac{1}{2}} \bigg/ \frac{1}{N} \sum_{n=1}^{N} F_2(x)_n \qquad (5\text{-}3)$$

where i is the parameter of interest, N is the total number of realizations, n is the current realization, $F_1^i(x)_{n/N}$ is the $(n/N)^{th}$ quantile of the basecase ($0<n<N$) and $F_2^i(x)_{n/N}$ is the $(n/N)^{th}$ quantile for the sensitivity case. Equation (5-3) shows the method used to compute the metric distance in this report.

5.3　　　　　Implementation Procedure

For the distributional sensitivity analysis, first the sensitivity cases are designed and then the TPA code is run for the sensitivity cases.

The sensitivity case can be created in several ways:

•　　　　Change the variance of the distribution function. This changes the range of the data.

•　　　　Shift the mean of the distribution without changing the data range (i.e., fixed variance).

•　　　　Change the mean of the distribution while keeping the end points fixed (the variance and other moments may change).

In this report, Case 3 (the third bullet) has been used. The changes have been accomplished by

•　　　　Changing the mean by 10 percent of the range while keeping the minimum and maximum values fixed (see Figure 5-1). (Note: The shifted distribution function will not be symmetrical because the maximum and minimum values are forced to remain fixed.)

•　　　　Changing the distribution function from one type to another while keeping the minimum and maximum values fixed (see Figure 5-2).

A 10-percent shift to the mean changes the entire distribution function. As a convention in this report, the 10-percent shift in the mean is always positive. For example, if the original distribution function is normal, the new distribution function, after a 10-percent shift to the mean, is no longer a normal distribution. Therefore, another distribution function must be used to represent the new distribution function with a new mean value but fixed endpoints. Beta distributions have been chosen to represent the new distribution function because the four parameters that define a beta distribution provide sufficient flexibility to represent a large suite of distribution functions. The logbeta distribution function is used if the original distribution is a log distribution (e.g., log-uniform or lognormal). The beta distribution is used primarily to represent shifts to normal, uniform, and exponential distribution functions. Several distribution functions in the TPA Version 4.1 code representing the basecase data set do not need beta or logbeta representation of the new distribution function. For example, in a triangular distribution, a 10-percent shift to the mean can easily be accomplished by appropriately shifting the distribution apex.

The sensitivity cases in which the entire distribution function is changed are obtained by changing the original uniform to normal, log-uniform to logbeta, and lognormal to logbeta. The sensitivity case for the parameters with log distributions can be created by switching from log-uniform to lognormal or vice versa; however, such switching shifts the mean of the distribution, even if the means are identical in the log scale. Therefore, logbeta distributions with appropriate shape parameters are used so the sensitivity case has the same mean value as the basecase. This process is illustrated in Figure 5-3. All changes to symmetric distributions preserve the mean value, thus no special treatment is necessary. Note that the change from uniform to normal decreases the frequency of values near the high and low limits, and from normal to uniform increases the frequency of the values near the high and low limits
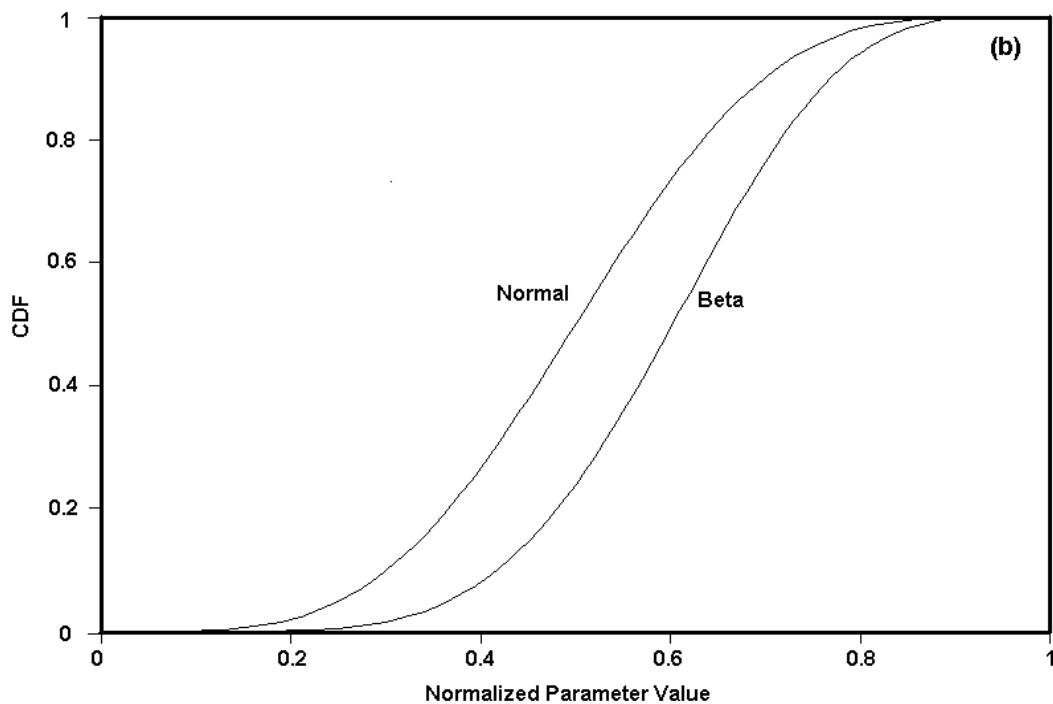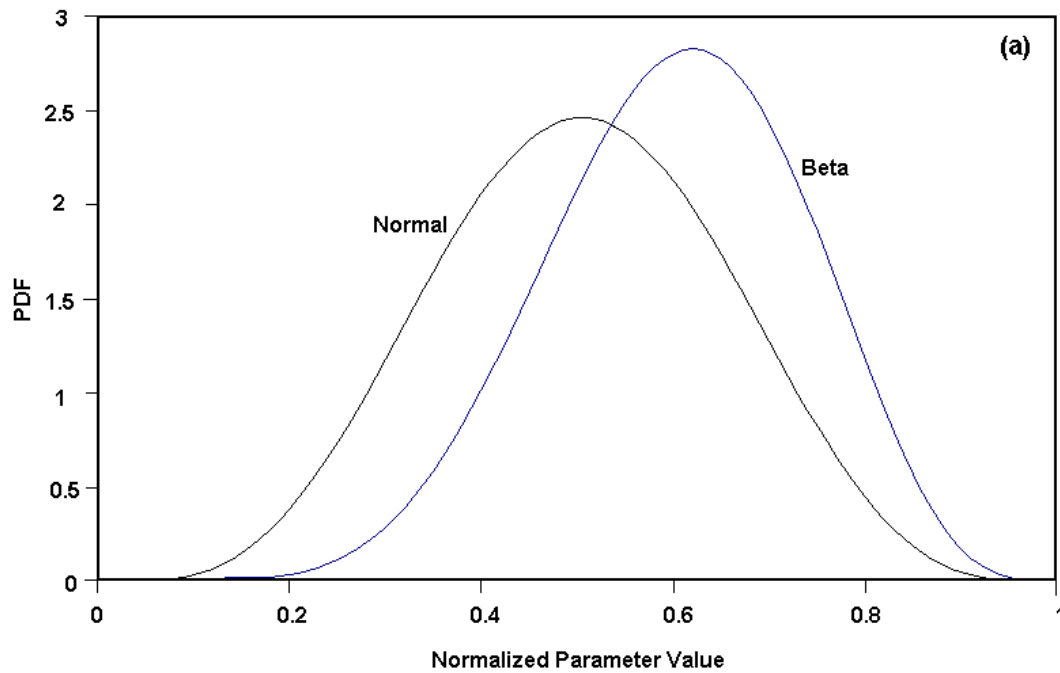
Figure 5-1. Example of (a) Changing the Probability Density Function for an Input Parameter by Shifting the Mean Value of a Normal Distribution Without Changing the End Points and (b) the Corresponding Changes to the Cumulative Distribution Functions. The New Distribution is Approximated by a Beta Distribution.
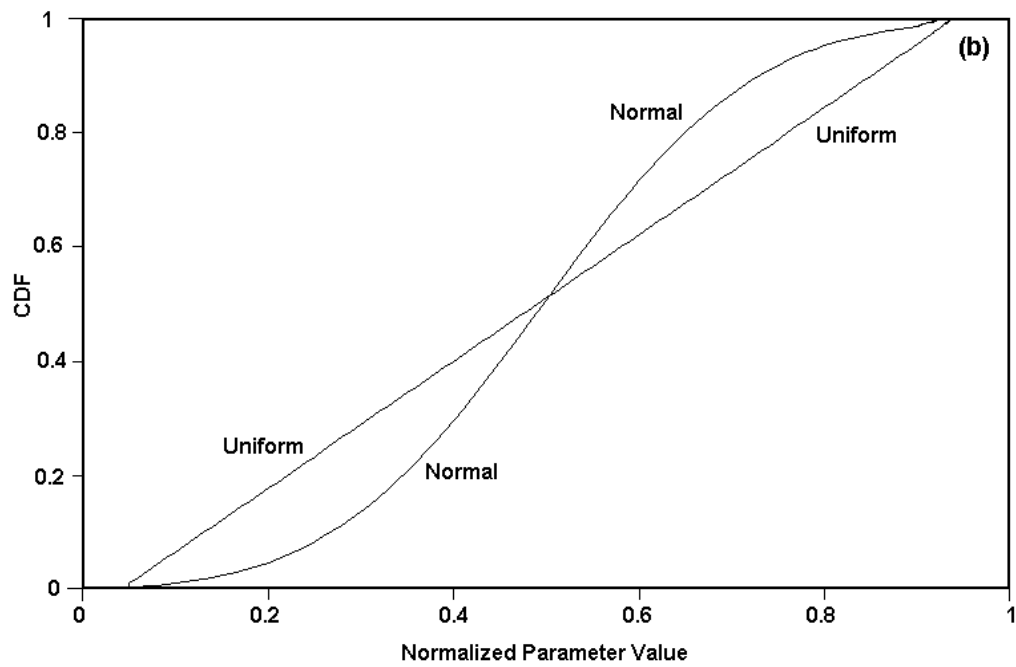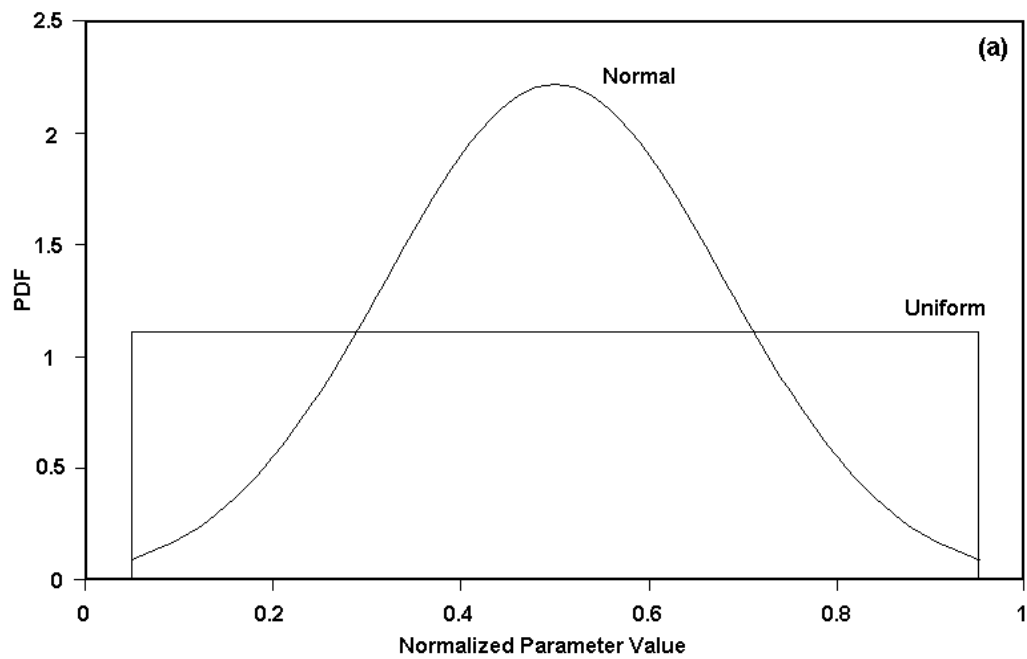
Figure 5-2. Example of (a) Changing the Probability Density Function by Changing the Distribution Type from Uniform to Normal and (b) the Corresponding Changes to the Cumulative Distribution Functions.
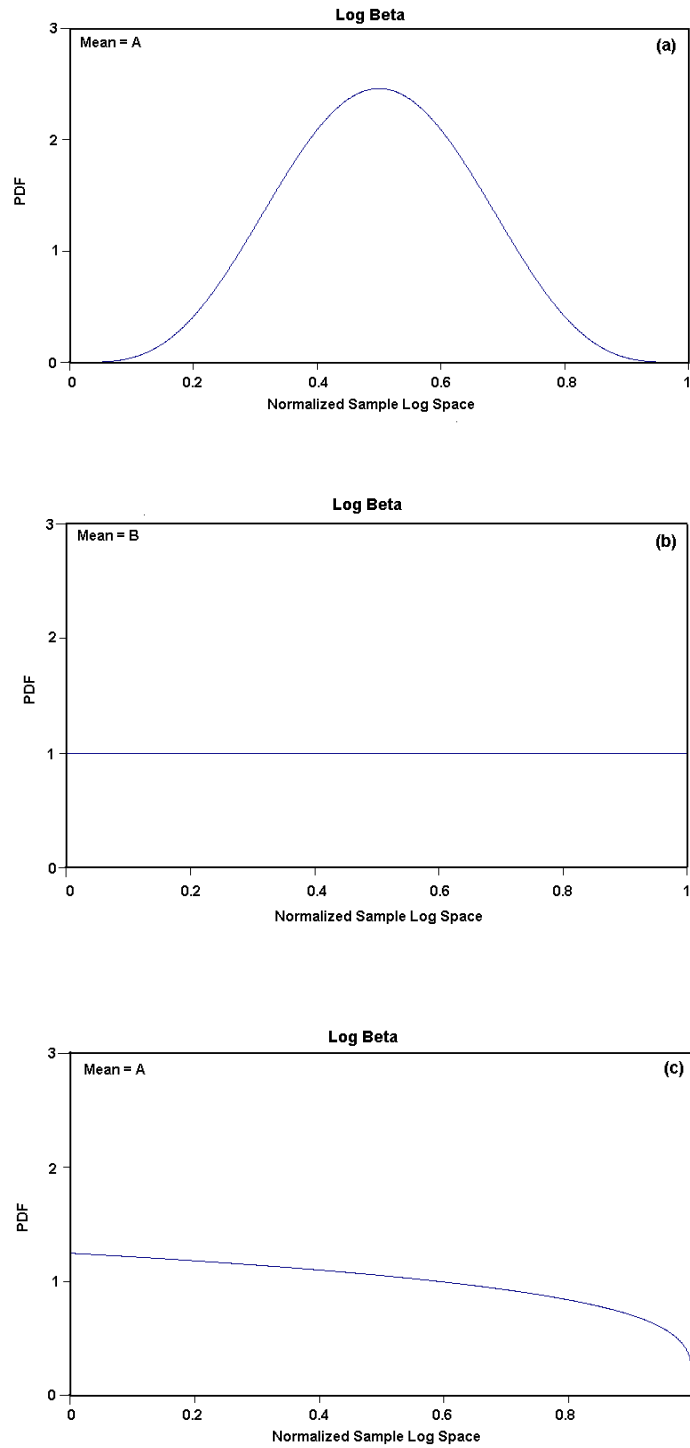
Figure 5-3. (a) Logbeta Representation of Lognormal with Mean A, (b) Logbeta Representation of Log-Uniform with Mean B, (c) Logbeta (d) with Shape Parameters Adjusted to Obtain Mean A

5-6

while keeping the mean value unchanged. The shape parameters in the logbeta distribution provide numerous possibilities for the shape of the distribution function while the mean is invariant. Therefore, while switching from lognormal to logbeta, the shape parameters are selected so that the logbeta distribution is as close as possible to the log-uniform distribution. Similarly, while switching from log-uniform to logbeta, the shape parameters for the logbeta distribution are selected so the shape of the logbeta distribution is as close as possible to the lognormal distribution. Figure 5-2 shows the minimum and maximum for the sensitivity case (i.e., the uniform distribution) are identical to the basecase (i.e., the normal distribution).

The sensitivity case was obtained by a 330-vector run after changing the distribution function for one parameter. To implement this method, the distribution function for only one parameter was changed for a given sensitivity case. The peak expected dose for the sensitivity case was computed using the same procedure used in computing peak expected dose from the basecase.

Because Latin hypercube sampling is used, the sampling sequence changes for other parameters when the distribution function is changed for the parameter of interest. Therefore, the original distribution is represented by a beta-equivalent approximation to obtain a modified basecase so that when the mean of the original distribution is shifted by 10 percent, there is no difference in the sampled values for the parameters other than the one that is changed. In effect, two Monte Carlo run sets were needed to perform consistent comparisons between the basecase and the sensitivity case.

Distributional sensitivity analysis was performed for the top 10 most influential parameters identified by the parametric sensitivity analysis methods described in Chapter 4. For the top 10 parameters, ideally, 3,630 realizations (i.e., 330 × 10 + 330 for the basecase) would be needed for constructing cumulative distribution functions and obtaining peak expected dose. Because of the need to obtain a modified basecase corresponding to each parameter, however, 6,600 realizations (i.e., 330 × 10 for the sensitivity case + 330 × 10 for the basecase) were needed to estimate the metric distance and the differences in the peak expected dose values.

5.4 Results

In this section, results are presented for the 10-percent shift to the mean of the input parameter distribution functions for the top 10 influential parameters. Then, the results for the change in the distribution type are presented. For both cases, results are presented for the 10,000-year simulation period.

Changes to the distribution function for the parameter set (i.e., 10-percent change to the mean for the top 10 parameters previously identified by the parametric sensitivity analysis methods) are shown in Table 5-1. The top 10 parameters used in the distributional sensitivity studies are the top 10 influential parameters based on the 10,000-year simulation period. In this table, column three shows the basecase distribution, column four shows the beta distribution equivalent of the basecase distribution, and column five shows the 10-percent shift to the means in the sensitivity case beta distribution. As mentioned before, this shift is 10 percent of the range of the distribution function.

Table 5-1. Modified Distribution Functions for the Top 10 Influential Parameters for Creating Sensitivity Cases				
Parameter		**Basecase Distribution**	**Revised Basecase Distribution**	**Sensitivity Case Distribution**
Abbreviation	**Description**			
WPFlowMF	Waste Package Flow Multiplication Factor	lognormal 3.15×10^{-2}, 1.05×10^{3}	logbeta 3.15×10^{-2}, 1.05×10^{3}, 5.0,5.0	logbeta 3.15×10^{-2}, 1.05×10^{3}, 8.2, 3.0
PSFDM1	Preexponential term for the spent nuclear fuel dissolution Model 2	log-uniform 1.2×10^{3}, 1.2×10^{6}	logbeta 1.2×10^{3}, 1.2×10, 1.0,1.0	logbeta 1.2×10^{3}, 1.2×10^{6}, 1.97,1.0
SbArWt%	Subarea wet fraction	uniform 0.0, 1.0	beta 0.0,1.0, 1.0,1.0	beta 0.0,1.0, 1.5,1.0
AAMAI@S	Areal average mean annual infiltration at start, [mm/yr]	uniform 4.0,13.0	beta 4.0,13.0, 1.0,1.0	beta 4.0,13.0, 1.5,1.0D
DSFailTi	Drip shield failure time [yr]	lognormal 2700.0, 20400.0	logbeta 2700.0, 20400.0, 5.0, 5.0	logbeta 2700.0, 20400.0, 7.8, 5.0
WPRRG@20	Well pumping rate at the 20-km [12.4 mi] receptor Group location [gal/day]	uniform 4.5×10^{6}, 1.3×10^{7}	beta 4.5×10^{6}, 1.3×10^{7}, 1.0, 1.0	beta 4.5×10^{6}, 1.3×10^{7}, 1.5, 1.0
WP-Def%	Fraction of total waste packages in a subarea that fails at time t = 0	uniform 1.0×10^{-4}, 1.0×10^{-2}	beta 1.0×10^{-4}, 1.0×10^{-2}, 1.0, 1.0	beta 1.0×10^{-4}, 1.0×10^{-2}, 1.5, 1.0
DTFFAVIF	Distance traveled in tuff [km]	uniform 10.0, 19.9	beta 10.0, 19.9, 1.0, 1.0	beta 10.0, 19.9, 1.5, 1.0
FOCTR	Fraction of water condensate moving toward repository	uniform 0.05, 1.0	beta 0.05, 1.0, 1.0, 1.0	beta 0.05, 1.0, 1.5, 1.0
ARDSAVNp	Matrix retardation for neptunium in the saturated zone of the Amargosa Valley alluvium	lognormal 1.0, 3.9×10^{3}	logbeta 1.0, 3.9×10^{3}, 5.0, 5.0	logbeta 1.0, 3.9×10^{3}, 8.2, 3.5

Table 5-2 shows that a 10-percent shift to the mean of the input distribution function toward high values resulted in a definite shift of the peak dose cumulative distribution function for each input parameter. The sensitivity case cumulative distribution functions shifted in such a way that, in all cases, the metric distance and peak expected dose changed. The minus sign for the peak expected dose implies there is an inverse relationship between the input and output parameters. This shift in the cumulative distribution function to higher values appears to be intuitively correct because a positive shift of the mean in the input distribution corresponds to sampling smaller values less frequently and sampling larger values more frequently. If the output value is directly proportional to the input value, the sensitivity case peak expected dose cumulative distribution function also shifts toward higher values and vice versa. The more pronounced the separation between the basecase and the sensitivity case cumulative distribution functions, the larger the magnitude of the metric distance. Because the whole cumulative distribution function shifted in the increasing direction without significant overlap, the metric distance is expected to correlate well with the magnitude of the change in the peak expected dose. Table 5-2 shows good correlation between metric distance and the relative change to the peak expected dose indicating, for the top 10 influential parameters, a shift in the mean of the input distribution directly resulted in a correspondingly large shift in the mean and variance of the dose values.

Table 5-2 shows that in 10,000 years, the WPFlowMF parameter is most sensitive to the change in the distribution function. For this parameter, the peak expected dose changed nearly 150 percent, with a metric distance of 4.78 [ft]. Recall that a metric distance of zero means no effect of the distributional change to the input on the output. Another parameter that showed a large change to the peak expected dose (i.e., 57.2 percent) is PSFDM1. Parameters with a moderate metric distance and change in peak expected dose are DSFailTi, WP-Def%, DTFFAVIF, and SbArWt%. Anomalous results have been observed only for ARDSAVNp. Although ARDSAVNp showed a change in peak expected dose comparable to WPRRG@20, its metric distance was much smaller compared to the latter. Such a difference in metric distance, with almost identical changes in peak expected dose, reveals that WPRRG@20 equally affected the realization peak doses as well as the peak expected dose, and ARDSAVNp affected the realization peak doses much less than the peak expected dose.

The next set of analyses involved changing the distribution type. Table 5-3 shows the basecase and the sensitivity case distributions with the associated parameters defining these distribution functions. Table 5-4 shows metric distance and the percentage changes to the peak expected dose for the 10,000-year simulation period corresponding to the sensitivity cases presented in Table 5-3. The percentage change in peak expected dose did not appear to correlate well with the metric distance for the parameters with lower metric distances, (i.e., less than 1.0). Three of six parameters (DTFFAVIF, SbArWt%, and WP-Def%) that have linear (i.e., nonlogarithmic) distribution functions showed a reasonably high metric distance (~0.7). Only one (DTFFAVIF) of the three showed greater than a 10-percent change to the peak expected dose. FOCTR showed a higher (i.e., ~10 percent) change in peak expected dose, while its corresponding metric distance was lowest among all parameters. This combination implies that the FOCTR parameter affected the peak expected dose but had minimal impact on peak dose. Only two parameters (ARDSAVNp and WPFlowMF) had metric distances greater than 1.0 and appear to have good correlation to the percentage change to the peak expected dose.

Table 5-2. Metric Distances for the 10,000-Year Simulation Period for the Top 10 Influential Parameters with 10 Subareas and 330 Realizations Where the Mean of the Distribution Is Shifted by 10 Percent of the Range				
Top 10 Parameters			**Metric Distance (mrem/yr)**	**Change in Peak Expected Dose (percent)**
Abbreviation	**Description**	**Distribution Type**		
WPFlowMF	Waste package flow multiplication factor	Lognormal	4.78×10^0	149.88
PSFDM1	Preexponential term for the spent nuclear fuel dissolution Model 2	Log-uniform	1.40×10^0	57.20
SbArWt%	Subarea wet fraction	Uniform	4.98×10^{-1}	24.93
AAMAI@S	Areal average mean annual-infiltration at start [mm/yr]	Uniform	2.09×10^{-1}	5.28
DSFailTi	Drip shield failure time [yr]	Lognormal	9.98×10^{-1}	-24.83
WPRRG@20	Well pumping rate at the 20-km [12.4-mi] receptor group location [gal/day]	Uniform	3.24×10^{-1}	-8.62
WP-Def%	Fraction of total waste packages in a subarea that fails at t = 0	Uniform	5.30×10^{-1}	22.06
DTFFAVIF	Distance traveled in tuff [km]	Uniform	5.16×10^{-1}	19.89
FOCTR	Fraction of water condensate moving toward the repository	Uniform	2.15×10^{-1}	4.41
ARDSAVNp	Matrix retardation for neptunium in the saturated zone of the Amargosa Valley alluvium	Lognormal	8.88×10^{-2}	-8.35

In the case of the uniform-to-normal change, the metric distance will change, but it is possible that the peak expected dose did not change because the mean of the distribution was preserved. The frequency values on both sides of the mean near the limits decrease symmetrically. The same is true for the normal to uniform case except that the frequency of values on both sides of the mean near the limits increased symmetrically. If the relationship between the input parameter and the peak expected dose is linear, the metric distance can be large even if the peak expected dose does not change; such is the case for AAMAI@S. If a change in the peak expected dose does occur, it is an indication the relationship between the dose and the parameter being studied is nonlinear.

Table 5-4 also shows that changing the distribution from lognormal to log-uniform and vice versa resulted in larger changes in the peak expected dose and overall larger metric distances. The percentage change in peak expected dose for the logarithmic distributions (4 of 10 parameters) ranged between 12.41 and 94.98 percent; whereas, for the parameters

Table 5-3. Changes to Distribution Type (One Parameter at a Time) to Create the Sensitivity Case in Which the Entire Distribution Function Is Changed; Metric Distances for the 10,000-Year Simulation Periods Using 10 Subareas and 330 Realizations Where the Distribution Type Is Changed Only One Parameter at a Time

Top 10 Parameters		Basecase	Sensitivity Case
Abbreviation	**Description**	**Basecase**	**Sensitivity Case**
WPFlowMF	Waste package flow multiplication factor	logbeta 3.15×10^{-2}, 1.05×10^{3}, 5.0, 5.0	logbeta 3.15×10^{-2}, 1.05×10^{3}, 1.0, 2.096
PSFDM1	Preexponential term for the spent nuclear fuel dissolution Model 2	logbeta 1.2×10^{3}, 1.2×10^{6}, 1.0, 1.0	logbeta 1.2×10^{3}, 1.2×10^{6}, 4.0, 2.35
SbArWt%	Subarea wet fraction	uniform 0.0, 1.0	normal 0.0, 1.0
AAMAI@S	Areal average mean annual-infiltration at start [mm/yr]	uniform 4.0, 13.0	normal 4.0, 13.0
DSFailTi	Drip shield failure time [yr]	logbeta 2700.0, 20400.0, 5.0, 5.0	logbeta 2700.0, 20400.0, 1.0, 1.247
WPRRG@20	Well pumping rate at the 20-km [12.4 mi] receptor group location [gal/day]	uniform 4.5×10^{6}, 1.3×10^{7}	normal 4.5×10^{6}, 1.3×10^{7}
WP-Def%	Fraction of total waste packages in a subarea that fails at time $t = 0$	uniform 1.0×10^{-4}, 1.0×10^{-2}	normal 1.0×10^{-4}, 1.0×10^{-2}
DTFFAVIF	Distance traveled in tuff [km]	uniform 10.0, 19.9	normal 10.0, 19.9
FOCTR	Fraction of water condensate moving toward repository	uniform 0.05, 1.0	normal 0.05, 1.0
ARDSAVNp	Matrix retardation for neptunium in the saturated zone of the Amargosa Valley alluvium	logbeta 1.0, 3.9×10^{3}, 5.0, 5.0	logbeta 1.0, 3.9×10^{3}, 1.0, 1.91

with linear (i.e., nonlogarithmic) distributions (6 of 10), the range is 0.86 to 16.89 percent. Note that 3 of 4 parameters with logarithmic distributions showed the 3 largest metric distances and changes in peak expected dose when the mean of the distributions is shifted by 10 percent. This analysis, however, revealed that the appropriate selection of distribution functions, especially for the parameters with logarithmic distribution is important. A wrong selection of a lognormal distribution instead of a log-uniform distribution may have a greater impact than the wrong selection of a uniform distribution for a normal distribution.

Table 5-4. Metric Distances for the 10,000-Year Simulation Period for the Top 10 Influential Parameters with 10 Subareas and 330 Realizations Where Distribution Type Is Changed

Top 10 Parameters			Metric Distance (mrem/yr)	Changes in Peak Expected Dose (Percent)
Abbreviation	**Description**	**Distribution Type**		
WPFlowMF	Waste package flow multiplication factor	Logbeta to logbeta (See Table 5-3)	1.24×10^0	−44.10
PSFDM1	Spent nuclear fuel dissolution (Preexponential term)	Logbeta to logbeta (See Table 6-5)	6.94×10^{-1}	42.09
SbArWt%	Subarea wet fraction	Uniform to normal	7.01×10^{-1}	−6.13
AAMAI@S	Areal average mean annua-infiltration at start [mm/yr]	Uniform to normal	2.50×10^{-1}	−0.86
DSFailTi	Drip shield failure time [yr]	Logbeta to logbeta (See Table 5-3)	6.22×10^{-1}	−12.41
WPRRG@20	Well pumping rate at the 20-km [12.4-mi] receptor group location [gal/day]	Uniform to normal	3.77×10^{-1}	−3.56
WP-Def%	Fraction of total waste packages in a subarea that fails at time t = 0	Uniform to normal	6.08×10^{-1}	−3.31
DTFFAVIF	Distance traveled in tuff [km]	Uniform to normal	7.81×10^{-1}	−16.89
FOCTR	Fraction of water condensate moving toward repository	Uniform to normal	2.13×10^{-1}	9.25
ARDSAVNp	Neptunium retardation in alluvium	Logbeta to logbeta (See Table 5-3)	2.30×10^0	94.98

In summary, distributional sensitivity analyses showed that improper choice of distribution function for certain variables can affect significantly the dose responses. Distributional sensitivity also reveals important information about the input-output relationship. For some parameters, the output was affected at all cumulative distribution function levels. For some other parameters, the output was affected at all cumulative distribution function levels except at the mean values. The two dose measures showed high distributional sensitivity, especially when the mean values were changed for the most influential parameters identified by the parametric sensitivity analysis methods. The two parameters are (i) the flow multiplication factor that determines the quantity of water entering the waste package (a 10-percent change to the parameter mean resulted in a 150-percent change in the dose) and (ii) the preexponential term for the spent nuclear fuel model used in the basecase (a 10-percent change to the parameter mean resulted in a 57-percent change in the dose). The analysis also revealed that, for some parameters (e.g., FOCTR), the output may not be affected significantly at any cumulative distribution function level although the peak expected dose can be affected substantially.

This combination revealed that the FOCTR parameter could influence the dose curve throughout (especially where the peak expected dose occurred) except where the realization peak occurred.

6 REPOSITORY COMPONENT SENSITIVITY ANALYSIS

6.1   Background

This chapter focuses on repository component sensitivity analysis in which the change in repository performance in response to a specified level of degradation in the functionality of the repository component is assessed. The repository system can be categorized into components in many ways. In this report, the components or subsystems are defined as physical entities of the repository. Because physical entities are easy to visualize, insights into repository performance can be readily gained. Although the repository has been divided into physical components to facilitate visualization of system performance, the repository system performance is still best described as the interaction of the physical features and processes that represent the natural and engineered systems with driving forces in the repository environment.

Repository component sensitivity analysis is different from standard sensitivity analysis in several ways. Generally, sensitivity analysis is used in the context of studying the effect of parameters, conceptual models, and scenario definitions on the system model response. Parametric, model, and scenario sensitivity analyses, however, do not readily get at the structural role of repository components. Also, if a component is modeled conservatively, parametric or conceptual model sensitivity analyses will fail to identify the true influence of the component or the overall system performance. An example is the role of the invert as a repository component. If the flow in the invert is conservatively assumed to be high, fracture flow would dominate, and, thus, the model parameters for transport processes in the invert would not be sensitive. Consequently, it can be concluded the invert is not important. Besides, the model predicts the waste package will last beyond the simulation period; parametric sensitivity analysis also will not identify the waste package as important because the waste package does not fail during that period. Sensitivity analysis, however, does not provide an understanding of the level of performance attributable to the waste package because in the system-level model, great effort is made to include as many process couplings as possible, which leads to masking the importance of one repository component or process by another. Sensitivity analysis is limited only to the model or submodels used in the system-level model. System-level modeling makes two inherent assumptions: all scenarios have been evaluated and the abstraction model appropriately accounts for all important scenarios, together with the couplings among processes in the presence of all features and events. Some residual uncertainty always remains in spite of the best effort, the scenario analysis and the model representation may have errors. In such a case, repository component sensitivity analysis provides an added degree of confidence by answering the following question: How will the system perform under assumed errors in modeling repository components?

Repository component analysis in this report was conducted by comparing the repository-system performance loss (or improvement) for a repository component case (i.e., the sensitivity case) with the basecase performance. A sensitivity case involves suppression or elimination of a repository component functions or functions of a combination of components from the performance assessment calculation. After the repository component functions are suppressed, the performance assessment calculations are performed as usual. The suppression of a repository component function is accomplished by (i) selection of an appropriate alternative conceptual model (that already exists in the system-level performance assessment model) and (ii) appropriate modifications to model parameters.

The suppression of a repository component only implies that the component no longer performs its intended function. It does not mean the component is physically removed because the removal would completely alter the conceptual framework. In this sense, the estimated repository component sensitivity is dependent on the modeling approaches, assumptions, variability, and uncertainty in the system model for the repository components that are not suppressed.

The performance metric used for repository component sensitivity analyses is the ratio between peak expected doses in the sensitivity case and in the basecase. The sensitivity cases are run for 10,000 years with the critical group located 20 km [12.4 mi] from the proposed repository footprint. The sensitivity cases represent either treatment of one repository component or a group of repository components. Because this approach requires one or more large sets of Monte Carlo calculations for each repository component or group of repository components tested, computational requirements are large. It should be noted that completely suppressing the functions of a repository component is clearly not realistic and therefore any dose results from such an analyses must not be compared to the regulatory standard. However, this device of suppressing repository component functions provides another powerful tool for understanding system behaviors under conditions not envisioned to exist in the completed case.

The repository component sensitivity analysis described is not intended to provide either guidance to the U.S. Department of Energy or describe a preferred approach for demonstrating the capabilities of barriers. These analyses were performed to further the staff efforts to understand the TPA Version 4.1 code and to explore ways to improve understanding of the repository system.

6.2 Description of Repository Components

For the purposes of this report, the repository system was divided into the following components: (i) drip shield, (ii) waste package, (iii) spent nuclear fuel, and (iv) invert. For the natural barrier, only the unsaturated zone and saturated zone as repository components will be studied.

In the following subsections, the functionality of the repository components selected for the repository component sensitivity analysis and the approach taken to suppress a repository component are briefly described. Discussions are provided as applicable whenever modification to one repository component will require changes to another repository component.

6.2.1 Drip Shield

By design, the drip shield, which is made of titanium, is expected to prevent aggressive chemicals in the flowing water during the early stage of repository closure from contacting the waste package. An intact drip shield is expected to prevent water from the drift wall from contacting waste packages, although the presence of the drip shield may lead to condensation of water underneath it. Corrosive chemicals (e.g., the deliquescence effect) could lead to early waste package failure because of corrosion and could readily dissolve already exposed spent nuclear fuel. The drip shield is also expected to prevent the waste package from damage by rockfall resulting from seismic events. Rockfall could lead to direct mechanical failure of the waste package, augment stress corrosion cracking, or create permanent deformation on the waste package where water could accumulate for an early start of corrosion after drip-shield failure.

The drip shield itself can undergo localized corrosion, uniform corrosion, or both. Effects, such as displacement of drip shields or development of a stress state in the materials that can lead to stress corrosion cracking, are not included in the model. The degradation of the drip shield is specified by a failure-time distribution that already accounts for any potential exposure to a stressful environment or degradation process.

The drip shield failure time in the basecase ranges between 2,700 and 20,400 years and is described by a lognormal distribution with a mean failure time of 7,241 years. For repository component sensitivity analysis, the suppression of the drip shield as a repository component is achieved by forcing the drip shield to fail immediately after closure of the repository. Consequently, the waste package is now exposed to the chemical environment that the drip shield was exposed to in the most likely scenario. Because the drip shield in the basecase is assumed completely suppressed at the time of failure, it does not limit the dripping water from entering a failed waste package.

6.2.2   Waste Package

By design, the waste package prevents water and dissolved chemicals from contacting the spent nuclear fuel. The waste package comprises an outer overpack of Alloy 22 to provide corrosion resistance and an inner overpack of stainless steel to provide mechanical strength. Mechanical disruption of the waste package includes residual stress and seismically induced rockfall that could hit the waste package and the drip shield, or, if the drip shield is not present, the rock could hit the waste package directly. Effects, such as mechanically deformed drip shields impinging on the waste package and development of a stress state in the materials that can lead to stress corrosion cracking, are not currently included in the performance assessment model.

The thermo-hydro-chemical environment dictates the nature of the waste package failure, which could be either small-diameter pits if localized corrosion is dominant or large patches if uniform corrosion is dominant. In the absence of igneous activity and faulting disruptive events, three failure modes occur: seismic rockfall, initial defects, and corrosion. These failure modes may create bathtubs after waste package failure. Basecase calculations show most waste packages fail from uniform corrosion. Therefore, large patches instead of pits are expected on the waste package.

For repository component sensitivity analysis, suppression of the waste package as a repository component is achieved by forcing the two waste package overpacks to fail at the time of repository postclosure. Therefore, all waste packages, including the packages that fail immediately after closure of the repository, are available for potential release. In the basecase, these remaining 8,828 (8,877 – 49) waste packages fail on average, at year 59,637. In the basecase, when the waste package fails naturally as a function of corrosion, it forms a bathtub. For the waste package repository component suppression case, however, the waste package is assumed to be completely removed. Consequently, the water contact mode is changed from bathtub to flow-through, and, instead of only a fraction of spent nuclear fuel being wet, all spent nuclear fuel is wet. Because the waste package layers are assumed to be completely removed, no flow diversion will occur. Therefore, all water impinging on a waste package in a basecase now contacts the spent nuclear fuel.

6.2.3 Waste Form

The spent nuclear fuel in the waste package consists of UO_2 pellets inside zircaloy clad fuel rods, hence, water must penetrate the fuel clad before contacting the spent nuclear fuel. In the basecase scenario, fuel clads are assumed not present; therefore, water will contact spent nuclear fuel as soon as it enters the waste package. Spent nuclear fuel must dissolve in the contacting water for release to take place. Water may contact the spent nuclear fuel pellets at their surface and the walls of the interconnected pores. In the release model, it is assumed the radionuclides will be released congruently with the dissolution of the UO_2 matrix that forms the spent nuclear fuel pellet.

The basecase spent nuclear fuel-dissolution model is a function of temperature and assumes that Ca^{2+} and Si^{2+} are present in the water. With this dissolution model, spent nuclear fuel takes more than 10,000 years for complete dissolution. For the repository component sensitivity analysis, suppression of the waste form as a repository component is achieved by forcing all spent nuclear fuel in the waste package to dissolve instantaneously at the first contact with water. Because the radionuclides are released from the spent nuclear fuel congruently, the associated radionuclides are available for instantaneous release from the waste package. Because the release is solubility controlled for some nuclides, however, those nuclides are not expected to be released any faster than the basecase if the flow rates are identical for the two cases. As in the basecase, only the spent nuclear fuel immersed in the bathtub will contribute to release.

6.2.4 Invert

Releases from the waste package will travel through the invert before entering the drift floor. Water running off or passing through the waste package would fall onto the invert. The current design shows the waste package on a v-shaped pallette held together by stainless steel supports over a porous invert made of carbon steel with a sand or gravel ballast. The invert material is expected to sorb several radionuclide species, thereby providing an additional repository component to impede their release into the geosphere. Flow through the invert or mass transfer can be both advective and diffusive. Sorption of radionuclides from the flowing water may offer a significant reduction in releases. In the model, if the water flow rate exceeds the hydraulic conductivity of the invert material, the invert model becomes a passthrough with no radionuclide holdup or retardation. In the current design, with a porous medium invert, this bypass is unlikely. The model does not account for colloidal transport and the possibility that radionuclides in the water might be captured along the liquid-water pathway by precipitation or sorption on material inside the waste package.

For repository component sensitivity analysis studies, the functions of the 0.75-m [2.5-ft] thick invert as a repository component is suppressed by specifying the invert thickness as zero at the time of repository closure; thus, there is no delay in fluid flow, and there is no retardation of the radionuclides.

6.2.5 Unsaturated Zone

The repository is located in the unsaturated zone, roughly halfway between the ground surface and the water table. The unsaturated zone is a repository component because it has the potential to substantially reduce flow of water and delay the transport of radionuclides to the

water table. The portion of the unsaturated zone above the repository is a repository component relevant only to flow of water, whereas the unsaturated zone below the repository is relevant as a repository component to both flow of water and transport of radionuclides. In this report, the unsaturated zone above and below the repository level are jointly referred to as the unsaturated zone. Hydrology of the unsaturated zone is represented as flow in both porous and fractured media, considering fracture versus matrix flow, groundwater velocity, moisture content, stratigraphic thickness, and fracture and matrix porosity and permeability. Time-varying, deep percolation is derived from the time-varying climate and shallow infiltration. Deep percolation is perturbed at the near field by decay heat at the repository level, resulting in alterations to the amount, arrival time, and chemical composition of the fluid to which the waste packages and waste forms may be exposed. Movement of water toward or away from the waste package is expected to take place by potential large-scale (external to the drift) focusing or diversion, film flow at the surface of the drift, capillary diversion in the fractures near the drift, and diversion of flow caused by the presence of corrosion products in corroded waste packages.

Radionuclide transport in the unsaturated zone between the repository horizon and the water table is primarily a function of groundwater traveltime, sorption, matrix diffusion, and longitudinal dispersion. Retardation of radionuclides in fractures caused by sorption is expected to be small and, therefore, is not represented in the basecase. Although the mathematical model can handle matrix diffusion in the unsaturated zone, it is expected to be minor on the basis of off-line modeling studies. Therefore, it is conservatively assumed not to occur for the basecase.

Suppression of the unsaturated zone repository component requires consideration of its characteristics as a flow repository component (above and below the repository) and its characteristics as a transport repository component below the repository. In the total system performance assessment model, water is assumed to percolate directly through fractures to the repository near field after shallow infiltration in the surficial soil, which, to some degree, tempers the temporal variation of the infiltration. Suppression of the unsaturated zone as a flow repository component above the repository requires modifications to only the infiltration in the surficial soil, thermo-hydrological refluxing, and near-field flow convergence or divergence. The shallow infiltration rate is replaced with precipitation to reflect suppression of the unsaturated zone above the repository. To suppress the near-field flow diversion, parameters representing the thermal dryout zone thickness, the fraction of condensate removed from the reflux zone, the fraction of condensate moving toward the repository, and the fraction of condensate removed by other processes are adjusted in such a way that water from the deep percolation can reach the waste package without the delay or loss caused by the reflux. To suppress flow diversion, the flow multiplication factors (F_{ow}, together with its multiplier that reflects uncertainty) are adjusted so that all deep percolation will reach the waste packages, and waste packages in the repository are exposed to deep percolation.

Suppression of the unsaturated zone as an impediment to flow and transport below the repository requires modifications to the thicknesses of the stratigraphic units. Consequently, the effective distance between the repository and the saturated zone becomes zero. When only the unsaturated zone repository component is suppressed, the waste packages still form bathtubs for radionuclide release, though the filling time will be different compared with the basecase.

6.2.6   Saturated Zone

The alluvium unit layer of the saturated zone is expected to substantially delay transport of radionuclides. A two-dimensional horizontal flow model is used to construct the steady-state velocity fields represented through a series of three, one-dimensional flow tubes from the water table (at locations directly below the repository) to the receptor location. The model for radionuclide transport in the saturated zone considers longitudinal dispersion, retardation, and matrix diffusion. Lateral dispersion and sorption of radionuclides on fracture surfaces are not included.

Repository component analysis of the saturated zone repository component requires suppression of those characteristics that delay the transport of radionuclides, such as modifications to length of the flow path in the fractured tuff aquifer and length of the flow path in alluvium between the repository footprint and the receptor located 20 km [12.4 mi] from the repository. In the basecase, the projected radionuclide transport path length from the repository footprint to the tuff-alluvium contact (via the fractured tuff aquifer) ranges between 10 and 20 km [6.2 and 12.4 mi], has a uniform distribution, and has a mean distance of 15 km [9.3 mi], which results in an average alluvium length of 5 km [3.1 mi]. By specifying the alluvium length essentially 0 km [0 mi], the beneficial sorption capacity and high kinematic porosity of the saturated alluvium were excluded from the calculation. By adjusting the alluvium length, the tuff aquifer was extended to the 20-km [12.4-mi] compliance point so the reasonably maximally exposed individual at 20 km [12.4 mi] can be used. The flow in the fractured tuff aquifer is predominantly in fractures and is assumed to be fast. The nominal fracture porosity, which is log-uniformly distributed ranging between 1×10^{-3} and 1×10^{-2}, was changed to a constant value of 1×10^{-4}, and the fracture-to-matrix diffusion coefficient was changed from 1×10^{-3} to 0.0 so the traveltime in the artificially established 20-km [12.4-mi] fractured tuff was small (~12 to 15 years). Other parameters, such as (i) longitudinal dispersivity (sampled as a fraction of the transport path length), (ii) effective flow porosities, (iii) matrix (immobile) porosity, and (iv) fraction of the immobile porosity penetrated for the saturated tuff have little if any effect under the neutralized conditions, and did not need to be changed from the values used in the basecase.

6.3   Effects of Disruptive Events on Repository Components

Three disruptive events were included in the performance assessment model: seismicity, faulting, and volcanism. Although the primary effect of seismicity and faulting in the system performance calculation was to cause additional waste package failures, the effect of an igneous activity disruptive event was broader. An intrusive igneous activity event results in failure of waste packages, whereas an extrusive igneous activity event creates a new source term because of waste-form entrainment to the atmosphere and a new biosphere pathway resulting from airborne transport of radionuclides and redistribution of radionuclides in soil. Repository component sensitivities also may be influenced by these external events.

Because seismicity, faulting, and intrusive igneous activity are modeled primarily to disrupt waste packages, the waste package repository component sensitivity analysis already provides needed information. Repository component sensitivity analysis for extrusive igneous activity requires somewhat complicated calculations involving convolution of as many as 12 sets of Monte Carlo calculations completed for various time periods. In the current model, the 12 sets are computed at fixed volcanic event times: 100; 500; 1,000; 2,000; 3,000; 4,000; 5,000; 6,000;

7,000; 8,000; 9,000; and 10,000 years for a given repository component suppression case. In this report, simulations have been conducted for a 10,000-year simulation period, with the volcanic event time at 10,000 years omitted from each set. All volcanism runs were made with both ground surface and groundwater dose contributions. Normal igneous activity calculations assumed groundwater dose can be neglected because the dose consequence (not risk) for igneous activity far exceeds the groundwater dose, and the calculations are configured to consider only ground surface contributions.

6.4   Results

This section presents results from repository component sensitivity analyses using either individual repository components or a combination of repository components. For 6 repository components there can be 64 (i.e., 2^6) possible unique combinations. In this report, a selected list of combinations was used with the assumption that other combinations either (i) do not have significant sensitivity or (ii) do not help identify the influential repository components. Because the identification of influential repository components is based on relative change and because results from 100 realizations are comparable to results from 350 Latin Hypercube samples, performing the limited calculations of a single set of 100 realizations for each configuration of suppressed barriers is consistent with the goals for conducting this analysis. Results for the basecase {i.e., a peak expected annual dose of 2.0 × 10^{-4} Sv/yr [0.02 mrem/yr] within 10,000 years} are based on a single set of 350 realizations—the best estimate for peak expected dose may be higher or lower (see Appendix H for a related discussion on the stability of the results for limited realizations). Similarly, the results presented for each suppressed configuration may be higher or lower than the best estimate. Consequently, if the ratio of the peak expected dose for the suppressed configuration to the peak expected dose of the basecase is close to one, suppressing the barrier or barriers may have no effect or a slight effect on the calculated dose.

6.4.1   One-Off Repository Component Sensitivity Analysis

The one-off repository component results are presented in Figure 6-1.

6.4.1.1   Drip Shield

Suppression of the drip shield resulted in a 34-percent increase in the dose level compared with the basecase. Suppression of the drip shield can potentially hasten the corrosion process and permit early contact of infiltrating water with the spent nuclear fuel. Suppression of the drip shield did not result in early failure of the waste package from corrosion but did permit water to contact spent nuclear fuel at early times. On average, the drip shield delays water contacting spent nuclear fuel in the initially defective waste packages for 7,830 years.

6.4.1.2   Waste Package

The suppression of the waste package repository component resulted in a 68,200-percent increase in dose with respect to the basecase. In the basecase, only the initially defective waste packages contributed to dose. In the waste package repository component sensitivity case, all waste packages dripped on are available for release at the beginning of the simulation. The average waste package failure time in the basecase is 59,637 years.

Figure 6-1. Single Repository Component Suppression (One-Off Sensitivity Analysis) for the 10,000-Year Simulation Period. Each Row Represents a Monte Carlo Analysis with a Repository Component Suppressed. The First Column Represents the Basecase with Six Repository Components. The Gray Color Indicates the Corresponding Repository Component Has Been Suppressed. The Value at the Bottom of Each Column is the Relative Change to the Peak Expected Dose in Percent.

6.4.1.3   Waste Form

The suppression of the waste form as a repository component increased the dose by approximately 60 percent. The dissolution time was set at 50 years for numerical efficiency in this case. The suppression of the waste form repository component decreased the time in which the spent nuclear fuel completely dissolved in water from more than 100,000 years (for 60 percent of the cases) to 50 years. It could be assumed that this would result in a many fold increase in the dose, but this is not the case. The less than two-fold increase in dose implies that even if spent nuclear fuel dissolved quickly, the solubility limit of the radionuclides constrained their removal from the waste package.

6.4.1.4   Invert

The suppression of the invert as a repository component increased dose by 6 percent. This small change can be attributed to a short {0.75-m [2.5-ft]} transport path. Depending on the infiltration rate, flowthrough the invert is either predominantly matrix flow or predominantly fracture flow. Because the flow in the invert in the basecase was predominantly fracture flow (contrary to the original hypothesis) and because of the assumption that the radionuclides were not retarded in fractures, it comes as no surprise that the dose was insensitive to invert suppression.

6.4.1.5   Unsaturated Zone

For the purposes of this analysis, the upper unsaturated zone (above the repository) and the lower unsaturated zone (below the repository) are considered as a single repository component called the unsaturated zone. The suppression of the unsaturated zone as a repository component resulted in a nearly 2,000-percent increase in peak expected dose. Traveltimes were relatively fast through the lower unsaturated zone, and none of the radionuclides were retarded in the fractures. In subareas where the Calico Hills vitric layer was thin or absent, soluble, unretarded species such as Tc-99 and I-129, were minimally influenced by transport through the lower unsaturated zone matrix. The lower unsaturated zone matrix may retard some species, such as uranium and thorium, but because of the predominant fracture flow in most of the subareas, these nuclides did not travel much faster in the repository component sensitivity case. Therefore, radionuclide transport in the lower unsaturated zone does not influence repository component sensitivity. Consequently, the sensitivity of dose to this repository component can be attributed to the ability of the upper unsaturated zone to limit the amount of water reaching the waste packages. This both increases the transport of radionuclides from the waste packages, and reduces the filling time of those waste packages. On an average, approximately 6 percent of precipitation at the surface of Yucca Mountain infiltrates. The remaining 94 percent is either diverted at the surface or lost by evapotranspiration. With the unsaturated zone suppressed, 100 percent of the water moves toward the waste package. Moreover, the absence of fractures does not focus flow into limited repository areas; hence, all waste packages are dripped on. Therefore, the repository performance shows significant sensitivity to the upper unsaturated zone.

6.4.1.6   Saturated Zone

The suppression of the saturated zone as a repository component resulted in nearly a 900-percent increase in peak expected dose. The increase in dose resulted from the reduction in the length of alluvium, through which the radionuclides may be transported, and a variation in the flow fields. Tc-99, I-129, and Cl-36 are expected to be primary dose contributors in the basecase and are unretarded in porous alluvium, hence, variations in the flow fields (porosity, permeability, and such) have only a small effect on Tc-99 and I-129 arrival times in 10,000 years. For Np-237, which is moderately retarded in alluvium, however, the impact is more significant when the saturated zone repository component is suppressed. For the 10,000-year simulation period, 85.4 percent of the dose is composed of Np-237, and the unretarded species (Tc-99, I-129, and Cl-36) compose 14.5 percent of the dose. The remainder of the radionuclides never reach the critical group in the 10,000-year simulation period.

6.4.2   One-On Repository Component Sensitivity Analysis

One-on repository component sensitivity analysis was conducted by first suppressing all repository components and then adding only one repository component. The relative change in dose from the one-on repository component case and the case with all repository components suppressed was the sensitivity measure for the one-on repository component sensitivity analysis. The one-on repository component results are presented in Figure 6-2.

One-on sensitivity analysis showed that repository components influenced performance in the following order: waste package, unsaturated zone, saturated zone, waste form, drip shield, and invert. Calculations also clearly showed that only three repository components were most influential: waste package (>99.9-percent decrease in dose), unsaturated zone (96-percent decrease in dose), and saturated zone (94-percent decrease in dose). One-on repository component sensitivity analysis also showed that the invert barely made any contribution to performance. This information is important because with the knowledge of poor performance of the invert, it can be determined if excessive conservativeness could be responsible for this result. Drip shield and waste form repository components showed only moderate sensitivity. Although the analysis presented in Chapter 4 indicated that the drip-shield failure time uncertainty significantly influenced repository performance uncertainty, the calculation did not provide insight into the level of performance. One-on sensitivity analysis showed the peak expected dose decreased by 63 percent, a value that can be compared against performance of other individual repository components such as 99.9 percent for the waste package repository component. The absolute performance of the drip shield was not obvious in the one-off analysis because, even if the drip shield performance was suppressed, the waste package prevented water from contacting the spent nuclear fuel.

6.4.3   Cumulative One-On Repository Component Sensitivity Analysis

To illustrate the effects of repository component suppression more clearly, all repository components were suppressed sequentially and cumulatively. By proceeding in a sequence that represents the vertical spatial positions of the repository components from bottom to top, performance of the newly added repository component was not masked by the previously added repository components. The cumulative one-on repository component results are presented in Figure 6-3. The left-most column in Figure 6-3 reflects a case in which all repository
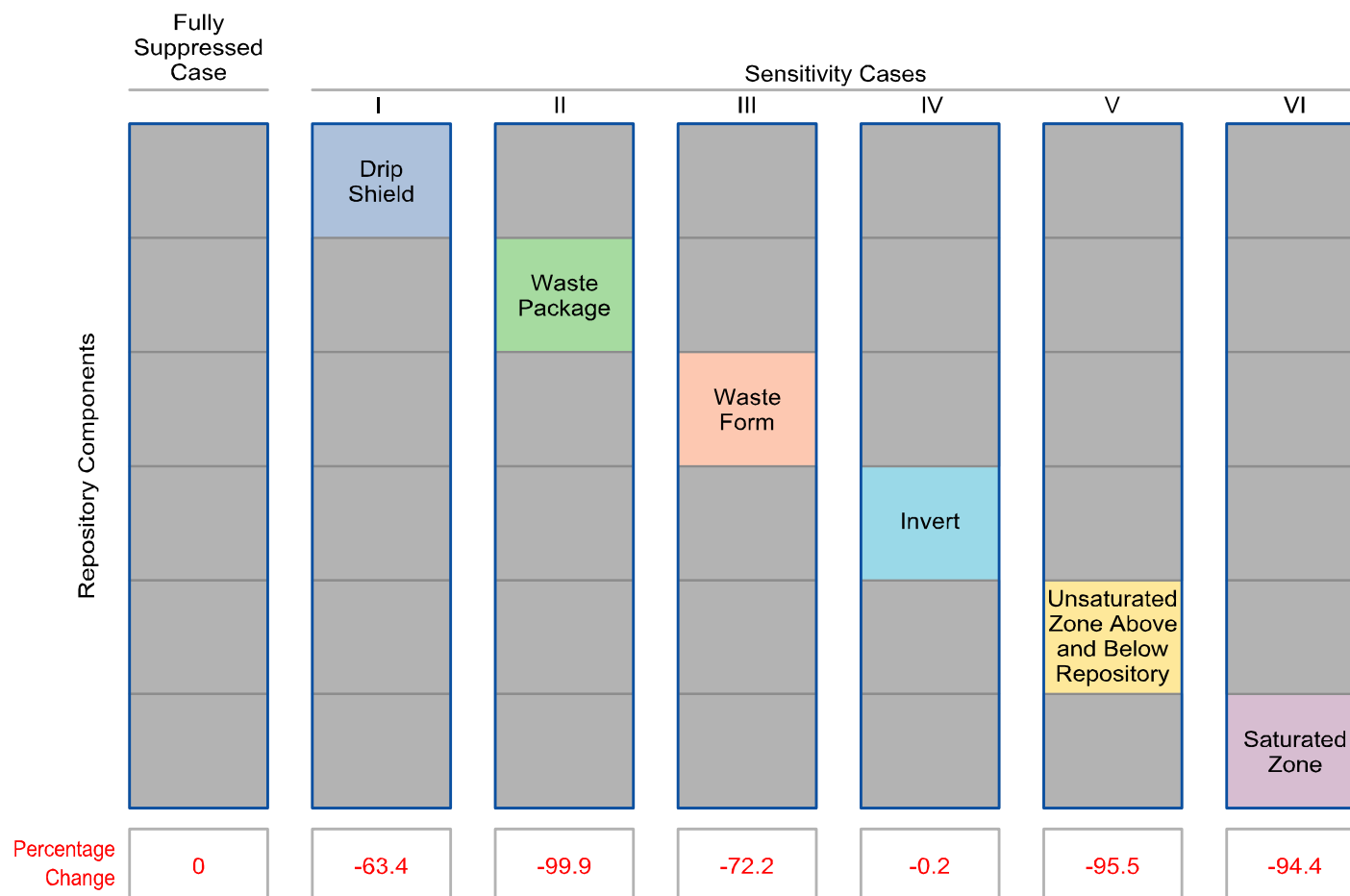
Figure 6-2. Single-Repository Component Added to a System in Which all Repository Components Have Been Suppressed (One-On Sensitivity Analysis) for the 10,000-Year Simulation Period. The Left-Most Column Represents the Case with all Repository Components Suppressed. The Gray Box Indicates the Corresponding Repository Component has Been Suppressed. The Values at the Bottom Represent Relative Change to the Peak Expected Dose in Percent.
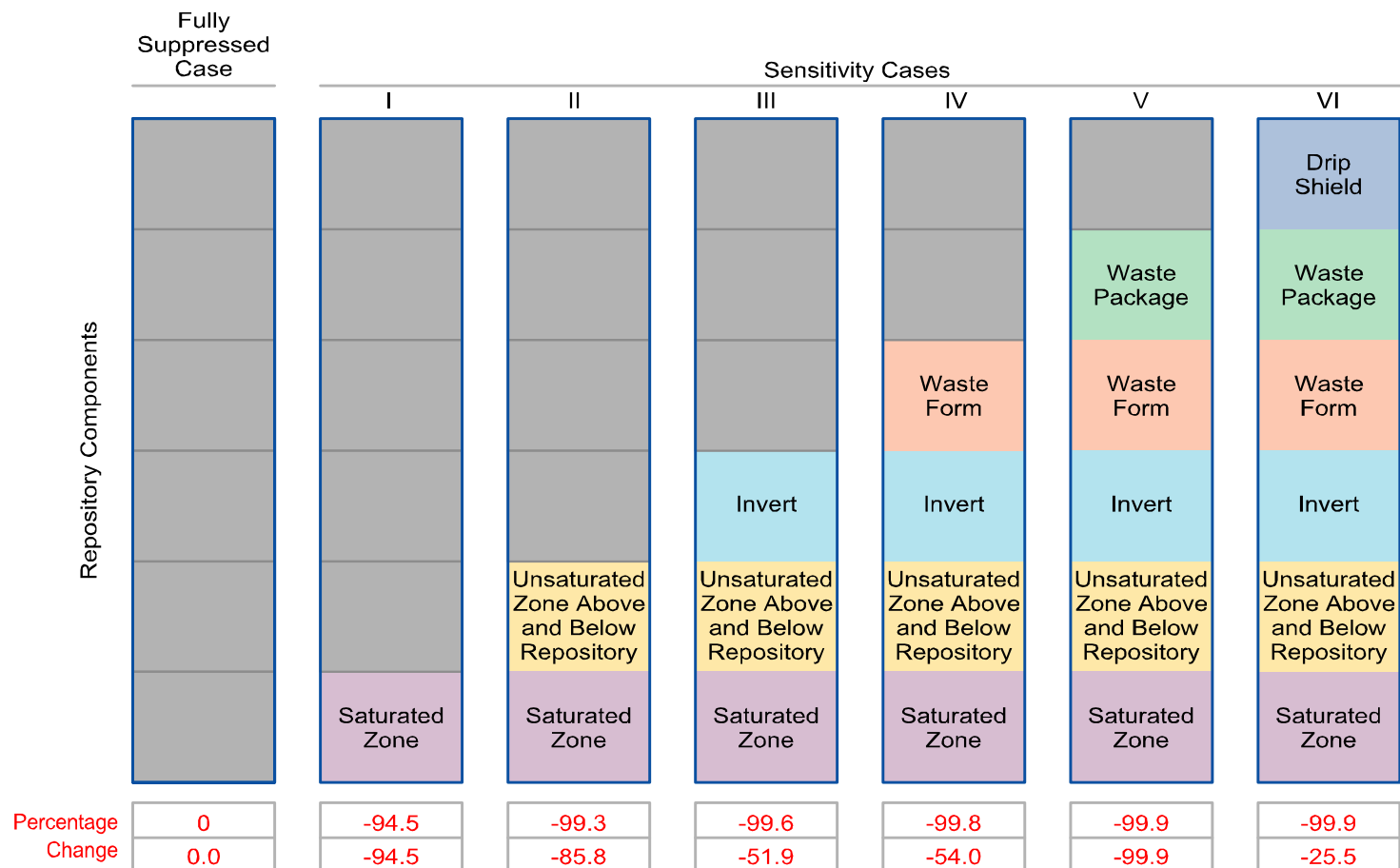
Figure 6-3. Addition of Repository Components to a Completely Suppressed System (10,000-Year Simulation Period). Each Column Represents a Monte Carlo Analysis with One Repository Component Added to the Suppressed System at a Time. The Left-Most Column Represents the System with all Six Barrier Components. The Gray Color Indicates that the Corresponding Repository Component Has Been Suppressed. The Right-Most Column Represents the Basecase in Which all Barrier Components are Present. The Bottom Row of Values Represents the Change in Peak Expected Dose Relative to the Case to its Immediate Left. The Values in the Next-Higher Row Represent Change to the Peak Expected Dose from 100 Realizations Relative to the Left-Most Column.

components are suppressed. When the saturated zone repository component was added, the peak expected dose decreased by nearly 94 percent. When the unsaturated zone repository component was added cumulatively to the saturated zone repository component, the peak expected dose decreased by nearly 99.3 percent.

Gradual addition of invert and waste form repository components only marginally changed the peak expected dose, whereas addition of the waste package repository component reduced the dose by 99.99 percent. Finally, adding the drip shield repository component reduced the peak expected dose by 99.999 percent.

The row 2 (i.e., the bottom row) values in Figure 6-3 shows the relative change in dose compared with the case to its immediate left. This change can be used to rank the repository components in their ability to decrease the dose. Again, it can be seen that the saturated and unsaturated zones and the waste package are the major contributors to dose reduction.

6.4.4   Repository Component Combination Sensitivity Analysis

In addition to the suppression of one repository component at a time (i.e., one-off analysis), as discussed previously, repository component sensitivity analysis was also performed with suppression of two or more repository components at a time, referred to in this report as the (i) drip shield + waste package, (ii) invert + unsaturated zone + saturated zone, and (iii) drip shield + waste package + waste form + invert. These three combinations are presented in Figure 6-4 using the relative change to the peak expected dose compared with the basecase. Analyses with combinations of repository components may reveal the cases where the performance of one component masks the performance of another component. For example, the presence of the drip shield may mask the determination of the waste package repository component sensitivity. Instead of using an exhaustive set of combinations for repository component combination sensitivity analysis, selected combinations were used.

The drip shield and waste package combination represents the main elements of the engineered barrier subsystem. A common characteristic is the ability to divert the in-drift flow of water. Analysis of this case showed an increase of nearly 179,000 percent (see Column III, Figure 6-4) when these 2 repository components are suppressed. As expected, this increase exceeded the sum or the product of the relative change to dose associated with the waste package and the drip-shield repository components individually as evident from the one-off analysis. Suppression of the waste package and drip shield repository components greatly magnified the dose despite the minor increase in dose when only the drip shield was suppressed. This increase is intuitively correct because when only the drip shield is suppressed, releases take place from the initially defective waste packages only. Likewise, when the waste package repository component was suppressed, the drip shield prevented water from entering these waste packages for an average of 7,800 years; thus, release takes place for an average of 2,200 years. When both barriers are suppressed, however, all waste packages (breached) are exposed to water from year zero. Thus, the analysis revealed the sensitivity of repository performance to the waste package repository component without the masking effect of the drip shield.

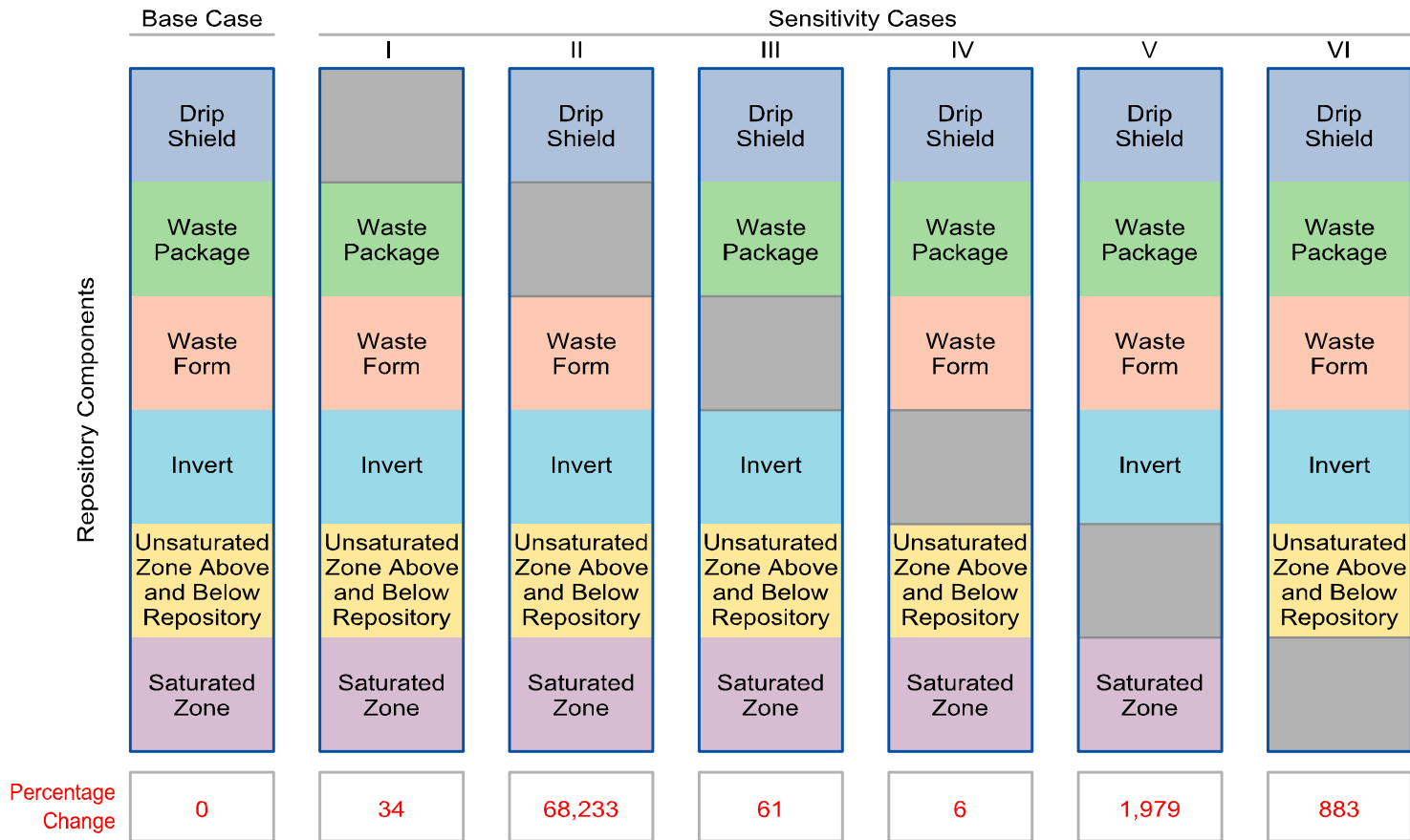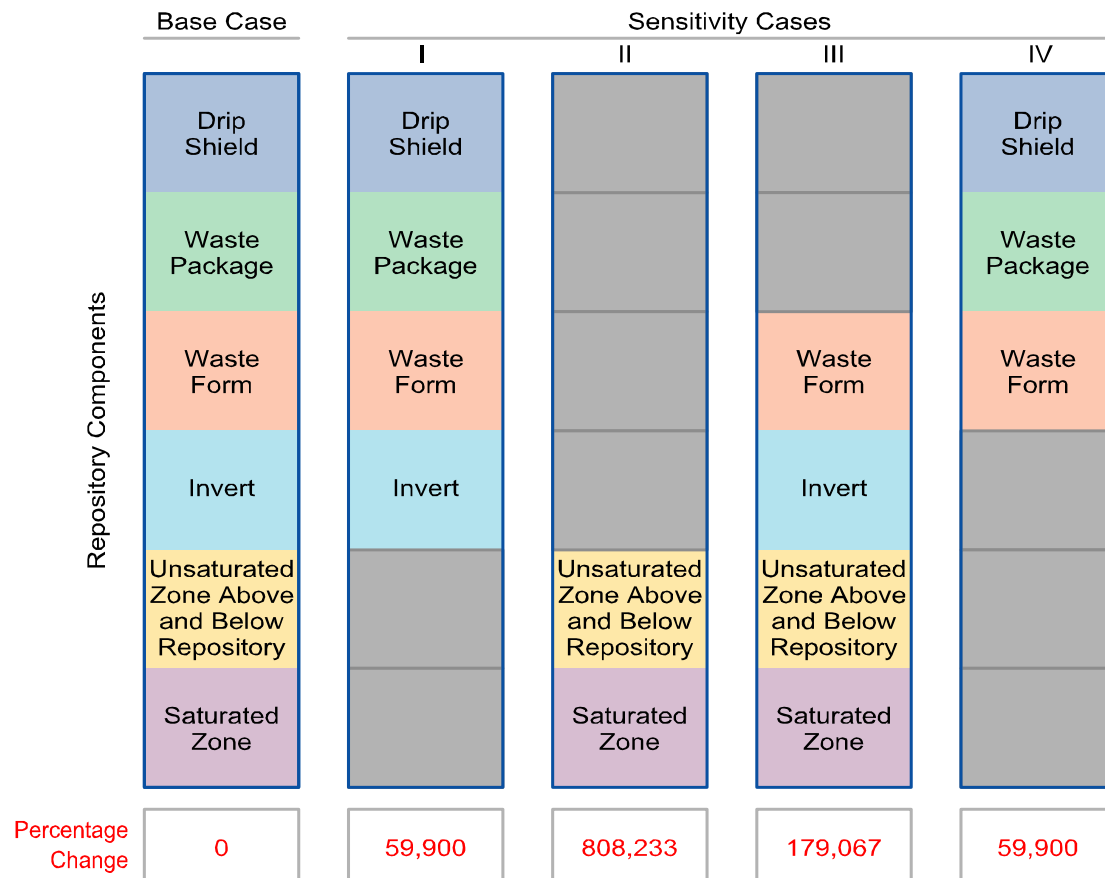**Figure 6-4. Combination Repository Component Suppression Sensitivity Analysis for the 10,000-Year Simulation Period. Each Row Represents a Monte Carlo Analysis with a Combination of Repository Component Suppressed. The First Column Represents the Basecase with Six Repository Components. The Gray Color Indicates the Corresponding Repository Component Has Been Suppressed. The Value at the Bottom of Each Column is the Relative Change to the Peak Expected Dose in Percent.**

A similar analysis can be performed with the remaining cases in Figure 6-4, however, it is not presented here. While performing barrier combination sensitivity analyses, it is important to note that when one repository component is suppressed, the suppression could influence how the repository components it is combined with are treated. For example, when the waste form repository component is suppressed in the single-repository component sensitivity analysis, the bathtub water contact mode is applied. In this model, not all spent nuclear fuel in the waste package is wet, and water diversion takes place on top of the waste package. When the waste package repository component is simultaneously suppressed with the waste form, however, a bathtub cannot form, and flow diversion cannot occur because the waste package is suppressed. Consequently, all spent nuclear fuel in a waste package will be contacted by water.

In summary, the repository component sensitivity analyses (i.e., one-off, one-on, cumulative one-on, and selected combination sets) provide useful information about the sensitivity of the repository performance to the repository subsystems. The influential repository components in order of influence are (i) waste package, (ii) unsaturated zone, (iii) saturated zone, (iv) waste form, and (v) drip shield. By analyzing the repository component sensitivity results in conjunction with the system-level results, it can be inferred that the waste package and the unsaturated and saturated zones substantially delay release. The repository component sensitivity results also showed the drip shield and waste form provide system resiliency. Because many scenarios presented in this analysis represent extreme and often physically unrealistic cases, caution should be exercised when interpreting the calculated dose.

7 SYNTHESIS OF RESULTS AND RISK INSIGHTS

This chapter synthesizes information from the analyses presented in Chapters 3, 4, 5, 6, and Appendixes F and G. Chapter 3 presented trends in repository system and subsystem responses to models and data, including the effects of input uncertainty and variability on the output uncertainty. Chapters 4–6 presented parametric, distributional, and subsystem (or repository component) sensitivity analyses and their results, as well as results from alternative conceptual models. Appendixes F and G present risk calculations for stylized human intrusion and in-package criticality. This chapter (7) focuses on identifying the important parameters, alternative models, and subsystems that significantly influence performance.

The following sections discuss the system-level overall performance results including the basecase, disruptive event cases, stylized human intrusion, and in-package criticality. Subsystem capability, as derived from the analysis of total system behavior calculations (Chapter 3), is presented next, followed by sensitivity analysis results from various methods (parametric, distributional, alternative conceptual model, and repository component). Parametric sensitivity analysis results from Chapter 4 are aggregated to extract the final list of the top 10 influential parameters from the basecase and the igneous activity case. These results are then verified by runs that demonstrate that most uncertainty in the dose is a result of uncertainty in the chosen parameters. Finally, the influential parameters, alternative conceptual models, and repository components are linked with integrated subissues to identify the parameters significant to performance for higher doses and maximum sensitivity to changes in parameters and conceptual models.

Although the radionuclide C-14 was included in the calculations of release, transport and dose, it will not be included in the synthesis of results. Currently, the TPA 4.1 code considers that C-14 would be in equilibrium between the water and gas phases, and would mostly partition into the gas stream, thereby being released primarily to the atmosphere (Codell, et al., 1992). The staff does not believe that the omission of C-14 from the results will alter any conclusions.

Insights gained from the risk analyses produced by the TPA Version 4.1 code must be tempered by the following considerations.

- There are many assumptions, uncertainties, conservatisms, and other limitations in the analyses.

- The results of the TPA Version 4.1 code are only pertinent to those conceptual models embodied in it (e.g., there is no diffusion from the waste packages and no cladding degradation, so no pertinent results on these phenomena can come directly from the analyses).

- The TPA Version 4.1 code was not developed as a tool to demonstrate compliance of the Yucca Mountain repository with 10 CFR Part 63 regulations; this is not the U.S. Nuclear Regulatory Commission (NRC) responsibility. Instead, the TPA code is a tool for use by NRC to better understand the functioning of the repository, and to allow independent review of the U.S. Department of Energy (DOE) performance assessment.

7.1 Overall Performance Analyses

7.1.1 Basecase

The results from the Monte Carlo sampling with 350 realizations using the basecase data set with a total of 950 parameters (330 sampled) show a peak risk value of 2.1×10^{-7} Sv/yr [0.021 mrem/yr] occurring at approximately 10,000 years. The peak dose from the mean value data set is 3.5×10^{-7} Sv/yr [0.035 mrem/yr]. Although the doses from these two cases are similar, they cannot be interpreted in the same way. For example, in the case of the 10,000-year simulation period, the major contributors to dose in the mean value data set case are I-129 and Tc-99. For multiple realizations, Np-237 is also a major contributor because Monte Carlo analysis allows the code to investigate regions of parameter space where Np-237 reaches the users in 10,000 years. Such an insight is not likely from a single, representative data set like the mean. Monte Carlo results show the doses at the time of peak expected dose in 10,000 years range from 0 to 6.95×10^{-6} Sv/yr [0.695 mrem/yr] {standard deviation = 7.1×10^{-7} Sv/yr [0.071 mrem/yr]} with 33 percent of realizations resulting in zero dose.

7.1.2 Disruptive Events

Igneous activity increases the peak risk from 2.1×10^{-7} Sv/yr [0.021 mrem/yr] for the basecase to 3.6 μSv/yr [0.36 mrem/yr], a 16-fold increase. Moreover, igneous activity shifts the time of occurrence of peak risk from ~10,000 for the basecase to 245 years. Probability-weighted faulting events do not influence the peak risk significantly. Seismic disruptive events did not contribute to peak risk in the Monte Carlo runs with 350 or 4,000 vectors for the 10,000-year simulation period.

7.1.3 Human-Intrusion Scenario Analysis

A stylized, very conservative and nonmechanistic analysis of the human-intrusion scenario calculations (see Appendix F) show a peak dose of approximately 10^{-6} Sv/yr [0.1 mrem/yr] in the 10,000-year simulation period. This peak dose is approximately one order of magnitude higher than the peak expected risk for the basecase but is still much smaller than 0.15 mSv/yr [15 mrem/yr] in the regulation. The results reflect limited spent nuclear fuel inventory available for additional release in this scenario. Only 1 waste package of 8,877, or less than 0.012 percent of the spent nuclear fuel, is made available for release by the stylized human-intrusion scenario. The conservative choice of the grain-size model for the human-intrusion analysis instead of the particle-size model for the basecase increases the surface area by a factor of approximately 150 for the TPA Version 4.1 code mean value data set. Because only 1 waste package is breached by human intrusion, compared with approximately 45 waste packages breached by initial defects, the net increase in available surface area is approximately a factor of 3 greater for human intrusion. As estimated in the TPA Version 4.0 code user's guide (Mohanty, et al., 2002), selection of fuel-dissolution Model 1 alone results in approximately a 100-times faster dissolution rate than Model 2 used in the basecase. This faster dissolution rate, along with the higher flow rate of water into the waste package for the human-intrusion scenario, and the high solubility of Cl-36, Tc-99, I-129, and Np-237 contribute significantly to the higher expected annual doses for the human-intrusion scenario.

7.1.4 In-Package Criticality Analysis

Both steady-state and transient criticality show an increase in the conditional peak expected dose following a criticality event (see Appendix G). The staff made no attempt to estimate the probability of criticality, although it is expected to be small. DOE used a probability of 0.001 to 0.005 criticality events in 10,000 years for its total system performance assessment analyses (DOE, 1998).

The steady-state case assumes the energy produced by the nuclear chain reaction is balanced exactly by the heat lost through thermal conduction in the rock and evaporation of water from the waste package. Several likely conservatisms are in this analysis: (i) criticality is assumed in all 32 initially defective waste packages starting at 5,000 years; (ii) all critical waste packages were under drips, and (iii) release continued to occur during the criticality, despite heat release from the spent nuclear fuel. Criticality in the prematurely failed waste packages results in a conditional peak expected dose higher than the basecase dose by approximately a factor of three.

In-package transient criticality calculations assume the contents of a waste package containing spent nuclear fuel undergo a fast transition to criticality, followed by an energetic steam explosion that destroys the container and disperses the spent nuclear fuel as fine, easily dissolved particles. The analysis used a highly conservative release rate model that led to a relatively fast release of the entire contents of the waste package. The conditional peak expected dose for this event exceeds that of the basecase in the 10,000-year simulation period by an order of magnitude but nonetheless is considerably smaller than the 0.15 mSv/yr [15 mrem/yr] standard in 10 CFR Part 63 (Code of Federal Regulations, 2002). Transient criticality gives rise to a relatively large peak in conditional dose shortly after the event is assumed to occur and quickly drops below the basecase peak expected dose. The staff considers the risk from this event to be small because the conditional dose is below the standard, and probability of the event is expected to be low. Therefore, the staff does not plan to refine this analysis further.

7.2 Subsystem Capability Analysis

The subsystem capabilities presented in this section are derived from the system-level and intermediate-level performance assessment results presented in Chapter 3. The intent is to emphasize how well the subsystems prevent or delay release of most radionuclides rather than to focus on the peak expected dose. Results presented below reflect the conceptual models in the TPA Version 4.1 code and the input parameters used.

7.2.1 Length of Time Waste Packages Remain Intact

The repository is specified to have 8,877 waste packages; 1 to 88 (an average of 44) of which are specified to have undergone initially defective failure (i.e., failure year 0). Aside from these initially defective waste packages, the other waste packages are subject to corrosion or mechanical failure because of seismicity, faulting, and igneous activity. No corrosion failure is observed within 10,000 years. The waste packages remain intact from corrosion for 37,900–100,000 years (and longer), with an average life of 68,000 years. Waste packages do not fail from seismicity during the 10,000-year simulation period. On an average, 33 waste packages fail from faulting events and 47 waste packages fail from igneous activity events

[4 from extrusive (range: 1–9) and 43 from intrusive (range: 6–88)]. These 47 waste packages could fail as early as 100 years; however, the event probabilities are low. Accounting for failures from the basecase and all disruptive event scenarios, on average, 124 waste packages could fail within 10,000 years. In other words, 8,753 (i.e., 8,877 – 44 – 33 – 47) waste packages that account for 98.6 percent of the total wastes would remain intact for 10,000 years.

7.2.2   Length of Time the Drip Shield Remains Intact

The drip shield is specified to remain intact for 2,700–20,400 years (lognormally distributed), with an average lifetime of 7,422 years. Depending on the type and location of failure, a partially failed drip shield could prevent water from entering the breached waste packages. The TPA Version 4.1 code, however, assumes that once the drip shield fails, it is no longer a barrier to flow.

The drip shield could lose its integrity more quickly because failure from rockfall has not been considered in the model. Failure of the drip shield in the first few thousand years, however, would be mitigated by thermal effects, which would reduce or eliminate dripping. The drip shield may minimize localized corrosion by preventing aggressive chemicals from contacting the waste package at high temperature. As modeled in the TPA Version 4.1 code, however, the corrosion models assume that aggressive chemistry would be present regardless of the effects of the drip shield, so the drip shield is given no credit for this protection. Drip-shield behavior, therefore, appears simply as a barrier to flow, redundant with the waste package and thermal effects, through the engineered barrier subsystem.

7.2.3   Amount of Meteoric Water Percolating into the Repository Horizon

For the models and parameters chosen, the cumulative amount of meteoric water percolating to the repository horizon in 10,000 years is 5.323×10^8 m^3 [1.88×10^{10} ft^3], which gives rise to an average rate of 53,230 m^3/yr [1.88×10^6 ft^3/yr]. This amount contrasts with the cumulative precipitation averaged for all realizations {8.771×10^9 m^3 [3.1×10^{11} ft^3]}, which gives rise to an average of 8.77×10^5 m^3/yr [3.1×10^7 ft^3/yr] and amounts to approximately 6 percent of the precipitation at the surface of Yucca Mountain. The remaining 94 percent is either diverted at the surface by runoff or lost because of evapotranspiration. The model assumes the infiltration outside the column representing the repository block is not diverted laterally toward the repository.

7.2.4   Packages That Experience Dripping

Waste packages that experience dripping are assumed to vary from 0 to 100 percent with a uniform distribution and an average of 50 percent. This assumption implies that, on average, 4,439 waste packages would experience dripping after the drip shield fails. Dripping is not expected on all waste packages because flow is contained primarily in channels through fractures, and not all fractures are flowing. The location of drips in tunnels could change with time because of changes in fracture dimensions caused by chemical, mechanical, or thermal effects, but this potential change is not modeled in the TPA Version 4.1 code.

7.2.5 Amount of Water that Contacts Waste

On average, 1.765×10^6 m^3 [6.23×10^7 ft^3] of water falls on to the drip shield (and eventually on to the waste package) in 10,000 years for the models and parameters assumed. This total amounts to an average rate of 176.5 m^3/yr [6.23×10^3 ft^3] of water, which is 0.02 percent of the precipitation and 0.332 percent of the 10,000-year average infiltrations. Dripping water will contact waste packages only after the drip shield fails. Some water would be diverted around the drift by capillarity in the rock. Another portion would flow along the drift wall. The remainder of the water would drip into the drift, with some of that falling onto the drip shield and subsequently onto the waste package after drip shield failure. Of the part that falls directly onto the waste package, only a fraction would enter through openings that were either directly under the drip or in the path of the runoff. Approximately 300 m^3 [10,600 ft^3] of water enter into failed waste packages during the 10,000-year simulation period after the drip shields fail {i.e., 6.71 m^3 [237 ft^3] per waste package}, which is 0.0037 percent of the infiltration and 0.002 percent of the precipitation.

7.2.6 Release Rates of Particular Radionuclides Based on Solubility Limits and Water Flow

The release of all but 7 of 19 radionuclides is controlled by the radionuclide solubility limits, for the models and parameters assumed. Radionuclides that experience a solubility-limited release are U-238, U-234, Pu-239, Pu-240, Nb-94, Am-241, Am-243, Np-237, Th-230, Cm-246, Cm-245, and Ra-226. The release is solubility limited greater than 90 percent of the time for U-238, U-234, Pu-239, Pu-240, and Nb-94. The release is solubility limited more than 50 percent of the time for Am-241, Am-243, and Np-237 and the release is solubility limited less than 50 percent of the time for Th-230, Cm-246, Cm-245 and Ra-226. The radionuclides that do not undergo solubility-limited release are Pb-210, Cs-135, I-129, Tc-99, Ni-59, Se-79, and Cl-36. The radionuclides that experience solubility-limited release are determined by the solubility limits, time-dependent flowrate, radionuclide half-life and the radionuclide inventory. Note that because of the time-varying flow rate, all of the nuclides having a solubility-limited release also switch between solubility-limited and dissolution-limited release from the waste package (see the 3rd and 5th columns in Table 7-1). Although subsystem capability analysis does not show the magnitude of decrease in the release rate because of the solubility limits, the analysis indicates that release of the majority of the radionuclides are limited at the specified solubility values. The degree to which solubility limits restrict release of radionuclides from the engineered barrier system can be found under the summary of alternative conceptual model results presented later in this chapter.

7.2.7 Delay in Release of Particular Radionuclides in the Engineered Barrier Subsystem

The percentage of the initial inventory of radionuclides specified for groundwater release that leaves the engineered barrier subsystem in 10,000 years is shown in Table 7-2 for the models and parameters chosen. Note that the releases of Pb-210 and Ra-226 exceed 100 percent of the initial inventory, caused by ingrowth of these radionuclides along the transport pathway from U-234 transport. Ingrowth from U-234 transport also causes the relatively high release of Th-230 for 7 percent of the initial inventory. The next greatest level of release is 0.02 percent of the initial inventory for seven radionuclides: I-129, Tc-99, Cl-36, Se-79, Np-237, Ni-59, and Cs-135, several of which ultimately reach the pumping well. For the three radionuclides that

Table 7-1. Time that Radionuclide Releases Are Controlled by the Solubility Limit and the Frequency of the Release Mode Switching from Solubility Limited to Dissolution Limited in 10,000 Years (All Isotopes of Radioelement Have the Same Solubility Limit)

Radionuclide	Average Length of Time Release Is Solubility Limited	Time Span (Out of 10,000 Years) that the Nuclide is Solubility Limit Controlled (%)	Rank by Average Length of Time Release is Solubility Limited	Average Number of Cycles Release Switches from Solubility Limited to Dissolution Limited	Ranking by the Average Number of Cycles Release Switches from Solubility Limited to Dissolution Limited
U-238	1,224	12.2	1	0.001	9
U-234	1,224	12.2	1	0.001	9
Pu-239	1,223.7	12.2	3	0.001	9
Pu-240	1,223.7	12.2	3	0.001	9
Nb-94	1,194.2	11.9	5	0.018	8
Am-241	1,065.5	10.7	6	0.073	6
Am-243	1,065.5	10.7	6	0.073	6
Np-237	764.85	7.6	8	0.149	1
Th-230	513.05	5.1	9	0.142	4
Cm-246	285.75	2.9	10	0.143	2
Cm-245	285.75	2.9	10	0.143	2
Ra-226	236.35	2.4	12	0.08	5
Pb-210	0	0	13	0	13
Cs-135	0	0	13	0	13
I-129	0	0	13	0	13
Tc-99	0	0	13	0	13
Ni-59	0	0	13	0	13
Se-79	0	0	13	0	13
Cl-36	0	0	13	0	13

contribute greatest to dose, approximately 0.02 percent of the inventory is released from the engineered barrier subsystem.

Delay in release is the result of several factors. First, most of the radionuclides are released from spent nuclear fuel congruently, which implies the delay in spent nuclear fuel-dissolution delays release of the radionuclides. With the fastest dissolution-rate model, the time for spent nuclear fuel dissolution is less than 1,300 years. Second, the bathtub formed in the failed waste package for several failure modes must fill before radionuclides can leave the waste package. Third, the invert may delay release of the radionuclides. Fourth, the radionuclides are restricted to leave the waste package at a rate less than or equal to the solubility limit times the flow rate. The analysis presented in Chapter 3 does not reveal the extent to which the invert delays

Groundwater Radionuclide	Initial Inventory (Ci)	Cumulative Release (Percentage of Initial Inventory)		
		Engineered Barrier Subsystem	Unsaturated Zone	Saturated Zone
I-129	3×10^3	2×10^{-2}	2×10^{-2}	2×10^{-2}
Tc-99	1×10^6	2×10^{-2}	2×10^{-2}	2×10^{-2}
Cl-36	8×10^2	2×10^{-2}	2×10^{-2}	2×10^{-2}
Se-79	2×10^3	2×10^{-2}	1×10^{-2}	4×10^{-4}
Np-237	3×10^4	1×10^{-2}	5×10^{-3}	3×10^{-5}
Ni-59	2×10^5	2×10^{-2}	1×10^{-2}	4×10^{-6}
Pb-210	4×10^{-3}	6×10^4	3×10^4	2×10^{-7}
Ra-226	3×10^{-2}	4×10^3	2×10^3	1×10^{-7}
Th-230	1×10^1	7×10^0	3×10^0	5×10^{-8}
U-234	8×10^4	7×10^{-6}	3×10^{-6}	7×10^{-9}
U-238	2×10^4	6×10^{-6}	3×10^{-6}	6×10^{-9}
Cm-246	5×10^3	5×10^{-3}	5×10^{-3}	0×10^0
Cm-245	3×10^4	8×10^{-3}	8×10^{-3}	0×10^0
Am-241	2×10^8	7×10^{-8}	4×10^{-8}	0×10^0
Am-243	2×10^6	4×10^{-4}	2×10^{-4}	0×10^0
Pu-239	3×10^7	1×10^{-5}	5×10^{-6}	0×10^0
Pu-240	4×10^7	6×10^{-6}	3×10^{-6}	0×10^0
Cs-135	4×10^4	2×10^{-2}	1×10^{-2}	0×10^0
Nb-94	6×10^4	1×10^{-4}	1×10^{-4}	0×10^0

Table 7-2. Percentage of Individual Radionuclides Released in 10,000 Years with Respect to Initial Inventory at Engineered Barrier Subsystem, Unsaturated Zone, and Saturated Zone Outlets

radionuclide transport. Information, however, can be extracted from the repository component sensitivity analysis results presented in Chapter 6.

Nineteen radionuclides in the TPA Version 4.1 code have been considered for groundwater releases. The minimum breakthrough from the engineered barrier subsystem time for all 19 radionuclides is 2,730 years. The average breakthrough time for all these radionuclides ranges between 16,225 and 19,614 years. The minimum, average, and maximum arrival times at the end of each subsystem for all 19 radionuclides are presented in Table 7-3.

7.2.8 Delay in Transport of Particular Radionuclides in the Unsaturated Zone

For the models and parameters chosen, the average groundwater traveltime in the unsaturated zone (averaged for time and realization) varies spatially among subareas between ~12 years (in Subarea 10) to 769 years (in Subarea 7), with a repository average of 209 years. These traveltimes may be artificially low because of assumptions made in the abstraction of transport in the unsaturated zone, particularly the deliberate bypassing of thin layers for computational efficiency. The shortest groundwater traveltime in any realization is 10 years (in Subarea 10), and the longest in any realization is 3,437 years (occurs in Subarea 7). The largest factor in the arrival time appears to be the presence of the Calico Hills vitric layer because of its high porosity and lack of fracture flow.

Table 7-3. Time of First Arrival of the Radionuclides at the Outlet of Engineered Barrier Subsystem, Unsaturated Zone, and Saturated Zone. Shown Are the Minimum, Average (Averaged over All Subareas and Realizations), and Maximum Breakthrough Times.

Radionuclide	Minimum Time Engineered Barrier Subsystem	Average Time Engineered Barrier Subsystem	Maximum Time Engineered Barrier Subsystem	Minimum Time Unsaturated Zone	Average Time Unsaturated Zone	Maximum Time Unsaturated Zone	Minimum Time Saturated Zone	Average Time Saturated Zone	Maximum Time Saturated Zone
Am-241	2,730	18,786	100,000	2,933	18,992	100,000	28,000	99,644	100,000
Am-243	2,730	17,388	100,000	3,635	66,496	100,000	100,000	100,000	100,000
Cl-36	2,730	16,225	100,000	2,933	16,271	100,000	3,076	16,379	100,000
Cm-245	2,730	18,525	100,000	2,933	18,577	100,000	17,200	98,697	100,000
Cm-246	2,730	18,525	100,000	2,933	18,607	100,000	26,200	99,832	100,000
Cs-135	2,730	16,268	100,000	3,635	38,466	100,000	8,490	82,744	100,000
I-129	2,730	16,225	100,000	2,933	16,271	100,000	3,076	16,379	100,000
Nb-94	2,730	16,460	100,000	2,933	16,503	100,000	7,376	45,385	100,000
Ni-59	2,730	16,243	100,000	3,635	36,628	100,000	4,291	46,693	100,000
Np-237	2,730	16,692	100,000	2,933	17,434	100,000	4,191	33,755	100,000
Pb-210	2,730	19,614	100,000	2,933	31,525	100,000	5,696	51,651	100,000
Pu-239	2,730	17,388	100,000	3,635	66,489	100,000	6,560	76,424	100,000
Pu-240	2,730	17,388	100,000	3,635	66,496	100,000	6,875	82,263	100,000
Ra-226	2,730	16,460	100,000	2,933	28,539	100,000	5,564	47,930	100,000
Se-79	2,730	16,225	100,000	3,635	22,087	100,000	4,191	32,367	100,000
Tc-99	2,730	16,225	100,000	2,933	16,271	100,000	3,076	16,379	100,000
Th-230	2,730	17,388	100,000	2,933	29,517	100,000	5,308	46,992	100,000
U-234	2,730	16,460	100,000	2,933	27,985	100,000	5,308	45,553	100,000
U-238	2,730	16,460	100,000	2,933	16,980	100,000	4,945	33,909	100,000

The minimum arrival time at the end of the unsaturated zone is 2,933 years for the radionuclides, which include Am-241, Cl-36, Cm-245, Cm-246, I-129, Nb-94, Np-237, Pb-210, Ra-226, Tc-99, Th-230, U-234, and U-238. The average arrival times for the same radionuclides vary between 16,271 and 31,525 years. The arrival time for the remaining six radionuclides (Am-243, Cs-135, Ni-59, Pu-239, Pu-240, and Se-79) is at least 3,635 years. The average arrival time for these radionuclides varies between 22,087 and 66,497 years.

The percentage of initial inventory of the radionuclides specified for groundwater release that leaves the unsaturated zone in 10,000 years is shown in Table 7-2. Pb-210 and Ra-226 leaving the unsaturated zone are 30,000 and 2,000 percent of the initial inventory, caused by ingrowth from U-234 transport. Aside from these two radionuclides, the largest amount of radionuclides leaving the unsaturated zone is Th-230, which is 3 percent of the initial inventory, also largely because of U-234 transport and ingrowth. The next level of release, 0.01–0.02 percent of the initial inventory, includes I-129, Tc-99, Cl-36, Se-79, Ni-59, and Cs-135, with several of these ultimately reach the pumping well. For the three radionuclides that contribute most to dose, only 0.02 percent of the inventory is released from the engineered barrier subsystem and the unsaturated zone. The difference in the cumulative 10,000-year release for unretarded radionuclides between the engineered barrier subsystem and the unsaturated zone can be seen only in the third or fourth decimal place, which is not shown in Table 7-2. This difference is consistent with the short arrival times in subareas of the unsaturated zone that do not contain the Calico Hills vitric unit.

Although relatively unretarded radionuclides like Tc-99, I-129, Cl-36, Se-79 and Ni-59 are not delayed greatly by the unsaturated zone, it would be a mistake to say that the unsaturated zone is not an effective barrier. For the 10 computed subareas, 6 include the Calico Hills vitric unit, and account for about half of the waste packages. For subareas where the Calico Hills vitric unit is present, there would be substantial delays for both unretarded and retarded radionuclides. Virtually no retarded radionuclides would escape those subareas in the regulatory period of 10,000 years.

The minimum, average, and maximum arrival times for all 19 radionuclides are presented in Table 7-3.

7.2.9   Delay in Transport of Particular Radionuclides in the Saturated Zone

The average groundwater traveltime in the saturated zone varies among subareas between 578 years (in Subareas 2 and 4) and 821 years (in Subarea 9) with a repository average of ~644 years. These averages are taken at a scale that reflects the interface area between an unsaturated zone subarea and a saturated zone streamtube. The shortest groundwater traveltime through the saturated zone for a single realization is 57 years (in Subarea 7). The longest groundwater traveltime through the saturated zone for a single realization is 1,790 years (in Subarea 9).

The combined unsaturated and saturated zones average traveltimes in the 10,000-year simulation period vary spatially between 598 and 1,395 years, with a repository average value of 926 years. Therefore, the radionuclides will be delayed an average of at least 926 years in the natural system.

The minimum arrival time at the end of the saturated zone for Am-241, Am-243, Cm-245, and Cm-246 is greater than 10,000 years (see Table 7-3). Three of the remaining 15 radionuclides (i.e., Tc-99, I-129, and Cl-36) travel at the groundwater velocity. Therefore, the earliest time these three radionuclides can reach the production well is 3,076 years. The earliest arrival time for the remainder of the radionuclides (i.e., Cs-135, Nb-94, Ni-59, Np-237, Pb-210, Pu-239, Pu-240, Ra-226, Se-79, Th-230, U-234, and U-238) ranges between 4,191 (for Np-237 and Se-79) and 8,490 years (for Cs-135). Average arrival times for all the radionuclides is greater than 10,000 years.

One hundred percent of the inventory of 9 of 19 radionuclides is delayed from reaching the pumping well in 10,000 years. Five of the remaining 11 radionuclides (i.e., Pb-210, Ra-226, Th-230, U-234, and U-238) experience only small releases from the saturated zone and a small fraction of the initial inventory of these radionuclides (see Table 7-2) enters the well. These radionuclides are unretarded. Therefore, these three radionuclides leaving the waste packages travel at the velocity of water and reach the wellbore in the 10,000-year simulation period. Note that in spite of substantial ingrowth of Pb-210 and Ra-226, only a small amount reaches the user's well because of retardation in the saturated zone. Also note that a small fraction of the initial inventory of Se-79, Np-237, and Ni-59 enters the wellbore because most of the mass is retarded in the saturated zone. The 3 primary radionuclides contributing to dose in the 10,000-year simulation period are Tc-99, I-129, and Cl-36. These radionuclides are unretarded. Therefore, these three radionuclides leaving the waste packages travel at the velocity of water and reach the wellbore in the 10,000-year simulation period. Approximately 99.98 percent of the initial inventory of these unretarded radionuclides do not reach the pumping well.

7.3   Synthesis of Sensitivity Analysis Results

7.3.1   Influential Parameters from Parametric Sensitivity

Parametric sensitivity analyses have been used to identify influential parameters in the basecase and in the igneous activity case. The influential parameters are the ones for which a unit change in the value leads to a large variation in performance (i.e., dose). In the absence of a suitable sensitivity analysis method that appropriately accounts for event probability, sensitivity analysis is performed using conditional dose for igneous activity.

For the 10,000-year simulation period, the parameters found most influential for the basecase (the basecase is defined as the undisturbed scenario and the effects of rockfall caused by seismicity) are

- Areal average mean annual infiltration at start (AAMAI@S)
- Drip shield failure time (DSFailTi)
- Preexponential term for spent nuclear fuel-dissolution Model 2 (PSFDM1)
- Subarea wet fraction (SbArWt%)
- Waste package flow multiplication factor (WPFlowMF)
- Well pumping rate at 20-km [12.4-mi] receptor group (WPRRG@20)
- Alluvium R_d for Np-237 (ARDSAVNp)
- Distance to tuff-alluvium interface (DTFFAVIF)
- Fraction of condensate toward repository (FOCTR)
- Waste package initially defective fraction (WP-Def%)

The definition of these parameters is given in Appendix A.

For the 10,000-year simulation period, the parameters found most influential for the igneous activity (based on conditional dose, which is not probability weighted) are

- Airborne mass load above the fresh ash blanket (ABMLAAsh)
- Wind speed (WindSpd)
- Diameter of volcanic conduit (VC-Dia)
- Volcanic event power (VE-Power)
- Volcanic event duration (VE-Durat)
- Time of next volcanic event in the region of interest (VEROI-Tn)
- Ash mean particle diameter (AshMnPLD)
- Random number to determine if the event is extrusive or intrusive (VEi/e-R#)
- Spent nuclear fuel wetted fraction for intrusive igneous activity (SFWt%V0)
- Preexponential term for spent nuclear fuel-dissolution Model 2 (PSFDM1)

7.3.2   Influential Parameters Based on Distributional Sensitivity

Distributional sensitivity analyses are performed for 2 sets of parameters, the first consisting of the top 10 influential parameters identified by the parametric sensitivity analysis methods described in Chapter 4 and the second, the last 5 of the 20 most influential parameters. The distributional sensitivities were determined by changing distribution functions by shifting the mean of the distribution by 10 percent of the data range toward higher values (Figure 5-2) and by completely changing the type of distribution function (Figure 5-3).

Several parameters show high distributional sensitivity, especially when the mean values are changed for the two most influential parameters identified by the parametric sensitivity analysis methods. For example, a 10-percent change to the WPFlowMF parameter results in a 150-percent change in the dose. The parameters that show the greatest sensitivity to distributional changes (data range not changed) are

- Waste package flow multiplication factor (WPFlowMF)
- Drip shield failure time (DSFailTi)
- Alluvium R_d for Np-237 (ARDSAVNp)
- Areal average mean annual infiltration at start (AAMAI@S)
- Preexponential term for spent nuclear fuel-dissolution Model 2 (PSFDM1)
- Distance to tuff-alluvium interface (DTFFAVIF)
- Subarea wet fraction (SbArWt%)
- Waste package initially defective fraction (WP-Def%)

7.3.3   Influential Alternative Conceptual Models

For the 10,000-year simulation period, several alternative conceptual models, and combinations thereof, were found most influential for the basecase. The 12 models encompass 3 processes: (i) spent nuclear fuel dissolution (rate and particle size), (ii) spent nuclear fuel wetting type (bathtub versus flowthrough), and (iii) radionuclide transport. Details of the analyses can be found in Chapters 2, 3, and 4. Several alternative conceptual models or their combinations increased and others decreased dose. The alternative conceptual models are shown in order of their influence. The values in the parentheses show qualitatively the relative change in peak

expected dose compared to the basecase. The minus (−) sign indicates that the dose decreased compared to the basecase. Consequently, from the risk standpoint, the models that increase dose need to be evaluated carefully. The influential alternative conceptual models in order of their influence are

- No retardation of americium, thorium, and plutonium in saturated zone (+++++)
- Flow-through spent nuclear fuel water contact mode with spent nuclear fuel-dissolution Model 1 (+++)
- Grain particle-size model with spent nuclear fuel-dissolution Model 1 (+++)
- Spent nuclear fuel-dissolution Model 1 (+++)
- Flow-through spent nuclear fuel water contact mode with spent nuclear fuel-dissolution Model 2 (++)
- Cladding credit with spent nuclear fuel-dissolution Model 1 (− −)
- Schoepite spent nuclear fuel-dissolution model (− −)
- Natural analog spent nuclear fuel-dissolution model (− −)
- Focused flow (− −)

7.3.4 Influential Subsystems Based on Repository Component Sensitivity

Dose shows most sensitivity to the waste package and little sensitivity to the invert subsytem component. The group of natural repository components (i.e., unsaturated zone and saturated zone together) shows approximately the same level of sensitivity as the waste package repository component. Drip shield and waste form engineered repository components show comparable level of influence on dose (waste form slightly more influential). Between the two natural repository components, the unsaturated zone is slightly more influential than the saturated zone. The main influence of the unsaturated zone is in preventing water from coming into contact with the waste. The main influence of the saturated zone is retarding radionuclide transport. The influential repository components in order of their influence are (i) waste package, (ii) unsaturated zone, (iii) saturated zone, (iv) waste form, and (v) drip shield. By analyzing the repository component sensitivity results in conjunction with the system-level results, it can be inferred that the waste package and the unsaturated and saturated zones substantially delay release. The component sensitivity results, however, show that the drip shield and waste form provide system resiliency. Additionally, the drip shield would also serve to protect the waste package from falling rocks and preventing aggressive precipitates from dripping onto its surface. These phenomena, however, are not modeled in the TPA Version 4.1 code; rock fall does not affect waste package failure time, and aggressive chemicals are already assumed to come into contact with the waste package nonmechanistically.

7.4 Linking Influential Parameters, Models, and Repository Components to Integrated Subissues

The influential parameters, alternative conceptual models, and repository components identified previously are linked to the NRC integrated subissues (NRC, 2002). The linking of the influential variables, parameters, alternative conceptual models, and repository components is presented in Table 7-4.

Table 7-4. A Crosswalk Between the Integrated Subissues, Alternative Conceptual Models, and the Influential Parameters (10,000 Years)			
Integrated Subissues	**Influence of Alternative Conceptual Models**	**Influential Parameters**	**Influence of Repository Components**
Degradation of engineered barriers (ENG1)	Not evaluated	• Initially defective fraction of waste packages • Drip shield failure time	Waste package (+++++) drip shield (+)
Mechanical disruption of engineered barriers (ENG2)	Not evaluated	—	Waste package (+++++)
Quantity and chemistry of water contacting waste packages and waste forms (ENG3)	Clad-M1 (−) Focflow (−)	• Waste package flow multiplication factor • Fraction of condensate toward repository	Unsaturated zone (+++)
Radionuclide release rates and solubility limits (ENG4)	Grain1 (+) NoSolLim-FT (++++) NoSolLim-BT (++) Model1 (++) Flwthru-1 (++) Flwthru-2 (+) Natan (-) Schoepite (−)	• Spent nuclear fuel-dissolution preexponential term in Model 2 (PSFDM1)	Waste form (+) Invert (○)
Climate and infiltration (UZ1)	Not evaluated	• Areal average mean annual infiltration at start	Unsaturated zone (+++)
Flow paths in the unsaturated zone (UZ2)	Focflow (−)	• Subarea wet fraction	Unsaturated zone (+++)
Radionuclide transport in the unsaturated zone (UZ3)	Not evaluated	—	—
Flow rates in the saturated zone (SZ1)	Not evaluated	—	—
Radionuclide transport in the saturated zone (SZ2)	NoRet (+++++) Matdif (○)	• Alluvium matrix R_d for Np-237 • Distance to tuff-alluvium interface	Saturated zone (+++)
Volcanic disruption of waste packages (DIRECT1)	Evaluated as a special case	• Volcanic event power* • Diameter of volcanic conduit* • Volcanic event duration*	—

Table 7-4. A Crosswalk Between the Integrated Subissues, Alternative Conceptual Models, and the Influential Parameters (10,000 Years) (continued)			
Integrated Subissues	**Influence of Alternative Conceptual Models**	**Influential Parameters**	**Influence of Repository Components**
Airborne transport of radionuclides (DIRECT2)	Evaluated as a special case	• Airborne mass load above fresh ash blanket* • Ash mean particle log diameter* • Wind Speed*	—
Representative volume (DOSE1)	Not evaluated	• Well pumping rate at receptor group at 20 km [12.4 mi]	No repository component analysis permitted because it is fixed by regulation
Redistribution of radionuclides in soil (DOSE2)	Not evaluated	—	—
Biosphere characteristics (DOSE3)	Not evaluated	—	—
*Sensitive parameters obtained directly from disruptive event scenario calculations without any consideration of event probability			

7.4.1 Key Integrated Subissues for 10,000-Year Simulation Period

The influential integrated subissues identified in Table 7-4, listed in order of approximate importance, based on the models and parameters assumed in the TPA Version 4.1 code analyses, are

*   Volcanic disruption of waste packages (DIRECT1)
*   Airborne transport of radionuclides (DIRECT2)
*   Radionuclide transport in the saturated zone (SZ2)
*   Degradation of engineered barriers (ENG1)
*   Flow paths in the unsaturated zone (UZ2)
*   Quantity and chemistry of water contacting waste packages and waste forms (ENG3)
*   Radionuclide release rates and solubility limits (ENG4)
*   Climate and infiltration (UZ1)
*   Mechanical disruption of engineered barriers (ENG2)

Because many such assumptions and processes (sometimes overlapping) influence the performance assessment results and the process of identifying influential parameters, models, and repository components, it is critical that the key technical issues consider all information in determining whether and where additional refinements could increase confidence.

Based on the system-level results and the parametric, distributional, alternative conceptual model, and repository component sensitivity analysis results, the following specific points can be made for the integrated subissues for the 10,000-year simulation period.

7.4.1.1 Integrated Subissue—Volcanic Disruption of Waste Packages (DIRECT1)

Igneous activity makes the largest contribution to risk in the 10,000-year simulation period. The risk from the igneous activity is more than one order of magnitude higher than the risk in the absence of igneous activities. The diameter of the volcanic conduit that determines the number of waste packages available for airborne transport of radionuclides and the duration and power of the volcanic event that determine the height of the eruption column have significant influence on repository performance. The time of the next volcanic event in the region of interest, which determines the time of the volcanic event in the 10,000-year simulation period, also has significant influence on repository performance.

The alternative conceptual model, which accounts for mechanistic consideration of waste package response to rapid influx of basaltic magma, increases the risk by one order of magnitude compared to the original model that uses the volcanic conduit diameter model to determine waste package failure for airborne transport. The increase in risk is directly related to an increase in the number of waste packages available for airborne transport of radionuclides.

7.4.1.2 Integrated Subissue—Airborne Transport of Radionuclides (DIRECT2)

Airborne entrainment of waste in the volcanic ash and the effect on the receptor group of the subsequent deposition of ash on ground surface play important roles in the determination of peak risk.

7.4.1.3 Integrated Subissues—Radionuclide Transport in the Saturated Zone (SZ2)

The dose shows strong sensitivity to the parameters defining the volume of alluvium in the saturated zone (defined in the model through the alluvium length) through which radionuclides must travel before reaching the pumping well. The dose is primarily from the non-sorbing radionuclides. Np-237 sorption plays an important role in the performance of the repository system. Np-237 is the only radionuclide with a nonzero sorption characteristic that still contributes to dose within 10,000 years. Other radionuclides and their associated retardation coefficients do not turn out to be important in the sensitivity analyses because little or none of each of these radionuclides reach the pumping well. This fact points to the importance of the geologic subsystem to isolating most of the radionuclides released from the repository. Uncertainty in the retardation of Np-237 significantly influences the uncertainty in repository performance. The subsystem component sensitivity analysis suggests that alluvium length plays an important role in substantially delaying the release of all sorbing radionuclides and also delaying traveltime of nonsorbing radionuclides. Because of this delay, radionuclides that are sorbed make either little or no contribution to dose in 10,000 years. The alternative conceptual model for no retardation of colloid-forming radionuclides shows that the dose can be highly sensitive to colloidal transport of colloid-forming radionuclides, if those conditions can exist. Matrix diffusion in fractured media does not have as pronounced an effect on the system performance compared to sorption in porous media. However, the model results do not show sensitivities to strongly retarded radionuclides because almost none of them arrive at the pumping well, so it is possible that matrix diffusion might be more significant for those radionuclides.

7.4.1.4 Integrated Subissues—Degradation of Engineered Barriers (ENG1) and Mechanical Disruption of Engineered Barriers (ENG2)

Factors causing waste packages to fail early by mechanisms other than corrosion are important to the 10,000-year simulation period because of the otherwise long waste package lifetime. Corrosion-resistant material significantly increases the life of the container, thus pushing the onset of release from most of the waste packages to beyond 10,000 years. Total system performance is sensitive to the percent of initially defective waste packages. Consistent with the analyses in Chapter 3, repository performance is not sensitive to seismic rockfall or instantaneous fault displacement on new or under-appreciated faults. Subsystem component sensitivity analysis suggests that if the waste packages fail early from corrosion or mechanical failure, groundwater dose would increase substantially.

Uncertainty in drip shield failure time moderately influences the uncertainty in repository performance. The drip shield delays water contacting spent nuclear fuel for thousands of years for the initially defective waste packages, during which time the repository temperature falls substantially, thus slowing spent nuclear fuel dissolution. The drip shield has a greater impact on peak dose than on peak expected dose. As a subsystem component, the drip shield has less impact compared with other subsystem components because (i) the drip shield is a redundant subsystem component; (ii) the drip shield failure assumptions are conservative; or (iii) when the drip shield is intact, the spent nuclear fuel release would not have been significant because of reduced flow rates from thermal effects on flow in the repository near field. It is important to note that decreasing uncertainty in drip shield failure time increases uncertainty in repository performance. The probable cause for this observation is that a narrow drip shield

failure time distribution increases the peak of the expected dose, thereby influencing the uncertainty caused by other parameter variations.

7.4.1.5   Integrated Subissue—Flow Paths in the Unsaturated Zone (UZ2)

Repository performance is sensitive to the unsaturated zone subsystem primarily because (i) it limits the amount of water that can reach the waste packages and waste form; evapotranspiration and capillary diversion are the main features of the unsaturated zone expected to divert water; and (ii) for those subareas where the Calico Hills vitric unit is present, retardation of sorbing radionuclides is substantial (see Section 7.2.8)

7.4.1.6   Integrated Subissue—Quantity and Chemistry of Water Contacting Waste Packages and Waste Forms (ENG3)

The amount of dripping water entering the waste package is important to system performance and depends strongly on the number of fractures intersecting the drift, capillary diversion around the drift wall, and the geometry of the defect (e.g., cracks on the waste package and drip shield). Note that increased focusing of flow into fewer waste packages leads to a smaller dose than the case where more waste packages get the same volume of water but at a lesser rate.

The amount of condensate that moves toward the drift is a function of the net infiltration. Because the thermal period lasts for several thousand years, thermally modified flow plays an important role in repository performance.

The alternative conceptual model that assumes partial cladding protection produces a much lower peak expected dose than the basecase.

7.4.1.7   Integrated Subissue—Radionuclide Release Rates and Solubility Limits (ENG4)

Uncertainty in the spent nuclear fuel-dissolution rate has a significant effect on uncertainty in total system performance in the basecase as well as the igneous activity case. The alternative conceptual model studies show that the choice of the flow-through model for spent nuclear fuel wetting, when coupled with a spent nuclear fuel-dissolution model (Model 1), significantly increases risk and uncertainty. The bathtub model takes several hundreds to thousands of years to fill, thereby delaying releases. The natural analog dissolution (Model 3) and schoepite dissolution (Model 4) alternative conceptual models for spent nuclear fuel dissolution both decrease dose.

Model 2 was the default dissolution rate model for these analyses. However, the sampled preexponential term for the Model 2 rate equation was taken from a lognormal distribution with a wide range. This one term alone caused major problems in statistical convergence, since its value varied so broadly (see Figure 7-1) and the sensitivity of dose to the parameter was strong. The large range destabilizes the system-level results by requiring a very large number of Latin Hypercube Sampling samples for convergence.

Parameters representing (i) the fraction of the spent nuclear fuel wet and (ii) the spent nuclear fuel-dissolution rate associated with the groundwater release from the intrusive igneous activity influence repository performance. Parametric and distributional sensitivity analyses reveal that

both the range and distribution function type of the preexponential term (PSFDM1) controlling the dissolution rate of spent nuclear fuel influence repository performance uncertainty.

In the absence of solubility limits, the peak expected dose increased by 42 percent compared to the basecase. This small change occurred because most of the primary dose contributors in the basecase (Tc-99, I-129, and Cl-36) are not solubility limited. Np-237 is the only major contributor to the basecase peak expected dose for which release is controlled by the solubility limit throughout the 10,000-year simulation period. Because the release is delayed by sorption in the saturated zone, however, the significance of its solubility is mitigated. Also note that in the basecase, all active failure modes (i.e., the modes under which waste packages failed) are specified to form bathtubs. Changing water contact mode for these failed waste packages from bathtub to flow-through resulted in a 544-percent increase in the peak expected dose.

Radionuclides available for instantaneous release (specified through gap fraction) make only a moderate contribution to the peak expected dose. Neglecting the radionuclides specified through the gap fraction decreases dose by only 3.5 percent.

7.4.1.8   Integrated Subissue—Climate and Infiltration (UZ1)

The amount of water entering the waste package depends strongly on infiltration at the surface. Higher infiltration leads to greater release from the engineered barrier subsystem because the bathtub fills faster, and in the case of solubility limited releases, the rate depends directly on the outflow. Higher infiltration also leads to an increased likelihood of fracture flow and faster transport in the unsaturated zone.

7.4.1.9   Discussion

The prominence of the top 8 of 14 integrated subissues resulted from the sensitivity analyses presented. Although parametric, distributional, alternative conceptual model, and subsystem component sensitivity analyses complement one another in determining what drives system performance, these techniques also focus on different aspects of the system. For example, the uncertainty in dose is significantly driven by the uncertainty in the preexponential term for spent nuclear fuel dissolution (PSFDM1) because of which the radionuclide release rates and solubility limits (ENG4) integrated subissue appears important. In addition, sensitivity of dose to seven different alternative conceptual models and two subsystem components is evaluated for this integrated subissue. Because the sensitivities to the alternative conceptual models and the subsystem components are not significant (see Table 7-4), the importance of the radionuclide release rates and solubility limits (ENG4) integrated subissue is primarily supported by the significant sensitivity of dose to the PSFDM1 parameter. In contrast, the degradation of engineered barriers (ENG1) integrated subissue has been identified as important primarily because of the sensitivity of dose to the waste package subsystem components. Although, Table 7-4 shows initial defective fraction of waste packages as an influential parameter, the decision that ENG1 is important is primarily based on the significant sensitivity of dose to waste package subsystem component. Another example is the radionuclide transport in the saturated zone (SZ2) integrated subissue. This integrated subissue is identified as important because the dose shows strong sensitivity to the related parameters, the alternative conceptual models, and the subsystem component. Distinctly different information can be derived from these three sensitivity types, however. The sensitivity analysis suggests that the alluvium length is influential. The subsystem component analysis suggests the same, but it also provides

assurance that the importance of alluvium length would not have been missed if a constant value was specified. Sensitivity analysis and the uncertainty analysis methods used in this report cannot identify a parameter as important unless the parameter is specified as a random variable. The alternative conceptual model sensitivity provides yet another relevant piece of information. The dose showing high sensitivity to the no-retardation model indicates that mechanisms like colloid transport of radionuclides may be important, providing that colloids are present in sufficient quantity in the groundwater and filtration is small.

Finally, the influential parameters, alternative conceptual models, and subsystem components identified in Table 7-4 must be viewed in the proper context of the assumptions made in the TPA Version 4.1 code and the assumptions made to facilitate sensitivity analyses. The following are some key points to consider when examining these tabulated results:

- All analysis results are based on the models and reference input values used in the TPA Version 4.1 code. The TPA Version 4.0 code user's guide (Mohanty, et al., 2002) presents the key assumptions for the conceptual models. Chapter 3 of this report lists the reference input values.

- Unlike the DOE total system performance assessment analyses; the TPA Version 4.1 code does not consider diffusion through stress corrosion cracks by dissolved radionuclides or colloids. All transport is by advective flow.

- No credit is given to the drip shield as a partial flow barrier after its failure. The current assumption is that the drip shield loses 100 percent of its functionality as a flow barrier once the first failure takes place.

- Fracture-only flow occurs in the unsaturated zone if the flux exceeds the saturated hydraulic conductivity of the rock matrix of a stratigraphic unit. When fracture flow occurs, no credit is attributed to retardation in fractures or matrix diffusion in the unsaturated zone. Retardation in the fractures or diffusion into the matrix would increase traveltime and reduce the 10,000-year peak expected dose. Note that if the traveltime in a stratigraphic unit is less than 10 years, flow and transport in that unit is considered instantaneous. In the majority of the fracture-flow cases, the groundwater traveltime through a single unit is less than 10 years.

- The receptor group is located 20 km [12.4 mi] from the repository and uses groundwater that could become contaminated for drinking and farming. Calculations in this report predate the final publication of the regulation in which the receptor group is specified at 18 km [11.2 mi].

- Well pumping rate is a sampled parameter ranging between $1.7 \times 10^4 \, m^3/day$ [4.5×10^6 gal/day] and $4.92 \times 10^4 \, m^3/day$ [1.3×10^7 gal/day] at the 20-km [12.4-mi] receptor location. Calculations in this report predate the final publication of the regulation in which a fixed pumping rate of 10,140 m^3/day {2.68×10^6 gal/day or [3,000 acre ft/yr]} is specified.

- All waste packages that did not fail by other mechanisms in a subarea are assumed to fail from corrosion when the representative waste package fails. Numerous waste packages are available for corrosion failure, which does not imply that all failed waste packages contribute to radionuclide release. A more gradual failure time distribution would have the effect of spreading the release through time, thereby diminishing the

peaks. In the current model, none of the waste packages undergo corrosion failure in the 10,000-year simulation period.

8 SUMMARY AND CONCLUSIONS

This report describes a series of computations with the TPA Version 4.1 code with the objective of gaining risk insights with respect to the performance of the proposed repository at Yucca Mountain. Use of this model by the U.S. Nuclear Regulatory Commission (NRC) staff and Center for Nuclear Waste Regulatory Analyses (CNWRA) has allowed them to focus on the most important parts of the analysis of postclosure repository performance.

8.1   System-Level Results

8.1.1   Deterministic Results

The staff made numerous runs with the TPA Version 4.1 code to gain insight into the basic functionality of the models. The first set of runs was deterministic, using the mean value data set (i.e., a single run with all input variables represented as constants, chosen to be the mean value of each of the sampled parameter ranges). Restricting the code to mean value input data allowed the code to be analyzed in detail and check many intermediate data streams from one module that are fed into the next. Results from the mean value data set were also compared to Monte Carlo results but were not expected to be totally representative of the full-range Monte Carlo analyses, however. Results were produced for two simulation periods: 10,000 years, corresponding to the period of regulatory concern; and 100,000 years, looking at long-term processes where many or most of the waste packages would be expected to fail by corrosion.

The mean value data set produced a peak dose of 3.5×10^{-4} mSv/yr [0.035 mrem/yr] occurring at 10,000 years. The dose resulted from the initially defective waste packages only because there were no corrosion failures until after 10,000 years. Peak dose for the 10,000-year simulation period was dominated by the unretarded radionuclides I-129, Tc-99, and Cl-36. For the 100,000-year simulation period, the peak dose of 3.8×10^{-2} mSv/yr [3.8 mrem/yr] occurred at 72,000 years and was dominated by Np-237, which has a large inventory, large dose factor, but greater retardation than those radionuclides important at 10,000 years.

8.1.2   Monte Carlo Results

Most of the calculations with TPA Version 4.1 code were Monte Carlo, for which the values of as many as 330 parameters were sampled randomly from input distributions using the Latin Hypercube Sampling method. The remaining 620 model parameters were specified constant. Some of the sampled parameters were specified partially correlated to other sampled variables. Typically, a set consisted of 350 runs or vectors. The Monte Carlo results were produced for 10,000- and 100,000-year simulation periods. The main purpose of the Monte Carlo calculations was to demonstrate the performance of the repository under as realistic conditions as possible, including the full range of uncertainty in parameters. Monte Carlo results were also used in many of the sensitivity analyses and to look at the ranges of the intermediate outputs. The peak expected dose from the Monte Carlo cases was 2.1×10^{-4} mSv/yr [0.021 mrem/yr] for the 10,000-year simulation period and 9.9×10^{-2} mSv/yr [9.9 mrem/yr] for the 100,000-year simulation period.

8.2 Alternative Conceptual Models

Numerous alternative conceptual models were evaluated. This study considered alternative conceptual models for fuel dissolution, fuel wetting, and transport through the geosphere. These are not the preferred models but in some cases represent possible alternatives that could be supported by available information. In other cases (e.g., no retardation, no solubility limits) the alternative conceptual models represent conservative, bounding analyses that are not necessarily supported by factual information. Conceptual models may be activated in the code by changing the equations describing the model abstraction (e.g., Models 1–4 for the spent nuclear fuel-dissolution model) or changing parameter values (e.g., changing retardation coefficients to simulate no retardation). The range of the expected doses from the alternative conceptual models evaluated in this study spanned four orders of magnitude. The alternative conceptual models with the greatest deviation from the basecase data set peak dose are the no-retardation case, which is two orders of magnitude greater than the basecase peak dose, and the schoepite and Clad-M1 cases, which are two orders of magnitude less than the basecase expected dose.

Choice of the spent nuclear fuel-dissolution models produced a wide variation in expected dose. Model 1, which is based on fuel-dissolution experiments where carbonate ions are present, gives the highest release rate and, therefore, the highest dose, which is approximately three to seven times the basecase results. Model 2, which is the default case used for most other runs in this report, assumes the water in contact with the waste has significant levels of silicate and calcium ions similar to J–13 Well water and has a release rate one to two orders of magnitude less than Model 1. Model 3 is a user-defined rate and, for the purposes of comparison to the other alternative conceptual models, assumes release rates typical of the Peña Blanca natural analog data (Murphy and Codell, 1999). Release rates for this case were significantly smaller than those for Models 1 and 2. Model 4 assumes that the release of all important radionuclide species from the fuel is controlled by dissolution of the secondary uranium mineral schoepite (Murphy and Codell, 1999). Model 4 has the smallest release rates and doses. Assuming the fuel has a surface area equivalent to the size of uranium grains (microns to tens of microns) leads to doses 2 to 12 times higher than the default model, which assumes the fuel surface area is based on larger fuel particles.

Choice of the fuel wetting assumptions has a significant effect on the calculated peak expected dose. The default fuel wetting model is the bathtub, for which water must first fill the waste package and then overflow to release radionuclides. The flowthrough model assumes that water flowing into the waste package is released immediately. Assuming there is a focusing effect for infiltrating water so that fewer waste packages get proportionally more infiltrating water allows faster filling of the bathtub and greater release of solubility limited radionuclides. This higher dose is for times less than approximately 5,000 years, but lower doses result in the basecase model beyond 5,000 years. Credit for the protection of the fuel by cladding leads to peak doses that are approximately proportional to the degree of protection.

This report studied three alternative conceptual models for assumptions about transport in the engineered barrier subsystem, unsaturated zone, and saturated zone. Assuming no retardation of the elements plutonium, americium, and thorium in the unsaturated and saturated zones led to doses approximately one to three orders of magnitude greater than for the basecase dose throughout 100,000 years. These elements are normally highly retarded and, assuming they are easily transported in the geosphere, is a conservative bounding analysis that could only

be contemplated if mechanisms such as colloidal transport or fracture flow transport were highly effective.

Solubility limits of the radionuclides appear to play an important note in slowing radionuclide release rates for many radionuclides and therefore delaying dose to the receptor group. Twelve of 19 radionuclides show solubility-limited release over a portion of the 10,000-year simulation period.

Assuming no matrix diffusion (i.e., no diffusion of radionuclides from fractures into rocks) appears to be an important factor in determining the peak dose. The peak expected dose for the no-matrix diffusion case is 50-percent higher than the basecase peak expected dose for the 10,000-year simulation period.

8.3 Disruptive Events

Waste package failure caused by rockfall is considered part of the basecase scenario. For the presented definition of the basecase, there were no waste package failures (other than juvenile failures) calculated. Faulting contributes an increase up to a factor of two in peak dose until waste packages start to fail from general corrosion after about 50,000 years. Faulting does not increase risk for the 10,000-year simulation period because of its low probability of occurrence (5×10^{-6} per year).

Igneous activity causes the largest increase in dose conditionally from both groundwater and airborne pathways, but the risk is still small when the probability of the volcanic event is factored into the calculations. The probability-weighted dose from igneous activity is approximately 3.6 μSv/yr [0.36 mrem/yr], which is greater than the basecase groundwater dose of 0.00021 mSv/yr [0.021 mrem/yr], but still small compared to the regulatory criterion of 0.15 mSv/yr [15 mrem/yr].

Human intrusion is handled as a stylized, bounding case and is not part of the risk calculations from other disruptive scenarios. Human intrusion is based on the drilling of a borehole through a waste package and subsequent releases of waste to the groundwater. The borehole acts as a fast groundwater pathway from the Earth's surface to the water table. Modeling of this scenario gave a conditional dose of 0.001 mSv/yr [0.1 mrem/yr], which is small compared to the regulatory standard of 0.15 mSv/yr [15 mrem/yr].

8.4 Sensitivity Analyses

8.4.1 Parametric Sensitivity

The sensitivity analyses used a variety of statistical, regression, nonparametric, and nonstatistical techniques, building on previous reports on total system performance assessment results. Most of the statistical analyses relied on a 4,000-vector Monte Carlo set calculated for the uncertainty analysis in the basecase scenario. Sensitivities for igneous activity scenario relied on multiple smaller (350) Monte Carlo run sets. All nonstatistical sensitivity analysis techniques required sets of runs calculated for input variables specified by the method. Sensitivity analyses were used to identify sensitive parameters for which a small input change can have a large effect on estimated repository performance. Data were also scaled or

standardized to take into account the relative change in a variable to allow more accurate ranking of sensitivities.

The regression analyses used both raw and transformed variables, including logarithmic and rank transformations. Although the transformed variables generally led to better coefficients of regression, they also distorted the meaning of the results by giving too much weight to small doses. In addition, this study added a new reliability-based method know as the Cumulative Distribution Function-Based Sensitivity Method (Appendix D).

All the nonstatistical methods used in previous total system performance assessment sensitivity studies (Morris method, FAST, and differential analysis) were also employed in this study. In addition, this study added the fractional factorial design method.

Rankings for sensitivity took a consensus approach that determined the most sensitive variables according to the relative rank of that variable in each of the separate sensitivity analyses. The ranking of the variables for the 10,000-year simulation period is shown in Table 4-10.

Validation of whether the choice of the sensitive parameters by the various methods was correct was achieved by calculating and comparing Monte Carlo runs with all 330 parameters in the basecase sampled against new Monte Carlo runs for which only the reduced set of sensitive variables were either included or eliminated. Results show that keeping only the most sensitive variables gives results similar to the basecase results. Removing the most sensitive variables from sampling reduces the uncertainty in the results. Both observations demonstrate that the correct variables have been identified as being most sensitive.

8.4.2 Distributional Sensitivity

Another new technique in this study was distributional sensitivity. It was not used directly to rank sensitive variables but to determine the effect of estimation of parameter distributions for important variables on the performance results. In this technique, the input distributions were changed either by shifting the mean of a distribution by 10 percent or changing the shape of the distribution while keeping the minimum and maximum fixed. This study used the 10 most influential variables identified in the sensitivity analyses. In summary, the distributional analyses showed that improper choice of distribution functions can significantly affect the dose response. Two parameters that appear especially important in this regard are the flow multiplication factor that determines the quantity of water entering the waste packages and the preexponential term for the spent nuclear fuel-dissolution model.

8.5 Repository Component Sensitivity Analyses

Repository component sensitivity analyses look at the whole barrier at once, either performing or not performing. In the Monte Carlo uncertainty analysis used, the performance of barriers other than the waste package often could not be seen (e.g., there were never any corrosion failures of the waste packages within 10,000 years). Repository component sensitivity analysis, which assumes failure of specific barriers, allows the exploration of barrier performance by reducing the overlapping capabilities of multiple barriers. The six repository components of the engineered and natural barriers are drip shield, waste package, spent nuclear fuel, invert, unsaturated zone, and saturated zone.

Barrier failure or suppression was simulated by changing input parameters to degrade the performance severely (e.g., setting the alluvium distance to zero). There was no attempt to define a probability associated with the suppressed barrier, and the technique was never used to calculate risk.

The repository component sensitivity analyses considered several possibilities: (i) one-off component suppression, for which the performance was calculated with a single barrier suppressed; (ii) one-on analysis, for which only a single barrier was active at a time; and (iii) multiple barrier suppression.

From the one-off analysis, the largest decrease in performance came from suppression of the waste package, followed by unsaturated zone, saturated zone, waste form, drip shield, and invert. The relatively large impact of the unsaturated zone resulted from its role above the repository in diverting of water away from the waste package and fuel, thereby reducing the mobilization and transport of radionuclides. One-on analysis ranks the contribution to repository performance in the same order as the one-off analysis, but in some respects, the contribution to performance of a single barrier is clearer. For example, the one-on analysis shows that the unsaturated zone alone would reduce the peak dose by more than 95 percent of the value with none of the barriers effective.

Suppression of multiple repository components shows some interesting interactions. For example, when both the drip shield and waste package components are off, the increase exceeds the sum of either component individually, revealing the sensitivity to the drip shield that is otherwise masked in the one-off analysis. In this case, the drip shield and waste package can be seen to be redundant (i.e., the function of the drip shield in shedding water could be assumed by the waste package if the former failed).

8.6 Subsystem Capacity Analysis

Subsystem capacity analyses show for the basecase conceptual models (i) the majority of waste packages remains intact for greater than 10,000 years, (ii) the drip shield delays the onset of dripping from the drift wall reaching the waste packages for a large fraction of 10,000 years, (iii) more than 90 percent of meteoric water will be diverted by the unsaturated zone above the engineered barrier, (iv) the properties of the unsaturated zone in conjunction with the drifts will act to divert water from many of the waste packages, (v) the properties of the waste form itself will cause radionuclides to be released slowly once other barriers have failed, and (vi) the unsaturated and saturated zones below the repository will retard and retain many of the radionuclides released from the engineered barrier subsystem for greater than 10,000 years.

8.7 Criticality

A conservative consequence analysis showed that the conditional occurrence of a steady-state or transient criticality would increase doses by an order of magnitude above the basecase dose, but is still well below the regulatory dose limit of 0.15 mSv/yr [15 mrem/yr]. In addition, the probability of conditions leading to this event is believed to be low, so the risk significance of in-package criticality is not expected to be great.

8.8 Importance of Radionuclides

For the basecase, most of the peak expected dose came from the isotopes Np-237, I-129, and Tc-99. The biggest factor in the dominance of these radionuclides is their low retardations, long half-lives, abundance, and dose conversion factors. The vast majority of retarded radionuclides (i.e., plutonium, americium) never arrive at the downgradient pumping well. Therefore, none of the parameters associated with these radionuclides surface as being sensitive in traditional sensitivity analyses. Techniques such as repository component analysis are useful in these cases because they show the effects of the arbitrary elimination of a repository component such as retardation. For the 10,000-year simulation period, the isotope Np-237 was retarded enough in the geosphere that it barely began to arrive at the downgradient well by 10,000 years. Np-237 became overwhelmingly important for the 100,000-year simulation period for which retardation in the geosphere was less of an issue, however.

8.9 Synthesis of Results to Determine Importance of Key Integrated Subissues for 10,000-Year Simulation Period

The important key integrated subissues, as determined by the analyses presented in this report, are

- Volcanic disruption of waste packages (DIRECT1)
- Airborne transport of radionuclides (DIRECT2)
- Degradation of the engineered barriers (ENG1)
- Flow paths in the unsaturated zone (UZ2)
- Quantity and chemistry of water contacting waste packages and waste forms (ENG3)
- Radionuclide release rates and solubility limits (ENG4)
- Mechanical disruption of engineered barriers (ENG2)
- Climate and infiltration (UZ1)
- Radionuclide transport in the saturated zone (SZ2)

This identification of key integrated subissues should be treated with considerable caution, bearing in mind that the TPA Version 4.1 code can only determine the effect of a phenomenon correctly if the physical processes have been included and properly abstracted into the code. The list of important key integrated subissues may change as models embedded in the TPA Version 4.1 code and their associated parameter ranges become better understood.

8.10 Further Study

A TPA Version 5.0 code is planned for 2003. This version will have a variety of improvements to model abstractions. Changes will reflect improvement in our understanding of the conceptual models of the site and their effect on estimated risk.

New models that may be added are

- Drift Collapse—This model will potentially affect seepage, drip shield failure, and flow diversion.

- Vitrified Waste Form—This model will calculate the dissolution of the glass waste form and release of radionuclides to the engineered barrier subsystem.

- Weld Corrosion—This model will estimate the extent of corrosion in the end cap welds. Estimates of the extent of these failures will potentially be used subsequently in a diffusive transport model.

- Diffusive Release from Waste Packages—The current model does not account for the possible release of radionuclides through small cracks in the waste packages. This revision will consider diffusion through thin films and small stress corrosion cracks in end lid welds, for conditions that would allow a diffusive path to the invert.

- Colloid Source Term—This model will estimate the rate of release of radionuclides as real and pseudocolloids.

- Cladding Failure Model—The current model has a crude accounting for cladding protection, but not a mechanistic model that would predict the corrosion of cladding or unzipping because of fuel degradation. This revision will include time-dependent failure rates for cladding.

- Microbially Induced Corrosion—This model will estimate the enhanced corrosion caused by microbially induced corrosion.

- Plume Capture—This model will calculate the portion of the plume that would be captured by the reasonably maximally exposed individual, whether at the 18-km [11.2-mi] location or closer.

Potential modifications to existing models and data are

- Update climate and infiltration data.

- Add runoff effect to the infiltration model.

- Modify shallow infiltration estimate to account for vegetation.

- Add a factor to account for infiltration variance.

- Include a model that accounts for general corrosion, fluoride attack, and mechanical failure of the drip shield—TPA Version 4.1 code treats drip shield failure as simply a sampled parameter.

- Add variability of pH in waste package corrosion model.

- Represent K_ds and retardation factors as functions of the geochemistry.

- Include uncertainty in the Calico Hills nonwelded vitric layer thickness.

- Account for multiple fracture flow and matrix flow episodes.

- Allow variable dispersivity for transport in the unsaturated zone.

- Include uncertainty in the saturated zone streamtube dimensions.

- Allow changes in streamtube flux after climate change.

- Improve mass loading and occupancy factors for igneous activity.

- Modify igneous activity source term to better account for physical processes of mixing fuel and magma.

- Add a short-term ash redistribution model to consider remobilization of ash by overland flow of water.

- Add effects of rockfall on drip shield.

In addition to the technical changes to the TPA Version 4.1 code to address improved model abstractions, data and models will be adjusted where necessary to accommodate changes to the current U.S. Department of Energy (DOE) repository design and thermal loading strategy.

8.11   Conclusions

The TPA Version 4.1 code has been used successfully in a structured way to provide risk insights through investigating the performance of the proposed Yucca Mountain repository and the sensitivity of this performance to repository subsystems and parameters on which they rely. The calculated risk is small within the 10,000-year simulation period, determined with the staff best estimate of models and parameters. Extrusive volcanism was the scenario that produced the maximum calculated risk of 3.6 µSv/yr [0.36 mrem/yr]. Experimentation with a wide range of alternative conceptual models for waste form dissolution, waste package lifetime, and radionuclide transport never led to calculated risks that were close to exceeding the standard.

The NRC and CNWRA staff used a variety of statistical and nonstatistical methods to determine the sensitivity of dose to variations in the input parameters. Three new methods applied to the TPA Version 4.1 code proved useful in determining parametric sensitivities. Fractional factorial design provides a means of unambiguously determining the interactions among variables. Distributional sensitivity illustrates the effect of parameter estimation errors on risk. The cumulative distribution function-based method shows sensitivities in different dose ranges, particularly the high-dose responses. As in previous total system performance assessment studies, staff relied on a consensus approach for all the parametric sensitivity methods to determine the parameters that appeared most frequently and with the highest rank among all the methods. Using this procedure, a list of the 10 most influential parameters was developed for the regulatory period of 10,000 years. This list consisted of parameters that deal with flow of water to the waste, failure of barriers to flow, retardation along transport pathways of slightly retarded Np-237, fuel-dissolution rates, and dilution at the point of use. There were no parameters in this list that dealt with waste package corrosion because the models predicted that none of the waste packages failed by this mechanism within 10,000 years. A similar list was developed for the 100,000-year simulation period, which is not required by the regulations but serves the purpose of broadening understanding of failure modes for the repository.

Parameters dealing with waste package corrosion appeared on this list, together with the retardation factor for Pu-239.

Repository component sensitivity analysis evaluated how repository components behaved in the repository system. Suppression of the performance of the repository components, singly and in combinations, provided useful informational about the sensitivity of the performance to the repository components (i.e., subsystems) although the staff never attached probabilities to these suppressions, and such results had no direct bearing on the overall risk. Repository component analysis pointed out interesting features of the repository such as (i) the redundancy of the drip shield and waste package to shed dripping water, (ii) the capabilities of the unsaturated and saturated zones independent of the waste package, and (iii) the relative unimportance of the invert as a barrier. Important components were also identified based only on their capabilities rather than their direct bearing on dose or risk. In identifying these components, the staff demonstrated that for the conceptual models included in the TPA Version 4.1 code, the drip shield, waste package, waste form, unsaturated zone, and saturated zone all contributed to waste isolation.

The NRC and CNWRA staff evaluated two stylized scenarios for human intrusion and in-package nuclear criticality. Both analyses were conditional, with no assignment of probability although these probabilities are believed to be small. Both produced maximum conditional dose values well below the 0.15 mSv/yr [15 mrem/yr] dose limit specified by the regulations.

This report was prepared to document work performed by the CNWRA for the NRC under Contract No. NRC–02–02–012. The activities reported here were performed on behalf of the NRC Office of Nuclear Material Safety and Safeguards, Division of Waste Management. The report is an independent product of CNWRA and does not necessarily reflect the views or regulatory position of NRC.

9 REFERENCES

Beckman, R.J. and M.D. McKay. "Monte Carlo Estimation Under Different Distributions Using the Same Simulation." *Technometrics*. Vol. 29, No. 2. pp. 153–160. 1987.

Benjamin, J.R. and C.A. Cornell. *Probability, Statistics, and Decision for Civil Engineers*. New York City, New York: McGraw-Hill. 1970.

Bowen, W.M. and C.A. Bennett, eds. NUREG/CR–4604, "Statistical Methods for Nuclear Material Management." Washington, DC: NRC. December 1988.

Box, G.E.P. and J.S. Hunter. "The 2^{k-p} Fractional Factorial Designs Part 1, 1961." *Technometrics*. Vol. 42, No 1. pp. 28–47. 2000. (This is a reprint of *Technometrics*. Vol. 3. pp. 311–351. 1961.)

Campbell, J. E. and C.D. Leigh. NUREG/CR–5618, "User's Manual for the NEFTRAN II Computer Code." Washington, DC: NRC. February 1991.

Chun, M.H., H.S.J. Han, and N.I. Tak. "An Uncertainty Importance Measure Using a Distance Metric for the Change in a Cumulative Distribution Function." *Reliability Engineering and System Safety*. Vol. 70. pp. 313–321. 2000.

Code of Federal Regulations. "Environmental Radiation Protection Standards for Management and Disposal of Spent Nuclear Fuel, High-Level and Transuranic Radioactive Waste." Title 40—Protection of the Environment, Chapter 1—Environmental Protection Agency, Part 191. Washington, DC: U.S. Government Printing Office. 2003.

———. "Disposal of High-Level Radioactive Waste in Geologic Repositories." Title 10—Energy, Chapter 1—Nuclear Regulatory Commission, Part 60. Washington, DC: U.S. Government Printing Office. 1991b

———. "Disposal of High-Level Radioactive Wastes in a Proposed Geological Repository at Yucca Mountain, Nevada." Title 10—Energy, Chapter 1—NRC, Part 63. Washington, DC: U.S. Government Printing Office. 2002.

———. "Public Health and Environmental Radiation Protection Standards for Yucca Mountain, Nevada." Title 40—Protection of Environment, Chapter 1—EPA, Part 197. Washington, DC: U.S. Government Printing Office. 2001.

Codell, R.B, N. Eisenberg, D. Fehringer, W. Ford, T. Margulies, T. McCartin, J. Park, and J. Randall. NUREG–1327, "Initial Demonstration of the NRC's Capability to Conduct a Performance Assessment for a High-Level Waste Repository." Washington, DC: NRC. May 1992.

CRWMS M&O. "License Application Design Selection Report." B00000000–01717–4600–00123. Rev. 01. Las Vegas, Nevada: CRWMS M&O. 1999.

———. "Total System Performance Assessment—Viability Assessment (TSPA-VA) Analyses Technical basis Document." B00000000–01717–4301–00002. Las Vegas, Nevada: TRW Environmental Safety Systems, Inc. 1998.

Cukier, R.I., J.H. Schaibly, and K.E. Schuler. "Study of the Sensitivity of Coupled Reaction Systems to Uncertainties in Rate Coefficients. III: Analysis of the Approximation." *Journal of Chemical Physics.* Vol. 63, No. 3. pp. 1,140–1,149. 1975.

Cukier, R.I., C.M. Fortuin, K.E. Schuler, A.G. Petschek, and J.H. Schaibly. "Study of the Sensitivity of Coupled Reaction Systems to Uncertainties in Rate Coefficients. I: Theory." *Journal of Chemical Physics*. Vol. 59, No. 8. pp. 3,873–3,878. 1973.

DOE. DOE/RW–0508/V3, "Viability Assessment of a Repository at Yucca Mountain. Vol. 3: Total System Performance Assessment."   Washington, DC: DOE, Office of Civilian Radioactive Waste Management. 1998.

Draper, N.R. and H. Smith, Jr. *Applied Regression Analysis*. 2nd Edition. New York City, New York: John Wiley and Sons. 1981.

Helton, J.C., J.W. Garner, R.D. McCurley, and D.K. Rudeen. "Sensitivity Analysis Techniques and Results for Performance Assessment at the Waste Isolation Pilot Plant." SAND90–7103. Albuquerque, New Mexico: Sandia National Laboratories. 1991.

Iman, R.L. and W.J. Conover. "The Use of the Rank Transform in Regression." *Techtonometrics*. Vol. 21. pp. 499–509. 1979.

Iman, R.L. and S.C. Hora. "A Robust Measure of Uncertainty Importance for Use in Fault Tree System Analysis." *Risk Analysis*. Vol. 10, No. 3. pp. 401–406. 1990

Iman, R.L., J. Davenport, and D. Ziegler. "Latin Hypercube Sampling (Program User's Guide)." SAND–1473. Albuquerque, New Mexico: Sandia National Laboratories.   1980.

Jarzemba M.S. and B. Sagar. "A Parameter Tree Approach to Estimating System Sensitivities to Parameter Sets." *Reliability Engineering and System Safety*. Vol. 67. pp. 89–102. 2000.

Jarzemba, M.S., P.A. LaPlante, and K.J. Poor. "ASHPLUME Code Version 1.0 Model Description and User's Guide." CNWRA 97-004. San Antonio, Texas: CNWRA. 1997.

Khatib-Rahbar, M., E. Cassoli, M. Lee, H. Nourbakhsh, R. Davis, and E. Schmidt. "A Probabilistic Approach to Quantifying Uncertainties in the Progression of Severe Accidents." *Nuclear Science Engineering*. Vol. 102. pp. 219–259. 1989.

Kahn, H. and A.W. Marshall. "Methods of Reducing Sample Size in Monte Carlo Computations." *Journal of the Operations Research Society of America*. Vol. 1. pp. 263–271. 1953.

Kennedy, W.J. and J.E. Gentle. "Statistical Computing." New York City , New York: Marcel Dekker. 1980.

Lichtner, P.C., M.S. Seth, and S. Painter. "MULTIFLO User's Manual MULTIFLO Version 1.2—Two-Phase Nonisothermal Coupled Thermal-Hydrologic-Chemical Flow Simulator." Rev. 2, Change 1. San Antonio, Texas: CNWRA. 2000.

Mason, R.L., R.F. Gunst, and J.L. Hess. *Statistical Design & Analysis of Experiments with Applications to Engineering and Science*. New York City, New York: John Wiley and Sons. 1989.

Mohanty, S. and T.J. McCartin. "Total-system Performance Assessment (TPA) Version 3.2 Code: Module Description and User's Guide." San Antonio, Texas: CNWRA. 1998.

Mohanty, S. and Y-T. (Justin) Wu. "CDF Sensitivity Analysis Technique for Ranking Influential Parameters in the Performance Assessment of the Proposed High-Level Waste Repository at Yucca Mountain, Nevada, USA." *Reliability Engineering and System Safety*. Vol. 73, No. 2. pp. 167–176. 2001.

Mohanty, S., T.J. McCartin, and D.W. Esh. "Total-system Performance Assessment (TPA) Version 4.0 Code: Module Descriptions and User's Guide." San Antonio, Texas: CNWRA. 2002.

Mohanty, S., R. Codell, R.W. Rice, J. Weldy, Y. Lu, R.M. Byrne, T.J. McCartin, M.S. Jarzemba, and G.W. Wittmeyer. "System-Level Repository Sensitivity Analyses Using TPA Version 3.2 Code." CNWRA 99-002. San Antonio, Texas: CNWRA. 1999.

Morgan, M.G. and M. Henrion. *Uncertainty: A Guide to Dealing with Uncertainty in Quantitative Risk and Policy Analysis*. New York City, New York: Cambridge University Press. 1990.

Morris, M.D. "Factorial Sampling Plans for Preliminary Computational Experiments." *Technometrics*. Vol. 33, No. 2. pp. 161–174. 1991.

Murphy, W.M. and R.C. Codell. "Alternate Source Term Models for Yucca Mountain Performance Assessment Based on Natural Analog Data and Secondary Mineral Solubility." Scientific Basis for Nuclear Waste Management XXII. D.J. Wronkiewicz and J.H. Lee, eds. Materials Research Society Symposium Proceedings. Boston, Massachusetts: Materials Research Society. Vol. 556. p. 551–558. 1999.

Napier, B.A., R.A. Peloquin, D.L. Strenge, and J.V. Ramsdell. "GENII: The Hanford Environmental Radiation Dosimetry Software System. Vols. 1, 2, and 3: Conceptual Representation, User's Manual, and Code Maintenance Manual." PNL–6584. Richland, Washington: Pacific Northwest National Laboratory. 1988.

NRC. NUREG–1804, "Yucca Mountain Review Plan: Final Report." Rev. 2. Washington, DC: NRC. July 2003.

———. NUREG–1762, "Integrated Issue Resolution Status Report." Washington, DC: NRC. July 2002.

———. NUREG–1668, "NRC Sensitivity and Uncertainty Analyses for a Proposed HLW Repository at Yucca Mountain, Nevada Using TPA 3.1. Volume II: Results and Conclusions." Washington, DC: NRC. March 1999a.

———. "Disposal of High-Level Radioactive Wastes in a Proposed Geological Repository at Yucca Mountain, Nevada: Proposed Rule." *Federal Register*. Vol. 64, No. 34. pp. 8640–8679. 1999b.

Nuclear Waste Policy Act of 1982. Pub. L. 97–425. 96 Stat. 2201 (1982).

Olague, N.E., D.E. Longsine, J.E. Wescott, M.P. Lee, N.A. Eisenberg, T.J. McCartin, and R.G. Baca, eds. NUREG–1464, "NRC Iterative Performance Assessment Phase 2." Washington, DC: NRC. October 1995.

Park, C.K. and K.I. Ahn. "A New Approach for Measuring Uncertainty Importance and Distributional Sensitivity in Probabilistic Safety Assessment." *Reliability Engineering and System Safety*. Vol. 46. pp. 253–261. 1994.

Schmidt, S.R. and R.G. Launsby. "Understanding Industrial Designed Experiments." Colorado Springs, Colorado: Air Force Academy Press. 1991.

Seitz, R.R., A.S. Rood, G.A Harris, S.J. Maheras, and M. Kotechi. "Sample Application of Sensitivity/Uncertainty Analysis Techniques to a Groundwater Transport Problem." DOE/LLW–108. Idaho Falls, Idaho: Idaho National Engineering Laboratory. 1991.

Sen, A. and M. Srivastava. *Regression Analysis Theory, Methods, and Applications*. New York City, New York: Springer-Verlag, Inc. 1990.

Stothoff, S.A. "Infiltration Abstraction for Shallow Soil Over Fractured Bedrock in a Semi-Arid Climate." San Antonio, Texas: CNWRA. 1999.

Stothoff, S.A., H.M. Castellaw, and A.C. Bagtzoglou. "Simulating the Spatial Distribution of Infiltration at Yucca Mountain, Nevada." San Antonio, Texas: CNWRA. 1997.

Suzuki, T. "A Theoretical Model for Dispersion of Tephra." *Arc Volcanism: Physics and Tectonics*. Tokyo, Japan: Terra Scientific Publishing. pp. 95–113. 1983.

Westcott, R.G., M.P. Lee, N.A. Eisenberg, T.J. McCartin, and R.G. Baca, eds. NUREG–1464 "NRC Iterative Performance Assessment Phase 2." Washington, DC: NRC. October 1995.

Wu, Y-T. "Computational Methods for Efficient Structural Reliability and Reliability Sensitivity Analysis." *AIAA Journal*. Vol. 32, No. 8. pp. 1,717–1,723. 1994.

Zimmerman, D.A. NUREG/CR–5395, "A Review of Techniques for Propagating Data and Parameter Uncertainties in High-Level Waste Performance Assessment Models." Washington, DC: NRC. 1991.

APPENDIX A

DESIGN MATRIX FOR THE MORRIS METHOD

This appendix explains the steps necessary to obtain the matrix used by the Total-system Performance Assessment (TPA) code as the input parameters. Let x_i, i = 1, 2, ..., I, be the elements of x, where x is the input parameter vector with I elements. Assuming $0 \leq x_i \leq 1$, the interval [0, 1] is now divided into p discrete levels. A randomly chosen base vector, x^*, is then obtained by assigning each element of x randomly from a set of discrete values: $\{0, 1/(p-1), 2/(p-1), \cdots, 1-\Delta\}$, where Δ = $p/2(p-1)$. To obtain the matrix, first, a (I + 1)-by-I sampling matrix, B, with elements of 0's and 1's is selected:

$$B = \begin{bmatrix} 0 & 0 & 0 & \cdots & 0 \\ 1 & 0 & 0 & \cdots & 0 \\ 1 & 1 & 0 & \cdots & 0 \\ \cdots & \cdots & \cdots & \cdots & \cdots \\ 1 & 1 & 1 & \cdots & 1 \end{bmatrix} \tag{A–1}$$

Matrix B has an important property, namely, that any row differs from its immediate neighboring rows only in one column. For instance, the second row differs from the first row only in the first column and the third row in the second column. A matrix obtained by multiplying B with Δ can be used to produce I values of $\partial y/\partial x_i$, based on (I + 1) runs. But the elements of the matrix are not randomly selected.

To randomize the matrix ΔB, the following operations are performed

$$B^* = J_{(I+1),I} \ x^* + (\Delta / 2)[(B - J_{(I+1),I}) D^* + J_{(I+1),I}] \tag{A–2}$$

where J is an (I+1)-by-I matrix of 1's and D^* is an I-dimensional diagonal matrix in which each diagonal element is either +1 or -1 with equal probability. The operations defined in Eq. (A–2) randomize the matrix ΔB. The matrix B* is called the design matrix.

Since the input variables are considered random, so is the output $y(x)$. If a distribution of r samples is required for each $\partial y/\partial x_i$, the previous process defined in Eq. (A–2) can be repeated r times to produce an r(I+1)-by-I design matrix X

$$X_{r(I+1),I} = \begin{bmatrix} B_1^* \\ B_2^* \\ \dots \\ B_r^* \end{bmatrix} \tag{A–3}$$

Each row of X will next be used as input to the TPA code, to calculate $y(x)$, and the matrix X will be used to produce rI number of $\partial y/\partial x_i$, which, in turn, will produce I distributions for the input variables, each with r samples.

APPENDIX B

ELSEVIER

Sensitivity analysis of a complex, proposed geologic waste disposal system using the Fourier Amplitude Sensitivity Test method

Yichi Lu[1], Sitakanta Mohanty*

Center for Nuclear Waste Regulatory Analyses, Southwest Research Institute, 6220 Culebra Road, San Antonio, TX 78238, USA

Abstract

The Fourier Amplitude Sensitivity Test (FAST) method has been used to perform a sensitivity analysis of a computer model developed for conducting total system performance assessment of the proposed high-level nuclear waste repository at Yucca Mountain, Nevada, USA. The computer model has a large number of random input parameters with assigned probability density functions, which may or may not be uniform, for representing data uncertainty. The FAST method, which was previously applied to models with parameters represented by the uniform probability distribution function only, has been modified to be applied to models with nonuniform probability distribution functions. Using an example problem with a small input parameter set, several aspects of the FAST method, such as the effects of integer frequency sets and random phase shifts in the functional transformations, and the number of discrete sampling points (equivalent to the number of model executions) on the ranking of the input parameters have been investigated. Because the number of input parameters of the computer model under investigation is too large to be handled by the FAST method, less important input parameters were first screened out using the Morris method. The FAST method was then used to rank the remaining parameters. The validity of the parameter ranking by the FAST method was verified using the conditional complementary cumulative distribution function (CCDF) of the output. The CCDF results revealed that the introduction of random phase shifts into the functional transformations, proposed by previous investigators to disrupt the repetitiveness of search curves, does not necessarily improve the sensitivity analysis results because it destroys the orthogonality of the trigonometric functions, which is required for Fourier analysis. © 2001 Elsevier Science Ltd. All rights reserved.

Keywords: Sensitivity analysis; Fourier amplitude sensitivity test; Performance assessment; Waste management; Nonlinear model; System simulation

1. Introduction

A total-system performance assessment (TPA) code has been developed by the Nuclear Regulatory Commission (NRC) and the Center for Nuclear Waste Regulatory Analyses (CNWRA) as a tool for reviewing the license application for the proposed high-level waste (HLW) repository at Yucca Mountain, Nevada, USA. The TPA code is designed to simulate probable complex behavior of the repository over long time periods (e.g. 10,000 years). Because of the simplifying assumptions to the governing physical processes, the coupling among these processes, the uncertainties in the parameters defining the physical system, and the boundary conditions that prevail over the long time period of interest (TPI), significant uncertainties are introduced in the future state of the repository simulated by the computer model. The TPA code is designed so that conceptual model uncertainties can be analyzed by using alternative conceptual models (not studied in this paper), and the parameter uncertainties can be studied by assigning them appropriate probability distribution functions. Identification of the most influential parameters among a large number of input parameters, which is usually performed by sensitivity analysis, can lead to a better understanding of the physical processes that control the performance of a repository; attention and resources could then be concentrated on investigating further these controlling physical parameters.

Many sensitivity analysis methods exist such as linear regression [1–4], nonparametric schemes [5–7], or one-at-a-time analysis [8,9]. Each method has its advantages and disadvantages. For example, while the linear regression methods are simple and easy to use, they cannot assess nonlinear effects. Nonparametric methods do not require the input parameters to have well-defined statistical descriptions, but when the input parameters have adequate statistical descriptions, the nonparametric methods usually result in less accurate estimates. The one-at-a-time approaches can clearly attribute the change in output to the change in each input parameter, but they may not be able to study the

---

* Corresponding author. Tel.: +1-210-522-5185; fax: +1-210-522-5155.
E-mail address: smohanty@swri.org (S. Mohanty).
[1] Current address: 9218 Balcones Club Dr., Austin, TX 78750, USA.

interactive effects (mathematically represented by products of two or more parameters) well because they only allow one parameter to change at any time, and the output is essentially a function of a single parameter at the time of change.

In this paper, a global sensitivity analysis method, the Fourier Amplitude Sensitivity Test (FAST) method [10–14], that determines the sensitivity of the output by averaging it over all input parameters, is investigated. The FAST method allows all input parameters to be varied simultaneously so that the interactive effects (i.e. the mutual or reciprocal effects) among input parameters on the output can be adequately studied. The method was first developed by Cukier, Schaibly, and Shuler, et al. [10–14], to investigate the sensitivity of the solutions of large sets of coupled nonlinear equations to uncertainties in the input parameters. Rather than investigating each individual input parameter separately, the FAST method varies all input parameters simultaneously to conduct the sensitivity analysis. This is in contrast to a differential analysis (a one-at-a-time analysis approach) where the sensitivity is analyzed near a local point in the input parameter space [9].

The FAST method was modified and used by Saltelli and his colleagues on many computer models [15–19]. Although Saltelli et al. [16] have since advocated the use of this method, applications so far appear to have been limited to computer models that have a small parameter set (~10 parameters), and all parameters are assumed to have a uniform distribution function [13,19]. Many real-world computer models, especially the models that conduct performance assessment of a HLW repository, have a far greater number of input parameters and more diverse distribution types for the input parameters.

In this paper, the FAST method, together with the Morris method [9], is used to conduct a sensitivity analysis on a computer model with a large number of sampled parameters (~250) characterized by diverse probability distribution functions. In Section 2, the major functions and components of the NRC/CNWRA computer model (the TPA code) that will be used to evaluate the performance of the proposed geologic HLW repository at Yucca Mountain (YM) are briefly described to give the reader a general idea of the computer model to be analyzed. In Section 3, a short description of the FAST method is presented, In the FAST method, a functional transformation is applied to each model input parameter. To the best of the authors' knowledge, the functional transformations have been presented in the literature only for uniform distribution [13,19]. Also in Section 3, a general functional transformation applicable to uniform and other probability distribution functions is derived. In Section 4, the FAST method is applied to an example problem with a small parameter set for which the importance of each parameter to the output of the example problem is known a priori. This enables us to investigate the effectiveness of the FAST method via its major components: (i) functional transformations applied to either uniform or other distribution functions, (ii) the integer frequency sets characterizing the search paths in the parameter space, (iii) random phase shift introduced in the functional transformations to disrupt the repetitiveness of the search curve, and (iv) number of discrete sampling points used in the FAST method. Application of the FAST method to the TPA computer code to rank model parameters is covered in Section 5 after screening less important parameters. Section 6 presents the results of sensitivity analysis. Verification of these results is presented in Section 7. A summary and conclusions are presented in Section 8.

2. The computer model

The computer model used in this study was developed by the NRC and CNWRA to guide the review of a potential license application for the proposed HLW repository at YM. The TPA computer code [20–22] considers uncertainties and spatial variability of system attributes, model parameters, and future system states (i.e. scenario classes). To capture the effects of uncertainties in system characteristics and future system states, the TPA code operates in a probabilistic manner (i.e. input parameters are sampled from assigned probability distributions). The TPA code estimates radiation doses from released radionuclides during specified time periods (e.g. regulatory compliance TPI) at designated receptor locations (e.g. 20 km downgradient of YM). Only a brief discussion of the processes in the code is presented in the paper. For a complete description of the methods and assumptions, refer to Mohanty and McCartin [22].

The TPA code simulates physical and chemical processes of the repository system. Calculations of the most likely scenarios include the degradation of waste packages (WPs), in which HLWs are disposed in an underground repository, and the release of radionuclides when the water precipitating on top of the mountain finds its way into the failed WPs and transports the radionuclides through a partially water-saturated geologic medium to the water table and, subsequently, to a designated receptor group. The calculation involves several steps including the computation of (i) time-varying precipitation resulting from postulated climate changes, water percolation from the land surface to the subsurface, and subsequently into the emplacement drifts and onto WPs; (ii) the chemical and physical processes (e.g., temperature, humidity, pH, chloride concentration, and carbonate concentration) affecting engineered barrier degradation, including the WPs and radionuclide releases; (iii) corrosion phenomena for determining a WP lifetime; (iv) the number of containers affected by seismicity-induced rock falls; (v) the radionuclide release rate from the EBS to the groundwater pathway as a function of time; (vi) flow and transport of radionuclides through the unsaturated zone; (vii) flow and transport of radionuclides through the saturated zone; and (viii) dose to a specified receptor from groundwater radioactivity concentrations

taking into account lifestyle characteristics of the receptor group at a designated location.

In addition to simulating the physical processes for the most likely scenario, the TPA code also simulates the processes involved with high-consequence-low-probability events that include (i) the number of WPs failed because of the displacement of yet unknown faults intersecting the repository, (ii) magmatic intrusions resulting from igneous activity, and (iii) extrusive igneous activity leading to dose to the receptor group from airborne transport of contaminated ash particles.

The TPA code samples the input parameters using a Latin hypercube sampling (LHS) algorithm [23], post processes time-dependent risk curves, and synthesizes statistical distributions (e.g. cumulative distribution functions (CDFs) and complementary cumulative distribution function (CCDFs)) for appropriate performance measures. Although the TPA code is designed to conduct Monte Carlo simulations, the user may specify input parameter values and perform a single realization. In this paper, the processes associated with high-consequence-low-probability events are not considered. In addition to numerous input files containing time-dependent parameters, the code also contains 838 input parameters out of which 246 are sampled from specified distribution functions. Eleven different distribution functions are used in the code to describe the statistical distribution of the input parameters.

Standard TPA calculations are performed at 10,000 years, the proposed compliance period in the draft regulation [24]. To investigate the performance beyond 10,000 years, calculations are also performed at 50,000 years.

3. The FAST method

The FAST method [10–14] applies a functional transformation to each input parameter, assigns each input parameter a distinct integer frequency, and introduces a common independent variable to all input parameters. The input parameters vary simultaneously with this independent variable in such a way that the output becomes a periodic function of the independent parameter. Fourier analysis is performed on the output, which produces Fourier amplitudes for each frequency. The magnitudes of the Fourier amplitudes are then taken to be the sensitivity measures of the output to the input parameter with which the particular frequency is associated. A large Fourier amplitude indicates that the output is sensitive to the parameter, while a small amplitude indicates that the output is less (or not) sensitive to the parameter.

Consider a computer model whose output is a nonlinear function of its input parameters:

$$y = y(x_1, x_2, ..., x_I),$$ (1)

where I is the number of input parameters. The input parameters are assumed to be random variables described by

assigned probability density functions (PDFs). The FAST method defines the sensitivity measure as the ensemble average of the change of output due to a small change in the ith input parameter averaged over the entire input parameter space [11]:

$$\left\langle \frac{\partial y}{\partial x_i} \right\rangle = \int_x \frac{\partial y(\mathbf{x})}{\partial x_i} P(x) \, d\mathbf{x},$$ (2)

where $P(x)$ is the joint probability density function of $\mathbf{x}$, where $\mathbf{x} = (x_1, x_2, ..., x_I)$. Assuming all input parameters are statistically independent, then

$$P(\mathbf{x}) = \prod_{i=1}^{I} f_i(x_i),$$ (3)

where $f_i(x_i)$ represents the PDF of x_i.

One way to determine the sensitivity measure would be to integrate Eq. (2) using a multi-dimensional Monte Carlo integration procedure. But such an integration is cumbersome [12], especially for a large I. An alternative approach is to use transformations to convert the I-dimensional integral in Eq. (2) into a one-dimensional integral [10–14]. In the FAST method, the transformation used is represented as [13]:

$$x_i = g_i[\sin(\omega_i s)], \qquad i = 1, 2, ..., I,$$ (4)

where each input parameter, x_i, is assigned an arbitrarily selected, but distinct, incommensurate frequency, ω_i, and s is an independent parameter for all x_i. As s varies, all input parameters vary simultaneously in their own regions of variance at the rates according to the frequencies assigned to them. After substituting Eq. (4) into Eq. (2), the I-dimensional integral in Eq. (2) over x_i becomes a one-dimensional integral over s:

$$\left\langle \frac{\partial y}{\partial x_i} \right\rangle = \int_s \frac{\partial y[x_1(s), x_2(s), ..., x_I(s)]}{\partial x_i(s)} P[x_1(s), x_2(s), ..., x_I(s)] \, ds.$$ (5)

To ensure that as s varies, the parameter x_i obtained in Eq. (4) traverses its region in accordance with the probability distribution function assigned to it, the function, g_i, in Eq. (4) must satisfy the equation [13,25]

$$\pi\sqrt{1 - u^2} f_i(g_i(u)) \frac{dg_i(u)}{du} = 1, \qquad g_i(0) = 0.$$ (6)

If the frequencies ω_i are incommensurate, as defined in Eq. (7), and the functions g_i satisfy Eq. (6), then it can be shown [13,25] that the one-dimensional integral in Eq. (5) yields the same result as that in Eq. (2).

The incommensurate frequencies, which are nonintegers, have an important property that no single frequency in a frequency set can be expressed as a linear combination of any other frequencies. Mathematically, a frequency set, $\{\omega_1, \omega_2, ..., \omega_I\}$, is said to be incommensurate if the equation

$$\sum_{i=1}^{I} a_i \omega_i = 0$$ (7)

can be satisfied only if $a_i = 0$ for every i, where a_i are integers. The use of incommensurate frequencies, however, would require that the integral in Eq. (5) be carried out over an infinitely long interval of s, which is not computationally feasible [11–14]. Therefore, integer frequencies are used in practice so that the integral in Eq. (5) can be evaluated over the finite interval from $-\pi$ to π.

When integer frequencies are used, all x_i and output y in Eq. (1) are periodic functions of s with period 2π:

$$y(s + 2\pi) = y(s). \tag{8}$$

Because the output is now a periodic function of s, it can be expanded into a Fourier series

$$y(s) = \sum_{i=1}^{I} A_i \sin(\omega_i s), \tag{9}$$

where A_i, $i = 1, 2, ..., I$ are the Fourier amplitudes that can be obtained from

$$A_i = \frac{1}{2\pi} \int_{-\pi}^{\pi} y(s) \sin(\omega_i s) \, \mathrm{d}s. \tag{10}$$

In the FAST method, the sensitivity measure of the model output to the input parameters, x_i, $i = 1, 2, ..., I$, are represented by the Fourier amplitudes A_i, $i = 1, 2, ..., I$. But the use of the integer frequencies causes errors [10–14], and the Fourier amplitude A_i will not be unambiguously related to x_i. To reduce the errors, the integer frequencies are still restricted by Eq. (7), but the condition imposed on a_i is loosened to

$$\sum_{i=1}^{I} |a_i| \le M + 1, \tag{11}$$

where M is an integer. No integer frequencies can satisfy Eq. (7) without loosening the condition imposed on a_i.

A frequency set that satisfies Eqs. (7) and (11) is said to be free of interference through Mth order, implying that no single frequency in the set can be expressed as a linear combination of any other M frequencies. In other words, no approximation errors would exist in using A_i as sensitivity measures of x_i if the frequency set is applied to a computer model with only $M + 1$ input parameters. But errors would occur if the model has more than $M + 1$ input parameters.

The functional form of g_i in Eq. (4) must be determined by solving Eq. (6). When applying the FAST method, previous investigators [13,19] assumed a uniform distribution for x_i. But in practice, most computer models, including the TPA code, use both uniform and other distribution functions to represent model parameters.

To solve for g_i, we first rewrite Eq. (6) as

$$f_i(g_i) \, \mathrm{d}g_i = \frac{1}{\pi} \frac{\mathrm{d}u}{\sqrt{1 - u^2}} \tag{12}$$

then, we integrate both sides to yield

$$F_{f_i}(g_i) = \int_{-\infty}^{g_i} f_i(t) \, \mathrm{d}t = \frac{1}{\pi} \arcsin u + C, \tag{13}$$

where F is the CDF for $f_i(x)$ and C is an integration constant.

If the inverse cumulative distribution function (ICDF) exists for $f_i(x)$, we can solve for g_i as a function of x_i from Eq. (13):

$$g_i(u) = F_{f_i}^{-1}\left(\frac{1}{\pi} \arcsin u + C\right), \tag{14}$$

where F^{-1} is the ICDF for the PDF $f_i(x)$. Combining Eqs. (4) and (14) then yields

$$x_i = F_{f_i}^{-1}\left(\frac{1}{\pi} \arcsin[\sin(\omega_i s)] + C\right). \tag{15}$$

If the distribution of x_i is uniform, Eq. (15) reduces to

$$x_i = \frac{1}{\pi} \arcsin[\sin(\omega_i s)] + C, \tag{16}$$

which agrees with Eq. (4.2) in Cukier et al. [13] and Eq. (19) in Saltelli et al. [19]. Eq. (15) indicates that the transformation function of the FAST method requires both an integer frequency, ω_i, and the knowledge of the ICDF. The 246 input parameters sampled by the TPA code have nine different PDF types that include Uniform, Log-uniform, Normal, Log-normal, Log-triangular, Beta, Exponential, Finite-exponential, and User defined. The PDFs, CDFs, and the ICDFs of the first eight distributions are described in Appendix A.

When the independent parameter, s, varies from $-\pi$ to π, Eq. (15) generates sampled input parameters for all x_i. In the FAST method, the sampled input parameters are called search paths. Using a single independent parameter to generate multiple search paths allows one to replace the I-dimensional integral in Eq. (2) with the one-dimensional integral in Eq. (5), as illustrated in Fig. 1. To demonstrate that when s varies, Eq. (15) indeed generates sampled input parameters with necessary distribution characteristics, the histograms of sampled input parameters of the first eight PDFs used in the TPA code are plotted in Fig. 2a–h, where the upper bounds are 1, and the lower bounds are either 0 for nonlogarithmic type distribution or 1.0×10^{-8} for logarithmic type distribution, and $\omega = 11$, which is arbitrarily chosen.

The histograms in Fig. 2a–h show that Eq. (15) generates sampled input parameter points that possess the essential characteristics specified by the PDFs of the input parameters. Eqs. (14) and (15) ensure that the sampled points satisfy the requirements of the FAST method for the transformation functions, g_i, also. The transformation functions represented by Eq. (15) are therefore more general than the one obtained by Saltelli et al. [19] because, strictly speaking, the latter should be applied only to parameters with a uniform distribution.
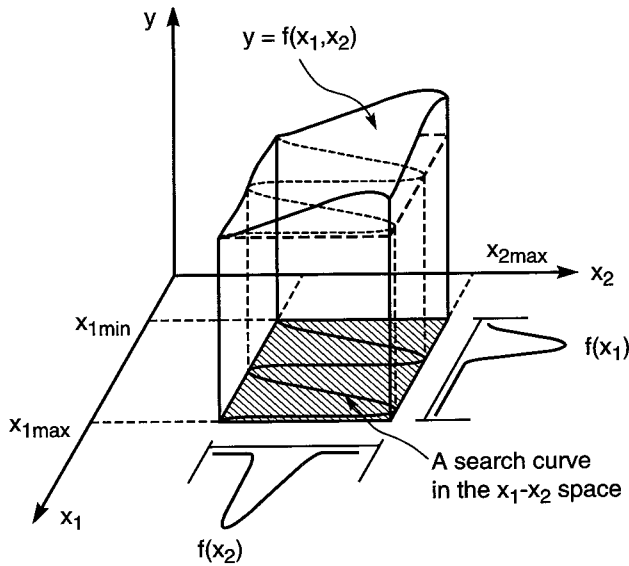
Fig. 1. An integral of $y = f(x_1, x_2)$ over a rectangular area in the x_1–x_2 plane. In the FAST method, the integral over $x_{1min} \leq x_1 \leq x_{1max}$, $x_{2min} \leq x_2 \leq x_{2max}$ is replaced by a line integral along the search curve in the x_1–x_2 plane.

3.1. Search paths based on integer and incommensurate frequencies

As mentioned earlier, theoretically incommensurate frequencies should be used in Eq. (4). But this would require an integration over an infinitely long interval, which is computationally not feasible. Therefore, in practice, integer frequencies, which are not incommensurate, are used. The difference between the integer frequencies and the incommensurate frequencies can be illustrated by a simple example. Let us consider two input parameters x_1 and x_2. We first select two integer frequencies $\omega_1 = 5$ and $\omega_2 = 11$. Notice these two frequencies can be made to satisfy Eq. (7) by selecting $a_1 = 11$ and $a_2 = -5$. These two frequencies are used to generate two sampled parameters:

$$x_1 = \frac{1}{2} + \frac{\arcsin[\sin(\omega_1 s)]}{\pi}, \qquad -\pi \leq s \leq \pi,$$

$$0 \leq x_1 \leq 1, \tag{17a}$$

$$x_2 = \frac{1}{2} + \frac{\arcsin[\sin(\omega_2 s)]}{\pi}, \qquad -\pi \leq s \leq \pi,$$

$$0 \leq x_2 \leq 1. \tag{17b}$$

Fig. 3 shows the search path in the x_1–x_2 plane along which the integration presented in Eq. (5) must be performed. Because integer frequencies are used, the path in Fig. 3 repeats itself along the same trace as s increases; it will never fill the whole sample space between $0 \leq x_i \leq 1$, $0 \leq x_2 \leq 1$. As mentioned earlier, this will result in an inadequate coverage of the sample space.

Next, we select two incommensurate frequencies: $\omega_1 = \sqrt{2}$ and $\omega_2 = 10\sqrt{3}$. Notice these two frequencies can never be made to satisfy Eq. (7) with integer coefficients. Fig. 4 shows the search path generated by using the two incommensurate frequencies. The path in Fig. 4 does not repeat itself; it fills the space between $0 \leq x_i \leq 1$, $0 \leq x_2 \leq 1$, as s becomes large and larger (i.e. as s approaches an infinitely long period).

Figs. 5 and 6 show the search paths after using the transformations defined by Eq. (15), where x_1 has a normal distribution and x_2 has a log-normal distribution. Notice the dramatic change in the search path shape when the distribution functions are nonuniform.

For the one-dimensional integral in Eq. (6) to be equal to the I-dimensional integral in Eq. (2), the search paths generated by Eq. (4) must be able to fill the parameter space [10–14]. Based on Figs. 3–6, the difference between using the incommensurate frequencies and using the integer frequencies is clear. With the incommensurate frequencies, as s increases, the sampled parameter space can be fully covered because a path with incommensurate frequencies will never repeat itself. With integer frequencies, the path continues to repeat itself and will never fill the parameter space.

Saltelli et al. [19] suggested introducing random phase shifts in Eq. (16) to disrupt the repetitiveness of the search paths with integer frequencies:

$$x_i = \frac{1}{\pi} \arcsin[\sin(\omega_i s + r_i)] + C, \tag{18}$$

where r_i is a random number, representing a random phase shift. A search path with a random phase shift does not appear to repeat itself anymore. The errors associated with using integer frequencies remain, however, and the random phase shifts destroy the orthogonality of trigonometric functions, which is needed for Fourier amplitude determination.

3.2. Aliasing and interference errors

There are at least two types of errors caused by using integer frequencies. First, there is a possibility that one particular frequency could be expressed as a linear combination of other frequencies. This would lead to interferences from other frequencies in the evaluation of the Fourier amplitude corresponding to this particular frequency. For instance, if $\omega_4 = \omega_1 + \omega_2 + \omega_3$, then $A(\omega_4) = A(\omega_1 + \omega_2 + \omega_3)$, then A_4 is not only related to x_4 but also to x_1, x_2, and x_3, and there will be errors if A_4 is used as a sensitivity measure of y to x_4. This type of error is called the interference error.

Second, in numerical calculations, N evenly spaced s points for $-\pi < s < \pi$ are used in both Eqs. (4) and (8):

$$s = -\pi + \frac{2\pi j}{N}, \qquad j = 1, 2, ..., N. \tag{19}$$

But if a linear combination of integer frequencies equals an integer multiplier of N

$$\omega_1 + \omega_2 = mN, \qquad m : \text{integer} \tag{20}$$
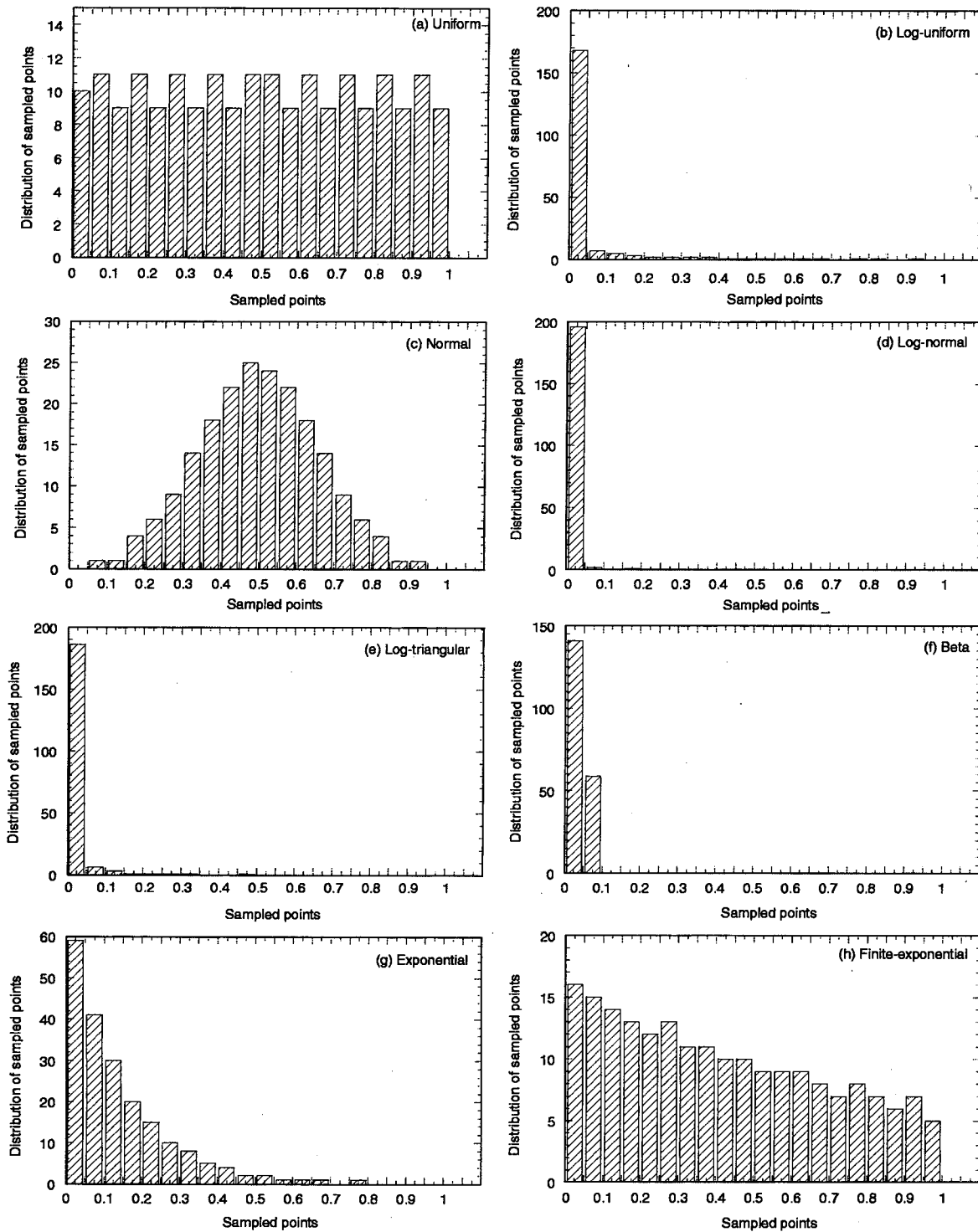
Fig. 2. Distribution of sampled points produced by Eq. (14): (a) Uniform, (b) Log-uniform, (c) Normal, (d) Log-normal, (e) Log-triangular, (f) Exponential, (g) Finite-exponential, and (h) Beta.

then

$$\sin(\omega_1 s) = \sin[(mN - \omega_2)s] = -\sin(\omega_2 s). \qquad (21)$$

Therefore, the input parameter x_1 would influence not only the amplitude A_1 but also the amplitude A_2, and so would x_2. This type of error is called the aliasing error. To

control the aliasing error, the number N is chosen to be the smallest integer such that

$$\sum_{i=1}^{I} b_i \omega_i \neq mN, \qquad m : \text{integer} \qquad (22)$$
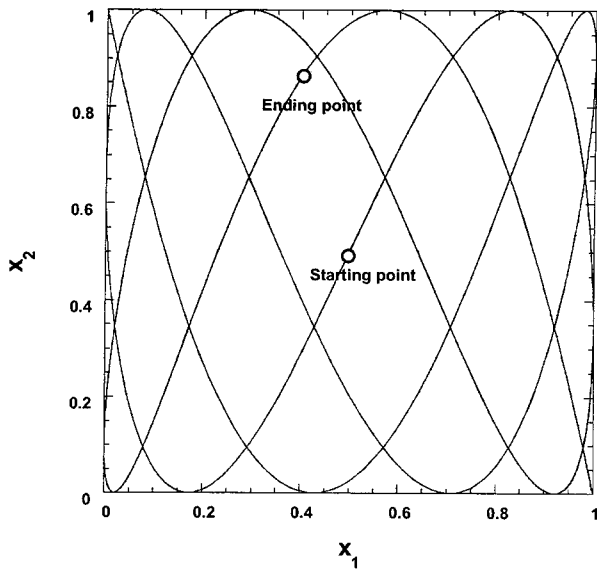
Fig. 3. A curve in the x_1–x_2 plane with integer frequencies. The start point is (0.5, 0.5). There is no end point because the curve is periodic.

where b_1 are integers satisfying Eq. (11). Physically, it means that the number of s points is chosen such that there is no aliasing error among any M Fourier amplitudes, but it would exist for any $(M + 1)$ or more amplitudes. As M and the number of input parameters to be investigated increases, the number N (or, number of realizations) becomes larger and larger to control the aliasing error. Using N number of five points and the output values calcu-
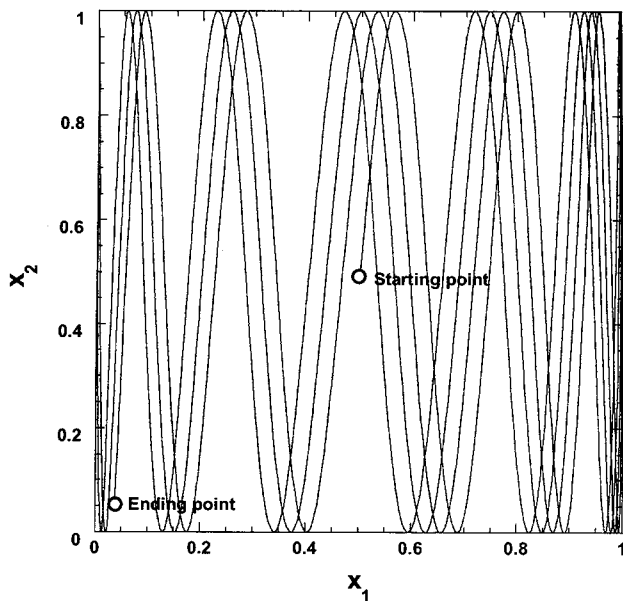
Fig. 4. A curve in the x_1–x_2 plane with noninteger frequencies. The start point is (0.5, 0.5); the end point is at (0.04, 0.06). Since the curve will never repeat itself if the parameter s is allowed to increase indefinitely, the curve will eventually fill the whole rectangle between $0 \leq x_1 \leq 1$, $0 \leq x_2 \leq 1$.
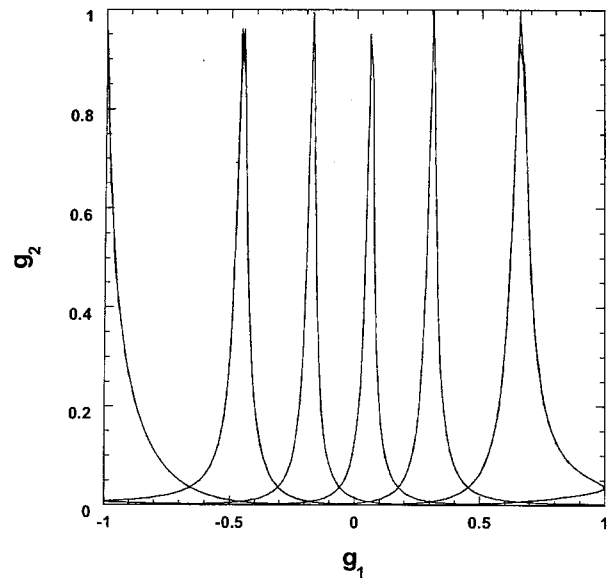
Fig. 5. A search curve in the g_1–g_2 plane with integer frequencies corresponding to the curve in Fig. 3. The curve is periodic.

lated at the corresponding x_1 values, the Fourier amplitudes in Eq. (9) can be obtained as

$$A_i = \frac{2}{N} \sum_{q=1}^{N} y(s_q)\, \sin\omega_i s_q, \qquad i = 1, 2, ..., I. \tag{23}$$

4. Application of the FAST method to an example problem

To assess the effectiveness of the FAST method as a sensitivity analysis tool, the method was first applied to a simple
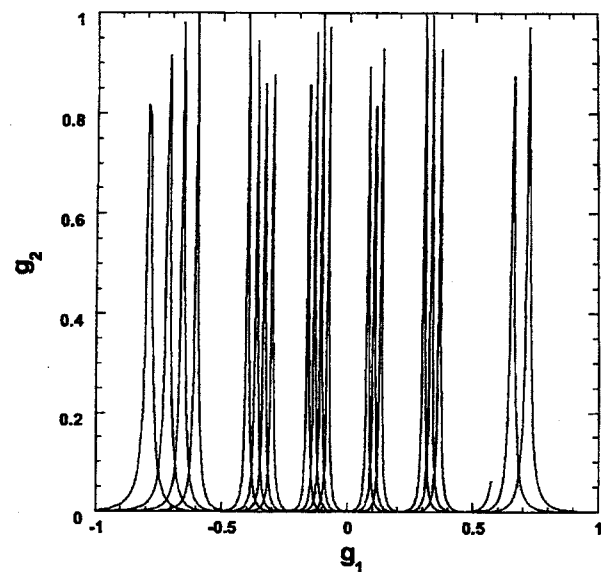
Fig. 6. A search curve in the g_1–g_2 plane with noninteger frequencies corresponding to the curve in Fig. 4. The curve never repeats itself.

Table 1
Parameter ranking using Eq. (15) without random phase shifts, number of realizations

Ranking	50	100	500	1000	5000	1×10^4	5×10^4	1×10^5	5×10^5	1×10^6
1	7	1	1	1	1	1	1	1	1	1
2	2	2	2	2	2	2	2	2	2	2
3	4	3	3	3	3	3	3	3	3	3
4	3	4	8	5	5	5	5	5	5	5
5	8	10	5	4	4	4	4	4	4	4
6	5	8	6	10	6	9	9	9	9	9
7	10	5	4	8	9	6	6	6	6	6
8	6	7	9	9	10	10	7	7	7	7
9	9	6	7	6	7	7	10	10	10	10
10	1	9	10	7	8	8	8	8	8	8

example problem prior to applying it to the TPA code. The transformation functions defined by both Eqs. (15) and (16) with or without random phase shift are investigated for their ability to rank input parameters. The example problem, which has only 10 input parameters, is represented through an explicit function:

$$y = \sum_{i=1}^{10} a_i(x_i + x_i^3) + 50(x_1 x_2 x_3)^2,$$

(24)

$$0 \le x_1, x_2, ..., x_{10}, \le 1.0$$

where $a_1 = 100$, $a_2 = 80$, $a_3 = 60$, $a_4 = 40$, $a_5 = 20$, $a_6 = 0.1$, $a_7 = 0.08$, $a_8 = 0.06$, $a_9 = 0.02$, $a_{10} = 0.01$. The coefficients a_i were selected so that $a_i < a_{i+1}$, $i = 1, 2, ..., 9$, and $a_1, a_2, ..., a_5$ are much larger than a_6, a_7, ..., a_{10}. In addition, all input parameters $x_1, x_2, ..., x_5$ have nonlinear effects (represented by the cubic terms), whereas x_1, x_2, and x_3 have an interactive effect (represented by the product of x_1, x_2, and x_3) on y. Four different distribution functions are assigned to input parameters: a uniform distribution for x_1, x_5, and x_9; log-uniform distribution for x_2, x_6, and x_{10}; normal distribution for x_3 and x_7; and log-normal distribution for x_4 and x_8. Based on the numerical values assigned to the coefficients of Eq. (24), if the FAST method is effective, it would always rank the parameter x_i ahead of x_{i+1}, $i = 1, 2, ..., 9$. The motivation of this simple example, therefore, is to use the a priori information about the actual ranking of the

model input parameters to determine the accuracy of the ranking produced by the FAST method.

Four different transformation functions are used in the FAST method: (i) the transformation defined by Eq. (15); (ii) that defined by Eq. (16); (iii) same as (i) but with random phase shift added; and (iv) same as (ii) but with random phase shift added. The frequency set free of interferences through 4th order for 10 input parameters [12] was used. Tables 1–4 list the ranking of the 10 parameters as a function of N and the number of s points, where the ranking was based on the magnitudes of the Fourier amplitudes. For a computer model with 10 parameters, the FAST method requires a minimum of 806 s points [12]. The same frequency set produced a perfect ranking when it was applied to the model

$$y = \sum_{i=1}^{4} a_i(x_i + x_i^3), \qquad 0 \le x_1, x_2, ..., x_{10} \le 1.0,$$

(25)

$$a_1 = 10.0, \quad a_2 = 8.0, \quad a_3 = 6.0, \quad a_4 = 4.0$$

with 78 realizations.

As mentioned earlier, a correct ranking should place the parameter x_i ahead of x_{i+1}, $i = 1, 2, ..., 9$. The rankings in Tables 1–4 indicate that no transformation function can produce a perfect ranking of all 10 parameters no matter how many realizations are used. This should be attributed to the fact that the frequency set used is

Table 2
Parameter ranking using Eq. (16) without random phase shifts, number of realizations

Ranking	50	100	500	1000	5000	1×10^4	5×10^4	1×10^5	5×10^5	1×10^6
1	7	1	1	1	1	1	1	1	1	1
2	2	2	2	2	2	2	2	2	2	2
3	3	3	3	3	3	3	3	3	3	3
4	4	4	4	4	4	4	4	4	4	4
5	8	5	5	5	5	5	5	5	5	5
6	5	10	8	9	6	6	6	6	6	6
7	10	7	10	6	9	9	9	9	9	9
8	9	8	6	8	7	7	7	7	7	7
9	6	6	7	10	10	10	10	10	10	10
10	1	9	9	7	8	8	8	8	8	8

Table 3
Parameter ranking using Eq. (15) with random phase shifts, number of realizations

Ranking	100	500	1000	5000	1×10^4	5×10^4	1×10^5	5×10^5	1×10^6
1	3	4	1	1	1	6	1	1	1
2	5	1	8	5	9	1	2	2	2
3	10	6	9	7	5	3	3	3	3
4	1	7	2	2	8	5	5	5	4
5	2	10	6	3	10	4	10	4	5
6	4	9	3	8	4	10	7	7	6
7	9	3	7	10	7	8	8	8	10
8	6	8	5	4	6	2	9	9	7
9	7	5	10	6	3	7	6	10	9
10	8	2	4	9	2	9	4	6	8

free of interferences through order 4, whereas, our example problem has 10 parameters. When the frequency set is used on a model with five or more parameters, interference, aliasing, or both errors will occur in the Fourier amplitudes. The size of the interference and aliasing errors depends upon the number of input parameters and the number of realizations employed. It could be reduced (but not eliminated) by increasing the number of realizations.

In Table 1, the transformation function defined in Eq. (15) produced a stable (but not entirely correct) ranking of the first five parameters with 1000 realizations, first seven with 5000, and all 10 parameters with 50,000 realizations. In comparison, in Table 2, it takes the transformation function defined in Eq. (16) 5000 realizations to achieve the stable ranking for all 10 parameters. When random phase shifts are added in the transformation function, it takes 100,000 realizations to produce a stable ranking for the first three parameters if Eq. (15) is used and for the first four parameters when Eq. (16) is used. The fact ranking is poorer when the random phase shifts are added into the phase of the transformation functions can be attributed to the loss of orthogonality of trigonometric functions when the random phase shifts are introduced into the transformation functions, where the trigonometric functions are also used in Eq. (23) for determination of the Fourier amplitudes.

5. Application of the FAST method to the TPA code

To apply the FAST method to the TPA code, we used the frequency sets and the number of s points obtained by Cukier, Schaibly and Shuler [12], where $M = 4$ for Eq. (11). The frequency sets can be applied to computer models with up to 50 input parameters using a minimum of 43,606 s points. Because the number of s points equals the number of realizations, if a computer model has 50 input parameters to be investigated, the computer model must be run with a minimum of 43,606 realizations. The minimum number of s points (i.e. the number of realizations), N, required by Eq. (22) increases drastically as the number of input parameters to be investigated and M increase.

The current version of the TPA code samples 246 input parameters that cannot be investigated by the FAST method because of the previously mentioned limitations. As a compromise, the Morris method [8] was first used to conduct a screening of the input parameters, and then the FAST method was applied to the 20 parameters deemed influential by the Morris method, which required a minimum of 4174 realizations. The Morris method was chosen because it was found to be a good screening tool for computer models with large numbers of input parameters [26], although the method is not used as a ranking tool. The readers are referred to the original paper for further details. The peak total effective dose equivalent (TEDE), or peak dose, in short, was used as the output variable. Peak

Table 4
Parameter ranking using Eq. (16) without random phase shifts, number of realizations

Ranking	100	500	1000	5000	1×10^4	5×10^4	1×10^5	5×10^5	1×10^6
1	3	4	7	7	2	1	1	1	1
2	1	3	3	5	1	6	2	2	2
3	5	5	1	4	3	3	3	3	3
4	9	10	8	3	5	2	4	4	4
5	8	7	4	10	9	5	10	5	5
6	4	8	10	2	4	4	6	7	9
7	7	9	9	8	8	9	9	6	7
8	6	1	6	1	7	7	8	10	8
9	2	2	2	6	10	8	5	9	10
10	10	6	5	9	6	10	7	8	6

Table 5

The top 20 most influential parameters identified by the Morris method, their distribution types and their minima and maxima. Full descriptions of the abbreviated parameter names are presented in Appendix B

10,000-year TPI	Distribution (min, max)	50,000-year TPI	Distribution (min, max)
AAMAI@S	Uniform (1.0, 10.0)	FOCTR	Uniform (0.0, 1.0)
MAPM@GM	Uniform (1.5, 2.5)	AA_2_1	Uniform $(0.2 \times 10^5, 0.63 \times 10^5)$
MATI@GM	Uniform $(-10.0, -5.0)$	OO-CofLC	Uniform $(0.866 \times 10^{-3}, 0.866 \times 10^{-2})$
FOC-R	Log-uniform $(0.1 \times 10^{-7}, 1.0)$	Fow	Log-normal $(0.1 \times 10^{-1}, 0.3 \times 10^1)$
FOCTR	Uniform (0.0, 1.0)	Fmult	Log-normal $(0.1 \times 10^{-1}, 0.2)$
FOCTR-R	Log-uniform $(0.1 \times 10^{-7}, 1.0)$	SbArWt%	Uniform (0.0, 1.0)
TempGrBI	Uniform (1.0, 100.0)	InitRSFP	Normal $(0.7 \times 10^{-3}, 0.3 \times 10^{-2})$
YMR-TC	Uniform (1.8, 2.2)	SFWt%C1	Uniform (0.0, 1.0)
SSMO-RE	Normal $(0.276 \times 10^{11}, 0.414 \times 10^{11})$	SFWt%C3	Uniform (0.0, 1.0)
Fow	Log-normal $(0.1 \times 10^{-1}, 0.3 \times 10^1)$	SFWt%C4	Uniform (0.0, 1.0)
Fmult	Log-normal $(0.1 \times 10^{-1}, 0.2)$	SFWt%C5	Uniform (0.0, 1.0)
SbArWt%	Uniform (0.0, 1.0)	SFWt%C6	Uniform (0.0, 1.0)
WP-Def%	Uniform $(1.0 \times 10^{-3}, 0.1 \times 10^{-1})$	SFWt%C7	Uniform (0.0, 1.0)
InitRSFP	Normal $(0.7 \times 10^{-3}, 0.3 \times 10^{-2})$	MKD_CHvU	Log-normal $(0.13 \times 10^{-8}, 3.3)$
SFWt%I3	Uniform (0.0, 1.0)	ARDSAVNp	Log-normal $(1.0, 0.39 \times 10^4)$
MPrm_PPw	Log-normal $(0.1 \times 10^{-17}, 0.1 \times 10^{-15})$	ARDSAVTc	Log-uniform (1.0, 30.0)
ARDSAV_1	Log-uniform (1.0, 4.0)	ARDSAV_U	Log-normal $(1.0, 0.19 \times 10^5)$
ARDSAV_Tc	Log-uniform (1.0, 30.0)	ARDSAVTh	Log-normal $(1.9, 0.45 \times 10^8)$
APrs_SAV	Uniform (0.1, 0.15)	APrs_SAV	Uniform (0.1, 0.15)
WPRRG@20	Uniform $(0.45 \times 10^7, 0.13 \times 10^8)$	WPRRG@20	Uniform $(0.45 \times 10^7, 0.13 \times 10^8)$

dose data were collected at both 10,000- and 50,000-year TPIs.

The Morris method is a one-at-a-time sensitivity analysis method that aims at isolating the influential parameters from a large number of input parameters [8,26,27]. The Morris method determines the statistical information of the random variable $\partial y/\partial x_i$ and uses the mean and standard deviation of $\partial y/\partial x_i$ at several points in the sample space to determine the sensitivity of y to x_i. A large value of the mean and a small value of the standard deviation of $\partial y/\partial x_i$ imply that x_i has a large overall influence on y and its influence on y is linear. A large value of the standard deviation implies that either x_i has significant interaction with other input parameters (i.e. x_k, $k = 1, 2, ..., I$ $k \neq i$) or its influence is highly nonlinear. The 20 most influential input parameters selected by the Morris method are listed in Table 5.

6. Analysis of the FAST method results

The 20 input parameters selected by the Morris method were sampled by first selecting 4174 equally spaced s points from $-\pi$ to π and then substituting these points into the transformations defined by Eq. (15). The sampled parameter data points were then used in the TPA code to produce model output. Both the sampled parameter points and the TPA output were used in Fourier amplitude determination (see Eq. (23)). To further study the effect of random phase shift as was proposed by Saltelli et al. [19], transformations with and without random phase shifts were used. To provide a visual impression of how the parameter values are chosen from the distribution function, the data points selected by the FAST method along a search path are mapped on the

distribution function. Fig. 7 shows snapshots of 25–4174 sampled points for an input parameter with a normal distribution. As evident in Fig. 7, the sampled points were not evenly distributed due to the presence of random phase shift. But as the number of points increases, the sampled points gradually spread over the region of the parameter and eventually cover the whole region.

When using the FAST method to rank the 20 parameters, the parameters that were screened out by the Morris method

Table 6

Ranking of the 20 parameters produced by the FAST method with random phase shift. Full descriptions of the abbreviated parameter names are presented in Appendix B

Ranking	10,000 years	50,000 years
1	YMR-TC	ARDSAVNp
2	ARDSAVTc	SbArWt%
3	WPRRG@20	AA_2_1
4	Fmult	WPRRG@20
5	AAMAI@S	InitRSFP
6	MPrm_PPw	APrs_SAV
7	InitRSFP	OO-CofLC
8	SbArWt%	SFWt%C3
9	SFWt%I3	SFWt%C4
10	APrs_SAV	SFWt%C1
11	TempGrBI	SFWt%C5
12	SSMO-RE	Fmult
13	MAPM@GM	ARDSAVTc
14	ARDSAV_I	SFWt%C7
15	FOCTR	ARDSAV_U
16	FOC-R	MKD_ChvU
17	WP-Def%	ARDSAVTh
18	MATI@GM	Fow
19	FOCTR-R	SFWt%C6
20	Fow	FOCTR
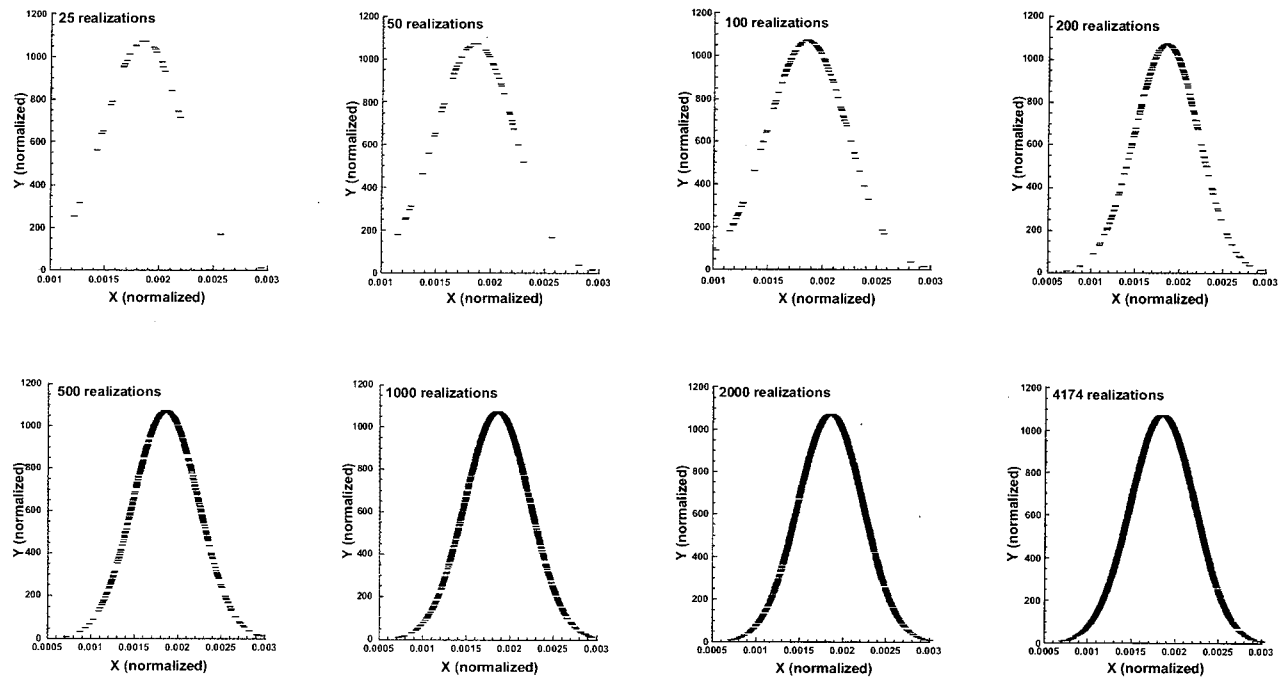
Fig. 7. Distributions of sampling points for an input parameter as the number of realizations increases. The parameter has a normal distribution density function.

were fixed at their median values, any interactions of the 20 sampled parameters with those fixed parameters were ignored. The search paths used by the FAST method lie in the subspace of the 20 sampled parameters, rather than that of the original 246 parameters.

The rankings of the influential parameters by the FAST

Table 7
Ranking of the 20 parameters produced by the FAST method with random phase shift. Full descriptions of the abbreviated parameter names are presented in Appendix B

Ranking	10,000 years	50,000 years
1	YMR-TC	ARDSAVNp
2	ARDSAVTc	SbArWt%
3	WPRRG@20	WPRRG@20
4	AAMAI@S	AA_2_1
5	MPrm_PPw	InitRSFP
6	Fmult	SFWt%C3
7	InitRSFP	APrs_SAV
8	SbArWt%	SFWt%C1
9	SFWt%I3	OO-CofLC
10	SSMO-RE	SFWt%C4
11	APrs_SAV	ARDSAV_U
12	FOCTR	SFWt%C5
13	TempGrBI	ARDSAVTh
14	ARDSAV_I	Fow
15	MAPM@GM	FOCTR
16	FOC-R	SFWt%C6
17	FOCTR-R	SFWt%C7
18	WP-Def%	ARDSAVTc
19	Fow	MKD_ChvU
20	MATI@GM	Fmult

method are presented in Tables 6 and 7, with and without the random phase shift. In both tables the most influential parameters are listed at the top. For the 10,000-year TPI in both Tables 6 and 7, whether or not the random phase shift was added, the top three parameters were always the thermal conductivity of the YM rock material (YMR-TC), the alluvium retardation coefficient for technetium (ARDSAVTc), and the well pumping rate for the farming receptor group located at 20 km from YM(WPRRG@20). Table 6 differs from Table 7 starting from the 4th ranked parameter. Overall, the difference is not significant.

For the 50,000-year TPI in both Tables 6 and 7, the first parameters are alluvium retardation coefficient for neptunium (ARDSAVNp) and the subarea wet fraction (SbArWt%) with or without random phase shift. When there is no random phase shift, Table 7, the third parameter is WPRRG@20 and the fourth parameter is the corrosion related passive current density for WP inner material (AA_2_1). For the 50,000-year TPI, the influence of random phase shift on ranking shows, beginning with the third ranked parameters. Similar to the 10,000-year TPI, the overall influence is not significant for the 50,000-year TPI.

7. Verification of fast results

Conditional complementary cumulative distribution functions [22] of the model output are used to verify the ranking of the influential parameters produced by the FAST
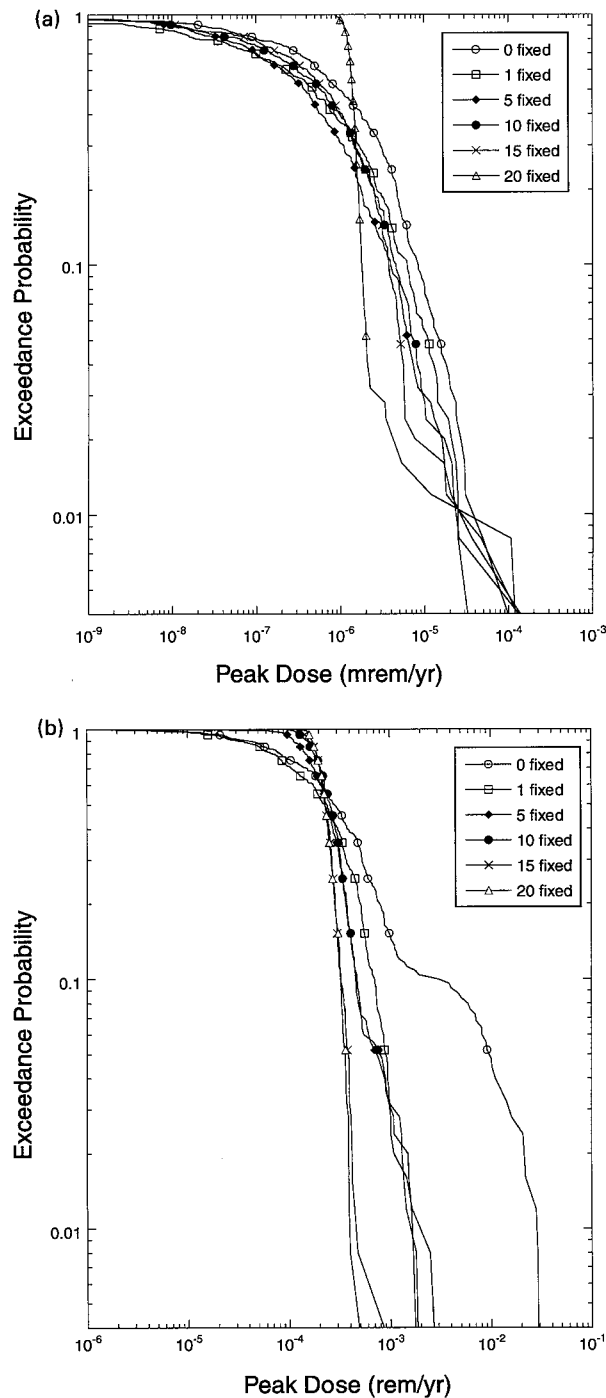
Fig. 8. Conditional complementary cumulative distribution function with random phase shift added into the transformation functions. The output peak total effective dose equivalents were conditioned by holding 0, 1, 5, 10, 15, and 20 most influential parameters fixed at their mean values. (a) 10,000-year TPI and (b) 50,000-year TPI.

Fig. 9. Conditional complementary cumulative distribution function without random phase shift added into the transformation functions. The output peak total effective dose equivalents were conditioned by holding 0, 1, 5, 10, 15, and 20 most influential parameters fixed at their mean values. (a) 10,000-year TPI and (b) 50,000-year TPI.

method. Because the output y is a random variable, each value of y has a probability of occurrence of $1/N$, where N is the number of realizations or input parameter vectors. A CDF is first constructed from these N values of y. The

complementary function, CCDF, to the CDF is then constructed based on CDF.

To use the CCDF to study the FAST results, a subset of influential parameters was selected in decreasing order of

influence. Validity of ranking produced by the FAST method was studied by holding the selected parameters at their mean values and performing *N* realizations. If by holding one or more parameters at their mean values there is a decrease in the spread of *N* values of *y*, then it is concluded that the parameters are indeed influential. If the ranking produced by the FAST method is correct, one would expect a systematic decrease in spread when more and more influenial parameters are held at their mean values (with the decreasing order of influential parameters), and the transition between the highest and lowest probability of exceedance values will be sharp. Of course, when all ranked parameters are fixed at their mean values, the variance of the output would be zero and the CCDF will assume the shape of a step function (no spread in output).

The CCDF results are presented for two cases: (i) TPA runs with random phase shift in the FAST transformation function, Fig. 8a and b, and (ii) TPA runs without the random phase shift, Fig. 9a and b. For each case, results are plotted for 10,000- and 50,000-year TPIs. In these figures the outputs are conditioned by holding at their fixed values (mean values) 0, 1, 5, 10, 15, and 20 top most influential parameters, and the remaining of 246 input parameters were allowed to be sampled within their ranges of variation. Each curve represents the output from 250 runs using an LHS sampler.

Figs. 8 and 9 appear to be similar. For the 10,000-year TPI in Figs. 8a and 9a, fixing the top one and five parameters reduced the spread of the output and narrowed the spread of the CCDF curve. The output, however, appears to have similar spread when the number of top parameters being fixed is increased from 5 to 10. When the top 15 and 20 parameters are fixed, the spread is again further narrowed. This observation indicates that the FAST method identifies the top five parameters correctly. But it may not do well when the size of the parameters is expanded to 10. For the 50,000-year TPI in Figs. 8b and 9b, the top parameter appears to have been correctly identified as ARDSAVNp, because there is a significant drop in spread by fixing the parameter. The spread in the CCDF drops further as more influential parameters are held at their mean values, but the rate of drop in the spread is less than that when ARDSAVNp is fixed. There are several crisscross points in Figs. 8 and 9, but they all occur in the regions with lower probability of exceedance.

Based on Tables 6 and 7 and the CCDF results shown in Figs. 8 and 9, it appears that the FAST method ranks the top parameters correctly (e.g. the top three parameters for the 10,000-year TPI and the top two for the 50,000-year TPI). But it could not consistently rank a larger set of parameters (e.g. the parameter set is expanded into 5 or 10 parameters). For both 10,000- and 50,000-year TPIs, the most important parameter seems to be correctly identified (YMR-TC for the 10,000-year TPI; ARDSAVNp for the 50,000-year TPI). It is difficult to see any definitive benefits of introducing the random phase shift into the transformation functions.

8. Summary and conclusions

The FAST method was used to conduct a sensitivity analysis for a computer model that performs a total system performance assessment that will be used in evaluating the proposed HLW repository at YM. This method was selected for the study because of its recently growing popularity as an accurate sensitivity analysis tool for highly nonlinear problems.

A short description of the method was presented and several key properties and performance measures were investigated. A general transformation function applicable to any probability distribution was derived and used. A simple example problem with only 10 input parameters demonstrated that it was difficult to produce a perfect ranking when the integer frequency set free of interference to *M*th order is applied to a model with more then *M* number of input parameters. As the number of realizations increases, however, ranking of top parameters may be achieved.

Although the method is suitable for highly nonlinear problems, the method is computationally expensive compared to most statistical but less accurate methods. Therefore, the FAST method appears to be limited to problems with a small number of input parameters. However, the usefulness of the method for problems with large parameter sets can be improved by prescreening less important parameters. The current version of the FAST method can only be applied to computer models with no more than 50 input parameters. Consequently, the Morris method was first used to select the most influential input parameters, and the FAST method was then used to rank the most influential parameters for both 10,000- and 50,000-year TPIs. Based on conditional CCDFs, the FAST method correctly ranked the top influential parameters for both 10,000- and 50,000-year TPIs. The results suggest that at least for the TPA code, introducing a random phase shift into the transformation functions does not improve the sensitivity analysis results.

The results also show that the FAST method can be used to determine the individual importance of input parameters to the output of a computer model; however, more effort will be needed to use the FAST method to determine the influence of products of two or more parameters (parameters that have mutual and reciprocal influence). For a large complex computer model like the TPA code, it is entirely possible that the influence of the product of parameters A and B is much greater than either A or B or their arithmetic sum.

The current version of the FAST method can handle at most 50 parameters with a minimum of 43,606 realizations. Therefore, a screening technique, such as the Morris method, should be used first to reduce to below 50 the number of parameters to be investigated. The FAST method also requires a large number of realizations to control the interference error and aliasing error.

The derivation of the transformation functions presented for parameters with nonuniform probability distribution has expanded the range of the FAST method to computer models with nonuniformly distributed parameters.

Acknowledgements

Appendix A

In this section, we present the probability density functions, $f(x)$, cumulative probability distribution func-

Log-uniform, $0 \le a \le x \le b$

$$f(x) = \begin{cases} 0, & x \le a, \\ \dfrac{1}{(x[\log(b) - \log(a)]}, & a \le x \le b \\ 0, & b \le x \end{cases} \qquad (A4)$$

$$y = F(x) = \begin{cases} 0, & x \le a \\ \dfrac{[\log(x) - \log(a)]}{[\log(b) - \log(a)]}, & a \le x \le b \\ 1, & x \le b \end{cases} \qquad (A5)$$

$$x = F^{-1}(y) = \exp\{\log(a) + [\log(b) - \log(a)]y\} \qquad (A6)$$

Normal Distribution [28]

$$f(x) = \frac{1}{\sqrt{2\pi}\sigma} \exp\left[-\frac{(x - \mu^2)}{2\sigma^2} \right] \qquad (A7)$$

$$y = F(x) = \frac{1}{\sqrt{2\pi}} \int_{-\infty}^{x} e^{-t^2/2} \, dt \qquad (A8)$$

$$x = F^{-1}(y) = \begin{cases} t - [(c_0 + c_1 t + c_2 t^2)/(1 + d_1 t + d_2 t^2 + d_3 t^3)], & t = \sqrt{-\ln(y^2)}, & 0 < y \le 0.5 \\ -t + [(c_0 + c_1 t + c_2 t^2)/(1 + d_1 t + d_2 t^2 + d_3 t^3)], & t = \sqrt{-\ln(1 - y^2)}, & 0.5 < y < 1.0 \end{cases} \qquad (A9)$$

tions, $F(x)$, and inverse cumulative probability distribution functions, $F^{-1}(x)$, that are used in this paper. They are Uniform, Log-uniform, Normal, Log-normal, Log-triangular, Beta, Exponential, Finite-exponential, and User defined.

Uniform Distribution, $a \le x \le b$

$$f(x) = \begin{cases} 0, & x \le a \\ \dfrac{1}{b - a}, & a \le x \le b \\ 0, & b \le x \end{cases} \qquad (A1)$$

$$y = F(x) = \begin{cases} 0, & x \le a \\ \dfrac{x - a}{b - a}, & a \le x \le b \\ 1, & x \le b \end{cases} \qquad (A2)$$

$$x = F^{-1}(y) = a + (b - a)y \qquad (A3)$$

where t is an integration variable, μ and σ are mean and standard deviation of the normal distribution function and

$$c_0 = 2.515517, \qquad c_1 = 0.802853, \qquad c_2 = 0.010328 \qquad (A10)$$

$$d_1 = 1.432788, \qquad d_2 = 0.189269, \qquad d_3 = 0.001308. \qquad (A11)$$

Log-normal Distribution

$$f(x) = \frac{1}{\sqrt{2\pi}\sigma x} \exp\left\{ -\frac{[\log(x) - \mu]^2}{2\sigma^2} \right\} \qquad (A12)$$

$$y = F(x) = \frac{1}{\sqrt{2\pi}} \int_{-\infty}^{\log(x)} e^{-t^2/2} \, dt \qquad (A13)$$

$$x = F^{-1}(y) = \begin{cases} \exp\left(t - \dfrac{c_0 + c_1 t + c_2 t^2}{1 + d_1 t + d_2 t^2 + d_3 t^3}\right), & t = \sqrt{-\ln(y^2)}, \quad 0 < y \le 0.5 \\ \exp\left(-t + \dfrac{c_0 + c_1 t + c_2 t^2}{1 + d_1 t + d_2 t^2 + d_3 t^3}\right), & t = \sqrt{-\ln(1 - y^2)}, \quad 0.5 < y < 1.0 \end{cases} \tag{A14}$$

Log-triangluar Distribution, $a \le x \le c, 0 < a < b < c$

$$f(x) = \begin{cases} \dfrac{2[\log(x) - \log(a)]}{x[\log(c) - \log(a)][\log(b) - \log(a)]}, & a \le x \le b \\ \dfrac{2[\log(c) - \log(x)]}{x[\log(c) - \log(a)][\log(c) - \log(b)]}, & b \le x \le c \end{cases} \tag{A15}$$

$$y = F(x) = \begin{cases} \dfrac{[\log(x) - \log(a)]}{[\log(c) - \log(a)][\log(b) - \log(a)]}, & a \le x \le b \\ \dfrac{[\log(x) - \log(b)][2\log(c) - \log(x) - \log(b)]}{[\log(c) - \log(a)][\log(c) - \log(b)]} + \dfrac{[\log(b) - \log(a)]}{[\log(c) - \log(a)]}, & b \le x \le c \end{cases} \tag{A16}$$

$$x = F^{-1}(y) = \begin{cases} \exp\left[\log(a) + \sqrt{y[\log(c) - \log(a)][\log(b) - \log(a)]}\right], & a \le x \le b \\ \exp\left(\dfrac{-b_1 - \sqrt{b_1^2 - 4a_1 c_1}}{2a_1}\right), & b \le x \le c \end{cases} \tag{A17}$$

where

$a = 1.0$

$b = 2\log(c)$

$c = y\log^2(c) + (1 - y)[\log(c)\log(b) + \log(c)\log(a)]$

$\quad - \log(b)\log(a)$

Beta Distribution [29], $0 \le x \le 1$, p and q: shape factors

$$f(x) = \frac{\Gamma(p + q)}{\Gamma(p)\Gamma(q)} x^{p-1}(1 - x)^{q-1} \tag{A18}$$

$$y = F(x) = \frac{\Gamma(p + q)}{\Gamma(p)\Gamma(q)} \int_0^x t^{p-1}(1 - t)^{q-1}\, dt \tag{A19}$$

$$x = F^{-1}(y) = \frac{p}{p + q\, e^{2\omega}} \tag{A20}$$

where $\Gamma(x)$ is the Gamma function,

$$w = \frac{y_p \sqrt{h + \lambda}}{h} - \left(\frac{1}{2q - 1} - \frac{1}{2p - 1}\right)\left(\lambda + \frac{5}{6} - \frac{2}{3h}\right) \tag{A21}$$

$$h = 2\left(\frac{1}{2p - 1} + \frac{1}{2q - 1}\right)^{-1} \tag{A22}$$

$$\lambda = \frac{y_p^2 - 3}{6} \tag{A23}$$

$$y = \frac{1}{\sqrt{2\pi}} \int_{y_p}^{\infty} e^{-t^2/2}\, dt \tag{A24}$$

Exponential Distribution, $x > 0$

$$f(x) = \lambda\, e^{-\lambda x} \tag{A25}$$

$$y = F(x) = 1 - e^{-\lambda x} \tag{A26}$$

$$x = F^{-1}(y) = \frac{\log(1 - y)}{\lambda} \tag{A27}$$

Finite-exponential Distribution, $0 \le a \le x \le b$.

$$f(x) = \frac{\lambda e^{-\lambda x}}{e^{-\lambda a} - e^{-\lambda b}} \tag{A28}$$

$$y = F(x) = \frac{e^{-\lambda a} - e^{-\lambda x}}{e^{-\lambda a} - e^{-\lambda b}} \tag{A29}$$

$$x = F^{1}(y) = -\frac{\log[e^{-\lambda a} - y(e^{-\lambda a} - e^{-\lambda b})]}{\lambda} \tag{A30}$$

Appendix B

Parameter abbreviation	Full parameter description
AAMAI@S	Areal averaged mean annual infiltration for the (current) climate
MAPM@GM	Mean average precipitation multiplier at glacier maximum
MATI@GM	Mean average temperature increase at glacial maximum
FOC-R	Fraction of water condensate removed in each reflux time step
FOCTR	Fraction of condensate moving toward the repository
FOCTR-R	Fraction of condensate moving toward the repository but escaped before entering the repository
TempGrBI	Temperature gradient in the vicinity of the boiling isotherm
YMR-TC	Thermal conductivity of rock
AA_2_1	Passive electric current density for waste package inner overpack
OO-CofLC	Coefficient for localized corrosion rate of outer overpack
SSMO-RE	Rock modulus of elasticity
Fow	Flow convergence/divergence factor
Fmult	Flow multiplication factor
SbArWt%	Subarea wet fraction
WP-Def%	Fraction of total waste packages in a subarea that fails at time $t = 0$
InitRSFP	Initial radius of UO_2 particle
SFWt%I3	Spent fuel wet fraction for initial failures in subarea 3
SFWt%C1	Spent fuel wet fraction for corrosion failures in subarea 1
SFWt%C3	Spent fuel wet fraction for corrosion failures in subarea 3
SFWt%C4	Spent fuel wet fraction for corrosion failures in subarea 4
SFWt%C5	Spent fuel wet fraction for corrosion failures in subarea 5
SFWt%C6	Spent fuel wet fraction for corrosion failures in subarea 6
SFWt%C7	Spent fuel wet fraction for corrosion failures in subarea 7
MKD_CHvU	Matrix distribution coefficient for uranium for Calico Hills nonwelded vitric
MPrm_PPw	Matrix permeability for Prow pass-welded (unsaturated zone)
ARDSAVNp	Alluvium retardation coefficient for neptunium
ARDSAVTc	Alluvium retardation coefficient for technetium
ARDSAV_U	Alluvium retardation coefficient for uranium
ARDSAVTh	Alluvium retardation coefficient for thorium
Aprs_SAV	Alluvium porosity of Amargosa Valley alluvium
WPRRG@20	Well pumping rate for residential receptor group located ≤ 20 km from YM

References

[1] Iman RL, Helton JC. A comparison of uncertainty and sensitivity analysis techniques for computer models. Risk Anal 1988;8:71–90.

[2] Draper NR, Smith Jr H. Applied regression analysis. 2nd edn. New York: Wiley, 1981.

[3] Iman RL, Connover WJ. The use of the rank transform in regression. Technometrics 1979;21:499–509.

[4] Saltelli A, Anderes JH, Homma T. Sensitivity analysis of model output—an investigation of new techniques. Comput Stat Data Anal 1993;15:211–38.

[5] Connover WJ. Practical nonparametric statistics. 2nd edn. New York: Wiley, 1980.

[6] Bowen WM, Bennet CA, editors. Statistical methods for nuclear materials management, NUREG/CR-4604. Washington, DC: US Nuclear Regulatory Commission, 1988.

[7] Jarzemba MS, Sagar B. A parameter tree approach to estimating system sensitivities to parameter sets. Reliab Engng Syst Safety 2000;67:89–102.

[8] Morris MD. Factorial sampling plans for preliminary computational experiments. Technometrics 1991;33(2):161–74.

[9] Helton JC. Uncertainty and sensitivity analysis techniques for use in performance assessment for radioactivce waste disposal. Reliab Engng Syst Safety 1993;42:327–67.

[10] Cukier RI, Fortuin CM, Schuler KE, Petschek AG, Schaibly JH. Study of the sensitivity of coupled reaction systems to uncertainties in rate coefficients I. Theory. J Chem Phys 1973;59(8):3873–8.

[11] Schaibly JH, Schuler KE. Study of the sensitivity of coupled reaction systems to uncertainties in rate coefficients II. Applications. J Chem Phys 1973;59(8):3879–88.

[12] Cukier RI, Schaibly JH, Schuler KE. Study of the sensitivity of coupled reaction systems to uncertainties in rate coefficients III. Analysis of the approximation. J Chem Phys 1975;63(3):1140.

[13] Cukier RI, Levine RB, Schuler KE. Nonlinear sensitivity analysis of multiparameter model systems. J Comp Phys 1978;26:1–42.

[14] McRae GJ, Tiden JW, Seinfeld JH. Global sensitivity analysis—a computational implementation of the Fourier amplitude sensitivity test (FAST). Comput Chem Engng 1982;6(1):15–25.

[15] Saltelli A, Bolado R. An alternative way to computer Fourier amplitude sensitivity test (FAST). Comp Stat Data Anal 1998;26:445–60.

[16] Saltelli A, Andres TH, Homma T. Sensitivity analysis of model output: an investigation of new techniques. Comp Stat Data Anal 1993;15:211–38.

[17] Saltelli A, Hjorth J. Uncertainty and sensitivity analysis of OH-initiated dimethylsulphide (DMS) oxidation kinetics. J Atmos Chem 1995;21:187–221.

[18] Campolongo F, Saltelli A. Sensitivity analysis of an environmental model. An application of different analysis methods. Reliab Engng Syst Safety 1997;52(1):49–69.

[19] Saltelli A, Tarantola S, Chan K. A quantitative, model independent method for global sensitivity analysis of model output. Technometrics 1999;41(1):39–56.

[20] Mohanty S, McCartin TJ. NRC sensitivity and uncertainty analyses for a proposed HLW repository at Yucca Mountain, Nevada using

TPA 3.1-Volume 1: conceptual models and data. NUREG-1668. US Nuclear Regulatory Commission, 2001.

[21] US Nuclear Regulatory Commission. NRC sensitivity and uncertainty analyses for a proposed HLW repository at Yucca Mountain, Nevada, using TPA 3.1-Volume II: results and conclusions. NUREG-1688. US Nuclear Regulatory Commission, 1999.

[22] Mohanty S, McCartin TJ, Total-system performance assessment (TPA) version 3.2 code: module descriptions and user's guide. Center for Nuclear Waste Regulatory Analyses, Southwest Research Institute, 1998.

[23] Iman RL, Connover WJ. Small sample sensitivity analysis techniques for computer models with an application to risk assessment. Part A-Theory and Methods. Commun Stat 1980;9:1749–842.

[24] US Nuclear Regulatory Commission. Disposal of high-level radioactive wastes in a proposed geological repository at Yucca Mountain, Nevada; proposed rule. Federal Register, Washington, DC: US Government Printing Offices 1999;64(34):8640–8679.

[25] Weyl H. Mean motion. Am J Math 1938;60:889–96.

[26] Mohanty S, Lu Y, Menchaca JM. Screening of sensitive parameters for a complex geologic waste disposal system using Morris method, in preparation.

[27] Mohanty S, Codell R, Rice R, Weldy J, Lu Y, Byrne R, McCartin TM, Jarzemba MJ, Wittmeyer G. System-level repository sensitivity analysis using TPA version 3.2 code. Washington, DC: US Nuclear Regulatory Commission, 1999 to be published as a NUREG document.

[28] Abramowitz M, Stegun I, editors. Handbook of mathematical functions with formulas, graphs, and mathematical tables, National Bureau of Standards, Formulae, 26.2.23, 1964.

[29] Abramowitz M, Stegun I, editors. Handbook of Mathematical Function with Formulas, Graphs, and Mathematical Tables, National Bureau of Standards, Formulae 26.5.22, 1964.

APPENDIX C

ELSEVIER

A parameter tree approach to estimating system sensitivities to parameter sets

M.S. Jarzemba, B. Sagar*

The Center for Nuclear Waste Regulatory Analyses, Southwest Research Institute, 6220 Culebra Road, San Antonio, TX 78238-5166, USA

Abstract

A post-processing technique for determining relative system sensitivity to groups of parameters and system components is presented. It is assumed that an appropriate parametric model is used to simulate system behavior using Monte Carlo techniques and that a set of realizations of system output(s) is available. The objective of our technique is to analyze the input vectors and the corresponding output vectors (that is, post-process the results) to estimate the relative sensitivity of the output to input parameters (taken singly and as a group) and thereby rank them. This technique is different from the design of experimental techniques in that a partitioning of the parameter space is not required before the simulation. A tree structure (which looks similar to an event tree) is developed to better explain the technique. Each limb of the tree represents a particular combination of parameters or a combination of system components. For convenience and to distinguish it from the event tree, we call it the parameter tree.

To construct the parameter tree, the samples of input parameter values are treated as either a "+" or a "−" based on whether or not the sampled parameter value is greater than or less than a specified branching criterion (e.g., mean, median, percentile of the population). The corresponding system outputs are also segregated into similar bins. Partitioning the first parameter into a "+" or a "−" bin creates the first level of the tree containing two branches. At the next level, realizations associated with each first-level branch are further partitioned into two bins using the branching criteria on the second parameter and so on until the tree is fully populated. Relative sensitivities are then inferred from the number of samples associated with each branch of the tree.

The parameter tree approach is illustrated by applying it to a number of preliminary simulations of the proposed high-level radioactive waste repository at Yucca Mountain, NV. Using a Total System Performance Assessment Code called TPA, realizations are obtained and analyzed. In the examples presented, groups of five important parameters, one for each level of the tree, are used to identify branches of the tree and construct the bins. In the first example, the five important parameters are selected by more traditional sensitivity analysis techniques. This example shows that relatively few branches of the tree dominate system performance. In another example, the same realizations are used but the most important five-parameter set is determined in a stepwise manner (using the parameter tree technique) and it is found that these five parameters do not match the five of the first example. This important result shows that sensitivities based on individual parameters (i.e. one parameter at a time) may differ from sensitivities estimated based on joint sets of parameters (i.e. two or more parameters at a time).

The technique is extended using subsystem outputs to define the branches of the tree. The subsystem outputs used in this example are the total cumulative radionuclide release (TCR) from the engineered barriers, unsaturated zone, and saturated zone over 10,000 yr. The technique is found to be successful in estimating the relative influence of each of these three subsystems on the overall system behavior. © 2000 Elsevier Science Ltd. All rights reserved.

Keywords: Sensitivity analysis; Parameter interactions; Post processor; System simulation

1. Introduction

Sensitivity analysis is a general term used to describe any study that quantifies how a given system output variable is modified with changes in system input variables. Many techniques for sensitivity analysis are described in the literature, some of the popular ones being differential analysis [1], stepwise regression [2,3], rank regression [4,5], Kolmogorov–Smirnov test [6], and signs test [6]. Excellent reviews on sensitivity analysis techniques are available in Helton [1]. A special issue of this journal was also devoted to sensitivity analysis [7]. Homma and Saltelli [8] classify various techniques into two main groups. The techniques in the first group which may be termed local sensitivity analysis aim to determine the derivative of the output with respect to an input parameter at a specific (or nominal) value of the parameter (see Pastres et al. and Turanji in Ref. [7]). While

---
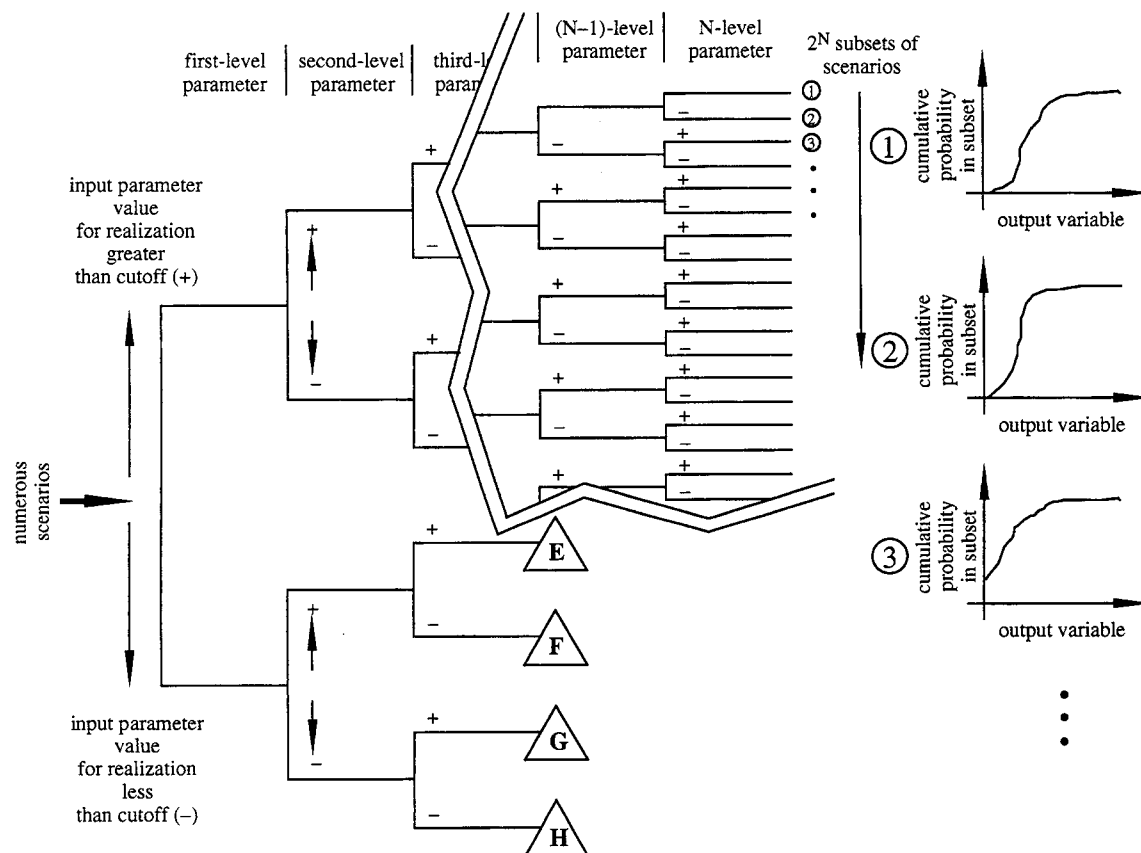
Fig. 1. A general parameter tree.

rarely done with such techniques, higher order mixed derivatives may be used to estimate the output sensitivity to a pair or a set of larger number of parameters. The second group of techniques may be called global sensitivity analysis. These techniques seek to determine the sensitivity of the output with respect to the variation of a parameter over its entire possible range which is usually described as a probability distribution [9]. In the global sensitivity techniques, the change in output variance due to variation of the parameter over its range may be taken as the sensitivity measure although it is possible to define other measures. A generalized sensitivity measure based on the work of Sobol' [9] is described by Homma and Saltelli [8]. The Sobol' measure is especially useful in making transparent the contribution to the overall output variance by each parameter variance and covariance of all orders although the contributions of covariance are usually neglected in most sensitivity analyses.

One problem with estimating the sensitivities of combinations of two or more variables is the significant increase in computational effort. Homma and Saltelli [8] tackle this problem by using the Sobol' [9] formulation and partitioning the overall sensitivity into two parts. The first part is the contribution by an input parameter considered alone and the second part is the contribution by the interactions of this parameter with all the remaining parameters. This formulation reduces the number of function evaluations drastically

and leads to efficient computations. However, a price for the computational efficiency is paid in lumping the effect of all interactions into a single term and thus foregoing the determination of importance of a particular interaction.

The sensitivity analysis approach described in this paper belongs to the global sensitivity analysis techniques and our emphasis is on determining the effect of parameter interactions, i.e. sensitivity of system output to parameter sets. The approach is based on partitioning the input parameter space (or subsystem output space if sensitivity is sought with respect to subsystem outputs) into subsets based on some criteria and analyzing the outputs that are associated with various bins. We found that the depiction of the partitioning process in the form of a tree (similar to the event trees) makes the process transparent and easier to understand and have named the technique the parameter tree approach. However, it should be noted that the construction of a parameter tree is not essential to the technique and the process can also be explained with the help of tables. One characteristic of our technique is that it is developed as a means to post-process results obtained from a Monte Carlo simulation of a complex system. That is, no a priori constraints with respect to problem formulation, function evaluations, or choice of sets of parameters are imposed on the analyst. The objective is to extract sensitivity information from the output already obtained by the analyst. This distinguishes

our approach from the Design of Experiments [10] techniques which do require the partitioning of the parameter space before the conduct of the experiments. In addition, in our approach the partitioning of the output associated with second and subsequent parameters is conditional on the partitioning obtained from the earlier parameters. Another aspect of our approach is that it is not restricted to estimation of sensitivity with respect to input parameters only but it can be also used to estimate the sensitivity with respect to certain subsystem outputs, as one of our example shows. The examples described in this paper are based on Monte Carlo simulations of a proposed geologic high level waste repository at Yucca Mountain (YM) using a model embodied in a computer code called TPA [11,12].

2. General approach: development of the parameter tree

Consider a system whose output (Y) is a random variable. In the following, we follow the convention of representing random variables in upper case and their particular samples (or realizations) in lower case symbols. In general, Y is a function of random parameters X_i, deterministic parameters d_k, and model assumptions a_m. We assume that the behavior of the system is simulated by appropriately sampling the random parameters and then computing the system output or realizations of Y for each parameter vector. For the purposes of this paper, which is to outline a method for analyzing simulation output to identify important random parameters and develop understanding of their relationship to the output, it is assumed that the decisions about appropriate model assumptions and deterministic parameters have been made a priori. As a result, we do not consider the dependence of Y on d_k and a_m any further and focus on the dependence of Y on the X_is only. Thus, for the jth realization of Y,

$$y_j = f(x_{1,j}, x_{2,j}, ..., x_{I,j}) \tag{1}$$

where I is the total number of sampled parameters in the model.

We want to analyze the outputs y_j to determine the sensitivity and correlations of Y to subgroups of the input parameters X_n, $n = 1, 2, ..., N$, where $N < I$. This can be depicted in a tree structure as explained in the following paragraphs.

Our approach for examining system output sensitivity to combinations of input parameters is to construct a parameter tree. Similar in appearance to an event tree, the parameter tree partitions parameter space into bins (each bin forming a branch of the tree) based on a partitioning (or branching) criterion. The simplest form of a branching criterion is a classification based on parameter magnitude which treats sampled values as either a "+" or a "−" depending upon whether the sampled value is greater or less than the branching criteria value. The event tree analogy is appropriate if one considers a "+" as a parameter failure and a "−" as a

parameter success, or vice-versa. Fig. 1 depicts a general parameter tree. To explain Fig. 1 using a system model, a number of output realizations are generated for a given scenario class (e.g. airplane crashes into an operating nuclear reactor). Next, the realizations are partitioned into two subsets determined by whether the first important parameter (how to choose the first important parameter will be discussed later) is greater than or less than a specified level (e.g. airplane crashes of craft more or less massive than a fully fueled and loaded Boeing model 727, or of craft more massive than the national median value for fully fueled and loaded aircraft, or of craft more massive than the national mean value for fully fueled and loaded aircraft, etc.). Realizations with a high value are all treated as "+" and low as a "−", regardless of their position within the subset. The procedure is repeated in each of these two subsets with the next important parameter to be considered (i.e. the second-level parameter, say, the thickness of the reactor containment system) and so on until each of the important parameters is considered. This procedure determines 2^M bins of realizations where M is the number of important parameters where M is less than or equal to the number of sampled parameters. Note that not every sampled parameter in the system model need be considered if a subset of the sampled parameters satisfactorily explains system behavior of interest. In terms of our previous example, if an aircraft more massive than a fully loaded Boeing model 727 crashes into a reactor with a pressure vessel less than six inches thick always produces a system failure (i.e. a reactor breach and release of radioactive material) in all realizations, then no more variables need be considered.

In the following, we develop a formal explanation of this method. Let $\hat{X}_i$ be the median value of $\hat{X}_i$, $\hat{Y}$ be the median value of Y, and I be the total number of sampled parameters. In explaining the approach, we use median values for partitioning criteria, but any other appropriate statistical or physical branching criterion can be used, as will be explained later through an example. Note that any criterion that will partition the parameter space into two disjoint sets will work. However, the selection of a branching criteria is problem specific and depends mainly on the information sought from a post processing analysis such as proposed in this paper. For the examples presented, the relation (if any) between the high (or low) values of the parameters to the high (or low) values of the output are of main interest, hence the selection of a statistical value (e.g. median). The first step in the procedure is to partition all of the realizations into two bins:

$$x_{1^+} = [\forall \text{ realizations with } x_{1,j} \geq \hat{X}_1] \tag{2a}$$

$$x_{1^-} = [\forall \text{ realizations with } x_{1,j} < \hat{X}_1] \tag{2b}$$

Assume that the two bins contain N_{1^+} and N_{1^-} members, respectively, where $N_{1^+} + N_{1^-} = N$ is the total number of samples or realizations. Note that when the partitioning

criterion is the median value, $N_{1^+} = N_{1^-} = N/2$ but that will not be true for other branching criteria.

Now consider the N_{1^+} realizations of Y that are produced by the x_{1^+} set. From these N_{1^+} realizations, we select those that meet the following criterion:

$$y_{1^+} = [\forall \text{ realizations with } y_j \geq \hat{Y} | x_{1,j} \in x_{1^+}] \tag{3}$$

Let the number of realizations satisfying this criteria be L_{1^+}. It follows that:

$$p_{1^+} = P\{Y \geq \hat{Y} | X_1 \geq \hat{X}_1\} = \frac{L_{1^+}}{N_{1^+}} \tag{4}$$

The second branch of the tree is associated with the y_{1^-} bin containing L_{1^-} members, where:

$$y_{1^-} = [\forall \text{ realizations with } y_j \geq \hat{Y} | x_{1,j} \in x_{1^-}] \tag{5}$$

In this case, similar to Eq. (4),

$$p_{1^-} = P\{Y \geq \hat{Y} | X_1 < \hat{X}_1\} = \frac{L_{1^-}}{N_{1^-}} \tag{6}$$

Equal values of p_{1^+} and p_{1^-} would imply that whether X_1 takes values greater or smaller than its median does not effect the bin into which Y values fall, thus indicating a lack of correlation or lack of sensitivity of Y to X_1. Consequently, a measure of relative sensitivity of Y with respect to X_1 can be constructed as $|p_{1^+} - p_{1^-}|$. It is noted that the proposed measure provides only relative sensitivity since it does not provide a precise description of the change in Y for a given change in X_1, as a measure for absolute sensitivity would provide. However, the relative sensitivity measure is sufficient for ranking important parameters. In general, one can partition the $x_{i,j}$ (and subsequent parameter realizations) into more than two bins but such a generalization will lead to a complicated tree structure (i.e. with potentially large numbers of branches per level) and is not pursued further in this paper.

The branching strategy explained above is now implemented for the second, third, and subsequent parameters until most of the output is sufficiently explained. For the second parameter, proceed as follows. Partition the bin x_{1^+} containing N_{1^+} realizations into two bins:

$$x_{1^+2^+} = [\forall \text{ realizations with } x_{1,j} \geq \hat{X}_1 \bigcap x_{2,j} \geq \hat{X}_2] \tag{7a}$$

and

$$x_{1^+2^-} = [\forall \text{ realizations with } x_{1,j} \geq \hat{X}_1 \bigcap x_{2,j} < \hat{X}_2] \tag{7b}$$

Similarly, the x_{1^-} bin can also be partitioned into two bins:

$$x_{1^-2^+} = [\forall \text{ realizations with } x_{1,j} < \hat{X}_1 \bigcap x_{2,j} \geq \hat{X}_2] \tag{7c}$$

and

$$x_{1^-2^-} = [\forall \text{ realizations with } x_{1,j} < \hat{X}_1 \bigcap x_{2,j} < \hat{X}_2]. \tag{7d}$$

Note that the partitioning for the second parameter is dependent on the partitioning of the first parameter. That is value

of $X_2 \geq \hat{X}_2$ are contained in not just one bin but two, i.e. $x_{1^+2^+}$ and $x_{1^-2^+}$.

Therefore, the joint sensitivity (or interaction affects in the parlance of design of experiments [10]) of Y to X_1 and X_2 determined here is different from that of Sobol' [9].

Let the number of members in each of the four bins be $N_{1^+2^+}$, $N_{1^+2^-}$, $N_{1^-2^+}$, and $N_{1^-2^-}$, respectively. The output realizations associated with members of a bin are now scrutinized to count the number of realizations in which $Y \geq \hat{Y}$. Thus, the four output bins associated with the four branches of the tree at the second parameter level are:

$$y_{1^+2^+} = [y_j \geq \hat{Y} | x_{1,j}, x_{2,j} \in x_{1^+2^+}] \tag{8a}$$

$$y_{1^+2^-} = [y_j \geq \hat{Y} | x_{1,j}, x_{2,j} \in x_{1^+2^-}] \tag{8b}$$

$$y_{1^-2^+} = [y_j \geq \hat{Y} | x_{1,j}, x_{2,j} \in x_{1^-2^+}] \tag{8c}$$

$$y_{1^-2^-} = [y_j \geq \hat{Y} | x_{1,j}, x_{2,j} \in x_{1^-2^-}] \tag{8d}$$

Let the number of realizations associated with the four bins of Eq. (8) be $L_{1^+2^+}, L_{1^+2^-}, L_{1^-2^+}$ and $L_{1^-2^-}$, respectively. Then at the second level of the tree, we can make the following probability statements:

$$p_{1^+2^+} = P\{Y \geq \hat{Y} | x_{1,j} \geq \hat{X}_1 \cap X_{2,k} \geq \hat{X}_2\} = \frac{L_{1^+2^+}}{N_{1^+2^+}} \tag{9a}$$

and with similar interpretations

$$p_{1^+2^-} = \frac{L_{1^+2^-}}{N_{1^+2^-}} \tag{9b}$$

$$p_{1^-2^+} = \frac{L_{1^-2^+}}{N_{1^-2^+}} \tag{9c}$$

$$p_{1^-2^-} = \frac{L_{1^-2^-}}{N_{1^-2^-}}. \tag{9d}$$

If $p_{1^+2^+} = p_{1^+2^-}$ then the second parameter, X_2, (given $X_1 \geq \hat{X}_1$) has no influence on Y. Thus, relative sensitivities of X_2 can be partially measured by $|p_{1^+2^+} - p_{1^+2^-}|$ and $|p_{1^-2^+} - p_{1^-2^-}|$ for the cases of $X_1 \geq \hat{X}_1$ and $X_1 < \hat{X}_1$, respectively. The total relative sensitivity of Y to X_2 can be determined from:

$$S_{X_2} = |p_{1^+2^+} - p_{1^+2^-}| P\{X_1 \geq \hat{X}_1\} + |p_{1^-2^+} - p_{1^-2^-}| P\{X_1 < \hat{X}_1\} \tag{10}$$

Also, $p_{1^+2^+}$ equal to $p_{1^-2^-}$, implies that whether the first two parameters together had high (greater than their medians) or low (smaller than their medians) values, there is an equal chance of producing a Y lower or higher than its median value. We propose the quantity $(|p_{1^+2^+} - p_{1^-2^-}|)/(1 - |p_{1^+2^+} - p_{1^-2^-}|)$ as a measure of the relative sensitivity of Y jointly to X_1 and X_2. It is possible to define other measures to quantify interactions when one parameter assumes a low value and the other a high value. The usefulness of such measures is currently being investigated and
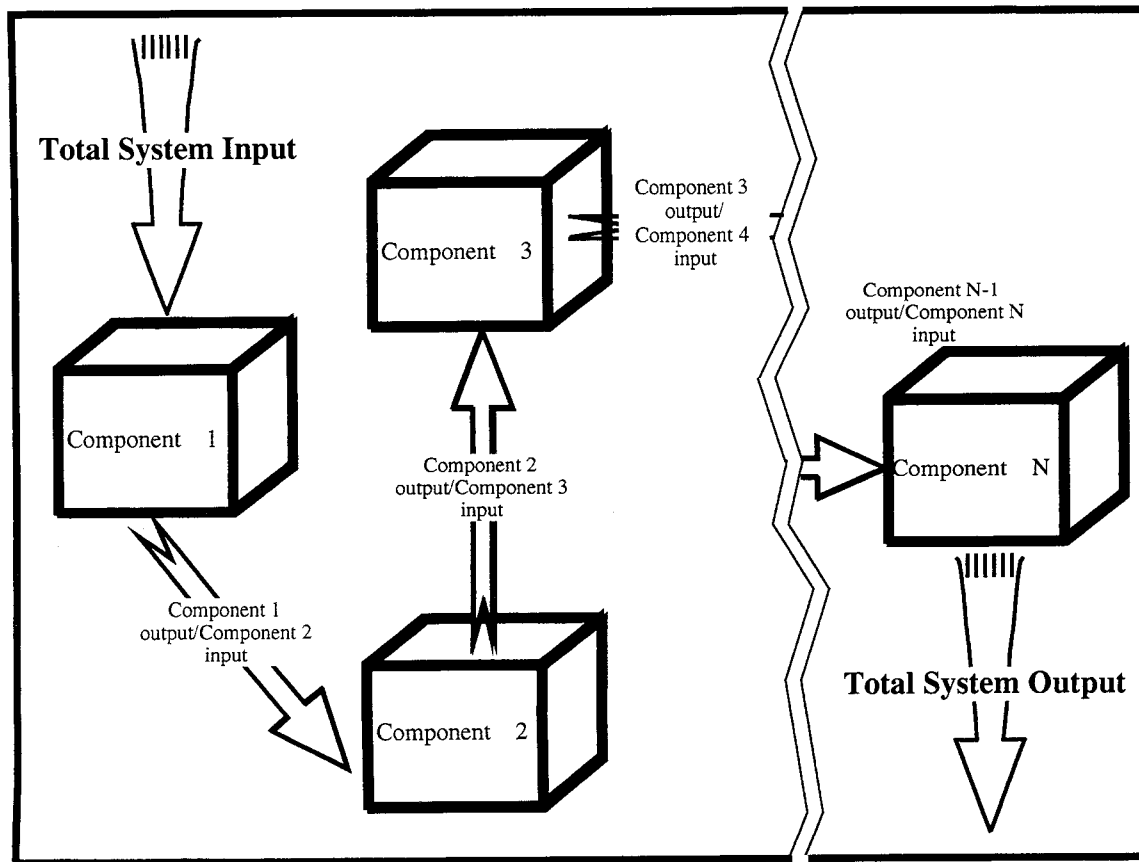
Fig. 2. A diagram showing the breakdown of a total system into subsystem components and their intermediate outputs.

not elaborated upon further in this paper. For this example, we have assumed that both X_1 and X_2 are positively correlated with Y (i.e. large values of X_1 and X_2 lead to large values of Y and vice-versa). In general, this is not a valid assumption and input parameters can be positively or negatively correlated with the output variable. Hence, we now change our nomenclature for the joint relative sensitivity such that the coefficient is now defined as $(|p_H - p_L|)/(1 - |p_H - p_L|)$, where p_H and p_L are the greatest and least values of p among the bins. In this formulation, the numerator represents the "distance" of the output variable from "perfect" non-correlation with the input parameter set (i.e. if Y has no correlation with the input parameter set under study, then p is the same in all bins and the numerator is zero). Similarly, the denominator represents the distance of the output variable from perfect correlation with the input parameter (i.e. if Y shows perfect correlation with the input parameter set under study, p is unity in the highest bin and zero in the lowest bin and the denominator is zero). With this formulation, the joint relative sensitivity is on the range $[0,\infty]$. This formulation can be extended to any number of parameters as is evident from the examples given later.

Another measure of influence of a subset of parameters may be defined through the contribution that realizations in a bin make to a specific statistic of the output. For example,

one can compute the expected value of Y for realizations associated with each branch of the tree and compare these means to the overall mean of Y. Of course, statistics other than the mean can be used or probability distributions can be developed for each branch and compared to the overall probability distribution of Y. If for example, the probability of Y exceeding a certain limiting value (perhaps specified by regulations) is of interest, one could find the value of such exceedance probability for each branch and estimate (in a relative sense) the contribution that each parameter set makes to such a probability. In fact, provided there are sufficient number of realizations associated with a branch, a cumulative distribution function (CDF) can be constructed and compared to the CDF of the overall system output to estimate the contribution of a branch to the overall system CDF. Formally then, if T is a statistic (e.g. mean, mode, median, exceedance probability) of interest, for the second level of the tree, the ratios of $T_{1^+2^+}$, $T_{1^+2^-}$, $T_{1^-2^+}$, $T_{1^-2^-}$ to T of Y as a whole provide measures of relative sensitivity.

Consider now the earlier suggestion that the branching criterion can be something other than the magnitude of a parameter. One of the more useful possibilities is to envision the system as being made up of several components such that the output from one component becomes an input to the second and so on as indicated in Fig. 2. With this conceptualization, the branching criterion can be stated in terms of
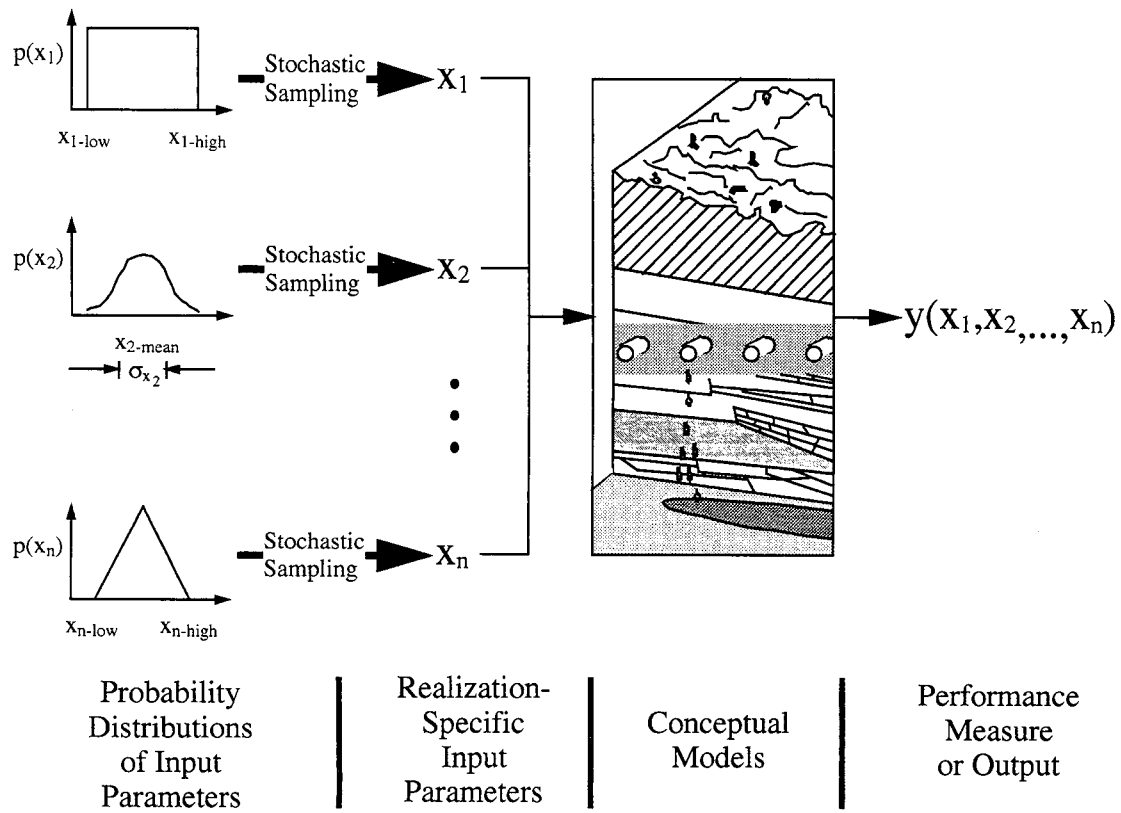
Fig. 3. A diagram illustrating the US Nuclear Regulatory Commission performance assessment model.

Number of Parameters Included in Fit
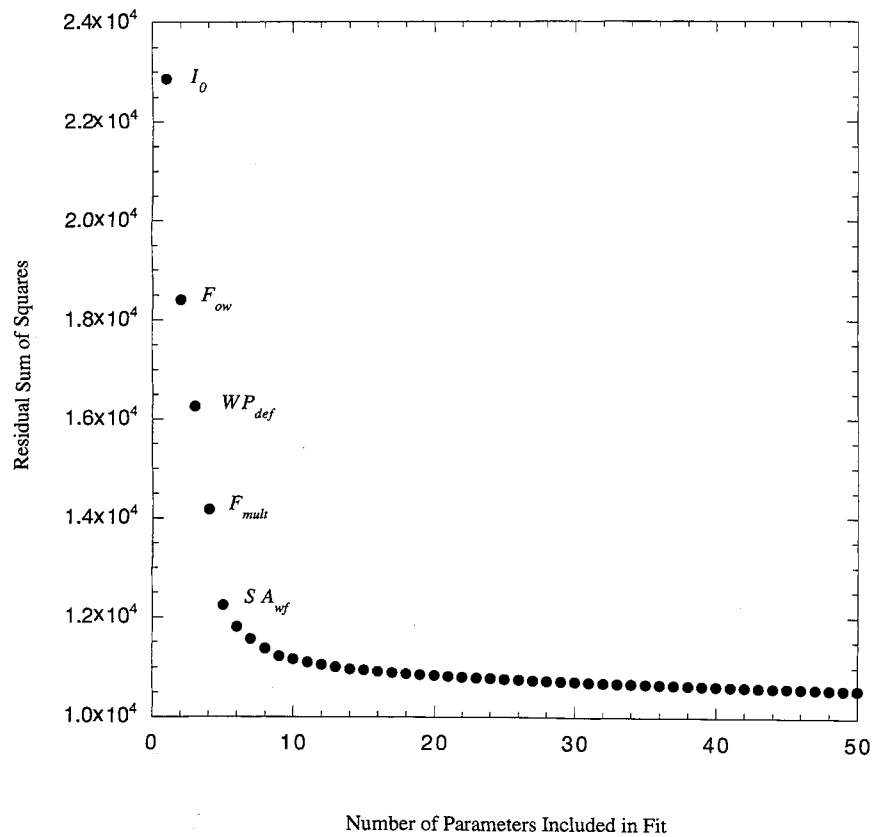
Fig. 4. Results of the stepwise multilinear regression showing the parameters with most influence on residual sum of squares.

the magnitude of the output of a component. In this case, each branch of the tree will represent the contribution of a component or a set of components to overall system performance. Relative sensitivity measures can be defined in exactly the same manner as explained above.

In general, the list of important (or most important) parameters is not known a priori, to develop such a list is, in fact, an important aspect of sensitivity analysis. The rest of this paper presents examples of the method using the US Nuclear Regulatory Commission (NRC) TPA code, which was developed to evaluate the proposed High-Level radioactive Waste (HLW) repository at Yucca Mountain, NV. In these examples, the list of important parameters is determined in two ways: (i) using traditional sensitivity analyses and (ii) using the parameter tree approach in a stepwise manner.

3. Examples of parameter tree applications

This section provides example applications of the parameter tree approach. These examples use simulation data developed using the NRC TPA code. Several trees are presented, each using different branching criteria for the important input parameters. A stepwise implementation of the approach is also presented.

3.1. Background

The TPA code used in these examples was jointly developed by the NRC and the Center for Nuclear Waste Regulatory Analyses. The TPA code has been used to conduct more traditional sensitivity analyses of repository performance [11,12]. In summary, this code includes models to predict the degradation and disruption of emplaced waste packages (WPs) loaded with commercial spent nuclear fuel, transport of radionuclides in groundwater to locations down gradient, and subsequent radiation doses that may occur from contaminated groundwater over long time periods (e.g. 10 kyr). Fig. 3 provides a simplified description of the repository system and of how PA is conducted. Since the current version of this code has many hundreds of parameters with 244 being sampled in the nominal case input data set [11], the results of the more traditional analyses are used as a starting point in the first example in order to limit the number of input parameters investigated.

For the purposes of this paper, the output variable of the model is the peak annual total effective dose equivalent (peak dose) in 10 kyr following repository closure. Input variables to the model are numerous [11]. Fig. 4 shows the results of a stepwise multilinear regression [13] of the residual sum of squares versus the number of parameters included in a multilinear fit of the logarithm of peak dose versus the logarithm of input parameters where the input parameters (i.e. the X_is) also appear only in first order in the fit [e.g. as in Eq. (1)]. This figure was generated using the S-PLUS statistical software package [13]. Because the data

range over orders of magnitude and the results of the model are largely multiplicative rather than additive in the input mechanisms modeled (i.e. the calculated peak doses could be thought of as the product of release from the engineered barrier system times protection afforded from the geosphere surrounding the WP, times a factor that converts releases from the geosphere to dose), fits to the logarithm of the variables tend to produce better results. The form of the fitting function is:

$$\log[Y] = m_1 \log[X_1] + m_2 \log[X_2] + \cdots + m_I \log[X_I] + b \quad (11)$$

where the m_i are the slopes and b is the intercept. All other variables are as previously defined. The stepwise regression routine in S-PLUS organizes the results so that the parameter that explains the greatest reduction in residual sum of squares (in the multilinear fit) appears first. As can be seen from Fig. 4, only about five sampled parameters provide significant reduction in the residual sum of squares, hence initially these are the important input parameters. A short description of these parameters is provided in the following paragraph.

The first-level parameter, I_0, is the areal average mean annual infiltration of groundwater at the start of the simulation period. Infiltration at later times is modeled as a linear multiple of the starting infiltration depending on climate change. The second and fourth parameters, F_{ow} and F_{mult}, account for flow diversion or funneling in the unsaturated zone (UZ) above the repository and in the near field environment toward or away from the WP. The third parameter, WP_{def} is the fraction of initially defective WPs. The fifth parameter, SA_{wf}, is the fraction of the subarea that experiences wetting from infiltrating groundwater. Since flow in the UZ is primarily in fractures, this fraction may be less than unity. A multilinear regression also showed that the regression coefficients of these five parameters [i.e. the m_i in Eq. (11)] were large with high confidence.

3.2. Analytical methods

As described previously, the method used for examining system sensitivity to combinations of parameters found to be most important is to treat each realization of a parameter value as either a "+" or a "−" depending on whether the realized value is greater than or less than a specified value. This is similar to the procedure followed in a signs test [6]. Next, the realizations are sorted based on the commonality of their input parameters being either a "+" or a "−". For example, realizations with all the five important input parameters sampled above the median would be placed in the same bin. Similarly, all realizations where the first four parameters are "+", and the last one is a "−" would be placed in another bin and so on.

For this example, a set of 4000 realizations of the NRC TPA code was used where 244 input parameters were sampled for the nominal case, which is considered to be the most likely evolution of the repository system [11].

Table 1
Statistical information about the 4000 realizations

Parameter	Median value	Mean value	90th percentile	Distribution type [bounds]
I_0 (mm/yr)	5.5	5.5	9.1	Uniform [1,10]
F_{ow}	0.173	0.264	0.566	Lognormal [0.1,3.0]
WP_{def}	0.00505	0.00505	0.00901	Uniform [0.0001,0.01]
F_{mult}	0.0447	0.0503	0.0833	Lognormal [0.01,0.2]
SA_{wf}	0.5	0.5	0.9	Uniform [0.0,1.0]
Realization peak dose (rem/yr)	2.82E−06	1.84E−05	4.97E−05	–

The nominal case includes estimation of WP lifetimes from corrosion and seismically induced rockfall, estimation of radionuclide transport to receptor group locations, and conversion of radionuclide concentration at the receptor location to dose. Table 1 shows some statistical information for these 4000 realizations. In this introductory example, the branching criterion is the median of the parameter distribution for input variables, and the median of the realized distribution for the output variable (i.e. peak dose in 10 kyr), although other statistical quantities for characterizing the distribution of realizations in a bin are also given. Later in this paper, other branching criteria (e.g. mean, percentiles) will be used with the same data set. Although peak dose for the realization whenever that peak may occur is used in this example, using dose for a realization at the

time of the peak of the average dose history curve (i.e. the performance measure in draft versions of the proposed YM implementing regulation 10 CFR Part 63 [14]) would not significantly alter the results since ~ 90 percent of the realizations have their peak dose at 10 kyr, and for those realizations with earlier peak doses, the peak dose does not significantly differ from the dose at 10 kyr.

Fig. 5 shows the parameter tree based on median values as the branching criterion. In Fig. 5, column A is the number of realizations of peak dose that were above the overall median value (i.e. over all 4000 realizations) in that bin. For example, row one in column A shows that 129 out of 4000 realizations had all five of the important parameters with values above their median. Of these 129 realizations, 128 had peak doses above the median value for all 4000

I_0	F_{ow}	WP_{def}	F_{mult}	SA_{wf}	A	B	C	D
					103/129	1.20E-04	0.2107	6.52
					31/97	6.11E-05	0.0803	3.32
					65/140	6.64E-05	0.1261	3.61
					11/68	2.27E-05	0.0209	1.23
					44/141	4.68E-05	0.0894	2.54
					4/70	1.52E-05	0.0114	0.83
					16/133	2.19E-05	0.0395	1.19
					3/87	9.63E-06	0.0114	0.52
					41/224	4.04E-05	0.1226	2.20
					4/58	1.78E-05	0.0140	0.97
					6/216	9.78E-06	0.0286	0.53
					0/59	3.73E-06	0.0030	0.20
					6/223	1.05E-05	0.0317	0.57
					0/62	4.19E-06	0.0035	0.23
					0/230	3.19E-06	0.0099	0.17
					0/63	1.05E-06	0.0009	0.06
					21/67	4.34E-05	0.0395	2.36
					25/226	1.72E-05	0.0528	0.93
					5/53	1.79E-05	0.0129	0.97
					3/230	5.86E-06	0.0186	0.33
					1/60	1.18E-05	0.0096	0.64
					2/227	6.11E-06	0.0188	0.33
					5/54	1.29E-05	0.0094	0.70
					0/218	2.19E-06	0.0065	0.12
					3/73	8.52E-06	0.0084	0.46
					1/125	4.00E-06	0.0068	0.22
					0/87	1.90E-06	0.0022	0.10
					0/148	7.60E-07	0.0015	0.04
					0/96	2.23E-06	0.0029	0.12
					0/122	1.03E-06	0.0017	0.06
					0/74	6.33E-07	0.0006	0.03
					0/140	4.47E-07	0.0008	0.02

Parameter value for realization greater than median (+)

4,000 Realizations

Parameter value for realization less than median (-)

Fig. 5. A tree describing the new technique for examining system sensitivity to groups of parameters. Input parameters divided based on their median values and output variable divided based on its median value from all 4000 realizations.

Table 2
Sensitivity coefficients for the example trees in this paper

Coefficient	Example 1: Fig. 5	Example 2: Fig. 6	Example 3: Fig. 7	Example 4: Fig. 8	Example 5: Fig. 9
Unconditional sensitivities of individual parameters					
S_{X_1}	0.351	0.26	0.134	0.351	0.772
S_{X_2}	0.31	0.28	0.16	0.31	0.692
S_{X_3}	0.202	0.173	0.119	0.202	0.192
S_{X_4}	0.204	0.178	0.0839	0.204	N/A
S_{X_5}	0.192	0.15	0.102	0.081	N/A
Joint sensitivities of parameter groups					
$\dfrac{\|p_H - p_L\|}{1-\|p_H - p_L\|}$	0.541	0.351	0.155	0.541	3.39
	2.37	1.63	0.462	2.37	9.53
	6.75	4.68	0.938	6.75	19.8
	26.0	9.42	1.46	26.0	N/A
	33.5	249	3.95	26.8	N/A

realizations (1.84E−05 rem/yr, Table 1). Column B shows that for these 129 realizations, the mean value of peak dose was 1.20E−04 rem/yr and column C shows that these 129 realizations accounted for 21.07 percent of the population mean of peak doses. This analysis reinforces the notion that these are indeed important parameters since slightly less than 3 percent of the realizations account for over 21 percent of the mean from all realizations. Column D shows an "importance factor" which is determined as the ratio of the contribution to the overall mean from realizations in

that bin to the average contribution of the same number of realizations to the overall mean, i.e.

$$A = \frac{\text{fractional contribution}}{\left(\dfrac{\text{number of realizations in bin}}{\text{total number of realizations}}\right)}$$

$$= \frac{\text{mean peak dose in bin}}{\text{mean peak dose overall realizations}} \tag{12}$$

All of the data in columns A through D serve as figures of
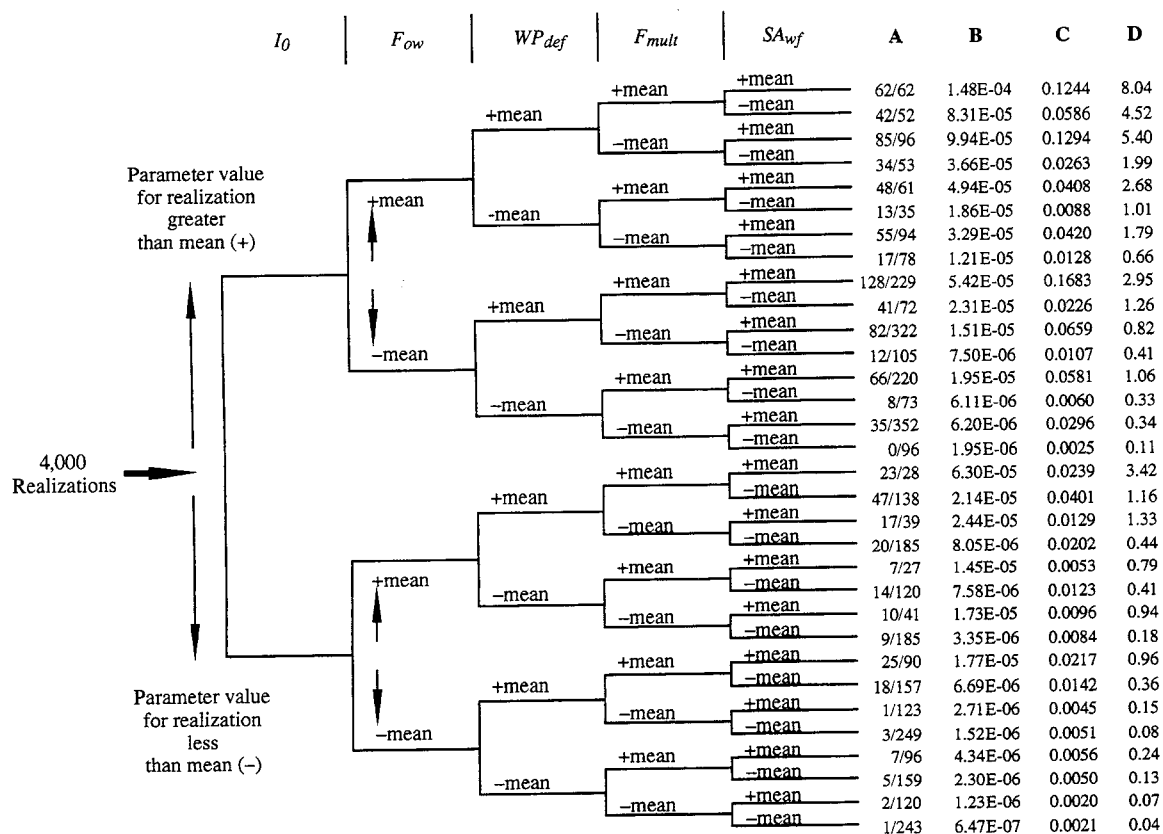
Fig. 6. Another tree describing the new technique for examining system sensitivity to groups of parameters. Input parameters divided based on their mean values and output variable divided based on its mean value from all 4000 realizations.
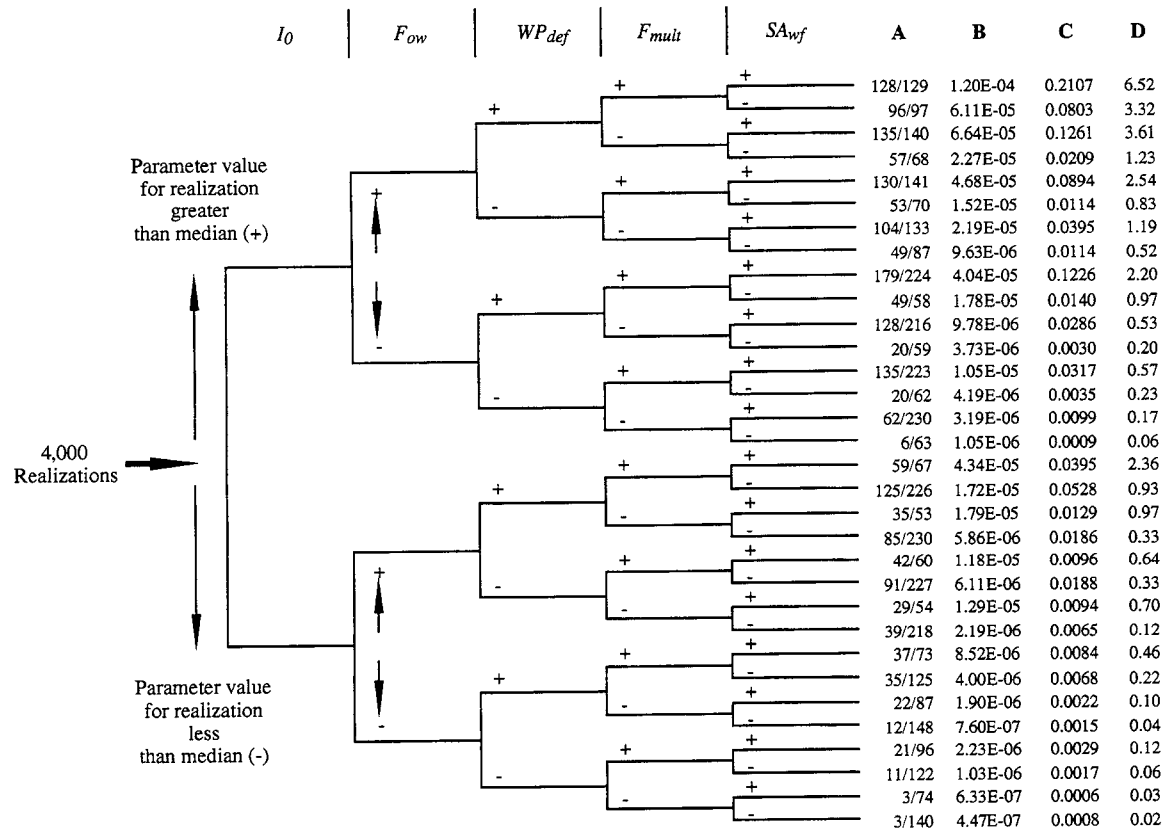
Fig. 7. Another tree describing the new technique for examining system sensitivity to groups of parameters. Input parameters divided based on their median values and output variable divided based on its 90th percentile value from all 4000 realizations.

merit for characterizing the group of realizations in a bin. Other measures of importance can be defined, the most common and quite useful is dependent on the contribution of each parameter to the variance of the output. Such a measure would indicate the contribution of a branch (i.e. set of parameters combined in a certain manner) to the uncertainty in the output. The Sobol' [10] measure essentially relates the variance of the output to the variance (and covariances) of the input parameters. Obviously such measures could be further generalized to include the sensitivity of the output variance (and mean or other statistic) to the means (or other statistics) of the input parameters. For illustration of the parameter tree approach, the importance measure presented is sufficient. Some other interesting observations that can be made about Fig. 5 are:

- The realizations where none or one of the input parameters is "−" account for 67 percent of the mean from all realizations (798 out of 4000 realizations).
- Only 8 out of 32 bins have importance factors above unity, indicating that the output variable distribution is skewed (the eight bins include 999 out of 4000 realizations).

In column 2 of Table 2, the sensitivity coefficients calculated based on equations in Section 2 are presented for this example (example 1). The ranking of individual parameters

matches the ranking obtained from using the regression analysis with the exception that parameters X_3 and X_4 have been reversed. We emphasize that these sensitivity coefficients provide only the relative sensitivities, so for example, from Table 2, Column 2, one can infer that the system is 1.8 times (0.351/0.192) more sensitive to parameter X_1, than it is to parameter X_5. In the lower portion of Table 2, the system sensitivities to joint sets of parameters are presented. As can be seen in the table, the system shows relatively greater sensitivity to parameter sets of increasing size. Again, one should keep in mind that such results are necessarily dependent on conceptual models embodied in the simulation model as well as on the many fixed value (deterministic) parameters in the TPA code. Other columns of Table 2 pertain to examples described below.

3.3. Parameter trees using different branching criteria

As mentioned briefly in the previous section, different branching criteria may be used to determine a "+" or a "−" value for a given parameter or the output variable. Fig. 6 shows a tree where both the input parameters and the output variable have been partitioned based on their mean values. Again, the bins toward the top of the tree account for a disproportionate amount of the mean from

I_0	F_{ow}	WP_{def}	F_{mult}	PR_{20}	A	B	C	D
					124/124	6.59E-05	0.1109	3.58
					100/102	1.30E-04	0.1801	7.06
					82/90	4.31E-05	0.0526	2.37
					110/118	5.90E-05	0.0944	3.20
					84/102	2.81E-05	0.0389	1.53
					99/109	4.39E-05	0.0649	2.38
					74/109	1.44E-05	0.0213	0.78
					79/111	1.96E-05	0.0295	1.06
					102/137	1.86E-05	0.0345	1.01
					126/145	5.19E-05	0.1021	2.82
					66/134	5.51E-06	0.0100	0.30
					82/141	1.13E-05	0.0216	0.61
					66/135	6.78E-06	0.0124	0.37
					89/150	1.12E-05	0.0228	0.61
					23/145	1.71E-06	0.0034	0.09
					45/148	3.73E-06	0.0075	0.20
					84/153	1.55E-05	0.0321	0.84
					100/140	3.17E-05	0.0601	1.72
					57/145	6.93E-06	0.0136	0.38
					63/138	9.55E-06	0.0179	0.52
					54/133	5.69E-06	0.0103	0.31
					79/154	8.67E-06	0.0181	0.47
					29/148	2.97E-06	0.0060	0.16
					39/124	5.92E-06	0.0100	0.32
					30/95	4.11E-06	0.0053	0.22
					42/103	7.10E-06	0.0099	0.39
					17/115	1.23E-06	0.0019	0.67
					17/120	1.13E-06	0.0018	0.06
					17/111	1.53E-06	0.0023	0.08
					15/107	1.60E-06	0.0023	0.09
					2/124	3.23E-07	0.0005	0.02
					4/90	7.70E-07	0.0009	0.04

Parameter value for realization greater than median (+)

4,000 Realizations

Parameter value for realization less than median (-)

Fig. 8. A tree developed using a stepwise implementation of the technique based on the importance factor.

all 4000 realizations. In this example, sampling all five of the important input parameters above their mean values assures a peak dose above its mean value (see column A, row 1 in Fig. 6). The realizations where none or one of the input parameters is "−" account for 55 percent of the mean from all realizations (528 out of 4000 realizations) which is a greater fraction on a per realizations basis than the example presented in Fig. 5. Column 3 (Example 2) of Table 2 shows that the ranking of the parameters according to sensitivity is slightly different with the mean as the branching criterion; in this case X_2 is the most sensitive parameter.

Fig. 7 presents an example of the technique where the input parameters are partitioned based on their median values and the output variable is partitioned based on its 90th percentile. Columns B, C and D of this figure contain numeric entries that are identical to those in Fig. 5. Row 1 of column A, however, shows that if all five of the important parameters are sampled above their median values (129 out of 4000 realizations), then the output variable is above its 90th percentile (4.97E−05 rem/yr) in 103 of these realizations. That is only 79.8 percent of the output above its 90th percentile is provided by the set of five parameters taking on values greater than their median. Comparing to corresponding values for Examples 1 and 2, it is clear that a significant number of extreme values (i.e. above 90th percentile) of the output are produced by combinations of parameters not

represented by the group of five used in our examples. Following the stepwise implementation described in the next section, it is possible to determine a set of parameters, different from the above group, that most influence the 90th or other percentiles.

Although these examples use parameter statistics as the branching criteria, other quantities could also be used. For example, total system failure could be defined as a peak dose to the hypothetical receptor greater than a predetermined limit defined by the regulation [14]. Similarly, input parameters could be partitioned based on a value that has some physical significance. For example, in the NRC TPA code, flow in fractures in the UZ is initiated when the infiltration exceeds the saturated matrix conductivity, currently estimated at about 3 mm/yr. This cutoff is important in terms of performance of this subsystem because flow in fractures occurs more rapidly and dissolved contaminants experience much less chemical retardation than flow in the rock matrix. Hence, initiation of fracture flow in the UZ could be thought of as a transition from one performance regime to another for the UZ.

3.4. Stepwise implementation of the technique

The parameter tree technique was implemented in a stepwise fashion with the importance factor (Column D of
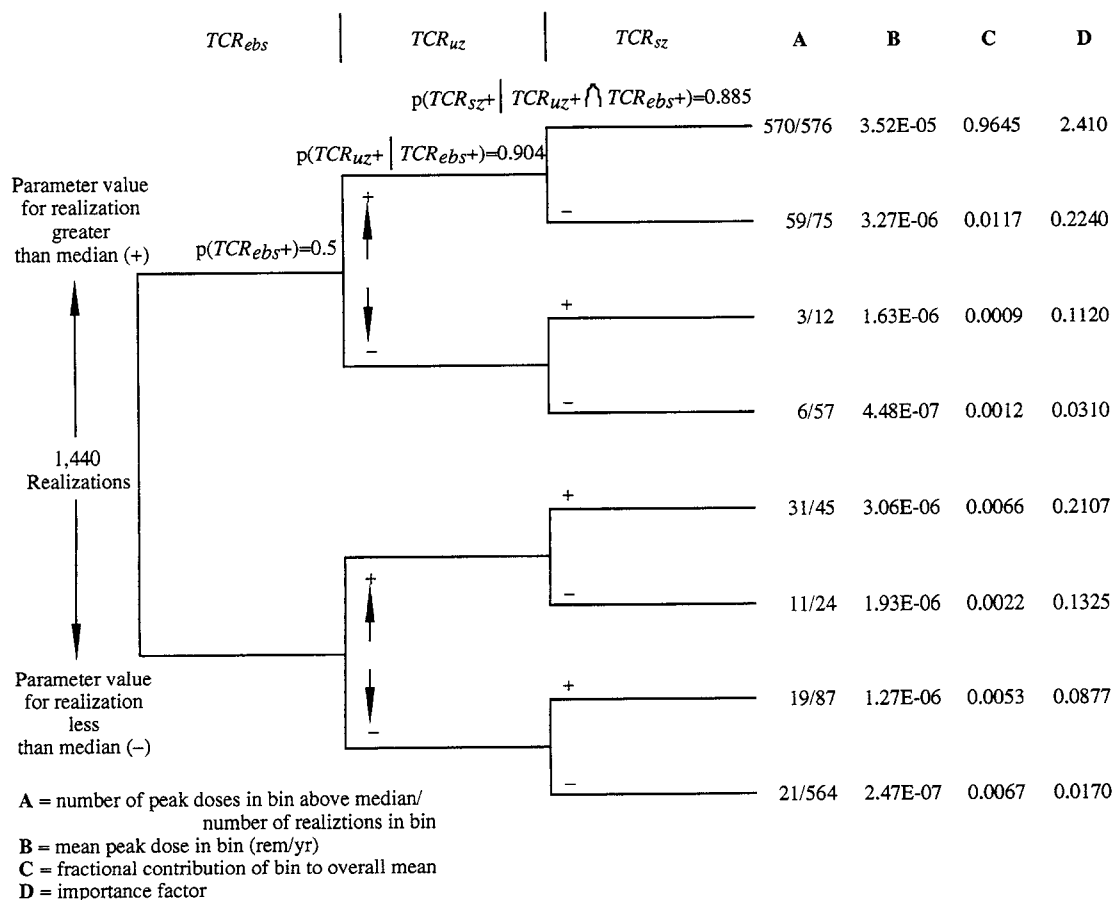
Fig. 9. An intermediate output tree developed using total cumulative radionuclide release from the engineered barrier system, unsaturated zone, and saturated zone based on 1440 realizations of the TPA code.

Figs. 5–8) as the figure of merit for determining maximum polarity of the bins and the median value as the branching criterion. First, a one-parameter-depth tree was drawn for each sampled parameter. The parameter that yielded the greatest importance factor for one of the two branches was then used as the first-level parameter for the following iteration in the stepwise implementation. Next, for all remaining sampled parameters, a two-parameter-depth tree was drawn where the first-level parameter was as determined from the previous iteration. In this second iteration, the parameter that yielded the greatest importance factor on any branch of the tree was used as the second-level parameter for the third iteration. The procedure was repeated until the number of realizations in any bin dropped below 50, with the results of that iteration being discarded. This procedure resulted in a tree that was five parameters deep as shown in Fig. 8. The reader will note that the first four parameters appear in the same order as in the stepwise regression shown in Fig. 4, however, the fifth parameter is the well pumping rate at the receptor located 20 km down gradient—(PR_{20}) instead of the subarea wet fraction (SA_{wf}). This result is important because it shows that these parameters comprise the most important five-parameter set,

which differs from the five individually most important parameters as determined by traditional methods (used in the previous example). Also, note that PR_{20} is negatively correlated with the output variable (because in the NRC TPA model increased pumping merely increases the dilution volume and not the interception fraction of the contaminant plume by the well) and the procedure for assigning "+" and "−" was not reversed so the "+ + + + −" bin represents the most pessimistic case in this example (i.e. the bin with the largest peak doses). In Fig. 8, note that this group of five parameters together produces a higher value of importance factor (7.06) for one of the branches (second branch from top of the tree) as compared to that in Fig. 5 (6.52 for the topmost branch). In contrast, the sensitivity measures in Table 2 for Example 4 show that the combination of these five parameters (i.e. the last row) have a joint relative sensitivity less than that of Example 1 (26.8 versus 33.5). Thus, the nature of information provided by each sensitivity measure is somewhat different. In other words, if we had decided to implement the stepwise procedure using the joint relative sensitivity measure, the five parameters would match exactly those of Example 1.

3.5. Example using intermediate system outputs

As mentioned in a previous section, the technique described in this paper can also be implemented using intermediate system outputs for the branches of the tree as opposed to input parameters. Previous experience indicates that for the HLW repository example, total cumulative radionuclide release (TCR) from the engineered barrier system (EBS), unsaturated zone (UZ), and saturated zone (SZ) are intermediate outputs that are well correlated with peak dose for the compliance period [12] (the output variable), and as such would make excellent examples to use in an "intermediate output" tree. TCR is defined as the integrated release from the subsystem of all radionuclides, measured by activity (Ci), no matter when that release occurs during the compliance period.

Fig. 9 shows an intermediate output TCR_{ebs} tree using TCR_{uz} and TCR_{sz} for the branches of the tree. As can be seen in the figure, realizations with all three of these intermediate outputs sampled above their medians dominate performance. In fact, 96.45 percent of the mean value over all realizations is from realizations in this bin. Also, the mean value for realizations in this bin is an order of magnitude higher than in any other bin.

Previously, we did not discuss the issue of correlations between parameters (i.e. between branches of the tree) because these correlations are known a priori when the sampling mechanisms in the model are created. However, for the case of intermediate outputs, these correlations are not known. Fig. 9 shows that the intermediate outputs considered in this example are correlated. For example, when TCR_{ebs} is greater than its median value or high, TCR_{uz} is also high in 90.4 percent of the realizations. When TCR_{ebs} and TCR_{uz} are both high, TCR_{sz} is high in 88.5 percent of the realizations. In terms of our previous nomenclature, these probabilities are given as:

$$p(TCR_{uz}+|TCR_{ebs}+) = \frac{N_{1^+2^+}}{N_{1_+}} \qquad (13a)$$

$$p(TCR_{sz}+|TCR_{uz}+ \cap TCR_{ebs}+) = \frac{N_{1^+2^+3^+}}{N_{1^+2^+}} \qquad (13b)$$

The magnitudes of these probabilities determine the correlations of the intermediate outputs. The fact that these three subsystem outputs are correlated is expected because in the NRC TPA model, if no release occurs from the EBS, then by definition, no release can occur from the UZ or SZ. Similarly, if no release occurs from the UZ, no release occurs from the SZ. Also, for large EBS releases, the UZ and SZ provide infrequent protection (i.e. they reduce doses by a meaningful amount in only a handful of realizations) which will also lead to correlation of these intermediate outputs. These results, of course, are subject to the assumptions and conceptual models used to generate them and may change as the assumptions and models are updated. The sensitivity

coefficients of Section 2 are also calculated and shown in the last column of Table 2.

4. Summary and conclusions

This paper describes a post-processing technique for estimating the sensitivity of system output variables to groups of system input parameters via the development of parameter trees. Examples are presented using 4000 realizations of the NRC TPA code. The technique involves assigning realization-specific parameter values either a "+" or a "−" based on whether or not they are greater or less than a statistic (e.g. median, mean, percentile) or some other branching criterion. Similar to event trees, parameter trees are then formed that group realizations into bins (or branches) based on the commonality of their parameter values being either a "+" or a "−". In this manner, groups of parameters can be examined (e.g. realizations where several important parameters are all "+") to determine statistical information about the realizations in a particular bin.

The technique was implemented in a stepwise fashion to determine if the most important (with contribution to the mean as the criterion for importance) five-member parameter set is different from the five individually most important parameters determined using traditional sensitivity analysis techniques. It was found that the fifth member of the stepwise constructed set differed from the set constructed with the five individually most important parameters, suggesting that the most sensitive input parameter set may not be the one composed of the individually most sensitive parameters. We examined whether the model output (dose) was a monotonic function of the five important parameters identified in the examples and determined that not to be the case. In fact a few low and few high values of a parameter could be found to produce high value of the dose.

The technique was also used with intermediate system outputs on the branches of the tree. It was shown for the NRC TPA code that if total cumulative radionuclide release from the three subsystems (engineered barrier system, unsaturated zone, and saturated zone) were high, then the corresponding peak doses from these realizations dominated total system performance. This tree also clearly showed the strong correlations between these subsystem outputs for this model.

The parameter tree approach of post processing results of Monte Carlo simulations provides a useful tool to rank the most important individual parameters and subgroups of parameters from among all subgroups that may be formed. It is relatively simple to implement and provides important insights about the system behavior. Its strength and uniqueness is that it can consider combination of parameters jointly in estimating sensitivities. Techniques based on design of experiments [10] are also capable of estimating parameter

interactions. However, such techniques have not been adopted to post-processing of results. The primary weakness of the parameter tree approach is the very large number of realizations required if many parameters are considered.

It is worth reiterating that multiple measures of sensitivity and importance can be defined, each providing different information about system behavior. We defined two in this paper, one based on the number of realizations that meet a specified criterion and the other based on the contribution that a set of parameters makes to the mean of the output. Parameters may differ in their ranking depending upon the criterion used.

Acknowledgements

References

[1] Helton JC. Uncertainty and sensitivity analysis techniques for use in performance assessment for radioactive waste disposal. Reliability Engineering and System Safety 1993;42:327–67.

[2] Draper NR, Smith Jr. H. Applied regression analysis, 2. New York, NY: Wiley, 1981.

[3] Iman RL, Davenport J, Ziegler D. Latin Hypercube Sampling (Program User's Guide). SAND-1473, 1980. Sandia National Laboratories, Albuquerque, NM.

[4] Iman RL, Connover WJ. The use of the rank transform in regression. Technometrics 1979;21:499–509.

[5] Saltelli A, Anderes JH, Homma T. Sensitivity analysis of model output—an investigation of new techniques. Computational Statistics & Data Analysis 1993;15:211–38.

[6] Bowen WM, Bennet CA. (eds.). Statistical methods for nuclear material management. NUREG/CR-4604 (1988), US Nuclear Regulatory Commission, Washington, DC.

[7] Saltelli A, Scott M, editors. The role of sensitivity analysis in the corroboration of models, and its links to model structural and parameter uncertainty. Reliability Engineering and System Safety 1997;57(1).

[8] Homma T, Saltelli A. Importance measures in global sensitivity analysis of nonlinear models. Reliability Engineering and System Safety 1996;52:1–17.

[9] Sobol' IM. Sensitivity estimates for nonlinear mathematical models. Mathematical Modeling & Computational Experiment 1993;1:407–14.

[10] Box GFP, Hunter WG, Hunter JS. Statistics for experiments, an introduction to design, data analysis, and model building, Wiley, 1978.

[11] Mohanty S, McCartin TJ, editors. Conceptual models and data. NUREG-1668 NRC sensitivity and uncertainty analyses for a proposed HLW repository at Yucca Mountain, Nevada using TPA 3.1, I. Washington, DC: US Nuclear Regulatory Commission, 1998.

[12] Jarzemba MS, Codell R, Deere L, firth J, Lui C, Mohanty S, Poor K, Weldy J. Results and conclusions, NUREG-1668, NRC sensitivity and uncertainty analyses for a proposed HLW repository at Yucca Mountain, Nevada Using TPA 3.1, II. Washington, DC: US Nuclear Regulatory Commission, 1999.

[13] StatSci, S-PLUS User's Manual—Version 3.2, Seattle, WA: MathSoft, Inc, 1993.

[14] US Nuclear Regulatory Commission. Disposal of high-level radioactive wastes in a proposed geological repository at Yucca Mountain, Nevada; proposed rule. Federal Register 1999;64(34):8640–79.

APPENDIX D

ELSEVIER

CDF sensitivity analysis technique for ranking influential parameters in the performance assessment of the proposed high-level waste repository at Yucca Mountain, Nevada, USA

Sitakanta Mohanty[a,*], Y-T. (Justin) Wu[b,1]

[a]Center for Nuclear Waste Regulatory Analyses, Southwest Research Institute, 6220 Culebra Road, San Antonio, TX 78238, USA
[b]Structural Integrity and Reliability Section, Southwest Research Institute, 6220 Culebra Road, San Antonio, TX 78238, USA

Abstract

A cumulative distribution function (CDF)-based method has been used to perform sensitivity analysis on a computer model that conducts total system performance assessment of the proposed high-level nuclear waste repository at Yucca Mountain, and to identify the most influential input parameters affecting the output of the model. The performance assessment computer model referred to as the TPA code, was recently developed by the US nuclear regulatory commission (NRC) and the center for nuclear waste regulatory analyses (CNWRA), to evaluate the performance assessments conducted by the US department of energy (DOE) in support of their license application. The model uses a probabilistic framework implemented through Monte Carlo or Latin hypercube sampling (LHS) to permit the propagation of uncertainties associated with model parameters, conceptual models, and future system states. The problem involves more than 246 uncertain parameters (also referred to as random variables) of which the ones that have significant influence on the response or the uncertainty of the response must be identified and ranked. The CDF-based approach identifies and ranks important parameters based on the sensitivity of the response CDF to the input parameter distributions. Based on a reliability sensitivity concept [AIAA Journal 32 (1994) 1717], the response CDF is defined as the integral of the joint probability-density-function of the input parameters, with a domain of integration that is defined by a subset of the samples. The sensitivity analysis does not require explicit knowledge of any specific relationship between the response and the input parameters, and the sensitivity is dependent upon the magnitude of the response. The method allows for calculating sensitivity over a wide range of the response and is not limited to the mean value. © 2001 Elsevier Science Ltd. All rights reserved.

Keywords: Sensitivity analysis; Risk assessment; Uncertainty analysis; Waste management; Influential parameters

1. Introduction

The US nuclear regulatory commission (NRC) and the center for nuclear waste regulatory analyses (CNWRA) recently developed a general computer model [2,3] for conducting total-system performance assessments of the proposed high-level waste repository at Yucca Mountain (YM) in Nevada, USA. This computer model is a tool for evaluating the performance assessments conducted by the US department of energy (DOE) in support of their license application. The relationship between the output and the input parameters in such a model is highly nonlinear and involves strong interactions among the input parameters.

Since it is often difficult to describe precisely the governing physical processes, coupling among these processes, parameters defining the physical system, and the evolution of the repository system over the long time period of interest (TPI), significant uncertainties exist in the computer model. The performance assessment model is then designed in such a way that these uncertainties can be analyzed by using alternative conceptual models and assigning uncertainties to model parameters. The performance assessment model also has a large number of input parameters that are described by ranges of variance and probability distribution functions representing uncertainties and variability. Sensitivity analysis of the performance assessment model is conducted to determine the uncertainty in the output due to uncertainties in the model (not considered in the paper) and input parameters and to determine the most influential input parameters that control the behavior of the output. Knowledge of the most influential input parameters is

---

* Corresponding author. Tel.: +1-210-522-5160; fax: +1-210-522-5155.
  E-mail address: smohanty@swri.org (S. Mohanty).
[1] Current address: Applied Research Associates, 811 Forest Road, Raleigh, NC 27609, USA.

important because it can be used for (i) providing an insight on where more efforts should be devoted to reduce the uncertainties of the output to significantly improve the understanding of the system, (ii) comparing results from calculations conducted by different research groups involved in solving the same problem, and (iii) aiding in design improvements by interactively improving the design criteria or requirements to reduce vulnerability to a particular design parameter.

Methods that are available to identify influential parameters such as linear and step-wise regression [4], non-parametric approaches [5,6], one-at-a-time approaches [7,8], response surface analysis, and Fourier amplitude sensitivity test (FAST) have their advantages and disadvantages. For example, while the linear regression-based sensitivity analysis methods provide ranking of the parameters regardless of the values of the response (an advantage), these methods are most suitable when the response is approximately a linear function of the input parameters (a disadvantage). Similarly, while a one-at-a-time approach has an unambiguous way to relate output parameter sensitivity to an input parameter, the method may not be able to study the interaction effects well. The limitation of other methods are documented in Mohanty et al. [9] and Lu and Mohanty [10].

This paper presents an alternative approach to identify and rank influential parameters based on the sensitivity of the cumulative distribution function (CDF) of model response to the parameter distribution. The approach does not assume a linear or other explicit functional relationship between the response and the input parameters, and the sensitivity is dependent upon the magnitude of the response. The feature of this method is that it allows calculating sensitivity over a wide range of the response and is not limited to the mean value. This approach is more general and provides more information than the regression-based methods. In the alternative approach, the responses and the corresponding random samples of the parameters are ordered so that for each selected response percentile, a corresponding subset of the ordered samples can be identified. Based on a reliability sensitivity concept [1], the response CDF is defined as the integral of the joint probability-density-function of the parameters, with a domain of integration defined by a subset of the samples. The response CDF sensitivities are then calculated from the derivatives of the probability integral. The derivatives are statistically estimated from the samples and used to identify and rank the influential random variables.

Section 2 presents the major functions and components of the performance assessment model for a geologic high-level nuclear waste repository, to give the reader a background of the computer model to be analyzed. Section 3 presents the details of the CDF-based method that is used to conduct sensitivity analysis on the computer model. The application of the CDF-based method to the performance assessment model is presented in Section 4 along with verification of the results, and the conclusion is presented in Section 5.

2. The performance assessment computer model

The performance assessment computer model used in this study was developed by the NRC and the CNWRA to study the uncertainty in estimating the post-closure performance of the proposed high-level waste (HLW) repository at Yucca Mountain (YM) over long time periods (e.g. 10,000 years). The computer code, referred to as the total-system performance assessment (TPA) code [2,3], considers uncertainties and spatial variability of system attributes, model parameters, and future system states (i.e. scenario classes). To capture spatio-temporal and temporal variability and future system state, the TPA code operates in a probabilistic manner (i.e. input parameter sampled from assigned probability distributions). The TPA code estimates dose from released radionuclides during specified time periods (e.g. regulatory compliance TPI) at designated receptor locations. This paper presents only a brief discussion of the processes modeled in the code. For a complete description of the methods and assumptions, the reader is referred to Mohanty and McCartin [2,3].

The TPA code simulates physical and chemical processes of the repository system. The calculations of the most likely scenario involve the degradation of a waste package (WP) in which HLW (e.g. spent nuclear fuel) is disposed approximately 300 m below the surface of YM in the engineered barrier system (EBS), the release of radionuclides when the water infiltrating the ground surface contacts exposed SNF and transports the radionuclides through the partially water-saturated geologic medium beneath the repository and subsequently in the saturated zone to a designated receptor group 20 km down-gradient of the repository. The system-level computation involves estimation of (i) time varying precipitation resulting from climate changes, water percolation from the land surface to the subsurface and subsequently into the emplacement drifts and onto WPs; (ii) the evolution of the chemical and physical processes (e.g. temperature, humidity, pH, chloride ion concentration, and carbonate ion concentration) affecting engineered barrier degradation including the WPs and radionuclide releases; (iii) the time of failure and the number of WPs failed based on corrosion phenomena and rockfalls in the unbackfilled repository; (iv) rockfalls induced by seismic events; (v) the rate of radionuclide release from the EBS to the groundwater pathway as a function of time; (vi) the rate of flow and transport of radionuclides through the unsaturated zone and the saturated zone (water tables); and (vii) radioactive dose to a designated receptor group from groundwater based on the group's lifestyle characteristics.

In addition to calculating the physical processes associated with the most likely scenario, the TPA code also computes the processes that involve high-consequence-low-probability events that include the dose consequences of (i) the WP failure from the displacement of yet unknown faults intersecting the repository; and (ii) intrusive igneous activities (WPs failed in place after coming in contact with

magmatic intrusion as well as extrusive igneous activities (WPs ejected out of the repository and radionuclides become airborne).

The TPA code uses Latin hypercube sampling (LHS) for sampling input parameters. The code contains 838 input parameters out of which 246 are sampled from specified distribution functions. Several sampled input parameters are specified as correlated to multiple parameters. Because special calculations are needed to combine dose from high-consequence-low-probability scenarios with the most likely scenario to compute total dose, only the results from the most-likely scenario are presented in this paper.

3. The CDF-based sensitivity analysis method

Let the performance function or the transfer function (e.g. the TPA code) be defined as

$$Y = Y(\underline{X}) \tag{1}$$

where $\underline{X} = (X_1, X_2, ..., X_L)$ is a vector of L input random variables (also referred to as parameters). Given this performance function and the joint probability distribution of $\underline{X}$, the CDF of Y can be represented as

$$p = P(Y < y_0) = F_y(y_0) = \int_\Omega \cdots \int f_{\underline{X}}(\underline{X}) \, d\underline{X} \tag{2}$$

where y_0 is a specific value of the random variable Y, the integrand $f_{\underline{X}}(\underline{X})$ is the joint probability density function of $\underline{X}$, and the domain of integration, Ω, is the region of $\underline{X}$ that satisfies the performance function constraint $Y(\underline{X}) < y_0$. Eq. (2) provides a convenient way to study the sensitivity of CDF to input variables at any desirable percentile including the extreme values by simply varying y_0. However, the multiple integral that represents the CDF, in general, is very difficult to evaluate for large L. Efficient approximate solutions which require the identification of approximation points (i.e. values of y_0) and the subsequent first- or second-order polynomial approximation of the $Y(\underline{X})$-function have been proposed in the literature [1,11,12] for many engineering problems with a special focus on analyzing very low probability of failure. However, the approximation methods only provide probability estimates and do not give error bounds and, in addition, the efficiency of the methods decrease significantly as a function of the number of input random variables. Therefore, when the performance function $Y(\underline{X})$ is complicated and the region of interest is not the extremes of the CDF, such as CDF > 0.999, it is more effective to compute the integral in Eq. (2) using random sampling techniques such as the LHS and Monte Carlo methods. In this paper, the LHS method is used to study the sensitivity of performance CDF ranging from 0.1 to 0.9. If a study of the extremes of the performance CDF is needed, the efficient approximation methods may be used after a small number of influential random variables have been identified from the results of the CDF sensitivities [13].

From Eq. (2), the sensitivity of p with respect to a distribution parameter θ (mean or standard deviation of the input variables) can be formulated as

$$\frac{\partial p}{\partial \theta} = \int_\Omega \cdots \int \frac{\partial f_{\underline{X}}}{\partial \theta} \, d\underline{X} \tag{3}$$

The partial derivative $\partial p / \partial \theta_i$ represents the sensitivity, which is the change in probability due to the change in a statistical parameter such as mean or standard deviation characterizing the distribution function of the input parameters. Eq. (3) can be represented by an expected function

$$\frac{\partial p / p}{\partial \theta / \theta} = \int_\Omega \cdots \int \frac{\theta \partial f_{\underline{X}}}{f_{\underline{X}} \partial \theta} \left[\frac{f_{\underline{X}}}{p} \right] d\underline{x} = E \left[\frac{\theta \partial f_{\underline{X}}}{f_{\underline{X}} \partial \theta} \right]_\Omega \tag{4}$$

in which $(f_{\underline{X}}/p)$ is the sampling density function that corresponds to the sampling region Ω. The expected value in Eq. (4) is evaluated using the samples in the region of interest, Ω, as indicated. In risk assessment, when the interest is at the right tail of the CDF (i.e. CDF $\gg$ 0.5), a commonly used approach is to compute the sensitivities of CCDF (i.e. the complementary CDF or the probability of exceedance) and then switch the signs to obtain the results for the sensitivities of CDF. This approach is particularly useful when combining it with an importance sampling method that focuses the sampling in the tail region of the CDF. In this paper, the CCDF approach has been adopted for the TPA application problem such that for CDF > 0.5 the samples (Ω) corresponding to $Y > y_0$ are used to compute the sensitivities.

By repeatedly applying the above method for a number of different percentiles, the sensitivities for the entire CDF of Y can be constructed. Thus, sensitivities of model output to input variables can be studied over the whole range, including low dose, most likely dose, and high dose. For example, CDF can be specified as 0.9 to study parameter sensitivities in the region of high dose and the parameters that are most influential in high dose regions.

In general, the function within the expectation operator in Eq. (4) can be computed by using standard numerical differentiation methods to differentiate the density function. The computation of the function, however, becomes difficult when the random variables X_i's are non-normal and mutually dependent. The sensitivity analysis can be greatly simplified if the original random variables are transformed to independent random variables. In general, the non-normal, dependent variables X_i's can be transformed to mutually independent, normal variables $\underline{u}$ using the following transformation [14]:

$$u_1 = \Phi^{-1}[F_1(x_1)]$$

$$u_2 = \Phi^{-1}[F_2(x_2|x_1)]$$

$$\vdots \tag{5}$$

$$u_L = \Phi^{-1}[F_L(x_L|x_1, x_2, ..., x_{L-1})]$$

where F_i is the original CDF, Φ^{-1} is the inverse standardized normal CDF, and u_i's are the standard normal variables with zero mean and unit standard deviation. As a special case, when the X_i variables are mutually independent, Eq. (5) reduces to

$$u_i = \Phi^{-1}[F_i(x_i)] \tag{6}$$

It is important to note that in Eq. (5), the numbering of the random variables is arbitrary such that any random variable can be assigned as X_1.

In most engineering applications, because of the inadequacy of data, only marginal distributions and covariances are available. In such cases, the joint PDF of $\underline{X}$ is not completely defined and a multivariate distribution model must be prescribed. One such model is the Nataf model which was discussed by Liu and Der Kiureghian [15]. If this model is used, the first step in generating a set of independent variables is to define a vector of dependent normal variables $\underline{u}$ using Eq. (6). Then the covariances of the u_i variables are computed from the covariances of the X_i variables. Finally a standard transformation procedure [11] can be applied to generate the independent normal variables from the dependent normal variables. The LHS method used for the TPA analysis does not require a specific prescription of a multivariate distribution model. Instead, the samples are generated based both on the marginal distributions and the input covariances. If the number of samples is sufficiently large, the samples can be used to define a joint PDF. Therefore, the joint PDF and the conditional CDFs in Eq. (6) can be regarded as implicitly defined from the LHS samples.

To account for the dependencies, Eq. (5) will be used to compute the sensitivities with respect to the mean and the standard deviation of any input random variables regardless of whether the random variables $\underline{X}$ are independent or dependent. However, to simplify the analysis and without losing generality, only the first formula in Eq. (5) will actually be used repeatedly such that each new random variable under investigation will be assigned as X_1. This process will result in generating u_i samples for each random variable for the sensitivity analyses. For correlated X_i's, the u_i variables thus produced will remain correlated and their sensitivities will be correlated as well.

Based on Eq. (4), Wu [1] proposed two types of probabilistic sensitivity coefficients for probabilistic performance assessment and design. One is the mean sensitivity coefficient, S_{μ_i}, and the other is the standard-deviation sensitivity coefficient, S_{σ_i}. The two sensitivity coefficients are defined as

$$S_{\mu_i} = \frac{\partial p/p}{\partial \mu_i/\sigma_i} \tag{7}$$

$$S_{\sigma_i} = \frac{\partial p/p}{\partial \sigma_i/\sigma_i} \tag{8}$$

where μ_i and σ_i are the mean and the standard deviation,

respectively, of the random variable X_i. In Eqs. (7) and (8), σ_i is used as a standardization factor to make the coefficients both dimensionless and more comparable. Other standardization factors may be used (e.g. the range of X_i that covers 99% of the population).

For high-level repository performance assessment, several sensitivity measures have been proposed by Eisenberg and Sagar [16] that include two important measures, $\partial \mu_Y/\partial \mu_i$ and $\partial \mu_Y/\partial \sigma_i$. These are closely related to $\partial p/\partial \theta_i$ because the change of the mean response, μ_Y, is a result of the change in the CDF of Y. However, $\partial p/\partial \theta_i$ are suitable for studying the sensitivities over a wide range of performance, including the mean performance.

By applying Eq. (5) to define the joint PDF function in Eq. (4), the sensitivity coefficients in Eqs. (7) and (8) can be simplified as

$$S_{\mu_i} = \frac{\partial p/p}{\partial \mu_i/\sigma_i} = \int_\Omega \cdots \int \frac{\partial \phi(\underline{u})}{\partial \mu_i} \frac{\sigma_i}{p} \, d\underline{u}$$

$$= \int_\Omega \cdots \int \frac{u_i \phi(\underline{u})}{\sigma_i} \frac{\sigma_i}{p} \, d\underline{u} = \int_\Omega \cdots \int u_i \left(\frac{\phi(\underline{u})}{p} \right) d\underline{u}$$

$$= E[u_i]_\Omega \tag{9}$$

$$S_{\sigma_i} = \frac{\partial p/p}{\partial \sigma_i/\sigma_i} = \int_\Omega \cdots \int \frac{\partial \phi(\underline{u})}{\partial \sigma_i} \frac{\sigma_i}{p} \, d\underline{u}$$

$$= \int_\Omega \cdots \int \frac{(u_i^2 - 1)\phi(\underline{u})}{\sigma_i} \frac{\sigma_i}{p} \, d\underline{u}$$

$$= \int_\Omega \cdots \int (u_i^2 - 1) \left(\frac{\phi(\underline{u})}{p} \right) d\underline{u} = E[u_i^2]_\Omega - 1 \tag{10}$$

in which $\phi(\underline{u})$ is the joint PDF of independent, standard normal variables. The two sensitivity coefficients can take positive, negative, or zero values. For the purposes of identifying influential variables, the absolute values should be used. A relatively large magnitude implies that the performance is probabilistically more sensitive with respect to a change in the input distribution, which, in turn, implies that the random variable is influential.

To estimate the sensitivities using a sampling-based approach, the empirical CDF of the performance function Y is first established by ordering the samples of Y from the smallest to the largest. When a percentile is selected, the corresponding subset of the Y samples with the associated input vectors can be easily identified. Then for each sample of Y the input x_i values are converted to u_i using the transformation described above (Eq. (6)). Finally, using Eqs. (9) and (10), the sensitivity coefficients are computed by taking the averages of the samples inside the expectation operator.

To identify and rank important random variables from the samples, the test-of-hypothesis approach can be used with the following null hypotheses:

$$H_0 : S_\mu = S_\sigma = 0 \tag{11}$$
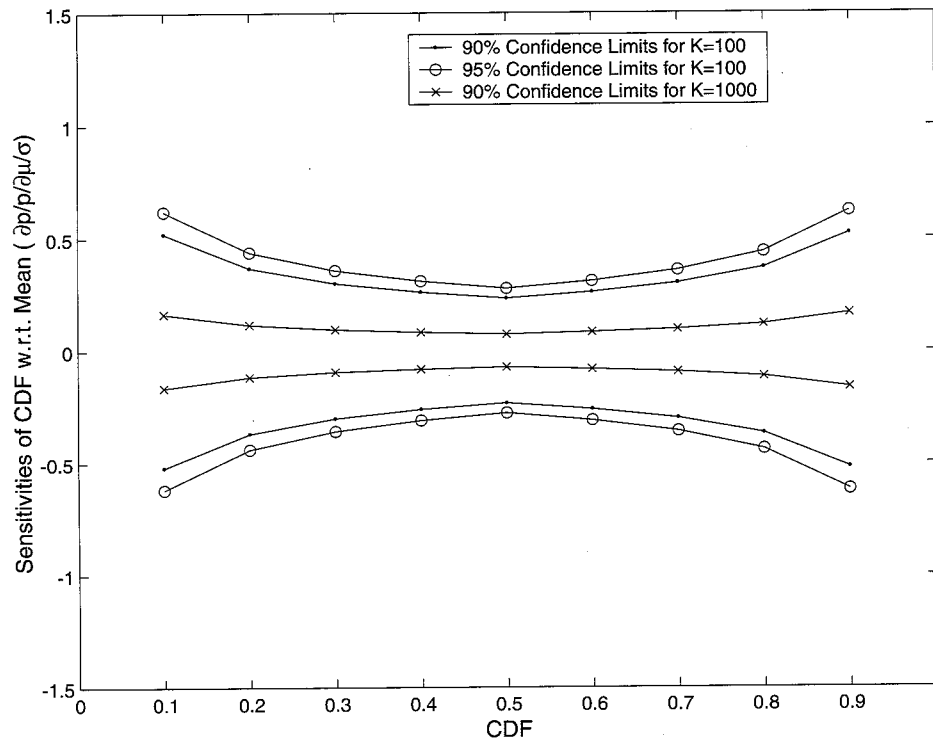
Fig. 1. Examples of confidence limits for identifying influential variables.

The alternative hypotheses are that the absolute sensitivities are greater than zero. When the sensitivities are zero, the standard normal random variable, u, is unrelated to the performance Y, therefore, the samples of u should follow the original distribution of u, i.e. standard normal.

Based on Eqs. (9) and (10), the sampling estimates are

$$\bar{S}_\mu = \frac{1}{k} \sum_1^k u_k \qquad (12)$$

$$\bar{S}_\sigma = \frac{1}{k} \sum_1^k u_k^2 - 1 \qquad (13)$$

It can be observed that $\bar{S}_\mu$ has a normal distribution and $\bar{S}_\sigma + 1$ has a chi-square distribution. These lead to the following probability statements:

$$P\left[-\frac{Z_{\alpha/2}}{\sqrt{k}} \le \bar{S}_\mu \le \frac{Z_{\alpha/2}}{\sqrt{k}} \right] \le 1 - \alpha \qquad (14)$$

$$P\left[\frac{\chi^2_{\alpha/2,k-1}}{k} - 1 \le \bar{S}_\sigma \le \frac{\chi^2_{1-\alpha/2,k-1}}{k} - 1 \right] \le 1 - \alpha \qquad (15)$$

where α is the significant probability level or the risk of making a wrong conclusion about the null hypothesis that the sensitivities are zero. As an example, the 90% ($1 - \alpha = 0.9$) test-of-hypothesis acceptance-limits for S_σ for $K = 100$ and 1000 samples are plotted in Fig. 1. In generating Fig. 1, the k value was the number of samples in the $Y \le y_0$ region for CDF ≤ 0.5 and in the $Y > y_0$ region if CDF > 0.5.

Consequently the test-of-hypothesis acceptance limits are symmetric around CDF $= 0.5$. The figure shows that the ranges of the acceptance limits are narrower for larger K, as expected.

If the calculated data points are within the limits, there is a high probability that the variable is not significant and the null hypothesis (Eq. (11)) will be accepted. On the other hand, if the calculated data points are outside the limits, we will accept the alternative hypothesis that the variable is significant (i.e. has nonzero sensitivity). In the latter case, the magnitude of the calculated sensitivities can be used to rank the influential variables with more confidence. In any case, the number of samples can be increased to reduce the sampling error, and to identify the influential variables and their ranking with improved confidence.

4. Results and discussions

Eleven different distribution functions are used in the TPA code to describe the statistical behavior of the input parameters. As indicated earlier, the particular data set selected for the analysis using this method, is referred to as the basecase because it excludes the consideration of dose contributions from the high-consequence low probability scenarios. The data in the basecase are represented by 4 out of 11 distribution functions used in the TPA code. These four distribution functions include uniform, normal, log-uniform, and lognormal. Based on Eq. (6), the transformations
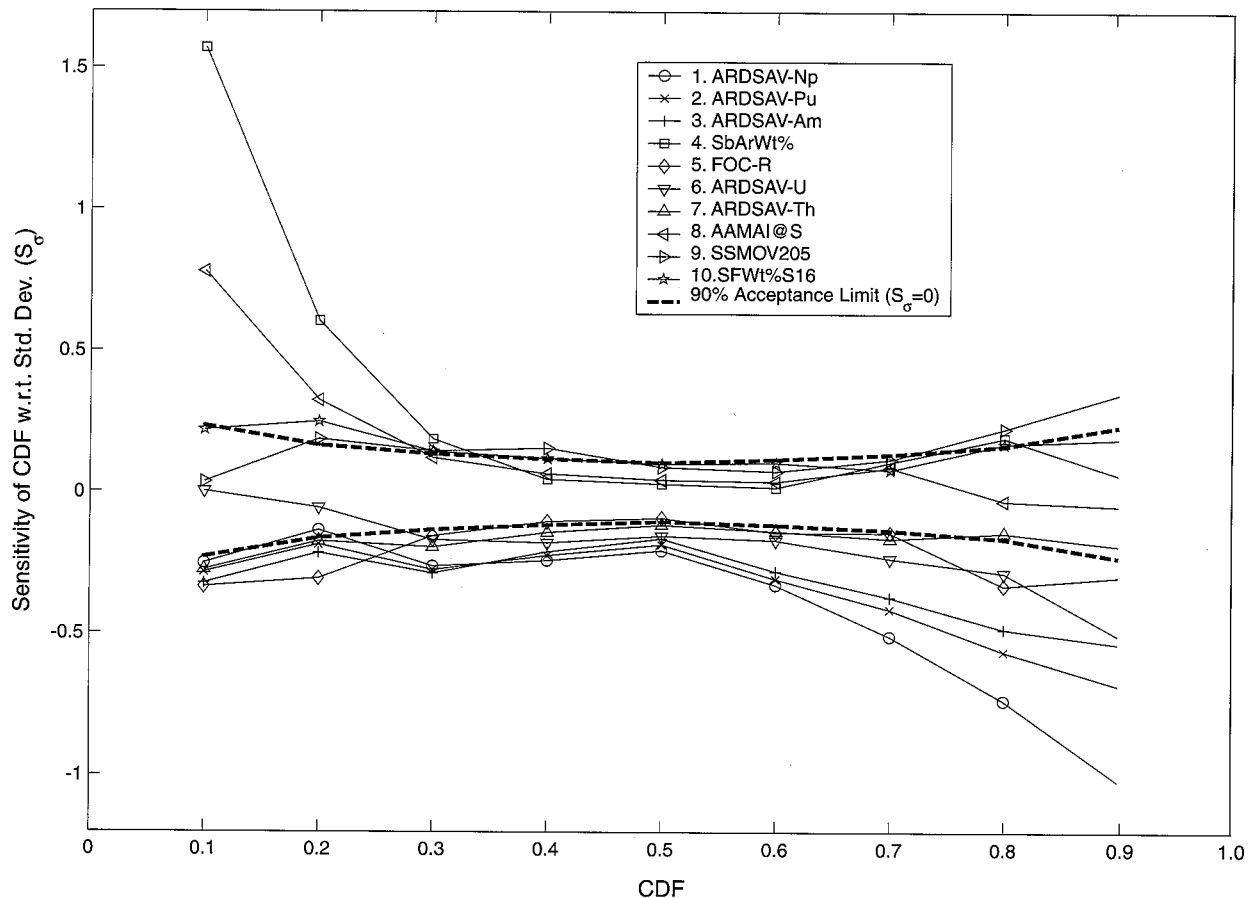
Fig. 2. Sensitivity of performance CDF to input variable standard deviation for top 10 variables having highest average.

to standard normal distribution have been obtained for the 246 random variables to implement the CDF-based method.

The sampled performance was ordered and divided into 10 regions and the performance was evaluated from 10 to 90 percentiles with a 10% increment. Figs. 2 and 3 show the results of S_σ and S_μ, respectively, for the top-10 influential variables based on sensitivity averages over the nine CDF levels. The figures also show the 90% test-of-hypothesis acceptance limits. As noted earlier, the parameters that are not influential are close to the zero sensitivity line and within the 90% limits. The farther the curve is outside of the test-of-hypothesis acceptance limits, the more sensitive is the performance CDF to the corresponding input parameter. The influential parameters can be ranked based on this departure from the zero line which could be different for a given random variable at different CDF levels. The top 10 influential parameters at CDF values of 0.1, 0.5, and 0.9 are presented in Table 1 for 50,000 year TPI. The table also presents the ranking based on the average sensitivity computed over the entire CDF (i.e. the selected nine CDF levels). The table only lists the abbreviated names of the parameters. A short description of what the parameters represent is included in Appendix A.

Figs. 2 and 3 and Table 1 show that the ranking varies for

Table 1
Top 10 influential variables based on three CDFs or average of nine CDFs

CDF	0.1	0.5	0.9	Avg.
S_σ				
1	SbArWt%	ARDSAV-Np	ARDSAV-Np	ARDSAV-Np
2	AAMAI@S	ARDSAV-Pu	ARDSAV-Pu	ARDSAV-Pu
3	MPrm_TSw	ARDSAV-Am	ARDSAV-Am	ARDSAV-Am
4	SSMOV506	ARDSAV-U	ARDSAV-U	SbArWt%
5	MKDCHzPb	SFWt%13	ARDSAV-I	FOC-R
6	WP-Def%	MPrm_UCF	SSMOV507	ARDSAV-U
7	SFWt%S11	ARDSAV-Th	MKDCHzNp	ARDSAV-Th
8	FOC-R	SFWt%C3	MPrm-BFw	AAMAI@S
9	ARDSAV-Am	SFWt%S25	SSMOV205	SSMOV205
10	SSMOV301	OO-CofLC	SSMOV308	SFWt%S16
S_μ				
1	SbArWt%	ARDSAV-Np	ARDSAV-Np	ARDSAV-Np
2	AAMAI@S	ARDSAV-Pu	ARDSAV-Pu	ARDSAV-Pu
3	Mprm_TSw	ARDSAV-Am	ARDSAV-Am	SbArWt%
4	ARDSAV-Np	ARDSAV-U	ARDSAV-U	ARDSAV-Am
5	Fow	SbArWt%	SbArWt%	ARDSAV-U
6	ARDSAV-U	AAMAI@S	Mprm_TSw	AAMAI@S
7	ARDSAV-Pu	WPRRG@20	WPRRG@20	Mprm_TSw
8	ARDSAV-Am	Mprm_TSw	ARDSAV-Th	WPRRG@20
9	WPRRG@20	ARDSAV-Th	AAMAI@S	Fow
10	SFWt%C1	SFWt%C3	OO-CofLC	ARDSAV-Th
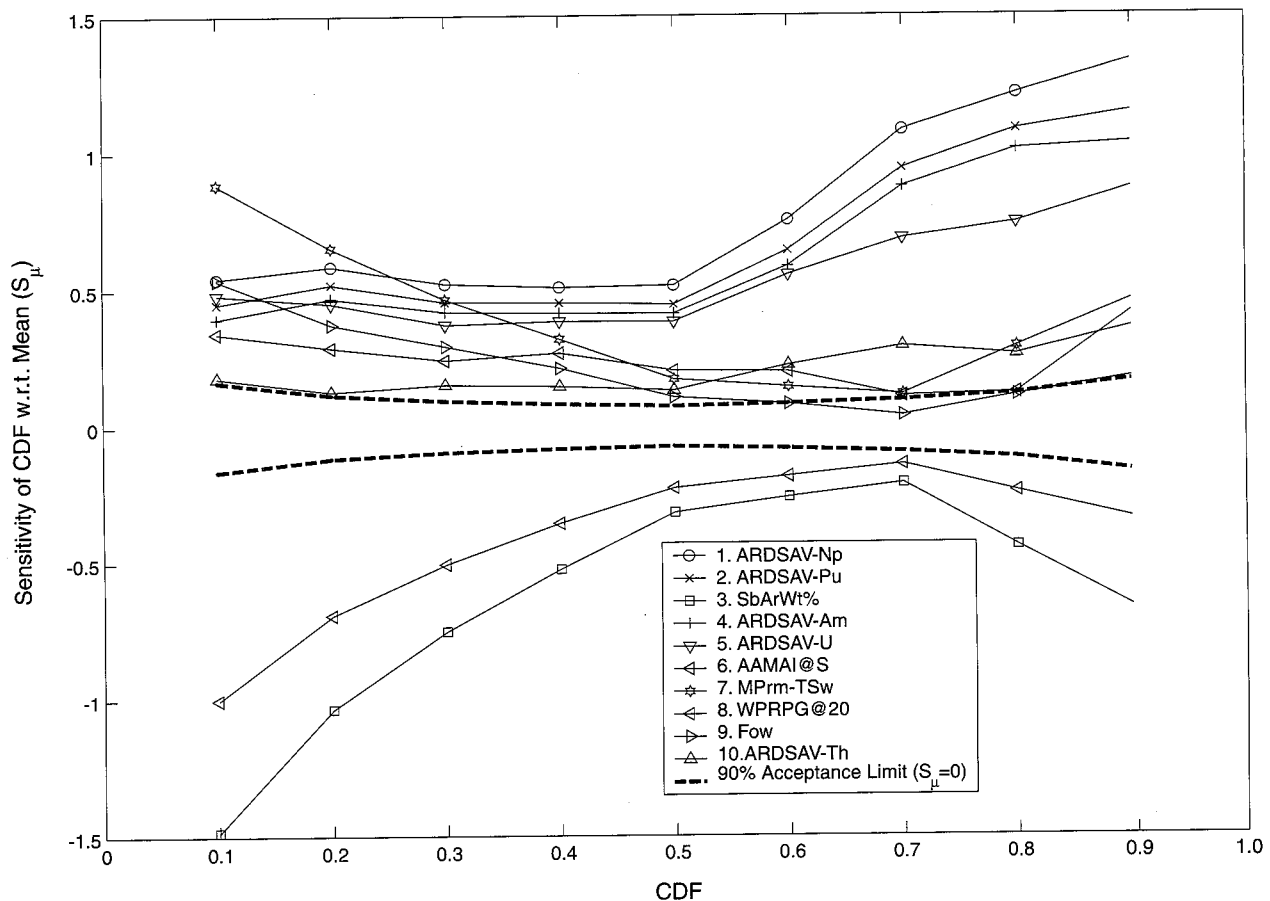
Fig. 3. Sensitivity of performance CDF to input variable mean value for top-ten variables having highest average.

different CDFs. This implies that the functional relationships between the performance and the input variables are not linear (i.e. the sensitivity varies over the range of performance). For example, the variable SbArWt% (subarea wet fraction or the fraction of the WPs in the repository wetted by the infiltrating water) has the highest sensitivity for CDF = 0.1 while the variable ARDSAVNp (Alluvium retardation coefficient for neptunium) has the highest sensitivity for both CDF = 0.5 and 0.9. Except for the top four variables, the ranking based on S_σ is different from that based on S_μ. This result is not surprising since S_σ and S_μ are, after all, different sensitivity measures, and, additionally, the sensitivities are subjected to statistical errors.

Using the 90% test-of-hypothesis acceptance limits as a guide, Fig. 2 suggests that there are four significantly influential variables. These top four parameters, in the order of influence are (1) ARDSAVNp (Alluvium retardation coefficient for neptunium), (2) ARDSAVPu (Alluvium retardation coefficient for Pu), (3) ARDSAVAm (Alluvium retardation coefficient for Am), and (4) SbArWt% (subarea wet fraction). These are the same top four variables identified by S_μ except that the ranking of ARDSAVAm and SbArWt% are in a reverse order. Based on S_σ the performance CDF will be significantly changed if the

input standard deviations of the identified top four variables are reduced. Because the performance variability will be reduced when we reduce the standard deviations of the input variables, and the fact that the performance variation is most affected by the four variables identified with the sensitivity analysis, it can be predicted that the performance standard deviation will be significantly reduced if the input standard deviations of these four variables are reduced.

Not all the top 10 random variables are independent. In fact, the top three variables identified above are highly correlated with the following inputs:

Correlation coefficient = 0.964 for ARDSAVPu and ARDSAVAm.

Correlation coefficient = 0.837 for ARDSAVNp and ARDSAVAm.

Correlation coefficient = 0.881 for ARDSAVPu and ARDSAVNp.

To verify the result by these CDF-based sensitivity analysis methods, several additional TPA analyses were conducted. The standard deviations of the performance were computed after holding at fixed values (mean values)

0, 1, 2, 3, 4, and 10 top most influential parameters (based on the S_σ average); the remaining of 246 input parameters were allowed to be sampled within their ranges of variation. The correlation coefficients were unchanged.

The standard deviation of the performance is plotted in Fig. 4. Each point on the curve represents the output from 250 runs using an LHS sample. It is shown that when the top parameter is fixed at its mean value, there is a significant drop (approximately 94% reduction) in the standard deviation. The curve remains flat after fixing variables 2 and 3 because the top three parameters are correlated. Apparently, it is because the top three variables are highly correlated and their correlation coefficients were fixed, forcing the variables to be dependent. The performance standard deviation drops to about 2% after fixing the top 10 variables. This result verifies that both S_σ and S_μ correctly identified the most influential random variables. Additional analyses are required to further verify the ranking for the correlated random variables.

It is important to note that while the average sensitivity over the entire CDF was effective in the above analysis to identify the most influential variables in the above TPA example, in general the ranking of the influential variable should depend on the analysis objective. The average of S_σ, for example, appears to be a good choice if the analysis objective is to investigate the impact of the input uncertainty (or variability) to the distribution of the performance. On the other hand, if we are more interested in investigating the impact of the input mean value change, then using S_μ offers a more direct answer. Also, if we are more interested in the sensitivity at the high end (e.g. at CDF ≥ 0.9 or high dose in the TPA code) of the performance, then the sensitivity at the tail end of the CDF, rather than the average, should be used to rank the variables.

The above analysis was based on 1000 random samples generated by the LHS method. The method should be equally applicable to the regular Monte Carlo random sampling method. In dealing with complex mathematical models such as the TPA code, it is desirable to use a small sample size to minimize the CPU time. In the above analysis, although 1000 samples (i.e. LHS realizations) were used, it was found that 100 samples were sufficient to identify the most influential variables. In fact, when using the average of the S_μ sensitivities over the entire CDF, it was found that the top five variables identified from the 100 samples were identical to those from the 1000 samples. Furthermore, the 100 samples identified 7 out of the top 10 variables from the 1000 samples. This suggests that when variables are highly significant, the number of samples required to identify them can be relatively small. To minimize the number of samples, one approach is to start from a small number, such as 100, and, by comparing the sensitivity with the test-of-hypothesis acceptance limits, incrementally add the number of samples and update the sensitivity until the results become stable.
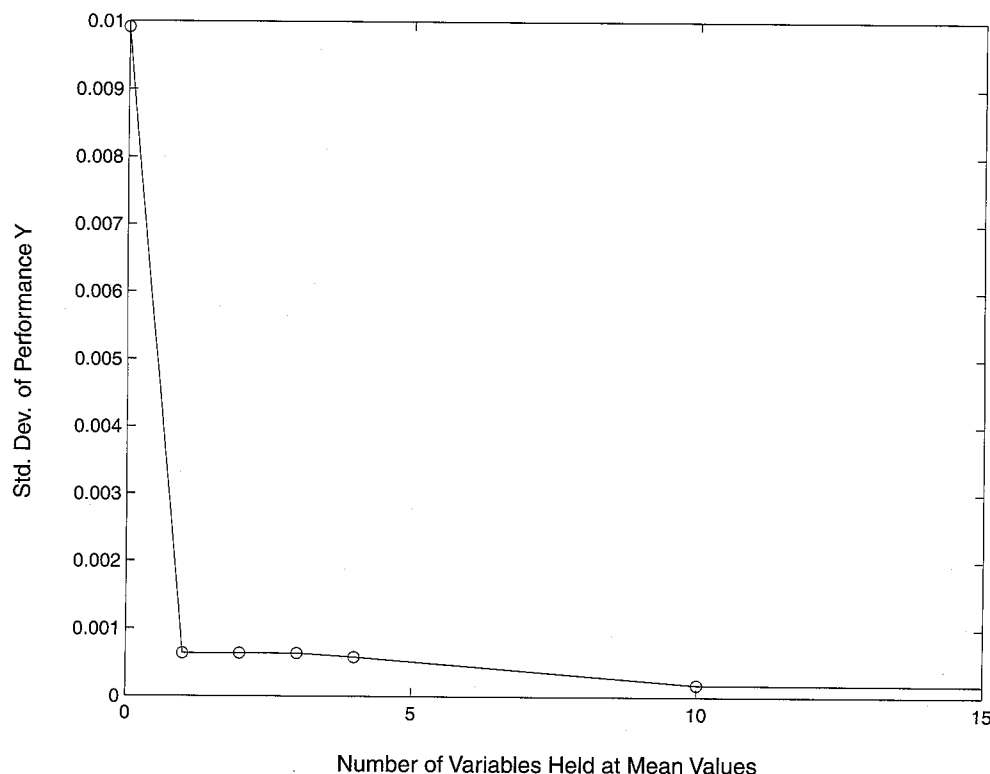
Fig. 4. Performance standard deviation after fixing 1–10 influential variables.

5. Summary and conclusions

The CDF-based method was used to conduct a sensitivity analysis on a computer model that performs a TPA of the proposed HLW repository at Yucca Mountain, Nevada, USA. A description of the method was first presented, and several key properties and performance measures of the CDF-based method were investigated. One feature of this method is that it allows calculating sensitivity at any designated level of the CDF of the response and is not limited to the mean value. One thousand TPA code realizations were used to demonstrate the applicability of the method for conducting sensitivity analysis for a large and complex problem.

Two sensitivity measures, S_μ (CDF sensitivity with respect to mean) and S_σ (CDF sensitivity with respect to standard deviation), were discussed. These measures provide a useful analysis tool to explore a repository design by identifying the influential input variables and by investigating the potential impact of the uncertainties in the input variables to the performance CDF.

The results of the TPA *basecase* show that at different performance CDF levels, the top influential variables may be different. For example, a variable very sensitive at CDF = 0.1 may be insensitive at CDF = 0.9. In general, the ranking of random variables at tail CDF levels can be different from the ranking obtained around the mean typically used in other sensitivity analysis methods.

Based on the average of the S_σ sensitivities taken over the entire CDF, the method identified four most influential variables ((1) ARDSAVNp, (2) ARDSAVPu, (3) ARDSA-VAm, and (4) SbArWt%) for 50,000 years TPI. These four variables were expected to be most sensitive to performance variability. When verified through the reduction of the variance in the performance by fixing the variables at their mean values, the performance standard deviation dropped to 6% after fixing the top four variables and dropped to 2% after fixing the top 10 variables.

The TPA sensitivities were computed based on 1000 LHS samples. However, the method can be applied to the regular Monte Carlo or other random sampling methods and a much smaller number of samples may be sufficient as long as the calculated sensitivity is statistically significant. In fact, it was found that for the TPA basecase, 100 LHS samples were sufficient to identify the same top five variables. This suggests that, in general, an integrated LHS-sensitivity analysis approach can be designed to adaptively determine and minimize the number of samples for sensitivity analysis purposes.

It should be cautioned that the TPA analysis is presented in this paper to demonstrate how the most influential variables may be efficiently and effectively identified in a large and complex problem and is not intended at this stage to make suggestions about what may be the most influential variables for the proposed repository at YM.

The future efforts will focus on determining the combined influence of two or more statistically correlated parameters and on developing other useful sampling-based sensitivity measures.

Acknowledgements

Appendix A

List of short names of the parameters and the short description of what the parameters represent. Only the short names of 27 out of 246 sampled parameters that appeared in the paper have been listed in this appendix

Abbreviation	Description
AAMAI@S	Areally averaged mean annual infiltration for the present day climate
ARDSAV_I	Matrix retardation for iodine in the saturated zone of Amargosa Valley alluvium
ARDSAV_U	Matrix retardation for uranium in the saturated zone of Amargosa Valley alluvium
ARDSAVAm	Matrix retardation for americium in the saturated zone of Amargosa Valley alluvium
ARDSAVNp	Matrix retardation for neptunium in the saturated zone of Amargosa Valley alluvium
ARDSAVPu	Matrix retardation for plutonium in the saturated zone of Amargosa Valley alluvium
ARDSAVTh	Matrix retardation for thorium in the saturated zone of Amargosa Valley alluvium
FOC-R	Fraction of water condensate removed in each reflux time step
Fow	A flow focusing factor which expresses the flow potentially reaching a wetted WP (can be greater or less than 1.0)
FPrm_UCF	Upper crater flat fracture permeability
MKDCHzNp	Matrix K_d for neptunium in the Calico Hills (zeolitic) stratigraphic unit
MKDCHzPb	Matrix K_d for lead in the Calico Hills (zeolitic) stratigraphic unit
MPrm_BFw	Matrix permeability for the Bull Frog stratigraphic unit
MPrm_TSw	Matrix permeability for the Topopah Springs stratigraphic unit
OO-CofLC	Coefficient for localized corrosion of outer overpack of the waste package

(*continued*)

Abbreviation	Description
SbArWt%	Fraction of a subarea wetted by water infiltrating into the repository
SFWt%C1	Fraction of spent fuel that is wet from encroaching water after the WP failed from corrosion process in subarea 1
SFWt%C3	Fraction of spent fuel that is wet from encroaching water after the WP failed from seismic activities in the first time interval in subarea 1
SFWt%I3	Fraction of spent fuel that is wet from encroaching water after the WP failed from seismic activities in the subarea 3
SFWt%S11	Fraction of spent fuel that is wet from encroaching water after the WP failed from seismic activities in the first time interval in subarea 1
SFWt%S16	Fraction of spent fuel that is wet from encroaching water after the WP failed from seismic activities in the first time interval in subarea 6
SFWt%S25	Fraction of spent fuel that is wet from encroaching water after the WP failed from seismic activities in the second time interval in subarea 5
SSMOV205	Vertical extent of rockfall due to seismicity for rock condition 2 and ground acceleration 0.25 g
SSMOV301	Vertical extent of rockfall due to seismicity for rock condition 3 and ground acceleration 0.05 g
SSMOV308	Vertical extent of rockfall due to seismicity for rock condition 3 and ground acceleration 0.4 g
SSMOV506	Vertical extent of rockfall due to seismicity for rock condition 5 and ground acceleration 0.3 g
SSMOV507	Vertical extent of rockfall due to seismicity for rock condition 5 and ground acceleration 0.35 g
WP-Def%	Fraction of WPs in each subarea that are initially defective
WPRRG@20	Well pumping rate at the 20 km receptor group

References

[1] Wu Y-T. Computational methods for efficient structural reliability and reliability sensitivity analysis. AIAA J 1994;32(8):1717–23.

[2] Mohanty S, McCartin TJ (coordinators). NRC Sensitivity and uncertainty analyses for a proposed HLW repository at Yucca Mountain, Nevada using TPA 3.1-vol. I: conceptual models and data, NUREG-1668, US nuclear regulatory commission, Washington, DC, 2001.

[3] Mohanty S, McCartin TJ (coordinators). Total-system performance assessment (TPA) version 3.2 Code: module descriptions and user's guide. Center for nuclear waste regulatory analyses, southwest research institute, prepared for US Nuclear Regulatory Commission, 1998.

[4] Draper NR, Smith Jr. H. Applied regression analysis. 2nd ed.. New York: Wiley, 1981.

[5] Jarzemba M, Sagar B. A parameter tree approach to estimating system sensitivities to parameter sets. Rel Engng Syst Saf 2000;67:89–102.

[6] Bowen WM, Bennet CA, editors. Statistical methods for nuclear materials management. NUREG/CR-4604, US Nuclear Regulatory Commission, 1988.

[7] Helton JC. Uncertainty and sensitivity analysis techniques for use in performance assessment for radioactive waste disposal. Rel Engng Syst Saf 1993;42:327–67.

[8] Cukier RI, Fortuin CM, Schuler KE, Petschek AG, Schaibly JH. Study of the sensitivity of coupled reaction systems to uncertainties in rate coefficients. I Theory. J Chem Phys 1973;59(8):3873–8.

[9] Mohanty S, Codell R, Rice R, Weldy J, Lu Y, Byrne R, McCartin T, Jarzemba M, Wittmeyer G. System-level repository sensitivity analysis using TPA version 3.2 code. Center for nuclear waste regulatory analyses, southwest research institute, Report CNWRA 99-002, prepared for US Nuclear Regulatory Commission 1999.

[10] Lu Y, Mohanty S. Sensitivity analysis of a complex, proposed geologic waste disposal system using the Fourier amplitude sensitivity test. Rel Engng Syst Saf 2001;72:275–291.

[11] Ang AH-S, Tang WH. Probability concepts in engineering planning and design, volume II: decision, risk, and reliability. New York: Wiley, 1984.

[12] Madsen HO, Krenk S, Lind NC. Methods of structural safety. Englewood Cliffs, NJ: Prentice-Hall, 1986.

[13] Wu Y-T. Methods for efficient probabilistic analysis of systems with large numbers of random variables. 7th AIAA/USAF/NASA/ISSMO Symposium on multidisciplinary analysis and optimization, St. Louis, MO, September, Paper 98-4908, 1998.

[14] Rosenblatt M. Remarks on a multivariate transformation. The Annals Math Statist 1952;23(3):470–2.

[15] Liu P-L, Der Kiureghian A. Multivariate distribution models with prescribed marginals and covariances. Probabilistic Engng Mech 1986;1(2):105–12.

[16] Eisenberg NA, Sagar B. Importance measures for nuclear waste repositories. Rel Engng Saf 2000;70:217–39.

APPENDIX E

Description of Abbreviations Used for TPA Version 4.1 Code Sampled Input Parameters

Parameter Identification	Short Name	Full Name	Description
10	AA_1_1	AA_1_1[C/m2/yr]	A corrosion rate (passive current density) for the waste package outer overpack in EBSFAIL
1	AAMAI@S	ArealAverageMeanAnnualInfiltrationAtStart[mm/yr]	Mean areal average infiltration into the subsurface at the start of a TPA Version 4.1 code run
329	ABMLAAsh	AirborneMassLoadAboveFreshAshBlanket[g/m3]	Mass of soil in the air above a fresh volcanic ash blanket
330	AMLASoil	AirborneMassLoadAboveSoil[g/m3]	Mass of soil in air above Amargosa Valley soil
236	APrs_SAV	AlluviumMatrixPorosity_SAV	Amargosa Valley alluvium saturated zone matrix porosity
241	AqThick5	AquiferThickness5km[m]	Thickness of the aquifer at a location 5 km [3.1 mi] south of Yucca Mountain
226	ARDSAV_U	AlluviumMatrixRD_SAV_U	Matrix retardation for uranium in the saturated zone of the Amargosa Valley alluvium

Description of Abbreviations Used for TPA Version 4.1 Code Sampled Input Parameters

Parameter Identification	Short Name	Full Name	Description
224	ARDSAVAm	AlluviumMatrixRD_SAV_Am	Matrix retardation for americium in the saturated zone of the Amargosa Valley alluvium
231	ARDSAVCs	AlluviumMatrixRD_SAV_Cs	Matrix retardation for cesium in the saturated zone of the Amargosa Valley alluvium
234	ARDSAVNb	AlluviumMatrixRD_SAV_Nb	Matrix retardation for niobium in the saturated zone of the Amargosa Valley alluvium
232	ARDSAVNi	AlluviumMatrixRD_SAV_Ni	Matrix retardation for nickel in the saturated zone of the Amargosa Valley alluvium
225	ARDSAVNp	AlluviumMatrixRD_SAV_Np	Matrix retardation for neptunium in the saturated zone of the Amargosa Valley alluvium
230	ARDSAVPb	AlluviumMatrixRD_SAV_Pb	Matrix retardation for lead in the saturated zone of the Amargosa Valley alluvium

Description of Abbreviations Used for TPA Version 4.1 Code Sampled Input Parameters

Parameter Identification	Short Name	Full Name	Description
227	ARDSAVPu	AlluviumMatrixRD_SAV_Pu	Matrix retardation for plutonium in the saturated zone of the Amargosa Valley alluvium
229	ARDSAVRa	AlluviumMatrixRD_SAV_Ra	Matrix retardation for radium in the saturated zone of the Amargosa Valley alluvium
233	ARDSAVSe	AlluviumMatrixRD_SAV_Se	Matrix retardation for selenium in the saturated zone of the Amargosa Valley alluvium
228	ARDSAVTh	AlluviumMatrixRD_SAV_Th	Matrix retardation for thorium in the saturated zone of the Amargosa Valley alluvium
328	AshMnPLD	AshMeanParticleLogDiameter[d_in_cm]	Relative size of ash/SF particulates from a volcanic event
11	*Chlorid	ChlorideMultFactor	Factor by which chloride concentration in matrix is multiplied to compensate for dripping and drying that would lead to salt accumulation

Description of Abbreviations Used for TPA Version 4.1 Code Sampled Input Parameters

Parameter Identification	Short Name	Full Name	Description
8	CritRHAC	CriticalRelativeHumidityAqueousCorrosion	Critical relative humidity above which aqueous corrosion may initiate
12	DSFailTi	DripShieldFailureTime[yr]	Time of failure of the dripshield (year)
237	DTFFAVIF	DistanceToTuffAlluviumInterface[km]	Distance traveled in Tuff
308	FEROI-Tn	TimeOfNextFaultingEventinRegionOfInterest[yr]	Time of the next faulting event in the repository area (years from present)
310	FEROI-X	XlocationOfFaultingEventInRegionOfInterest[m]	X location of the center of the faulting event within the repository area
311	FEROI-Y	YlocationOfFaultingEventInRegionOfInterest[m]	Y location of the center of the faulting event within the repository area
312	FO-Rn#Sd	RntoDetermineFaultOrientation	Random number selected to determine the orientation of the fault within the repository area
4	FOC-R	FractionOfCondensateRemoved[1/yr]	Fraction of water condensate removed in each reflux3 time step
5	FOCTR	FractionOfCondensateTowardRepository[1/yr]	Fraction of water condensate moving towards the repository

Description of Abbreviations Used for TPA Version 4.1 Code Sampled Input Parameters

Parameter Identification	Short Name	Full Name	Description
214	FPrm_BFw	FracturePermeability_BFw_[m2]	Bullfrog-welded fracture permeability (UZ)
210	FPrm_CHv	FracturePermeability_CHnv[m2]	Calico Hills-nonwelded vitric fracture permeability (UZ)
211	FPrm_CHz	FracturePermeability_CHnz[m2]	Calico Hills-nonwelded zeolitic fracture permeability (UZ)
212	FPrm_PPw	FracturePermeability_PPw_[m2]	Prow Pass-welded fracture permeability (UZ)
209	FPrm_TSw	FracturePermeability_TSw_[m2]	Topopah Spring-welded fracture permeability (UZ)
213	FPrm_UCF	FracturePermeability_UCF_[m2]	Upper Crater Flat fracture permeability (UZ)
215	FPrm_UFZ	FracturePermeability_UFZ_[m2]	Unsaturated Fracture Zone fracture permeability (UZ).
221	FPrs_BFw	FracturePorosity_BFw_	Bullfrog-welded fracture porosity (UZ)
217	FPrs_CHv	FracturePorosity_CHnv	Calico Hills-nonwelded vitric fracture porosity (UZ)

Description of Abbreviations Used for TPA Version 4.1 Code Sampled Input Parameters

Parameter Identification	Short Name	Full Name	Description
218	FPrs_CHz	FracturePorosity_CHnz	Calico Hills-nonwelded zeolitic fracture porosity (UZ)
219	FPrs_PPw	FracturePorosity_PPw_	Prow Pass-welded fracture porosity (UZ)
235	FPrs_STF	FracturePorosity_STFF	Fracture porosity of saturated tuff (SZ)
216	FPrs_TSw	FracturePorosity_TSw_	Topopah Spring-welded fracture porosity (UZ)
220	FPrs_UCF	FracturePorosity_UCF_	Upper Crater Flat fracture porosity (UZ)
222	FPrs_UFZ	FracturePorosity_UFZ_	Unsaturated Fracture Zone fracture porosity (UZ)
297	genKDsAm	KD_Soil_Am[cm3/g]	Soil K_d for americium (cm^3/g)
306	genKDsC	KD_Soil_C[cm3/g]	Soil K_d for carbon (cm^3/g)
294	genKDsCm	KD_Soil_Cm[cm3/g]	Soil K_d for curium (cm^3/g)
302	genKDsCs	KD_Soil_Cs[cm3/g]	Soil K_d for cesium (cm^3/g)
303	genKDsI	KD_Soil_I[cm3/g]	Soil K_d for iodine (cm^3/g)
305	genKDsNi	KD_Soil_Ni[cm3/g]	Soil K_d for nickel (cm^3/g)

Description of Abbreviations Used for TPA Version 4.1 Code Sampled Input Parameters

Parameter Identification	Short Name	Full Name	Description
298	genKDsNp	KD_Soil_Np[cm3/g]	Soil K_d for neptunium (cm^3/g)
301	genKDsPb	KD_Soil_Pb[cm3/g]	Soil K_d for lead (cm^3/g)
295	genKDsPu	KD_Soil_Pu[cm3/g]	Soil K_d for plutonium (cm^3/g)
300	genKDsRa	KD_Soil_Ra[cm3/g]	Soil K_d for radium (cm^3/g)
307	genKDsSe	KD_Soil_Se[cm3/g]	Soil K_d for selenium (cm^3/g)
304	genKDsTc	KD_Soil_Tc[cm3/g]	Soil K_d for technetium (cm^3/g)
299	genKDsTh	KD_Soil_Th[cm3/g]	Soil K_d for thorium (cm^3/g)
296	genKDsU	KD_Soil_U[cm3/g]	Soil K_d for uranium (cm^3/g)
293	gen_AUSF	AnimalUptakeScaleFactor	Animal uptake scaling factor used to scale animal transfer factors in *gftrans.dat*
292	gen_PUSF	PlantUptakeScaleFactor	Plant uptake scaling factor used to scale plant transfer factors in *gftrans.dat*
275	gen_bfdf	BeefFreshForageDietFraction	Beef cattle fresh forage diet fraction

Description of Abbreviations Used for TPA Version 4.1 Code Sampled Input Parameters

Parameter Identification	Short Name	Full Name	Description
277	gen_bfgt	BeefFreshForageGrowTime[day]	Beef cattle fresh forage growing time (day)
287	gen_dwc1	DrinkingWaterConsumptionRate1[L/yr]	Drinking water consumption rate for infant (liters per year)
288	gen_dwc2	DrinkingWaterConsumptionRate2[L/yr]	Drinking water consumption rate for toddler (liters per year)
289	gen_dwc3	DrinkingWaterConsumptionRate3[L/yr]	Drinking water consumption rate for preteen (liters per year)
290	gen_dwc4	DrinkingWaterConsumptionRate4[L/yr]	Drinking water consumption rate for teen (liters per year)
291	gen_dwc5	DrinkingWaterConsumptionRate5[L/yr]	Drinking water consumption rate for adult:ICRP72 (liters per year)
261	gen_firC	FruitIrrigationRateCB[in/yr]	Fruit irrigation rate for current biosphere (liters per year)
247	gen_firP	FruitIrrigationRatePB[in/yr]	Fruit irrigation rate for pluvial biosphere (liters per year)

Description of Abbreviations Used for TPA Version 4.1 Code Sampled Input Parameters

Parameter Identification	Short Name	Full Name	Description
268	gen_fitC	FruitIrrigationTimeCB[mo/yr]	Fruit irrigation time for current biosphere (months per year)
254	gen_fitP	FruitIrrigationTimePB[mo/yr]	Fruit irrigation time for pluvial biosphere (months per year)
262	gen_girC	GrainIrrigationRateCB[in/yr]	Grain irrigation rate for current biosphere (liters per year)
248	gen_girP	GrainIrrigationRatePB[in/yr]	Grain irrigation rate for pluvial biosphere (liters per year)
269	gen_gitC	GrainIrrigationTimeCB[mo/yr]	Grain irrigation time for current biosphere (months per year)
255	gen_gitP	GrainIrrigationTimePB[mo/yr]	Grain irrigation time for pluvial biosphere (months per year)
274	gen_hfgt	HenFeedGrowTime[day]	Egg-laying hen feed growing time (day)
263	gen_hirC	HomeIrrigationRateCB[in/yr]	Residential irrigation rate for current biosphere (liters per year)

Description of Abbreviations Used for TPA Version 4.1 Code Sampled Input Parameters

Parameter Identification	Short Name	Full Name	Description
249	gen_hirP	HomeIrrigationRatePB[in/yr]	Residential irrigation rate for pluvial biosphere (liters per year)
270	gen_hitC	HomeIrrigationTimeCB[mo/yr]	Residential irrigation time for current biosphere (months per year)
256	gen_hitP	HomeIrrigationTimePB[mo/yr]	Residential irrigation time for pluvial biosphere (months per year)
244	gen_ifi	InterceptionFraction/Irrigate	Irrigation interception fraction
245	gen_lirP	LeafyVegetableIrrigationRatePB[in/yr]	Leafy vegetable irrigation rate for pluvial biosphere (inches per year)
276	gen_mfdf	MilkFreshForageDietFraction	Dairy cattle fresh forage diet fraction
278	gen_mfgt	MilkFreshForageGrowTime[day]	Dairy cattle fresh forage growing time (day)
246	gen_oirP	OtherVegetableIrrigationRatePB[in/yr]	Other vegetable irrigation rate for pluvial biosphere (liters per year)
273	gen_pfgt	PoultryFeedGrowTime[day]	Poultry feed growing time (day)

Description of Abbreviations Used for TPA Version 4.1 Code Sampled Input Parameters

Parameter Identification	Short Name	Full Name	Description
283	genbfirC	BeefFreshForageIrrigationRateCB[in/yr]	Beef cattle fresh forage irrigation rate for current biosphere (inches per year)
279	genbfirP	BeefFreshForageIrrigationRatePB[in/yr]	Beef cattle fresh forage irrigation rate for pluvial biosphere (liters per year)
285	genbfitC	BeefFreshForageIrrigationTimeCB[mo/yr]	Beef cattle fresh forage irrigation time for current biosphere (months per year)
281	genbfitP	BeefFreshForageIrrigationTimePB[mo/yr]	Beef cattle fresh forage irrigation time for pluvial biosphere (months per year)
265	genhfirC	HenFeedIrrigationRateCB[in/yr]	Egg-laying hen feed irrigation rate for current biosphere (liters per year)
251	genhfirP	HenFeedIrrigationRatePB[in/yr]	Egg-laying hen feed irrigation rate for pluvial biosphere (liters per year)
272	genhfitC	HenFeedIrrigationTimeCB[mo/yr]	Egg-laying hen feed irrigation time for current biosphere (months per year)

Description of Abbreviations Used for TPA Version 4.1 Code Sampled Input Parameters

Parameter Identification	Short Name	Full Name	Description
258	genhfitP	HenFeedIrrigationTimePB[mo/yr]	Egg-laying hen feed irrigation time for pluvial biosphere (months per year)
259	genlvirC	LeafyVegetableIrrigationRateCB[in/yr]	Leafy vegetable irrigation rate for current biosphere (liters per year)
266	genlvitC	LeafyVegetableIrrigationTimeCB[mo/yr]	Leafy vegetable irrigation time for current biosphere (months per year)
252	genlvitP	LeafyVegetableIrrigationTimePB[mo/yr]	Leafy vegetable irrigation time for pluvial biosphere (months per year)
284	genmfirC	MilkFreshForageIrrigationRateCB[in/yr]	Dairy cattle fresh forage irrigation rate for current biosphere (liters per year)
280	genmfirP	MilkFreshForageIrrigationRatePB[in/yr]	Milk fresh forage irrigation rate for pluvial biosphere (liters per year)
286	genmfitC	MilkFreshForageIrrigationTimeCB[mo/yr]	Dairy cattle fresh forage irrigation time for current biosphere (months per year)

Description of Abbreviations Used for TPA Version 4.1 Code Sampled Input Parameters

Parameter Identification	Short Name	Full Name	Description
282	genmfitP	MilkFreshForageIrrigationTimePB[mo/yr]	Dairy cattle fresh forage irrigation time for pluvial biosphere (months per year)
260	genovirC	OtherVegetableIrrigationRateCB[in/yr]	Other vegetable irrigation rate for current biosphere (liters per year)
267	genovitC	OtherVegetableIrrigationTimeCB[mo/yr]	Other vegetable irrigation time for current biosphere (months per year)
253	genovitP	OtherVegetableIrrigationTimePB[mo/yr]	Other vegetable irrigation time for pluvial biosphere (months per year)
264	genpfirC	PoultryFeedIrrigationRateCB[in/yr]	Poultry feed irrigation rate for current biosphere (liters per year)
250	genpfirP	PoultryFeedIrrigationRatePB[in/yr]	Poultry feed irrigation rate for pluvial biosphere (liters per year)
271	genpfitC	PoultryFeedIrrigationTimeCB[mo/yr]	Poultry feed irrigation time for current biosphere (months per year)
257	genpfitP	PoultryFeedIrrigationTimePB[mo/yr]	Poultry feed irrigation time for pluvial biosphere (months per year)

Description of Abbreviations Used for TPA Version 4.1 Code Sampled Input Parameters

Parameter Identification	Short Name	Full Name	Description
9	H2O-FThk	ThicknessOfWaterFilm[m]	Thickness of water film on waste package surface
223	IPPFSTFF	ImmobilePorosityPenetrationFraction_STFF	Effective fraction of saturated rock matrix accessible to matrix diffusion; during the time scale for transport from source to receptor, used to calculate effective immobile porosity and matrix diffusion mass-transfer rate coefficient in NEFTRAN
64	InitRSFP	InitialRadiusOfSFParticle[m]	Initial radius of spent nuclear fuel particle—affects spent nuclear fuel alteration rate and transport out of a failed waste package in EBSREL
131	InvMPerm	InvertMatrixPermeability[m^2]	Matrix permeability of the invert
2	MAPM@GM	MeanAveragePrecipitationMultiplierAtGlacialMaximum	Mean annual precipitation increase at glacial maximum—affects infiltration from the land surface in UZFLOW

Description of Abbreviations Used for TPA Version 4.1 Code Sampled Input Parameters

Parameter Identification	Short Name	Full Name	Description
3	MATI@GM	MeanAverageTemperatureIncreaseAtGlacialMaximum[degC]	Magnitude of mean annual temperature change at glacial maximum—affects infiltration from the land surface in UZFLOW
151	MKD_BFwU	MatrixKD_BFw_U[m3/kg]	Bullfrog-welded matrix K_d for uranium
147	MKD_CHvU	MatrixKD_CHnvU[m3/kg]	Calico Hills-nonwelded vitric matrix K_d for uranium
148	MKD_CHzU	MatrixKD_CHnzU[m3/kg]	Calico Hills-nonwelded zeolitic matrix K_d for uranium
149	MKD_PPwU	MatrixKD_PPw_U[m3/kg]	Prow Pass-welded matrix K_d for uranium
146	MKD_TSwU	MatrixKD_TSw_U[m3/kg]	Topopah Spring-welded matrix K_d for uranium
150	MKD_UCFU	MatrixKD_UCF_U[m3/kg]	Upper Crater Flat matrix K_d for uranium
137	MKDBFwAm	MatrixKD_BFw_Am[m3/kg]	Bullfrog-welded matrix K_d for americium
186	MKDBFwCs	MatrixKD_BFw_Cs[m3/kg]	Bullfrog-welded matrix K_d for cesium

Description of Abbreviations Used for TPA Version 4.1 Code Sampled Input Parameters

Parameter Identification	Short Name	Full Name	Description
193	MKDBFwNi	MatrixKD_BFw_Ni[m3/kg]	Bullfrog-welded matrix K_d for nickel
144	MKDBFwNp	MatrixKD_BFw_Np[m3/kg]	Bullfrog-welded matrix K_d for neptunium
179	MKDBFwPb	MatrixKD_BFw_Pb[m3/kg]	Bullfrog-welded matrix K_d for lead
158	MKDBFwPu	MatrixKD_BFw_Pu[m3/kg]	Bullfrog-welded matrix K_d for plutonium
172	MKDBFwRa	MatrixKD_BFw_Ra[m3/kg]	Bullfrog-welded matrix K_d for radium
200	MKDBFwSe	MatrixKD_BFw_Se[m3/kg]	Bullfrog-welded matrix K_d for selenium
165	MKDBFwTh	MatrixKD_BFw_Th[m3/kg]	Bullfrog-welded matrix K_d for thorium
133	MKDCHvAm	MatrixKD_CHnvAm[m3/kg]	Calico Hills-nonwelded vitric matrix K_d for americium
182	MKDCHvCs	MatrixKD_CHnvCs[m3/kg]	Calico Hills-nonwelded vitric matrix K_d for cesium
189	MKDCHvNi	MatrixKD_CHnvNi[m3/kg]	Calico Hills-nonwelded vitric matrix K_d for nickel
140	MKDCHvNp	MatrixKD_CHnvNp[m3/kg]	Calico Hills-nonwelded vitric matrix K_d for neptunium

Description of Abbreviations Used for TPA Version 4.1 Code Sampled Input Parameters

Parameter Identification	Short Name	Full Name	Description
175	MKDCHvPb	MatrixKD_CHnvPb[m3/kg]	Calico Hills-nonwelded vitric matrix K_d for lead
154	MKDCHvPu	MatrixKD_CHnvPu[m3/kg]	Calico Hills-nonwelded vitric matrix K_d for plutonium
168	MKDCHvRa	MatrixKD_CHnvRa[m3/kg]	Calico Hills-nonwelded vitric matrix K_d for radium
196	MKDCHvSe	MatrixKD_CHnvSe[m3/kg]	Calico Hills-nonwelded vitric matrix K_d for selenium
161	MKDCHvTh	MatrixKD_CHnvTh[m3/kg]	Calico Hills-nonwelded vitric matrix K_d for thorium
134	MKDCHzAm	MatrixKD_CHnzAm[m3/kg]	Calico Hills-nonwelded zeolitic matrix K_d for americium
183	MKDCHzCs	MatrixKD_CHnzCs[m3/kg]	Calico Hills-nonwelded zeolitic matrix K_d for cesium
190	MKDCHzNi	MatrixKD_CHnzNi[m3/kg]	Calico Hills-nonwelded zeolitic matrix K_d for nickel
141	MKDCHzNp	MatrixKD_CHnzNp[m3/kg]	Calico Hills-nonwelded zeolitic matrix K_d for neptunium

Description of Abbreviations Used for TPA Version 4.1 Code Sampled Input Parameters

Parameter Identification	Short Name	Full Name	Description
176	MKDCHzPb	MatrixKD_CHnzPb[m3/kg]	Calico Hills-nonwelded zeolitic matrix K_d for lead
155	MKDCHzPu	MatrixKD_CHnzPu[m3/kg]	Calico Hills-nonwelded zeolitic matrix K_d for plutonium
169	MKDCHzRa	MatrixKD_CHnzRa[m3/kg]	Calico Hills-nonwelded zeolitic matrix K_d for radium
197	MKDCHzSe	MatrixKD_CHnzSe[m3/kg]	Calico Hills-nonwelded zeolitic matrix K_d for selenium
162	MKDCHzTh	MatrixKD_CHnzTh[m3/kg]	Calico Hills-nonwelded zeolitic matrix K_d for thorium
135	MKDPPwAm	MatrixKD_PPw_Am[m3/kg]	Prow Pass-welded matrix K_d for americium
184	MKDPPwCs	MatrixKD_PPw_Cs[m3/kg]	Prow Pass-welded matrix K_d for cesium
191	MKDPPwNi	MatrixKD_PPw_Ni[m3/kg]	Prow Pass-welded matrix K_d for nickel
142	MKDPPwNp	MatrixKD_PPw_Np[m3/kg]	Prow Pass-welded matrix K_d for neptunium
177	MKDPPwPb	MatrixKD_PPw_Pb[m3/kg]	Prow Pass-welded matrix K_d for lead

Description of Abbreviations Used for TPA Version 4.1 Code Sampled Input Parameters

Parameter Identification	Short Name	Full Name	Description
156	MKDPPwPu	MatrixKD_PPw_Pu[m3/kg]	Prow Pass-welded matrix K_d for plutonium
170	MKDPPwRa	MatrixKD_PPw_Ra[m3/kg]	Prow Pass-welded matrix K_d for radium
198	MKDPPwSe	MatrixKD_PPw_Se[m3/kg]	Prow Pass-welded matrix K_d for selenium
163	MKDPPwTh	MatrixKD_PPw_Th[m3/kg]	Prow Pass-welded matrix K_d for thorium
132	MKDTSwAm	MatrixKD_TSw_Am[m3/kg]	Topopah Spring-welded matrix K_d for americium
181	MKDTSwCs	MatrixKD_TSw_Cs[m3/kg]	Topopah Spring-welded matrix K_d for cesium
188	MKDTSwNi	MatrixKD_TSw_Ni[m3/kg]	Topopah Spring-welded matrix K_d for nickel
139	MKDTSwNp	MatrixKD_TSw_Np[m3/kg]	Topopah Spring-welded matrix K_d for neptunium
174	MKDTSwPb	MatrixKD_TSw_Pb[m3/kg]	Topopah Spring-welded matrix K_d for lead
153	MKDTSwPu	MatrixKD_TSw_Pu[m3/kg]	Topopah Spring-welded matrix K_d for plutonium
167	MKDTSwRa	MatrixKD_TSw_Ra[m3/kg]	Topopah Spring-welded matrix K_d for radium

Description of Abbreviations Used for TPA Version 4.1 Code Sampled Input Parameters

Parameter Identification	Short Name	Full Name	Description
195	MKDTSwSe	MatrixKD_TSw_Se[m3/kg]	Topopah Spring-welded matrix K_d for selenium
160	MKDTSwTh	MatrixKD_TSw_Th[m3/kg]	Topopah Spring-welded matrix K_d for thorium
136	MKDUCFAm	MatrixKD_UCF_Am[m3/kg	Upper Crater Flat matrix K_d for americium
185	MKDUCFCs	MatrixKD_UCF_Cs[m3/kg]	Upper Crater Flat matrix K_d for cesium
192	MKDUCFNi	MatrixKD_UCF_Ni[m3/kg]	Upper Crater Flat matrix K_d for nickel
143	MKDUCFNp	MatrixKD_UCF_Np[m3/kg]	Upper Crater Flat matrix K_d for neptunium
178	MKDUCFPb	MatrixKD_UCF_Pb[m3/kg]	Upper Crater Flat matrix K_d for lead
157	MKDUCFPu	MatrixKD_UCF_Pu[m3/kg]	Upper Crater Flat matrix K_d for plutonium
171	MKDUCFRa	MatrixKD_UCF_Ra[m3/kg]	Upper Crater Flat matrix K_d for radium
199	MKDUCFSe	MatrixKD_UCF_Se[m3/kg]	Upper Crater Flat matrix K_d for selenium
164	MKDUCFTh	MatrixKD_UCF_Th[m3/kg]	Upper Crater Flat matrix K_d for thorium

Description of Abbreviations Used for TPA Version 4.1 Code Sampled Input Parameters

Parameter Identification	Short Name	Full Name	Description
152	MKDUFZ_U	MatrixKD_UFZ_U[m3/kg]	Unsaturated Fracture Zone matrix K_d for uranium
138	MKDUFZAm	MatrixKD_UFZ_Am[m3/kg]	Unsaturated Fracture Zone matrix K_d for americium
187	MKDUFZCs	MatrixKD_UFZ_Cs[m3/kg]	Unsaturated Fracture Zone matrix Kd for cesium
194	MKDUFZNi	MatrixKD_UFZ_Ni[m3/kg]	Unsaturated Fracture Zone matrix K_d for nickel
145	MKDUFZNp	MatrixKD_UFZ_Np[m3/kg]	Unsaturated Fracture Zone matrix K_d for neptunium
180	MKDUFZPb	MatrixKD_UFZ_Pb[m3/kg]	Unsaturated Fracture Zone matrix K_d for lead
159	MKDUFZPu	MatrixKD_UFZ_Pu[m3/kg]	Unsaturated Fracture Zone matrix K_d for plutonium
173	MKDUFZRa	MatrixKD_UFZ_Ra[m3/kg]	Unsaturated Fracture Zone matrix K_d for radium
201	MKDUFZSe	MatrixKD_UFZ_Se[m3/kg]	Unsaturated Fracture Zone matrix K_d for selenium

Description of Abbreviations Used for TPA Version 4.1 Code Sampled Input Parameters

Parameter Identification	Short Name	Full Name	Description
166	MKDUFZTh	MatrixKD_UFZ_Th[m3/kg]	Unsaturated Fracture Zone matrix K_d for thorium
207	MPrm_BFw	MatrixPermeability_BFw_[m2]	Bullfrog-welded matrix permeability
203	MPrm_CHv	MatrixPermeability_CHnv[m2]	Calico Hills-nonwelded vitric matrix permeability
204	MPrm_CHz	MatrixPermeability_CHnz[m2]	Calico Hills-nonwelded zeolitic matrix permeability
205	MPrm_PPw	MatrixPermeability_PPw_[m2]	Prow Pass-welded matrix permeability
202	MPrm_TSw	MatrixPermeability_TSw_[m2]	Topopah Spring-welded matrix permeability
206	MPrm_UCF	MatrixPermeability_UCF_[m2]	Upper Crater Flat matrix permeability
208	MPrm_UFZ	MatrixPermeability_UFZ_[m2]	Unsaturated Fracture Zone matrix permeability
242	MixZnT20	MixingZoneThickness20km[m]	Mixing zone thickness at 20 km [12.4 mi].
314	NEFZnW	NEFaultZoneWidth[m]	Northeast fault zone width
316	NELCDAmt	NEAmountOfLargestCredibleDisplacement[m]	Northeast largest credible displacement

Description of Abbreviations Used for TPA Version 4.1 Code Sampled Input Parameters

Parameter Identification	Short Name	Full Name	Description
313	NWFZnW	NWFaultZoneWidth[m]	Northwest fault zone width
315	NWLCDAmt	NWAmountOfLargestCredibleDisplacement[m]	Northwest largest credible displacement
63	PSFDM1	Preexponential_SFDissolutionModel2	Preexponential factor for spent nuclear fuel dissolution rate from (mg m^{-2} d^{-1})
243	PWPRRG20	PluvialWellPumpingRateAtReceptorGroup20km[gal/day]	Well pumping rate at 20 km [12.4 milocation during pluvial period [gal/day]
240	PlumeTh5	PlumeThickness5km[m]	Plume thickness at 5 km [3.1 mi]
61	SbArWt%	SubAreaWetFraction	Subarea wet fraction
65	SbGFRATF	SubGrainFragmentRadiusAfterTransFrac[m]	Subgrain fragment radius of UO$_2$ particle after transgranular fracture; used only if fuel conversion takes place from UO$_2$ to UO$_{2.4}$ and U$_3$O$_8$; used only by the spent nuclear fuel dissolution models dependent on exposed surface area

Description of Abbreviations Used for TPA Version 4.1 Code Sampled Input Parameters

Parameter Identification	Short Name	Full Name	Description
121	SFWt%C1	SFWettedFraction_Corrosion_1	Spent nuclear fuel wet fraction for corrosion failures in subarea 1
122	SFWt%C2	SFWettedFraction_Corrosion_2	Spent nuclear fuel wet fraction for corrosion failures in subarea 2
123	SFWt%C3	SFWettedFraction_Corrosion_3	Spent nuclear fuel wet fraction for corrosion failures in subarea 3
124	SFWt%C4	SFWettedFraction_Corrosion_4	Spent nuclear fuel wet fraction for corrosion failures in subarea 4
125	SFWt%C5	SFWettedFraction_Corrosion_5	Spent nuclear fuel wet fraction for corrosion failures in subarea 5
126	SFWt%C6	SFWettedFraction_Corrosion_6	Spent nuclear fuel wet fraction for corrosion failures in subarea 6
127	SFWt%C7	SFWettedFraction_Corrosion_7	Spent nuclear fuel wet fraction for corrosion failures in subarea 7
128	SFWFC1	SFWettedFraction_Corrosion_8	Spent nuclear fuel wet fraction for corrosion failures in subarea 8

Description of Abbreviations Used for TPA Version 4.1 Code Sampled Input Parameters

Parameter Identification	Short Name	Full Name	Description
129	SFWt%C9	SFWettedFraction_Corrosion_9	Spent nuclear fuel wet fraction for corrosion failures in subarea 9
130	SFWt%C10	SFWettedFraction_Corrosion_10	Spent nuclear fuel wet fraction for corrosion failures in subarea 10
79	SFWt%F0	SFWettedFraction_FAULTO	Spent nuclear fuel wet fraction for faulting failures
69	SFWt%I1	SFWettedFraction_Initial_1	Spent nuclear fuel wet fraction for initial failures in subarea 1
70	SFWt%I2	SFWettedFraction_Initial_2	Spent nuclear fuel wet fraction for initial failures in subarea 2
71	SFWt%I3	SFWettedFraction_Initial_3	Spent nuclear fuel wet fraction for initial failures in subarea 3
72	SFWt%I4	SFWettedFraction_Initial_4	Spent nuclear fuel wet fraction for initial failures in subarea 4
73	SFWt%I5	SFWettedFraction_Initial_5	Spent nuclear fuel wet fraction for initial failures in subarea 5

Description of Abbreviations Used for TPA Version 4.1 Code Sampled Input Parameters

Parameter Identification	Short Name	Full Name	Description
74	SFWt%I6	SFWettedFraction_Initial_6	Spent nuclear fuel wet fraction for initial failures in subarea 6
75	SFWt%I7	SFWettedFraction_Initial_7	Spent nuclear fuel wet fraction for initial failures in subarea 7
76	SFWFI1	SFWettedFraction_Initial_8	Spent nuclear fuel wet fraction for initial failures in subarea 8
77	SFWt%I9	SFWettedFraction_Initial_9	Spent nuclear fuel wet fraction for initial failures in subarea 9
78	SFWt%I10	SFWettedFraction_Initial_10	Spent nuclear fuel wet fraction for initial failures in subarea 10
81	SFWt%S11	SFWettedFraction_SEISMO1_1	Spent nuclear fuel wet fraction for seismic failures for seismic interval 1 in subarea 1
82	SFWt%S12	SFWettedFraction_SEISMO1_2	Spent nuclear fuel wet fraction for seismic failures for seismic interval 1 in subarea 2

Description of Abbreviations Used for TPA Version 4.1 Code Sampled Input Parameters

Parameter Identification	Short Name	Full Name	Description
83	SFWt%S13	SFWettedFraction_SEISMO1_3	Spent nuclear fuel wet fraction for seismic failures for seismic interval 1 in subarea 3
84	SFWt%S14	SFWettedFraction_SEISMO1_4	Spent nuclear fuel wet fraction for seismic failures for seismic interval 1 in subarea 4
85	SFWt%S15	SFWettedFraction_SEISMO1_5	Spent nuclear fuel wet fraction for seismic failures for seismic interval 1 in subarea 5
86	SFWt%S16	SFWettedFraction_SEISMO1_6	Spent nuclear fuel wet fraction for seismic failures for seismic interval 1 in subarea 6
87	SFWt%S17	SFWettedFraction_SEISMO1_7	Spent nuclear fuel wet fraction for seismic failures for seismic interval 1 in subarea 7
88	SFWFSEIS	SFWettedFraction_SEISMO1_8	Spent nuclear fuel wet fraction for seismic failures for seismic interval 1 in subarea 8

Description of Abbreviations Used for TPA Version 4.1 Code Sampled Input Parameters

Parameter Identification	Short Name	Full Name	Description
89	SFWt%S19	SFWettedFraction_SEISMO1_9	Spent nuclear fuel wet fraction for seismic failures for seismic interval 1 in subarea 9
80	SFWt%S1A	SFWettedFraction_SEISMO1_10	Spent nuclear fuel wet fraction for seismic failures for seismic interval 1 in subarea 10
91	SFWt%S21	SFWettedFraction_SEISMO2_1	Spent nuclear fuel wet fraction for seismic failures for seismic interval 2 in subarea 1
92	SFWt%S22	SFWettedFraction_SEISMO2_2	Spent nuclear fuel wet fraction for seismic failures for seismic interval 2 in subarea 2
93	SFWt%S23	SFWettedFraction_SEISMO2_3	Spent nuclear fuel wet fraction for seismic failures for seismic interval 2 in subarea 3
94	SFWt%S24	SFWettedFraction_SEISMO2_4	Spent nuclear fuel wet fraction for seismic failures for seismic interval 2 in subarea 4

Description of Abbreviations Used for TPA Version 4.1 Code Sampled Input Parameters

Parameter Identification	Short Name	Full Name	Description
95	SFWt%S25	SFWettedFraction_SEISMO2_5	Spent nuclear fuel wet fraction for seismic failures for seismic interval 2 in subarea 5
96	SFWt%S26	SFWettedFraction_SEISMO2_6	Spent nuclear fuel wet fraction for seismic failures for seismic interval 2 in subarea 6
97	SFWt%S27	SFWettedFraction_SEISMO2_7	Spent nuclear fuel wet fraction for seismic failures for seismic interval 2 in subarea 7
98	SFWFSEI	SFWettedFraction_SEISMO2_8	Spent nuclear fuel wet fraction for seismic failures for seismic interval 2 in subarea 8
99	SFWt%S29	SFWettedFraction_SEISMO2_9	Spent nuclear fuel wet fraction for seismic failures for seismic interval 2 in subarea 9
100	SFWt%S2A	SFWettedFraction_SEISMO2_10	Spent nuclear fuel wet fraction for seismic failures for seismic interval 2 in subarea 10

Description of Abbreviations Used for TPA Version 4.1 Code Sampled Input Parameters

Parameter Identification	Short Name	Full Name	Description
101	SFWt%S31	SFWettedFraction_SEISMO3_1	Spent nuclear fuel wet fraction for seismic failures for seismic interval 3 in subarea 1
102	SFWt%S32	SFWettedFraction_SEISMO3_2	Spent nuclear fuel wet fraction for seismic failures for seismic interval 3 in subarea 2
103	SFWt%S33	SFWettedFraction_SEISMO3_3	Spent nuclear fuel wet fraction for seismic failures for seismic interval 3 in subarea 3
104	SFWt%S34	SFWettedFraction_SEISMO3_4	Spent nuclear fuel wet fraction for seismic failures for seismic interval 3 in subarea 4
105	SFWt%S35	SFWettedFraction_SEISMO3_5	Spent nuclear fuel wet fraction for seismic failures for seismic interval 3 in subarea 5
106	SFWt%S36	SFWettedFraction_SEISMO3_6	Spent nuclear fuel wet fraction for seismic failures for seismic interval 3 in subarea 6

Description of Abbreviations Used for TPA Version 4.1 Code Sampled Input Parameters

Parameter Identification	Short Name	Full Name	Description
107	SFWt%S37	SFWettedFraction_SEISMO3_7	Spent nuclear fuel wet fraction for seismic failures for seismic interval 3 in subarea 7
108	SFWFSEI6	SFWettedFraction_SEISMO3_8	Spent nuclear fuel wet fraction for seismic failures for seismic interval 3 in subarea 8
109	SFWt%S39	SFWettedFraction_SEISMO3_9	Spent nuclear fuel wet fraction for seismic failures for seismic interval 3 in subarea 9
110	SFWt%S3A	SFWettedFraction_SEISMO3_10	Spent nuclear fuel wet fraction for seismic failures for seismic interval 3 in subarea 10
111	SFWt%S41	SFWettedFraction_SEISMO4_1	Spent nuclear fuel wet fraction for seismic failures for seismic interval 4 in subarea 1
112	SFWt%S42	SFWettedFraction_SEISMO4_2	Spent nuclear fuel wet fraction for seismic failures for seismic interval 4 in subarea 2

Description of Abbreviations Used for TPA Version 4.1 Code Sampled Input Parameters

Parameter Identification	Short Name	Full Name	Description
113	SFWt%S43	SFWettedFraction_SEISMO4_3	Spent nuclear fuel wet fraction for seismic failures for seismic interval 4 in subarea 3
114	SFWt%S44	SFWettedFraction_SEISMO4_4	Spent nuclear fuel wet fraction for seismic failures for seismic interval 4 in subarea 4
115	SFWt%S45	SFWettedFraction_SEISMO4_5	Spent nuclear fuel wet fraction for seismic failures for seismic interval 4 in subarea 5
116	SFWt%S46	SFWettedFraction_SEISMO4_6	Spent nuclear fuel wet fraction for seismic failures for seismic interval 4 in subarea 6
117	SFWt%S47	SFWettedFraction_SEISMO4_7	Spent nuclear fuel wet fraction for seismic failures for seismic interval 4 in subarea 7
118	SFWFSEI9	SFWettedFraction_SEISMO4_8	Spent nuclear fuel wet fraction for seismic failures for seismic interval 4 in subarea 8

Description of Abbreviations Used for TPA Version 4.1 Code Sampled Input Parameters

Parameter Identification	Short Name	Full Name	Description
119	SFWt%S49	SFWettedFraction_SEISMO4_9	Spent nuclear fuel wet fraction for seismic failures for seismic interval 4 in subarea 9
120	SFWt%S4A	SFWettedFraction_SEISMO4_10	Spent nuclear fuel wet fraction for seismic failures for seismic interval 4 in subarea 10
80	SFWt%V0	SFWettedFraction_VOLCANO	Spent nuclear fuel wet fraction for volcanic failures
66	Solbl-Am	SolubilityAm[kg/m3]	Solubility limit for americium
67	Solbl-Np	SolubilityNp[kg/m3]	Solubility limit for neptunium
68	Solbl-Pu	SolubilityPu[kg/m3]	Solubility limit for plutonium
15	SSMO-JS1	SEISMOJointSpacing1[m]	Joint spacing for rock condition 1. Not all rocks falling from roof of emplacement will impact waste packages. Effective size of rock that impacts waste packages will be controlled by joint spacing.

Description of Abbreviations Used for TPA Version 4.1 Code Sampled Input Parameters

Parameter Identification	Short Name	Full Name	Description
16	SSMO-JS2	SEISMOJointSpacing2[m]	Joint spacing for rock condition 2
17	SSMO-JS3	SEISMOJointSpacing3[m]	Joint spacing for rock condition 3
18	SSMO-JS4	SEISMOJointSpacing4[m]	Joint spacing for rock condition 4
19	SSMO-JS5	SEISMOJointSpacing5[m]	Joint spacing for rock condition 5
13	SSMO-RE	RockModulusOfElasticityforSEISMO[Pa]	Rock modulus of elasticity
14	SSMO-RPR	RockPoissonRatioforSEISMO[]	Rock poisson ratio
20	SSMOV201	VerticalExtentOfRockFall2_1[m]	Vertical extent of rockfall for rock condition 2 and ground acceleration 0.05g. Lower limit approximately equivalent to average rock joint spacing of rock condition 1. Upper limit estimated from numerical results.
21	SSMOV202	VerticalExtentOfRockFall2_2[m]	Same as above except with ground acceleration 0.10g
22	SSMOV203	VerticalExtentOfRockFall2_3[m]	Same as above except with ground acceleration 0.15g

Description of Abbreviations Used for TPA Version 4.1 Code Sampled Input Parameters

Parameter Identification	Short Name	Full Name	Description
23	SSMOV204	VerticalExtentOfRockFall2_4[m]	Same as above except with ground acceleration 0.20g
24	SSMOV205	VerticalExtentOfRockFall2_5[m]	Same as above except with ground acceleration 0.25g
25	SSMOV206	VerticalExtentOfRockFall2_6[m]	Same as above except with ground acceleration 0.30g
26	SSMOV207	VerticalExtentOfRockFall2_7[m]	Same as above except with ground acceleration 0.35g
27	SSMOV208	VerticalExtentOfRockFall2_8[m]	Same as above except with ground acceleration 0.40g
28	SSMOV209	VerticalExtentOfRockFall2_9[m]	Same as above except with ground acceleration 0.45g
29	SSMOV210	VerticalExtentOfRockFall2_10[m]	Same as above except with ground acceleration 0.50g
30	SSMOV301	VerticalExtentOfRockFall3_1[m]	Vertical extent of rockfall for rock condition 3 and ground acceleration 0.05g

Description of Abbreviations Used for TPA Version 4.1 Code Sampled Input Parameters

Parameter Identification	Short Name	Full Name	Description
31	SSMOV302	VerticalExtentOfRockFall3_2[m]	Same as above except with ground acceleration 0.10g
32	SSMOV303	VerticalExtentOfRockFall3_3[m]	Same as above except with ground acceleration 0.15g
33	SSMOV304	VerticalExtentOfRockFall3_4[m]	Same as above except with ground acceleration 0.20g
34	SSMOV305	VerticalExtentOfRockFall3_5[m]	Same as above except with ground acceleration 0.25g
35	SSMOV306	VerticalExtentOfRockFall3_6[m]	Same as above except with ground acceleration 0.30g
36	SSMOV307	VerticalExtentOfRockFall3_7[m]	Same as above except with ground acceleration 0.35g
37	SSMOV308	VerticalExtentOfRockFall3_8[m]	Same as above except with ground acceleration 0.40g
38	SSMOV309	VerticalExtentOfRockFall3_9[m]	Same as above except with ground acceleration 0.45g

Description of Abbreviations Used for TPA Version 4.1 Code Sampled Input Parameters

Parameter Identification	Short Name	Full Name	Description
39	SSMOV310	VerticalExtentOfRockFall3_10[m]	Same as above except with ground acceleration 0.50g
40	SSMOV401	VerticalExtentOfRockFall4_1[m]	Vertical extent of rockfall for rock condition 4 and ground acceleration 0.05g
41	SSMOV402	VerticalExtentOfRockFall4_2[m]	Same as above except with ground acceleration 0.10g
42	SSMOV403	VerticalExtentOfRockFall4_3[m]	Same as above except with ground acceleration 0.15g
43	SSMOV404	VerticalExtentOfRockFall4_4[m]	Same as above except with ground acceleration 0.20g
44	SSMOV405	VerticalExtentOfRockFall4_5[m]	Same as above except with ground acceleration 0.25g
45	SSMOV406	VerticalExtentOfRockFall4_6[m]	Same as above except with ground acceleration 0.30g
46	SSMOV407	VerticalExtentOfRockFall4_7[m]	Same as above except with ground acceleration 0.35g

Description of Abbreviations Used for TPA Version 4.1 Code Sampled Input Parameters

Parameter Identification	Short Name	Full Name	Description
47	SSMOV408	VerticalExtentOfRockFall4_8[m]	Same as above except with ground acceleration 0.40g
48	SSMOV409	VerticalExtentOfRockFall4_9[m]	Same as above except with ground acceleration 0.45g
49	SSMOV410	VerticalExtentOfRockFall4_10[m]	Same as above except with ground acceleration 0.50g
50	SSMOV501	VerticalExtentOfRockFall5_1[m]	Vertical extent of rockfall for rock condition 5 and ground acceleration 0.05g
51	SSMOV502	VerticalExtentOfRockFall5_2[m]	Same as above except with ground acceleration 0.10g
52	SSMOV503	VerticalExtentOfRockFall5_3[m]	Same as above except with ground acceleration 0.15g
53	SSMOV504	VerticalExtentOfRockFall5_4[m]	Same as above except with ground acceleration 0.20g
54	SSMOV505	VerticalExtentOfRockFall5_5[m]	Same as above except with ground acceleration 0.25g

Description of Abbreviations Used for TPA Version 4.1 Code Sampled Input Parameters

Parameter Identification	Short Name	Full Name	Description
55	SSMOV506	VerticalExtentOfRockFall5_6[m]	Same as above except with ground acceleration 0.30g
56	SSMOV507	VerticalExtentOfRockFall5_7[m]	Same as above except with ground acceleration 0.35g
57	SSMOV508	VerticalExtentOfRockFall5_8[m]	Same as above except with ground acceleration 0.40g
58	SSMOV509	VerticalExtentOfRockFall5_9[m]	Same as above except with ground acceleration 0.45g
59	SSMOV510	VerticalExtentOfRockFall5_10[m]	Same as above except with ground acceleration 0.50g
6	TempGrBI	TemperatureGradientInVicinityOfBoilingIsotherm[K/m]	Temperature gradient in vicinity of boiling isotherm, (parameter specific to reflux3 model)
322	VC-Dia	DiameterOfVolcanicCone[m]	Cone diameter
319	VD-Angle	AngleOfVolcanicDikeMeasuredFromNorthClockwise[degrees]	Volcanic dike angle
320	VD-Length	LengthOfVolcanicDike[m]	Volcanic dike length
321	VD-Width	WidthOfVolcanicDike[m]	Volcanic dike width
326	VE-Durat	VolcanicEventDuration[s]	Volcanic event duration

Description of Abbreviations Used for TPA Version 4.1 Code Sampled Input Parameters

Parameter Identification	Short Name	Full Name	Description
327	VE-Power	VolcanicEventPower[W]	Volcanic event power
318	VEi/e-R#	RNtoDetermineIfExtrusiveOrIntrusiveVolcanicEvent	Random number to determine volcanic event type
317	VEROI-Tn	TimeOfNextVolcanicEventinRegionOfInterest[yr]	Time of next volcanic event
325	WindSpd	WindSpeed[cm/s]	Wind speed
62	WP-Def%	DefectiveFractionOfWPs/cell	Fraction of total waste packages in a subarea that fail at time = 0
309	WPFD-ThD	ThresholdDisplacementforFaultDisruptionOfWP[m]	Threshold fault displacement for disruption. Data input order: number of fault displacement values to be provided followed by equiprobable displacement values
60	WPFlowMF	WastePackageFlowMultiplicationFactor	Factor that is multiplied by flow rate hitting waste package. Resulting flow rates written to ebsflow.dat, which is an input file to releaset.f stand-alone code

Description of Abbreviations Used for TPA Version 4.1 Code Sampled Input Parameters

Parameter Identification	Short Name	Full Name	Description
324	WPMeFail	NumberOfMagmaInducedMechanicalFailuresRemainingInDrift[]	Number of waste package that fail during intrusive event and remain in disrupted drifts (process-based model)
238	WPRRG@10	WellPumpingRateAtReceptorGroup10km[gal/day]	Well-pumping rate for residential receptor group located less than 10 km [6.2 mi] from Yucca Mountain
239	WPRRG@20	WellPumpingRateAtReceptorGroup20km[gal/day]	Well-pumping rate for residential receptor group located less than 20 km [12.4 mi] from Yucca Mountain
7	YMR-TC	ThermalConductivityofYMRock[W/(m-K)]	Thermal conductivity of rock

APPENDIX F

HUMAN-INTRUSION ANALYSIS

F.1   Background

The National Academy of Sciences recommended that a precribed scenario of human intrusion of the repository be modeled to judge if the repository system is inherently resilient to such disruption (National Research Council, 1995). The U.S. Nuclear Regulatory Commission prescribed human-intrusion scenario is described by 10 CFR 63.322 (Code of Federal Regulations, 2002), and makes the following assumptions:

•   There is a single human intrusion as a result of exploratory drilling for groundwater.

•   The intruders drill a borehole directly through a degraded waste package into the uppermost aquifer underlying the proposed Yucca Mountain repository.

•   The drillers use common techniques and practices currently employed in exploratory drilling for groundwater in the region surrounding Yucca Mountain.

•   Careful sealing of the borehole does not occur, instead, natural degradation processes gradually modify the borehole.

•   No particulate waste material falls into the borehole.

•   The exposure scenario includes only those radionuclides transported to the saturated zone by water (e.g., water enters the waste package, releases radionuclides, and transports radionuclides by way of the borehole to the saturated zone).

•   No releases caused by unlikely natural processes and events are included.

This study was to determine risk significance of a human-intrusion event. The TPA code was used to evaluate the impact of a prescribed human-intrusion scenario at Yucca Mountain. The results were compared to the TPA Version 4.1 code basecase results and previous human intrusion analyses performed using TPA Version 3.2 code (Smith, et al., 1999).

In the sections to follow, the method implemented is described, and results from the analyses are presented. The risk significance of human intrusion is discussed last.

F.2   Method

With guidance from 10 CFR 63.322, a human-intrusion scenario was developed that could be modeled using the TPA Version 4.1 code (Mohanty, et al., 2002). When assumptions are required, beyond those specified by regulation, the calculation uses a conservative approach because the primary purpose is to gauge the potential importance of the human-intrusion scenario. A conceptual image of this precribed human-intrusion scenario is depicted as Figure F–1. The following additional assumptions were made to complete the scenario:

•   The disruptive event is conservatively assumed to occur just 100 years after closure.
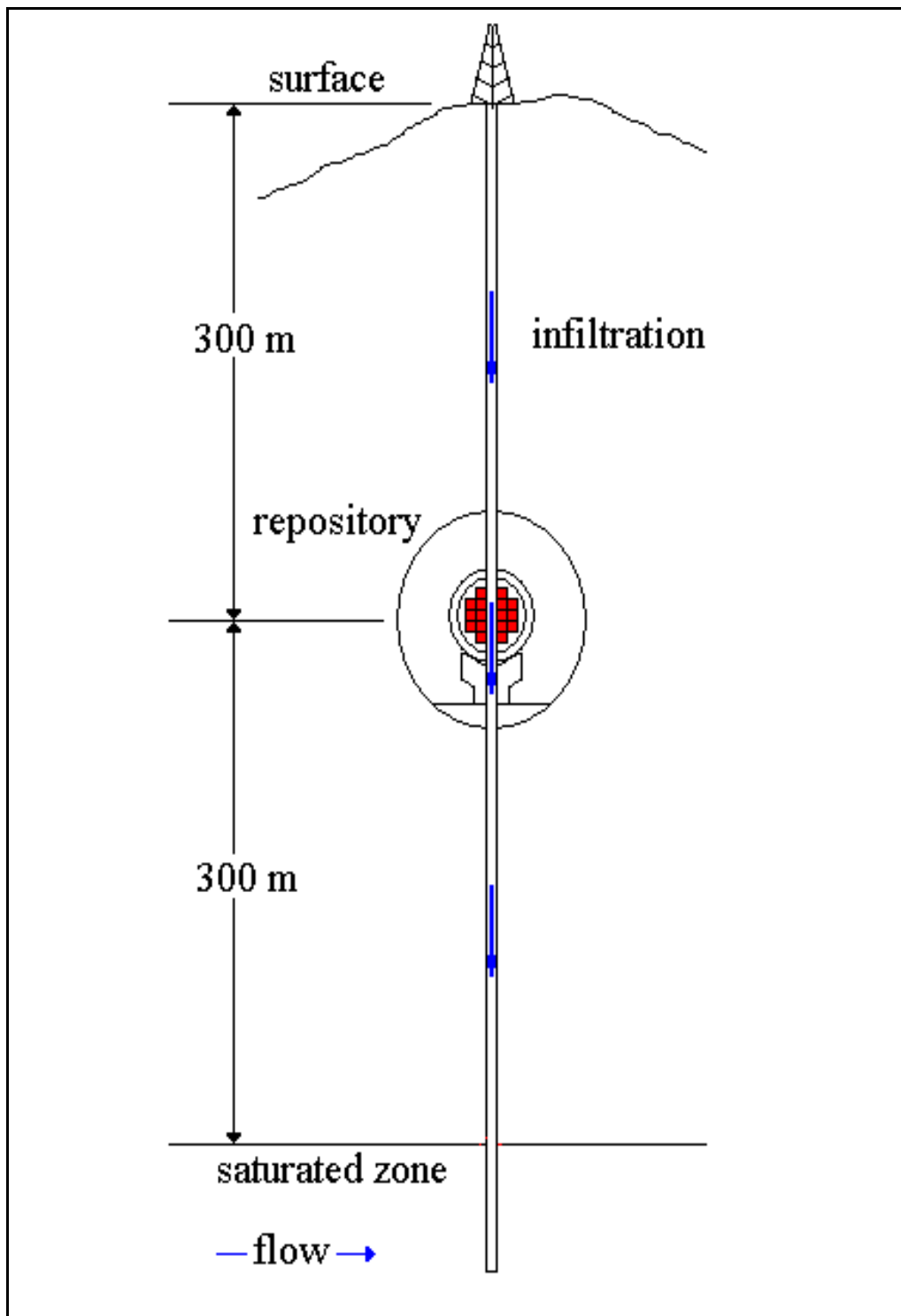
Figure F–1. Conceptual Image of Yucca Mountain Prescribed Human-Intrusion Scenario Modeled Using TPA Version 4.1 Code

- A 14.0-cm [5.5-in] borehole penetrates a waste package and continues to the saturated zone, creating a zero-time pathway from the waste package to the saturated zone. The size of the borehole is not specified by regulation.

- One hundred percent of the spent nuclear fuel remains in the waste package at the repository horizon.

- The spent nuclear fuel remaining in the waste package experiences chemical and flow conditions prevailing in the unsaturated zone.

- The spent nuclear fuel is conservatively assumed to be unprotected by cladding and is subgranular.

- The spent nuclear fuel travels toward the reasonably maximally exposed individual via the groundwater, which is used for drinking water, irrigation, and as the water source for livestock.

The human-intrusion scenario modeling is described conceptually in the following three subsections: timing and number of waste package failures, unsaturated zone flow and transport, and spent nuclear fuel degradation and release. The total-system performance assessment parameters modified to conduct the human-intrusion analysis are detailed in Table F–1.

7.2.1 Timing and Number of Waste Package Failures

The human intrusion scenario is described by a single event assumed to occur 100 years after closure. To simulate this event in the TPA Version 4.1 code, parameter selections were made to force the code to incur only one waste package failure at the desired time (100 years). The single waste package failure accomplished by allowing one juvenile waste package failure to occur 100 years after closure. The potential for additional waste package failures was removed by eliminating disruptive events and eliminating corrosion failure of waste packages.

7.2.2 Unsaturated Zone Flow and Transport

The human-intrusion event is described by a single borehole that pierces a waste package and continues to the saturated zone. No spent nuclear fuel falls to the saturated zone, but the borehole acts as a fast transport pathway from the ground surface to the saturated zone. The temperature, pH, oxygen partial pressure, and carbonate concentration values for the prevailing unsaturated zone environment were used. The volumetric flow of water entering the breached waste package was adjusted to equal the amount of surface water that could enter the borehole from a 10-m^2 [32.8-ft^2] catchment area. To simulate the fast pathway through the unsaturated zone, the following flow and transport barriers were removed: drip shield, invert, and unsaturated zone stratigraphy.

	Table F–1. TPA Version 4.1 Code Input Parameters Modified to Conduct the Human-Intrusion Analysis		
Parameter	**Default Distribution and Value**	**Modified Distribution and Value**	**Explanation for Change**
Seismic Disruptive Scenario Flag	iflag 1	iflag 0	Desire to look at impact of human-intrusion event only.
Stop at Subarea	iconstant 10	iconstant 1	Changed to look at one subarea with one failure (human-intrusion event). Identical TPA Version 4.1 code runs were repeated for each subarea and showed that subarea 1 results in the earliest dose and highest peak dose.
Number of Realizations	iconstant 1	iconstant 250	250 realizations sufficient for stability.
Critical Relative Humidity Air Corrosion	constant 0.55	constant 1.0	Set to 1.0 to eliminate nonjuvenile failures due to humid air corrosion.
Critical Relative Humidity Aqueous Corrosion	normal 0.6, 0.65	constant 1.0	Set to 1.0 to eliminate nonjuvenile failures due to aqueous corrosion.
Drip-Shield Failure Time	lognormal 2700.0, 20400.0	constant 100.0	Set to coincide with timing of human-intrusion event.
Waste Package Flow Multiplication Factor	lognormal 3.15×10^{-2}, 1.05×10^{3}	constant 167.0	Parameter adjusted to match unsaturated zone volumetric flux rate experienced down borehole assuming that precipitation falling over a given catchment area enters the borehole and reaches the repository horizon.

Assuming a 10-m^2 catchment area and a 17.5-cm/yr[*] precipitation rate gives a 1.75-m^3/yr volumetric flux rate. A separate TPA Version 4.1 code input file[†] was created to eliminate the effects of reflux and the changing climate conditions and resulted in a volumetric flux of 1.36 m^3/yr reported in the *ebsflo.dat* file. Given the default values for Fmult = 0.0447, Fow = 0.173, and Fwet set = 1.0, the waste package flow multiplication factor was set to 167.0 to give an adjusted volumetric flux of 1.75 m^3/yr. |
| Subarea Wet Fraction | uniform 0.0, 1.0 | constant 1.0 | Set to 1.0 so that all breached waste packages are dripped on. |

Table F–1. TPA Version 4.1 Code Input Parameters Modified to Conduct the Human-Intrusion Analysis (continued)			
Parameter	Default Distribution and Value	Modified Distribution and Value	Explanation for Change
Initial Failure Time	constant 0.0	constant 100.0	Set to coincide with timing of human intrusion event.
Defective Fraction of Waste Packages Per Cell	uniform 1.0×10^{-4}, 1.0×10^{-2}	constant 6.8729×10^{-4}	Set to give one failure in subarea 1 that contains 1,455 waste packages.
Surface Area Model (selection of model for computing surface area of spent nuclear fuel)	iconstant 1	iconstant 2	Spent nuclear fuel is assumed subgranular and dependent on grain radius and width of oxidation zone.
I Model (selection of model for computing spent nuclear fuel dissolution)	iconstant 2	iconstant 1	This dissolution model provides the fastest dissolution rate and assumes the absence of calcium and silicon.
Spent Nuclear Fuel Wetted Fraction	uniform 0.0, 1.0	constant 1.0	Assumes 100-percent spent nuclear fuel of breached waste package is contacted by water.
Invert Bypass	iflag 0	iflag 1	Transport through invert is skipped, consistent with the human-intrusion scenario borehole
Unsaturated Zone Stratigraphic Layer Thicknesses for All 10 Subareas	constant various	constant 0	All unsaturated zone stratigraphic layers set to 0-m thickness to simulate direct pathway provided by the human-intrusion scenario borehole.

*Precipitation rate reported to range from 10–25 cm/yr in draft environmental impact statement for Yucca Mountain (U.S. Department of Energy, 1999).
† The additional parameters modified for the separate TPA Version 4.1 code input file are displayed as Table F–2 of this appendix.
‡Note: All correlated parameters related to the unsaturated zone were commented out (essentially removed) to ensure no impact on the model results from unsaturated zone-related parameters.

F.3   Spent Nuclear Fuel Degradation and Release

For spent nuclear fuel degradation, the first of four spent nuclear fuel degradation models available in the TPA Version 4.1 code was selected. This model provides the fastest dissolution rate and is a function of temperature, pH, oxygen partial pressure, and carbonate concentration. For the spent nuclear fuel dissolution, it is conservatively assumed that the spent nuclear fuel is crushed to grain size by the human-intrusion event and that the total surface area contributes to spent nuclear fuel dissolution. A granular model is used in the basecase, but a subgranular model was selected for the human-intrusion scenario to account for disruption of spent nuclear

fuel that could occur during the drilling event. The 20 radionuclides tracked for the total system performance basecase analyses were also used for this analysis (C-14, Cl-36, Ni-59, Se-79, Nb-94, Tc-99, I-129, Cs-135, Pb-210, Ra-226, Th-230, U-234, Np-237, U-238, Pu-239, Pu-240, Am-241, Am-243, Cm-245, and Cm-246). The flow and transport modeling in the saturated zone and beyond matched that done for the basecase. All releases from the proposed repository are assumed uniformly mixed in the groundwater supply used by a reasonably maximally exposed individual. The reasonably maximally exposed individual is assumed to be a rural resident located 20-km [12.4-mi] downgradient from the repository whose diet consists of TPA Version 4.1 code default food consumption rates based on a survey of Armagosa Valley residents (CRWMS M&O, 2000). Note that 10 CFR Part 63 (Code of Federal Regulations, 2002) locates the reasonably maximally exposed individual no further than 18-km [11.2-mi] downgradient from the repository, and it is anticipated that future versions of the TPA code will be modified to include an 18-km [11.2-mi] compliance boundary.

F.4   Results

Modeling this human-intrusion scenario using the TPA Version 4.1 code gave peak total expected annual doses to the reasonably maximally exposed individual near 10^{-6} Sv [0.1 mrem] in 10,000 years. As indicated in Table F–3, TPA Version 4.1 code human-intrusion dose calculation results are near the results for the TPA Version 3.2 code human-intrusion analyses (Smith, et al., 1999). As expected, only radionuclides with higher solubility rates and lower retardation rates (i.e., Cl-36, Tc-99, I-129, and Np-237) contribute significantly to the dose within 10,000 years of the event. The primary contributors to the expected annual dose in 10,000 years for the human-intrusion scenario are presented in Table F–4. The primary contributors to the expected annual dose in 10,000 years for the human-intrusion and basecase scenarios are also shown graphically in Figures F–2 and F–3. For the human-intrusion scenario (Figure F–2), the primary contributor to the expected annual dose is Tc-99 for approximately the first 2,000 years and then Np-237 afterward. For the basecase (Figure F–3), the primary contributor remains as Tc-99 in 10,000 years.

F.5   Risk Significance

As reported in the previous section, the total-system performance assessment human-intrusion scenario calculations show peak annual total expected doses to the reasonably maximally exposed individual near 10^{-6} Sv [0.1 mrem] during the 10,000-year simulation period. The calculated dose remains low primarily because of the limited spent nuclear fuel inventory available in this scenario. Only one of 8,877 waste package, or less than 0.012 percent of the spent nuclear fuel expected to be placed at Yucca Mountain, is made available for release by the scenario. As indicated by Figure F–4, the additional contribution to the expected annual dose from this prescribed human-intrusion event in 10,000 years is approximately one order of magnitude above the expected annual dose from the total-system performance assessment basecase analyses. The primary difference in 10,000 years is that the initial expected dose from the human-intrusion scenario arrives approximately 4,000 years earlier than for the total-system performance assessment basecase, and Np-237 becomes the dominant radionuclide.

Table F–2. Additional TPA Version 4.1 Code Input Parameters Modified to Eliminate the Effects of Reflux and Changing Climate Conditions to Facilitate the Calculation of an Appropriate Value for the Waste Package Flow Multiplication Factor

Parameter	Default Distribution and Value	Modified Distribution and Value	Explanation for Change
Areal Average Mean Annual Infiltration at Start	uniform 1.0, 10.0	constant 5.5	Set to constant value to eliminate impact on flow rate into waste package.
Mean Average Precipitation Multiplier at Glacial Maximum	uniform 1.5, 2.5	constant 1.0	Set to constant value to eliminate impact on flow rate into waste package.
Mean Average Temperature Increase at Glacial Maximum	uniform −10, −5	constant 0.0	Set to constant value to eliminate impact on flow rate into waste package.
Reflux Model	iconstant 3	iconstant 1	Set to constant value to eliminate impact on flow rate into waste package.
Length of Reflux Zone	constant 20	constant 0.0	Set to constant value to eliminate impact on flow rate into waste package.
Perched Bucket Volume per Subarea	constant 0.5	constant 0.0	Set to constant value to eliminate impact on flow rate into waste package.

Table F–3. Peak Expected Annual Dose in 10,000 Years for Human-Intrusion and Basecase Scenarios Using TPA Versions 4.1 and 3.2 Codes

Scenario	Peak Expected Dose (mrem/yr)
TPA Version 4.1 Code Basecase	1.77×10^{-2}
TPA Version 4.1 Code Human Intrusion	5.73×10^{-2}
TPA Version 3.2 Code Human Intrusion[*]	1.23×10^{-2}
[*]Smith, M., T. McCartin, and S. Mohanty. "Demonstration of TPA Version 3.2 Code's Capability to Evaluate the Effects of Human Intrusion." Transactions of the American Nuclear Society 1999 Winter Meeting. Vol. 81. Long Beach, California: American Nuclear Society. November 14–18, 1999.	

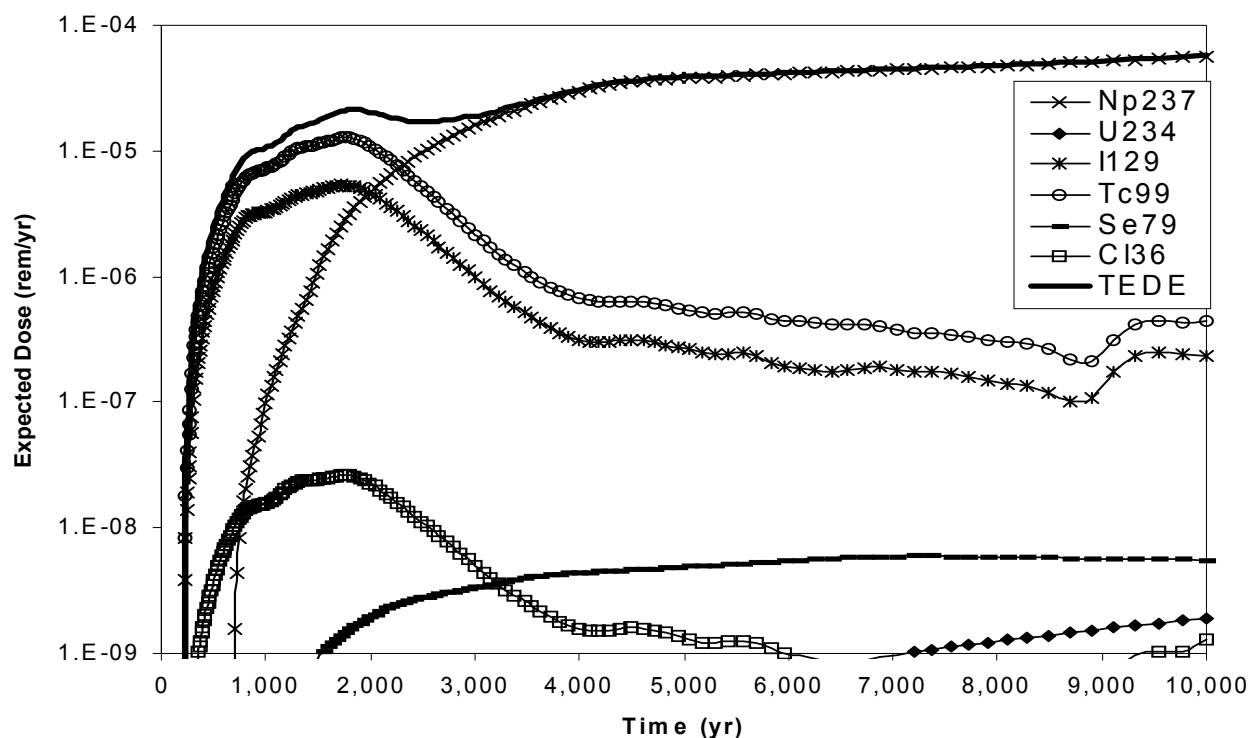| Table F–4. Primary Contributors to Peak Expected Annual Dose in 10,000 Years for TPA Version 4.1 Code Basecase and Human-Intrusion Scenario with 250 Realizations		
Radionuclide*	TPA Version 4.1 Code Basecase (%)	TPA Version 4.1 Code Human Intrusion (%)
Tc-99	57.4	0.8
I-129	28.1	0.4
Np-237	14.3	98.8
Cl-36	—	0.2
*Radionuclides considered: C-14, Cl-36, Ni-59, Se-79, Nb-94, Tc-99, I-129, Cs-135, Pb-210, Ra-226, Th-230, U-234, Np-237, U-238, Pu-239, Pu-240, Am-241, Am-243, Cm-245, and Cm-246.		

Figure F–2. Primary Contributors to the Expected Dose in 10,000 Years for the TPA Version 4.1 Code Human-Intrusion Scenario
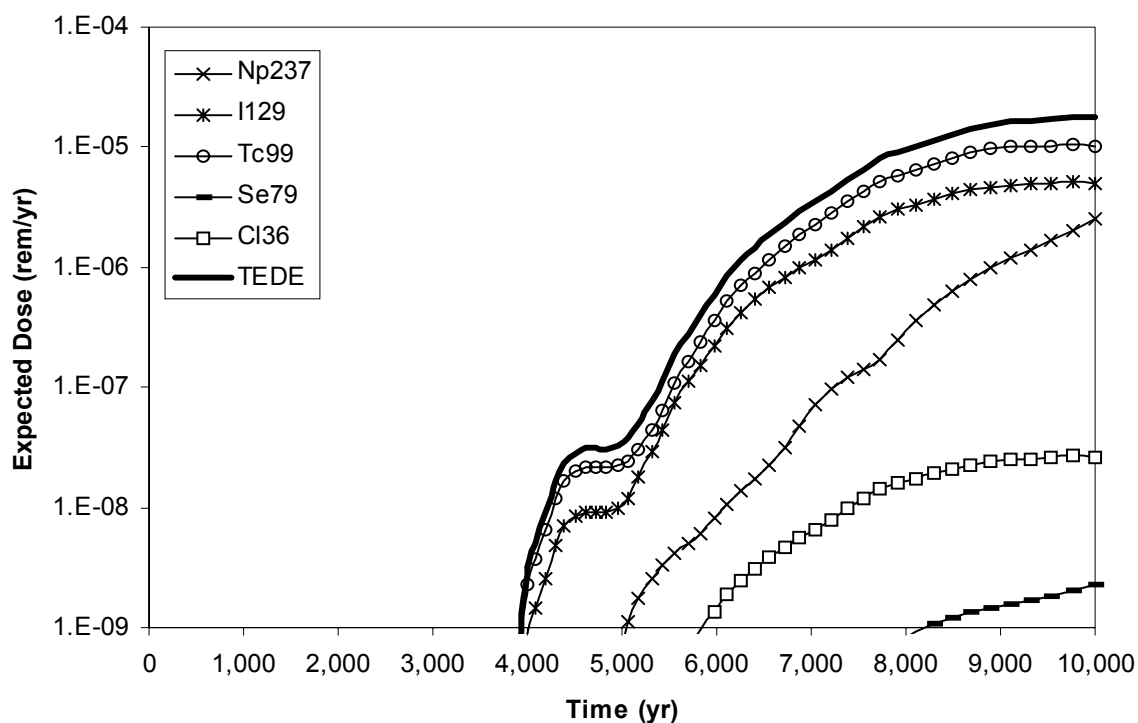
Figure F–3. Primary Contributors to the Expected Dose in 10,000 Years for the TPA Version 4.1 Code Basecase
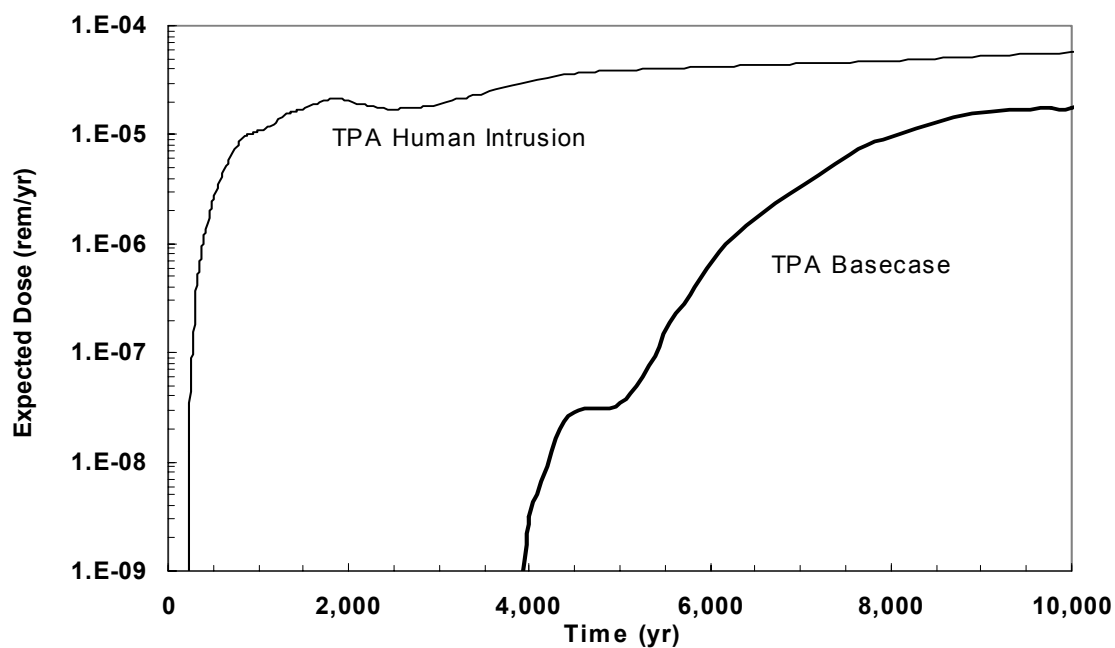

Figure F–4. Expected Total Dose in 10,000 Years for TPA Version 4.1 Code Basecase and Human-Intrusion Scenarios with 250 Realizations

F–9

F.6   References

Mohanty, S., T. McCartin, D. Esh (co-ordinators). "Total-system Performance Assessment (TPA) Version 4.0 Code: Module Descriptions and User's Guide." San Antonio, Texas: CNWRA. 2002.

CRWMS M&O. "Identification of Critical Group (Consumption of Locally Produced Food and Tap Water)." ANL–MGR–MD–000005. Revision 0. Las Vegas, Nevada: CRWMS M&O. 2000.

National Research Council. "Technical Bases for Yucca Mountain Standards." Washington, DC: National Research Council. 1995.

Smith, M., T. McCartin, and S. Mohanty. "Demonstration of TPA Version 3.2 Code's Capability to Evaluate the Effects of Human Intrusion." Transactions of the American Nuclear Society 1999 Winter Meeting. Vol. 81. Long Beach, California: American Nuclear Society. November 14–18, 1999.

APPENDIX G

IMPACT OF IN-PACKAGE CRITICALITY ON REPOSITORY PERFORMANCE

Analyses reported in this appendix quantify the consequences of postclosure criticality events on the expected dose. Consequences of nuclear criticality can be an increase in the inventory of radionuclides in the waste package, elevation of the temperature of the waste package, and mechanical damage to the engineered barriers of the repository. Because the criticality event is expected to occur with low probability, the processes leading to criticality have not been included in the basecase performance assessment model. Similar to the igneous activity and faulting event calculations, risk from a criticality event also requires the knowledge of the event probability. Analyses in this appendix are limited to obtaining an estimate of only the consequence of an in-package criticality event (i.e., criticality occurring within the waste package) without consideration of event probabilities. In this regard, the information presented in this appendix does not provide a direct measure of risk. Although probabilities exist in the literature [e.g., DOE, 1998] uses 5×10^{-3} and 1×10^{-3} for probability of criticality for pressurized water reactor and Boiling water reactor waste packages for 10,000 years with certain assumptions), NRC staff and the CNWRA continue to focus only on the consequence estimates.

Criticality outside the waste package is not considered in this report but is currently being investigated. In-package criticality is considered more likely than criticality occurring outside of the waste package, because of reduced concentrations of important radionuclides and the difficulty in obtaining the accumulations and configurations necessary to permit criticality to occur.

In-package criticality may occur if certain conditions are met. A possible scenario for which in-package criticality can occur is described next. As shown in Figure G–1, after waste package breach, water can fill the waste package as long as the bottom of the waste package is intact. As water collects in the waste package, the internal structures of the waste package will corrode, releasing some of the neutron poison into solution. If sufficient water collects in the waste package allowing the water level to rise to where the breach exists, the neutron poison can be removed gradually as water exits the waste package. If the waste package bottom remains intact until a sufficient fraction of the poison is removed, some spent nuclear fuel could go critical (depending on configuration of the fuel, amount of water in the waste package, and so on). Seismic events could cause a rapid insertion of reactivity by shaking the waste package so that several fuel assemblies held above the water level by degraded internal structures would drop into the water. This rapid insertion of reactivity could result in a transient criticality with a rapid increase in temperatures and pressures in the waste package. Potentially, this reaction could cause mechanical damage to the fuel, waste package, and surrounding engineered barriers.

These analyses used the TPA code with appropriate adjustment of model parameters to mimic an in-package criticality condition. Because criticality can occur from a variety of configurations, the probability of this particular configuration occurring was less than the cumulative probability of criticality. Because the calculations were limited by the options currently available within the existing total-system performance assessment framework, emphasis was placed on obtaining a
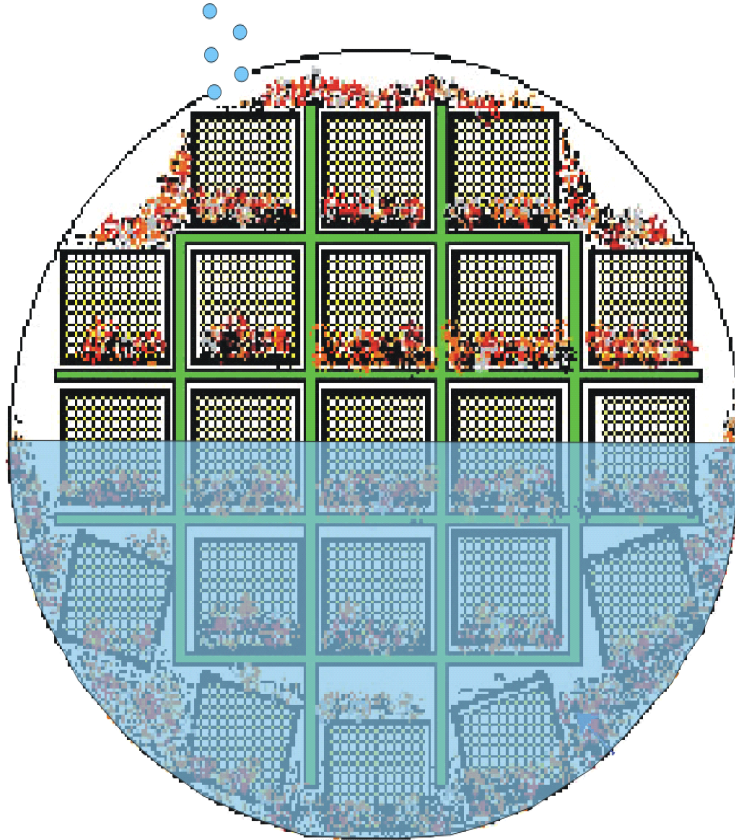
**Figure G–1. Schematic of a Degraded Waste
Package Prior to an In-Package Criticality Event
(DOE, 1998)**

conservative estimate. The rationale for using a conservative analysis was that, if the
consequence of the criticality event is low, in spite of the conservatism, there will be no further
need to focus on the quantitative accuracy of the criticality event probability.

Two types of criticality events may occur: steady-state criticality and transient criticality. The
scenario of a steady-state criticality inside the waste package would involve failure of the waste
package, subsequent intrusion of water into the waste package, and corrosion, dissolution, and
removal of the criticality control system (i.e., borated stainless steel). Subsequent to gradual
removal of the borated stainless steel, the waste package will approach a critical condition. As
the result of a critical condition, additional heat, above and beyond the decay heat, will be
produced that will cause the waste package temperature to increase and the water inside the
waste package to start to evaporate. The evaporation continues until the water level decreases
and causes the criticality condition to cease. This sequence of water intrusion, approach to
critical condition, evaporation, and return to subcritical condition will be repeated whenever
water enters the waste package. At steady state, the power level will be determined by the heat
transfer away from the waste package. This heat transfer will include the mechanisms of
thermal conduction, convection, radiation, and latent heat loss by evaporation of water dripped
into the waste package.

The process for the transient criticality scenario would begin similar to the steady-state criticality. On removal of the criticality control system, however, there could be a configuration in which the system suddenly becomes critical or supercritical. For example, in a bathtub model when the water level inside the waste package reaches a height where the system is close to critical condition, and a seismic event could cause shuffling of the stacked spent nuclear fuel assemblies, a reactivity insertion could be introduced into the system that could produce significant kinetic energy. This kinetic energy could unzip the spent nuclear fuel rods and create openings in the bottom of the waste package and the invert. The adjacent waste packages may also be damaged. Therefore, the consequences of a transient criticality may include an impact on the barriers.

In the following sections, steady-state criticality consequence modeling is described, followed by a description of the technique used to capture the consequences of a transient criticality event. The procedure presented is a formalization of the approach presented in Weldy, et al. (2001). The procedure fully relies on the framework of the TPA Version 4.0 code (Mohanty, et al., 2002) and does not rely on any external model calculations. The criticality event is minimal in the TPA Version 4.1 code, appropriately adjusting the parameters to provide conservative estimates of the consequence. The procedure described was used to determine the power level and the resulting increase in radionuclide inventory from the steady-state criticality cycles and the subsequent impact on the expected dose. The parameters in the TPA Version 4.1 code that were changed and the magnitude of these changes are described for both steady-state and transient criticality scenarios. Finally, results from the two criticality consequence models are described.

Steady-State Criticality

The sustainable power level of a steady-state criticality will be limited by the rate of water infiltration into the waste package. As the power level increases, more water will be evaporated, the water level will fall, and the system will lose reactivity. Therefore, the maximum sustainable power level cannot exceed the power required to evaporate water entering the waste package plus the power required to make up for heat lost to the surrounding rock.

To bound the potential effects of criticality, a conservative case was analyzed. It was assumed at year 5,000 all failed waste packages would go critical and remain critical for 10,000 years. The analysis evaluated whether the generation of additional radionuclides and the increased temperature from the criticality event would significantly affect repository performance.

From Sonntag and van Wylen (1991), the power level in the waste package can be calculated by

$$P_{WP} = Q_{WP} + \dot{m}\left(h_2 - h_1\right) \tag{G-1}$$

where

P_{WP} — power level from in-package steady-state criticality (W)
Q_{WP} — heat loss from the waste package to surrounding area (no backfill) (W)
$\dot{m}$ — water mass flow rate into the waste package (g/s)

h_2 —   enthalpy of water before evaporation (J/g)
h_1 —   enthalpy of water after evaporation (J/g)

The heat loss from the waste package can be calculated according to the TPA Version 4.0 code user's guide (Mohanty, et al., 2002)

$$Q_{WP} = \left(G_{conv} + G_{cond} + G_{rad}\right)\left(T_{wp} - T_{rock}\right) \tag{G–2}$$

where

G_{conv} —   effective thermal conductance for convective heat transfer (W/°C)
G_{cond} —   effective thermal conductance for conductive heat transfer (W/°C)
G_{rad} —   effective thermal conductance for radiative heat transfer (W/°C)
T_{wp} —   waste package surface temperature (°C)
T_{rock} —   drift rock wall temperature (°C)

The effective thermal conductance for convective, conductive, and radiative heat transfer coefficients can be calculated from the following formulae, also in the TPA Version 4.0 code user's guide (Mohanty, et al., 2002)

$$G_{conv} = f_c \frac{2\pi k_{eff-nc}\left(L_{wp} - 2\delta\right)}{\ln\left(\dfrac{D_{rw}}{D_{wp}}\right)} \tag{G–3}$$

where

f_c —   fractional area not covered by the floor = 0.75 (Mohanty, et al., 2000)
$k_{effi-nc}$ —   effective thermal conductivity for natural convection = 0.9 W/m-°C (Mohanty, et al., 2000)
D_{rw} —   Diameter of drift = 5.5 m [18 ft] (CRWMS M&O, 2000)
D_{wp} —   Diameter of waste package = 1.579 m [5.2 ft] (CRWMS M&O, 2000)
L_{wp} —   Length of waste package = 5.275 m [17.3 ft] (CRWMS M&O, 2000)
δ —   Spacing between waste package = 0.1 m [0.33 ft] (CRWMS M&O, 2000)

$$G_{cond} = \left(1 - f_c\right)\frac{2\pi k_{floor}\left(L_{wp} - 2\delta\right)}{\ln\left(\dfrac{D_{rw}}{D_{wp}}\right)} \tag{G–4}$$

where

f_c —   fractional area not covered by the floor = 0.75 (Mohanty, et al., 2000)
k_{floor} —   thermal conductivity of floor = 0.6 W/m-°C (Incropera and DeWitt, 1995)

$$G_{rad} = F_c \cfrac{4\sigma\left(273.15 + T_{rock}\right)^3}{\cfrac{1 - \varepsilon_{wp}}{\varepsilon_{wp}\pi D_{wp}L_{wp}} + \cfrac{1}{F_{wp-rw}\pi D_{wp}\left(L_{wp} + 2\delta\right)} + \cfrac{1 - \varepsilon rw}{\varepsilon_{rw}\pi D_{rw}\left(L_{wp} + 2\delta\right)}} \qquad (G\text{–}5)$$

where

σ	—	Stefan-Boltzman constant = 5.67×10^{-8} W/m^{2}K^4 (Mohanty, et al., 2000)
ε_{wp}	—	emissivity of the waste package = 0.87 (Mohanty, et al., 2000)
F_{wp-rw}	—	radiative view factor from the waste package to the rock wall = 1 (Mohanty, et al., 2000)
T_{rock}	—	drift rock wall temperature (°C)

A rock wall temperature at t = 5,000 years of 70 °C [158 °F] from total-system performance assessment results and an increase in the temperature of the waste package from the criticality of 25 °C [77 °F] from U.S. Department of Energy (DOE) calculations (DOE, 1998) were used. A reasonably conservative value for the flow rate of water into the waste package of 0.1 m^3/yr [3.5 ft^3/yr] from CRWMS M&O (2000) was used. Enthalpy values for 70 °C [158 °F] water and 100 °C [212 °F] steam from Sonntag and van Wylen (1991, Table A.1.2SI) were obtained. These values result in the calculation of a power level of 4.78 kW [6.4 hp].

This power level was used in ORIGEN2 (Oak Ridge National Laboratory, 1991) calculations for 10,000 years to calculate the inventory generation for this event (note that the ORIGEN2 calculations do not account for differences in moderator density or temperatures between a reactor and a waste package, which could have a moderate effect on the results). The goal is to get an increase in inventory at 15,000 years, for all total-system performance assessment nuclides considered, that matches the 10,000-year criticality inventory increase calculated using ORIGEN2.1. For radionuclides that are not daughter products in a decay chain series, the inventory at 10 years is increased by that same percentage. Chain nuclides need to consider the effects of parent decay on inventory. If the inventory from the parent decay dominates the amount of radionuclides present at 15,000 years, only the inventory of the parent needs to be increased by the appropriate percentage. If the inventory of the daughter dominates, only the inventory of the daughter needs to be increased. If the contribution of the parent and daughter are comparable, changes to inventory will have to be divided between the two. The radionuclide inventory was increased to reflect the criticality contribution, as shown in Table G–1. Changes to other total-system performance assessment input files for simulating steady-state criticality consequences are described in the following sections and shown in Table G–2.

The steady-state criticality event was modeled as a 10,000-year steady-state criticality that starts at year 5,000. It was assumed all initially defective waste packages (an average of approximately 32) go critical at year 5,000, and all waste packages that go critical are under drips (otherwise, they could not go critical). The analysis was performed in such a way to show only the incremental dose from steady-state criticalities. Therefore, to obtain the total dose, the dose from the basecase needed to be added to the criticality dose. In addition, all the radionuclides produced by the steady-state criticality were assumed available for instantaneous release.

Table G–1. Increase in Radionuclide Inventory from Steady-State Criticality				
Radionuclide	**15,000-Year Inventory Dominated By**	**Base Inventory (Ci/MTU)**	**Percent Increase**	**PostCriticality Inventory (Ci/MTU)**
Cm-246	Self	7.62×10^{-2}	374	0.361
U-238	Self	0.315	−1.1	0.3115
Cm-245	Self	0.366	Leave same—not important to performance	No change
Am-241	Parent (Cm-245)	2,080	Leave same—not important to performance	No change
Np-237	Parent (Am-241)	0.434	71 – 1.65 Ci/MTU from parents, need to increase initial inventory to raise to 2.823 Ci/MTU at 15,000 years	1.173
Am-243	Self	26.4	313.7	109.2
Pu-239	Self	369	28.8	475.4
Pu-240	Self	544	160.2	1,415
U-234	50% self, 50% Pu-238	1.18	251 – 2.636 Ci/MTU from parents, need to increase initial inventory to raise to 9.267 Ci/MTU at 15,000 years	6.63
Th-230	Parent (U-234)	No change	No change	No change—inventory will be wrong because of U-234 change; model separately if necessary

Radionuclide	15,000-Year Inventory Dominated By	Base Inventory (Ci/MTU)	Percent Increase	PostCriticality Inventory (Ci/MTU)
Ra-226	Parent (Th-230)	No change	No change	No change—inventory will be wrong because of U-234 change; model separately, if necessary
Pb-210	Parent (Ra-226)	No change	No change	No change—inventory will be wrong because of U-234 change; model separately, if necessary
Cs-135	Self	0.536	87.4	1.00
I-129	Self	3.57×10^{-2}	22.1	4.36×10^{-2}
Tc-99	Self	14.5	11.5	16.2
Ni-59	Self	2.44	45	3.54
C-14	Self	1.44	310.3	5.91
Se-79	Self	0.458	11.2	0.509 (corrected to 0.03 because of half-life change)
Nb-94	Self	0.848	65.1	1.4
Cl-36	Self	1.15×10^{-2}	31.5	1.47×10^{-2}

Table G–1. Increase in Radionuclide Inventory from Steady-State Criticality (continued)

	Table G–2. TPA Version 4.1 Code Input Parameters Modified to Simulate In-Package Steady-State Criticality Consequences		
File/Parameter	**Default Distribution Value**	**Modified Distribution and Value**	**Explanation for Change**
tpa.inp			
Seismic Disruptive Scenario Flag	iflag 1	iflag 0	Desire to look at impact of steady-state criticality events
Number of Realizations	iconstant 1	iconstant 250	250 realizations sufficient for stability
AA_1_1 (Passive Current Density for Waste Package Outer Overpack)	Normal 1.6×10^3, 1.7×10^4	Normal 1.6, 1.7	To eliminate nonjuvenile failure caused by corrosion
Coefficient for Localized Corrosion of Outer Overpack	Constant 2.5×10^{-4}	Constant 2.5×10^{-8}	To eliminate nonjuvenile failure caused by corrosion
Subarea Wet Fraction	Uniform 0.0, 1.0	Uniform 0.999999, 1.0	To make all juvenile failed waste packages to be dripped on
Initial Failure Time	Constant 0.0	Constant 5000.0	Assuming it takes 5,000 years for the breached waste packages to lose its criticality control system
Gap Fraction	Default values in column three of Table G–1	Changed default values by the fractions in column four of Table G–1	To simulate the incremental increase in radionuclide inventory available for release
burnup.dat			
Heat Generation (lines added to input) Boiling water reactor (W/MTIHM) Pressurized Water Reactor (W/MTIHM)		<u>5,000 10,000 15,000</u> 56.54 35.52 25.0 64.1 46.27 28.0	To simulate the increase in temperature from steady-state criticality

Table G–2. TPA Version 4.1 Code Input Parameters Modified to Simulate In-Package Steady-State Criticality Consequences (continued)			
File/Parameter	Default Distribution Value	Modified Distribution and Value	Explanation for Change
wpflow.def			
Flow Diversion Factor (F_{mult})	0.044721 for t = 0.0 to 100,000 years.	0.044721 for t = 0.0 to 7,000 years 0.0 for t = 7,000 to 15,000 years	To simulate water evaporation with no release during criticality period
nuclides.dat			
	column three of Table G–1	column five of Table G–1	To simulate increase in radionuclide inventory from steady-state criticality

The heat produced by the steady-state criticality was also included in the consequence model. The values of heat generation were modified to produce a heat increase of approximately 25 °C [77 °F] between the years 5,000 and 15,000. The 25 °C [77 °F] increase in temperature was taken from calculations performed by DOE (1998). Specifically, the heat-generation rate at year 5,000 was changed to 56.54 W/MTHM for boiling water reactor fuel and 64.1 W/MTHM for pressurized water reactor fuel. At year 10,000, the heat-generation rate was changed to 35.52 W/MTIHM for boiling BWR fuel and 46.27 W/MTIHM for pressurized water reactor fuel, and the heat-generation rate was set to 25.00 W/MTIHM for boiling water reactor fuel and 28.00 W/MTIHM for pressurized water reactor fuel at year 15,000.

To simulate the steady-state criticality, the bathtub model in the TPA code was used. It was assumed water enters the waste package and accumulates until a critical condition is reached. The water then evaporates until the system goes subcritical. This cycle repeats until the year 15,000, and no radionuclides are released before 15,000 years. At year 15,000, when the steady-state criticality ends, the water that contains dissolved radionuclides starts leaving the waste package.

Transient Criticality

The transient criticality was modeled as an extreme event in which the fuel maintains its geometry and sufficient water remains in the waste package to generate a very large pressure pulse. This pressure pulse is assumed sufficient to very quickly degrade the spent nuclear fuel inside the waste package, cause serious damage to the waste package so the water contact model is a flowthrough model, fail one waste package on either side of the critical waste package, and blast a hole in the invert material below the waste package such that the performance of the invert is bypassed. The drip shield above the waste package would also be failed by the blast but was already assumed failed for the waste package to accumulate water

and go critical. The total number of fissions will be limited enough that changes in radionuclide inventory or long-term heat generation can be ignored.

The calculation required two runs of the TPA code to perform the modeling—one for the waste package in which the transient criticality occurs and one for the two additional waste packages, which are failed by the transient criticality. The required modifications for the total-system performance assessment input file for the source package are shown in Table G–3. The results of the analysis can be added with the basecase dose to compare the results to the basecase. Therefore, the simulation for the source package was performed by turning off the corrosion-induced and seismic-induced waste package failures, setting the number of initially failed waste packages to 1, and forcing it to be dripped on and become critical at year 5,000. At year 5,000, the impact of a transient criticality event was modeled by switching to the flowthrough model and bypassing the invert. Switching to a flowthrough model simulates the hole that could be created from a pressure pulse. Bypassing the invert is a way of mimicking the hole that the pressure pulse could create in the invert.

With respect to simulating the impact of the pressure pulse on the adjacent waste packages, a separate total-system performance assessment run with no corrosion-induced and seismic-induced waste package failures and two waste packages with initial failure. In the simulation, it was also assumed the blast would make ineffective the invert under the two adjacent waste packages. The changes to the TPA.INP file for the adjacent packages are similar to those shown in Figure G–1 except the default-dissolution model for the spent nuclear fuel model is used, and defective waste package fractions are changed to 4.5×10^{-4} to ensure that only two waste packages are failed initially (one located in Subarea 2 and one located in Subarea 1). The release model also removes all controls on radionuclide release such as solubility limits, cladding and waste package filling time.

Results

Both the steady-state and transient criticality cases showed an increase in dose following a criticality event. These results, however, do not incorporate the probability of a criticality event occurring in the repository. Factors such as the long projected lifetime of the waste package, variations in initial enrichment and burnup of the fuel, the limited fraction of waste packages that will be dripped on, and the potential for failures to occur on the bottom of the waste package need to be considered in calculating the probability of criticality within a waste package.

Figure G–2 shows the effect of steady-state criticality in those waste packages with premature failure on the repository performance. The analysis indicates the conditional dose rate at the critical group would not exceed basecase dose rate by more than a factor of three. Half this increase reflects the modeling assumption that all failed waste packages are located under a drip.

Figure G–3 shows the effect of the in-package transient criticality on the repository by dose. The analysis shows that the event results in a relatively large peak dose shortly after the event is assumed to occur and quickly drops below the basecase results. The peak projected dose exceeds the peak basecase dose within 10,000 years by one order of magnitude. These effects are larger immediately after the event, primarily because of the assumption the fuel is

Table G–3. TPA Version 4.1 Code Input Parameters Modified to Simulate In-Package Transient Criticality Consequences			
File/Parameter	**Default Distribution Value**	**Modified Distribution and Value**	**Explanation for Change**
tpa.inp			
Seismic Disruptive Scenario Flag	iflag 1	iflag 0	Desire to look at impact of transient criticality event
Number of Realizations	iconstant 1	iconstant 250	250 realizations sufficient for stability
AA–1–1 (Passive Current Density for Waste Package Outer Overpack)	normal 1.6×10^3, 1.7×10^4	normal 1.6, 1.7	To eliminate nonjuvenile failure caused by corrosion
Coefficient for Localized Corrosion of Outer Overpack	constant 2.5×10^{-4}	constant 2.5×10^{-8}	To eliminate nonjuvenile failure caused by corrosion
Subarea Wet Fraction	uniform 0.0, 1.0	uniform 0.999999, 1.0	To make the juvenile-failed waste package to be dripped on
Defective Fraction of Waste Packages	uniform 1.0×10^{-4}, 1.0×10^{-2}	uniform 4.299×10^{-4}, 4.3×10^{-4}	To simulate only one waste package would go critical
Initial Failure Time	constant 0.0	constant 5000.0	Assuming it takes 5,000 years for the breached waste package to lose its criticality control system
Water Contact Mode for Initial Failure	iflag 0	iflag 1	To simulate the switch from bathtub to flowthrough model after the transient criticality

| Table G–3. TPA Version 4.1 Code Input Parameters Modified to Simulate In-Package Transient Criticality Consequences (continued)			
File/Parameter	Default Distribution Value	Modified Distribution and Value	Explanation for Change
Invert Bypass	iflag 0	iflag 1	To simulate the hole created in the invert after the transient criticality event
I Model (selection of model for computing spent nuclear fuel dissolution)	iconstant 2	iconstant 3	Spent nuclear fuel is assumed to disintegrate completely after transient criticality event
User Leach Rate	User provided leaching rate if I Model = 3	2.5×10^{-2}	To simulate disintegration of spent nuclear fuel and increased solubility as the result
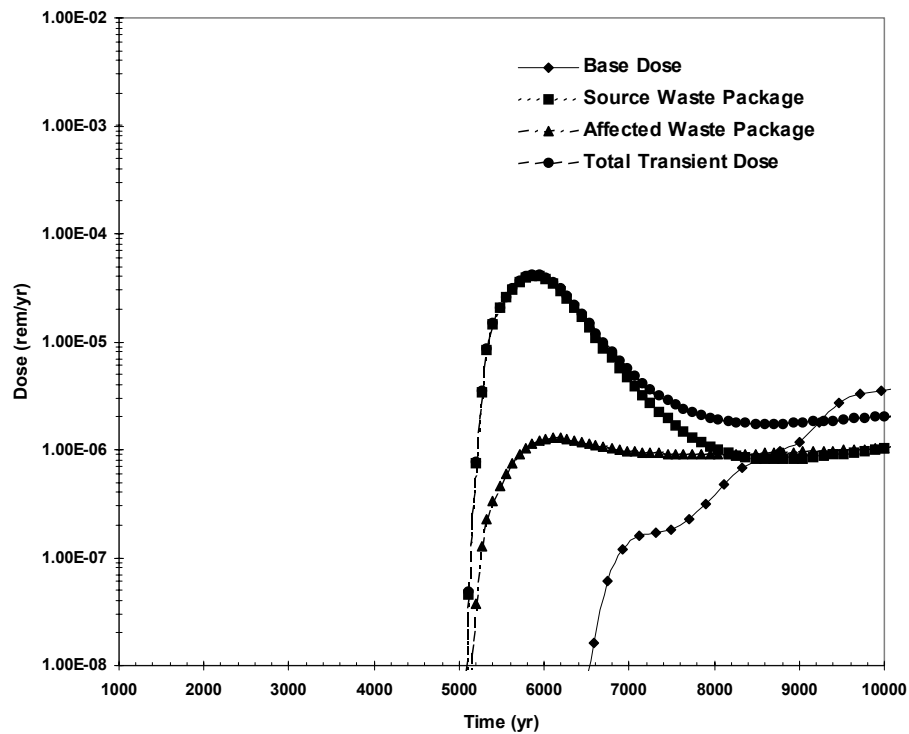
Figure G–2. Dose Consequence of In-Package Steady-State Criticality
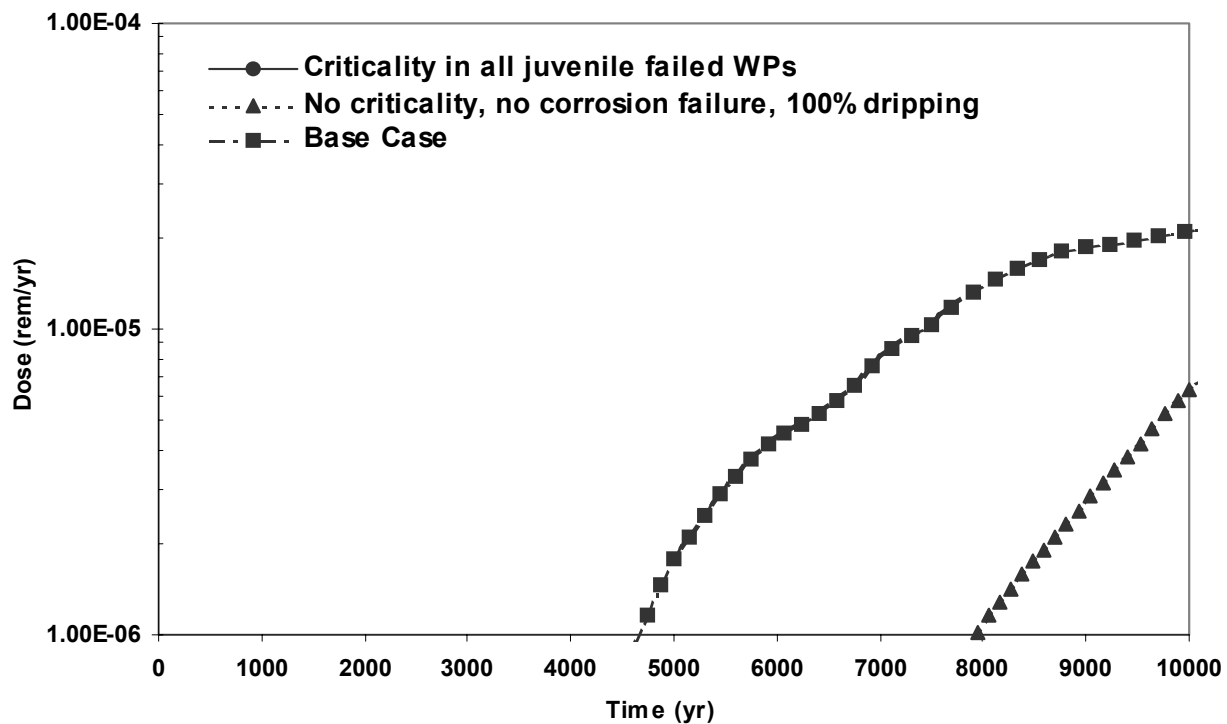
G–12

Figure G–3. Dose Consequence of In-Package Transient Criticality

destroyed by the event. As indicated earlier, these effects do not include the probabilities of the event and pulverization of the fuel.

Significance

The results indicated that, in the absence of probability, the consequence of transient criticality appeared to be an increase in the peak basecase dose for the 10,000-year simulation period by one order of magnitude. As described in the previous section, however, the assumptions made in simulating the transient criticality may be overly conservative. This is a simplistic approach in attempting to bound the consequence of criticality

References

CRWMS M&O. "Total System Performance Assessment for the Site Recommendation." TDR–WIS–PA–000001. Rev. 00 ICN 01. Las Vegas, Nevada: CRWMS M&O. 2000.

DOE. "Disposal Criticality Analysis Methodology Topical Report." YMP/TR–004Q. Rev. 0. Las Vegas, Nevada: DOE, Office of Civilian Radioactive Waste Management. 1998.

Incropera, F.P., and D.P. DeWhitt. *Fundamentals of Heat and Mass Transfer*. 3rd Edition. New York: John Willey and Sons. 1995.

Mohanty, S., T.J. McCartin, and D.W. Esh. "Total-system Performance Assessment (TPA) Version 4.0 Code: Module Descriptions and User's Guide." San Antonio, Texas: CNWRA. 2002.

Mohanty, S., T.J. McCartin, and D.W. Esh. "Total-system Performance Assessment Version 4.0 Code: Module Descriptions and User's Guide." San Antonio, Texas: CNWRA. 2000.

Oak Ridge National Laboratory. "ORIGEN 2.1–Isotope Generation and Depletion Code." CCC–371. Oak Ridge, Tennessee: Oak Ridge National Laboratory. 1991.

Sonntag, R. and G. van Wylen. *Introduction to Thermodynamics: Classical and Statistical*. New York City, New York: John Wiley and Sons. 1991.

APPENDIX H

CONVERGENCE OF THE TOTAL-SYSTEM PERFORMANCE ASSESSMENT CODE RESULTS

When the TPA code is executed for a realization of the parameter vector, dose to the receptor is calculated. The expected dose is computed by averaging the doses at each time from all realizations from a Monte Carlo TPA code run that uses the Latin Hypercube Sampling method. The resulting curve is a time-dependent dose curve that represents the expected dose. The peak expected dose within the compliance period of 10,000 years, which is identified as a performance objective in the 10 CFR Part 63 (Code of Federal Regulations, 2002), is the largest expected dose obtained from the expected dose versus time curve. Another value that is used in the sensitivity analysis is the peak dose which is the largest dose of a particular realization. These two estimates must be stable. The results are considered stable at a certain number of realizations, if the expected dose (and the mean peak dose) does not change after a certain number of Monte Carlo realizations. Because the Latin Hypercube Sampling method is used and the TPA code has 330 sampled parameters, at least 331 realizations are required to appropriately account for the parameter correlations. Chapter 3 is based on 350 realizations because with that many realizations, the peak expected dose appears to provide representative values to express peak expected dose. Most information presented in this report is comparative results, which is not affected by the number of realizations as long as the sampling sequence in the Latin Hypercube Sampling is not changed. A more careful study reveals that as the number of realizations is increased the convergence in the results from the TPA Version 4.1 code is lost. This appendix investigates the convergence of the peak expected dose and the mean peak dose as a function of the sample size.

Three approaches were adopted to study the stability issue: perform independent Latin Hypercube Sampling runs with different numbers of realizations, perform Monte Carlo resampling from the 4,000-vector data prior to computing the mean peak dose, and perform independent Latin Hypercube Sampling runs with different numbers of realizations and 6 different seeds with each set (500; 1,000; 2,000; 3,000; and 4,000 realizations) using a different seed. The results from the first approach are shown in Table H–1. This table shows peak expected dose as a function of the number of realizations, in which each data point is a separate Latin Hypercube Sampling run. As this table indicates, the peak expected dose has a random pattern with the number of realizations and the time when the peak expected dose occur. Monte Carlo resampling analysis (i.e., the second approach) also showed similar random behavior. Figure H–1 shows the mean peak dose calculated using an increasing number of realizations from a 4,000-vector run. The mean peak dose varies between 0.108 and 0.275 mSv/yr [10.8 and 27.5 mrem/yr]; the latter value occurring with a very few realizations (i.e., less than 100). The 0.108 mSv/yr [10.8 mrem/yr] is obtained with 500 realizations. Thereafter, the mean peak dose appears to climb almost steadily to 4,000 realizations, which is the maximum number of realizations used in the investigation.

Figure H–2 shows that, for the majority of cases, the variance of the mean peak dose decreases as the number of realizations increases. However, the data show an undesirable amount of fluctuation which leads to significant difficulties in implementing several sensitivity analysis methods.
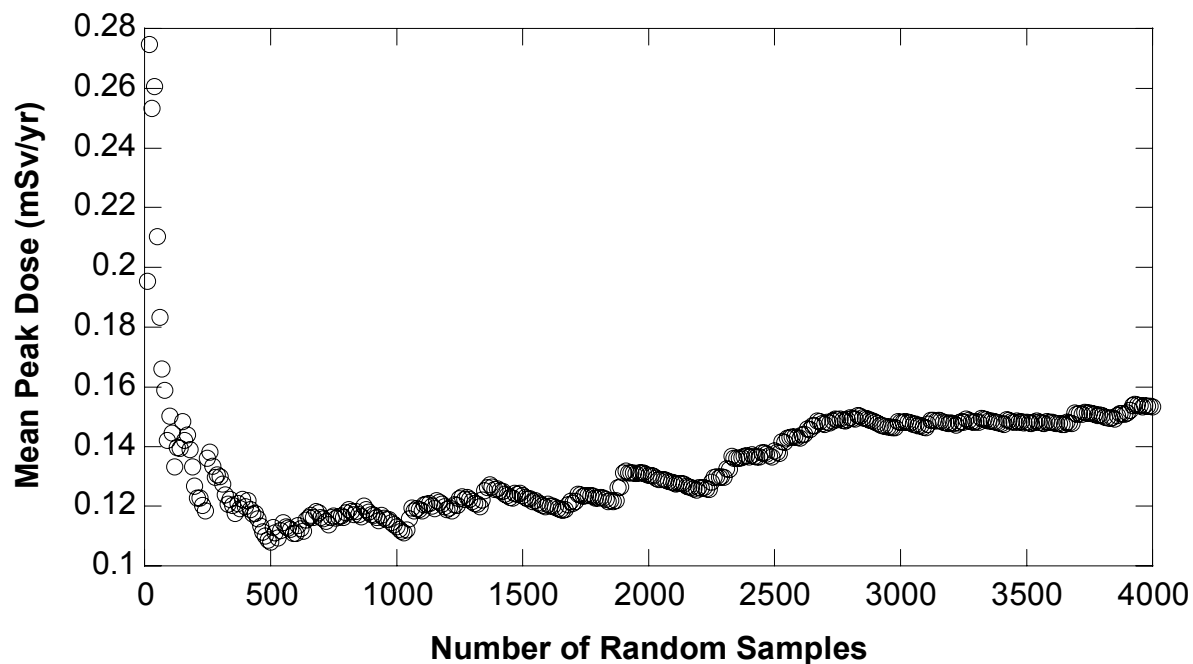
Figure H–1. Mean Peak Dose as a Function of Sample Size Using the TPA Version 4.1 Code

Table H–1. Peak Expected Dose as a Function of the Number of Realizations; Each Data Row Represents an Independent Latin Hypercube Sampling Run		
Realizations	Peak Expected Dose (mSv/yr)	Peak Occurs (yr)
500	2.48×10^{-4}	10,000
1,000	3.05×10^{-4}	8,490
2,000	3.24×10^{-4}	10,000
3,000	2.46×10^{-4}	10,000
4,000	2.94×10^{-4}	10,000

As part of these analyses, a comparison was made with the previous version of the TPA code. Figure H–3 shows the results from the TPA Version 3.2 code (previous version) for one set of 4,000 Latin Hypercube Samplings (compare with Figure H–1). The old result converges nicely with the increasing number of realizations showing stability. Consequently, analyses of the results from the current TPA Version 4.1 code focused on parameters that were newly introduced and on parameters that had their ranges revised. The effects of these parameters were investigated by focusing on the top 25 percent (i.e., high doses) of the realizations.

The analysis revealed that the parameter named Preexponential_SFDissolutionModel2 (variable identification = 63), which affects the mass release rate from the engineered barrier system, was responsible for the increasing trend in the mean peak dose with the increase in the number of realizations. This parameter has a log-uniform distribution with values ranging over three orders of magnitude and has a significant impact on the spent nuclear fuel-dissolution
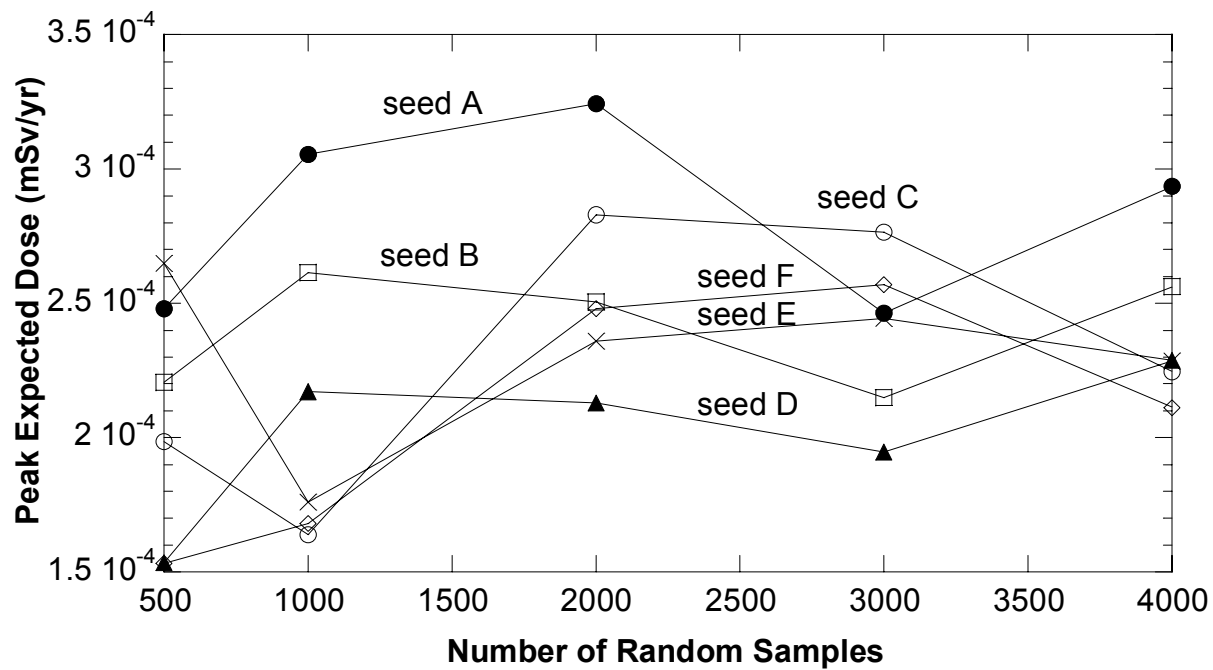
Figure H–2. Peak Expected Dose as a Function of the Number of Realizations; Each Data Point for a Realization Set Represents a Different Random Seed
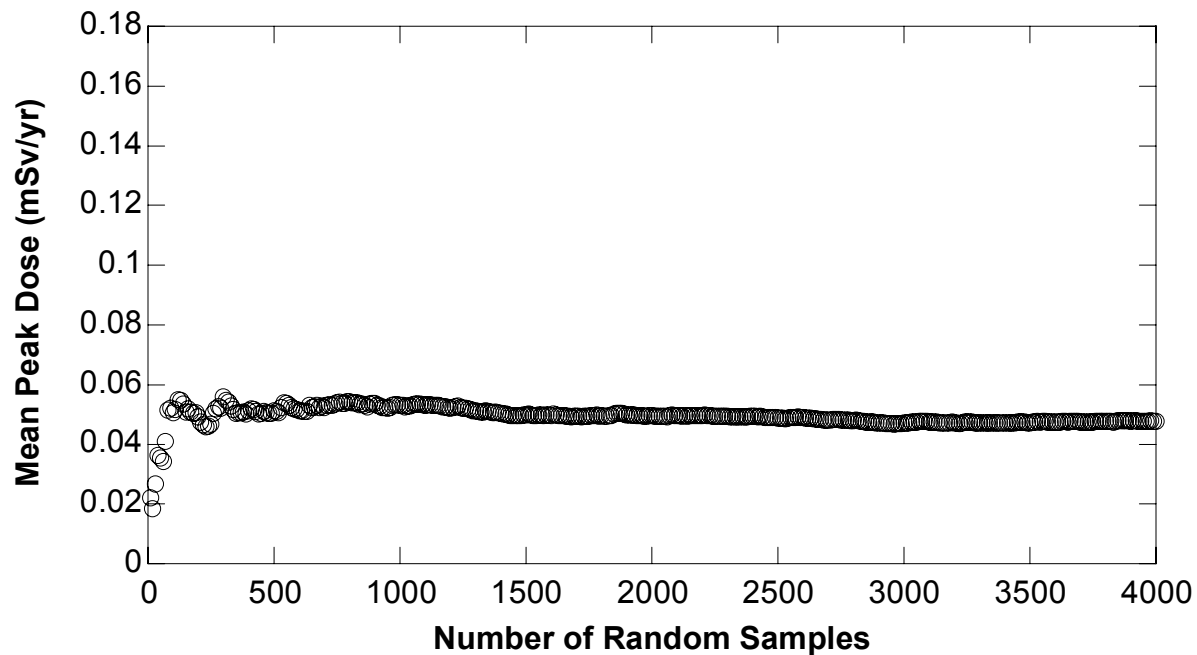

Figure H–3. Mean Peak Dose as a Function of Sample Size Using the TPA Version 3.2 Code

H–3

time, varying from 0 to more than 100,000 years. This parameter makes a large contribution to dose in combination with several other parameters.

Figure H–4 shows the mean peak dose for the remaining realizations after the realizations corresponding to the highest 25 percent of the sampled values for this parameter are removed from the set of 4,000. The difference between Figures H–1 and H–4 suggests that the large variations in the mean peak dose as a function of the number of realizations are caused by the preexponential spent fuel dissolution Model 2 parameter.

This investigation lead to the following findings: (i) the sampling technique used in the current NRC code needs to be carefully examined, (ii) sets much larger than the set of 4,000 realizations should be used to reach a stable peak expected dose or mean peak dose, (iii) the parameter ranges should be carefully screened to ensure that the long-tail distributions for influential parameters are not arbitrarily specified, (iv) sensitivity analyses should be performed carefully, especially when estimating the number of realizations needed to reach a specified confidence level, and (v) multiple sets of realizations of the same size (length) generated using different random seeds should be used for a variety of sample sizes to assure convergence.

References

Code of Federal Regulations. "Disposal of High-Level Radioactive Wastes in a Proposed Geological Repository at Yucca Mountain, Nevada." Title10—Energy, Chapter 1—NRC, Part 63. Washington, DC: U.S. Government Printing Office, 1991.
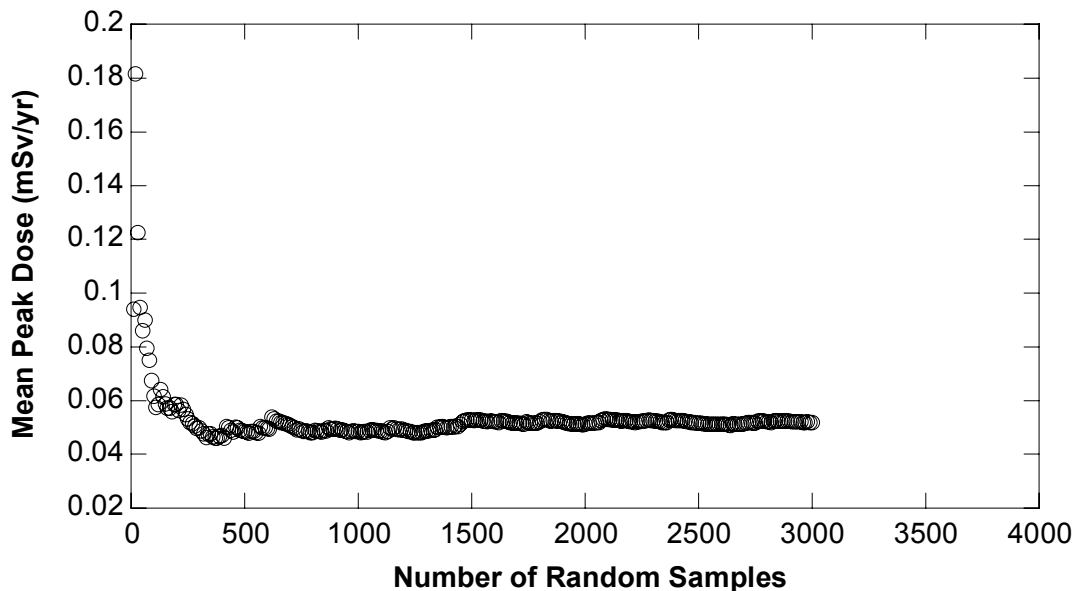

Figure H–4. Mean Peak Dose as a Function of Number of Realizations Remaining After the Realizations Corresponding to the Highest 25 Percent of the Sampled Values for the Preexponential_SFDissolutionModel2 Parameter are Removed from the Set of 4,000